

VOLUME 79

JULY 3, 1975

✓ NUMBER 14

JPCHAx

---

THE JOURNAL OF  
PHYSICAL  
CHEMISTRY

---

PUBLISHED WEEKLY BY THE AMERICAN CHEMICAL SOCIETY

# THE JOURNAL OF PHYSICAL CHEMISTRY

---

**BRYCE CRAWFORD, Jr.**, *Editor*  
**STEPHEN PRAGER**, *Associate Editor*  
**ROBERT W. CARR, Jr.**, **FREDERIC A. VAN-CATLEDGE**, *Assistant Editors*

**EDITORIAL BOARD:** C. A. ANGELL (1973-1977), F. C. ANSON (1974-1978), V. A. BLOOMFIELD (1974-1978), J. R. BOLTON (1971-1975), L. M. DORFMAN (1974-1978), H. L. FRIEDMAN (1975-1979), E. J. HART (1975-1979), W. J. KAUZMANN (1974-1978), R. L. KAY (1972-1976), D. W. McCLURE (1974-1978), R. M. NOYES (1973-1977), J. A. POPLER (1971-1975), B. S. RABINOVITCH (1971-1975), S. A. RICE (1969-1975), F. S. ROWLAND (1973-1977), R. L. SCOTT (1973-1977), A. SILBERBERG (1971-1975), J. B. STOTHERS (1974-1978), W. A. ZISMAN (1972-1976)

**AMERICAN CHEMICAL SOCIETY**, 1155 Sixteenth St., N.W., Washington, D.C. 20036

## Books and Journals Division

**JOHN K CRUM** *Director*  
**VIRGINIA E. STEWART** *Assistant to the Director*

---

**CHARLES R. BERTSCH** *Head, Editorial Processing Department*  
**D. H. MICHAEL BOWEN** *Head, Journals Department*  
**BACIL GUILLEY** *Head, Graphics and Production Department*  
**SELDON W. TERRANT** *Head, Research and Development Department*

©Copyright, 1975, by the American Chemical Society. Published biweekly by the American Chemical Society at 20th and Northampton Sts., Easton, Pa. 18042. Second-class postage paid at Washington, D.C., and at additional mailing offices.

All manuscripts should be sent to *The Journal of Physical Chemistry*, Department of Chemistry, University of Minnesota, Minneapolis, Minn. 55455.

*Additions and Corrections* are published once yearly in the final issue. See Volume 78, Number 26 for the proper form.

*Extensive or unusual alterations in an article after it has been set in type are made at the author's expense*, and it is understood that by requesting such alterations the author agrees to defray the cost thereof.

The American Chemical Society and the Editor of *The Journal of Physical Chemistry* assume no responsibility for the statements and opinions advanced by contributors.

Correspondence regarding accepted copy, proofs, and reprints should be directed to Editorial Processing Department, American Chemical Society, 20th and Northampton Sts., Easton, Pa. 18042. Department Head: CHARLES R. BERTSCH. Associate Department Head: MARIANNE C. BROGAN. Assistant Editors: CELIA B. MCFARLAND, JOSEPH E. YURVATI.

Advertising Office: Centcom, Ltd., 50 W. State St., Westport, Conn. 06880.

## Business and Subscription Information

Send all new and renewal subscriptions *with payment to:* Office of the Controller, 1155 16th Street, N.W., Washington, D.C. 20036. Subscriptions should be renewed promptly to avoid a break in your series. All correspondence and telephone calls regarding

changes of address, claims for missing issues, subscription service, the status of records, and accounts should be directed to Manager, Membership and Subscription Services, American Chemical Society, P.O. Box 3337, Columbus, Ohio 43210. Telephone (614) 421-7230. For microfiche service, contact ACS Journals Department, 1155 16th St. N.W., Washington, D.C. 20036. Telephone (202) 872-4444.

On changes of address, include both old and new addresses with ZIP code numbers, accompanied by mailing label from a recent issue. Allow four weeks for change to become effective.

Claims for missing numbers will not be allowed (1) if loss was due to failure of notice of change in address to be received before the date specified, (2) if received more than sixty days from date of issue plus time normally required for postal delivery of journal and claim, or (3) if the reason for the claim is "issue missing from files."

Subscription rates (hard copy or microfiche) in 1975: \$20.00 for 1 year to ACS members; \$80.00 to nonmembers. Extra postage \$4.50 in Canada and PUAS, \$5.00 other foreign. Supplementary material (on microfiche only) available on subscription basis, 1975 rates: \$15.00 in U.S., \$19.00 in Canada and PUAS, \$20.00 elsewhere. All microfiche airmailed to non-U.S. addresses; air freight rates for hard-copy subscriptions available on request.

Single copies for current year: \$4.00. Rates for back issues from Volume 56 to date are available from the Special Issues Sales Department, 1155 Sixteenth St., N.W., Washington, D.C. 20036.

Subscriptions to this and the other ACS periodical publications are available on microfilm. For information on microfilm write Special Issues Sales Department at the address above.

Notice to Authors printed in this issue

# THE JOURNAL OF PHYSICAL CHEMISTRY

Volume 79, Number 14 July 3, 1975

JPCHAx 79(14) 1327-1482 (1975)

ISSN 0022-3654

- Gas to Liquid to Solid Transition in Halogen Hot Atom Chemistry. II. Systematics of Bromine Reactions Activated by Radiative Neutron Capture and Isomeric Transition with Halomethanes . . . . . M. E. Berg, W. M. Grauer, R. W. Helton, and E. P. Rack\* 1327
- Variations of Fluorescence Quantum Yields with pH or Hammett Acidity. Near Equilibrium Vs. Nonequilibrium Excited State Proton Exchange . . . . . Stephen G. Schulman\* and Anthony C. Capomacchia 1337
- Excited State  $pK^*$  Values for Fluorimetry . . . . . Nechama Lasser and Jehuda Feitelson\* 1344
- A Spectroscopic Study on Benzenethiol and Thioanisole by Photoselection . . . . . Philip G. Russell 1347
- Some Observations on the Photoproduct Formation in Benzenethiol, Diphenyl Disulfide, and Diphenyl Sulfide . . . . . Philip G. Russell 1353
- Metal Precipitation from Pulse Irradiated Solutions of Cadmium(II) and Similar Cations . . . . . Aaron Barkatt\* and Joseph Rabani 1359
- Solute Environmental Effects in the One-Electron Reduction of Lysozyme in Aqueous Solution . . . . . Morton Z. Hoffman\* and E. Hayon\* 1362
- Solvent and Temperature Effects on the Fluorescence of *all-trans*-1,6-Diphenyl-1,3,5-hexatriene . . . . . E. D. Cehelnik, R. B. Cundall,\* J. R. Lockwood, and T. F. Palmer 1369
- An Investigation of Isomerization of 1,3-Pentadiene Sensitized by Solid Benzophenone Using Internal Reflection Photolysis . . . . . José S. DeGuzman and G. R. McMillan\* 1377
- Dye Binding and Its Relation to Polyelectrolyte Conformation . . . . . J. S. Tan\* and R. L. Schneider 1380
- Effects of Ion Association upon the Solubilities of the Cyclooctatetraene Dianion . . . . . Gerald R. Stevenson\* and Ignacio Ocasio 1387
- Thermodynamic Quantities for the Transfer of Urea from Water to Aqueous Electrolyte Solutions . . . . . Martha Y. Schrier, Peter J. Turner, and Eugene E. Schrier\* 1391 ■
- Wave-Damping and Film-Pressure Studies of Polydimethylsiloxane Monolayers on Organic Liquid Substrates . . . . . R. L. Shuler and W. A. Zisman\* 1397
- Conjugation between Unsaturated Systems through a Heteroatom. II. Molecular Stereolability of Reacting Para-Substituted Phenyl Isobutenyl Ethers . . . . . R. H. Donnay, F. Garnier, and J. E. Dubois\* 1406
- Deuteron Nuclear Magnetic Resonance in Amphiphilic Liquid Crystals. Alkali Ion Dependent Water and Amphiphile Orientation . . . . . Nils-Ola Persson\* and Björn Lindman 1410
- Electron Spin Resonance Studies of Phenyl and Pyridyl Radicals in Aqueous Solution . . . . . Haya Zemel and Richard W. Fessenden\* 1419
- The Nature of the Potential Function for Internal Rotation about Carbon-Sulfur Bonds in Disulfides . . . . . H. E. Van Wart, L. L. Shipman, and H. A. Scheraga\* 1428
- Theoretical and Experimental Evidence for a Nonbonded 1,4 Carbon-Sulfur Interaction in Organosulfur Compounds . . . . . H. E. Van Wart, L. L. Shipman, and H. A. Scheraga\* 1436 ■
- A Statistical Thermodynamical Approach to the Distribution of Cations in Silicate Minerals . . . . . W. J. Mortier 1447

ห้องสมุด กรมวิทยาศาสตร์  
26.๗.๒518

Conductivity Anomalies of Aqueous Carboxylic Acid Solutions. Dimerization or Effect of Solvent Medium? . . . . .	<b>R. B. Simpson</b>	1450
Capacitance and Conductance of Solutions of Optically Active Amino Acid Ion Pairs in 1-Octanol . . . . .	<b>Stefan Highsmith</b>	1456
Evaluation of Dielectric Behavior of Time Domain Spectroscopy. I. Dielectric Response by Real Time Analysis . . . . .	<b>Robert H. Cole</b>	1459
Evaluation of Dielectric Behavior of Time Domain Spectroscopy. II. Complex Permittivity . . . . .	<b>Robert H. Cole</b>	1469

### COMMUNICATIONS TO THE EDITOR

Evidence for an Exciton Interaction in the Low-Lying Singlets of Diphenyl Sulfide . . . . .	<b>Philip G. Russell</b>	1475
Ethylamine Behavior on 3A Zeolite Surface . . . . .	<b>Ubavka Mioč* and Nadezda Petranović</b>	1476
Chemistry of Nuclear Recoil $^{18}\text{F}$ Atoms. VII. Detection of Caging Reactions in Liquid Phase $\text{CF}_3\text{CH}_3$ and $\text{CHF}_2\text{CH}_3$ . . . . .	<b>Ronald G. Manning and John W. Root*</b>	1478
Selective Oxidation of Nickel in Copper-Nickel Alloys in Nitric Oxide . . . . .	<b>Yoshio Takasu,* Yoshiharu Matsuda, Shun-ichi Maru, Nobutoshi Hayashi, Hiroshi Yoneyama, and Hideo Tamura</b>	1480
Absolute Viscosity of $\text{D}_2^{18}\text{O}$ between 15 and $35^\circ$ . . . . .	<b>D. Wolf and A. I. Kudish*</b>	1481

■ Supplementary material for this paper is available separately, in photocopy or microfiche form. Ordering information is given in the paper.

\* In papers with more than one author, the asterisk indicates the name of the author to whom inquiries about the paper should be addressed.

### AUTHOR INDEX

Barkatt, A., 1359	Hayashi, N., 1480	Ocasio, I., 1387	Shipman, L. L., 1428, 1436
Berg, M. E., 1327	Hayon, E., 1362	Palmer, T. F., 1369	Shuler, R. L., 1397
Capomacchia, A. C., 1337	Helton, R. W., 1327	Persson, N.-O., 1410	Simpson, R. B., 1450
Cehelnik, E. D., 1369	Highsmith, S., 1456	Petranović, N., 1476	Stevenson, G. R., 1387
Cole, R. H., 1459, 1469	Hoffman, M. Z., 1362	Rabani, J., 1359	Takasu, Y., 1480
Cundall, R. B., 1369	Kudish, A. I., 1481	Rack, E. P., 1327	Tamura, H., 1480
DeGuzman, J. S., 1377	Lasser, N., 1344	Root, J. W., 1478	Tan, J. S., 1380
Donnay, R. H., 1406	Lindman, B., 1410	Russell, P. G., 1347, 1353, 1475	Turner, P. J., 1391
Dubois, J. E., 1406	Lockwood, J. R., 1369	Scheraga, H. A., 1428, 1436	Van Wart, H. E., 1428, 1436
Feitelson, J., 1344	Manning, R. G., 1478	Schneider, R. L., 1380	Wolf, D., 1481
Fessenden, R. W., 1419	Maru, S., 1480	Schrier, E. E., 1391	Yoneyama, H., 1480
Garnier, F., 1406	Matsuda, Y., 1480	Schrier, M. Y., 1391	Zemel, H., 1419
Grauer, W. M., 1327	McMillan, G. R., 1377	Schulman, S. G., 1337	Zisman, W. A., 1397
	Mioč, U., 1476		
	Mortier, W. J., 1447		

# NOTICE TO AUTHORS

---

## I. General Considerations

*The Journal of Physical Chemistry* is devoted to reporting both experimental and theoretical research dealing with fundamental aspects of physical chemistry. Space limitations necessitate giving preference to research articles dealing with previously unanswered basic questions in physical chemistry. Acceptable topics are those of general interest to physical chemists, especially work involving new concepts, techniques, and interpretations. Research that may lead to reexaminations of generally accepted views is, of course, welcome.

Authors reporting data should include an interpretation of the data and its relevance to the theories of the properties of matter. However, the discussion should be concise and to the point and excessive speculation is to be discouraged. Papers reporting redeterminations of existing data will be acceptable only if there is reasonable justification for repetition: for example, if the more recent or more accurate data lead to new questions or to a reexamination of well known theories. Manuscripts that are essentially applications of chemical data or reviews of the literature are, in general, not suitable for publication in *The Journal of Physical Chemistry*. Detailed comparisons of methods of data analysis will be considered only if the paper also contains original data, or if such comparison leads to a genesis of new ideas.

Authors should include an introductory statement outlining the scientific rationale for the research. The statement should clearly specify the questions for which answers are sought and the connection of the present work with previous work in the field. All manuscripts are subject to critical review. It is to be understood that the final decision relating to a manuscript's suitability rests solely with the editors.

Symposium papers are sometimes published as a group, but only after special arrangement with the editor.

Authors' attention is called to the "Handbook for Authors," available from the Special Issues Sales Department, American Chemical Society, 1155 Sixteenth St., N.W., Washington, D. C. 20036, in which pertinent material is to be found.

## II. Types of Manuscripts

*The Journal of Physical Chemistry* publishes two types of manuscripts: *Articles* and *Communications*.

A. *Articles* should cover their subjects with thoroughness, clarity, and completeness. However, authors should also strive to make their *Articles* as concise as possible, avoiding unnecessary historical background. Abstracts to *Articles* should be brief—300 words is a maximum—and should serve to summarize the significant data and conclusions. The abstract should convey the essence of the *Article* to the reader.

B. *Communications* are of two types, *Letters* and *Comments*. Both types are restricted to three-quarters of a page (750 words or the equivalent) including tables, figures, and text, and both types of *Communications* are subject to critical review, but special efforts will be made to expedite publication.

*Letters* should report preliminary results whose immediate availability to the scientific community is deemed important, and whose topic is timely enough to justify the double publication that usually results from the publication of a *Letter*.

*Comments* include significant remarks on the work of others. The editors will generally permit the authors of the work being discussed to reply.

The category of *Notes* has been discontinued since the handling of such manuscripts was precisely the same as that of *Articles* save for the requirement of an Abstract, and since even a short *Article* will need an Abstract ultimately, it seems as well to ask the author to provide this. Short *Articles* will of course continue to be welcome contributions.

## III. Introduction

All manuscripts submitted should contain brief introductory remarks describing the purpose of the work and giving sufficient background material to allow the reader to appreciate the state-of-knowledge at the time when the work was done. The introductory remarks in an *Article* should constitute the first section of the paper and should be labeled accordingly. In *Communications*, the introductory material should not be in such a separate section. To judge the appropriateness of the manuscript for *The Journal of Physical Chemistry*, the editors will place considerable weight on the author's intentions as stated in the Introduction.

## IV. Microform Material

From time to time manuscripts involve extensive tables, graphs, spectra, mathematical derivations, expanded discussions of peripheral points, or other material which, though essential to the specialized reader who needs all the data or all the detail, does not help and often hinders the effective presentation of the work being reported. Such "microform material" can be included in the *microfilm* edition of this Journal, available in many scholarly libraries, and also in the *microfiche* edition. In some instances the microform material may also be included in the printed issue in *miniprint*, in which the manuscript pages are reproduced directly in reduced size. All microform material may be obtained directly by the interested reader at nominal cost, either in full size photocopy or in microfiche (in which miniprint material appears at standard reduction, i.e., one manuscript page per microfiche frame). Authors are encouraged to make use of this resource, in the interest of shorter articles (which mean more rapid publication) and clearer more readable presentation.

Microform material should accompany a manuscript at the time of its original submission to an editor. It should be clipped together and attached at the end of the manuscript, along with a slip of paper clearly indicating that the material is "microform material." Copy for microform material should preferably be on 8½ × 11 in. paper, and in no case on sheets larger than 11 × 14 in.; if typed it should be one and

one-half spaced, and in any event the smallest character should be at least one-eighth inch in size; good contrast of black characters against a white background is required for clear photoprocess reproduction.

A paragraph should appear at the end of the paper indicating the nature of the material and the means by which the interested reader may obtain copies directly. The following is an example.

*Supplementary Material Available.* A listing of structure factor amplitudes will appear following these pages in the microform editions of this volume of the Journal. Photocopies of this material from this paper only, or microfiche (105 × 148 mm, 24× reduction, negatives) containing all material for the papers in this issue, may be obtained from the Business Office, Books and Journals Division, American Chemical Society, 1155 Sixteenth Street N.W., Washington, D. C. 20036. Remit check or money order for \$0.00 for photocopy or \$0.00 for microfiche, referring to code number JPC-00-0000.

The amount of money to be indicated in the blanks will be filled in by the Editorial Office at Easton, Pa. after the acceptance of an article.

## V. Functions of Reviewers

The editors request the scientific advice of reviewers who are active in the area of research covered by the manuscript. The reviewers act only in an advisory capacity and the final decision concerning a manuscript is the responsibility of the editors. The reviewers are asked to comment not only on the scientific content, but also on the manuscript's suitability for *The Journal of Physical Chemistry*. With respect to *Communications*, the reviewers are asked to comment specifically on the urgency of publication. **Authors are encouraged to suggest, when submitting a manuscript, names of scientists who could give a disinterested and informed and helpful evaluation of the work.** All reviews are anonymous and the reviewing process is most effective if reviewers do not reveal their identities to the authors. An exception arises in connection with a manuscript submitted for publication in the form of a comment on the work of another author. Under such circumstances the first author will, in general, be allowed to review the communication and to write a rebuttal, if he so chooses. The rebuttal and the original communication may be published together in the same issue of the journal. Revised manuscripts are generally sent back to the original reviewers, who are asked to comment on the revisions. If only minor revisions are involved, the editors examine the revised manuscript in light of the recommendations of the reviewers without seeking further opinions. For the convenience of reviewers, authors are advised to indicate clearly, either in the manuscript or in a covering letter, the specific revisions that have been made.

## VI. Submission of Manuscripts

**All manuscripts must be submitted in triplicate to expedite handling. Manuscripts must be typewritten, double-spaced copy, on 8½ × 11 in. paper. Legal sized paper is not acceptable.** Authors should be certain that copies of the manuscript are clearly reproduced and readable. **Authors submitting figures must include the original drawings or photographs thereof, plus three xerographic copies for review purposes. These reproductions of the figures should be on 8½ × 11 in. paper.** Graphs must be in black ink on white or blue paper. Figures and tables should be held to a minimum consistent with adequate presentation of information. All original

data which the author deems pertinent must be submitted along with the manuscript. For example, a paper reporting a crystal structure should include structure factor tables for use by the reviewers.

**All references and explanatory notes, formerly set up as footnotes on individual pages, are now grouped at the end of the article in a section called "References and Notes."** They should be numbered consecutively in the order in which they are first mentioned in the text, and the complete list of notes and literature citations should appear at the end of the manuscript. Nomenclature should conform to that used in *Chemical Abstracts* and mathematical characters should be underlined for italics, Greek letters should be annotated, and subscripts and superscripts clearly marked.

Papers should not depend for their usefulness on unpublished material, and excessive reference to material in press is discouraged. References not readily available (*e.g.*, private technical reports, preprints, or articles in press) that are necessary for a complete review of the paper must be included with the manuscript for use by the reviewers.

## VII. Revised Manuscripts

A manuscript sent back to an author for revision should be returned to the editor within 6 months; otherwise it will be considered withdrawn and treated as a new manuscript when and if it is returned. Revised manuscripts returned to the editor must be submitted in triplicate and all changes should be made by typewriter. **Unless the changes are very minor, all pages affected by revision must be retyped.** If revisions are so extensive that a new typescript of the manuscript is necessary, it is requested that a copy of the original manuscript be submitted along with the revised one.

## VIII. Proofs and Reprints

Galley proofs, original manuscript, cut copy, and reprint order form are sent by the printer directly to the author who submitted the manuscript. The attention of the authors is directed to the instructions which accompany the proof, especially the requirement that all corrections, revisions, and additions be entered on the proof and not on the manuscript. Proofs should be checked against the manuscript (in particular all tables, equations, and formulas, since this is not done by the editor) and returned as soon as possible. No paper is released for printing until the author's proof has been received. Alterations in an article after it has been set in type are made at the author's expense, and it is understood that by entering such alterations on proofs the author agrees to defray the cost thereof. The filled-out reprint form must be returned with the proof, and if a price quotation is required by the author's organization a request for it should accompany the proof. Since reprinting is generally done from the journal press forms, all orders must be filed before press time. None can be accepted later, unless a previous request has been made to hold the type. Reprint shipments are made a month or more after publication, and bills are issued by the printer subsequent to shipment. Neither the editors nor the Washington office keeps any supply of reprints. Therefore, only the authors can be expected to meet requests for single copies of papers.

A page charge is assessed to cover in part the cost of publication. Although payment is expected, it is not a condition for publication. Articles are accepted or rejected only on the basis of merit, and the editor's decision to publish the paper is made before the charge is assessed. The charge per journal page is \$50.

# THE JOURNAL OF PHYSICAL CHEMISTRY

Registered in U. S. Patent Office © Copyright, 1975, by the American Chemical Society

VOLUME 79, NUMBER 14 JULY 3, 1975

## Gas to Liquid to Solid Transition in Halogen Hot Atom Chemistry. II. Systematics of Bromine Reactions Activated by Radiative Neutron Capture and Isomeric Transition with Halomethanes<sup>1</sup>

M. E. Berg, W. M. Grauer, R. W. Helton, and E. P. Rack\*

Department of Chemistry, University of Nebraska, Lincoln, Nebraska 68508 and General Medical Research, V.A. Hospital, Omaha, Nebraska 68105 (Received December 23, 1974)

Publication costs assisted by the U.S. Energy Research and Development Administration

Bromine reactions activated by  $^{79}\text{Br}(n,\gamma)^{80}\text{Br}$ ,  $^{81}\text{Br}(n,\gamma)^{82}\text{Br}^m + ^{82}\text{Br}$ , and  $^{82}\text{Br}^m(\text{I.T.})^{82}\text{Br}$  nuclear transformations were studied in halomethanes as functions of mole fraction of  $\text{Br}_2$ , phase, density, and intermolecular distance. Gas phase systematics coupled with the density and mole fraction of  $\text{Br}_2$  studies demonstrate the existence of systematic trends in the condensed phases as evidenced by the Richardson-Wolfgang effect. A definitive difference due to activation that is independent of system and suggests the importance of caging at higher densities is shown by the variation of total and individual organic product yields with density. The study of total organic product yield vs. intermolecular distance provides both a means of separating cage and molecular reactions and suggests the importance of molecular properties in the caging event.

### Introduction

A fundamental question in condensed phase hot atom chemistry is whether reactions activated by nuclear transformations in organic media proceed by caging or molecular mechanisms, or both. Since Franck and Rabinowitsch<sup>2</sup> postulated the cage event there have been many studies<sup>3</sup> directed at characterization of radical reactions in the cage; yet no direct evidence of the caging process has been presented. In the condensed phase the concept of the caging process suggests complex and diverse kinetic events for both hot atom<sup>4-6</sup> and photochemistry.<sup>7-10</sup>

Recent analytic studies<sup>8,9</sup> and computer simulations<sup>7,10</sup> have cast doubt upon the adequacy of bulk properties such as viscosity to describe the caging process. Bunker and Jacobson<sup>7</sup> have suggested that recoil energy, molecular size, and intermolecular forces play a more important role in the determination of cage recombination reactions. It is unfortunate that those experimental techniques most sensitive to molecular properties, e.g., molecular beam and ion cyclotron resonance studies, are ill-suited to high density or pressure regions where the caging event occurs. Photochemical studies have provided a wealth of information on

\* Address correspondence this author at the Department of Chemistry, University of Nebraska, Lincoln, Nebr. 68508.

reactions within the cage but cannot provide simultaneous data on cage and molecular reactions since, in the majority of events, the reactant species is born within the cage.

One of the most significant studies demonstrated the Richardson-Wolfgang effect.<sup>11</sup> In their study of  $^{18}\text{F}$  reaction activated by the  $(n,2n)$  process in  $\text{CH}_3\text{F}$ , Richardson and Wolfgang found an increase in product yields with increasing density in the gas to liquid to solid transition. Above a density of  $0.1 \text{ g cm}^{-3}$  the product yields were essentially constant, giving a continuous plateau through the critical density region, before rising again, above a density of  $0.5 \text{ g cm}^{-3}$  where mean intermolecular distances shrink to about half the diameter of the fluorine atom. If the plateau that Richardson and Wolfgang observe is due to collisional stabilization of molecular products, then the subsequent increase in product yields with increasing density must be the result of caging reactions involving the hot atom and organic radicals it has produced in the medium.

In this paper we report on studies of the effects of bromine concentration, density, phase, and intermolecular distance on bromine reactions activated by radiative neutron capture and isomeric transition on halomethane systems in an attempt to learn more about the characteristics and systematics of molecular and radical cage reactions.

## Experimental Section

**Materials.**  $\text{CH}_3\text{F}$ ,  $\text{CH}_3\text{Cl}$ , and  $\text{CH}_3\text{Br}$  were obtained from Matheson Chemical Co. with a stated purity level greater than 98, 99.5, and 99.5 mol %, respectively. Prior to filling the sample ampoules the halomethanes were purified by repeated bulb-to-bulb distillation cycles on the vacuum line. Matheson  $\text{ICl}$  was used as received. Bromine prepared from Mallinckrodt reagent grade  $\text{K}_2\text{Cr}_2\text{O}_7$ ,  $\text{KBr}$ , and  $\text{H}_2\text{SO}_4$  was used after three distillations over  $\text{P}_2\text{O}_5$ , collecting middle fractions. Airco assayed reagent He, Ar, Kr, and Xe were used without further purification.

**Preparation of Reaction Systems.** Gas-phase radiative neutron capture and isomeric-transition activated reactions of bromine with halomethanes were studied in the presence of rare-gas moderators or  $\text{Br}_2$  additive in order to determine the "thermal" and "hot" (requiring high translational energy)<sup>3d</sup> contribution to the total organic product yield (TOPY). Quadruplicate thin-wall quartz ampoules of about 10 ml size were prewashed<sup>12</sup> and filled with the reactants and moderator using vacuum line techniques. All samples (with rare-gas moderators) contained 5 Torr of  $\text{Br}_2$  vapor except where indicated. The total pressure of these systems was 1 atm. All samples, wrapped in aluminum foil, were kept frozen under liquid nitrogen until neutron irradiation. Exposure to light was minimized before, during, and after irradiation. High pressure gas samples were prepared by the usual vacuum line techniques except thick-walled quartz ampoules were employed.

Condensed-phase systems containing  $\text{Br}_2$  or  $\text{ICl}$  and the halomethane were prepared in a similar manner to that described for gaseous systems. Small (less than 1 ml volume) thick-walled quartz ampoules, capable of withstanding several tens of atmospheres of internal pressure, were filled with  $\text{Br}_2$  or  $\text{ICl}$  and the halomethane. Bromine or  $\text{ICl}$  was introduced into the quartz ampoule by freezing down a relatively large quantity from a large glass flask attached to the vacuum line. The halomethane was then introduced in a similar fashion. The ampoule was immersed under liquid nitrogen at all times. The relative amounts of gases used were metered by the manometer prior to freezing down into the ampoule so that mole fractions could readily be calculated. For all reaction mixtures in the study of the effects of varying density on TOPY and individual organic product yields (IOPY), densities of the reaction mixture as a function of temperature were determined by the method of Rice and Willard.<sup>13</sup>

**Neutron Irradiation.** All irradiations were performed in the Omaha Nebraska, V.A. Hospital TRIGA reactor at a thermal neutron flux of  $1.1 \times 10^{11}$  neutrons  $\text{cm}^{-2} \text{sec}^{-1}$  and an accompanying  $\gamma$ -radiation flux of  $3 \times 10^{17}$  eV  $\text{g}^{-1} \text{min}^{-1}$ . Irradiation times varied from a few seconds for TOPY determinations to 3 min for IOPY determinations employing chromatographic techniques. We did not find any radiation damage in such short irradiation times. Irradiation procedures for studying the  $(n,\gamma)$ -activated reactions of  $^{80}\text{Br}$ ,  $^{82}\text{Br}$ , and  $^{38}\text{Cl}$  are similar to those previously reported.<sup>12,14,15</sup> The "in-reactor" techniques<sup>16</sup> was used for TOPY and IOPY determinations produced by the  $^{82}\text{Br}^m(\text{I.T.})^{82}\text{Br}$  reaction in the various gas and condensed phase samples.

The densities of the condensed phase reaction mixtures were varied by changing the temperature of the ampoule. For temperatures greater than 25°, the ampoule was immersed in preheated mineral oil in the TRIGA irradiation "rabbit". For the short irradiation times employed there

was little change in temperature. Other ampoules were irradiated immersed in ice water and Dry Ice. It was not feasible to irradiate samples under liquid nitrogen. For the  $(n,\gamma)$ -activated bromine or chlorine systems, ampoules initially at liquid nitrogen temperatures were irradiated for times less than 10 sec. We found that the temperature rose to only 80°K at 30 sec after being removed from the liquid nitrogen, 83°K at 45 sec, and 103° at 55 sec.<sup>21</sup> Handling of bromine samples by (I.T.) activation was similar to that previously described except the irradiated ampoule was allowed to stand for 2 hr under heated mineral oil, room temperature, ice water, Dry Ice, or liquid nitrogen, allowing greater than 99.9% of the  $^{82}\text{Br}^m$  to undergo isomeric transition.

**Extraction Procedure.** Total organic product yields (TOPY) for both the  $(n,\gamma)$ - and (I.T.)-activated systems were determined by breaking the irradiated bubblet in a separatory funnel containing a two-phase mixture of  $\text{CCl}_4 + \text{I}_2$  and 0.5 M aqueous  $\text{Na}_2\text{SO}_3$  in the usual manner.<sup>12,14,16</sup> For  $^{38}\text{Cl}$  determinations in the  $\text{ICl} + \text{CH}_3\text{Cl}$  system, a Harshaw 12.2% efficient  $\text{Ge}(\text{Li})$  detector<sup>17,18</sup> coupled to a Nuclear Data 2400 1024-channel analyzer was used. The TOPYs were determined in the usual manner.<sup>12,14,16</sup> In order to prevent any volatilization of  $^{82}\text{Br}$  labeled products, the polyethylene counting vials were stored over Dry Ice for 48 hr before counting the  $^{82}\text{Br}$  activity.

**Radiogas Chromatographic Separations of the Activated Mixtures.** Before the irradiated samples were analyzed in the radiogas chromatograph, they were subjected to a solvent extraction procedure to remove the inorganic halogen products. The labeled organic products were extracted into 5–10 ml of  $\text{CCl}_4$ , depending on the activity level of the sample. Samples for  $^{80}\text{Br}$  or  $^{38}\text{Cl}$  determinations [ $(n,\gamma)$ -activation] were analyzed immediately. Samples for  $^{82}\text{Br}$  determinations [(I.T.)-activation] were extracted 48 hr after irradiation. Small quantities of the organic phase with added product carriers were injected directly into the radiogas chromatograph, which has been previously described in detail.<sup>12,22,23</sup> For low-activity gas systems we employed a modified flow-through proportional counter of the type described by Wolf et al.,<sup>24</sup> and previously used by us. For high activity condensed phase systems a  $\gamma$ -ray scintillation counter<sup>12,22</sup> was employed.

All separations were performed on a 3-m stainless steel coil containing 5% by weight di(2-ethylhexyl) sebacate on 50–60 mesh firebrick, linear temperature programmed from 15 to 125° at 4°/min, with a helium flow rate of 100 ml/min for  $\text{CH}_3\text{Br}$  systems and 75 ml/min for  $\text{CH}_3\text{Cl}$  and  $\text{CH}_3\text{F}$  systems. For the (a)  $\text{CH}_3\text{F}$ , (b)  $\text{CH}_3\text{Cl}$ , and (c)  $\text{CH}_3\text{Br}$  systems the labeled products observed in their order of elution were: (a)  $\text{CH}_3\text{Br}$ ,  $\text{CH}_2\text{FBr}$ ,  $\text{CH}_2\text{Br}_2$ ,  $\text{CHBr}_3$ ,  $\text{CFBr}_3$ , and  $\text{CBr}_4$ ; (b)  $\text{CH}_3\text{Br}$ ,  $\text{CH}_2\text{ClBr}$ ,  $\text{CH}_2\text{Br}_2$ ,  $\text{CHClBr}_2$ , and  $\text{CHBr}_3$ ; (c)  $\text{CH}_3\text{Br}$ ,  $\text{CH}_2\text{Br}_2$ ,  $\text{CHBr}_3$ , and  $\text{CBr}_4$ .

In our initial communication<sup>15</sup> reporting a density effect on  $^{80}\text{Br}$  reactions with  $\text{CH}_3\text{F}$  we employed C-22A firebrick coated with 13% by weight of DC-550 silicone oil, operated at 50°. Under these conditions the  $\text{CH}_3\text{Br}$  and  $\text{CH}_2\text{FBr}$  appeared as one peak followed by  $\text{CH}_2\text{Br}_2$ , with no other products separated. However, the general trends in product yield with density previously found<sup>15</sup> are similar to those found using the sebacate column. Our chromatographic results for both  $(n,\gamma)$ - and (I.T.)-activated bromine with condensed phase  $\text{CH}_3\text{Br}$  (Figures 7 and 8) are quite similar to those of Milman et al.<sup>25</sup> using a discontinuous radiogas chromatographic procedure.



## Results and Discussion

*Activation of Bromine by Radiative Neutron Capture and Isomeric Transition.* It is generally recognized that an atom can acquire a spectrum of kinetic energies as a result of its nucleus capturing a neutron with a subsequent emission of  $\gamma$  rays. We have calculated the kinetic energy spectrum of  $^{128}\text{I}^{26}$  using three-dimensional random-walk equations and found that the  $^{128}\text{I}$  atoms acquire a kinetic energy ranging from 0 to 194 eV reaching a maximum at 152 eV. There is insufficient  $\gamma$ -ray spectral data for the  $^{79}\text{Br}(n,\gamma)^{80}\text{Br}^m$ ,  $^{79}\text{Br}(n,\gamma)^{80}\text{Br}$ , and  $^{81}\text{Br}(n,\gamma)^{82}\text{Br}^m + ^{82}\text{Br}$  activations to allow a calculation of a probability distribution vs. recoil energy. However, it is known from neutron binding energy data<sup>27</sup> that the kinetic energy spectrum for  $^{80}\text{Br}$  and  $^{82}\text{Br}^m + ^{82}\text{Br}$  range from 0 to 417 eV, and from 0 to 378 eV, respectively. This is similar to  $(n,\gamma)$ -activated  $^{38}\text{Cl}^{27}$  which ranges from 0 to 530 eV.

Reactions of  $^{80}\text{Br}$ ,  $^{80}\text{Br}^m$ , and  $^{82}\text{Br}^m + ^{82}\text{Br}$  can occur with various organic molecules by virtue of a high kinetic energy acquired in the  $(n,\gamma)$ -activation process. In addition to kinetic energy there is some evidence<sup>28</sup> that a fraction of the Br acquires a positive charge resulting from internal conversion. However, Rack and Gordus<sup>29</sup> and Tachikawa and Saeki<sup>30</sup> found that the reactions of  $^{80}\text{Br}$  with  $\text{CH}_4$  occurred mainly as a result of the kinetic energy, with charge of the Br atom not being a requirement for reaction.

Geissler and Willard<sup>5</sup> proposed that halogen reactions in the liquid state, especially heavy halogens (Br and I), could be the result of the formation of low-lying nuclear states produced in the emission of internal conversion and auger electrons, similar to what occurs in isomeric transition (I.T.) activation. If this is true then the kinetic energy of the activated Br or I atom or ion is not the result of  $(n,\gamma)$ -activation but that resulting from the emission of auger and internal conversion electrons. In their study of the reactions of  $^{130}\text{I}^m + ^{130}\text{I}$  activated by radiative neutron capture and  $^{130}\text{I}$  by isomeric transition, Nicholas et al.<sup>31</sup> found that the radiative neutron capture "hot" yields were consistently higher than those of "hot" isomeric transition-activated yields. This result was consistent with the fact that  $(n,\gamma)$ -activated  $^{130}\text{I}$  species are formed with larger kinetic energies than  $^{130}\text{I}$  activated by (I.T.).<sup>16,32</sup> These results suggested that the higher "hot" organic yields were predominantly due to kinetic energy imparted to the recoil  $^{130}\text{I}$  atoms or ions as a result of  $\gamma$  ray cascades. A similar effect was found for reaction of  $^{82}\text{Br}$  activated by radiative neutron capture and isomeric transition. Since it has previously been shown<sup>29,30</sup> that positive charge is not a requirement for reaction and from the previous considerations we feel that it is safe to assume that the reactions of  $(n,\gamma)$ -activated bromine are mainly the result of hot (requiring high translational energy) Br atoms.

It is generally recognized that by virtue of the  $^{80}\text{Br}^m(\text{I.T.})^{80}\text{Br}$  reactions the bromine atom can acquire a high positive charge<sup>28</sup> from +1 to +13 as a result of auger and secondary electron radiolysis. In the gaseous state this high positive charge can be distributed within the molecule by intramolecular electron transfer resulting in two positive centers within the molecule. The Br ion can then acquire a spectrum of kinetic energies as a consequence of the intramolecular coulombic explosion.

We can calculate a probability distribution of Br ions vs. recoil energies. The probability distribution of the ion's charge states as a result of internal conversion is known.<sup>28</sup> However the intramolecular redistribution of charge can-

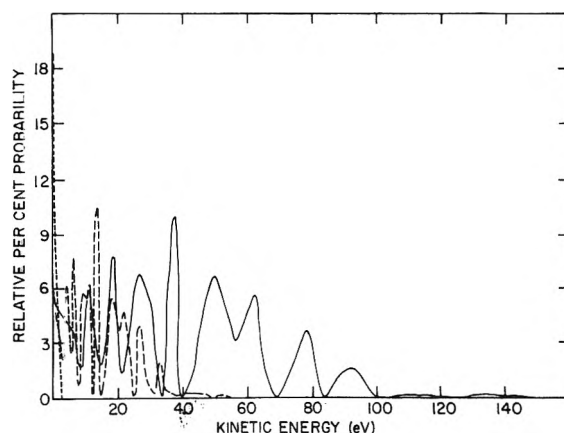


**Figure 1.** Probability distribution of bromine ions vs. recoil energy (in eV) from  $^{82}\text{Br}^m(\text{I.T.})^{82}\text{Br}$ : HBr (---);  $\text{CH}_3\text{Br}$  (- -);  $\text{Br}_2$  (—).

not be determined experimentally since a highly charged ion will rapidly undergo charge transfer with its medium. Conservation of momentum requirements dictate that the bromine recoil energy be dependent on the molecule in which it is born. Three molecules of interest as sources of activated bromine are HBr,  $\text{CH}_3\text{Br}$ , and  $\text{Br}_2$ . The kinetic energy spectra of these molecules were calculated from several intramolecular redistribution models<sup>33</sup> which allowed for extreme and intermediate redistributions. The resulting spectra are shown in Figure 1. These spectra range from a minimum value of 0 eV to maximum of 1.3, 55, and 158 eV, respectively for HBr,  $\text{CH}_3\text{Br}$ , and  $\text{Br}_2$ , the most probable energies being 0.75, 14, and 37 eV. It appears that  $\text{Br}_2$  is the most significant source of translationally excited bromine ions.

*Gas Phase Systematics. The Kinetic Energy Degradation Factor.* Presented in Table I are the various "hot" total organic product yields (TOPY) for the reaction of  $(n,\gamma)$ -activated  $^{80}\text{Br}$  and  $^{82}\text{Br}^m + ^{82}\text{Br}$  and (I.T.)-activated  $^{82}\text{Br}$  with  $\text{CH}_4$ ,  $\text{CH}_3\text{F}$ ,  $\text{CH}_3\text{Cl}$ , and  $\text{CH}_3\text{Br}$ . The "hot" TOPY values are the percent of Br stabilized as organic products by virtue of the kinetic energy acquired in the activation process. When  $\text{Br}_2$  is used as the scavenger, only for the (I.T.)-activated bromine reactions in  $\text{CH}_4$ <sup>16</sup> and  $\text{CH}_3\text{F}$ <sup>14</sup> do we find TOPY value contributions which are the result of thermal (kinetic energy independent) reactions of bromine species, probably as ions; and these contributions were minor compared to the "hot" contributions. In all systems studied the predominant organic product was the halogen substitution product,  $\text{CH}_3\text{Br}$ . The only other product of consequence was the hydrogen substitution product,  $\text{CH}_2\text{XBr}$ . Because of the rapid exchange between HBr and  $\text{Br}_2$  we could not determine the individual yields of the hot abstraction products.

Our results in Table I show a progressive decrease in hot TOPY values for  $\text{CH}_4 > \text{CH}_3\text{F} > \text{CH}_3\text{Cl} > \text{CH}_3\text{Br}$ . By employing arguments similar to Yoong et al.,<sup>26</sup> we find there is no simple or systematic relation between hot TOPY values and steric factors.<sup>34</sup> The observed decrease in hot TOPY values appears independent of a bond energy effect. In a highly moderated system and in the absence of any scavenger, Daniel and Ache<sup>35</sup> studied the systematics of (I.T.)-activated  $^{80}\text{Br}$  reactions with the halomethanes. Under these conditions the trend in bromine substitution organic products (only thermal) is in the order  $\text{CH}_3\text{F} < \text{CH}_3\text{Cl} < \text{CH}_3\text{Br} < \text{CH}_3\text{I}$ . Compared to our hot TOPY values it is obvious that the systematics of hot and thermal

TABLE I:

Target molecules	CH <sub>4</sub>		CH <sub>3</sub> F		CH <sub>3</sub> Cl		CH <sub>3</sub> Br	
	<sup>80</sup> Br	<sup>82</sup> Br + <sup>82</sup> Br <sup>m</sup> (I.T.)	<sup>80</sup> Br	<sup>82</sup> Br + <sup>82</sup> Br <sup>m</sup> (I.T.)	<sup>80</sup> Br	<sup>82</sup> Br + <sup>82</sup> Br <sup>m</sup> (I.T.)	<sup>80</sup> Br	<sup>82</sup> Br + <sup>82</sup> Br <sup>m</sup> (I.T.)
Hot TOPY <sup>a</sup>	12.1	10.5	7.4	5.75	5.0	4.5	4.3	3.9
TOPY from steric factors	(12.4) <sup>b</sup>	(6.1) <sup>c</sup>					(4.3) <sup>d</sup>	
Energy degradation factor	0.556	0.546	8.8	0.829	0.949	8.8	8.8	0.995
C-X bond energy, kcal/mol		104	108		84			70
IP, eV		12.99	12.8		11.22			10.54

<sup>a</sup> Relative standard deviation  $\pm 0.5\%$ , average of at least six determinations extrapolated to zero mole fraction of Br<sub>2</sub> and corrected for thermal yields. Samples irradiated for 5 sec at room temperature. All irradiated systems contained 760 Torr total pressure. <sup>b</sup> M. Saeki, Numakura, and E. Tachikawa, *Bull. Chem. Soc. Jpn.*, **45**, 1715 (1972). <sup>c</sup> L. Spicer and A. A. Gordius, *Proc. Symp. Chem. Eff. Nucl. Trans.*, **2**, 195 (1965). <sup>d</sup> Reference 53. <sup>e</sup> Reference 39.

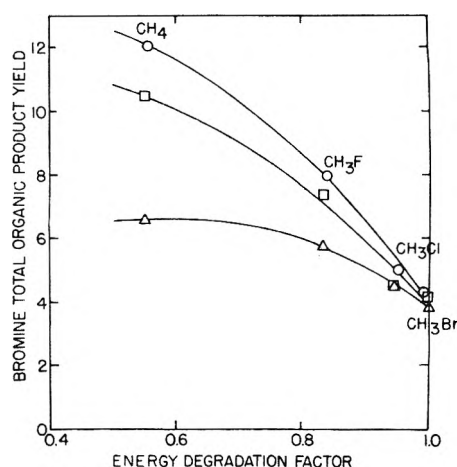


Figure 2. Total organic product yields vs. energy degradation factor for halomethanes: <sup>82</sup>Br(n,γ), O; <sup>82</sup>Br<sup>m</sup> + <sup>82</sup>Br(n,γ), □; <sup>82</sup>Br(I.T.), Δ.

bromine reactions are quite different involving at least two different mechanisms.

There is no experimental evidence to indicate<sup>29</sup> that bromine reactions activated by radiative neutron capture occur (to any extent) by positive ions; however, as a result of the (I.T.)-activation process, bromine reactions in CH<sub>4</sub>, CH<sub>3</sub>F, and CH<sub>3</sub>Cl occur (see previous section) as bromine positive ions. In methyl bromide, in the presence of Br<sub>2</sub> scavenger where charged transfer is possible the reaction of bromine probably occurs as a neutral atom. The only systematic trend we were able to find was between the hot TOPY values and the halomethane system energy degradation factor.<sup>26,36</sup> The progressive decrease in hot TOPY values for (n,γ)-activated <sup>80</sup>Br and <sup>82</sup>Br<sup>m</sup> + <sup>82</sup>Br and (I.T.)-activated <sup>82</sup>Br with increasing energy degradation factor can be seen in Figure 2. It is important to note that for atoms born with high kinetic energies such as (n,p)-activated tritium ( $\sim 10^5$  eV) we would not expect the energy degradation factor to be of importance since the loss of energy upon collision may still result in the atoms having energy in or above the reactive zone E<sub>2</sub>-E<sub>1</sub>.<sup>3d</sup> As pointed out previously and from inspection of Figure 1, a significant fraction of the bromine atoms or ions are born in or near the region E<sub>2</sub>-E<sub>1</sub>. For atoms or ions born with these low kinetic energies such as (n,γ)-activated <sup>80</sup>Br or <sup>82</sup>Br<sup>m</sup> + <sup>82</sup>Br and (I.T.)-activated <sup>82</sup>Br, the energy degradation factor becomes significant because one or two collisions with the halomethane molecule may result in bromine atoms or ions having energy below the reactive zone, removing them from hot organic combination. While the energy degradation factor depends on the mass of the hot atom and the mass of the medium (see, equation, ref 36) the significance of the energy degradation factor in a reaction system depends upon the recoil energy possessed by the hot atoms<sup>37</sup> (i.e., the kinetic energy spectra of the hot atoms).

Compared to the plot of <sup>128</sup>I hot TOPY vs. the energy degradation factors of the halomethane systems reported previously,<sup>26</sup> the plot depicted in Figure 2 differs in two respects; the decrease in TOPY with increasing energy degradation factor (EDF) is not linear but parabolic in shape and extrapolates to a value of 4.0 and not zero as reported for the <sup>128</sup>I systems. It is interesting to observe that the isotope separation for the halomethane systems diminishes with increasing EDF disappearing for CH<sub>3</sub>Br systems. Even though the <sup>128</sup>I plot decreases linearly with increasing EDF there is no reason to assume that it should be linear a

TABLE II: Approximate Maximum Kinetic Energies (eV) after 0, 1, or 2 Collisions<sup>a</sup>

Activation (zero collisions)	EDF ( <sup>80</sup> Br)	<sup>80</sup> Br( <i>n, γ</i> ) 1st/2nd collisions, 417 eV	EDF ( <sup>82</sup> Br)	<sup>82</sup> Br + <sup>82</sup> Br <sup>m</sup> ( <i>n, γ</i> ) 1st/2nd collisions, 378 eV	<sup>82</sup> Br(I.T.) 1st/2nd collisions, 158 eV
CH <sub>4</sub>	0.556	185/82	0.546	171/78	69/32
CH <sub>3</sub> F	0.837	68/11	0.829	65/11	26/4.5
CH <sub>3</sub> Cl	0.949	21/1.1	0.942	22/1.3	9/0.5
CH <sub>3</sub> Br	0.990	4/0.04	0.993	3/0.02	1/0.01

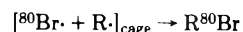
<sup>a</sup>  $KE_{\max} = (1 - EDF)^n E_{\text{Act}}$ , where  $KE_{\max}$  is maximum kinetic energy after the  $n$ th collision,  $n$  is the number of collisions, EDF is the energy degradation factor (see equation ref 36), and  $E_{\text{Act}}$  is the maximum kinetic energy imparted at activation.

priori for the bromine-halomethane systems. Since the reaction of iodine probably occurs as a result of iodine ions in ground and/or excited electronic states<sup>38</sup> and it has been shown that bromine reactions occur mainly as neutral atoms<sup>29,30</sup> we would not expect a zero TOPY for the CH<sub>3</sub>Br system.

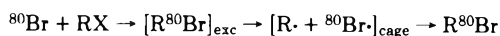
Since bromine hot atoms are born in or near the reactive zone,  $E_2 - E_1$ ,<sup>3d</sup> the observed TOPY should be sensitive to the energy spectra of the hot atom, i.e., a kinetic energy isotope effect should be observed. As seen in Table II, the maximum recoil energies of <sup>79</sup>Br(*n, γ*)/<sup>80</sup>Br, <sup>81</sup>Br(*n, γ*)/<sup>82</sup>Br<sup>m</sup> + <sup>82</sup>Br, and <sup>82</sup>Br<sup>m</sup>(I.T.)/<sup>82</sup>Br are 417, 378, and 158 eV, respectively. This difference in recoil spectra supports the supposition of a kinetic energy isotope effect. One or two collisions of the hot atom or ion with halomethane molecules may remove sufficient energy to prevent stable organic combination; yet logic dictates that a collisional efficiency of one (every collision leads to stable organic combination) cannot be possible since some significant fraction of hot atoms or ions are born above the reactive zone. Therefore, collisional deactivation of recoil energy must be considered. A study of approximate recoil energies after collisions with halomethane molecules is presented in Table II. Examination reveals that in the CH<sub>4</sub> system (low EDF) after one or two collisions the various isotopes have distinguishable (significantly different) kinetic energy spectra, corresponding to the large kinetic energy isotope effect seen for CH<sub>4</sub> in Table I and Figure 2. CH<sub>3</sub>F shows distinguishability only between (*n, γ*)- and (I.T.)-activation and in CH<sub>3</sub>Br, collisional deactivation suggests, as is observed, the disappearance of a kinetic energy isotope effect. Tachikawa<sup>39</sup> observes an isotope effect for isomeric transition activated reactions of <sup>80</sup>Br<sup>m</sup> and <sup>82</sup>Br<sup>m</sup> in CH<sub>4</sub>. While that author argued his results as being due to differences in the decay schemes, the isotope effect may be the result of the difference in kinetic energy of the two isotopes. These results suggest that one of the prime factors in determining the extent of reaction for (*n, γ*)-activated <sup>80</sup>Br and <sup>82</sup>Br<sup>m</sup> + <sup>82</sup>Br and (I.T.)-activated <sup>82</sup>Br atoms or ions is the system's energy degradation factor.

*The Gas to Condensed Phases Transition.* One of the most important questions asked in the study of halogen reactions in the condensed state media is the relative role of displacement (molecular) and radical formation (caging) mechanisms; and if caging reactions do occur what are the specific mechanisms by which the radicals are formed. It has long been realized that the borderline between cage and molecular reactions may be difficult to establish not only experimentally but also in principle, e.g., stabilization of an excited product of the halogen hot atom reaction by collision with the cage "walls" may not be distinguished in any qualitative sense from combination of a caged atom

with a radical it had created, i.e.



or recombination after excitation decomposition of a first formed hot substitution product, i.e.



It is unfortunate that in the early work only caging mechanisms were considered, such as the Libby billiard-ball collision and billiard-ball collision-epithermal collision hypothesis.<sup>4</sup> When we consider the number of mechanisms advanced in the last 10 years to explain bromine and iodine reactions with hydrocarbons and alkyl halides, such as Willard's "random-fragmentation" hypothesis,<sup>40</sup> the Geissler-Willard "auto-radiation" hypothesis,<sup>5</sup> Shaw's thermal-spike model,<sup>6</sup> Milman's modified impact on molecule model,<sup>41</sup> and Stöcklin's direct replacement with collisional stabilization of caged complex model,<sup>42</sup> it is obvious that there is no good understanding of bromine or iodine reactions activated by radiative neutron capture or isomeric transition in the condensed phase. Therefore, there is no definitive view of caging and molecular reactions.

It is our purpose, not to affirm or deny any specific model, but rather to attempt to observe the caging event. Regardless of the system we feel that it is impossible to define complex condensed state mechanisms strictly based on TOPY and individual organic product yields (IOPY) values, scavenger-mixture experiments, and comparison between various nuclear activation modes and radiolysis. In order to gain insight as to condensed phase mechanisms we studied the reactions of (*n, γ*)-activated <sup>80</sup>Br and <sup>82</sup>Br<sup>m</sup> + <sup>82</sup>Br and (I.T.)-activated <sup>82</sup>Br with CH<sub>3</sub>F, CH<sub>3</sub>Cl, and CH<sub>3</sub>Br with increasing density from low pressure gas systems to high density solid state systems. It is in our favor that these systems are not self-scavenging with respect to thermal bromine atoms or ions, as is the case of <sup>18</sup>F and possibly <sup>38</sup>Cl. Noyes<sup>43</sup> has shown that the presence of a reactive cage wall (scavenger present) leads to complications difficult to describe in any quantitative way, tending to further confuse the distinction between molecular and cage reactions. The only system that we were able to do extensive work over a wide range of densities was the CH<sub>3</sub>F system because of its low critical temperature. Because of an explosion hazard in the reactor we were unable to run samples near the critical temperature region<sup>44</sup> for both CH<sub>3</sub>Cl and CH<sub>3</sub>Br.

*The Methyl Fluoride System.* Presented in Figures 3 and 4 are the effects of added Br<sub>2</sub> on TOPY and IOPY values for bromine reactions activated by radiative neutron capture and isomeric transition in the CH<sub>3</sub>F liquid system at 23°.

Ever since the discovery by Willard and Levey<sup>45</sup> that

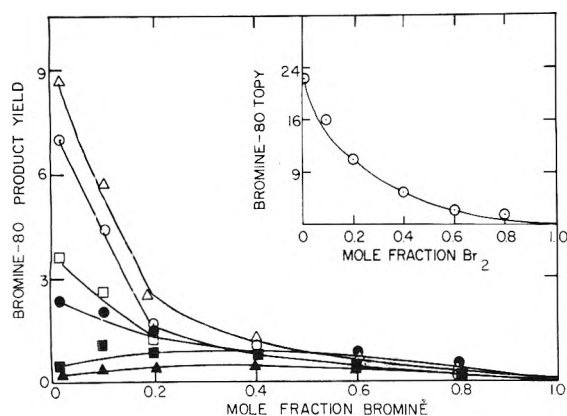


**Figure 3.** Effect of mole fraction of  $\text{Br}_2$  on total and individual organic product yields of  $^{80}\text{Br}(n,\gamma)$  in liquid  $\text{CH}_3\text{F}$  at room temperature: TOPY (insert);  $\text{CH}_2\text{FBr}$ ,  $\Delta$ ;  $\text{CH}_3\text{Br}$ ,  $\circ$ ;  $\text{CH}_2\text{Br}_2$ ,  $\square$ ;  $\text{CHBr}_3$ ,  $\bullet$ ;  $\text{CBr}_4$ ,  $\blacksquare$ ;  $\text{CFBr}_3$ ,  $\blacktriangle$ .

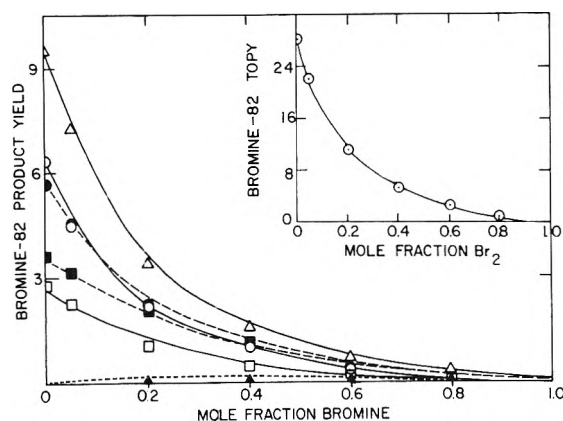


**Figure 4.** Effect of mole fraction of  $\text{Br}_2$  on total and individual organic product yields of  $^{82}\text{Br}(\text{I.T.})$  in liquid  $\text{CH}_3\text{F}$  at room temperature: TOPY (insert);  $\text{CH}_2\text{FBr}$ ,  $\Delta$ ;  $\text{CH}_3\text{Br}$ ,  $\circ$ ;  $\text{CHBr}_3$ ,  $\bullet$ ;  $\text{CBr}_4$ ,  $\blacksquare$ ;  $\text{CH}_2\text{Br}_2$ ,  $\square$ ;  $\text{CFBr}_3$ ,  $\blacktriangle$ .

TOPY values of iodine or bromine hot atom reactions in liquid alkyl halide systems could be reduced by the addition of small amounts of radical scavengers such as  $\text{I}_2$  or  $\text{Br}_2$ , this "scavenger-effect" has had general applicability in heavy halogen hot atom chemistry<sup>46-48</sup> of liquid alkyl halides and hydrocarbons. For these systems the thermal radical reaction contribution to the TOPY values was simply found. The "scavenger-effect" may not be readily observed in all systems; e.g., Milman et al.<sup>25</sup> have shown that the bromine scavenger curve for bromine reactions activated by radiative neutron capture and isomeric transition in liquid  $\text{CH}_3\text{Br}$  does not define a rapid TOPY decrease at low mole fraction of  $\text{Br}_2$  but a smooth curve not decreasing linearly until about 0.6 mol fraction of  $\text{Br}_2$ .

From observing the TOPY curves in Figures 3 and 4 it is obvious that we cannot make a simple empirical back extrapolation to lower mole fraction of  $\text{Br}_2$  defining a diffusive (thermal) or hot component to the TOPY values. It seems improbable that  $\text{Br}_2$  concentrations as high as 0.6 mol fraction are necessary to completely suppress the diffusive thermal reactions. A more meaningful presentation may be to look at the effects of added  $\text{Br}_2$  on the individual organic product yields (IOPY).

Bromine reactions in liquid  $\text{CH}_3\text{F}$  appear more complex than gas-phase  $\text{CH}_3\text{F}$  where only two bromine-labeled products,  $\text{CH}_3\text{Br}$  (major) and  $\text{CH}_2\text{FBr}$  (minor), were ob-

served. As can be seen in Figures 3 and 4 six labeled bromine products for the  $(n,\gamma)$ - and (I.T.)-activated systems were observed. For the  $^{80}\text{Br}(n,\gamma)$  reactions in order of increasing IOPY at zero mole fraction of  $\text{Br}_2$ :  $\text{CFBr}_3$  (0.1%),  $\text{CBr}_4$  (0.5%),  $\text{CHBr}_3$  (2.4%),  $\text{CH}_2\text{Br}_2$  (3.8%),  $\text{CH}_3\text{Br}$  (7.0%), and  $\text{CH}_2\text{FBr}$  (8.6%) and for the  $^{82}\text{Br}(\text{I.T.})$  reactions, in order of increasing IOPY:  $\text{CFBr}_3$  (0.1%),  $\text{CH}_2\text{Br}_2$  (2.8%),  $\text{CBr}_4$  (3.6%),  $\text{CHBr}_3$  (5.8%),  $\text{CH}_3\text{Br}$  (6.4%), and  $\text{CH}_2\text{FBr}$  (9.6%). It is not unusual to find from bromine hot atom reactions with condensed organic systems highly halogenated products. For example, Hornig and Willard<sup>48</sup> and Merrigan et al.<sup>52</sup> have shown that all possible brominated products are produced by virtue of bromine reactions activated by both radiative neutron capture and isomeric transition in liquid carbon tetrachloride. In all alkyl halide systems studied employing halogen hot atom the major product involved halogen substitution<sup>6,14,23,24,28</sup> regardless of phase. In liquid  $\text{CH}_3\text{F}$  the major product is surprisingly not  $\text{CH}_3\text{Br}$  but the hydrogen-substituted  $\text{CH}_2\text{FBr}$  for both  $(n,\gamma)$ - and (I.T.)-activated reactions.

A close inspection of Figures 3 and 4 shows that there is a marked product distribution difference between  $(n,\gamma)$ - and (I.T.)-activated reactions. In Figure 3 we can see that the products  $\text{CH}_2\text{FBr}$ ,  $\text{CH}_3\text{Br}$ ,  $\text{CH}_2\text{Br}_2$ , and  $\text{CHBr}_3$  decrease with increasing mole fraction of  $\text{Br}_2$  while  $\text{CFBr}_3$  and  $\text{CBr}_4$  increase reaching a maximum in the scavenger curve. Undoubtedly, the maximum in this scavenger curve can only be explained if part of the diffusive IOPY is directly dependent on the presence of inactive  $\text{Br}_2$  contributing to its formation.<sup>25</sup> Because of the shape of the scavenger curves for  $\text{CH}_2\text{FBr}$ ,  $\text{CH}_3\text{Br}$ ,  $\text{CH}_2\text{Br}_2$ , and  $\text{CHBr}_3$  it is impossible to distinguish between thermal, hot radical, or hot molecular reactions. As  $\text{CH}_3\text{Br}$  and  $\text{CH}_2\text{FBr}$  were the only observed products in the gas phase it is difficult to imagine that the other four products were the result of  $\text{Br}$  hot atom reactions with molecular  $\text{CH}_3\text{F}$ . For the (I.T.)-activated system shown in Figure 4, unlike the  $(n,\gamma)$ -activated system, all products except  $\text{CFBr}_3$  decrease with increasing mole fraction of  $\text{Br}_2$ . As in the  $(n,\gamma)$ -activated system we cannot readily distinguish between radical or molecular reactions. Nothing conclusive can be said about the relative roles of thermal and hot reactions in liquid  $\text{CH}_3\text{F}$  employing a scavenger plot. In order to find the relative importance of molecular vs. radical reactions a more informative study may be a determination of the effects of increasing system density to the bromine TOPY values. We chose to measure TOPY rather than IOPY at various system densities for several reasons: (1) the complex distribution of IOPY values, (2) small changes in IOPY values may not be observed due to experimental errors, particularly for the minor products, and most importantly (3) we feel that TOPY values are a more informative factor in the density plot which attempts to differentiate caging reactions from molecular reactions. If a hot atom reacts with a radical in a cage it makes no difference if it reacts as a thermalized species or just prior to loss of appreciable kinetic energy. If bromine does react with organic radicals in the cage it will because the radicals were produced as a result of recoil energy from the  $\text{Br}$  atom's (or ion's) activation. Therefore, we feel that the TOPY increment corresponding to the caging of radicals phenomenon is more meaningful than considering the caging of particular radicals.<sup>49</sup>

Depicted in Figure 5 are the TOPY values for the reactions of  $^{80}\text{Br}$  and  $^{82}\text{Br}^m + ^{82}\text{Br}$  activated by radiative neutron capture and  $^{82}\text{Br}$  activated by isomeric transition as a

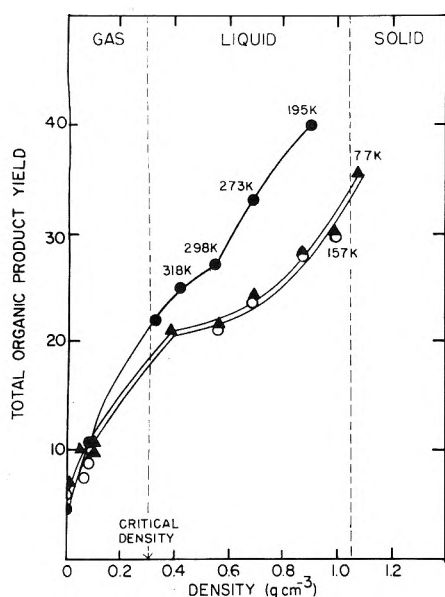


**Figure 5.** Total organic product yields as a function of density in the  $\text{CH}_3\text{F}$ -0.0167 mole fraction of  $\text{Br}_2$  system:  $^{82}\text{Br}(\text{I.T.})$ ,  $\bullet$ ;  $^{80}\text{Br}(\text{n},\gamma)$ ,  $\blacktriangle$ ;  $^{82}\text{Br}^{\text{m}} + ^{82}\text{Br}(\text{n},\gamma)$ ,  $\blacktriangle$ ,  $\circ$ . All samples unless otherwise indicated at  $25^\circ\text{C}$  (298K).

function of density employing bromine at 0.0167 mol fraction in  $\text{CH}_3\text{F}$ .<sup>50</sup> It is interesting to note that regardless of the activation mode there is a general increase in TOPY with increasing density to approximately  $0.5 \text{ g cm}^{-3}$  with a subsequent plateau (approximate) and secondary rise starting at approximately  $0.6 \text{ g cm}^{-3}$ . This behavior is similar to that originally reported by Richardson and Wolfgang<sup>11</sup> for  $^{18}\text{F}$  activated by the  $(\text{n},2\text{n})$  reaction with  $\text{CH}_3\text{F}$ .

We note what appears to be a kinetic energy isotope effect between  $(\text{n},\gamma)$ -activated  $^{80}\text{Br}$  and  $^{82}\text{Br}^{\text{m}} + ^{82}\text{Br}$  throughout the density range. This effect is small and on the fringes of experimental error; however, the  $^{80}\text{Br}$  TOPYs are higher than the corresponding  $^{82}\text{Br}^{\text{m}} + ^{82}\text{Br}$  TOPYs. This is in agreement with arguments based on the kinetic energy spectra (see previous section) and the temptation exists to ascribe this to such an effect. We feel, however, that this small isotope separation cannot conclusively be due to a kinetic energy isotope effect due to its size with respect to the experimental error and the difficulty in assigning the molecular vs. radical contributions.

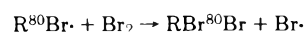
Since we are unable to assign the molecular and radical contributions and because of the obvious difficulties in assigning all the decomposition channels we have not been able to apply unimolecular decay theory to the primary rise. We do not feel that the secondary rise in TOPY is mainly the result of stabilization of excited products because at these high densities it would imply that a major fraction of the excited products would become stabilized before moving a fraction of an ångström, this implying lifetime shorter than a period of vibration; hence, the molecule would not have existed.<sup>11</sup> It is important to realize that this does not exclude increased stabilization of products observed at lower density but rather the introduction of newly observed stabilization products or channels.

In order to obtain a variation in density we varied the temperature over wide limits. There may be some question as to whether the observed variations are a true density effect or a temperature effect, either in addition to or in lieu

of a density effect. Lampe and Noyes<sup>9</sup> in their photochemical caging studies found that there was a general decrease in TOPY with increasing temperature. This was especially true for heavier solvents, attributable to thermal agitation. This increase in temperature would have resulted in a decrease in density. In their caging study, Rice and Willard<sup>51</sup> concluded that the observed temperature effect was in reality a density effect since an increase in density necessitated more kinetic energy expenditure in radical production since there was constraint by the cage wall as well as a lowering of diffusive reactions. Richardson and Wolfgang<sup>11</sup> felt the secondary rise in the density plot of  $\text{CH}_3\text{F}$  with  $^{18}\text{F}$  could not be attributed to a temperature effect since temperature effects of that magnitude were not observed nor expected in hot atom chemistry. They found the temperature coefficient of the reactions approximately zero, as current caging theories suggest,<sup>3d</sup> much less than needed to produce the rise observed. In a temperature-pressure study by Shaw et al.<sup>6</sup> the diffusive yield was found to decrease with decreasing temperature or increasing pressure (increasing constraint by the cage walls) while the scavenger insensitive yield were found to increase with decreasing temperature or increasing pressure. In general yields of the individual fractions at constant bromine concentration varied linearly with pressure (density).

As mentioned previously, the gas-phase (I.T.)-activated bromine TOPY value is less than the  $(\text{n},\gamma)$ -activation value. Both increase with increasing density, the (I.T.) increasing more rapidly, with the two TOPY curves crossing at a density of approximately  $0.1 \text{ g cm}^{-3}$  and the (I.T.)-TOPY being greater from that density upward. We also note a difference in shapes between the radiative neutron capture and the isomeric transition activated TOPY curves. This suggests an application of the Geissler-Willard "auto-radiation" hypothesis<sup>5</sup> may not be valid since if low-lying metastable nuclear states were formed from  $(\text{n},\gamma)$ -activated atoms or ions with the subsequent emission of auger and internal-conversion electrons the  $(\text{n},\gamma)$  and (I.T.) curves would, of necessity, be identical. Indeed as gas-phase reactions are supportive of a kinetic energy requirement for hot atom (molecular) reactions we must conclude that there exists a quantitative difference between radiative neutron capture and isomeric transition activations in radical production.

*The Methyl Bromide System.* Milman et al.<sup>25</sup> were the first to determine scavenger curves for Br reactions activated by radiative neutron capture and isomeric transition in liquid  $\text{CH}_3\text{Br}$ . Our experimental data are quantitatively supporting in its nature of the work of Milman et al.<sup>25</sup> Compared to the  $\text{CH}_3\text{F}$  system the TOPY plots are less complicated. Regardless of mode of activation the  $\text{CH}_3\text{Br}$  product decreases gradually with added  $\text{Br}_2$  while the products  $\text{CH}_2\text{Br}_2$ ,  $\text{CHBr}_3$ , and  $\text{CBr}_4$  exhibit a progressive maximum in their scavenger curves suggesting the importance of inactive  $\text{Br}_2$  for product formation. From similar data Milman et al.<sup>25</sup> suggest that the  $\text{CH}_3\text{Br}$  product for both  $(\text{n},\gamma)$ - and (I.T.)-activated bromine are mainly the result of kinetic energy acquired by the recoiling atom or ion while the minor products,  $\text{CH}_2\text{Br}_2$ ,  $\text{CHBr}_3$ , and  $\text{CBr}_4$ , because of the maximum in their scavenger plots are mainly the result of thermal radical reactions of the kind



We have found for gas-phase Br reactions in  $\text{CH}_3\text{Br}$  at zero mole fraction of  $\text{Br}_2$  the product distribution for (I.T.)-

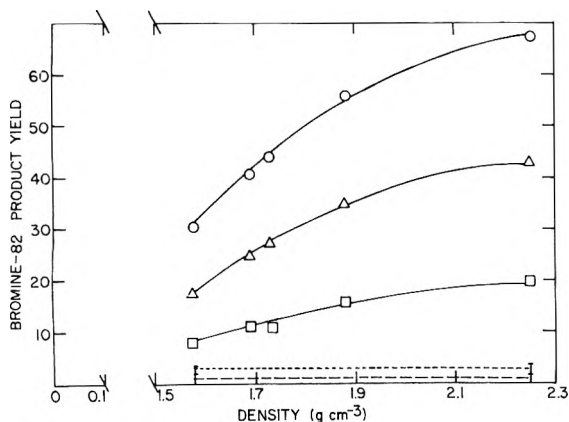


Figure 6. Total and individual organic product yields as a function of density in the  $^{82}\text{Br}(\text{I.T.})\text{-CH}_3\text{Br}$  system at 0.0167 mole fraction of  $\text{Br}_2$ : TOPY, O;  $\text{CH}_3\text{Br}$ ,  $\Delta$ ;  $\text{CH}_2\text{Br}_2$ ,  $\blacksquare$ ;  $\text{CHBr}_3$  (---);  $\text{CBr}_4$  (- -).

activated reactions are:  $\text{CH}_3\text{Br}$  (2.8%),  $\text{CH}_2\text{Br}_2$  (0.9%),  $\text{CHBr}_3$  (0.2%), and  $\text{CBr}_4$  (>0%). For  $(n,\gamma)$ -activated  $^{80}\text{Br}$  Alfassi et al.<sup>53</sup> found:  $\text{CH}_3\text{Br}$  (3.0%),  $\text{CH}_2\text{Br}_2$  (1.0%),  $\text{CHBr}_3$  (0.3%), and  $\text{CBr}_4$  (0%). In the liquid state from stabilization of excited products we would expect an enhancement in the product yields of  $\text{CH}_3\text{Br}$  and  $\text{CH}_2\text{Br}_2$ ; therefore, we could not agree with Milman that the  $\text{CH}_2\text{Br}_2$  yield is due strictly to scavenger reactions. However, it would appear that the minor products  $\text{CHBr}_3$  and  $\text{CBr}_4$  are due exclusively to scavenger reactions in the liquid state. In our opinion it is not possible to conclude anything about the nature of the  $\text{CH}_3\text{Br}$  yield. Undoubtedly both radical and molecular reactions are involved.

Because of  $\text{CH}_3\text{Br}$ 's high critical temperature (194°) it was not possible to define a density plot over the wide range of densities possible in  $\text{CH}_3\text{F}$ . Because of the less complex product distribution, we were able to study the effects of density on the  $\text{CH}_3\text{Br}$  and  $\text{CH}_2\text{Br}_2$  IOPYs. Presented in Figures 6 and 7 are the TOPY and IOPY values for (I.T.)- and  $(n,\gamma)$ -activated Br in  $\text{CH}_3\text{Br}$  at 0.0167 mole fraction of  $\text{Br}_2$ . Unlike the scavenger plots there are marked differences between  $(n,\gamma)$ - and (I.T.)-activated systems. Similar to the  $\text{CH}_3\text{F}$  system, the (I.T.) values increase convexly while the  $(n,\gamma)$  values increase in a concave fashion. As in the  $\text{CH}_3\text{F}$  system the two activation processes appear not identical giving additional evidence as to the nonapplicability of the Geissler-Willard "auto-radiolysis" hypothesis.<sup>5</sup>

Because of experimental problems involving the nuclear reactor we were not able to extend the plot to lower densities. We were able to observe the general increase in IOPY values similar to that found in the  $\text{CH}_3\text{F} + ^{18}\text{F}$  system.<sup>11</sup> It is interesting to note that our  $(n,\gamma)$  data exhibit the same type of increase as was found by Richardson and Wolfgang<sup>11</sup> while the (I.T.) data increased in a convex fashion. No meaningful variation could be found for the two minor products because of their small yield.

We extended the density study of  $(n,\gamma)$ -activated  $^{80}\text{Br}$  to 0.21 mole fraction of  $\text{Br}_2$ . We observed that the effect of increasing mole fraction of  $\text{Br}_2$  was to diminish the yield of  $\text{CH}_3\text{Br}$ , probably as a result of scavenging of thermal Br atoms, while maintaining the general feature of the IOPY curves at 0.0167 mole fraction of  $\text{Br}_2$ .

*The Effect of Varying Intermolecular Distances.* While density plots are interesting in showing differences between  $(n,\gamma)$ - and (I.T.)-activation and demonstrating the

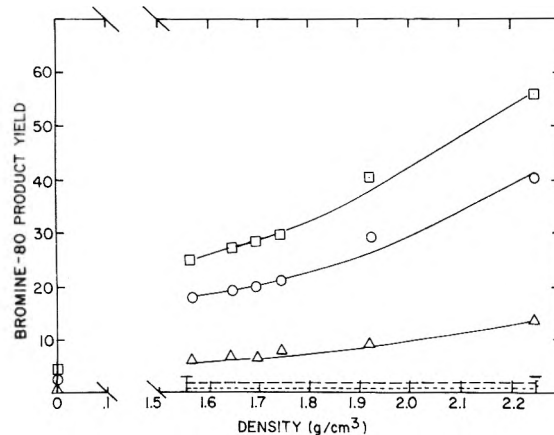


Figure 7. Total and individual organic product yields as a function of density in the  $^{80}\text{Br}(n,\gamma)\text{-CH}_3\text{Br}$  system at 0.0167 mole fraction of  $\text{Br}_2$ : TOPY,  $\square$ ;  $\text{CH}_3\text{Br}$ , O;  $\text{CH}_2\text{Br}_2$ ,  $\Delta$ ;  $\text{CHBr}_3$  (---);  $\text{CBr}_4$  (- -).

original characteristics observed by Richardson and Wolfgang,<sup>11</sup> it is not really possible to compare systems, not atoms, or modes of activation readily. It may be more meaningful to observe the effect of decreasing the intermolecular distance,  $\lambda$ , on the various TOPY values. To provide direct comparison of different systems, Root<sup>54</sup> has suggested a normalization factor,  $\sigma$ , defined as the molecular diameter of the medium. The quantity  $\lambda/\sigma$  provides a unitless quantity to observe decreasing intermolecular distance in terms of the system's own size. The intermolecular distance,  $\lambda$ , is readily calculated from the experimentally determined system density as follows:

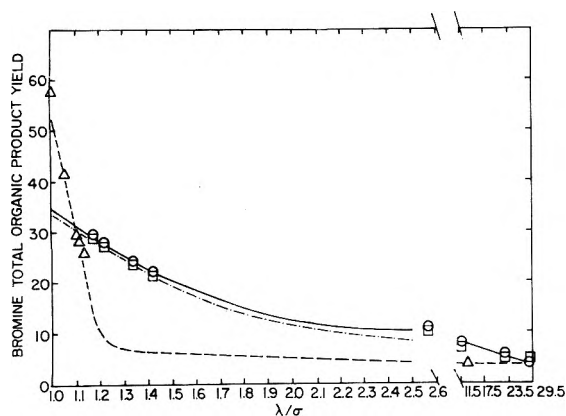
$$\lambda = (\rho N/M)^{-1/3}$$

where  $\rho$  is the system density in  $\text{g cm}^{-3}$ ,  $N$  is Avogadro's number, and  $M$  is the molecular weight (or "averaged" molecular weight) of the medium. This equation yields the intermolecular distance between "point" or "center of mass" molecules.<sup>55</sup> Since the molecules are actually spheroids with radii  $\sigma/2$ , the closest approach is  $\lambda = 2(\sigma/2) = \sigma$ ; a  $\lambda/\sigma$  value equal to 1.

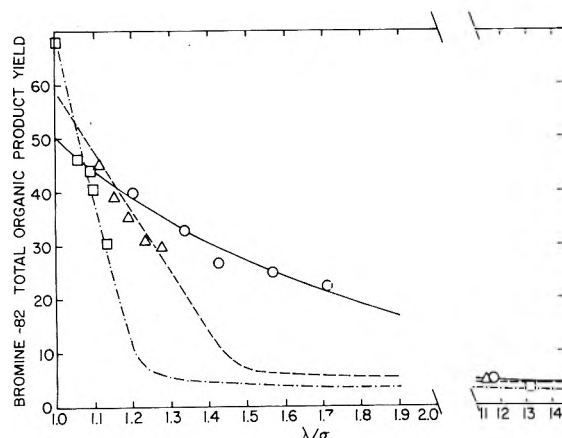
Depicted in Figure 8 is a plot of TOPY vs.  $\lambda/\sigma$  for  $(n,\gamma)$ -activated Br in  $\text{CH}_3\text{F}$  and  $\text{CH}_3\text{Br}$ .<sup>56</sup> We again note what appears to be a kinetic energy isotope effect between  $^{80}\text{Br}$  and  $^{82}\text{Br}^m + ^{82}\text{Br}$  in  $\text{CH}_3\text{F}$ . The parallel curvature, with  $^{80}\text{Br}$  TOPY greater than  $^{82}\text{Br}^m + ^{82}\text{Br}$  TOPY, supports this idea; however, since the separation is on the fringe of experimental error we feel that this is not conclusive. We also note the difference in shapes between the  $\text{CH}_3\text{F}$  and  $\text{CH}_3\text{Br}$  systems. While both may be imagined as the merging of two approximately linear segments,<sup>57</sup> the slopes and intercept of these segments vary greatly. We may safely assume that some qualitative difference exists between these segments.

Figure 9, a plot of TOPY vs.  $\lambda/\sigma$  for (I.T.)-activated  $^{82}\text{Br}$  in  $\text{CH}_3\text{F}$ ,  $\text{CH}_3\text{Cl}$ , and  $\text{CH}_3\text{Br}$ , provides further evidence of systematic differences. Again there appears the merging of two linear segments<sup>57</sup> for each system, but with differing slopes and intercepts, seeming to vary in a systematic way from  $\text{CH}_3\text{F}$  to  $\text{CH}_3\text{Cl}$  to  $\text{CH}_3\text{Br}$ .

For  $\text{CH}_3\text{Br}$  and  $\text{CH}_3\text{Cl}$  there appears to be a large angle of intersection between the two line segments. This may be due to some definite difference in the chemical processes commencing at this point. We believe that the near horizontal segment may be indicative of molecular reactions while the angled segment indicates cage reactions as im-



**Figure 8.** Effect of  $\lambda/\sigma$  on the total organic product yields of  $(n,\gamma)$ -activated Br in halomethanes at 0.0167 mole fraction of  $\text{Br}_2$ :  $^{80}\text{Br}$  in  $\text{CH}_3\text{F}$ , O (—);  $^{82}\text{Br}^m + ^{82}\text{Br}$  in  $\text{CH}_3\text{F}$ ,  $\square$  (---);  $^{80}\text{Br}$  in  $\text{CH}_3\text{Br}$ ,  $\Delta$  (- - -).



**Figure 9.** Effect of  $\lambda/\sigma$  on the total organic product yields of (I.T.)-activated  $^{82}\text{Br}$  in halomethanes at 0.0167 mole fraction of  $\text{Br}_2$ :  $\text{CH}_3\text{F}$ , O (—);  $\text{CH}_3\text{Cl}$ ,  $\Delta$  (---);  $\text{CH}_3\text{Br}$ ,  $\square$  (- - -).

plied by the differences in slope. Although the exact nature of the caging mechanisms cannot be predicted from the data we feel that the angled segment corresponds to caging rather than stabilization of an excited product due to the definite break between line segments. The existence of such complexes is somewhat in doubt since the mean free path of the atom ( $\lambda - \sigma$ , due to our "center of mass" molecules) in this close-packed region is in general much less than the molecular diameter ( $\sigma$ ). This implies a lifetime of the complex less than a period of vibration, hence the complex did not exist.<sup>11</sup>

As mentioned earlier the (I.T.)-activated  $^{82}\text{Br}$  TOPY in  $\text{CH}_3\text{F}$  equals the  $(n,\gamma)$  TOPY at a density of approximately  $0.1 \text{ g cm}^{-3}$ . This corresponds to a  $\lambda/\sigma$  value of 2.52. Extension of the  $\lambda/\sigma$  plots for  $\text{CH}_3\text{F}$  suggests that there may be a contribution to the TOPY due to the angled segment. This is supportive of the idea that the angled segment corresponds to caging reactions since we must attribute the increasing (I.T.) yield, at least in part, to radical cage reactions. It is unfortunate that our experimental technique did not allow us to observe the density where the TOPYs for  $(n,\gamma)$ - and (I.T.)-activated bromine in  $\text{CH}_3\text{Br}$  were equal. Back extrapolation of the density plots (Figures 6 and 7) suggest that (I.T.) and  $(n,\gamma)$  TOPYs are equal at approximately  $1.5 \text{ g cm}^{-3}$ , corresponding to a  $\lambda/\sigma$  value of 1.14. Examination of Figures 8 and 9 show that this is indeed true and that both the  $(n,\gamma)$ - and the (I.T.)-activated bromine TOPYs lie on the angled segment of the graph.

The question naturally arises as to why from system to system the intersection and slopes vary. There is no a priori reason why the slopes and intersection must be constant. It must be realized that  $\lambda/\sigma$  is a unit of convenience and that  $\sigma$  varies from system to system such that the intermolecular distances ( $\lambda$ ) are not equal for a constant  $\lambda/\sigma$  value. We feel that two effects may be at work within a system, a degradation effect and a packing effect.

If the angled segment is indeed indicative of caging reactions then the slope of this segment must suggest the strength of the systems ability to cage. It is not entirely correct to say that the TOPY intercept at  $\lambda/\sigma$  equal to one is indicative of the systems ability to produce radicals. We must remember that liquid state TOPYs are the result of both radical cage reactions and molecular reactions. As was mentioned previously we are unable to assign the relative molecular and radical contributions because of the difficulties in assigning all the decomposition channels and hence the inability to apply unimolecular theory to find the extent of molecular reactions via stabilization modes. However from our previously described gas phase systematics studies the TOPYs decreased in the order  $\text{CH}_3\text{F} > \text{CH}_3\text{Cl} > \text{CH}_3\text{Br}$ . Therefore the extrapolations at  $\lambda/\sigma$  equal to one units TOPYs decreasing in the order  $\text{CH}_3\text{Br} > \text{CH}_3\text{Cl} > \text{CH}_3\text{F}$  would suggest that the best radical producer is  $\text{CH}_3\text{Br}$ , as we, of course, would suspect. To produce a hot atom, either thermalized or with diminished recoil energy, trapped in a cage of radicals, the hot atom must lose kinetic energy to the extent that it can no longer escape (diffuse) from the cage; the energy lost by the cooling hot atom should be expended in the production of radicals.<sup>51</sup> This collisional degradation of kinetic energy suggests the importance of the kinetic energy degradation factor. Reexamination of Tables I and II show that the ability of the medium to collisionally "cool" the hot atom decreases in the order  $\text{CH}_3\text{Br} > \text{CH}_3\text{Cl} > \text{CH}_3\text{F}$ , the same order as steepness of slope.

While  $\text{CH}_3\text{Br}$  is the most effective system to "cool" a bromine hot atom,  $\text{CH}_3\text{Br}$  is the system with the largest molecular diameter ( $\sigma$ ).<sup>58</sup> The reactive cage is envisioned as a "packing" of spheroid molecules around the reactants. Large  $\sigma$  values must lead to a less tightly meshed cage, since such molecules cannot approach each other or the reactants as closely, resulting in "holes" in the cage. Thus, for a hot atom recoiling within the cage, a loosely packed system impedes the hot atom less than a tightly packed medium. This impediment is displayed (see Figures 8–10) in the shifting of the intersection of line segments to large values of  $\lambda/\sigma$  for tighter packed systems. Thus one sees a systematic trend between intersection values of  $\lambda/\sigma$  and relative packing in the order  $\text{CH}_3\text{F} > \text{CH}_3\text{Cl} > \text{CH}_3\text{Br}$ . We suggest that this packing effect must contribute to conditions which lead to caging although contributing little energetically or mechanistically to the caging event. Therefore the loss in degradation (EDF) for a light-weight, small-size system is partially compensated by the increased number of collisions (packing effect) (see, equation, ref. 37).

In Figure 10 the TOFY vs.  $\lambda/\sigma$  is plotted for the systems  $^{18}\text{F}(n,2n) + \text{CH}_3\text{F}$ ,<sup>11</sup>  $^{38}\text{Cl}(n,\gamma) + \text{CH}_3\text{Cl}$ , and  $^{80}\text{Br}(n,\gamma) + \text{CH}_3\text{Br}$ . The similarity of the curves suggests the near identity of the methyl halide-halogen systems. The near parallel slopes correspond to small variations in EDF.<sup>59</sup> Similarly, the intersections correspond to the near equality of packing with respect to the hot atom's size.

The degradation effect and the packing effect represent

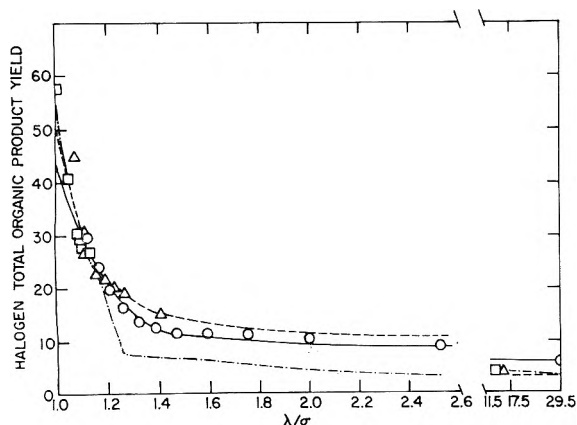


**Figure 10.** Effect of  $\lambda/\sigma$  on the total organic product yield of halogen-halomethane systems:  $^{18}\text{F}(n,2n)$  in  $\text{CH}_3\text{F}$ ,  $\circ$  (—);  $^{38}\text{Cl}(n,\gamma)$  in  $\text{CH}_3\text{Cl}$   $\Delta$  (---);  $^{80}\text{Br}(n,\gamma)$  in  $\text{CH}_3\text{Br}$ ,  $\square$  (- · - ·).

two of the molecular properties suggested by Bunker and Jacobson. In their paper<sup>7</sup> they reported on the Monte-Carlo simulation of the photochemical reaction of  $\text{I}_2$  with  $\text{CCl}_4$  which suggested the importance of molecular parameters rather than bulk properties in the determination of the cage event. Our  $\lambda/\sigma$  work correlates well with their ideas and provides an experimental basis for future development.

### Summary

As demonstrated by mole fraction studies, the condensed phase is a viable, although complex, source of information. In conjunction with density one observes changes in product production both in mode and in yield during the gas to condensed phase transition. Although no specific information on the relative contribution of molecular vs. radical reactions could be obtained from these studies, one can observe continuities both within a system and among the various halomethane systems, e.g., the duplication of the Richardson-Wolfgang<sup>11</sup> effect and the characteristic concavity/convexity of  $(n,\gamma)/(\text{I.T.})$ -activated density plots. These density studies, viewed with the gas phase systematics, demonstrate the importance of mode of activation in molecular reactions and in the caging event. The normalized intermolecular distance ( $\lambda/\sigma$ ) studies provide a method for the direct comparison of systems, hot atoms, and modes of activation and the means to separate cage and molecular events. The  $\lambda/\sigma$  work also suggests the importance of molecular parameters on caging events and demonstrates the importance of the degradation effect (EDF) in both gas and condensed state systematic studies.

**Acknowledgments.** The authors gratefully acknowledge discussions with Professor J.W. Root, especially his suggesting the use of  $\lambda/\sigma$  factor, and financial support from the USAEC.

### References and Notes

- This research was supported through an Atomic Energy Commission Contract, No. AT(11-1)-1617. This is AEC document COO-1617-39.
- J. Franck and E. Rabinowitsch, *Trans. Faraday Soc.*, **30**, 120 (1934).
- For examples and references see (a) J. E. Willard, *Annu. Rev. Nucl. Sci.*, **3**, 193 (1953); (b) J. E. Willard, *Proc. Symp. Chem. Eff. Nucl. Trans.*, **1**, 215 (1961); (c) *ibid.*, **1**, 221 (1965); (d) R. Wolfgang, *Prog. React. Kinet.*, **3**, 99 (1935).
- W. F. Libby, *J. Am. Chem. Soc.*, **69**, 2523 (1947).
- P. R. Geissler and J. E. Willard, *J. Phys. Chem.*, **67**, 1615 (1963).
- A. J. Cole, M. D. Mia, G. E. Miller, and P. F. D. Shaw, *Radiochim. Acta*, **9**, 194 (1968).
- D. L. Bunker and B. S. Jacobson, *J. Am. Chem. Soc.*, **94**, 1843 (1972).
- R. M. Noyes, *J. Chem. Phys.*, **18**, 999 (1950).
- F. W. Lampe and R. M. Noyes, *J. Am. Chem. Soc.*, **76**, 2140 (1954).
- C. Walling and A. R. Lepley, *Int. J. Chem. Kinet.*, **3**, 97 (1971).
- A. E. Richardson and R. Wolfgang, *J. Am. Chem. Soc.*, **92**, 3480 (1970).
- J. A. Merrigan and E. P. Rack, *J. Phys. Chem.*, **69**, 2795 (1965).
- W. E. Rice and J. E. Willard, *J. Am. Chem. Soc.*, **75**, 6156 (1953).
- R. W. Helton, M. Yoong, and E. P. Rack, *J. Phys. Chem.*, **75**, 2072 (1971).
- R. W. Helton, W. M. Grauer, and E. P. Rack, *Radiochim. Acta*, **19**, 44 (1973).
- J. B. Nicholas and E. P. Rack, *J. Chem. Phys.*, **48**, 4085 (1968).
- A. J. Blotcky, L. J. Arsenault, and E. P. Rack, *Anal. Chem.*, **45**, 1056 (1973).
- A. J. Blotcky, D. M. Duven, W. M. Grauer, and E. P. Rack, *Anal. Chem.*, **46**, 838 (1974).
- O. U. Anders, *Phys. Rev.*, **138**, B1 (1965).
- E. Tachikawa and J. Okamoto, *Radiochim. Acta*, **13**, 159 (1970).
- R. L. Ayres, E. J. Kernitz, R. M. Lambrecht, and E. P. Rack, *Radiochim. Acta*, **11**, 1 (1969).
- J. A. Merrigan, J. B. Nicholas, and E. P. Rack, *J. Chem. Educ.*, **43**, 543 (1966).
- R. L. Ayres, Ph.D. Thesis, The University of Nebraska, 1970.
- M. Welch, R. Withnell, and A. P. Wolf, *Anal. Chem.*, **39**, 275 (1967).
- Z. Abedinzadeh, R. Radicella, K. Tanaka, and M. Milman, *Radiochim. Acta*, **12**, 4 (1969).
- M. Yoong, Y. C. Pao, and E. P. Rack, *J. Phys. Chem.*, **76**, 2685 (1972).
- J. H. E. Mattauch and W. Thiele, *Nucl. Phys.*, **67**, 32 (1965).
- S. Wexler and G. R. Anderson, *J. Chem. Phys.*, **33**, 850 (1960).
- E. P. Rack and A. A. Gordus, *J. Phys. Chem.*, **65**, 944 (1961).
- M. Saeki and E. Tachikawa, *Bull. Chem. Soc. Jpn.*, **46**, 839 (1973).
- J. B. Nicholas, M. Yoong, and E. P. Rack, *Radiochim. Acta*, **19**, 25 (1973).
- We have calculated the spectra of  $^{130\text{m}}(\text{I.T.})^{130\text{I}}$  in  $\text{I}_2$  and found it to range from 0 to 76 eV.
- The three models of intramolecular redistribution were (1) equal probability, (2) maximum redistribution, and (3) rapid explosion. (1) The equal probability model gives equal statistical weighting to all possible charge redistributions. For example, the molecular ion  $^{80}\text{Br}^{7+}\text{Br}^0$  can remain 7-0 or redistribute its charges 6-1, 5-2, or 4-3. In this model each redistribution has equal probability. (2) In the maximum redistribution model it is assumed that the electron transfer is much faster than the motion of the ions; thus maximum repulsion is favored. To simulate this, binomial expansion coefficients were used as statistical weighting coefficients; thus, for the above example the coefficients are 1, 7, 21, and 35, respectively. (3) At the other extreme, the rapid explosion model assumes that electron transfer occurs within a finite time scale which is governed by the energetics of electron transfer. *Repulsive acceleration of the ions may terminate electron transfer prior to charge equalization.* As a statistical weight a ratio of the ionization potential of the donor to the electron affinity of the receptor was used. The spectra shown in Figure 1 has been calculated by the rapid explosion model. Although this is not in absolute agreement with models 1 and 2 they are qualitatively similar and disagree by no more than 10%.
- L. Spicer and R. Wolfgang, *J. Am. Chem. Soc.*, **90**, 2426 (1968).
- S. H. Daniel and H. J. Ache, *Radiochim. Acta*, **19**, 132 (1973).
- The energy degradation factor represents the fraction of recoil energy lost by a hot atom in collision with another body. From conservation of momentum requirements the equation becomes:
 
$$\text{EDF} = 4M_H M_T / (M_H + M_T)^2$$
 where EDF is the energy degradation factor,  $M_H$  is the mass of the hot atom, and  $M_T$  is the mass of the struck molecule.
- $$E_N = E_0(1 - \text{EDF})^N \prod_{i=1}^N \cos \theta_i$$
 The recoil energy after the  $N$ th collision ( $E_N$ ) equals the recoil energy acquired in activation ( $E_0$ ) times the fraction of energy retained. Note the dependence on the angles of collision ( $\cos \theta_i$ ).
- E. P. Rack and A. A. Gordus, *J. Chem. Phys.*, **34**, 1855 (1961).
- E. Tachikawa, *Bull. Chem. Soc. Jpn.*, **43**, 63 (1970).
- S. Goldhaber and J. E. Willard, *J. Am. Chem. Soc.*, **74**, 318 (1952).
- M. Milman, *Radiochim. Acta*, **1**, 15 (1963).
- H.-J. Machulla and G. Stocklin, *J. Phys. Chem.*, **78**, 658 (1974).
- R. M. Noyes, *J. Am. Chem. Soc.*, **77**, 2042 (1954).
- The critical temperatures and pressures of halomethanes are:  $\text{CH}_3\text{F}$ , 44.9°, 62.0 atm;  $\text{CH}_2\text{Cl}$ , 143.8°, 65.8 atm;  $\text{CH}_3\text{Br}$ , 194°, 51.6 atm.
- G. Levey and J. E. Willard, *J. Am. Chem. Soc.*, **74**, 6161 (1952).
- N. J. Parks, K. A. Krohn, and J. W. Root, *J. Chem. Phys.*, **55**, 2690 (1971).
- Z. B. Alfassi and S. Amiel, *Radiochim. Acta*, **15**, 201 (1971).
- J. F. Hornig and J. E. Willard, *J. Am. Chem. Soc.*, **75**, 461 (1953).
- The change of IOPY as a function of density may not be significant within the limits of experimental error, however, the sum of the IOPYs (TOPY) can be accurately measured and small variations as a function of density can be studied.
- The solubility of  $\text{Br}_2$  is limited in  $\text{CH}_3\text{F}$  and fractional crystallization may occur at low temperatures.
- W. E. Rice and J. E. Willard, *J. Am. Chem. Soc.*, **75**, 6156 (1953).
- J. A. Merrigan, W. K. Ellgren, Jr., and E. P. Rack, *J. Chem. Phys.*, **44**, 174 (1966).



- (53) Z. B. Alfassi, S. Amiel, and M. Baer, *J. Chem. Phys.*, **57**, 3519 (1972).  
 (54) J. W. Root, private communication.  
 (55) "Center of mass" molecules are chosen as a matter of mathematical convenience.  
 (56) The curves were computer fitted using polynomial regression analysis on the data points. All points shown in Figure 8-10 were experimentally determined and represent a minimum of six runs.  
 (57) Although several polynomials of different orders were applied to the data, two intersecting first-order polynomials provided the best fit.  
 (58) Molecular diameters ( $\sigma$ ): CH<sub>3</sub>Br, 4.13 Å; CH<sub>3</sub>Cl, 3.82 Å; CH<sub>3</sub>F, 3.28 Å.  
 (59) System kinetic energy degradation factors (EDF): CH<sub>3</sub>F + <sup>18</sup>F, 0.92; CH<sub>3</sub>Cl + <sup>36</sup>Cl, 0.98; CH<sub>3</sub>Br + <sup>80</sup>Br, 0.99.

## Variations of Fluorescence Quantum Yields with pH or Hammett Acidity. Near Equilibrium Vs. Nonequilibrium Excited State Proton Exchange

Stephen G. Schulman\* and Anthony C. Capomacchia

College of Pharmacy, University of Florida, Gainesville, Florida 32610

(Received May 14, 1973; Revised Manuscript Received January 29, 1975)

Proton transfer in the lowest excited singlet state may be much faster, much slower, or contemporaneous with fluorescence. In the first two cases, the variations of fluorescence quantum yields of excited acid and conjugate base, with pH or Hammett acidity, are indicative of no photoreaction and of photoequilibrium, respectively. In the case of fluorescence and excited state prototropism of comparable rate, the form of the fluorometric titration curve depends upon the rates of proton transfer relative to those of fluorescence in both excited conjugate species. It is shown that in concentrated acid or base solutions and in concentrated aqueous buffer solutions it is possible to observe excited state proton exchange even in many substances which do not demonstrate this phenomenon in poorly buffered aqueous media.

It has been recognized, for almost 3 decades, that the differences between the pH dependences of electronic absorption and fluorescence spectra are due to the origins of the former in ground state prototropism and of the latter in proton exchange in the lowest excited singlet state.<sup>1,2</sup> The alterations of the electronic charge distributions of molecules promoted to the lowest excited singlet state change the intrinsic Brønsted acidities and basicities of functionally substituted aromatic molecules and may therefore alter the fractional concentrations of acid and conjugate base species, in the excited state, relative to the fractional concentrations of acid and conjugate base in the ground state. Hence, the interconversion of the fluorescence spectra of acid and conjugate base may occur in a pH region different from  $\text{pH} \sim \text{p}K_a$  (the ground state equilibrium constant).

Although, the inflection points in the fluorometric pH titration curves of organic acids and bases have generally been taken to represent  $\text{pH} = \text{p}K_a^*$ , where  $\text{p}K_a^*$  is the dissociation constant for the excited state reaction corresponding to  $\text{p}K_a$ , it was shown by Weller<sup>3,4</sup> that if the rates of fluorescence and proton exchange in the excited state are comparable, the fluorometric titration curve depends upon the kinetics of excited state proton exchange, rather than upon the position of equilibrium in the excited state, represented by  $\text{p}K_a^*$ . This position has recently been reemphasized and affirmed by Lasser and Feitelson.<sup>5</sup> However, in our experience, the subject of pH dependent fluorometry envelopes, and is indicative of, several singlet-state photochemical phenomena. Each, depending upon the acid-base pair, the solvent, and the concentrations and identities of all proton donor and acceptor species, may represent no reaction, partial reaction, or, very nearly reaction until equilibrium in the excited state is attained.

The lifetimes of molecules in the lowest excited singlet

state are typically  $\sim 10^{-11}$  to  $10^{-7}$  sec. The pseudo-first-order rate constants ( $\bar{k}$ ) for proton transfer from acids to the solvent (dissociation) or to bases from the solvent (hydrolysis) are generally assumed to be less than  $10^{11} \text{ sec}^{-1}$ .<sup>6</sup> The second-order rate constants ( $k$ ) for proton transfer from the solvated proton to bases or from acids to the lyate anion are typical of the rate constants of diffusion limited reactions and are of the order of  $10^{11} \text{ M}^{-1} \text{ sec}^{-1}$  or less.<sup>6</sup> Thus, depending upon the lifetimes of excited acid and conjugate base, their rate constants and mechanisms of proton exchange and the concentrations of proton donor and acceptor species in solution, excited state proton exchange may not measurably occur, may occur to a limited extent, or may come very nearly to equilibrium as characterized by the thermodynamics of the excited state reaction ( $\text{p}K_a^*$ ). The actual dependence of the fluorescence spectrum of an excited acid or base upon pH (the variation of fluorescence quantum yield of excited acid or base with pH) is determined by which of these situations occurs in solution. This will now be considered in some detail.

### Excited State Proton Exchange Much Slower Than Fluorescence in Acid or Conjugate Base

If the rate of pseudo-first-order dissociation of an excited acid or protonation of an excited base is small by comparison with the reciprocal of the lifetime of the excited acid or base and the rate of second-order protonation of the excited conjugate base or deprotonation of the excited conjugate acid is small by comparison with the reciprocal of the lifetime of the excited conjugate base or acid, for all experimental purposes, fluorescence will take place from the species directly excited before appreciable proton transfer can occur in the excited state. Since in this case the quantum yield of fluorescence will generally be pH independent,

the intensity of fluorescence from acid and conjugate base will depend only upon the ground state concentration and molar absorptivity of each species at the wavelength of excitation. The variation of the intensity of fluorescence of acid or base will therefore depend only upon the thermodynamics of the ground state acid-base reaction and the absorptive properties of acid and conjugate base and will parallel the absorptiometric pH titrations of each species. This situation can be brought about by low rate constants for excited state proton exchange or by short excited state lifetimes, but in the mid pH region (pH 3–11) in unbuffered solutions, it is common because even if  $k$  is great, the low concentrations of  $H_3O^+$  and  $OH^-$  result in low overall rates of second-order protonation and proton abstraction. In concentrated acid, base, or buffer solutions it is less often observed because of the high concentrations of protonating or deprotonating species. A representative fluorometric titration of this type is seen in the pH dependences of the relative fluorescence quantum yields of the neutral molecule and monocation derived from *o*-phenanthroline (Figure 1) in which the inflection points in the fluorometric titration curves correspond to the ground state  $pK_a$  value of the neutral and singly protonated *o*-phenanthroline molecule.

#### Excited State Proton Exchange Much Faster Than Fluorescence in Acid or Conjugate Base

If the rates of dissociation of excited acid and of protonation of excited conjugate base are much greater ( $>10$  times) than the rates of their fluorescences, prototropic equilibrium will be nearly established in the lowest excited singlet state. In this event, it is the dissociation constant of the excited state proton exchange ( $pK_a^*$ ) which governs the fluorometric pH titration behavior of the analyte (the variations with pH or Hammett acidity of the relative quantum yields of fluorescence of acid and conjugate base). Because the electronic distribution of an electronically excited molecule is very different from that of its ground state,  $pK_a^*$  is generally very different from  $pK_a$ . Differences between  $pK_a^*$  and  $pK_a$  are commonly six or more logarithmic units and differences approaching twenty logarithmic units are not unknown. The difference between  $pK_a^*$  and  $pK_a$  means that the conversion of acid to conjugate base in the excited state occurs in a pH region (or Hammett acidity region) different from the corresponding ground state reaction so that the absorptiometric titration occurs in a pH or Hammett acidity region different from that in which the conversion of acid to conjugate base is observed by fluorometry (i.e., if  $pK_a^* < pK_a$  the excitation of only acid in the pH interval between  $pK_a$  and  $pK_a^*$  results in fluorescence only from the conjugate base while if  $pK_a^* > pK_a$  excitation of only base at  $pK_a^* > pH > pK_a$  results in only fluorescence of conjugate acid). The attainment of prototropic equilibrium in the excited state is characterized by a narrow fluorometric titration interval (about 4 pH or  $H_0$  units) yielding titration curves whose points fit the Henderson-Hasselbach equation in the form

$$pK_a^* = pH \text{ (or } H_0) - \log \frac{\phi_A^0 - \phi_A}{\phi_A - \phi_B^0} \quad (1)$$

(assuming that the excited acid-base equilibrium is represented in a straightforward manner by the Hammett acidity scale) where  $\phi_A$  is the quantum yield of fluorescence at any point in the fluorometric inflection region at the analytical wavelength of fluorescence and  $\phi_A^0$  and  $\phi_B^0$  are the

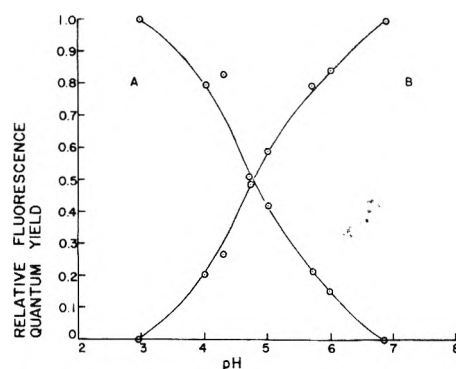


Figure 1. Variations of the relative quantum yields of fluorescence of the singly charged cation (A) and neutral species (B) derived from *o*-phenanthroline, in unbuffered aqueous solutions, with pH.

quantum yields of fluorescence at the analytical emission wavelength when  $pH \text{ (or } H_0) \ll pK_a^*$ , and when  $pH \text{ (or } H_0) \gg pK_a^*$ , respectively. A representative fluorometric titration curve which represents the attainment of equilibrium in the lowest excited singlet state is shown in Figure 2 for the excited state proton exchange between the doubly and singly charged cations derived from 9-aminoacridine. Because of the low concentrations of  $H_3O^+$  and  $OH^-$  in the mid pH region which result in low rates of diffusion-limited protonation and dissociation, the establishment of prototropic equilibrium in excited acid-base pairs whose fluorometric titration breaks occur in the mid pH region is never observed unless high concentrations of proton donors or acceptors other than  $H_3O^+$  or  $OH^-$  (buffers) are also present. Excited state prototropic equilibrium is, however, often established in concentrated sulfuric or perchloric acid solutions (where  $H_0$  of, e.g.,  $-10.0$  corresponds roughly to  $[H_3O^+] = 1 \times 10^{10} M$  in terms of protonating ability) and in concentrated NaOH solutions (where  $H_-$  of 18.0 corresponds roughly to  $[OH^-] = 1 \times 10^4 M$  in proton abstracting ability). In these strongly protonating and deprotonating media even nonfluorescent species (i.e., having very short lifetimes, e.g.,  $<10^{-11}$  sec) such as the excited zwitterion derived from 8-quinolinol<sup>7-12</sup> are capable of being protonated and deprotonated during the short lifetime of the lowest excited singlet state because  $k[H_3O^+]$  or  $k[OH^-]$  will usually be substantially greater than  $10^{11} \text{ sec}^{-1}$ . The accuracy of this statement is, of course, limited by the accuracy with which it is possible to interpret the Hammett acidity functions as  $H_0 = -\log [H_3O^+]$  and  $H_- = \log K_w + \log [OH^-]$ . However, the observation of fluorescence from species such as the cation and anion derived from 8-quinolinol and the cations derived from benzaldehyde and acetophenone<sup>13</sup> in Hammett acidity regions where they cannot thermodynamically exist, in the ground state, suggest that this argument is, at least qualitatively, accurate.

#### Excited State Proton Exchange and Fluorescence of Comparable Rates

If the rates of proton transfer between excited acid and solvent or lyate ion (e.g.,  $OH^-$ ) or between excited base and solvent or lyonium ion ( $H_3O^+$ ) are comparable to the rates of deactivation of acid and conjugate base, the variations of the relative quantum yields of fluorescence of acid and conjugate base with pH will be governed by the kinetics of the excited state reaction. Weller<sup>3</sup> has employed simple steady state kinetics to show that, to a good approximation, for the prototropic reactions

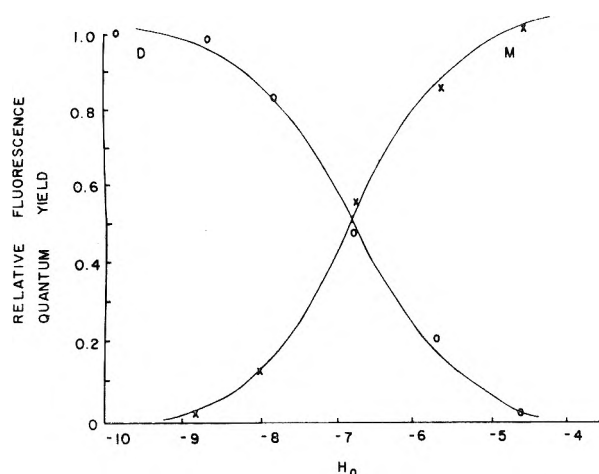
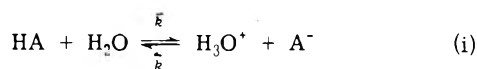
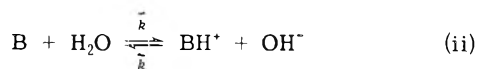


Figure 2. Variations of the relative quantum yields of fluorescence of the doubly charged cation (D) and monocation (M) derived from 9-aminoacridine, in concentrated sulfuric acid, with Hammett acidity.



and



the relative quantum yield of fluorescence ( $\phi/\phi_0$ ) of HA or B (reacting with the solvent) is given by

$$\frac{\phi}{\phi_0} = \frac{1 + \bar{k}\tau_0'c}{1 + \bar{k}\tau_0 + \bar{k}\tau_0'c} \quad (2)$$

where  $c = [\text{H}_3\text{O}^+]$  if  $\phi/\phi_0$  corresponds to HA,  $c = [\text{OH}^-]$  if  $\phi/\phi_0$  corresponds to B and  $\tau_0$  is the lifetime of HA or B while  $\tau_0'$  is the lifetime of  $\text{A}^-$  or  $\text{BH}^+$  in the lowest excited singlet state. The distinction between HA and  $\text{BH}^+$  and between  $\text{A}^-$  and B does not attach significance here to the charge types of acid and conjugate base, but rather, is intended to distinguish between proton transfer reactions with  $\text{H}_3\text{O}^+$  and  $\text{H}_2\text{O}$  as proton donor and acceptor, respectively, and with  $\text{H}_2\text{O}$  and  $\text{OH}^-$  as proton donor and acceptor, respectively. Correspondingly, if  $\phi'/\phi_0'$  is the relative fluorescence efficiency of the excited species conjugate to HA or B ( $\text{A}^-$  or  $\text{BH}^+$ ), then

$$\frac{\phi'}{\phi_0'} = \frac{\bar{k}\tau_0}{1 + \bar{k}\tau_0 + \bar{k}\tau_0'c} \quad (3)$$

A more refined treatment, by Weller,<sup>14</sup> takes into account the approximate nature of the steady state assumption in deriving expressions for  $\phi/\phi_0$  and  $\phi'/\phi_0'$ . However, this is beyond the scope of the present work.

The dependences of the relative quantum yields of fluorescence of excited acid and base upon the relative rates of proton exchange in the excited state and of fluorescence of acid and base are observed in the fluorometric titration curves as the stretching of the pH interval over which the fluorescence of the excited acid is converted to that of the conjugate base. The region in some cases extends over the entire pH interval between the ground and excited state  $\text{p}K_a$  values. In general, the faster the rates of excited state proton exchange relative to the rates of fluorescence, the closer to  $\text{pH} = \text{p}K_a^*$  will be the point where  $\phi/\phi_0 = \phi'/\phi_0' = 0.5$ . Conversely, the slower the rates of excited state proton exchange relative to the rates of fluorescence, the closer to

$\text{pH} = \text{p}K_a$  will be the point where  $\phi/\phi_0 = \phi'/\phi_0'$ . In the limit of very fast excited-state proton exchange  $\text{p}K_a^*$  defines the shape and position of the titration curve while in the limit of very slow excited-state proton exchange, relative to fluorescence,  $\text{p}K_a$  determines the shape and position of the fluorometric titration curve. The actual form of the fluorometric titration curve of any specific excited acid-base conjugate pair in which proton exchange is comparable in rate with fluorescence for at least one member of the conjugate pair depends upon whether the rates of proton exchange and fluorescence are comparable in both members or in only one member of the acid base pair. (a) If proton exchange is comparable in rate with fluorescence for both members of the conjugate pair or is comparable in rate with fluorescence for one member of the conjugate pair and much faster than fluorescence for the other member of the conjugate pair, the fluorometric titration curves will vary continuously with  $[\text{H}_3\text{O}^+]$  or  $[\text{OH}^-]$  over the entire titration interval. The fluorometric titrations will appear as stretched sigmoidal curves with their inflection points ( $\phi/\phi_0 = \phi'/\phi_0'$ ) lying very nearly between  $\text{p}K_a$  and  $\text{p}K_a^*$  in the former case and closer to  $\text{p}K_a^*$  in the latter case. This situation is frequently observed at  $\text{pH} < 3$  and in concentrated basic media (i.e., when the titration break occurs at  $\text{pH} > 11$ ) where the rates of the diffusion limited protonations and deprotonations are not severely limited by the lack of availability of  $\text{H}_3\text{O}^+$  or  $\text{OH}^-$ . (b) If the rate of the pseudo-first-order reaction with the solvent (i.e.,  $\text{HA} + \text{H}_2\text{O} \rightarrow \text{H}_3\text{O}^+ + \text{A}^-$  or  $\text{B} + \text{H}_2\text{O} \rightarrow \text{BH}^+ + \text{OH}^-$ ) is comparable to or much greater than the rate of fluorescence of HA or B but the rate of fluorescence of  $\text{A}^-$  or  $\text{BH}^+$  is much greater than the rate of protonation of  $\text{A}^-$  or deprotonation of  $\text{BH}^+$ , the reactions with the solvent (which are independent of pH) will occur partially (or completely if  $\bar{k} \gg 1/\tau_0$ ) between  $\text{pH} = \text{p}K_a$  and  $\text{pH} = \text{p}K_a^*$  but the back reaction will not occur measurably. This means that in the pH interval between  $\text{p}K_a$  and  $\text{p}K_a^*$  a fraction of the HA (or B) excited will ionize to  $\text{A}^-$  (or  $\text{BH}^+$ ) and fluoresce as such while the remaining fraction will fluoresce as HA (or B). Since no protonation of  $\text{A}^-$  (or dissociation of  $\text{BH}^+$ ) occurs during the lifetime of its excited state and since the dissociation of HA (and protonation of B) is pH independent, the relative quantum yields of fluorescence of HA and  $\text{A}^-$  (or B and  $\text{BH}^+$ ) will be constant through much or the pH interval between  $\text{p}K_a$  and  $\text{p}K_a^*$  or beyond, until a sufficiently high value of  $[\text{H}_3\text{O}^+]$  or  $[\text{OH}^-]$  is reached, that  $\bar{k}c$  is comparable to  $1/\tau_0'$ . In this circumstance eq 2 and 3 reduce to

$$\phi/\phi_0 = 1/(1 + \bar{k}\tau_0) \quad (4)$$

and

$$\phi'/\phi_0' = \bar{k}\tau_0/(1 + \bar{k}\tau_0) \quad (5)$$

in which  $\phi/\phi_0$  and  $\phi'/\phi_0'$  are, in fact, independent of pH. In the mid pH region (e.g., pH 3–11) the vanishing of the  $\bar{k}\tau_0'c$  term in eq 2 and 3 is invariable and is due to the low value of  $c$ . 6-Methoxyquinoline represents this type of behavior.<sup>15</sup> However, even in concentrated acid or base solutions  $\bar{k}$  may be small relative to  $\tau_0'c$  and therefore result in independence of  $\phi/\phi_0$  and  $\phi'/\phi_0'$  of the Hammett acidity. In the latter case and when  $\text{p}K_a^*$  lies outside the interval 3–11, the inflection point, in the region where  $\bar{k}\tau_0'c$  becomes comparable to  $\bar{k}\tau_0$  in eq 2 and 3, lies between  $\text{p}K_a$  and  $\text{p}K_a^*$  but very close to  $\text{p}K_a^*$ . However, if  $\text{p}K_a^*$  lies between 3 and 11 it is kinetically impossible for complete conversion between excited acid and conjugate base to occur within

the confines of the pH interval between  $pK_a$  and  $pK_a^*$ . In this case the inflection point in the fluorometric titration will lie at pH or  $H_0 < pK_a^*$  (for HA,  $A^-$ ) or at pH or  $H_- > pK_a^*$  (for B,  $BH^+$ ). (c) If the rate of the back reaction ( $A^- + H_3O^+ \rightarrow HA$  or  $BH^+ + OH^- \rightarrow B + H_2O$ ) is comparable to or much greater than the rate of fluorescence of  $A^-$  or  $BH^+$  but the rate of fluorescence of HA or B is much greater than the rate of dissociation of HA or protonation of B (i.e.,  $\bar{k}$  is small compared with  $1/\tau_0$  as occurs, for example, when HA and B are nonfluorescent) and if HA or B is excited, eq 2 and 3 are reduced to

$$\frac{\phi}{\phi_0} = \frac{1 + \bar{k}\tau_0'c}{1 + \bar{k}\tau_0'c} = 1 \quad (6)$$

and

$$\phi'/\phi_0' = 0 \quad (7)$$

Equations 6 and 7 indicate that direct excitation of HA or B results only in fluorescence from HA or B (i.e., no excited state proton exchange is possible). Thus if HA (or B) is fluorescent, excitation of these species yields ground state titration characteristics because only the absorbances and not the fluorescence quantum yields of these species are pH dependent. However, if  $A^-$  or  $BH^+$  is excited directly a somewhat different situation will result.

If  $A^-$  is the only species excited, the rate of loss of excited  $A^-$  is given by

$$-\frac{d[A^-(t)]}{dt} = \bar{k}[A^-(t)][H_3O^+] + \frac{[A^-(t)]}{\tau_0'} \quad (8)$$

If at time  $t = 0$ ,  $[A^-(0)] = 1$  and at  $t = \infty$ ,  $[A^-(\infty)] = 0$  we have

$$-\int_1^0 d[A^-(t)] = \bar{k}[H_3O^+] \int_0^\infty [A^-(t)] dt + \int_0^\infty \frac{[A^-(t)]}{\tau_0'} dt \quad (9)$$

but

$$\int_0^\infty \frac{[A^-(t)]}{\tau_0'} dt = \frac{\phi'}{\phi_0'} \quad (10)$$

so that

$$1 = \bar{k}[H_3O^+]\tau_0' \frac{\phi'}{\phi_0'} + \frac{\phi'}{\phi_0'} \quad (11)$$

or

$$\frac{\phi'}{\phi_0'} = \frac{1}{(1 + \bar{k}\tau_0'[H_3O^+])} \quad (12)$$

the rate of disappearance from the excited state is

$$-\frac{d[HA(t)]}{dt} = -\bar{k}[A^-(t)][H_3O^+] + \frac{[HA(t)]}{\tau_0} \quad (13)$$

at time  $t = 0$ ,  $[HA(t)] = 0$  and at  $t = \infty$ ,  $[HA(t)] = 0$  so that if HA is fluorescent

$$-\int_0^0 d[HA(t)] = -\bar{k}[H_3O^+] \int_0^\infty [A^-(t)] dt + \int_0^\infty \frac{[HA(t)]}{\tau_0} dt \quad (14)$$

but

$$\int_0^\infty \frac{[HA(t)]}{\tau_0} dt = \frac{\phi}{\phi_0} \quad (15)$$

so that

$$0 = -\bar{k}[H_3O^+]\tau_0'(\phi'/\phi_0') + (\phi/\phi_0) \quad (16)$$

or

$$\phi/\phi_0 = \bar{k}\tau_0'[H_3O^+](\phi'/\phi_0') \quad (17)$$

finally

$$\frac{\phi}{\phi_0} = \frac{\bar{k}\tau_0'[H_3O^+]}{1 + \bar{k}\tau_0'[H_3O^+]} \quad (18)$$

(if HA is nonfluorescent  $\phi/\phi_0$  is indeterminate). Similarly if  $BH^+$  is the only species excited and B is formed only by excited state proton abstraction by  $OH^-$  we have for the fluorescence of  $BH^+$

$$\frac{\phi'}{\phi_0'} = \frac{1}{1 + \bar{k}\tau_0'[OH^-]} \quad (19)$$

and for the fluorescence of B (if B is fluorescent)

$$\frac{\phi}{\phi_0} = \frac{\bar{k}\tau_0'[OH^-]}{1 + \bar{k}\tau_0'[OH^-]} \quad (20)$$

Thus the fluorescence of  $A^-$  can be altered by  $H_3O^+$  at pH higher than the ground state  $pK_a$  provided that  $\bar{k}\tau_0'[H_3O^+]$  is comparable to 1 in magnitude. This is favored by high  $[H_3O^+]$  (i.e., low  $pK_a$ ) and high  $\bar{k}$ . The latter circumstance is met when  $A^-$  is a stronger base in the excited state than in the ground state. If  $A^-$  is a weaker base than in the ground state (i.e., if  $pK_a^* < pK_a$ ),  $\bar{k}[H_3O^+]$  will be much smaller than  $1/\tau_0'$  at pH  $> pK_a$  and  $\phi'/\phi_0'$ , resulting from direct excitation of  $A^-$ , will follow ground state titration characteristics. Correspondingly, if  $BH^+$  is a stronger acid in the excited state than in the ground state,  $[OH^-]$  is large (i.e., the ground state  $pK_a$  is high), and  $\tau_0'$  is sufficiently long, the fluorometric titration of  $BH^+$  when the latter is directly excited (pH  $< pK_a$ ) will show a decrease in  $\phi/\phi_0$  at pH  $< pK_a$ . It may be noted that eq 12 and 19 are identical in form with the Stern-Volmer equation<sup>16</sup> for diffusional quenching with  $[H^+]$  or  $[OH^-]$  occupying the place of the concentration of quenching species. This is a reasonable result because quenching, in general, amounts to an irreversible reaction of the excited (fluorescing) species with an extraneous species in solution, so that the derivation of the Stern-Volmer equation evolves along the same lines as the derivations of eq 12 and 19. Equations 12 and 19 have the same shape as the titration curves obtained when equilibrium is attained in the excited state.

$$K_a^* = \frac{[H_3O^+][A^-]}{[HA]} = \frac{[H_3O^+](\phi'/\phi_0')}{(1 - \phi'/\phi_0')} \quad (21)$$

$$\frac{\phi'}{\phi_0'} = \frac{1}{1 + ([H_3O^+]/K_a^*)} \quad (22)$$

$$K_b^* = \frac{[BH^+][OH^-]}{[B]} = \frac{(\phi'/\phi_0')[OH^-]}{(1 - \phi'/\phi_0')} \quad (23)$$

and

$$\phi'/\phi_0' = \frac{1}{1 + ([OH^-]/K_b^*)} \quad (24)$$

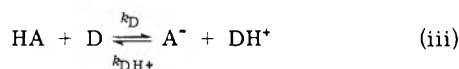
Thus plots of  $\phi_0'/\phi'$  vs.  $[H_3O^+]$  for  $A^-$  or of  $\phi_0'/\phi'$  vs.  $[OH^-]$  for  $[BH^+]$  yield straight lines whose slopes are  $\bar{k}\tau_0'$ , in the nonequilibrium case and  $1/K_a^*$  and  $1/K_b^*$ , respectively, in the equilibrium case. This renders the assessment of whether or not one is dealing with a system in excited-state equilibrium somewhat difficult. However, in many cases this dilemma can be resolved by estimating  $pK_a^*$  or  $pK_b^*$  from the Förster cycle,<sup>1,2</sup> employing the spectral shifts accompanying protonation or dissociation. Moreover, although the slope of  $\bar{k}\tau_0'$  obtained from the Stern-Volmer

plot is not truly a  $pK_a^*$ , it is a rough measure of the intrinsic basicity of  $A^-$  or acidity of  $BH^{+17}$  in the excited state, relative to that in the ground state.

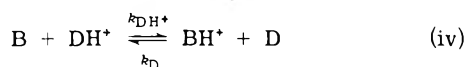
### Effect of Buffers

Up to the present the only proton donor and acceptor species considered have been the solvent, the lyonium ion ( $H_3O^+$ ), and the lyate ion ( $OH^-$ ). Thus, in the mid pH region, because of the very low concentrations of  $H_3O^+$  and  $OH^-$ , the only excited singlet state proton transfer reactions which were presumed to occur were those in which the analytes HA or B entered into pseudo-first-order proton transfer with the solvent. However, most analytical measurements performed upon aqueous solutions in the mid pH region, especially upon biological or model biological systems, are performed upon solutions containing buffer ions, often in high concentrations. The buffer ions are themselves proton donors or acceptors and may therefore enter into proton transfer reactions with excited, potentially fluorescent molecules. The rate constants for the interactions of many common buffer ions (e.g., acetate, monohydrogen phosphate, dihydrogen phosphate) with several fluorescent species have been shown to be comparable to the rate constants for the interaction of  $H_3O^+$ ,  $OH^-$ , and  $H_2O$  with these species.<sup>4</sup> Because the concentrations of buffer ions are considerably greater than those of  $H_3O^+$  or  $OH^-$  in buffered solutions, the probability of reaction of excited species with buffer ions is appreciable.

In the presence of the buffer system  $DH^+$ , D the reaction



can accompany the reaction of HA with  $H_2O$  while the reaction



can accompany the reaction of B with  $H_2O$  in the excited state, in solution. Weller<sup>4</sup> has shown by means of steady state kinetics, that when buffer species, as well as the solvent, react, with excited HA or B (at pH, e.g., between 3 and 11), the relative quantum yields of fluorescence of HA and  $A^-$  vary with  $[D]$  and  $[DH^+]$  according to

$$\frac{\phi}{\phi_0} = \frac{1 + k_{DH^+}[DH^+]\tau_0'}{1 + k_{DH^+}[DH^+]\tau_0' + (\bar{k} + k_D[D])\tau_0} \quad (25)$$

and

$$\frac{\phi'}{\phi_0'} = \frac{(\bar{k} + k_D[D])\tau_0}{1 + k_{DH^+}[DH^+]\tau_0' + (\bar{k} + k_D[D])\tau_0} \quad (26)$$

while the relative quantum yields of fluorescence of B and  $BH^+$  vary with  $[D]$  and  $[DH^+]$  according to

$$\frac{\phi}{\phi_0} = \frac{1 + k_D[D]\tau_0'}{1 + k_D[D]\tau_0' + (\bar{k} + k_{DH^+}[DH^+])\tau_0} \quad (27)$$

and

$$\frac{\phi'}{\phi_0'} = \frac{(\bar{k} + k_{DH^+}[DH^+])\tau_0}{1 + k_D[D]\tau_0' + (\bar{k} + k_{DH^+}[DH^+])\tau_0} \quad (28)$$

where  $k_D$  is the bimolecular rate constant for reaction of excited HA or  $BH^+$  with D and  $k_{DH^+}$  is the bimolecular rate constant for reaction of excited  $A^-$  or B with  $DH^+$ . If the reactions of excited HA or B with  $H_2O$  are too slow to occur during  $\tau_0$ , eq 25–28 reduce to

$$\frac{\phi}{\phi_0} = \frac{1 + k_{DH^+}[DH^+]\tau_0'}{1 + k_{DH^+}[DH^+]\tau_0' + k_D[D]\tau_0} \quad (29)$$

$$\frac{\phi'}{\phi_0'} = \frac{k_D[D]\tau_0}{1 + k_{DH^+}[DH^+]\tau_0' + k_D[D]\tau_0} \quad (30)$$

$$\frac{\phi}{\phi_0} = \frac{1 + k_D[D]\tau_0'}{1 + k_D[D]\tau_0' + k_{DH^+}[DH^+]\tau_0'} \quad (31)$$

and

$$\frac{\phi'}{\phi_0'} = \frac{k_{DH^+}[DH^+]\tau_0}{1 + k_D[D]\tau_0' + k_{DH^+}[DH^+]\tau_0'} \quad (32)$$

respectively. Equations 29–32 indicate that, in the presence of sufficiently high buffer concentrations with sufficiently high rate constants  $k_D$  and  $k_{DH^+}$ , excited state proton transfer is possible even if reaction with solvent species is not. If the concentration of buffer species is high enough, excited state equilibrium corresponding to reactions iii and iv may occur, the equilibrium constants for these reactions being given, respectively, by

$$K_{D-HA}^* = \frac{k_D}{k_{DH^+}} = \frac{[DH^+][A^-]}{[D][HA]} \quad (33)$$

and

$$K_{D-B}^* = \frac{k_{DH^+}}{k_D} = \frac{[BH^+][D]}{[B][DH^+]} \quad (34)$$

Since in the ground state, equilibrium exists between D and  $DH^+$  (equilibrium constant,  $K_D$ ), we have

$$K_{D-HA}^* = \frac{[A^-][H_3O^+]}{[HA]K_D} \quad (35)$$

and

$$K_{D-B}^* = \frac{[BH^+]}{[B]} \frac{K_D}{[H_3O^+]} \quad (36)$$

or

$$K_{D-HA}^*K_D = \frac{[A^-][H_3O^+]}{[HA]} \quad (37)$$

and

$$K_{D-B}^*K_w/K_D = \frac{[BH^+][OH^-]}{[B]} \quad (38)$$

where  $K_w$  is the autoprotolysis constant of water. In logarithmic form

$$pK_{D-HA}^* + pK_D = -\log \frac{[H_3O^+][A^-]}{[HA]} \quad (39)$$

and

$$pK_{D-B}^* + pK_w - pK_D = -\log \frac{[BH^+][OH^-]}{[B]} \quad (40)$$

However, eq 39 is equivalent to the sum of the standard state free energy changes of reaction iii and the buffer ionization ( $BH^+ + H_2O \rightleftharpoons B + H_3O^+$ ), which, in turn, is equivalent to the standard state free energy change of reaction i, in the excited state. Thus it is correct to write

$$pK_{D-HA}^* + pK_D = pK_a^* \quad (41)$$

By analogous reasoning we obtain

$$pK_{D-B}^* + pK_w = pK_b^* \quad (42)$$

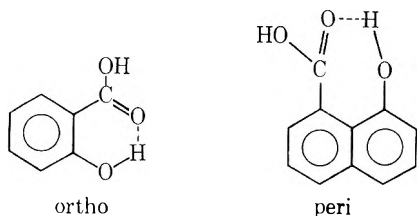
It is seen that the equilibria of HA and  $A^-$  and of B and  $BH^+$  with the solvent and lyonium and lyate ions, characterized by  $pK_a^*$  and  $pK_b^*$ , are coupled to the equilibria characterized by  $pK_{D-HA}^*$  and  $pK_{D-B}^*$ , respectively, and that excited-state equilibria in reactions iii or iv is suffi-

cient to cause excited-state equilibria in the former reactions. The buffer species have therefore altered the mechanism of attainment but not the position of excited state equilibrium. In reaction iii HA and  $A^-$  are the only fluorescent species while in reaction iv and B and  $BH^+$  are the only fluorescent species. Consequently, at buffer concentrations high enough to sustain excited-state equilibria in reactions iii and iv the variations of  $\phi/\phi_0$  and  $\phi'/\phi_0'$  with pH will reflect the equilibrium fluorometric curves corresponding to the equilibria involving  $H_3O^+$  and  $OH^-$ . Buffer systems may thus be useful in forcing to excited-state equilibrium acid-base pairs that by themselves in water cannot be studied under equilibrium conditions. In this regard, it is desirable to choose a buffer system whose  $pK_a^*$  is as close as possible to the excited state  $pK_a^*$  of the conjugate pair of interest in order to assure that sufficiently high concentrations of D and  $DH^+$  will be present, near the anticipated inflection region, to cause both excited acid and conjugate base to react. The effects of phosphate buffer concentration upon the fluorometric pH titrations of 1- and 2-anthroate are shown in Figures 3 and 4. In Figures 3 and 4, curve A (no buffer present) reflects ground state equilibrium titrimetry, curves B and C reflect partial excited state proton exchange in their protracted inflection regions, and curve D (very high buffer concentration) represents the near attainment of excited-state equilibrium in its narrow titration interval. The inflection points of curve D in Figures 3 and 4 occur at pH 6.3 and 6.5, respectively, in reasonably good agreement with the  $pK_a^*$  values of 6.9 and 6.6 calculated from the Förster cycle.<sup>18</sup>

### Phototautomerism

In certain molecules containing at least two ionizing functional groups, excitation to the lowest excited singlet state may result in the "simultaneous" loss of a proton from one group and gain a proton by another. Since no net ionization has occurred, the process amounts to a photoisomerization or phototautomerization. Phototautomerism is frequently observed in polyfunctional molecules containing at least one electron acceptor group (which becomes more basic in the excited state) and one electron donor group (which becomes more acidic in the excited state) and is usually observed as an anomalously large Stokes shift of the fluorescence (i.e., the fluorescence band lies at much longer wavelengths than would be anticipated on the basis of the electronic structure of the neutral molecule).

Two broad classes of excited singlet state phototautomerism may be distinguished. In intramolecular phototautomerism, the electron acceptor and donor groups are usually situated ortho or peri to one another on the aromatic ring, with an intramolecular hydrogen bond bridging the two functional groups. In some instances, however, intra-



molecular hydrogen bonding occurs between aryl substituent groups and acidic or basic groups on side chains. Upon excitation, the hydrogen atom belonging to the electron donor group is transferred predominately or entirely to the electron acceptor group. This process is very fast and may

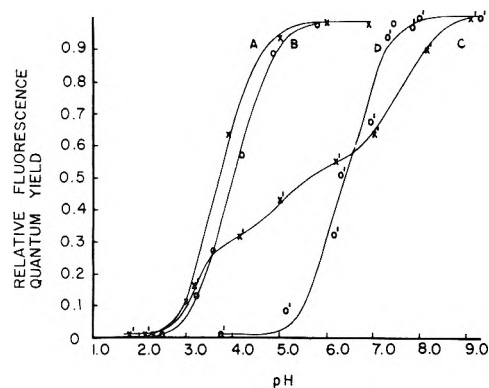


**Figure 3.** Variations of the relative quantum yields of fluorescence of the 1-anthroate anion with pH, in the presence of sodium dihydrogen phosphate buffer: (A)  $C_{NaH_2PO_4} = 0$ , (B)  $C_{NaH_2PO_4} = 0.010$  M, (C)  $C_{NaH_2PO_4} = 0.10$  M, (D)  $C_{NaH_2PO_4} = 1.0$  M. The pH dependence of the fluorescence of neutral 1-anthraic acid is omitted in the interest of graphical clarity.

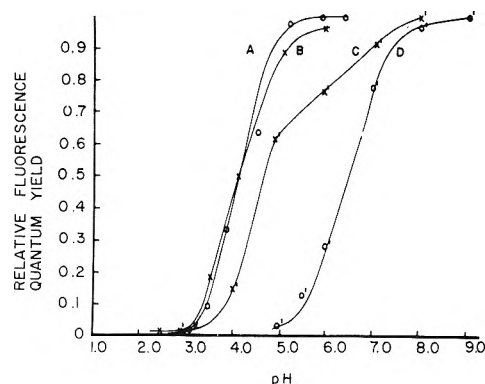


**Figure 4.** Variations of the relative quantum yield of fluorescence of the 2-anthroate anion with pH, in the presence of sodium dihydrogen phosphate buffer: (A)  $C_{NaH_2PO_4} = 0$ , (B)  $C_{NaH_2PO_4} = 0.010$  M, (C)  $C_{NaH_2PO_4} = 0.10$  M, (D)  $C_{NaH_2PO_4} = 1.0$  M. The pH dependence of neutral 2-anthraic acid is omitted in the interest of graphical clarity.

be complete within the lifetime of a few molecular vibrations ( $\sim 10^{-13}$  sec) after excitation. Intramolecular phototautomerism does not demonstrate a strong dependence on the solvent. It was first observed by Weller<sup>19</sup> who noted that the fluorescence of salicylic acid, in alcoholic and hydrocarbon solvents, occurred at much longer wavelengths ( $\sim 440$  nm) than the fluorescence of *o*-anisic acid ( $\sim 340$  nm), the latter having a similar electronic structure to salicylic acid but also having a methoxy group rather than a hydroxy group so that phototautomerism was not possible. The pH dependences of the fluorescence quantum yields of phototautomers, formed by the intramolecular route, follow the same general patterns as those of the molecules previously described. However, the sites of ionization in the excited state (if excited state protonation or dissociation is fast enough to occur) are different from the sites of ionization in the ground state.<sup>20</sup> For example, in concentrated sulfuric acid, the salicylic acid cation dissociates from the protonated carboxyl group in the ground state and from the phenolic group in the excited state, to form the excited zwitterion. Near pH 3 salicylic acid dissociates in the ground state from the carboxyl group to form the singly charged anion. Excited state dissociation of the salicylic acid zwitterion is not fast enough to compete with fluorescence. Thus, as the pH interval from 1 to 5 is traversed, the

fluorescence of the zwitterion (formed by direct excitation of the neutral molecule) changes to that of the excited singly charged anion ionized at the phenolic group, the latter being formed only by the direct excitation and rapid intramolecular phototautomerization of the singly charged ground state anion (ionized at the carboxyl group). An important point to be made here is that, because the sites of ionization are different in phototautomers, the excited state acid-base properties cannot be predicted from the Förster cycle employing fluorescence maxima which correspond to a different conjugate pair than that represented by the ground state  $pK_a$ .

Intermolecular phototautomerism is often observed in polyfunctional molecules in which the electron donor and electron acceptor groups are widely separated. In this case, subsequent to excitation, the electron acceptor group is protonated by the solvent or by  $H_3O^+$  while the electron donor group is deprotonated by the solvent or by  $OH^-$ . The time scale for intermolecular phototautomerism is thus comparable to that for ordinary excited state protonation and deprotonation. Tautomerism is, in the thermodynamic sense, pH invariant because no protons are gained or lost in the overall process. However, in some cases, the rate of a protonation or dissociation step in the phototautomerization process is slow, compared with fluorescence, because of low concentrations of  $H_3O^+$  or  $OH^-$  (as in the mid pH range). Yet the reaction may occur in concentrated acid or base solutions. The fluorometric titration curve will thus show a pH dependence as the acidity region in which the concentration of  $H_3O^+$  or  $OH^-$  becomes high enough for phototautomerism to occur is entered. Several quinoline-carboxylic acids have been shown to demonstrate this behavior<sup>21,22</sup> which is often difficult to distinguish from equilibrium excited state proton transfer.

The occurrence of kinetically pH-dependent phototautomerism can be identified by protonating, stepwise, all functional groups in the molecule and observing the absorption and fluorescence spectra as the pH is varied. In the absence of pH-dependent, intermolecular phototautomerism a molecule will demonstrate as many inflection regions in its absorptiometric and fluorometric titration

curves as the number of ionizing functional groups it has. However, for molecules undergoing pH-dependent intramolecular phototautomerism, each species involved in the phenomenon will yield one extra inflection region in the pH dependence of the fluorescence spectra (but not in that of the absorption spectra). For example, 1-hydroxy-2-naphthoic acid and 2-hydroxy-1-naphthoic acid each demonstrate three prototropic dissociations in the absorption spectra, cation = neutral molecule, neutral molecule = singly charged anion, and singly charged anion = doubly charged anion. However, the fluorescence spectra show four fluorescent transformations.<sup>23</sup> One of these (in each compound) has been attributed to phototautomerism of the neutral molecule to the zwitterion, which appears to require the protonation of the carboxyl group in the excited state as the first step.

## References and Notes

- (1) T. Förster, *Z. Elektrochem.*, **54**, 42 (1950).
- (2) T. Förster, *Z. Elektrochem.*, **54**, 531 (1950).
- (3) A. Weller, *Z. Elektrochem.*, **56**, 662 (1952).
- (4) A. Weller, *Prog. React. Kinet.*, **1**, 187 (1961).
- (5) N. Lasser and J. Feitelson, *J. Phys. Chem.*, **77**, 1011 (1973).
- (6) M. Eigen, W. Kruse, G. Maas, and L. De Maeyer, *Prog. React. Kinet.*, **2**, 285 (1964), and references contained therein.
- (7) R. E. Ballard and J. W. Edwards, *J. Chem. Soc.*, 4868 (1964).
- (8) S. Schulman and Q. Fernando, *J. Phys. Chem.*, **71**, 2668 (1967).
- (9) S. Schulman and Q. Fernando, *Tetrahedron*, **24**, 1777 (1968).
- (10) M. P. Bratzel, J. J. Aaron, J. D. Winefordner, S. G. Schulman, and H. Gershon, *Anal. Chem.*, **44**, 1240 (1972).
- (11) S. G. Schulman, *Anal. Chem.*, **43**, 285 (1971).
- (12) M. P. Bratzel, J. J. Aaron, J. D. Winefordner, S. G. Schulman, and H. Gershon, *J. Phys. Chem.*, **77**, 1595 (1973).
- (13) W. L. Paul, P. J. Kovi, and S. G. Schulman, *Spectrosc. Lett.*, **6**, (1973).
- (14) A. Weller, *Z. Phys. Chem. (Frankfurt am Main)*, **15**, 438 (1958).
- (15) S. G. Schulman, R. M. Threatte, A. C. Capomacchia, and W. L. Paul, *J. Pharm. Sci.*, **63**, 876 (1974).
- (16) O. Stern and M. Volmer, *Z. Phys.*, **20**, 183 (1919).
- (17) R. P. Bell, "The Proton in Chemistry", Cornell University Press, Ithaca, N.Y., 1959, Chapter X.
- (18) E. VanderDonckt and G. Porter, *Trans. Faraday Soc.*, **64**, 3215 (1968).
- (19) A. Weller, *Z. Elektrochem.*, **60**, 1144 (1956).
- (20) P. J. Kovi, C. L. Miller, and S. G. Schulman, *Anal. Chim. Acta*, **61**, 7 (1972).
- (21) P. J. Kovi, C. L. Miller, and S. G. Schulman, *Anal. Chim. Acta*, **62**, 59 (1972).
- (22) B. Zalis, A. C. Capomacchia, D. Jackman, and S. G. Schulman, *Talanta*, **20**, 33 (1973).
- (23) S. G. Schulman and P. J. Kovi, *Anal. Chim. Acta*, **67**, 259 (1973).

## Excited State $pK^*$ Values from Fluorimetry

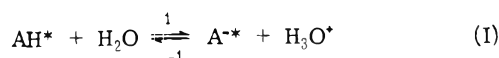
Nechama Lasser and Jehuda Feitelson\*

Department of Physical Chemistry, The Hebrew University, Jerusalem, Israel  
(Received June 14, 1973; Revised Manuscript Received February 24, 1975)

Publication costs assisted by the United States-Israel Binational Science Foundation

The reciprocal singlet state lifetimes are compared with the dissociation and protonation rates in the excited state of the reaction  $AH^* + H_2O = A^{-*} + H_3O^+$ . It is found that if one of the species  $AH^*$  or  $A^{-*}$  is nonfluorescent ( $\tau \leq 10^{-11}$  sec) the reaction in which it takes part cannot proceed to any appreciable extent during its very short lifetime. Although the presence of buffers, composed of an acid and its conjugate base, does increase the rates of protonation and of dissociation, it can be seen that at any reasonable buffer concentration the reaction rates in  $AH^* + B = A^{-*} + BH^+$  ( $B, BH^+ =$  buffer base and acid) are still far too low to compete with the rapid deactivation rate of a nonfluorescent molecule or ion ( $AH^*$  or  $A^{-*}$ ). It is concluded that, if in an aqueous solution (pH 0–14) only one of the species  $AH^*$  or  $A^{-*}$  is fluorescent, a pH vs. fluorescence intensity curve does not represent an excited state equilibrium and does not, therefore, allow us to determine the  $pK^*$  value of the above dissociation reaction. Both cases are discussed in detail. Tyramine is presented as an example for a system where the acidic form  $AH^*$  only is fluorescent and riboflavin monophosphate (FMN) for the case where only  $A^{-*}$  does fluoresce.

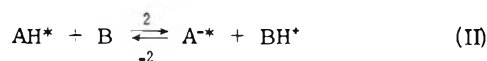
In a previous paper we had found that in those cases where only one species  $A^{-*}$  or  $AH^*$  in the dissociation equilibrium is fluorescent the dependence of fluorescence on pH does not in general yield the excited state equilibrium constant.<sup>1</sup> This conclusion was based on a comparison of excited singlet state lifetimes with the rates of dissociation and of protonation. It was shown that even if the energetics of the process differs in the ground and in the excited singlet states the fluorescence should still either follow the ground state dissociation curve or at most should measure the rate of the back reaction in the equilibrium



It has been stated by Schulman and Capomacchia<sup>2</sup> that the difficulty of attaining excited state equilibrium in aqueous solution (at pH 3 to 11) can be overcome by using buffer substances which act as proton donors or acceptors with respect to the excited molecules. We wish to discuss here the influence of buffers on the attainment of excited state dissociation equilibria and on the determination of  $pK^*$  values in aqueous solution with special emphasis on those cases where only one of the species  $AH^*$  or  $A^{-*}$  fluoresces.

### Both $HA^*$ and $A^{-*}$ Are Fluorescent

We denote the acidic form of the buffer by  $BH^+$  and its conjugate base by  $B$ . Since  $B$  is usually a better proton acceptor than water, the dissociation rate of an excited molecule  $AH^*$  in presence of  $B$ , namely of the forward reaction in



will exceed the rate of the dissociation step (reaction 1) in eq I. The rate of the back reaction (reaction -2), at low  $H^+$  ion concentrations, will compete successfully with the protonation by  $H^+$  ions (reaction -1).

The probability of approaching equilibrium can be estimated by comparing the product of the bimolecular rate constant by the concentration of the buffer species ( $k_2C_B$  and  $k_{-2}C_{BH^+}$ ) with the reciprocal lifetimes of the excited

states  $1/\tau_{AH^*}$  and  $1/\tau_{A^{-*}}$ . The values of the constants  $k_2$  and  $k_{-2}$  are usually smaller than  $3 \times 10^9 M^{-1} sec^{-1}$ .<sup>3,4</sup> It is therefore true that if both  $AH^*$  and  $A^{-*}$  have lifetimes in the nanosecond range an approach toward equilibrium in reaction II is possible at sufficiently high buffer concentrations. At equilibrium the dissociation constant is given by

$$K_{HA^*} = K_{BH^+}K_{II} = K_{BH^+} \left\{ \frac{[BH^+][A^{-*}]}{[B][HA^*]} \frac{f_{BH^+} + f_{A^{-*}}}{f_B f_{HA^*}} \right\}_{eq} \quad (III)$$

and can in principle be evaluated for a given buffer composition and fluorescence ratio of  $A^{-*}$  and  $AH^*$ .

There are, however, a number of serious difficulties in using eq III to obtain  $pK_{HA^*}$ .

(a) Even a state of near equilibrium is seldom achieved by the use of comparatively high buffer concentrations. For example, in the system 1-anthroic acid-anthroate ion both species are fluorescent. Figure 1 shows the fluorimetric behavior of the anthroate ion in various solutions of phosphate buffer. It is seen that in the presence of 0.46 M  $NaH_2PO_4$  (curve a) about 60% of the anthroate fluorescence is quenched (see pH 4–5). By increasing the  $K_2HPO_4$  concentration (pH >6) the back reaction  $AH^* + B \rightarrow A^{-*} + BH^+$  gains in importance and the anthroate fluorescence increases: i.e., both the forward and the back reactions take place to some extent. That the system is still far from equilibrium, however, is indicated by the fact that (1) even in 0.46 M  $NaH_2PO_4$  the forward reaction (2) is only 60% complete during the lifetime of the excited ion  $A^{-*}$ . (2) Increasing the overall buffer concentration over a given pH interval causes the fluorescence vs. pH curve to be displaced (curve b); it now tends toward an inflection point at a higher pH value. Curves a and b are not continued since in order to increase the pH, unreasonably high  $K_2HPO_4$  concentrations would be required. The broken line (c) at a total buffer concentration of 0.92 M cannot represent equilibrium conditions. Here the  $NaH_2PO_4$  concentration decreases above pH 6.5 to a value which cannot sustain the forward reaction (eq II,2), and hence an approach toward equilibrium, during the lifetime of  $A^{-*}$ .

(b) At high salt concentrations the activity coefficient



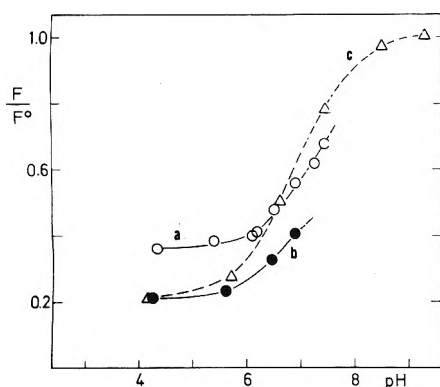


**Figure 1.** Relative fluorescence of 1-anthroate ion as a function of pH in presence of phosphate buffer: (a)  $\circ$ ,  $\text{NaH}_2\text{PO}_4$  concentration 0.46 M; (b)  $\bullet$ ,  $\text{NaH}_2\text{PO}_4$  concentration 0.92 M; (c)  $\Delta$  total  $\text{NaH}_2\text{PO}_4 + \text{K}_2\text{HPO}_4$  concentration 0.96 M.

ratio in eq III could differ appreciably from unity. There are no data available on activity coefficients of 1-anthroic acid and of the anthroate ion in high concentration salt solutions.

(c) High concentration buffers often act as fluorescence quenchers irrespective of any dissociation equilibrium.

Weller has shown<sup>3,5</sup> how the rate constants for the forward and the back reactions of eq II can be evaluated from the dependence of the  $\text{HA}^*$  and  $\text{A}^{-*}$  fluorescences upon buffer concentration. In this method comparatively low buffer concentrations can be used and excited state equilibrium does not have to be attained for the evaluation of  $pK_{\text{HA}^*}$ . Our calculations by Weller's approach yield for anthroic acid a value of  $pK_{\text{HA}^*} = 8.0$ – $8.6$ . This procedure, though computationally more complex than a titration curve, is, to our mind, much to be preferred to an attempt to attain near equilibrium in the excited state at high buffer concentrations.

The situation however is different if only one of the two forms HA or  $\text{A}^-$  fluoresce. Let us discuss separately the two cases.

#### $\text{HA}^*$ Only Is Fluorescent

As mentioned above, in presence of a buffer base, B, the dissociation rate of  $\text{HA}^*$  increases and its fluorescence intensity decreases correspondingly. On the other hand, if the ionic form  $\text{A}^{-*}$  is nonfluorescent, i.e., has a lifetime of  $\tau \leq 10^{-11}$  sec, even a concentration of  $\text{BH}^+$  or of  $\text{H}^+$  ions of up to 1 M will not suffice to protonate  $\text{A}^{-*}$  to any appreciable extent during its excited state lifetime ( $k_{-2}C_{\text{BH}^+} \leq 3 \times 10^9 \text{ sec}^{-1}$  to be compared with  $k_{\text{deexc}} \geq 10^{11} \text{ sec}^{-1}$ ). Under these conditions one cannot talk about equilibrium in the excited state and the fluorescence vs. pH curve should reflect only the dissociation step (reaction 2). An example for such a behavior can be found in the phenol–phenolate or tyramine–tyramine ion systems which do fluoresce only in their protonated form, PhOH, while  $\text{PhO}^-$  is nonfluorescent. The ground state  $pK$  values of phenol and of tyramine are close to  $pK \approx 10$ , while the Förster cycle predicts an excited state value of  $pK^* \approx 4.5$ . Acetate ions, acting as buffer base B, promote the dissociation of PhOH and thereby quench its fluorescence. If equilibrium in the excited state was established one would expect the protonation  $\text{PhO}^- + \text{BH}^+ \rightarrow \text{PhOH} + \text{B}$ , where  $\text{BH}^+$  is acetic acid, to predominate below pH 4.5. The reaction should be accompanied by an increase of the PhOH fluorescence. Figure 2

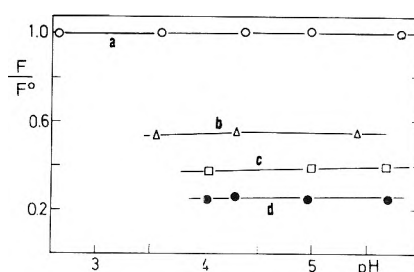


**Figure 2.** Relative fluorescence of tyramine as a function of pH in presence of acetic acid–acetate buffer:  $\text{CH}_3\text{COONa}$  concentration ( $\circ$ ) none; ( $\Delta$ ) 0.1 M; ( $\square$ ) 0.21 M; ( $\bullet$ ) 0.42 M.

shows no such effect. Any given concentration of acetate ions quenches the tyramine fluorescence to the same extent over the whole pH range between pH 3.5 and 7. No inflection, indicating protonation, in the fluorescence curve of PhOH is observed at the acidic side of the above pH range, although the concentration of acetic acid ( $\text{BH}^+$ ) increases to 0.9 M at the low pH end of curves b, c, and d. This can be interpreted in terms of eq II to mean that reaction 2 leads to the formation of the nonfluorescent anion  $\text{PhO}^-$ , but that no back reaction (reactions  $-1$  or  $-2$ ) takes place.

#### $\text{A}^{-*}$ Only Is Fluorescent

If only the dissociated form  $\text{A}^{-*}$  is fluorescent and the acidic form  $\text{AH}^*$  is nonfluorescent (i.e., has a lifetime of  $\tau \leq 10^{-11}$  sec) no appreciable dissociation of the latter will take place in the excited state unless  $\text{AH}^*$  is a fairly strong acid in aqueous solution ( $k_1 \geq 10^{10} \text{ sec}^{-1}$ ). The presence of up to 1 M buffer base, B, will not change the situation. No significant amount of  $\text{A}^{-*}$  will be formed since  $k_2C_{\text{B}} \leq 3 \times 10^9 \text{ sec}^{-1}$  while  $1/\tau_{\text{HA}^*} > 10^{11} \text{ sec}^{-1}$ . In such a case only excitation at pH values above the ground state  $pK$  will form the fluorescent species  $\text{A}^{-*}$ . On the other hand, it is possible that the acidic form of the buffer,  $\text{BH}^+$ , will lead to protonation of  $\text{A}^{-*}$  and to a corresponding decrease in its fluorescence yield. If the concentration of  $\text{BH}^+$  is kept constant, while the concentration of B is changed in order to alter the pH, the fluorescence yield of  $\text{A}^{-*}$  will be lower than in the absence of  $\text{BH}^+$  by a constant amount, commensurate with the concentration of  $\text{BH}^+$ . The concentration of B will have no effect on the fluorescence since, as mentioned above, it cannot influence the dissociation of  $\text{AH}^*$  (reaction 2). If the concentration of  $\text{BH}^+$  is allowed to change (for example, if the total buffer concentration is kept constant) lowering the pH will increase the  $\text{BH}^+$  concentration (at the expense of B). This in turn will cause the rate of protonation (reaction  $-2$ ) to increase, and a corresponding decrease in the  $\text{A}^{-*}$  fluorescence will be observed. The latter, however, will reflect only the change in concentration of  $\text{BH}^+$  but will be unrelated to the  $pK^*$  value of  $\text{HA}^*$ .

Again, as in the previous case ( $\text{HA}^*$  only fluorescent) one cannot talk about an excited state equilibrium since only one of the two reactions involved in eq II can proceed to any measurable extent.

Flavin mononucleotide can serve as an example for a case where the basic form (FMN) fluoresces while the acidic form ( $\text{FMNH}^+$ ) is nonfluorescent. The FMN fluorescence has attracted attention in the literature<sup>2,6</sup> and we shall therefore discuss it in some detail.

Curve a of Figure 3 shows the fluorescence of FMN as a function of pH in aqueous solution. This curve, when compared to the ground state titration, is displaced by about

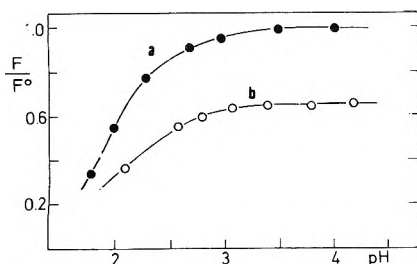


Figure 3. Fluorescence of FMN as a function of pH in presence of formic acid formate buffer: (a) pure aqueous solution; (b) HCOOH concentration 0.46 M.

two pH units toward higher pH values. We think that this fluorimetric titration curve is determined only by the protonation step in the excited state and does not therefore represent an equilibrium or even an approach toward equilibrium.<sup>1</sup> Moreover a sigmoid  $\phi/\phi_0$  vs. pH curve is no proof of equilibrium but can just as well describe quenching by  $H^+$  ions (as was done by us in ref 1). We showed that with decreasing lifetime (because of quenching by  $Br^-$  ions) the FMN fluorescence yield vs. pH curve shifts toward the ground state titration curve but does not change its shape. We see no reason to assume that the curve in the absence of  $Br^-$  ions, where the lifetime of FMN is  $\tau \approx 4.6$  nsec, has any special significance. Could one increase this lifetime by some means, the curve would probably move further toward higher pH values. No approach to equilibrium is achieved also by the use of formate buffer (curve b). Formic acid (0.46 M,  $BH^+$ ) quenches the fluorescence of FMN through reaction -2 by  $\sim 35\%$  (Figure 3). This is true over the whole pH range between pH 1.8 and 4.0 and does not depend on the concentration of formate ions (B). If the  $pK^*$  value of FMN were located in this region and indeed both reactions 2 and -2 were to take place, then the addition of formate ion (B) would lead to an increase in the rate of reaction 2 and thus would cause a corresponding increase in the fluorescence of FMN. Such an effect, however, is not observed although at pH 4 the formate ion concentration increases to 1.25 M. Hence, we think that in this pH range only reaction -2 proceeds in the excited state while reaction 2 does not take place during the short lifetime of  $FMNH^{*+}$ . We claim therefore that on the basis of these fluorescence measurements alone it is not possible to decide whether  $FMNH^{*+}$  is indeed a stronger acid than the ground state  $FMNH^+$ , as required by the Förster cycle, or not. Certainly the value of  $pK^*$  cannot be estimated from these data. By the way, we did recently find that in strongly acidic solution ( $HClO_4 \geq 4 N$ , 50% ethanol) a weak fluorescence of the  $FMNH^+$  cation can be observed. Although this might be taken to indicate an approach to excited state equilibrium (with  $pK^* \approx -1$  to  $-2$ ) we do not think, as will be explained presently, that such data can be used to determine the  $pK^*$  value. In our previous study as well as in the present communication we dealt with the dissociation equilibrium in aqueous solution *only* (see eq 1 and ref 1, eq 5

and 6). These studies therefore refer to systems in the ordinary pH range ( $0 < pH < 14$ ) and not to high acid or base concentrations described by the Hammett functions  $H_0$  and  $H_-$ . It is true that in extremely acid solutions protonation might take place in a time comparable to the excited state lifetime of a nonfluorescent species because the high  $H^+$  ion concentration causes protonation to become a very rapid process. However solutions of hydrogen ion concentration in the  $H_0 > 1$  range cannot, to our mind, be considered truly aqueous in the sense that both the structure of the solvent (water) and the solute-solvent interactions might differ appreciably between neutral and highly acidic solutions. These solvent effects become important when comparing  $pK^*$  values derived from the Förster cycle with those from a fluorimetric titration. In the former the absorption and/or fluorescence spectra of the acidic and of the ionized form of the molecule are usually determined within the range  $0 < pH < 14$  so that the  $pK^*$  derived refers to an aqueous solution. On the other hand,  $pK^*$  values determined from the inflection in the pH dependence of absorption (near, e.g., pH 1) and fluorescence (near  $H_0 = 5$ , for example) involves measurements in solvents of very different thermodynamic properties. Thus, the fluorescence vs. pH curve describes the acidic dissociation in a solvent whose proton acceptor or donor properties vary widely from those of a truly aqueous solution. For example, the fluorescence of the protonated 8-hydroxyquinoline and similar compounds has been described in terms of the anhydrous properties of sulfuric acid and alcoholic solvents.<sup>8,9</sup> It is the solvent which seems to promote the formation of the fluorescent species, an effect which cannot be directly correlated with the excited state properties of the molecule. Moreover  $pK$  values derived with the aid of Hammett functions are altogether known to be only approximately correct.<sup>10</sup> Because of these uncertainties in the determination of  $pK^*$  and in the true nature and the effects due to the solvent we choose to limit our discussion to the well-defined aqueous solutions in the above range ( $0 < pH < 14$ ). Our study therefore does not cover the quinolinium derivatives and aromatic ketones discussed by Schulman and Capomacchia.<sup>2</sup>

*Acknowledgment.* This research was sponsored in part by the United States-Israel Binational Science Foundation, Grant No. 81.

## References and Notes

- (1) N. Lasser and J. Feitelson, *J. Phys. Chem.*, **77**, 1011 (1973).
- (2) S. G. Schulman and A. C. Capomacchia, preceding article in this issue.
- (3) A. Weller, *Z. Elektrochem.*, **64**, 55 (1960), *Prog. React. Kinet.*, **1**.
- (4) J. Feitelson, *J. Phys. Chem.*, **68**, 391 (1964).
- (5) A. Weller, *Z. Phys. Chem. (Frankfurt am Main)*, **18**, 163 (1958).
- (6) S. G. Schulman and Q. Fernando, *Tetrahedron*, **24**, 1777 (1968).
- (7) N. Lasser and J. Feitelson, *Photochem. Photobiol.*, submitted for publication.
- (8) E. L. Wehry in "Fluorescence, Instrumentation and Practice", G. G. Guilbault, Ed., Marcel Dekker, New York, N.Y., 1967, Chapter 2.
- (9) O. Popovych and L. B. Rogers, *Spectrochim. Acta*, **15**, 584 (1959).
- (10) R. P. Bell, "The Proton in Chemistry", Cornell University Press, Ithaca, N.Y., 1959, Chapter VI.

## A Spectroscopic Study on Benzenethiol and Thioanisole by Photoselection

Philip G. Russell<sup>1</sup>

Department of Chemistry, C.W. Post College, P.O. Greenvale, New York 11548 (Received August 9, 1974; Revised Manuscript Received March 12, 1975)

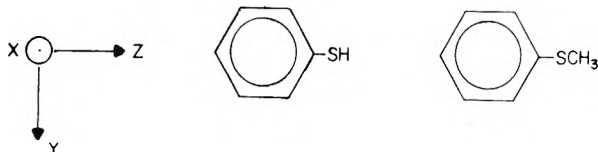
The polarization of the fluorescence and phosphorescence in benzenethiol (PhSH) and thioanisole (PhSCH<sub>3</sub>) at 77°K is studied in detail. Polarization of emission excitation experiments give the expected result that the first and second absorption bands are oppositely polarized. In each case the first weak absorption band is the <sup>1</sup>L<sub>b</sub> state while the strong absorption band is the <sup>1</sup>L<sub>a</sub> state. A large polarization peak (long-axis in-plane polarized) due to an intense vibronic transition is found in the phosphorescence for excitation in the 0-0 region of the <sup>1</sup>L<sub>a</sub> band. Some polarization detail is observed in the fluorescence also. The value of the polarization ratio (1.62) in the 0-0 region of PhSH (for excitation in the <sup>1</sup>L<sub>a</sub> band) indicates that the phosphorescing state is an n,π\* triplet. In PhSCH<sub>3</sub> the smaller value found for the polarization ratio (1.0) is interpreted in terms of a π,π\* emitting triplet.

### Introduction

The method of photoselection<sup>2</sup> has been used to obtain detailed polarization measurements on the fluorescence and phosphorescence in PhSH and PhSCH<sub>3</sub>. These experiments were carried out in 3-methylpentane (3MP) and EPA glasses at 77°K.

The method of photoselection (see Appendix for a brief description of the photoselection method and its application here) has been used previously in order to obtain values for the molecular emission parameters (probability for emission along individual molecular axes) in the lowest triplet state of benzene,<sup>3</sup> in the low-lying electronic states of dimethoxybenzene,<sup>4</sup> and in some amino-substituted benzene derivatives.<sup>5</sup> In these molecules the long phosphorescence lifetimes (seconds) and the values obtained for the polarization ratios indicate the absence of n,π\* states in the various pathways for obtaining emission from the lowest <sup>3</sup>π,π\* state. In contrast the smaller values found for the phosphorescence lifetimes<sup>6</sup> in PhSH and PhSCH<sub>3</sub> (0.007 and 0.0076 sec, respectively) indicate the importance of the n,π\* states and π,π\* states containing charge transfer (CT) character in the dominant spin-orbit vibronic coupling mechanisms. In this case the spin-orbit coupling is enhanced by one center contributions on the sulfur atom.<sup>7</sup>

Low-lying CT states have been observed in PhSH and confirmed by CI calculations.<sup>8</sup> For excitation in a CT state with <sup>1</sup>L<sub>a</sub> symmetry (long-axis in-plane or z direction)



values for the polarization ratios of 1.62 and 1.00, respectively, were found in the 0-0 region of the PhSH and PhSCH<sub>3</sub> phosphorescence bands. A value of 1.00 in the 0-0 region is usually indicative of a <sup>3</sup>π,π\* state while the much larger value of 1.62 could indicate an n,π\* lowest triplet.<sup>9</sup> In addition photoproduct formation (requiring only one photon) was found to occur rapidly in PhSH while no evidence for photoproduct formation was observed in PhSCH<sub>3</sub>. These observations would support the polarization results if one assumes that the photoreactivity found

in PhSH is linked in some way to the presence of a low-lying n,π\* triplet. However the photochemical observations found here (these are reported in a second paper) may be just a coincidence and in no way support the polarization results.

### Experimental Section

The apparatus for obtaining the polarization measurements is shown in Figure 1. The slit widths in the excitation monochromator and observing spectrometer were 2.0 and 0.4 mm, respectively, in these polarization experiments. All samples were less than  $1.0 \times 10^{-3}$  M at 77°K and were contained in 9-mm o.d. quartz test tubes. The samples were degassed with zero grade helium prior to cooling in liquid nitrogen. Any nitrogen bubbles present were directed away from the excitation and emission light paths inside the dewar. Details for performing low temperature photoselection experiments have been given elsewhere<sup>4</sup> (see Appendix).

Eastman PhSH and the Aldrich PhSCH<sub>3</sub> (99%) were vacuum distilled. Phillips Petroleum pure grade 3MP and isopentane were passed through a column of MCB activated alumina (8-14 mesh) previously heated overnight in a vacuum oven to approximately 200°. This procedure removed most of the low-temperature phosphorescing impurities. The EPA mixed solvent was made from the purified isopentane, MCB spectroquality ethyl ether, and U.S.I. reagent quality absolute ethyl alcohol in a ratio of 5:5:2 parts by volume respectively.

Low-temperature absorption spectra were obtained by aligning a deuterium lamp having a Supracil window (George W. Gates and Co.) with the condenser lens system on the entrance slit (0.1 mm width) of the spectrometer (containing a 2400 groove/mm grating blazed for 1500 Å; dispersion 13.3 Å/mm) while the dewar containing a square quartz cell (1 cm × 1 cm) was placed between the exit slit (0.1 mm width) and the phototube housing. For each solute material the molar absorptivity is found by comparing the transmission of a glass made from the solute solution using the low temperature concentration (1.28 times the room temperature concentration for these solvents) with that of a glass made from the pure solvent. In regions where the solute molecule absorbs the strongest, solutions one-tenth

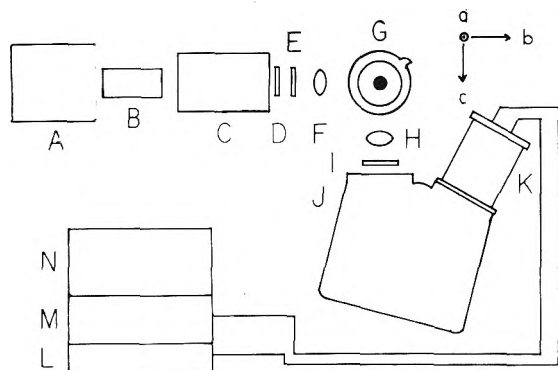


**Figure 1.** Apparatus for obtaining polarization ratios: (A) lamp housing containing quartz condenser lenses and a 500W/2 Osram Hg lamp. The lamp power supply (George W. Gates and Co.) plugs into a Sola constant voltage transformer; (B) 10-cm path of water with 2-in. diameter quartz windows cooled by water flow through a copper coil; (C) Bausch and Lomb high-intensity monochromator with a 2700 grooves/mm uv grating and variable slits, dispersion 32 Å/mm; (D) CS 7-54 filter; (E) polarizer, Polacoat formula PL 40 on G.E. 151 fused quartz; (F) quartz lens; (G) quartz dewar containing quartz sample tube; (H) quartz condenser lenses; (I) Polacoat 105 uv WRM polarizer; (J) McPherson Model 218 spectrometer with a 1200 groove/mm grating blazed for 5000 Å, dispersion 26.5 Å/mm; (K) housing with an EMI 9635 QB photomultiplier tube; (L) Sorensen Model 5002-10 high voltage supply; (M) Keithley 610 CR electrometer; (N) Hcneywell Electronik 194 Lab recorder. All quartz is of Supracil quality or equivalent.

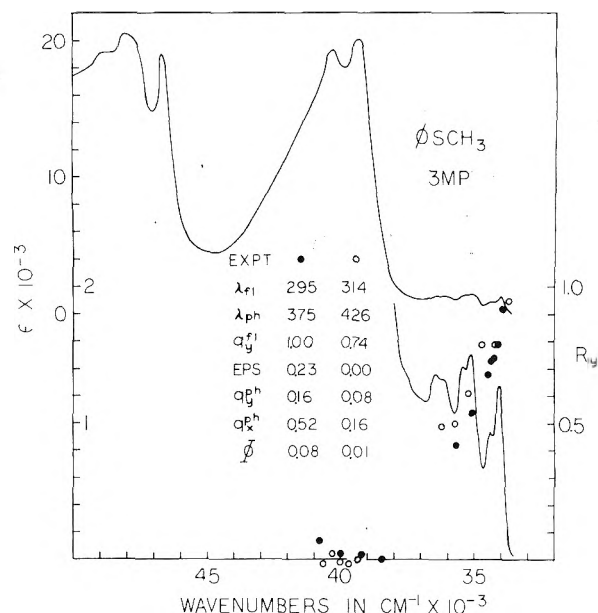


**Figure 2.** Low-temperature absorption spectra of PhSCH<sub>3</sub> in 3MP. Molar absorptivity,  $\epsilon$ . The values of  $R_y$  are found from the value of  $N^I$  obtained in the 0-0 region, ●, and at the wavelength of maximum emission intensity, ○, for each excitation wavelength in the POEE experiment. Each set of polarization ratios in the fluorescence or phosphorescence band is obtained on a single sample region. Each value of  $N$  used in the calculation is the average of two separate experiments done on different sample regions.

the original concentration are used in order to obtain the contours found in the absorption bands.

## Results and Discussion

Two types of polarization experiments are performed in this study. A description of each one is given here (see the Appendix for a discussion of the method used to interpret the photoselection studies). In each case the polarization ratio is obtained at one or more emission wavelengths. A polarization ratio,  $N$ , is defined as the ratio of the vertical component of emission to the horizontal component of emission observed at right angles to the direction of the excitation. The first type of experiment is a polarization of emission excitation (POEE) experiment. In a POEE experiment the observed wavelength region in an emission band is kept constant (then the emission parameters  $q_x$ ,  $q_y$ , and  $q_z$  are constant) and the value of  $N$  is obtained for excitation in different wavelength regions throughout one or more absorption bands. The values of  $N$  for the fluorescence and phosphorescence bands ( $N^f$  and  $N^{ph}$ , respectively) found in this manner are used to obtain best fit values of the emission parameters ( $q_y^f$ ,  $q_y^{ph}$ , and  $q_x^{ph}$ ). These best fit values are then used to obtain values for the absorption parameter (in this case  $R_y$  which is the intrinsic probability for absorption along the  $y$  molecular axis) throughout the absorption bands.

The absorption spectra of PhSH and PhSCH<sub>3</sub> along with the values of  $R_y$  calculated from eq 1a (Appendix) using the best fit values (also shown) found for the molecular parameters are shown in Figures 2-4. In each case two sets of  $R_y$  values were obtained which match each other closely. In one set of POEE experiments the values of  $N^f$  and  $N^{ph}$  were obtained in the 0-0 region of the fluorescence and phosphorescence spectra, respectively, while in a second set of experiments the values of  $N^f$  and  $N^{ph}$  were obtained at the wavelength of maximum intensity ( $\lambda_{max}$ ) in each band.

These results for  $R_y$  are based on the valid assumption that the first weak absorption band in these molecules is the  ${}^1I_b$  ( $y$  polarized) state. In addition the analysis of the photoselection results is limited to an orthogonal set of cartesian axes which belong to separate irreducible representations of the molecular point group.

The value of  $R_y$  is found to be 0.88 or larger for absorption near the 0-0 region in the lowest excited  ${}^1L_b$  state with the value decreasing to near zero for excitation approaching the 0-0 region in the first intense absorption band. This band has the same symmetry as the  ${}^1L_a$  state of benzene where the absorption is polarized along the long-axis in-plane, i.e.,  $R_z = 1.0$ . For PhSCH<sub>3</sub> in 3MP where the resolution of the absorption spectra is the sharpest  $R_y$  varies from a value of 0.95 in the 0-0 region of the  ${}^1L_b$  band to a value of 0.0 in the 0-0 region of the  ${}^1L_a$  band.

Both calculations and experimental results indicate the presence of CT character in the lower energy singlet states of these molecules. Kimura and Nagakura have found<sup>6</sup> that in PhSH the  ${}^1L_a$  band is about 54% intramolecular CT of a sulfur  $p_\pi$  electron to a ring  $\pi^*$  orbital whereas the lowest absorption band ( ${}^1L_b$ ) was found to be about 20% CT in nature. The presence of CT character for these same bands in the phenyl sulfides has been shown experimentally by observing the absorption spectra of phenyl  $n$ -propyl sulfide in 3MP both with and without HCl(g) present in the solution at 77°K.<sup>7</sup> Without HCl the absorption spectrum is almost identical with that of PhSCH<sub>3</sub> in 3MP. The emission spectrum is very similar also. With HCl present a large blue shift occurred (at low temperature) and the absorption and emission spectra were found to be similar to those of anisole and anisole + HCl at 77°K. In this case the phosphorescence lifetimes are similar also. Hydrogen bonding between the HCl and the nonbonding sulfur electron pairs at 77°K is thought to occur here. This has the effect of in-

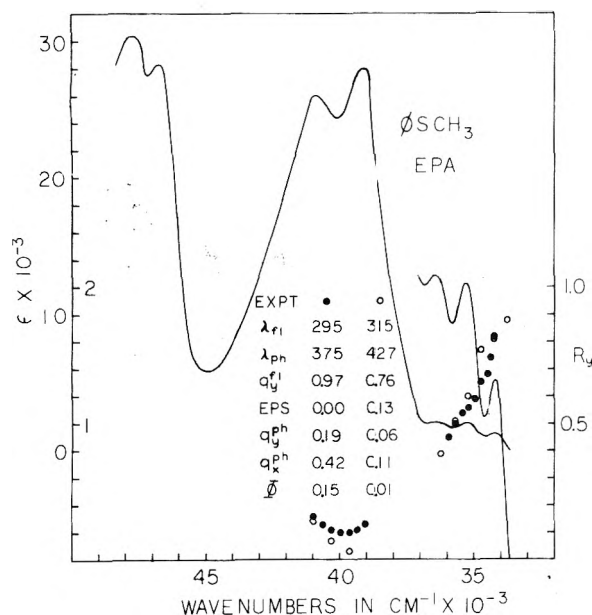


**Figure 3.** Low-temperature absorption spectra of PhSCH<sub>3</sub> in EPA. Molar absorptivity,  $\epsilon$ . The values of  $R_y$  are found from the value of  $N^f$  obtained in the 0-0 region, ●, and at the wavelength of maximum emission intensity, ○, for each excitation wavelength in the POEE experiment. Each set of polarization ratios in the fluorescence or phosphorescence band is obtained on a single sample region. Each value of  $N$  used in the calculation is the average of two separate experiments done on different sample regions.

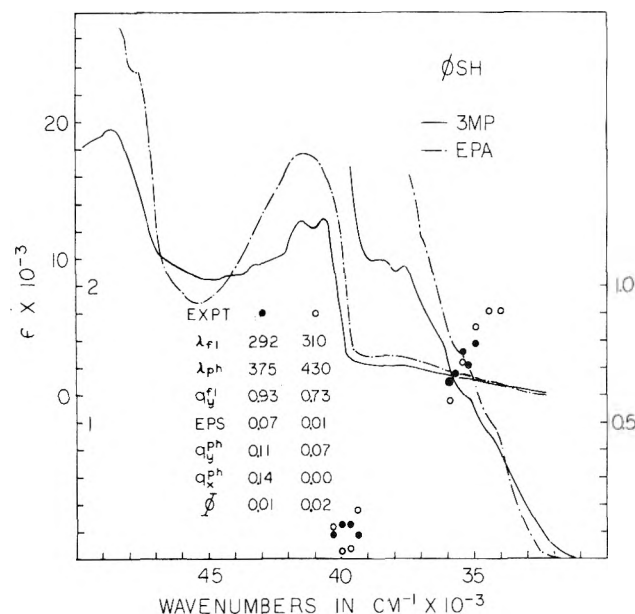


**Figure 4.** Low-temperature absorption spectra of PhSH in 3MP and EPA. Molar absorptivity,  $\epsilon$ . The values of  $R_y$  are found from the value of  $N^f$  obtained in the 0-0 region, ●, and at the wavelength of maximum emission intensity, ○, for each excitation wavelength in the POEE experiment performed in EPA. Only one polarization ratio is obtained on each sample region. Each value of  $N$  used in the calculation is the average of two separate experiments.

creasing the energy of the CT configurations which results in the appearance of only the lower energy  $\pi, \pi^*$  spectra similar to that found in anisole. These same results should be observed with PhSCH<sub>3</sub> also. The results obtained with phenyl *n*-propyl sulfide suggested the presence of a low-lying  $n, \pi^*$  triplet in the phenyl sulfides.

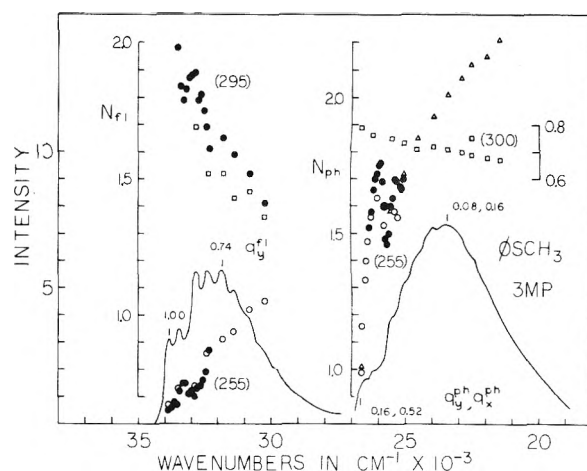


**Figure 5.** Fluorescence and phosphorescence spectra of PhSCH<sub>3</sub> in 3MP showing the POEE results. An entire set of polarization ratios for an emission band (designated by ●, ○, □, or Δ) is obtained on a single sample region. Each value of  $N$  shown is the average of two separate experiments done on different sample regions. Each excitation wavelength is given in parentheses ( $\lambda$  m $\mu$ ). The number pairs (each pair refers to  $q_y^{ph}$  and  $q_x^{ph}$ , respectively) and the values of  $q_y^f$  are the best fit values of the molecular parameters obtained from the two POEE experiments performed in the 0-0 and the  $\lambda_{max}$  regions of the emission bands (see Figure 2 for the values of the observed wavelengths in fluorescence and phosphorescence).

In contrast to the above results only a small blue shift was observed (at room temperature and 77°K) on the absorption spectra when anhydrous HCl(g) was added to a solution of PhSH. A low-lying  $^3n, \pi^*$  state should be present in PhSH also. In fact the polarization results obtained here indicate that the phosphorescence originates from an  $n, \pi^*$  triplet (see discussion on the phosphorescence polarization results). However in this case the presence of HCl(g) appears to have little effect on the energy of the CT configurations and the  $n, \pi^*$  states.

The second type of polarization experiment is the polarization of emission (POE) experiment. In a POE experiment the molecule is excited at a fixed wavelength (then the apparent absorption parameters  $r_x$ ,  $r_y$ , and  $r_z$  are constant) and the value of  $N$  is obtained at intervals throughout one or more emission bands.

The emission spectra and the results of the POE experiments are shown in Figures 5-7. No corrections have been made for phototube and spectrometer sensitivity or the effects of self-absorption on the shape of the emission bands. The parent emission of PhSH in 3MP and of diphenyl disulfide in both 3MP and EPA glasses was very weak and it was not possible to obtain accurate emission spectra or polarization ratios in these cases. Since photoproduct formation was found to be absent in PhSCH<sub>3</sub> it was possible to carry out an entire POE or POEE experiment on one sample region without serious depletion of the randomly oriented solute molecules. In PhSH on the other hand where the photoproduct buildup is rapid only one polarization ratio is obtained in a given sample region (with a total excitation time of approximately 1 min) using the following order for the measurement of the polarization components: vertical, horizontal for  $N_{cbds}$ , then horizontal, vertical for  $N_c$  (the correction ratio,  $N_c$ , for instrumental depolarization is discussed in the Appendix). When more than one ratio was measured in a given sample region and/or  $N_c$  was obtained before  $N_{obsd}$  the result was a lower than expected

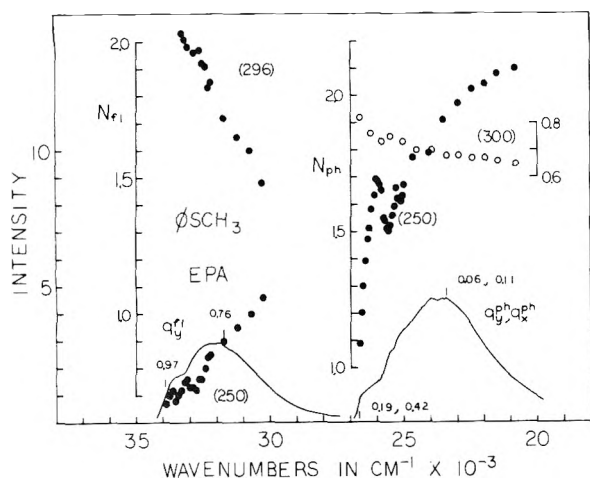


**Figure 6.** Fluorescence and phosphorescence spectra of PhSCH<sub>3</sub> in EPA showing the POE results. An entire set of polarization ratios for an emission band (designated by ● or ○) is obtained on a single sample region. Each value of  $N$  shown is the average of two separate experiments done on different sample regions. Each excitation wavelength is given in parentheses ( $\lambda$  m $\mu$ ). The number pairs (each pair refers to  $q_y^{\text{ph}}$  and  $q_x^{\text{ph}}$ , respectively) and the values of  $q_y^{\text{fl}}$  are the best fit values of the molecular parameters obtained from the two POEE experiments performed in the 0-0 and the  $\lambda_{\text{max}}$  regions of the emission bands (see Figure 3 for the values of the observed wavelengths in fluorescence and phosphorescence).

value for  $N$ . The largest error (approximately 0.3 polarization unit) found in this manner was observed in the phosphorescence spectra of PhSH in EPA for excitation at 252 m $\mu$  where the emission came from the front face of the glass because of the very large molar absorptivity. This results in a rapid depletion of the randomly oriented sample in the observed area of the glass which results in a depolarization of the emission. For excitation at 294 m $\mu$  this problem was not as serious (see Figure 7) for the same excitation time period. The small value for the molar absorptivity at 294 m $\mu$  results in emission being viewed from a larger sample region thereby diluting the depolarization effect (the four values of  $N$  obtained in each sample region in one experiment did not result in much depolarization). Each value of  $N$  plotted in the POE experiments represents an average of two experiments.

In these molecules the fluorescence is weaker than the phosphorescence by a factor of approximately 10 for PhSH and PhSCH<sub>3</sub>. The most intense emission spectrum was found for PhSCH<sub>3</sub> in EPA followed by PhSCH<sub>3</sub> in 3MP with PhSH in EPA having the weakest emission spectrum on which polarization measurements were made. As a consequence the largest scattering in the value of  $N$  is found in the POE experiments on the PhSH fluorescence spectra.

Upon examination of the phosphorescence POE experiments it is seen that for excitation in the 250-m $\mu$  region (long-axis in-plane absorption) the change in the value of  $N^{\text{ph}}$  throughout the band is increased by a factor of 10 (except for PhSCH<sub>3</sub> in EPA) over that change found for excitation in the <sup>1</sup>L<sub>b</sub> absorption band. This discloses a large peak in the  $N^{\text{ph}}$  curve approximately 700 cm<sup>-1</sup> from the 0-0 region in PhSCH<sub>3</sub> and about 600 cm<sup>-1</sup> from the 0-0 region in PhSH. For PhSCH<sub>3</sub> in 3MP the peak height is 0.3  $N^{\text{ph}}$  unit. Since the values of the  $q$ 's at an emission wavelength are independent of the excitation wavelength a corresponding dip of only 0.03  $N^{\text{ph}}$  unit should be observed in the  $N^{\text{ph}}$  curve when obtained by excitation in the <sup>1</sup>L<sub>b</sub> ab-

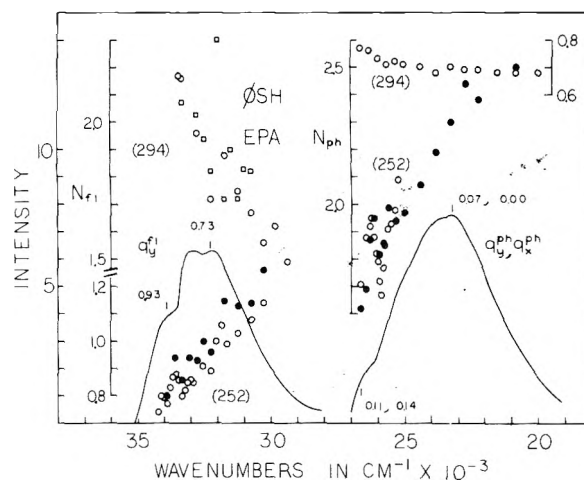


**Figure 7.** Fluorescence and phosphorescence spectra of PhSH in EPA showing the POE results. One or more sets of polarization ratios for an emission band (designated by ●, ○, or □) are obtained from a single glass. Only one polarization ratio is obtained on each sample region (except in one case, ○, where four values of  $N$  are obtained on each sample region in the fluorescence and phosphorescence bands for excitation at 294 m $\mu$ ). Each value of  $N$  shown is the average of two separate experiments. Each excitation wavelength is given in parentheses ( $\lambda$  m $\mu$ ). The number pairs (each pair refers to  $q_y^{\text{ph}}$  and  $q_x^{\text{ph}}$ , respectively) and the values of  $q_y^{\text{fl}}$  are the best fit values of the molecular parameters obtained from the two POEE experiments performed in the 0-0 and the  $\lambda_{\text{max}}$  regions of the emission bands (see Figure 4 for the values of the observed wavelengths in fluorescence and phosphorescence).

sorption band. This value is within the estimated 5% error for these measurements and no attempt was made to observe this small dip.

The presence of this peak in the  $N^{\text{ph}}$  curve is most likely due to a strong vibronic coupling bringing in a large amount of long-axis in-plane component to the phosphorescing state in PhSCH<sub>3</sub> and PhSH. This coupling is then followed by numerous other vibronic couplings which increase the  $z$  character until the value of  $q_z^{\text{ph}}$  approaches 1.0 in the tail end of the band. The polarization results obtained here however differ somewhat with those results for many aromatic carbonyl compounds (and in other molecules with <sup>3</sup> $\pi, \pi^*$  states<sup>5</sup>) where it is found in many cases that the polarization peaks are repeated at definite intervals and the average degree of polarization remains constant throughout the band outside of the 0-0 region for excitation in the <sup>1</sup>L<sub>a</sub> state.<sup>9,10</sup> There is no evidence for strong additional polarization peaks in PhSCH<sub>3</sub> and PhSH (however an additional small peak of 0.05  $N^{\text{ph}}$  unit is observed for PhSCH<sub>3</sub> in 3MP and maybe in EPA also) and the degree of polarization increases rapidly throughout the band. The large increase observed in the value of  $N^{\text{ph}}$  may result from the influence of the sulfur atom in these molecules. The <sup>3</sup> $\pi, \pi^*$  states contain CT configurations and low-lying <sup>3</sup>n,  $\pi^*$  states are available for vibronic and spin-orbit coupling in the various pathways for obtaining phosphorescence.

Vibronic transitions cause a large change in the value of  $N^{\text{fl}}$  (observed at wavelength intervals throughout the band) for excitation near the 0-0 region in either the <sup>1</sup>L<sub>b</sub> or <sup>1</sup>L<sub>a</sub> absorption band. Some polarization detail is found in each case for both molecules. This is most clearly observed for PhSCH<sub>3</sub> in 3MP. For excitation at 255 m $\mu$  a small peak is observed in the  $N^{\text{fl}}$  curve with a maximum at approximately 33,300 cm<sup>-1</sup> (this peak is clearly seen in PhSH also).

This is followed by a minimum at  $32,900\text{ cm}^{-1}$  and a shoulder in the steeply rising portion of the curve at  $32,350\text{ cm}^{-1}$ . This detail is confirmed by the amplified mirror image obtained for excitation at  $295\text{ m}\mu$ . In this case the value of  $N^{\text{fl}}$  decreases (with increasing wavelength) because of the  $z_x$  polarized vibronic transition. If one assumes that the molecule has  $C_{2v}$  point symmetry then a  $b_z$  vibration is required in order to couple the  ${}^1L_a$  and  ${}^1L_b$  states and add  $z$  character to the fluorescence.

The vibrational structure found in the fluorescence spectra and the polarization results indicate that two main vibrational progressions are observed (in a rigid glass) that give rise to different polarization components in the emission. The first one consists of a totally symmetric mode ( $a_1$  symmetry) of approximately  $1000\text{ cm}^{-1}$  while the second one is built on a  $b_2$  mode (approximately  $400\text{ cm}^{-1}$ ) followed by one or more quanta of a symmetric vibration. These progressions result in  $y$  and  $z$  polarized emission, respectively. The position of the  $b_2$  mode peak in the fluorescence spectra ( $0-0$  position  $-400\text{ cm}^{-1}$ ) does not coincide with the maximum or minimum obtained in the  $N^{\text{fl}}$  curve (for  ${}^1L_a$  and  ${}^1L_b$  excitation, respectively). However this could result from the use of larger slit widths in making the polarization measurements.

The polarization results can be used to indicate either a  $\pi, \pi^*$  or  $n, \pi^*$  type of emitting triplet in these molecules. The POE results for PhSCH<sub>3</sub> indicate that the emission in the  $0-0$  region is polarized along all three molecular axes (but polarized approximately 50% out-of-plane). In a true  $C_{2v}$  symmetry only an  $n, \pi^*$  triplet can spin-orbit couple directly to singlet states that would provide all three polarization components. However a  $\pi, \pi^*$  triplet state is more likely in this case.<sup>7,9</sup> In a lower than  $C_{2v}$  symmetry a  $y$  and  $z$  polarized component would be possible in the  $0-0$  region of a  ${}^3L_b$  and  ${}^3L_a$  state, respectively, so that each state would have all three allowed polarization components in the  $0-0$  region. In this case then no decision between a lowest  ${}^3L_b$  or  ${}^3L_a$  state can be made based solely on the polarization results.

In PhSH the polarization results in the  $0-0$  region are quite different. In this case the POEE results show that the emission is 75% long-axis in-plane polarized. These results alone indicate that the emission could come from a  ${}^3n, \pi^*$  state. In this case the  $0-0$  region is expected to be mostly long-axis in-plane polarized whereas for an emitting  ${}^3\pi, \pi^*$  state the in-plane polarized component is expected to appear through vibronic spin-orbit coupling involving  $n, \pi^*$  triplets as intermediate states.<sup>9</sup> Becker et al.<sup>7</sup> have shown experimentally the existence of a low-lying  ${}^3n, \pi^*$  state (proposed to be between the lowest singlet and triplet states) in the phenyl sulfides (see previous discussion). The one-center terms in the direct spin-orbit coupling of this state to a  ${}^1\pi, \pi^*$  state (containing CT) along with a heavy atom effect was found to be responsible for the large ratio of phosphorescence to fluorescence in the aromatic sulfides (compared to the ethers). These same terms are important in the second-order coupling mechanisms that also determine the phosphorescence lifetime. Since the phosphorescence lifetimes for both PhSCH<sub>3</sub> and PhSH are about one-third the value found<sup>7</sup> for phenyl  $n$ -propyl sulfide (0.023 sec) the above terms involving the  ${}^3n, \pi^*$  state also appear to be at least as important in these molecules.

The presence of photoreactivity in PhSH is worth mentioning here, although it may only be a coincidence that PhSH has a  ${}^3n, \pi^*$  state (as suggested by the polarization

results) and is photoreactive. The phenyl sulfonyl radical is produced in both EPA and 3MP by a one photon absorption mechanism when PhSH is excited in the  $0-0$  region of the  ${}^1L_b$  state at  $77^\circ\text{K}$ . In population of the  $n, \pi^*$  triplet the electron from the sulfur nonbonding orbital goes into a ring antibonding  $\pi$  orbital whereas scission of the S-H bond would be helped if the S-H antibonding orbital ( $\sigma^*$ ) was occupied instead. If the  $\sigma^* \leftarrow n$  configuration is low enough in energy (this may be the case since the lowest triplet appears to be an  $n, \pi^*$  state) it could become populated as either a singlet or triplet state. In  $C_{2v}$  the  $\sigma^* \leftarrow n$  configuration would have  $b_2$  symmetry and would mix with the  ${}^1, {}^3L_b$  states. In this way scission of the S-H bond could occur as a competing side reaction leading to the formation of a stabilized phenyl sulfonyl radical and molecular hydrogen. In durene a one-photon process is found to cause  $\beta$ -bond scission (methyl hydrogen) when a dilute solution of this molecule (in 3MP at  $77^\circ\text{K}$ ) absorbs light at energies corresponding to excited vibrational levels of the first excited singlet state (for excitation in the  $0-0$  region of this state the process was found to be biphotonic in nature).<sup>11</sup> In this case singlet states are involved in the scission process. Scission of the S-H bond in PhSH may also occur through population of the  ${}^1n, \sigma^*$  state.

If the  $\sigma^* \leftarrow n$  configuration plays an active role in the photoreactivity of PhSH then one would expect that these states could also be active in PhSCH<sub>3</sub>. However, no photoreactivity was observed in PhSCH<sub>3</sub>. In this case the  $\sigma^* \leftarrow n$  configuration would most likely involve the S-CH<sub>3</sub> bond. If this configuration is found at a higher energy (maybe due to a higher energy  $\sigma^*$  orbital) then one would not expect to find much photoreactivity.

*Acknowledgment.* The author is indebted to the Chemistry Department for most of the equipment used in these experiments. He is also grateful for a yearly NSF grant made available to him by the Research Committee. The machine shop work of Mr. Peter Amirato and use of the computer facilities are appreciated. The author is grateful to both referees for a careful reading of the original manuscript. This led to many critical comments which were valuable in revision.

## Appendix

In the photoselection method a sample of solute molecules, randomly oriented in a rigid glass, is excited by vertically polarized light with excitation direction along the  $b$  axis (see Figure 1 for the laboratory fixed axes  $a$ ,  $b$ , and  $c$ ). The vertical component,  $I_c$ , and the horizontal component,  $I_b$ , in an emission wavelength interval is observed at right angles (along the  $c$  axis) to the direction of excitation giving an observed polarization ratio,  $N_{\text{obsd}}$ , where  $N_{\text{obsd}}$  is  $(I_a)_{\text{obsd}}/(I_b)_{\text{obsd}}$ . The values of  $I_a$  and  $I_b$  depend upon the polarization of the exciting light and the apparent probabilities for absorption ( $r_x, r_y, r_z$  where  $r_x + r_y + r_z = 1$ ) and emission ( $q_x, q_y, q_z$  where  $q_x + q_y + q_z = 1$ ) along molecular fixed axes  $x$ ,  $y$ , and  $z$ . The values for the  $r$ 's and the  $q$ 's depend upon the excitation and emission wavelengths, respectively.

The value of  $N_{\text{obsd}}$  is not accurate in most cases and a correction ratio,  $N_c$ , is obtained by repeating the above experiment using horizontally polarized light. This time the ratio should be unity regardless of along which axes in the molecule the absorption and emission processes occur.<sup>2</sup> The value of  $N_c$  (when not unity) reflects the overall favor-

ing of the apparatus due to the depolarization of radiation by the various instrumental components. The value of  $N_c$  has been found to vary with the observed wavelength.<sup>4</sup> The use of  $N_c$  does not always give an ideal value for the polarization ratio,  $N$  (where  $N = N_{\text{obsd}}/N_c$ ), in a given experiment because of small unaccountable depolarizations which tend to randomize the intrinsic values of the absorption and emission probabilities (the  $R$ 's and  $Q$ 's, respectively). To account for this a single randomization factor,  $\epsilon$  (not to be confused with the molar absorptivity), has been defined<sup>2</sup> which relates the apparent and intrinsic values of the molecular absorption probabilities in a given experiment ( $r_i = R_i(1 - \epsilon) + \epsilon/3$  where  $\sum r_i = \sum R_i$  for  $i = x, y, z$ ). The calibration of each experiment in this manner has proved successful when comparing different experiments.<sup>2-5</sup>

Two types of polarization experiments are performed. The first is a polarization of emission (POE) experiment and the second is a polarization of emission excitation (POEE) experiment. In a POE experiment the molecule is excited at a fixed wavelength (with  $r_x, r_y, r_z$  constant) and the polarization ratio,  $N$ , is obtained at intervals throughout the emission band(s). In a POEE experiment the observed wavelength region in an emission band is constant (then  $q_x, q_y, q_z$  are constant) and  $N$  is obtained for excitation in different wavelength regions throughout one or more absorption bands.

In order to obtain values for the intrinsic molecular parameters (the values for the  $q$ 's are assumed to be intrinsic) it is necessary to carry out a POEE experiment where a value for  $N^{\text{fl}}$  and  $N^{\text{ph}}$  is obtained at each excitation wavelength (having a given value of  $R_y$ ). In addition it is necessary to make the assumption that there is no out-of-plane component due to vibronic coupling in absorption ( $R_x = 0$ ) for the  ${}^1L_b$  and  ${}^1L_a$  states nor in the fluorescence emission ( $q_x^{\text{fl}} = 0$ ). This is true for benzene and it was shown that  $R_x = q_x^{\text{fl}} = 0$  in the case of four aminobenzene derivatives.<sup>5</sup> Then  $R_z = 1 - R_y$  always. The values of  $R_y$  can be determined from either one of the following equations:<sup>4</sup>

$$R_y = \frac{-N^{\text{fl}}(1 + q_y^{\text{fl}} + \frac{5}{3}\epsilon') + 3 - 2q_y^{\text{fl}} + \frac{5}{3}\epsilon'}{(N^{\text{fl}} + 2)(1 - 2q_y^{\text{fl}})} \quad (1a)$$

for  $q_z^{\text{fl}} = 1 - q_y^{\text{fl}}$  and

$$R_y = \frac{-N^{\text{ph}}(1 + (q_y^{\text{ph}} + q_x^{\text{ph}}) + \frac{5}{3}\epsilon') + 3 - 2(q_y^{\text{ph}} + q_x^{\text{ph}}) + \frac{5}{3}\epsilon'}{(N^{\text{ph}} + 2)(1 - 2q_y^{\text{ph}} - q_x^{\text{ph}})} \quad (1b)$$

for  $q_z^{\text{ph}} = 1 - q_y^{\text{ph}} - q_x^{\text{ph}}$  where  $\epsilon' = \epsilon/1 - \epsilon$ . Upon equating eq 1a and 1b for  $R_y$  it is found that

$$N^{\text{fl}} = \frac{AN^{\text{ph}} + B}{CN^{\text{ph}} + D}$$

where  $A, B, C$ , and  $D$  are nonlinear functions of the three molecular parameters  $q_y^{\text{fl}}, q_y^{\text{ph}}, q_x^{\text{ph}}$ , and  $\epsilon$ . For  $L$  different excitation wavelengths there are  $2L$  equations from which to determine the  $L$  values of  $R_y$ , the three molecular parameters and  $\epsilon$  giving  $L + 4$  unknowns. The unknowns are over-determined for  $L > 4$ . A steepest descent method<sup>12</sup> is used to obtain acceptable best fit values for the three molecular parameters and  $\epsilon$ . This occurs when the value of the best fit parameter,  $\Phi$ , where  $\Phi = \sum (N_{\text{expt}}^{\text{fl}} - N_{\text{calcd}}^{\text{fl}})^2$  becomes a minimum. (Here  $N_{\text{expt}}^{\text{fl}} - N_{\text{calcd}}^{\text{fl}}$  is the difference between the experimental value and the calculated value of  $N^{\text{fl}}$  at a given excitation wavelength.) Then the  $L$  values of  $R_y$  are obtained from eq 1a. These calculations were done on an IBM 1130 computer.

## References and Notes

- (1) Address correspondence to the Department of Applied Science, Brookhaven National Laboratory, Upton, N.Y. 11973.
- (2) A. C. Albrecht, *J. Mol. Spectrosc.*, **6**, 84 (1961).
- (3) P. G. Russell and A. C. Albrecht, *J. Chem. Phys.*, **41**, 2536 (1964).
- (4) P. G. Russell, Ph.D. Thesis, Cornell University, Ithaca, N.Y., 1963.
- (5) A. H. Kalantar and A. C. Albrecht, *Ber. Bunsenges. Phys. Chem.*, **68**, 361, 377 (1964).
- (6) H. H. Perkampus and H. R. Vollbrecht, *Spectrochim. Acta*, **27**, 2173 (1971).
- (7) R. S. Becker, A. D. Jordan, and J. Kolc, *J. Chem. Phys.*, **59**, 4024 (1973).
- (8) K. Kimura and S. Nagakura, *Mol. Phys.*, **9**, 117 (1965).
- (9) E. C. Lim, Y. Kanda, and J. Stanislaus, "Molecular Luminescence", E. C. Lim, Ed., W. A. Benjamin, New York, N.Y., 1969, p 111.
- (10) M. E. Long, Y. H. Li, and E. C. Lim, *Mol. Photochem.*, **3**, 221 (1971).
- (11) F. P. Schwarz and A. C. Albrecht, *Chem. Phys. Lett.*, **9**, 163 (1971).
- (12) D. W. Marquardt, *Chem. Eng. Prog.*, **55**, 65 (1959).



## Some Observations on the Photoproduct Formation in Benzenethiol, Diphenyl Disulfide, and Diphenyl Sulfide

Phillip G. Russell<sup>1</sup>

Department of Chemistry, C. W. Post College, P. O. Greenvale, New York 11548 (Received August 9, 1974; Revised Manuscript Received March 12, 1975)

Benzenethiol (PhSH) and diphenyl disulfide (PhSSPh) undergo photolysis readily in EPA and 3-methylpentane (3MP) glasses to form the phenyl sulfyl radical and at least one other photoproduct species by a one-photon absorption mechanism. The red and blue emission bands observed in the photolyzed region are identified with this radical. The results of three-step photoselection experiments on the red and blue emission bands suggest <sup>2</sup>B<sub>2</sub> assignments (C<sub>2v</sub>) for the uv absorption, the blue emission, and the red emission bands. The green emission band observed in the photolyzed region of diphenyl sulfide (PhSPh) originates from a photoproduct species formed by a two-photon absorption process. The photoproduct is thought to be the phenyl sulfyl cation radical. Polarization results on the green emission band (assuming a three-step analysis) suggest that the uv absorption band and the green emission band have <sup>1</sup>A<sub>1</sub> symmetry.

### Introduction

When an EPA solution of PhSH at 77°K is excited in the 0–0 region of the <sup>1</sup>L<sub>b</sub> absorption band the visible emission gradually changes from a blue (PhSH phosphorescence) to a pink color as a result of photochemical changes occurring in the glass. A bright red emission is observed when this region of the glass is excited with 365-mμ radiation. In the original glass no emission is observed for excitation at this wavelength. A relatively weaker blue emission band is found to be present also. These same results are found when a PhSSPh solution is used in place of PhSH. It is found that only one photon is required to form the photoproduct(s) responsible for these emission bands.

A simple explanation of these observations is that the phenyl sulfyl (PhS) radical is formed in each case when the parent molecule undergoes photolysis. The absorption by this radical over a broad region (approximately 300–400 mμ) results in the characteristic red and blue emission bands. These emission bands do not appear to be from a cation species produced by photoionization since no recombination emission was observed with PhSH when the photoexcited sample region was exposed to 650-mμ light.<sup>2</sup>

Radicals have been detected by low-temperature ESR measurements when aromatic disulfides and thiophenols undergo photolysis. A red substance was found to condense on a cold finger (77°K) when PhSSPh vapor was photolyzed.<sup>3</sup> This substance was thought to be the PhS radical where the ESR measurements indicated that the electron was largely localized on the sulfur atom. The radical is stable at 77°K but was found to recombine forming PhSSPh within a few minutes at 165°K. When photolysis occurred in an EPA solution of PhSH at 77°K a new absorption band appeared with a maximum in absorption at 3875 Å. This band was attributed to the PhS radical.<sup>4</sup> In this same paper no radical formation was found when PhSSPh was photolyzed in an EPA glass. This was attributed to the cage effect in this high viscosity glass which prevented stabilization of the radicals by the matrix. However, in a glass of less viscosity (8 parts neohexane and 3 parts *n*-pentane) radical formation was found to occur upon prolonged photolysis accompanied by the expected absorption band at 3875 Å.<sup>5</sup> During the initial period of photolysis in this glass

a broad absorption band appeared near 3200 Å. A yellow color which formed in the glass during this period was traced to this band and not to the formation of the radical band which was thought to be the case previously. In this lab a yellow color is found to appear whenever an EPA or 3MP glass of PhSH or PhSSPh undergoes photolysis also. However no color is observed when PhSPh is photolyzed in either of the glasses. It appears then that at least two photoproduct species are formed whenever PhSH and PhSSPh undergo photolysis. These are the PhS radical (from which the red and blue emission bands originate) and a second product responsible for the yellow color produced in the glass.

When a sample region of PhSPh is excited in its near-uv band in an EPA glass for 1 hr or more one or more photoproducts are formed since on further excitation with 365-mμ light a green emission band is observed (a weaker blue emission band is found to be present also). No radical formation or other reaction products were observed in the previous work.<sup>4</sup> Again this is probably due to the low-power lamp used and to the limitation of excitation time to a maximum of 32 min. Much more excitation time is required to produce a comparable amount of photoproduct emission intensity in PhSPh than in PhSH or PhSSPh. It is found that two photons are required to form the photoproduct in PhSPh which gives rise to the green emission band. This photoproduct is tentatively identified as the phenyl sulfyl cation radical where the electron ejected from the PhS radical (this radical and a second photoproduct are formed and stabilized upon absorption of one photon by the PhSPh molecule) is trapped by the second photoproduct (maybe a phenyl radical).

### Experimental Section

The apparatus for obtaining the emission spectra and the polarization measurements has been described in a previous paper.<sup>6</sup> This apparatus is used here with minor modifications. In all experiments involving the photoproduct emission a visible grating was used in the excitation monochromator. This grating was used to produce the photoproducts also since it was found to give enough intensity in the uv region. An RCA C7164S photomultiplier tube was

used to observe the red emission. It was found necessary to subtract out background emission in all experiments. In the red band the only background emission found was that due to the dark current in the tube. A CS 3-67 filter was placed after the sample in order to remove second-order emission for excitation of the photoproduct with 365-m $\mu$  radiation. In the green and blue regions the background emission was obtained by lowering the dewar position to a fresh sample region and viewing the background emission of the lamp as observed by the spectrometer over the wavelength region of interest. This background emission is subtracted from the observed photoproduct emission at each wavelength. In this way mercury line spectra from the lamp normally reflected off surfaces in the dewar was removed from the photoproduct emission spectra. In the polarization experiments a similar correction was made on each observed polarization component.

Low-resolution excitation spectra of the photoproducts were obtained by comparing the intensity of each photoproduct emission band (observed at  $\lambda_{\max}$ ) to the intensity of the blue emission (observed at  $\lambda_{\max}$ ) from an esculin solution (1 g/l. of water) corrected for the molar absorbance at each excitation wavelength. A high-intensity xenon lamp was not available for these experiments. The Osram 500 W/2 Hg lamp was used here with 2-mm slits on the excitation monochromator. This gave a fairly smooth lamp intensity curve below 380 m $\mu$ .

The photon dependence of each photoproduct emission band was obtained by comparing the initial slope of the emission band intensity obtained for 100% lamp intensity to that value obtained when a neutral density filter (approximately 50% transmission) is placed in the excitation beam.

The photoproduct absorption spectra were obtained using a tungsten lamp (Bausch and Lomb) light source with the sample contained in a square cell with a 1-cm pathlength. The transmission of the cell before and after photolysis was compared over the 300-600-m $\mu$  region.

## Results and Discussion

The red and blue emission bands of the photoproduct(s) resulting from photolysis of PhSH and PhSSPh are shown in Figures 1 and 2. No corrections have been made for the spectrometer sensitivity or for the sensitivity of either phototube. The red emission band is found to have the same shape and origin in a given solvent regardless of whether PhSH or PhSSPh is the parent molecule undergoing photolysis with one exception. A weak peak seen at about 16,100 cm $^{-1}$  in PhSH (3MP) is absent when PhSSPh is the parent molecule. This may be the 0-0 region of this band. In addition the peak position is red shifted about 700 cm $^{-1}$  on going from a polar to a nonpolar solvent. The blue emission bands appear to have the same origin regardless of which molecule undergoes photolysis and appear to be the same in each solvent. Difficulty in subtracting out the mercury line spectra from the lamp accounts for the small differences found in the band shapes. In Figure 2 the photoproduct emission is pink in color (vs. red in EPA) because of the relative increase in the blue emission intensity.

The photoproduct emission spectra from PhSPh are shown in Figure 3. The prominent green emission band (EPA) has the same shape as the red emission band in Figure 1. By comparison the emission intensities for the red and blue bands in this case are found to be very weak making it difficult to determine the proper shape of the blue

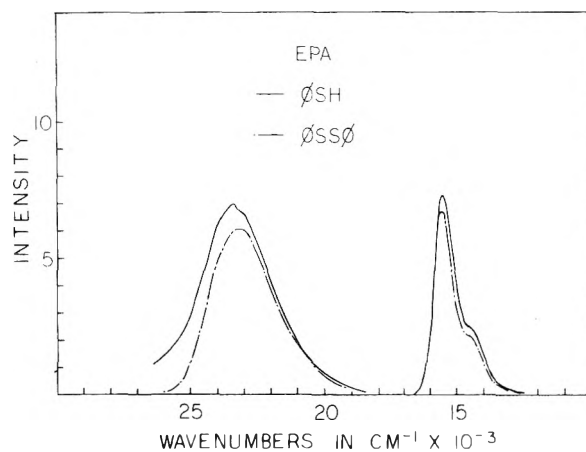


Figure 1. Red and blue photoproduct emission spectra of PhSH and PhSSPh in EPA.

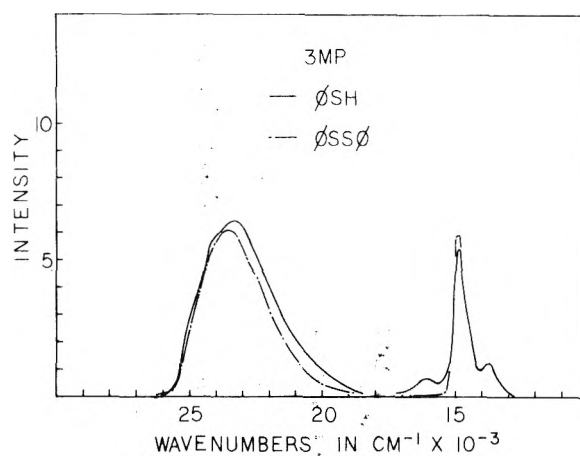


Figure 2. Red and blue photoproduct emission spectra of PhSH and PhSSPh in 3MP.

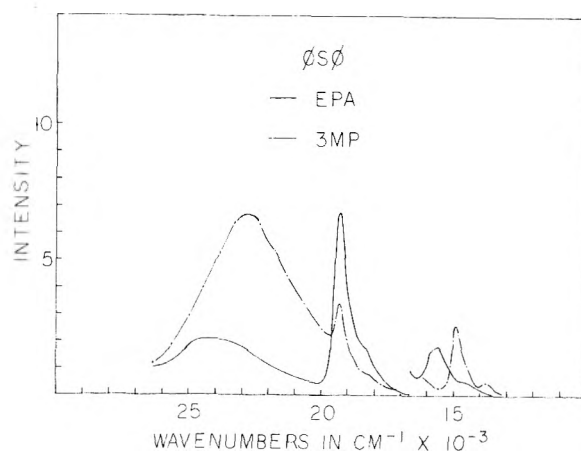


Figure 3. Red, green, and blue photoproduct emission spectra of PhSPh in EPA and 3MP. The red emission band is very weak in each case and is observed only by the phototube.

emission band. In 3MP the blue emission band is relatively more intense and the photoproduct emission takes on a blue-green color. The peak position of the green band remains the same in both solvents.

Photon dependence experiments on these bands (Table I) show that it takes one photon to produce the photoproduct

**TABLE I: Photon Dependence of the Photoproduct Emission Bands<sup>a</sup>**

	Photoproduct emission band			Pentamethylbenzyl radical <sup>f</sup>
	Red <sup>c</sup>	Green <sup>d</sup>	Blue <sup>e</sup>	
$n^b$	$1.8 \pm 0.2$	$3.3 \pm 0.4$	$2.0 \pm 0.2$	$3.3 \pm 0.2$

<sup>a</sup> With the exception of the green emission band the parent molecule and the photoproduct are excited simultaneously. The photon dependence of the photoproduct emission band,  $n$ , is the number of photons necessary to form the photoproduct plus one to excite it, so that  $n - 1$  is the photon dependence for photoproduct formation. <sup>b</sup> Five or six experimental values are used in each case. Both the mean value and the mean deviation are given. <sup>c</sup>  $\lambda_{ex}$  (PhSSPh and photoproduct) at 314 m $\mu$ .  $\lambda_{em}$  is 640 m $\mu$ . <sup>d</sup>  $\lambda_{ex}$  (PhSPh) at 296 m $\mu$ .  $\lambda_{ex}$  (photoproduct) at 369 m $\mu$ .  $\lambda_{em}$  is 519 m $\mu$ . The PhSPh phosphorescence intensity is very strong at 519 m $\mu$  compared to small increases in the emission intensity due to photoproduct formation which does not appear to absorb strongly at 296 m $\mu$ . The excitation was stopped periodically (the excitation time was recorded) in order to measure the emission intensity produced by the strong photoproduct absorption at 369 m $\mu$ . <sup>e</sup>  $\lambda_{ex}$  (PhSSPh and photoproduct) at 314 m $\mu$ .  $\lambda_{em}$  is 430 m $\mu$ . The phosphorescence intensity in PhSSPh is very weak at 430 m $\mu$  and the increase in the emission intensity due to photoproduct formation is readily observed. <sup>f</sup>  $\lambda_{ex}$  (hexamethylbenzene and the pentamethylbenzyl radical) at 277 m $\mu$ .  $\lambda_{em}$  is 540 m $\mu$ . The formation of this radical has been found to be a two photon process.<sup>8</sup> This experiment was repeated here in order to check the validity of the other results obtained in this lab. The value of 2.3 for  $n - 1$  agrees fairly well with the previous result.

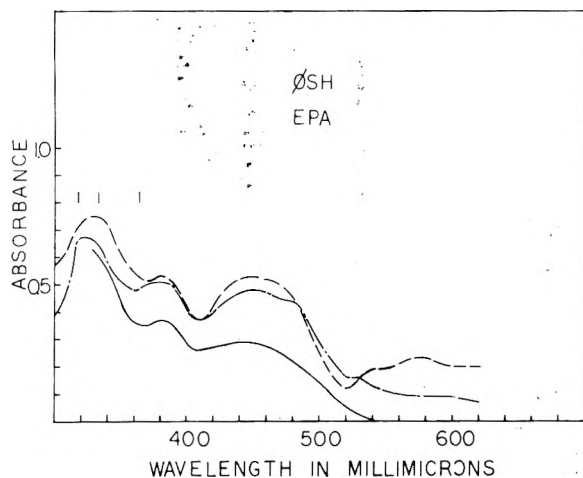


**Figure 4.** The photoproduct absorption spectra in PhSH. A commercial EPA solvent was used in these three separate experiments. The PhSH was not vacuum distilled. Essentially no absorption occurs beyond 540 m $\mu$ . Difficulty in obtaining the proper alignment of the dewar position for maximum transmission simultaneously with the correct position of the cell for maximum photoproduct absorption resulted in the addition of a spurious absorption throughout the entire band in two experiments. Each vertical line is the position of a peak in the excitation spectra obtained with PhSH (see Figure 6).

uct(s) responsible for the red and blue emission bands and that it takes two photons to make the photoproduct that gives rise to the green emission band.

The formation of the PhS radical in both PhSH and PhSSPh (two PhS radicals/molecule photolyzed) by a one-photon process resulting in the scission of the S-H bond and the S-S bond, respectively, is the most probable explanation for the presence of the red and blue emission bands. This radical has been detected when photolysis occurred in low-temperature glasses of these molecules.<sup>4</sup> A band that

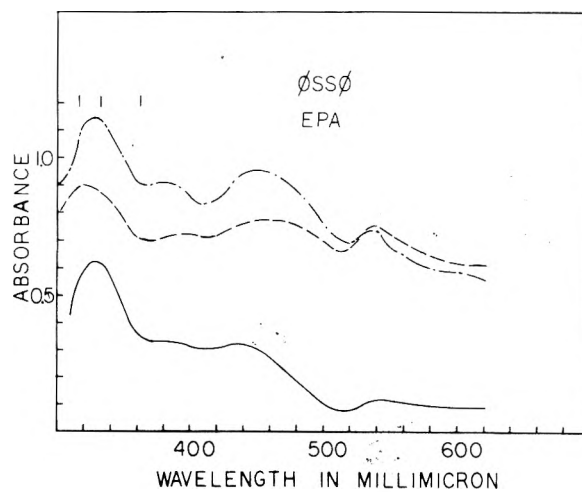


**Figure 5.** The photoproduct absorption spectra in PhSSPh. A commercial EPA solvent is used in these two separate experiments. The repeat run (—) made in one experiment (---) indicates the difficulty of obtaining the correct band contours. Both runs show a large spurious absorption due to the difficulty in obtaining the proper alignment of the dewar position for maximum transmission simultaneously with the correct position of the cell for maximum photoproduct absorption. Each vertical line is the position of a peak in the excitation spectra obtained with PhSSPh (see Figure 6).

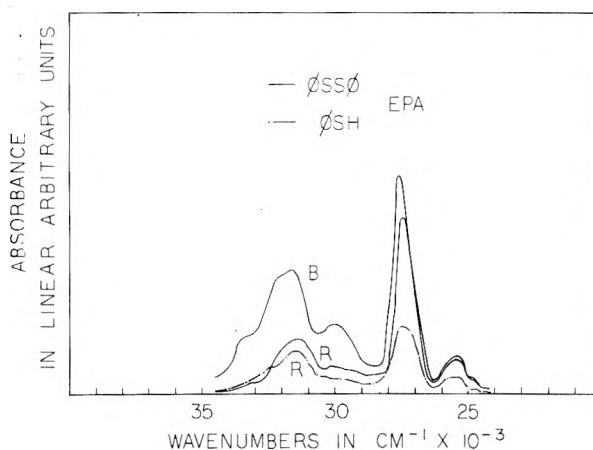


**Figure 6.** Excitation spectra for the red and blue emission bands in EPA: red band (R), blue band (B).

was found in the photoproduct absorption spectra of both PhSH in EPA and PhSSPh in a glass containing 8 parts neohexane and 3 parts *n*-pentane (but not in EPA) at 387.5 m $\mu$  was identified with the PhS radical while a broad band at 320 m $\mu$  was identified with the photoproduct(s) responsible for the yellow color found in the glass. Evidence that the red and blue emission bands originate with this radical can be found by comparing their excitation spectra with the photoproduct absorption spectra found in the glass after photolysis. The absorption spectra (of the photolyzed region in the glass) obtained in the 300–600-m $\mu$  region in both PhSH and PhSSPh are shown in Figures 4 and 5, respectively. In each case there appear to be three overlapping absorption bands with maxima at approximately 325, 380, and 450 m $\mu$ . The first two bands agree well with the previous results while the one at 450 m $\mu$  was not reported in the earlier work.<sup>4</sup> The band at 380 m $\mu$  (with greatest definition in PhSH) indicates that the PhS radical is produced during photolysis in an EPA glass containing either PhSH

**TABLE II: Polarization Results for Three-Step Photoselection Experiments on the Photoproduct Emission Bands<sup>a</sup>**

		Exciting near-uv band		Exciting second-uv band		
		create		create		
PhSH	E					
	x	↑ 2.12	→ 2.17	↑ 2.34	→ 2.36	
	c					
	i					
	t	→ 0.97	1.00	→ 1.02	1.00	
Red band	e					
	E					
	x	↑ 2.66	→ 2.80	↑ 2.80	→ 1.83	
	c					
	i					
Blue band	t	→ 1.09	1.00	→ 1.22	1.00	
	e					
	PhSPh <sup>b</sup>	E				
		x				
		c	↑ 4.10	→ 2.43		
i						
t		→ 2.28	1.00			
Green band	e					

<sup>a</sup> Reference 10. <sup>b</sup> The ratios 4.1:2.28:2.43 are close to the ratios 5:3:3 found in the ideal case for single axis absorption and emission (only in a three-step analysis). See text.

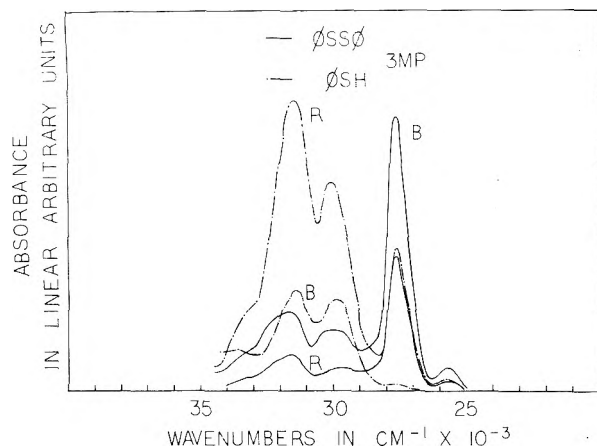


**Figure 7.** Excitation spectra for the red and blue emission bands in 3MP: red band (R), blue band (B).

or PhSPh. The excitation spectra (Figures 6 and 7) of the red and blue emission bands occur in the 300–400- $\mu$  region with peaks found at approximately 318, 333, and 363  $\mu$ . The peak at 363  $\mu$  which may be closer to 380  $\mu$  because of an overcorrection<sup>7</sup> indicates that the red and blue emission bands are associated with the PhS radical. The other two peaks in the excitation spectra indicate that at least part of the 325- $\mu$  band as well as the band at 380  $\mu$  in the photoproduct absorption spectra belong to the PhS radical formed during the photolysis. The remainder of the 325- $\mu$  band and the entire band at 450  $\mu$  belong to the absorption spectra of one or more other photoproducts

**TABLE III: Best Fit Values for the Molecular Parameters Using the Polarization Results**

	PhSH red band			PhSH blue band	PhSPh green band
	<i>a</i>	<i>b</i>	<i>c</i>	<i>d</i>	<i>e</i>
	<i>r<sub>y</sub></i> (near-uv)	0.60	0.74		0.64
<i>r<sub>y</sub></i> (second-uv)	0.23		0.51	0.17	
<i>t<sub>y</sub></i>	0.00	0.00	0.01	0.00	0.02
<i>t<sub>x</sub></i>	0.00	0.00	0.00	0.00	0.02
<i>q<sub>y</sub></i>	0.19	0.08	0.20	0.19	0.04
<i>q<sub>x</sub></i>	0.01	0.10	0.00	0.00	0.02
$\Phi^f$	0.157	0.008	0.038	0.715	0.002

<sup>a</sup> For  $r_y = r_y$  (near-uv),  $r_z = (1 - r_y)/2$ ,  $r_x = r_z$ , when  $r_y = r_y$  (second-uv),  $r_x = r_y$  and  $r_z = 1 - r_y - r_x$ . The six independent values of the polarization ratio obtained for excitation in the near-uv and the second-uv bands of PhSH are used. <sup>b</sup> For  $r_x = 0$ ,  $r_z = 1 - r_y$ ,  $t_x = 0$ ,  $t_z = 1 - t_y$ ,  $q_x = 0.1$ , and  $q_z = 1 - q_y - q_x$ . The three independent values of the polarization ratio obtained for excitation in the near-uv band of PhSH are used. <sup>c</sup> For  $r_x = 0.2$ ,  $r_z = 1 - r_y - r_x$ ,  $t_x = 0$ ,  $t_z = 1 - t_y$ ,  $q_x = 0$  and  $q_z = 1 - q_y$ . The three independent values of the polarization ratio obtained for excitation in the second-uv band of PhSH are used. In an approximate best fit  $\Phi = 0.174$  and  $r_y$  (second-uv) = 0.26 which is close to the value found when both polarization experiments were used together. <sup>d</sup> The poorest best fit was obtained in this case. For  $r_y = r_y$  (near-uv),  $r_z = 1 - r_y$ ,  $r_x = 0$  always,  $r_y = r_y$  (second-uv),  $r_z = 1 - r_y$ . The six independent values of the polarization ratio obtained for excitation in the near-uv and the second-uv bands of PhSH are used. <sup>e</sup> For  $r_y = r_y$  (near-uv),  $r_x = r_y$ ,  $r_z = 1 - r_y - r_x$ ,  $t_x = t_y$ ,  $t_z = 1 - t_y - t_x$ ,  $q_x = 0.02$  always,  $q_z = 1 - q_y - q_x$ . The three independent values of the polarization ratio obtained for excitation in the near-uv band of PhSH are used. These are the results for the  $x'$ ,  $y'$ ,  $z'$  axes. See text. In *a* and *e* above an attempt is made to account for depolarization effects. <sup>f</sup> See Appendix in previous paper for a discussion of the best fit parameter.

formed during the photolysis. It appears then that the PhS radical is the dominant photoproduct produced during the photolysis of both PhSH and PhSPh having emission bands in the visible region. Since these bands are the same in a glass containing either PhSH or PhSPh this would rule out the possibility of any strong interaction occurring between the two PhS radicals produced in the PhSPh glass. Each radical is stabilized by the solvent in this case.

The observation of two visible emission bands during excitation of the PhS radical is unusual since in two other studies involving aromatic type radicals (methyl-substituted benzyl radicals<sup>8</sup> and methyl-substituted azabenzyl radicals<sup>9</sup>) only one visible emission band was observed. The molecular structure of the PhS radical can be thought of as being similar to that of the benzyl radical where in this case the odd electron is in a sulfur  $p_\pi$  orbital. This would form an odd-alternate hydrocarbon in basic Hückel theory having a doublet ground state<sup>8</sup> ( ${}^2B_2$  in  $C_{2v}$  symmetry).

The three-step photoselection experiments on the red and blue emission can help in suggesting assignments for the lower energy levels in the PhS radical. The polarization ratios and the corresponding best fit values (see Appendix) of the molecular parameters are shown in Tables II and III, respectively. The values found for the molecular parameters in the red emission indicate a large noninstrumental depolarization.<sup>11</sup> However all the results tabulated here indicate that the photoproduct absorption and 80% or more of the emission occur along the  $z$  direction (see Chart I for the  $y$  and  $z$  directions in the phenyl ring). This suggests

**TABLE IV: Energy Levels (in eV for EPA) and Proposed Symmetry Assignments for the Phenyl Sulfyl Radical and the Phenyl Sulfyl Cation Radical<sup>a</sup>**

	Phenyl sulfyl radical	Phenyl sulfyl cation radical
Uv absorption	3.26 <sup>2</sup> B <sub>2</sub>	3.26 <sup>1</sup> A <sub>1</sub>
Blue emission	3.10 <sup>2</sup> B <sub>2</sub>	3.28 <sup>1</sup> A <sub>1</sub>
Green emission		2.39 <sup>1</sup> A <sub>1</sub>
Red emission	1.94 <sup>2</sup> B <sub>2</sub>	
Ground state	0.00 <sup>2</sup> B <sub>2</sub>	0.00 <sup>1</sup> A <sub>1</sub>

<sup>a</sup> The energy levels for the blue emission bands are approximate.

that the first excited state and the uv absorption band have <sup>2</sup>B<sub>2</sub> symmetry (see Table IV). In contrast the first excited state in the benzyl radical has a <sup>2</sup>A<sub>2</sub> assignment.<sup>12</sup> The blue band may be due to a second fluorescing state (this emission may originate with the uv absorption band) and has been given a tentative <sup>2</sup>B<sub>2</sub> assignment. This is based on the poor best fit results obtained with the polarization ratios. A large amount of noninstrumental depolarization is also present. If the oscillator strength of this state is large and if the gap between this state and the first excited state is large enough then the radiative process could be competitive with that of the first excited state.

The photoproduct responsible for the green emission band may result from formation of a separated charge transfer complex obtained by a two-photon absorption process. The following explanation presents a simple picture of the events that may occur in the formation of this photoproduct. In the first step the PhS radical and a second photoproduct species (the phenyl radical or other resulting photoproduct) are formed and stabilized by the solvent following the absorption of one photon by the PhSPh molecule.<sup>13</sup> Scission of the C-S bond could occur if an electron was excited into the  $\sigma^*$  orbital. The triplet state in PhSPh may be an  $n, \pi^*$  state.<sup>14</sup> This suggests that the  $\sigma^* \leftarrow n$  configuration may be low enough in energy (to mix with one of the lower  $\pi, \pi^*$  states) so that scission of the C-S bond could compete with other processes occurring here.<sup>6</sup> Either the PhS radical or the second photoproduct species could act as a stable intermediate and absorb an additional photon resulting in the formation of a final photoproduct species.<sup>15</sup> The PhS radical does not form an additional photoproduct species upon absorption of a photon when it is produced separately in a PhSH or PhSSPh glass. In addition the green emission band does not appear to originate from a cation species where the ejected electron is stabilized by traps in the glass.<sup>17</sup> However the second photoproduct species formed here may act as a stable electron trap<sup>18</sup> and possibly influence the photoionization process in the PhS radical. In an aqueous solution (but not in the gas phase<sup>19</sup>) the absorption spectra of the phenyl radical (assuming this to be the second photoproduct) resembles that of benzene<sup>20</sup> so that it is probably not being electronically excited here. In addition the ground state electronic configuration has been found to contain a hole in the nonbonding sp<sup>2</sup> orbital (at least for the gas phase)<sup>19</sup> which could act as a stable electron trap. In this case a one-photon ionization of the PhS radical<sup>21,22</sup> could lead to the formation of the PhS cation radical. This species would also have excited states in the visible region.<sup>8</sup> One may think of other explanations, but these will not be considered here.

The polarization ratios and the corresponding best fit

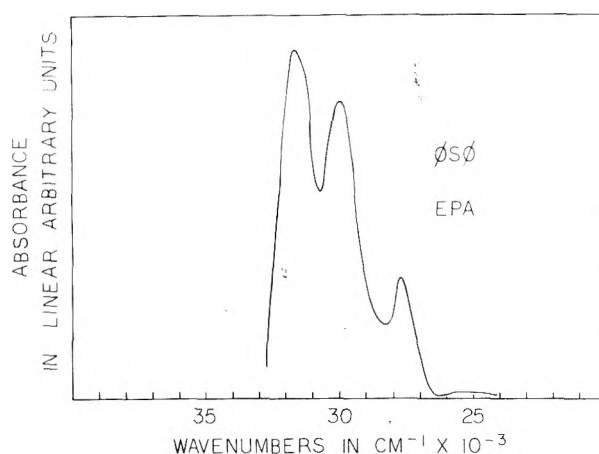
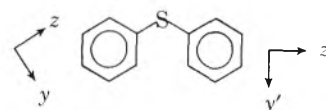


**Figure 8.** Excitation spectra for the green emission band in EPA. The phosphorescence intensity of PhSPh is very strong at 519 m $\mu$ . This emission is subtracted out from the green emission band (observed at 519 m $\mu$ ) for each excitation wavelength where necessary when determining the excitation spectra.

### Chart I



values of the molecular parameters obtained in the photo-selection experiments on the green emission band (Tables II and III, respectively) are close to those values found in one of the ideal cases for a three-step photo-selection experiment where the transition moment is along the same single axis in the parent absorption (the  $z'$  axis in PhSPh, see Chart I) and the photoproduct absorption and emission bands.<sup>8</sup> Values of 0.92, 0.96, and 0.94 were obtained for  $r_2'$ ,  $t_2'$ , and  $q_2'$ , respectively (see Appendix). However these results are valid only in a three-step photo-selection experiment. The photoproduct from which the green emission band originates is produced by a two-photon process so that the polarization data formally requires a four-step analysis where the additional step is for the absorption of a second photon. The high polarization ratios observed here could arise from a polarized second photon step. However if the second photon is absorbed isotropically then the polarization data can be analyzed in terms of three-step photo-selection. An experiment was not carried out here in order to determine whether or not the second photon was absorbed in an isotropic manner. The absorption of a second photon in the creation of benzyl radicals has been found to be completely isotropic (unpolarized).<sup>8</sup> This "has been interpreted as reflecting the near-continuum of states, with various polarizations, which must appear just below the ionization continuum."<sup>16</sup> One would expect similar states to be present in the PhSPh molecule so that the second photon absorption could occur in an isotropic way. It is assumed that this is the case in PhSPh.

If one assumes that the green emission band originates with the PhS cation radical then the polarization results can be used to make tentative assignments for some of the excited states. The ground state should have <sup>1</sup>A<sub>1</sub> symmetry (in C<sub>2v</sub>). The excitation spectrum for the green emission band (Figure 8) shows the presence of one uv absorption band. The parent molecule absorption occurs along the  $z'$  direction because of the exciton interaction between the

$^1L_b$  ring states.<sup>14</sup> The polarization results (for a three-step analysis) indicate that the PhS cation radical absorbs and emits along the same axis. In this case there is no longer any exciton interaction occurring between the lower energy ring states because both the PhS cation radical and the second photoproduct species (probably the phenyl radical) have been stabilized by the solvent. This suggests that the  $z$  and  $z'$  directions are similar<sup>23</sup> which would suggest  $A_1$  assignments (probably singlets) for the uv absorption and green emission bands.

No polarization studies were carried out or excitation spectra obtained on the blue emission band observed for excitation in the photoproduct region of the glass. In this case the blue emission band may also originate with the uv absorption band of the phenyl sulfonyl cation radical and is given a tentative  $A_1$  assignment.

*Acknowledgment.* The author is indebted to the Chemistry Department for most of the equipment used in these experiments. He is also grateful for a yearly NSF grant made available to him by the Research Committee. The machine shop work of Mr. Peter Amirato and use of the computer facilities are appreciated. The author is grateful to the referee for a careful reading of the original manuscript. This led to many critical comments which were valuable in revision.

## Appendix

A detailed discussion of the three-step photoselection method and derivation of the necessary equations are given in ref 8. An outline of this method and the procedure for finding best fit values of the molecular parameters for the polarization results obtained in this paper is given here.

In a three-step photoselection experiment a random sample of the parent molecules is excited in a uv absorption band. In addition to the fluorescence and phosphorescence one or more photoproducts are formed. The formation of a photoproduct species requires one or more photons. A two-step photoselection experiment is then performed on the oriented photoproduct sample (hopefully only one). Since the parent molecules can be excited with either vertically polarized ( $\uparrow$ ) or horizontally polarized ( $\rightarrow$ ) radiation two different photoselected samples of photoproduct species will be created. Each sample can then be excited with the  $\uparrow$  or  $\rightarrow$  component making a total of four polarization ratios that can be obtained at each set of wavelengths (for creation, excitation, and observation of the photoproduct). These values of  $N$  obtained in a single experiment may be identified by the polarization components used to create and excite the photoproduct. The four values of  $N$  (create, excite) are  $N(\uparrow, \uparrow)$ ,  $N(\uparrow, \rightarrow)$ ,  $N(\rightarrow, \uparrow)$ , and  $N(\rightarrow, \rightarrow)$ . The value of  $N(\rightarrow, \rightarrow)$  is independent of the values for the molecular parameters and should be unity in the absence of depolarization. When different from unity it can be used to correct the other three polarization ratios for any instrumental depolarization, i.e.,  $N(\uparrow, \uparrow) = N(\uparrow, \uparrow)_{\text{obsd}}/N(\rightarrow, \rightarrow)_{\text{obsd}}$ , etc.

The values of the three independent polarization ratios depend upon the values of the molecular parameters for absorption by the parent molecule and absorption and emission by the photoproduct which are the  $r$ 's,  $t$ 's, and  $q$ 's, respectively (where  $r_x + r_y + r_z = 1$ , etc.). The  $x$ ,  $y$ , and  $z$  molecular directions are the same as in the two-step photoselection experiments.

In order to determine values for the molecular param-

eters from a single three-step photoselection experiment one value each of the  $r$ 's,  $t$ 's, and  $q$ 's is held constant giving only three independent molecular parameters, one each from the  $r$ 's,  $t$ 's, and  $q$ 's. For example, if the out-of-plane absorption in the parent molecule is assumed to be zero ( $r_x = 0$ ) then  $r_z = 1 - r_y$  gives only one independent parameter from the  $r$ 's. This parameter along with one each from the  $t$ 's and the  $q$ 's is varied by the program in order to find the best fit values for all the parameters.

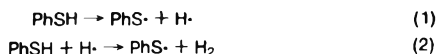
The values of the molecular parameters (Table III) found from the polarization results (Table II) in the green emission band of the photoproduct formed when PhSPh is excited in its near-uv band were obtained in this way using a steepest descent method.<sup>6</sup> The ratios among the three independent polarization ratios are close to the values found in the ideal case where the parent molecule absorbs and the photoproduct absorbs and emits along the same single axis (the  $z'$  axis in PhSPh, see text). The results are the apparent values of these parameters since the correction factor (epsilon) which relates the apparent values with the intrinsic values cannot be used as an additional parameter, one for each absorption step, in order to consider the effects of noninstrumental depolarization explicitly as was done in the two-step photoselection experiments so that the intrinsic values of the molecular parameters (the  $R$ 's and  $T$ 's) cannot be obtained here (see the previous paper<sup>6</sup> and references therein for a discussion of epsilon). Since  $R_x$ ,  $R_y$ ,  $T_y$ , and probably  $T_x$  are zero in this case an attempt was made to introduce an epsilon type correction by setting  $r_x = r_y$  and  $t_x = t_y$  each time a new value of  $r_y$  and  $t_y$  was found in the program before setting  $r_z = 1 - r_y - r_x$  and  $t_z = 1 - t_y - t_x$ . Also  $q_x$  is held constant,  $q_y$  is varied in the program and  $q_z = 1 - q_y - q_x$ .

The values of the molecular parameters found from the polarization ratios in the red emission band of the radical formed in PhSH were obtained in two different ways. In the first method (first column, Table III) six independent polarization ratios are used (for excitation in the 0-0 region of the near-uv and second-uv bands of PhSH). This method gives values for  $r_y$  (near-uv) and  $r_y$  (second-uv) which ideally should be 1.0 and 0.0, respectively, along with values for  $t_y$ ,  $t_x$ ,  $q_y$ , and  $q_x$ . In the second method the three polarization ratios obtained from a single experiment were used to determine the three independent values of the molecular absorption parameters, one each from the  $r$ 's,  $t$ 's, and  $q$ 's.

## References and Notes

- (1) Address correspondence to the Department of Applied Science, Brookhaven National Laboratory, Upton, N.Y. 11973.
- (2) Photoionization has been found to occur when phenol is excited in its  $^1L_b$  absorption band by observing the thermoluminescence which occurs upon warming. A. A. Gibbons, G. Porter, and M. I. Savadatti, *Nature (London)*, **206**, 1355 (1965). The emission from the parent molecule can be observed easily when the photoelectrons, ejected from traps in the glass by exposure to 650-m $\mu$  light, recombine with the cation species. This result was obtained in this lab on a helium degassed sample of phenol. An initially strong phosphorescence (observed at  $\lambda_{\text{max}}$ ) was obtained for a few seconds after the photoexcited sample region was exposed to 650-m $\mu$  light. An identical experiment on PhSH gave no evidence that photoionization had occurred previously.
- (3) U. Schmidt, *Angew. Chem.*, **76**, 629 (1964); *Angew. Chem., Intl., Edit., Engl.*, **3**, 602 (1964). This is a review paper on "Free Radicals and Free Radical Reactions of Monovalent and Divalent Sulfur".
- (4) F. Feher, T. Gladden, and D. Kurz, *Z. Naturforsch. B*, **25**, 1215 (1970).
- (5) The failure to detect radical formation for photolysis of PhSSPh in EPA may be due to the use of a low power (80 W) mercury lamp. In the present experiments a 500-W lamp is employed, and the intensity of the red emission (for excitation of the radical at 365 m $\mu$ ) is used as a measure of the quantity of radical formed. This may be a more sensitive method than the measurement of a change in the absorption spectra produced by the formation of a small amount of radical.

- (6) P. G. Russell, preceding article in this issue.
- (7) The first intense peak at about 363 mμ in the photoproduct excitation spectra does not coincide with the maximum found at 380 mμ in the corresponding absorption band. If the minimum found at 380 mμ in the excitation band is an error resulting from an overcorrection due to a very large inaccurate peak in the corrected lamp intensity curve then the first peak in the excitation spectra would probably be broader and have a maximum closer to 380 mμ. This would provide better agreement with the photoproduct absorption spectra. Since both the lamp intensity and the absorbance of esculin increase very rapidly in adjacent wavelength regions a large error can be obtained in the resulting peak found at 380 mμ in the corrected lamp intensity curve used in obtaining the excitation spectra band shape.
- (8) P. M. Johnson, Ph.D. Thesis, Cornell University, Ithaca, N.Y., 1967; P. M. Johnson and A. C. Albrecht, *J. Chem. Phys.*, **48**, 851 (1968).
- (9) P. M. Johnson, *J. Chem. Phys.*, **52**, 5745 (1970).
- (10) In the photoselection experiments on PhSPh the value of  $M(\rightarrow, \rightarrow)$  varied from a low of 0.6 to a high of 0.78 because of the low emission intensity available on which to make the measurements. Values of 0.7 or less gave values for  $M(\uparrow, \uparrow)$  greater than the maximum allowed value of 5.0 for a three-step analysis. The value of  $M(\rightarrow, \rightarrow)$  varies with the observed wavelength. A linear plot of  $M(\rightarrow, \rightarrow)$  vs. observed wavelength using information obtained from the polarization experiments on the red and blue emission bands (values of  $M(\rightarrow, \rightarrow)$  used were 1.12 and 0.52 at 430 and 640 mμ, respectively) gave a value of 0.87 for  $M(\rightarrow, \rightarrow)$  at 519 mμ. To check this result the mean value of  $M(\rightarrow, \rightarrow)$  obtained at 519 mμ in the blue emission band of PhSH in EPA was found to be 0.86 ± 0.05. A value of 0.86 was used to obtain the three corrected polarization ratios.
- (11) Hydrogen and PhSSPh were found in a PhSH solution which had been photolyzed at 77°K.<sup>4</sup> Two of the reactions which were proposed to have occurred during photolysis were



- The migration of hydrogen atoms through the glass followed by reaction 2 would result in a depolarization of the photoselected sample of PhS radicals. This would account for the low value of  $r_y$  (near-uv) and the high value of  $r_x$  (second uv).
- (12) D. M. Friedrich and A. C. Albrecht, *J. Chem. Phys.*, **58**, 4766 (1973).
- (13) Scission of the C-S bond is found to occur when a solution of PhSPh and other aromatic sulfides undergo photolysis at room temperature. F. C. Thyron, *J. Phys. Chem.*, **77**, 1478 (1973). The transient absorption spectra obtained by flash photolysis on a PhSPh solution was attributed to the formation of the PhS radical. In addition when a benzyl phenyl sulfide solution underwent photolysis an additional sharp band at 317 mμ was obtained which was attributed to the benzyl radical.
- (14) P. G. Russell, communication appearing in this issue.
- (15) The triplet state of PhSPh has a short lifetime, probably in milliseconds, and one would not expect it to be the intermediate. In contrast the triplet state of the methylated benzenes, with lifetimes in seconds, is the most likely intermediate state in the formation of the corresponding benzyl radical.<sup>16</sup>
- (16) P. M. Johnson and A. C. Albrecht, "The Chemistry of Ionization and Excitation", G. R. A. Johnson and G. Scholes, Ed., Taylor and Francis, London, 1967, p 91.
- (17) The intensity of the green emission band was not affected when the photolyzed region in the PhSPh glass was exposed to 650-mμ radiation for 10 min.<sup>2</sup>
- (18) D. K. Bohme and L. Brewster Young, *Can. J. Chem.*, **49**, 2918 (1971).
- (19) G. Porter and B. Ward, *Proc. R. Soc., Ser. A*, **287**, 457 (1965).
- (20) B. Cercek and M. Kongshaug, *J. Phys. Chem.*, **74**, 4319 (1970).
- (21) W. C. Meyer, *J. Phys. Chem.*, **74**, 2118, 2122, 2127 (1970).
- (22) If the final photoproduct species is formed in this manner most of the PhS radicals absorb an additional photon to form the cation radical since the red emission associated with the PhS radical is very weak (especially for PhSPh in EPA). This assumes that this emission does not result from the presence of an impurity in the PhSPh sample.
- (23) This was thought to be the case in the polarization study on the parent emission bands.<sup>14</sup>

## Metal Precipitation from Pulse Irradiated Solutions of Cadmium(II) and Similar Cations

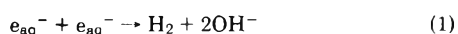
Aaron Barkatt\* and Joseph Rabani

Department of Physical Chemistry, The Hebrew University of Jerusalem, Jerusalem, Israel (Received September 5, 1974; Revised Manuscript Received April 7, 1975)

The precipitate obtained upon irradiating Ar-saturated Cd<sup>2+</sup> aqueous solutions containing alcohols or formate is shown to consist of pure cadmium metal. The yield of Cd<sup>0</sup> indicates that the principal reaction undergone by Cd<sup>2+</sup> ions is disproportionation to Cd<sup>0</sup> and Cd<sup>2+</sup>. The chemical properties and optical spectrum of Cd<sup>0</sup> in suspension were studied. The latter was found to consist of a large-grain dispersion by Cd<sup>0</sup>, with absorption peaks in the uv which are attributed to interaction between Cd<sup>0</sup> and dissolved Cd<sup>2+</sup>. This system makes it possible to analyze the kinetic processes associated with the nucleation and growth of metallic precipitates through the use of pulse radiolytic techniques. The amount of precipitate obtained from various divalent ions is correlated with their effectiveness in reducing G(H<sub>2</sub>).

### Introduction

Baxendale and Dixon<sup>1</sup> observed that several divalent cations, viz., Pb<sup>2+</sup>, Cd<sup>2+</sup>, Ni<sup>2+</sup>, Co<sup>2+</sup>, and Zn<sup>2+</sup>, are effective in reducing G(H<sub>2</sub>) in neutral, but not in acid, deaerated aqueous solutions of alcohols. In the cases of neutral Cd<sup>2+</sup> and Pb<sup>2+</sup> solutions, precipitates were reported, presumably consisting of the corresponding metals. In the case of Zn<sup>2+</sup> an opalescence was observed, which disappeared upon standing. The proposed mechanism for the reduction of G(H<sub>2</sub>) was as follows:



This mechanism was supported by additional work.<sup>2,3</sup> However, as Baxendale and Dixon pointed out, more experiments are required to establish reaction 3 and determine, e.g., whether M<sup>+</sup> ions disappear through disproportionation or through dimerization to form M<sub>2</sub><sup>2+</sup> or another stabilized species of the monovalent cations.

The purpose of the present work is the study of the kinetic processes of the nucleation and growth of metallic

precipitates, and the factors which determine the amount of precipitate in pulse irradiated  $\text{Cd}^{2+}$  aqueous solutions.

### Experimental Section

The accelerator, the optical analyzing system, and the handling of solutions were described previously.<sup>4</sup> When the optical analyzing system was used with an optical path of 12.3 cm, irradiations were performed in a 4 cm long, 8 ml volume, quartz (Spectrosil B) cell with an inlet for filling the cell with an Ar-saturated solution from a 100-ml syringe and an outlet for disposal of the irradiated solution. When it was desired to remove the irradiated solutions for subsequent analysis, irradiations were carried out in 5-ml syringes or in 1-cm long quartz cells fitted with a rubber septum cap.

Solutions were prepared using analytical grade reagents and triply distilled water. They were deaerated by saturation with high-purity argon (Matheson Co.).

Dosimetry of the electron pulse intensities employed in the present work was carried out through the use of the "super" Fricke dosimeter (0.01 M  $\text{Fe}(\text{NH}_4)_2(\text{SO}_4)_2$ ; 0.8 N  $\text{H}_2\text{SO}_4$ ;  $\text{O}_2$  saturated), and calculations were based on  $\epsilon_{\text{Fe}^{3+}}$  (302 nm)  $2197 \text{ M}^{-1} \text{ cm}^{-1}$  at  $25^\circ$  and  $G(\text{Fe}^{3+}) = 16.1$ .<sup>5</sup>

### Results and Discussion

Solutions containing 0.01 M  $\text{CdSO}_4$  and  $\text{Cd}(\text{ClO}_4)_2$  and 0.025 M alcohols (methanol, ethanol, 2-propanol, 2-methyl-2-propanol, ethylene glycol, polyethylene glycol (mol wt 10,000)) were irradiated with single 1.5- $\mu\text{sec}$ ,  $3 \times 10^{17} \text{ eV g}^{-1}$  pulses. After the decay of the  $\text{Cd}^+$  absorption within about  $10^{-4}$  sec, complete transmission was observed in the irradiated solutions up to about 100 msec. Thereafter the transmission decreased, reaching a plateau value at time  $> 10$  sec (see Figure 1). Upon visual observation it was found to contain a suspension which was white upon illumination with a strong beam of light from an Xe lamp and gray when examined under diffuse, indirect light. This suspension settled over a period of 1–2 hr, and the supernatant solution became transparent again. This process was accelerated by heating or centrifugation of the suspension.

In order to analyze the precipitate,  $1000 \times 10^{16} \text{ eV g}^{-1}$  pulses were applied to a solution of 0.025 M  $\text{Cd}^{2+}$ , 0.05 M alcohol at a rate of 15 pulses/sec. Upon settling, the precipitate was observed to consist of gray metallic pieces. The precipitate was washed several times with triply distilled water, once with 1 M  $\text{HClO}_4$ , and once with ethanol, and dried to constant weight at  $70^\circ$ .

The suspension was obtained in the presence of various OH scavengers (alcohols, phenol, benzene, and formate), but not in solutions of  $\text{Cd}^{2+}$  salts in pure water.

The quantity of the suspension and the ensuing precipitate was largest at pH 6–7.5 (higher pH's were not tested) and decreased gradually at lower pH. Below pH 2, no suspension was formed. The production of the suspension was independent of the anion (sulfate or perchlorate). The use of sodium formate at pH 6 as an OH and H scavenger resulted in an increase of the precipitate weight by a factor of  $(2.2 \pm 0.4)$  compared with that obtained in ethylene glycol at the same pH. (In a separate series of experiments,  $\text{CO}_2^-$  was found to reduce  $\text{Cd}^{2+}$  to  $\text{Cd}^+$  with a second-order rate constant of  $(5.1 \pm 0.3) \times 10^6 \text{ M}^{-1} \text{ sec}^{-1}$ .)

Analysis of the precipitate was carried out under the following conditions: solutions (4 ml each) of 0.05 M  $\text{CdSO}_4$  and 1 M  $\text{HCOONa}$  were irradiated, each with  $500 \times 10^{17} \text{ eV}$  pulses. The precipitates from 24 solutions were col-

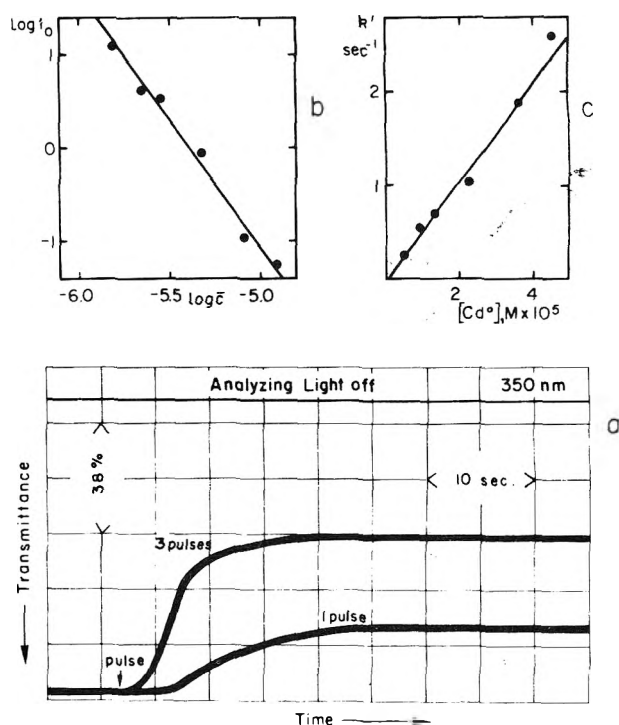


**Figure 1.** (a) Oscilloscope traces obtained in Ar-saturated solution of 0.01 M  $\text{CdSO}_4$  and 0.025 M ethylene glycol upon irradiation with  $1 \times 10^{17} \text{ eV g}^{-1}$  pulses ( $l = 12.3$  cm). (b) Pseudo-first-order rate constants for latter half of the precipitation process at different doses in the same solution. (c) Induction periods at different doses in the same solution.

lected, washed, and dried, and were found to weigh totally  $(25 \pm 2)$  mg. (The relatively small pulses used were to minimize the quantity of oxalate from the recombination of  $\text{CO}_2^-$  radicals; insoluble  $\text{CdC}_2\text{O}_4$ , which might have been formed from  $< 2\%$  of the  $\text{CO}_2^-$  radicals, was apparently removed by the washing with 1 M  $\text{HClO}_4$ .) Chemical analysis of such-collected precipitates was carried out using two methods. (1) Dissolution in a few drops of concentrated  $\text{HNO}_3$ , evaporation of the excess acid, dissolution of  $\text{Cd}(\text{NO}_3)_2$  in triply distilled water, and titration with 0.05 M EDTA solution in the presence of hexamethylenetetramine (pH 6), using Xylenol Orange as an indicator.<sup>6</sup> This method showed that the precipitate contained  $\geq 99\%$  Cd. (2) Dissolution of the precipitate in concentrated HCl and measurement of the evolved  $\text{H}_2$  volume under constant pressure. The amount of evolved  $\text{H}_2$  was equivalent to the presence of  $\geq 97.5\%$   $\text{Cd}^0$  in the precipitate. (This second method is more sensitive to the presence of monovalent cadmium, since  $\text{Cd}_2\text{O}$ , which would contain 93% Cd, would release only 47% of the  $\text{H}_2$  liberated by the same weight of  $\text{Cd}^0$ .) Results of  $\geq 98\%$   $\text{Cd}^0$  in the precipitate were also obtained when ethylene glycol was substituted for formate, and in the presence of 1 M NaCl (where  $\text{Cd}_2\text{Cl}_2$ , containing only 76% Cd, might have been formed, had  $\text{Cd}_2^{2+}$  been the product of reaction 3).

The results obtained in the 0.05 M  $\text{CdSO}_4$ –1 M  $\text{HCOONa}$  system lead to a result of  $G(\text{Cd}^0) = (2.8 \pm 0.2)$ . This result is in agreement with the value expected for  $0.5(G(e_{\text{aq}}^-) + G(\text{OH}) + G(\text{H}) - 2G(\text{H}_2\text{O}_2))$  in this range of scavenger concentrations. It should be noted that the irradiation dose applied to the solution results in reduction of 4.8% of the present  $\text{Cd}^{2+}$  to  $\text{Cd}^0$ .

*Chemical Properties and Spectrum of Radiation-Pro-*



duced  $\text{Cd}^0$ . After settling, the chemical reactivity of the precipitate is similar to that of cadmium metal grains of analytical grade. While present in suspension,  $\text{Cd}^0$  reacts within less than 10 sec with oxidizing agents ( $\text{O}_2$ ,  $\text{H}_2\text{O}_2$ ,  $\text{KMnO}_4$ ,  $\text{Fe}(\text{ClO}_4)_3$ ), i.e., much faster than do Cd grains, probably because of much larger surface area. It reduces benzoquinone to hydroquinone within less than 10 sec and quantitatively, but, like Cd grains, it cannot reduce weak oxidizing agents such as acetophenone and fluorenone. The reactivity of the suspension toward acid is similar to that of Cd grains: it dissolved within a few seconds upon the addition of concentrated  $\text{HNO}_3$ , and more slowly in concentrated  $\text{HCl}$ ,  $\text{H}_2\text{SO}_4$ , and  $\text{HClO}_4$ , and was quite inert toward dilute acids.

The optical spectrum of the suspension was taken with a Cary-14 recording spectrophotometer 10 min after irradiation of an Ar-saturated 0.01 M  $\text{CdSO}_4$  solution containing 0.025 M formate or ethylene glycol as measured against the unirradiated solution. Above 260 nm the spectrum was measured also 50 sec after the pulse, showing results identical with those obtained with the Cary-14 spectrophotometer. The spectrum is shown in Figure 2 to consist of two portions: a flat decrease in transmission over the 700–350-nm range, and discrete peaks in the uv (two doublets around 315 and 240 nm, and another band around 205 nm). It is possible to attribute the flat spectrum in the visible to dispersion by the Cd grains (the very gradual reduction of transmission upon going to shorter wavelengths indicates that the suspension is much coarser than that giving rise to Rayleigh dispersion; this is in agreement with the fast rate of settling). A very similar spectrum is observed upon shaking analytical grade cadmium grains in a 0.025 M  $\text{CdSO}_4$  solution and measuring the transmittance against a similar solution (see Figure 2). This is an additional confirmation of the fact that the radiation induced suspension consists of  $\text{Cd}^0$ . In the case of water or 0.025 M  $\text{Na}_2\text{SO}_4$  shaken with Cd grains, the flat spectrum in the visible resembles the one obtained in  $\text{CdSO}_4$  solution, but the discrete peaks in the uv are much less prominent. After a period of 10 hr these peaks can be observed, perhaps because they can be attributed to an association between  $\text{Cd}^0$  in suspension and  $\text{Cd}^{2+}$  in solution. No ESR signals were observed in the radiation produced suspension or precipitate as expected if the material is  $\text{Cd}^0$ .

**Pulse Radiolytic Measurements of the Kinetics of Formation of the  $\text{Cd}^0$  Suspension.** Pulse radiolysis can be used as a method for very fast production of species in concentrations larger than their solubility products and for following the subsequent precipitation processes. This method was previously employed by Schiller and Ebert<sup>7</sup> in the case of  $\text{AgCl}$ . In the present case, the following characteristics of the formation have been observed.

(1) An induction period  $t_0$ , corresponding to the time required for nucleation and growth to a grain size which displays turbidity,<sup>8</sup> was measured in accordance with Schiller and Ebert.<sup>7</sup> The induction period becomes shorter upon increasing the supersaturation  $\bar{c}$ , taken as proportional to the dose. Plotting  $\log t_0$  against  $-\log \bar{c}$  we obtain a slope  $n = 2.5 \pm 0.5$  (see Figure 1b). Comparison with previous results<sup>7</sup> indicates that  $n$  strongly depends on the nature of the precipitate.

(2) The shapes of the precipitation curves (Figure 1c) at different extents of supersaturation are very similar to those obtained by Turnbull<sup>9</sup> in the case of  $\text{BaSO}_4$  and may be interpreted accordingly. It is possible to approximate

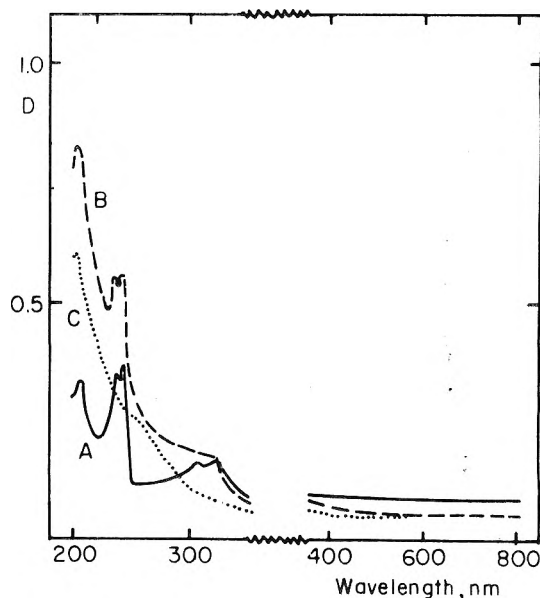


**Figure 2.** (A) Optical spectrum obtained in Ar-saturated solution of 0.025 M  $\text{CdSO}_4$  and 0.05 M ethylene glycol upon pulse irradiation. Dose =  $5 \times 10^{17}$  eV  $\text{g}^{-1}$  ( $l = 1$  cm). (B) Optical spectrum of Cd metal grains shaken with a 0.025 M  $\text{CdSO}_4$  solution. (C) Optical spectrum of Cd metal grains shaken with a 0.025 M  $\text{Na}_2\text{SO}_4$  solution.

the second half of a growth curve by a pseudo-first-order rate law with respect to  $\text{Cd}^0$ , with a rate constant of  $(5 \pm 2) \times 10^4 [\text{Cd}^0] \text{ sec}^{-1}$  (see Figure 1). (We assume that the solubility of  $\text{Cd}^0$  is very small compared with the produced concentrations of  $10^{-6}$  to  $10^{-5}$  M, and this is in accordance with the fact that the linear plot of the pseudo-first-order rate constant vs.  $[\text{Cd}^0]$  can be extrapolated to zero.)

(3) Upon increasing the initial  $[\text{Cd}^{2+}]$  from  $10^{-3}$  to  $10^{-1}$  M in the presence of  $10^{-1}$  M ethylene glycol the turbidity produced upon irradiation increases by about 30%, and this may be interpreted as the result of enhanced scavenging from the spurs. However, the kinetics of precipitation of metallic Cd is not influenced by the large change in ionic strength. The kinetics are also not influenced by changing the alcohol used to scavenge OH and H. Identical kinetics are observed upon irradiation with  $n 1 \times 10^{17}$  eV  $\text{g}^{-1}$  pulses and with  $10n 1 \times 10^{16}$  eV  $\text{g}^{-1}$  pulses (emitted at a rate of 15 pulses/sec). The effect of other additives is not clear—formate was observed to accelerate the growth rate (beyond the effect of increasing the amount of  $\text{Cd}^0$ ), while acetate retards the growth rate.

**Other Cations.** Pulse irradiation under similar conditions in the presence of 0.025 M ethylene glycol or formate at pH 5 was carried out on sulfates and perchlorates of other divalent cations. The intensity of the turbidity was found to depend on the cation in the following order:  $\text{Pb}^{2+} \approx \text{Cd}^{2+} \gg \text{Zn}^{2+} > \text{Ni}^{2+} > \text{Co}^{2+}$ .

Hardly any turbidity was observed in the case of  $\text{Co}^{2+}$  ions. Both molar quantities and kinetics of formation of the suspensions were very similar in the cases of  $\text{Pb}^{2+}$  and  $\text{Cd}^{2+}$ .

The intensity of turbidity may be influenced by the amount of the suspension and by grain size and structure. However, it is clear that the amount of suspension (both before and after settling) is much smaller in the cases of  $\text{Zn}^{2+}$ ,  $\text{Ni}^{2+}$ , and  $\text{Co}^{2+}$ . This can explain the much smaller effectiveness of these ions in reducing  $G(\text{H}_2)$ .<sup>1,2,10,11</sup> In

these cases, some  $M^+$  may react with water, alcohol, or alcohol radicals in competition with reaction 3. (In the case of  $Cd^{2+}$ , the second-order behavior of the decay of  $Cd^+$  shows that reaction 3 predominates. In all cases, some  $M^+$  is reoxidized by molecular  $H_2O_2$ .<sup>10</sup>)

This effect may be the principal cause for the discrepancy between the effectiveness of divalent ions as  $e_{aq}^-$  scavengers and their effectiveness in reducing  $G(H_2)$ .

Pulse radiolytic measurements were carried out with 1.5- $\mu$ sec pulses ( $3 \times 10^{17}$  eV  $g^{-1}$ ) in Ar-saturated 0.01 M  $M^{2+}$  ( $M = Cd, Zn, Pb, Ni, Co$ ), 0.025 M ethylene glycol solutions. Optical measurements in the range 260–400 nm showed that in all cases the spectra obtained 1  $\mu$ sec after the pulse at pH 4.5–5.5 and at pH 2 (acidified with  $HClO_4$ ) were identical, showing no evidence for early formation of  $Cd^0$ .<sup>12</sup> The absorption of  $M^+$  decayed to zero much before the start of nucleation of  $M^0$  in the seconds time scale, in agreement with previous results.<sup>13</sup>

*Acknowledgment.* The authors are grateful to Dr. D. Meyerstein, of the Negev University, Beer-Sheba, for helpful discussions.

## References and Notes

- (1) J. H. Baxendale and R. S. Dixon, *Proc. Chem. Soc. (London)*, 148 (1963); *Z. Phys. Chem. (Frankfurt am Main)*, **43**, 161 (1964).
- (2) E. Peled and G. Czapski, *J. Phys. Chem.*, **74**, 2903 (1970).
- (3) D. Meyerstein and W. A. Mulac, *J. Phys. Chem.*, **72**, 784 (1968).
- (4) D. Zehavi and J. Rabani, *J. Phys. Chem.*, **75**, 1738 (1971).
- (5) H. Fricke and E. J. Hart in "Radiation Dosimetry", H. Attix and E. G. Roesch, Ed., Academic Press, New York, N.Y., Chapter 12.
- (6) A. I. Vogel, "Quantitative Inorganic Analysis", 3rd ed, Longmans, London, 1961, p 444.
- (7) R. Schiller and M. Ebert, *Int'l. J. Radiat. Phys. Chem.*, **1**, 111 (1969).
- (8) F. C. Collins and J. P. Leinweber, *J. Phys. Chem.*, **60**, 389 (1956).
- (9) D. Turnbull, *Acta Met.*, **1**, 684 (1954).
- (10) D. Meyerstein and W. A. Mulac, *J. Phys. Chem.*, **72**, 784 (1968).
- (11) M. Faraggi and J. Desalos, *Int'l. J. Radiat. Phys. Chem.*, **1**, 335 (1969).
- (12) G. E. Adams, J. H. Baxendale, and J. W. Boag, *Proc. Chem. Soc. (London)*, 241 (1963).
- (13) J. H. Baxendale, J. P. Keene, and D. A. Stott, *Chem. Commun.*, 715 (1966).

## Solute Environmental Effects in the One-Electron Reduction of Lysozyme in Aqueous Solution<sup>1</sup>

Morton Z. Hoffman\*

Department of Chemistry, Boston University, Boston, Massachusetts 02215

and E. Hayon\*

Pioneering Research Laboratory, U.S. Army Natick Laboratories, Natick, Massachusetts 01760 (Received December 4, 1974)

The reaction of lysozyme with hydrated electrons generated pulse radiolytically produces an initial transient absorption with  $\lambda_{max}$  420 nm which can be attributed to the formation of the one-electron reduced lysozyme radical with the unpaired electron highly localized on one of the disulfide linkages. The value of  $k(e_{aq}^- + lys)$  ranges from  $1.4 \times 10^{11} M^{-1} sec^{-1}$  at pH 5.7 to  $1.5 \times 10^{10} M^{-1} sec^{-1}$  at pH 12 and is dependent upon the ionic strength of the solution. This initial transient absorption, which is also produced by the reaction of  $CO_2^-$  radicals with lysozyme, decays in less than  $10^{-3}$  sec to reveal a secondary absorption centered around 420 nm. The pH-dependent decay kinetics of this secondary absorption are mainly first order with  $k$  a function of the concentration of added solutes including phosphate buffer, *tert*-butyl alcohol, glycine, NaCl, and formate. The reduced lysozyme species is evidently very sensitive to its solution environment which suggests that ionic associations and solvent structure perturbations affect the conformation of the radical and its subsequent decay kinetics.

### Introduction

Lysozyme is an hydrolytic enzyme with a molecular weight of approximately 14,400, containing four disulfide linkages ( $-SS-$ ) among the 129 amino acid residues. The reaction of  $e_{aq}^-$ , generated in the pulse radiolysis of dilute aqueous solutions of the enzyme, has been observed to produce a transient optical absorption spectrum<sup>2</sup> with a maximum at 420 nm; this spectrum was attributed to the species formed by the trapping of electrons on a disulfide bridge inasmuch as the absorption was almost identical with that of the  $(-SS-)^-$  radical anion formed on reduction of simple disulfides.<sup>3</sup> The decay of the electron adduct to lysozyme was noted<sup>2</sup> to be slower than that of the corre-

sponding species from cystamine<sup>3</sup> but no kinetics data were presented. Electron transfer from  $CO_2^-$  to lysozyme was also shown to produce the  $(-SS-)^-$  absorption,<sup>4</sup> but again no data on the decay of that absorption were presented. Although the one-electron reduction of lysozyme by free radicals and  $e_{aq}^-$  has been demonstrated directly, this process does not cause appreciable inactivation of the enzyme.<sup>5</sup>

This study of the one-electron reduction of lysozyme had, as its rationale, our detailed examination of the kinetics behavior of the  $(-SS-)^-$  radical anion derived from simple aliphatic disulfides.<sup>6</sup> This radical decays via first-order kinetics forming  $RS\cdot$  and  $RS^-$  with a rate constant that is dependent on the state of protonation of the amino groups

$\alpha$  to the  $-\text{SS}-$  group. The radical anion is rapidly protonated which enhances its decay to the corresponding thyl radical. For lipoic acid, a cyclic disulfide, the  $(-\text{SS}-)^{\cdot-}$  radical decays via second-order kinetics, apparently due to the inability of the fragments to diffuse away into solution after S-S bond scission.

The four disulfide linkages in lysozyme bridge pairs of cysteine residues (6 and 127, 30 and 115, 64 and 80, 76 and 94) and the X-ray crystallographic examination of the enzyme shows that two such linkages are adjacent to the surface of the molecule while two are deep within the molecular structure.<sup>7</sup> The linkages establish and maintain at least part of the helical structure and conformation of the molecule. The purpose of the work reported here was to examine in detail the kinetics of the formation and decay of the  $(-\text{SS}-)^{\cdot-}$  radical in lysozyme and compare the results with those we obtained from aliphatic disulfides.<sup>6</sup> Because of the effect that ions have on the solution structure of biological macromolecules,<sup>8</sup> we were particularly concerned about similar effects of added solutes on the kinetics behavior of the one-electron reduced species.

### Experimental Section

Single pulses of 2.3-MeV electrons of  $\sim 30$ -nsec duration were generated by a Febetron 705 pulsed source (Field Emission Corp.). The absorption spectra of transient intermediates and their decay kinetics were determined as previously described.<sup>9</sup> Dosimetry was carried out using KSCN solutions and the extinction coefficients of intermediates were derived taking  $G(e_{\text{aq}}^-) = G(\text{OH}) = 2.8$  and  $G(\text{H}) = 0.55$ .

Hen egg white lysozyme (crystallized three times, A grade) was obtained from Calbiochem and used without further purification. The solid enzyme was always added to the deoxygenated solution containing the added solutes after which time the pH was adjusted using KOH or  $\text{HClO}_4$ . Alternatively, a neutral deoxygenated fresh stock solution of the enzyme was used to prepare the solutions for pulsing. A new sample of solution was used for each pulse. All other reagents were the highest purity research grade commercially available.

For the experiments involving other sulfur-containing enzymes, the following materials were used: trypsin (Calbiochem),  $\alpha$ -chymotrypsin (Worthington), papain (Calbiochem), pepsin (Worthington), and ribonuclease A (Worthington).

### Results and Discussion

The radiolysis of neutral aqueous solutions generates  $e_{\text{aq}}^-$ , OH, and H as the major reactive species with  $G$  values (number of molecules produced per 100 eV of energy absorbed by the solution) of 2.8, 2.8, and 0.55, respectively. The OH radical can be effectively scavenged by *tert*-butyl alcohol ( $k = 5.2 \times 10^8 \text{ M}^{-1} \text{ sec}^{-1}$ )<sup>10</sup> producing the generally inert and weakly absorbing  $\cdot\text{CH}_2\text{C}(\text{CH}_3)_2\text{OH}$  radical.<sup>9</sup> In acidic solution,  $e_{\text{aq}}^-$  is converted to H ( $k = 2.2 \times 10^{10} \text{ M}^{-1} \text{ sec}^{-1}$ ).<sup>11</sup> The reducing radicals  $\text{CO}_2^{\cdot-}$  and  $(\text{CH}_3)_2\dot{\text{C}}\text{OH}$  can be generated conveniently by the reaction of OH radicals and H atoms with  $\text{HCO}_2^-$  and  $(\text{CH}_3)_2\text{CHOH}$ , respectively ( $k = 10^7\text{--}10^9 \text{ M}^{-1} \text{ sec}^{-1}$ ).<sup>10,12</sup>

**Reaction of Lysozyme with  $e_{\text{aq}}^-$ . Rate Constants.** The rate constants for the reaction of  $e_{\text{aq}}^-$  with lysozyme were determined in deoxygenated solutions from the pseudo-first-order decay of  $e_{\text{aq}}^-$  monitored at 700 nm. From the slope of the straight line obtained when the pseudo-first-

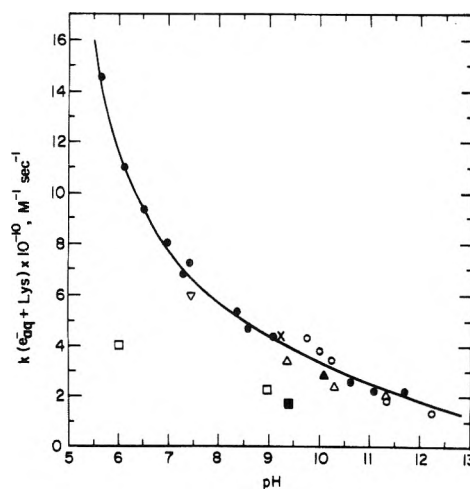


**Figure 1.** Dependence of  $k(e_{\text{aq}}^- + \text{lys})$  on pH; [lysozyme] =  $2 \times 10^{-5} \text{ M}$ ; O, no added solute; ●,  $1 \times 10^{-4} \text{ M}$  phosphate; X,  $1 \times 10^{-4} \text{ M}$  tetraborate; ▽,  $1 \times 10^{-4} \text{ M}$  phosphate +  $0.5 \text{ M}$  *tert*-butyl alcohol; Δ,  $1 \times 10^{-2} \text{ M}$  NaCl; ▲,  $1 \times 10^{-2} \text{ M}$  glycine; □,  $1 \times 10^{-2} \text{ M}$  phosphate; ■,  $1 \times 10^{-2} \text{ M}$  tetraborate.

order rate constant is plotted vs. [lysozyme] ( $1\text{--}4 \times 10^{-5} \text{ M}$ ), the value of  $k(e_{\text{aq}}^- + \text{lys})$  was calculated. Figure 1 shows the dependence of  $k(e_{\text{aq}}^- + \text{lys})$  upon pH as well as the effect of added solutes such as phosphate or borate buffers. These data were obtained at [lysozyme] =  $2 \times 10^{-5} \text{ M}$  in the absence of *tert*-butyl alcohol; preliminary experiments had shown that the presence of that alcohol as an OH radical scavenger had no effect on the observed value of  $k(e_{\text{aq}}^- + \text{lys})$ . It is evident that the value of  $k$  increases sharply to over  $10^{11} \text{ M}^{-1} \text{ sec}^{-1}$  as the acidity of the solution is increased. Under the conditions of the experiments, no competition from  $\text{H}^+$  for  $e_{\text{aq}}^-$  can occur. Furthermore, the presence of  $>10^{-4} \text{ M}$  ionic solutes has the effect of lowering the value of  $k$ ; the magnitude of the effect depends upon the concentration of ionic solute and is diminished in basic solution as the isoelectric point of lysozyme<sup>13</sup> at pH 10.5 is reached. Such a general dependence of  $k$  on pH had been noted previously but no correlation could be made between the observed value of  $k(e_{\text{aq}}^- + \text{lys})$  with the algebraic sum of the reactivities of the component amino acids.<sup>14</sup> Comparison of the data presented here with those reported by previous investigators<sup>11</sup> is quite good despite the retarding effect of buffer solutes and the often varying and unspecified buffer concentrations used in such measurements.

The pH dependence of  $k$  at low ionic strengths can be most easily rationalized in terms of the charge on the lysozyme molecule as a result of protonation-deprotonation equilibria involving the various functional groups. As the solution is made more basic, successive deprotonation of the carboxylic acid groups in the aspartic and glutamic acid residues and the free end of the protein, histidine, the phenol groups in tyrosine, and the amino groups in arginine, lysine, and the free end of the protein causes the charge on the molecule to become less positive in an almost continuous manner. In very alkaline solution, hydrolysis of the disulfide bonds is to be expected<sup>15</sup> which increases the overall negative charge through formation of deprotonated sulfhydryl groups at the eight cysteine residues. From strictly electrostatic considerations, the rate of reaction of a  $-1$  charged species with an increasingly less positive protein molecule should decrease. It should be noted that the variation of  $k(e_{\text{aq}}^- + \text{lys})$  as a function of pH cannot be attributed to major changes in the conformation of the enzyme

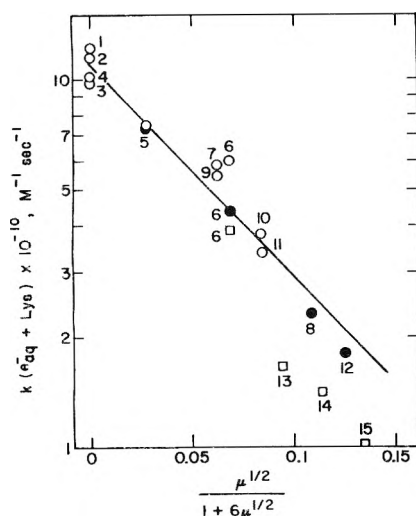


**Figure 2.** Plot of  $\log k(e_{aq}^- + \text{lys})$  as a function of ionic strength at pH 6.0.  $[\text{Lysozyme}] = 1 \times 10^{-5} M$  (○),  $2 \times 10^{-5} M$  (●),  $4 \times 10^{-5} M$  (□): (1) no additional solute; (2)  $1 \times 10^{-2} M$  urea; (3)  $1 \times 10^{-2} M$  glycine; (4)  $1 \times 10^{-4} M \text{NaH}_2\text{PO}_4$ ; (5)  $1 \times 10^{-3} M \text{NaH}_2\text{PO}_4$ ; (6)  $1 \times 10^{-2} M \text{NaH}_2\text{PO}_4$ ; (7)  $1 \times 10^{-2} M \text{LiCl}$ ; (8)  $8 \times 10^{-2} M \text{LiCl}$ ; (9)  $1 \times 10^{-2} M \text{NaO}_2\text{CCH}_3$ ; (10)  $1 \times 10^{-2} M \text{Na}_4\text{P}_2\text{O}_7$ ; (11)  $1 \times 10^{-2} M \text{K}_2\text{SO}_4$ ; (12)  $8 \times 10^{-2} M \text{K}_2\text{SO}_4$ ; (13)  $1.5 \times 10^{-2} M \text{K}_2\text{SO}_4$ ; (14)  $4 \times 10^{-2} M \text{K}_2\text{SO}_4$ ; (15)  $1.5 \times 10^{-1} M \text{K}_2\text{SO}_4$ .

inasmuch as lysozyme resists unfolding and maintains its conformation except in strongly acidic and strongly alkaline solutions.<sup>16</sup>

The results in Figure 1 show that increased ionic strength in acidic solution has a stronger retarding effect than in basic solution, consistent with the change in charge as pH is varied. A test was made of the kinetic salt effect at pH 6.0 on  $k(e_{aq}^- + \text{lys})$  by measuring  $k$  in the presence of added solutes. The results are shown in Figure 2 where a reasonably good linear plot is obtained for  $\log k$  vs.  $\mu^{1/2}/(1 + 6\mu^{1/2})$ . The constant  $\alpha$  is a function of the encounter distance and is defined as  $\alpha = (r_{e_{aq}^-} + r_{\text{lys}})/3$  where  $r_{e_{aq}^-}$  and  $r_{\text{lys}}$  are the radii of  $e_{aq}^-$  and lysozyme, respectively, in ångströms. The radius of charge distribution of  $e_{aq}^-$  is 2.5–3.0 Å and the species can be viewed as spherically symmetrical.<sup>17</sup> The lysozyme molecule in aqueous solution assumes a spherical or oblate ellipsoidal shape with an unhydrated molecular radius of approximately 16 Å and a radius in aqueous solution of approximately 19 Å.<sup>18</sup> On that basis, the value of  $\alpha = 6$  was chosen to test the fit of the data to the Brønsted-Bjerrum ionic salt effect relationship.<sup>19</sup> Figure 2 shows that the relationship is followed over a fairly wide range of solution ionic strengths, specifically from 0 to 0.24  $M$ . Distinct deviations from linearity are seen in high ionic strength solutions containing  $4 \times 10^{-5} M$  lysozyme. Lysozyme is known to dimerize at pH 5–9 in high ionic strength solutions with the degree of dimerization increasing with increasing monomer concentration.<sup>20</sup> Dimerization causes the concentration of reactive species in solution to be lower than that calculated on the basis of monomer resulting in low values for  $k(e_{aq}^- + \text{lys})$  when calculated from pseudo-first-order electron decays. The slope of the plot in Figure 2 is  $-6.4$  which corresponds to  $1.02Z_{e_{aq}^-} - Z_{\text{lys}}$  yielding an apparent charge of  $+6.4$  for lysozyme at pH 6.0 in aqueous solution. Considering that lysozyme at pH 6.0 contains 11 deprotonated carboxylate groups and 18 protonated amino groups (histidine and tyrosine are not deprotonated at this pH) the excess of positive charge over negative charge results in an overall ionic charge of  $+7$ .

The coincidence of the calculated and observed values of the ionic charge of the enzyme is excellent and probably remarkable in light of the size of the macromolecule and the underlying assumptions made in the derivation and application of the Brønsted-Bjerrum relationship.<sup>19</sup> It is recognized that the agreement of the values and the linearity of the relationship shown in Figure 2 may be fortuitous and further work with other enzymes and macromolecules is required to demonstrate the efficacy of the application of the kinetic salt effect to these systems. If, however, the relationship is valid, the results described here imply that the interaction of  $e_{aq}^-$  with lysozyme involves the charge on the entire molecule rather than a specific locus of charge on the surface of the molecule. It is interesting to note that in the case of the reaction of  $e_{aq}^-$  with simple aliphatic disulfides,<sup>6</sup> we concluded that the value of  $k$  is dictated by  $e_{aq}^-$  attack at the  $-\text{SS}-$  group and only to a relatively small extent on the net charge on the molecule. However, these experiments were not performed as a function of ionic strength. Furthermore, in the compounds examined,<sup>6</sup> the rate of electron attack on functional groups other than  $-\text{SS}-$  is very low. In lysozyme, on the other hand, the aromatic amino acids and the peptide linkages are also reactive toward  $e_{aq}^-$  so that virtually the entire molecule is susceptible to electron attack.

In some preliminary experiments with  $\alpha$ -chymotrypsin, the value of  $k(e_{aq}^- + \text{chy})$  was found to be dependent on pH ranging from  $2.5 \times 10^{10} M^{-1} \text{sec}^{-1}$  at pH 5.8 to  $7.0 \times 10^9 M^{-1} \text{sec}^{-1}$  at pH 11.5. Although these experiments, involving  $4 \times 10^{-5} M$  enzyme, were conducted at an uncontrolled, but low, ionic strength, it can be seen that the trend is similar to that shown by lysozyme. Trypsin, on the other hand, shows a pH-independent (7–10) value of  $k(e_{aq}^- + \text{trypsin}) = 3.9 \pm 0.3 \times 10^{10} M^{-1} \text{sec}^{-1}$ , virtually identical with that reported by Masuda et al.<sup>21</sup>

**Transient Spectra.** The reaction of  $e_{aq}^-$  with lysozyme ( $1 \times 10^{-4} M$ ) in Ar-purged 1  $M$  *tert*-butyl alcohol solution resulted in the transient absorption spectrum shown in Figure 3a (open circles) for which  $\lambda_{\text{max}} 420 \text{ nm}$  (apparent  $\epsilon_{420} 5.8 (\pm 0.2) \times 10^3 M^{-1} \text{cm}^{-1}$ ). In contrast, at pH 2.1, where  $e_{aq}^-$  is converted quantitatively to H, the initial transient spectrum exhibited  $\lambda_{\text{max}} 320 \text{ nm}$  (apparent  $\epsilon_{320} 2.9 \times 10^3 M^{-1} \text{cm}^{-1}$ ) as shown in Figure 3b. The spectrum of the initial electron-adduct to lysozyme,  $T_1$ , was unaffected by pH (4–12.3), the presence or absence of *tert*-butyl alcohol, or the presence of the other solutes used in this work.

$T_1$  decayed in a matter of tenths of milliseconds resulting in the absorption spectrum shown in Figure 3a (closed circles) attributed to a species designated as  $T_2$ . This secondary absorption showed  $\lambda_{\text{max}} 420 \text{ nm}$  with an apparent  $\epsilon_{420} 3.6 (\pm 0.5) \times 10^3 M^{-1} \text{cm}^{-1}$ . It must be recognized that inasmuch as the primary and secondary absorption spectra may themselves result from a composite of many species that may or may not be mechanistically interrelated, it is not possible to know the concentration of  $T_2$  and hence the value of  $\epsilon$  cannot be known with certainty. The apparent  $\epsilon_{420}$  value was independent of solution acidity in the range pH 5–11; above pH 11 the absorbance of  $T_2$  was significantly diminished.

$T_2$  exhibited a wide range of lifetimes depending on the pH and the presence of added solutes. When  $T_2$  decayed ( $\tau = 0.1\text{--}5 \text{ sec}$ ), a tertiary absorption spectrum could be observed in the 400–420-nm region (Figure 3a, open squares) with an apparent  $\epsilon_{420} \sim 300 M^{-1} \text{sec}^{-1}$  independent of pH

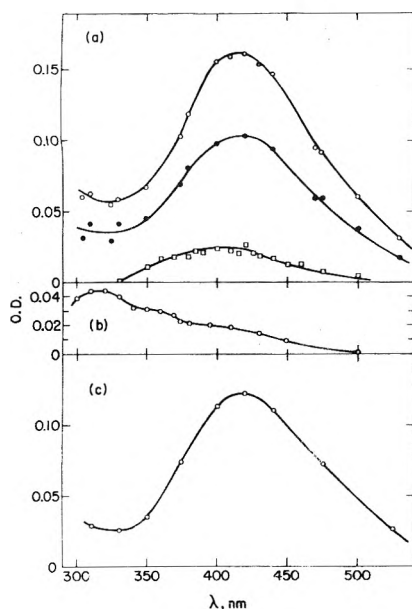


**Figure 3.** Transient absorption spectra from the pulse radiolysis of aqueous solutions of lysozyme; [lysozyme] =  $1 \times 10^{-4}$  M, optical path = 2.0 cm. (a) [*tert*-Butyl alcohol] = 1 M, Ar purged: O, initial spectrum at pH 7.4, dose/pulse = 8.0 krad; ●, secondary spectrum at 2 msec after the pulse at pH 7.4, dose/pulse = 8.0 krad; □, tertiary spectrum at 0.1 sec after the pulse at pH 8.6, dose/pulse = 16.0 krad. (b) [*tert*-Butyl alcohol] = 1 M, Ar purged: initial spectrum at pH 2.1, dose/pulse = 1.9 krad. (c) [ $\text{HCO}_2^-$ ] = 0.1 M,  $\text{N}_2\text{O}$  saturated; initial spectrum at pH 7.4, dose/pulse = 3.0 krad.

(5–12).  $T_3$  decayed slowly ( $\tau \sim 10$  sec) yielding a nonabsorbing solution ( $\lambda > 300$  nm); the kinetics of the decay of  $T_3$  could not be established due to its weak absorbance and exceedingly slow decay.

The 420-nm absorption band has been attributed to the addition of  $e_{aq}^-$  to a disulfide linkage resulting in the formation of the  $(-SS)^-$  radical.<sup>2</sup> We concur with this proposal but we wish to point out that neither the results reported here nor those from previous studies can establish which of the four disulfide linkages in the molecule is specifically involved. In fact, addition of  $e_{aq}^-$  may or may not occur statistically among the disulfide groups. Since there are many alternate sites at which  $e_{aq}^-$  can react, it is not necessary for the added electron to eventually reside at the disulfide linkage. Although  $\epsilon_{420}$  for the  $(-SS)^-$  radical has been shown to be somewhat dependent upon the molecular environment near the group,<sup>6</sup> the value for cystamine ( $\epsilon_{420}$   $9.0 \times 10^3$  M<sup>-1</sup> cm<sup>-1</sup>) can be taken as being representative of the absorptivity of the disulfide radical anion. The apparent  $\epsilon$  value for  $T_1$  can be interpreted<sup>22</sup> as demonstrating that the added electron can reside on other functional groups as well and that only ~62% of  $e_{aq}^-$  are actually localized on a disulfide group. In this regard, the absorption envelope of  $T_1$  shows a stronger absorption in the 300–500-nm region than exhibited by  $(-SS)^-$  from the simpler disulfides. Again, this could be the result of the environment of the radical within the molecule. However, electron adducts to aromatic, heterocyclic, and peptide systems show absorption in that spectral region<sup>23–26</sup> and could be the contributing factors. It should be noted that under the conditions of the experiment, the spectrum of the H atom adduct, which could also derive from multiple sites of attack involving aromatic, peptide, and disulfide groups, would not contribute significantly to the spectrum of  $T_1$ .

The spectrum of  $T_2$  is virtually identical with that of  $T_1$

except for its lower apparent absorptivity. The ratio of the absorbances of  $T_1$  and  $T_2$  is ~1.6 in the range 310–500 nm. Thus,  $T_2$  can be identified as arising also from electron addition to the disulfide linkage but the question of whether  $T_2$  arises from the decay of  $T_1$  or is generated independently of  $T_1$  in the initial  $e_{aq}^-$  reaction cannot be resolved. It is possible that intramolecular electron transfer from a  $(-SS)^-$  radical (or other radical site) to another disulfide linkage in the molecule occurs. Such intramolecular processes involving electron or hydrogen atom transfer have been suggested for other proteins.<sup>27</sup> Alternatively, initial electron addition occurs at various disulfide sites which have different intrinsic lifetimes. We have shown<sup>6</sup> that the kinetics of the decay of  $(-SS)^-$  are strongly dependent on the molecular environment of the radical; the unimolecular cleavage of the S–S bond in aliphatic disulfides is in contrast to the bimolecular decay of the radical in cyclic lipoic acid.

The origin of the absorption spectrum of  $T_3$  is less clear.  $T_3$  may be a radical derived from the decay of  $T_2$  or formed in the initial electron attack, or may be a radical (or non-radical) species involved in the change of the structure of the enzyme.

The reaction of  $e_{aq}^-$  with the other disulfide-containing enzymes (pepsin, trypsin,  $\alpha$ -chymotrypsin, papain, and ribonuclease A) in neutral solution generated the same general transient spectra as did lysozyme with  $\lambda_{max}$  420 nm. From the intensity of the 420-nm absorbance in comparison with that from the  $e_{aq}^-$ -cystamine reaction, the apparent percent of  $e_{aq}^-$  that generates the  $(-SS)^-$  radical in these enzymes was calculated. The values of 27, 56, 40, 19, and 12% for pepsin, trypsin,  $\alpha$ -chymotrypsin, papain, and ribonuclease A, respectively, compare favorably with those values obtained by other workers.<sup>21,22,28</sup> Furthermore, in modestly acidic *tert*-butyl alcohol solution (pH ~ 2), where H atoms are the predominant reactive species, these other enzymes gave a broad absorption with  $\lambda_{max}$  320 nm not unlike that shown by lysozyme. The apparent values of  $\epsilon_{320}$  are  $2.0 \times 10^3$ ,  $2.9 \times 10^3$ ,  $1.5 \times 10^3$ , and  $1.5 \times 10^3$  M<sup>-1</sup> cm<sup>-1</sup> for trypsin,  $\alpha$ -chymotrypsin, papain, and ribonuclease A, respectively. Finally, the initial electron adduct to these enzymes, designated as  $T_1$ , decayed within a millisecond to reveal a secondary absorption ( $T_2$ ) also centered around 420 nm. In the case of lysozyme  $T_1/T_2 \sim 1.6$ . For other enzymes, the ratio is 3.2, 3.6, 3.7, and 4.3 for papain,  $\alpha$ -chymotrypsin, trypsin, and pepsin, respectively.

One can see that although the individual enzymes have somewhat differing spectral and kinetics characteristics with regard to the radiation-generated intermediates, their general overall behavior is quite similar, no doubt arising from their common disulfide linkage.

**Reaction of Lysozyme with  $\text{CO}_2^-$ . Absorption Spectrum and Rate Constants.** The reaction of lysozyme with  $\text{CO}_2^-$ , generated in  $\text{N}_2\text{O}$ -saturated solutions containing  $\text{HCO}_2^-$ , produced the absorption spectrum shown in Figure 3c with  $\lambda_{max}$  420 nm (apparent  $\epsilon_{420}$   $3.6 \times 10^3$  M<sup>-1</sup> cm<sup>-1</sup>). Through the monitoring of the formation of this absorption band, the rate constant for the reaction of  $\text{CO}_2^-$  with lysozyme was evaluated (Figure 4). The values of  $k(\text{CO}_2^- + \text{lys})$  show many characteristics similar to those of  $k(e_{aq}^- + \text{lys})$ : pH dependence, ionic strength dependence, and effect of [lysozyme]. Again these effects can be rationalized in terms of the charges on the reacting species and the apparent dimerization of the enzyme at high ionic strengths. The values of  $k(\text{CO}_2^- + \text{lys})$  are over two orders of magnitude lower

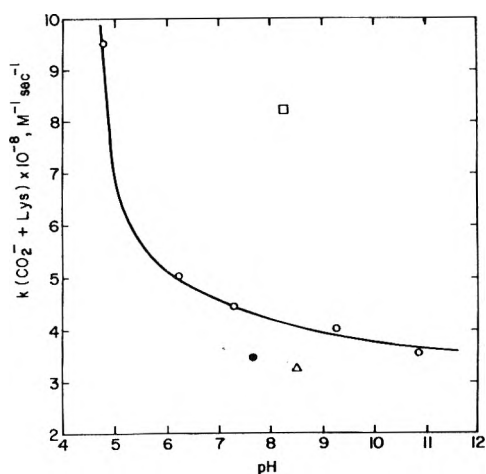


Figure 4. Dependence of  $k(\text{CO}_2^- + \text{lys})$  on pH;  $\text{N}_2\text{O}$ -saturated solutions:  $\circ$ ,  $2 \times 10^{-4} \text{ M}$  lysozyme,  $0.1 \text{ M HCO}_2^-$ ;  $\square$ ,  $2 \times 10^{-4} \text{ M}$  lysozyme,  $0.02 \text{ M HCO}_2^-$ ;  $\triangle$ ,  $2 \times 10^{-4} \text{ M}$  lysozyme,  $0.5 \text{ M HCO}_2^-$ ;  $\bullet$ ,  $5 \times 10^{-4} \text{ M}$  lysozyme,  $0.1 \text{ M HCO}_2^-$ .

than  $k(e_{\text{aq}}^- + \text{lys})$ , a fact reflecting the lower reducing ability of  $\text{CO}_2^-$  and increased structural barriers toward efficient electron transfer. It is interesting to note that no 420-nm absorption was observed from the reaction of  $(\text{CH}_3)_2\dot{\text{C}}\text{OH}$  radicals with lysozyme.

Under the conditions used to determine the transient absorption spectrum of the product of the reaction of  $\text{CO}_2^-$  with lysozyme, the bimolecular decay of  $\text{CO}_2^-$  is kinetically competitive. As a result, the spectrum shown in Figure 3c is less intense by an amount corresponding to the competitive loss of  $\text{CO}_2^-$  via the bimolecular process. Taking  $2k(\text{CO}_2^- + \text{CO}_2^-) = 1.5 \times 10^9 \text{ M}^{-1} \text{ sec}^{-1}$ ,<sup>29</sup> we estimate that ~40% of the  $\text{CO}_2^-$  radicals are lost in the combination reaction. Thus, the apparent  $\epsilon_{420}$  value for the transient becomes  $\sim 6 \times 10^3 \text{ M}^{-1} \text{ cm}^{-1}$ . This value compares very well with that of the primary absorption ( $T_1$ ) from the reaction of  $e_{\text{aq}}^-$ . The only spectral difference is seen in the 300–350-nm region where the product of the reaction of  $\text{CO}_2^-$  with lysozyme does not absorb as strongly as does  $T_1$ . In fact, the spectrum in Figure 3c resembles very closely that from the electron adduct to simple disulfides.<sup>6</sup> Apparently, the reaction with  $\text{CO}_2^-$  results in the formation of  $(-\text{SS}-)^-$  radicals to the same extent as the reaction with  $e_{\text{aq}}^-$ , albeit at a lower rate and without the added absorption in the ultraviolet.  $\text{CO}_2^-$  radicals have been considered<sup>30</sup> to be more selective in their reaction with lysozyme than are  $e_{\text{aq}}^-$  so that the distribution of radicals among the disulfide linkages or other functional groups may be different than that from  $e_{\text{aq}}^-$ . However, it appears that the total extent of formation of  $(-\text{SS}-)^-$  is the same from the two reducing agents.

The initially generated transient absorption does show some decay in the order of tenths of milliseconds resulting in a nearly identical residual absorption. The magnitude of the decay is very small owing to the fact that the  $\text{CO}_2^-$ -lysozyme reaction occurs in the same time range so that formation of the 420-nm absorption and its slight decay are almost superimposed. The decay of the secondary absorption resulted in a solution that showed no absorption in the 400-nm region.

**Kinetics of the Decay of the Intermediates. Initial Transient.**  $T_1$ , generated from the  $e_{\text{aq}}^-$ -lysozyme reaction in the presence or absence of *tert*-butyl alcohol, decayed via first-order kinetics with a pH-independent (5–10) rate constant of  $\sim 1 \times 10^4 \text{ sec}^{-1}$ . The relatively small absorbance

TABLE I: Second-Order Rate Constants for the Reaction of the One-Electron Reduced Lysozyme Radical in the Presence of Various Solutes

Solute	pH	$k$ , $\text{M}^{-1} \text{ sec}^{-1}$ <sup>a</sup>	
$\text{O}_2$	5.1	$2.7 \times 10^8$	
	Indigotetrasulfonate	5.1–7.4	$6.5 \times 10^8$
		8.9	$5.5 \times 10^8$
		9.8	$4.5 \times 10^8$
	11.0	$1.9 \times 10^8$	
$\text{H}_2\text{PO}_4^-$	4.9	$1.9 \times 10^2$	
	$\text{HPO}_4^{2-}$	10.0	$1.0 \times 10^3$
Glycine	6.2	$2.2 \times 10^2$	
	11–12	$2.6 \times 10^2$	
<i>tert</i> -Butyl alcohol	4.9	4.5	
$\text{HCO}_2^-$	5.0	$4.6 \times 10^4$	
	6.0	$6.0 \times 10^3$	
	6.4	$3.1 \times 10^3$	
	7.0	$6.8 \times 10^2$	
	8.0	$7.6 \times 10^1$	
	9–12	$1.6 \times 10^1$	

<sup>a</sup> Decay of  $(-\text{SS}-)^-$  monitored at 420 nm.

changes resulting from the decay of  $T_2$  did not permit a more precise determination of the value of  $k$ . However, it could be seen that  $k$  was independent of the presence of other added solutes such as phosphate, formate, glycine, acetate, and NaCl. Above pH 10, the rate of decay of  $T_1$  was perceptibly slower with  $k$  diminishing by about a factor of 2.

The initial transient decayed rapidly in the presence of  $\text{O}_2$  yielding a nonabsorbing solution in the 420-nm region. In an experiment conducted at pH 5.1 with  $5 \times 10^{-4} \text{ M}$  lysozyme in an air- ( $[\text{O}_2] = 2.5 \times 10^{-4} \text{ M}$ ) or  $\text{O}_2$ -saturated ( $[\text{O}_2] = 1.3 \times 10^{-3} \text{ M}$ ) solution, the rate of reaction of  $e_{\text{aq}}^-$  with lysozyme ( $k \geq 1.4 \times 10^{11} \text{ M}^{-1} \text{ sec}^{-1}$ ) is greater than that of  $e_{\text{aq}}^-$  with  $\text{O}_2$  ( $k = 1.9 \times 10^{10} \text{ M}^{-1} \text{ sec}^{-1}$ ).<sup>11</sup> Virtually the full absorption of  $T_1$  was generated which then decayed completely via pseudo-first-order kinetics with a rate that was almost an order of magnitude faster than the natural decay of  $T_1$  into  $T_2$ . The conclusion is reached that  $T_1$  reacts with  $\text{O}_2$  with a rate constant of  $2.7 \times 10^8 \text{ M}^{-1} \text{ sec}^{-1}$  (Table I). Whether the reaction occurs via electron transfer producing  $\text{O}_2^-$  or through  $\text{O}_2$  addition to the  $(-\text{SS}-)^-$  radical site has not been established.

$T_1$  also reacts with indigotetrasulfonate which has been shown to be an effective electron acceptor ( $E^0 = -0.046 \text{ V}$  at pH 7) reacting rapidly with reducing radicals.<sup>31</sup> In our experiments, Ar-purged neutral and alkaline solutions of  $2 \times 10^{-5} \text{ M}$  indigotetrasulfonate,  $5 \times 10^{-4} \text{ M}$  lysozyme, and  $1 \text{ M}$  *tert*-butyl alcohol were subjected to pulse radiolysis. Under these conditions, OH radicals are scavenged and all  $e_{\text{aq}}^-$  react with the lysozyme. The extent of the formation of the reduced acceptor, as monitored by its absorption maximum at 610 nm, from the reaction of indigotetrasulfonate with the reduced enzyme was identical with the formation of the reduced acceptor from the reaction of the dye with  $e_{\text{aq}}^-$  in the absence of the enzyme (all other conditions identical). The conclusion is reached that the reaction of the reduced lysozyme with the acceptor occurs quantitatively and that the standard oxidation potential of the reduced lysozyme species is more positive than +0.046 V. From the pseudo-first-order formation of the reduced acceptor, the rate constants for the electron transfer reaction as a function of pH have been evaluated (Table I). The de-

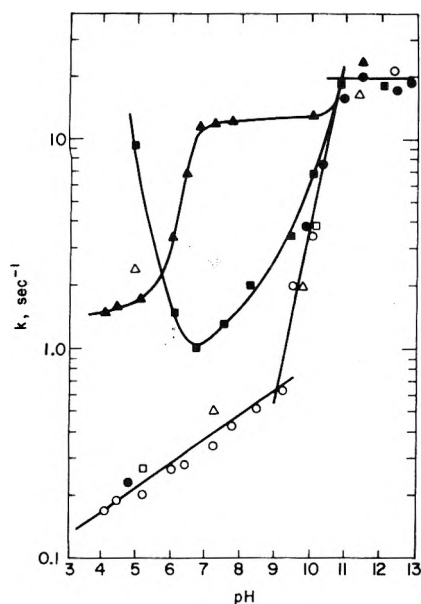


**Figure 5.** Dependence of the first-order rate constant for the decay of  $T_2$  on pH; [lysozyme] =  $1 \times 10^{-4}$  M, Ar-purged solutions,  $\lambda$  420 nm: ●, no additional solute; ○,  $1 \times 10^{-4}$  M phosphate; □,  $1 \times 10^{-2}$  M urea; ▲,  $1 \times 10^{-2}$  M phosphate; △, 0.5 M *tert*-butyl alcohol +  $1 \times 10^{-4}$  M phosphate; ■, 2 M *tert*-butyl alcohol +  $1 \times 10^{-4}$  M phosphate.

crease in  $k$  as pH is increased can be attributed to the increasingly more negative charge on the reduced lysozyme as its component amino acids are deprotonated.

**Secondary Absorbance.**  $T_2$  decayed via first-order kinetics with values of  $k$  that depended in a complex way upon pH and the presence of phosphate buffer and *tert*-butyl alcohol (Figure 5). In the absence of *tert*-butyl alcohol and a maximum of  $1 \times 10^{-4}$  M phosphate, the decay of  $T_2$  was extremely slow in acidic and neutral solution ( $k < 1 \text{ sec}^{-1}$ ), showed a 30-fold increase in  $k$  between pH 9 and 11, and reached an apparent plateau at pH >11. Urea, which causes unfolding of the enzyme at high concentrations,<sup>32</sup> had no effect at  $1 \times 10^{-2}$  M on  $k$  at pH 5.2 and 10.1.

We had shown<sup>6</sup> that the  $(-SS)^{\cdot-}$  radical produced from electron addition to aliphatic disulfides undergoes rapid protonation ( $k > 10^8 \text{ M}^{-1} \text{ sec}^{-1}$ ) causing a sharp increase in the rate of S-S bond scission in acidic solution. No such effect is seen in lysozyme; in fact, the most stable radical is seen at pH 4. Furthermore, it is not known if the mode of decay of  $T_2$  or any of the intermediates is via S-S bond scission, as has been pointed out previously.<sup>2</sup> One can only speculate that the successive deprotonation of adjacent carboxylic acid and histidine moieties enhances the apparent unimolecular decay of  $T_2$ . The rapid increase in  $k$  occurs in the pH range in which amino groups and tyrosine deprotonate.

The presence of phosphate accelerates the rate of decay of  $T_2$  while not changing its absorption spectrum. A plot of  $k$  as a function of pH for solutions containing  $1 \times 10^{-2}$  M phosphate (Figure 5) exhibits a "titration curve" with a midpoint at pH 6.2. The plateau of points at pH >7 appears to lead to the plateau at pH >11. Inasmuch as the value of  $k$  is a linear function of [phosphate] at constant pH (Figure 6), the apparent second-order rate constants  $k(\text{H}_2\text{PO}_4^- + T_2) = 1.9 \times 10^2 \text{ M}^{-1} \text{ sec}^{-1}$  at pH 4.9 and  $k(\text{HPO}_4^{2-} + T_2) = 1.0 \times 10^3 \text{ M}^{-1} \text{ sec}^{-1}$  at pH 10.0 (Table I) can be calculated. The "titration curve" in Figure 5 can be explained in terms of these values and the  $pK_a$  of

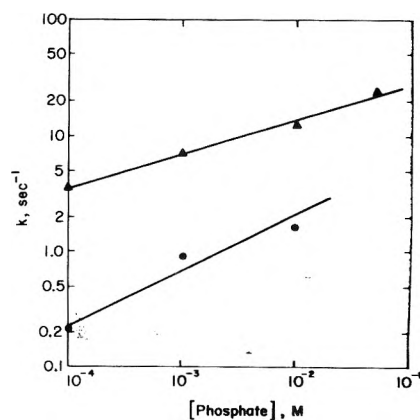


**Figure 6.** Dependence of the first-order rate constant for the decay of  $T_2$  on [phosphate]; [lysozyme] =  $1 \times 10^{-4}$  M, Ar-purged solutions,  $\lambda$  420 nm: ●, pH 4.9; ▲, pH 10.0. Each point is the average of two to three runs at different doses.

$\text{H}_2\text{PO}_4^-$  (7.2). Thus, at pH 6.2, where  $[\text{H}_2\text{PO}_4^-] = 10[\text{HPO}_4^{2-}]$ ,  $\text{rate}(\text{H}_2\text{PO}_4^- + T_2) \approx \text{rate}(\text{HPO}_4^{2-} + T_2)$ .

The mechanism of the decay of  $T_2$  in the presence of phosphate could involve a direct bimolecular reaction between  $T_2$  and phosphate or, alternatively, a slow rate-determining association of phosphate with  $T_2$  causing conformational changes that result in a very rapid unimolecular loss (say via S-S bond scission) of the  $(-SS)^{\cdot-}$  radical. Electron transfer from  $T_2$  and proton transfer from phosphate can probably be ruled out. On electrostatic grounds,  $\text{HPO}_4^{2-}$  should be more difficult to reduce than  $\text{H}_2\text{PO}_4^-$  and thus would not be expected to exhibit a higher scavenging rate constant. Similarly, the rate constant of proton transfer is generally a function of the acidity of the donor.<sup>33</sup> It is interesting to speculate that even such relatively low concentrations of phosphate could cause structural deformation in the protein radical to enhance the decay of the electron adduct.

The presence of  $\geq 0.5$  M *tert*-butyl alcohol had an effect on the rate of decay of  $T_2$  (Figure 5) which gave rise to a linear dependence of  $k$  on [*tert*-butyl alcohol] (Figure 7b). It can be seen from Figure 5 that the pseudo-first-order rate constant decreases with increasing pH up to pH 7 and the effect of the presence of the alcohol diminishes further in more basic solution. We recognize that the effect could be due to impurities in the alcohol which lead to the apparent value of  $k(\text{tert-butyl alcohol} + T_2) = 4.5 \text{ M}^{-1} \text{ sec}^{-1}$  at pH 4.9. On the other hand, the effect of the alcohol on the conformation of the protein radical must be considered; such protein-solvent interactions in native lysozyme are known.<sup>34</sup>

The presence of glycine also had an effect on the decay of  $T_2$ . Figure 7a shows that both the zwitterion and the fully protonated forms of the amino acid enhance the decay of  $T_2$  to approximately the same extent (Table I). The dependence of the pseudo-first-order rate constant for the decay of  $T_2$  on pH in the presence of 0.1 and 0.01 M glycine is shown in Figures 8a and 8b, respectively. The break in the curve in both cases occurs around pH 9 which corresponds very closely to the  $pK_a$  for the deprotonation of the  $-\text{NH}_3^+$  group of glycine. On the other hand, 0.01 M NaCl also shows a pH dependence of the rate constant for the decay of  $T_2$  (Figure 8b) although 0.1 M NaCl produces a totally different behavior (Figure 8a). Coordination of the solute to the enzyme radical through ion-pair interactions or modification of the enzyme radical conformation through

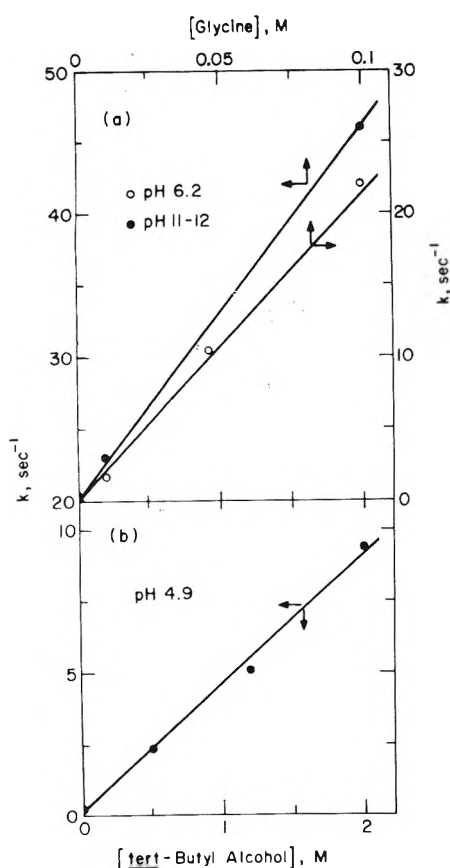


**Figure 7.** Dependence of the first-order rate constant for the decay of  $T_2$  on (a) [glycine] and (b) [tert-butyl alcohol]: [lysozyme] =  $1 \times 10^{-4}$  M, Ar-purged solutions,  $\lambda$  420 nm.

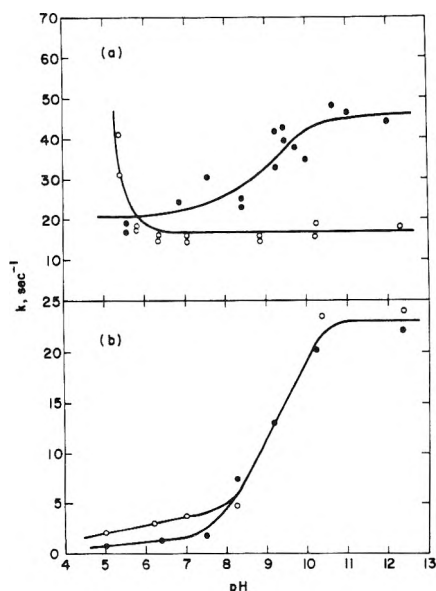


**Figure 8.** Dependence of the first-order rate constant for the decay of  $T_2$  on pH in the presence of glycine and NaCl; [lysozyme] =  $1 \times 10^{-4}$  M, [phosphate] =  $1 \times 10^{-4}$  M, Ar-purged solutions,  $\lambda$  420 nm: (a) O, 0.1 M NaCl; ●, 0.1 M glycine; (b) O, 0.01 M NaCl; ●, 0.01 M glycine.

direct interaction or through solvent structural transformation remain possibilities to explain these effects.

The presence of  $\text{HCO}_2^-$  had a very strong effect on the decay of the intermediate (Figure 9). In mildly acidic and neutral solution, a plot of  $\log k$  vs. pH was linear with a

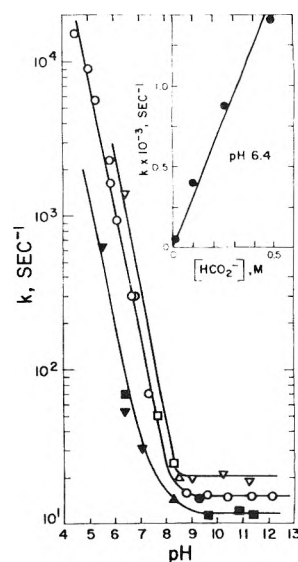


**Figure 9.** Dependence of the first-order rate constant for the decay of  $T_2$  on pH in the presence of  $\text{HCO}_2^-$ ;  $\text{N}_2\text{O}$ -saturated unless otherwise noted,  $\lambda$  420 nm: O,  $1 \times 10^{-4}$  M lysozyme, 0.1 M  $\text{HCO}_2^-$ ; ●,  $2 \times 10^{-4}$  M lysozyme, 0.1 M  $\text{HCO}_2^-$ ; △,  $2 \times 10^{-4}$  M lysozyme, 0.5 M  $\text{HCO}_2^-$ ; □,  $5 \times 10^{-4}$  M lysozyme, 0.5 M  $\text{HCO}_2^-$ ; ▽,  $1 \times 10^{-4}$  M lysozyme, 0.5 M  $\text{HCO}_2^-$ ; ▲,  $2 \times 10^{-4}$  M lysozyme, 0.02 M  $\text{HCO}_2^-$ ; ■,  $1 \times 10^{-4}$  M lysozyme, 0.02 M  $\text{HCO}_2^-$ ; ▽,  $1 \times 10^{-4}$  M lysozyme, 0.02 M  $\text{HCO}_2^-$ , 1 M *tert*-butyl alcohol, Ar purged. Insert shows the dependence of  $k$  on  $[\text{HCO}_2^-]$  at pH 6.4.

family of lines generated as a function of  $[\text{HCO}_2^-]$ . It should be noted that this particular behavior was not restricted to the intermediate arising from the reaction of  $\text{CO}_2^-$  with lysozyme. In the presence of 0.02 M  $\text{HCO}_2^-$  and 1 M *tert*-butyl alcohol, the reactive reducing radical in Ar-purged solution is mainly  $e_{\text{aq}}^-$ , yet the value of  $k$  correlated well with systems in which  $\text{CO}_2^-$  was generated in 0.02 M  $\text{HCO}_2^-$  solutions that were  $\text{N}_2\text{O}$  saturated. The effect must therefore be specific for the interaction of reduced lysozyme with  $\text{HCO}_2^-$ . The value of the observed rate constant is clearly a function of both  $[\text{H}^+]$  and  $[\text{HCO}_2^-]$  and  $k(\text{HCO}_2^- + T_2)$  values are given in Table I at fixed solution acidity. The tabulated values of  $k$  are nearly linearly dependent on  $[\text{H}^+]$  indicating that the decay step most probably involves protonation. From plots of the observed rate constants as a function of  $[\text{H}^+]$  at constant  $[\text{HCO}_2^-]$ , we obtain a value of  $1 \times 10^9 \text{ M}^{-1} \text{ sec}^{-1}$  for the apparent specific rate of protonation which is quite independent of  $[\text{HCO}_2^-]$ . These results provide a good indication that  $\text{HCO}_2^-$  associates with the reduced lysozyme possibly causing conformational changes which enhance the rate of S-S bond scission. They also clearly indicate that the effect of added solute is very specific.

## Conclusions

The reaction of  $e_{\text{aq}}^-$  with lysozyme occurs at a diffusion-controlled rate with a value of  $k$  that is dependent upon pH in a way that reflects the continuous deprotonation of acidic groups on the molecule as the pH is increased. The dependence of  $k(e_{\text{aq}}^- + \text{lys})$  on ionic strength suggests that the interaction of  $e_{\text{aq}}^-$  with the enzyme over the large molecular diameters involved may be a matter of the overall charges of the reacting species rather than perturbations due to the high surface charge on the macromolecule. The reaction of  $\text{CO}_2^-$  with lysozyme seems to follow the same general rules. The reduced enzyme has the free-radical site mainly localized on the disulfide linkages although other



sites in the molecule also appear to be involved. Intramolecular electron transfer may be an important mechanistic pathway. The decay kinetics of the transients observed, although mainly first order, are dependent in a complex way on the solution environment. Even the presence of modest concentrations of solutes (phosphate buffer, formate, NaCl, for example) has a marked effect on the observed value of  $k$ . Future investigators of the decay kinetics of radicals derived from the one-electron reduction and oxidation of macromolecules are cautioned to control the nature of the reaction medium and recognize the range of possible interactions between the radical and its environment.

## References and Notes

- (1) Presented in part at the Fifth International Congress of Radiation Research, Seattle, Wash., July 1974.
- (2) G. E. Adams, R. L. Willson, J. E. Aldrich, and R. B. Cundall, *Int. J. Radiat. Biol.*, **16**, 333 (1969).
- (3) G. E. Adams, G. S. McNaughton, and B. D. Michael, "The Chemistry of Ionization and Excitation", G. R. A. Johnson and G. Scholes, Ed., Taylor and Francis, London, 1967.
- (4) G. E. Adams, R. B. Cundall, and R. L. Willson, "Chemical Reactivity and Biological Role of Functional Groups in Enzymes", R. M. S. Smellie, Ed., Academic Press, London, 1970.
- (5) J. E. Aldrich and R. B. Cundall, *Int. J. Radiat. Biol.*, **16**, 343 (1969).
- (6) M. Z. Hoffman and E. Hayon, *J. Am. Chem. Soc.*, **94**, 7950 (1972).
- (7) C. C. F. Blake, D. F. Koenig, G. A. Mair, A. C. T. North, D. C. Phillips, and V. R. Sarma, *Nature (London)*, **206**, 757 (1965).
- (8) P. H. von Hippel and T. Schleich, *Acc. Chem. Res.*, **2**, 257 (1969).
- (9) M. Simic, P. Neta, and E. Hayon, *J. Phys. Chem.*, **73**, 3794 (1969).
- (10) L. M. Dorfman and G. E. Adams, *Natl. Stand. Ref. Data Ser., Nat. Bur. Stand.*, **No. 46** (1973).
- (11) M. Anbar, M. Bambenek, and A. B. Ross, *Natl. Stand. Ref. Data Ser., Nat. Bur. Stand.*, **No. 43** (1972).
- (12) P. Neta, *Chem. Rev.*, **72**, 533 (1972).
- (13) K. Brew, J. T. Canaman, and R. L. Hill, *J. Biol. Chem.*, **242**, 3747 (1967).
- (14) R. Braams, *Radiat. Res.*, **31**, 8 (1967).
- (15) R. Roxby and C. Tanford, *Biochemistry*, **10**, 3348 (1971).
- (16) C. Tanford, *Adv. Protein Chem.*, **23**, 121 (1968).
- (17) E. J. Hart and M. Anbar, "The Hydrated Electron", Wiley-Interscience, New York, N.Y., 1970.
- (18) A. J. Sophianopoulos, C. K. Rhodes, D. N. Holcomb, and K. E. Van Holde, *J. Biol. Chem.*, **237**, 1107 (1962).
- (19) S. W. Benson, "The Foundations of Chemical Kinetics", McGraw-Hill, New York, N.Y., 1960, p 525.
- (20) A. J. Sophianopoulos and K. E. Van Holde, *J. Biol. Chem.*, **239**, 2516 (1964).
- (21) T. Masuda, J. Ovadia, and L. I. Grossweiner, *Int. J. Radiat. Biol.*, **20**, 447 (1971).
- (22) G. E. Adams, J. L. Redpath, R. H. Bisby, and R. B. Cundall, *Isr. J. Chem.*, **10**, 1079 (1972).
- (23) R. C. Armstrong and A. J. Swallow, *Radiat. Res.*, **40**, 563 (1969).
- (24) M. Simic, P. Neta, and E. Hayon, *J. Am. Chem. Soc.*, **92**, 4763 (1970); P. S. Rao and E. Hayon, *J. Phys. Chem.*, **78**, 1193 (1974).
- (25) J. Feitelson and E. Hayon, *J. Phys. Chem.*, **77**, 10 (1973).
- (26) J. P. Mittal and E. Hayon, *J. Phys. Chem.*, **78**, 1790 (1974).
- (27) N. N. Lichtin, J. Ogdan, and G. Stein, *Biochim. Biophys. Acta*, **263**, 14 (1972); **276**, 124 (1972).
- (28) J. R. Clement, D. A. Armstrong, N. V. Klassen, and H. A. Gillis, *Can. J. Chem.*, **50**, 2833 (1972).
- (29) P. Neta, M. Simic, and E. Hayon, *J. Phys. Chem.*, **73**, 4207 (1969).
- (30) G. E. Adams in "Advances in Radiation Chemistry", Vol. 3, M. Burton and J. L. Magee, Ed., Wiley-Interscience, New York, N.Y., 1972, p 125.
- (31) P. S. Rao and E. Hayon, *J. Phys. Chem.*, **77**, 2753 (1973).
- (32) J. H. Bradbury and N. L. R. King, *Nature (London)*, **223**, 1154 (1969).
- (33) M. Eigen, *Angew. Chem., Intl. Ed., Engl.*, **3**, 1 (1964).
- (34) S. N. Timasheff, *Acc. Chem. Res.*, **3**, 62 (1970).

## Solvent and Temperature Effects on the Fluorescence of *all-trans*-1,6-Diphenyl-1,3,5-hexatriene

E. D. Cehelnik, R. B. Cundall,\* J. R. Lockwood, and T. F. Palmer

Department of Chemistry, The University, Nottingham NG7 2RD, England (Received December 26, 1974)

Fluorescence yields and lifetimes of *all-trans*-1,6-diphenyl-1,3,5-hexatriene have been measured over a range of temperatures in a number of different solvents. Fluorescence lifetimes increase with decrease of solvent polarity and above room temperature do not change markedly. Fluorescence efficiencies are high in nonpolar solvents and tend to unity at low temperatures. This behavior is explained by a mechanism which requires the lifetimes to be associated with configuration changes of the excited state, which are solvent dependent. In the polar solvents, ethanol and acetonitrile, there is evidence for a temperature-dependent solvent-induced radiationless transition which competes with fluorescence.

## Introduction

The influence of solvent environment on the molecular configuration of excited states and the consequent effect on the various primary processes is an important aspect of photochemistry which requires detailed study. Most of the published work has been concerned with the fluorescence properties of planar chromophores in which there is an approximate mirror image relationship between the fluorescence spectrum and the first absorption band. Under these conditions the value of  $q/\tau$ , where  $q$  and  $\tau$  are the fluorescence efficiency and measured decay time, provides a quantitative measure of the probability of emission from

the first excited singlet state. The radiative probability can, when the essential planarity of the chromophore is unchanged on excitation, compare closely with theoretical values calculated from the expressions due to Förster,<sup>1</sup> Strickler and Berg,<sup>2</sup> or Birks and Dyson,<sup>3</sup> which purport to relate the emission and absorption properties. Fluorescence yields and decay times usually decrease with increasing temperature due to enhancement of the probability for internal conversion and intersystem crossing to the triplet manifold. A combination of the appropriate quantum yields with the measured decay times allows the effect of both temperature and solvent on the different primary pro-

cesses to be examined. A more complex situation arises when there is a change in configuration between the lower vibrational levels of the ground and excited states. Changes in molecular geometry may become rate determining and the relative effects of fluorescence, intersystem crossing, and internal conversion processes can be affected. Berlman<sup>4</sup> has formulated a number of principles which give some indications of the expected correlations between the absorption and fluorescence properties for differing nuclear configurations. Differences in molecular geometry between electronic states can be as significant as other photophysical processes such as fluorescence, intersystem crossing, and internal conversion, for influencing the photochemical properties of some molecules.

The ring-polyene systems, which include as an example the well-known scintillator 1,6-diphenyl-1,3,5-hexatriene,<sup>5</sup> are instances of  $\pi$  bonded molecules in which photochemical excitation is expected to be followed by a rapid and marked change in configuration due to twisting around the carbon-carbon bonds of the polyene chain.<sup>6</sup> This is manifested by both the luminescence properties<sup>7-10</sup> and the geometrical isomerization effects of the type extensively studied in the case of stilbene derivatives.<sup>11,12</sup> Berlman<sup>4</sup> has suggested that the fluorescence properties of DPH are anomalous due to twisting of the excited state, but a detailed examination of temperature and solvent effects is necessary for the understanding of environmental influences on the change of shape which follows excitation and the consequent effects on radiative and nonradiative processes. This has been attempted in our investigation.

## Experimental Section

**Materials.** *all-trans*-1,6-Diphenyl-1,3,5-hexatriene (DPH, Koch-Light scintillation grade) was found to be pure, as previously reported.<sup>13</sup> Methylcyclohexane (Koch-Light puriss), heptane (BDH), and 3-methylpentane (Koch-Light) were purified using the methods described by Cundall and Pereira.<sup>14</sup> Benzene (Merck Spectrograde) was treated with concentrated sulfuric acid and washed with sodium carbonate solution. The sample was washed with distilled water, dried with magnesium sulfate, and subjected to fractional distillation, only the middle fraction being retained. Hexane (Hopkins and Williams Spectrosol) was used without further purification. Ethyl iodide (Koch-Light puriss) was distilled under vacuum. Perfluoro-*n*-hexane (Fluorochem) was treated with nitrating acid, washed with alkali and water, and dried over phosphorus pentoxide. The middle fraction from a vacuum distillation was retained. Acetonitrile (Koch-Light puriss) was purified as reported by Coetzee et al.<sup>15</sup> Ethanol (BDH Spectrograde) was fractionated from sodium hydroxide pellets in a continuous stream of nitrogen. 1,4-Dioxane (BDH Spectrograde) was distilled under vacuum. Solvent purity was checked in all cases by absorption and fluorescence spectroscopy under conditions of high sensitivity.

**Techniques.** In both the steady state and pulse excitation experiments on solutions at room temperature and above, the samples were contained in 1-cm square cross-section Spectrosil cuvettes. The cells were fitted with grease free taps and the solutions were purged with nitrogen and sealed before use. All solutions were freshly prepared before each experiment in 10-ml graduated flasks and diluted to the required concentrations ( $\approx 10^{-5}$  M). For the low temperature studies the solutions were sealed

under vacuum after repeated freeze-pump-thaw cycles in 1-cm diameter cylindrical ampoules.

Fluorescence decay measurements were made by using the single photon counting technique.<sup>16</sup> A detailed description of the apparatus is to be presented elsewhere.<sup>17</sup> A gated (20 kHz) nanosecond flash lamp filled with 350 Torr of hydrogen provided an instrumental response function of 1.7 nsec (full-width at half-maximum). Emission was viewed at 90° to the direction of excitation and in most cases the fluorescence was isolated with a Wratten 47B filter. For the experiments in which the decay time was measured as a function of emission wavelength a Bausch and Lomb high intensity monochromator with a 10-nm band pass was used in place of the Wratten filter. A grating monochromator (Rank Precision D330) was used to isolate a 2-nm bandpass for excitation, which was usually at 360 nm. Lifetimes greater than 10 nsec were analyzed by plotting on a semilogarithmic scale. A straight line computer analysis was used to give the best least-squares fit assuming a single exponential decay function. Lifetimes shorter than 10 nsec required the use of an iterative computation procedure to extract the lifetime.

Fluorescence spectra and quantum yields were measured using an improved version of a fully corrected spectrofluorimeter originally described by Cundall and Evans.<sup>18</sup> Absorption spectra were determined with a Pye-Unicam SP1800 spectrophotometer. Temperature control was achieved with an electrically heated aluminum block above room temperature and with an Oxford Instruments CF 103 cryostat (liquid N<sub>2</sub> flow) for experiments below room temperature. Quantum yields at room temperature were determined relative to a convenient standard by comparison of the integrated emission spectra. Measured emission intensities were multiplied by the square of the refractive index of the solvent in the wavelength region of the fluorescence emission before the comparison, as suggested by Parker.<sup>19</sup> The low concentrations of solute used made corrections for self absorption of fluorescence unnecessary. Quantum yields for a particular sample at different temperatures were determined relative to the room temperature yield. The true quantum yield  $\phi_F(T)$  at a temperature  $T$  is given by

$$\phi_F(T) = \frac{\phi_F^0 D_0 n^2(T) \int_0^\infty F(\nu, T) d\nu}{D(T) n_0^2 \int_0^\infty F_0(\nu) d\nu}$$

where  $\phi_F^0$  is the room temperature quantum yield at 25°.  $F(\nu, T)$  is the corrected fluorescence spectrum in relative quanta per unit wavelength at temperature  $T$  and  $F_0(\nu)$  is that for the spectrum at 25°.  $D(T)$  is the optical density at temperature  $T$  and  $D_0$  the ambient value.  $n^2(T)$  is the square of the refractive index at  $T$  and  $n_0^2$  the corresponding value at 25°. Variations in the refractive index with temperature were calculated as suggested by Mantulin and Huber<sup>20</sup> from values of solvent density and refractive index given in International Critical Tables.

## Results

Figure 1 shows the absorption spectra of the lowest energy transitions of *all-trans*-DPH in several solvents at 26°. The spectra are similar in general shape and consist of a series of overlapping bands giving rise to a region of continuous absorption between approximately 300 and 400 nm. A solvent shift is apparent in the wavelength maxima of the

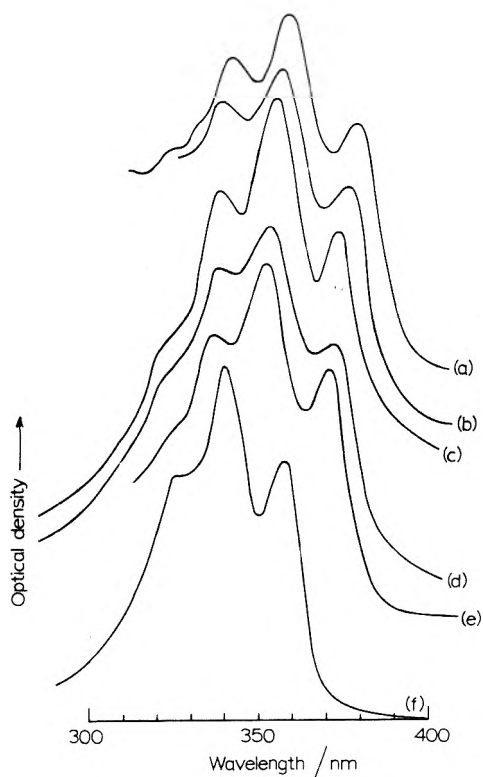


**Figure 1.** Absorption spectra of DPH in (a) benzene, (b) 1,4-dioxane, (c) methylcyclohexane, (d) 3-methylpentane, (e) acetonitrile, and (f) perfluoro-*n*-hexane.

various bands. In most solvents at room temperature the shift is small, for example, the wavelength of the maxima of the most intense band lies at  $354 \pm 2$  nm for the solvents methylcyclohexane, 3-methylpentane, acetonitrile, hexane, and heptane. In dioxane and benzene there are slightly larger shifts to the red with the maximum of the same band being at 358 and 361 nm, respectively. In perfluoro-*n*-hexane solutions the spectrum is shifted considerably to high frequency, the maximum of the most intense band occurring at 341 nm. The typical effect of temperature on the absorption spectra in different solvents is exemplified by the results for methylcyclohexane shown in Figure 2.

Fully compensated fluorescence excitation spectra of optically dilute ( $OD \approx 0.1$ ) solutions of DPH in 3-methylpentane, acetonitrile, and perfluoro-*n*-hexane at room temperature (Figure 3) are virtually identical in shape with the corresponding absorption spectra, the band maxima being located in the same position for each solvent. The results show that as the temperature is lowered each band in both the absorption and excitation spectra increases in peak intensity and the band maxima shift to lower frequencies. The relative intensities of the different maxima in the spectrum change in some, but not all, solvents.

Fluorescence spectra do not show a close mirror image relationship to absorption or excitation spectra. The fluorescence spectra are broad but show some structure and consist of a series of overlapping bands giving rise to an emission extending from just below 400 nm to slightly beyond 600 nm. The relative intensities of the bands vary with solvent but a distinct solvent shift is not apparent. Figure 4 compares the fluorescence spectrum of DPH in methylcyclohexane with the spectra in a number of other solvents. The fluorescence spectra, although similar, cannot be superimposed. The differences in the spectra appear

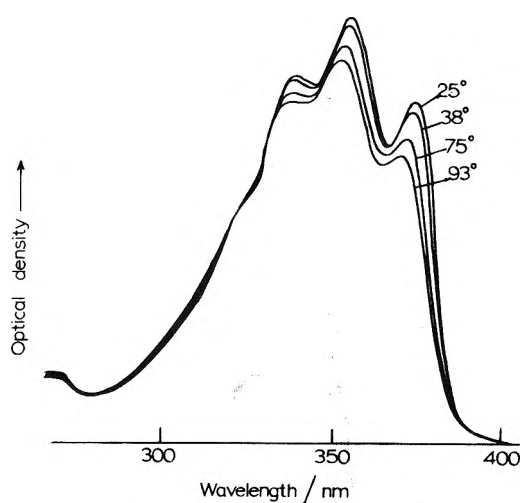


**Figure 2.** Effect of temperature on the absorption spectrum of DPH in methylcyclohexane.

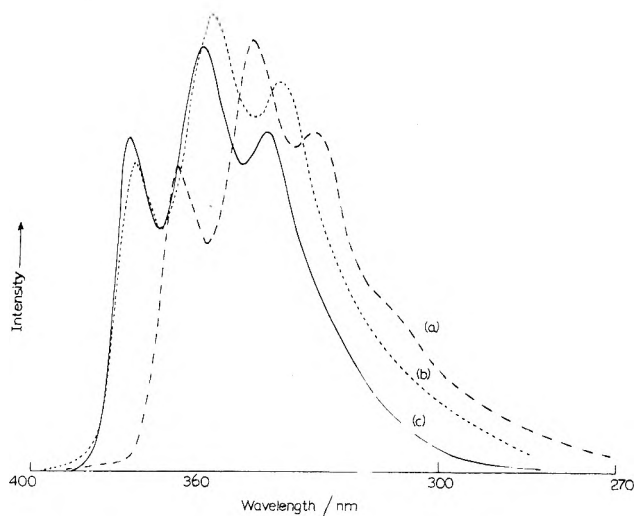


**Figure 3.** Excitation spectra of DPH in (a) perfluoro-*n*-hexane, (b) acetonitrile, and (c) methylcyclohexane, at 25° (emission wavelength 420 nm).

to be due to small changes in the relative intensities of the bands rather than being due to solvent shift effects.

At 77 K the excitation spectrum of DPH in 3-methylpentane glass (Figure 5) shows enhanced resolution and more structure is apparent. The maxima of the bands are shifted to lower frequencies and the relative intensities changed compared to the room temperature results. Fluorescence spectra of DPH in 3-methylpentane glass at 77 K (Figure 5) also show enhanced resolution compared to room temperature but no changes in the wavelengths of the band maxima can be observed.

Fluorescence yields in all solvents were measured by comparison with the emission spectra of DPH in methylcyclohexane at 25° using optical densities  $< 0.1$ . The value of 0.65 for the quantum yield,  $\phi_F$ , for DPH in methylcyclohexane at 25° was measured relative to a value of 0.83 for 9,10-diphenylanthracene in cyclohexane.<sup>21,22</sup> Quantum yields were found to be independent of excitation wavelength in all solvents at any particular temperature. Only in ethanol was evidence found for appreciable photochemical reaction within the time of measurement of the fluorescence quantum yields. Quantum yield measurements in

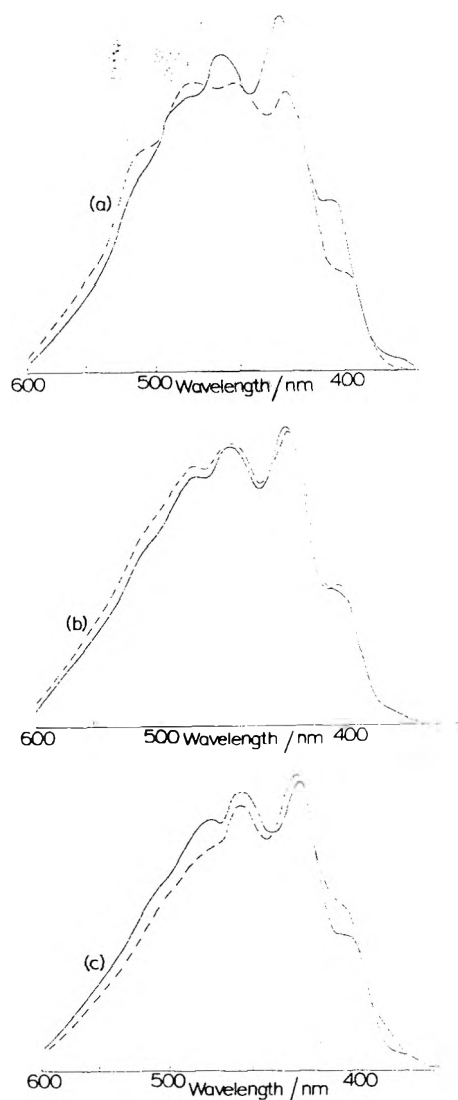


Figure 4. Comparison of the fluorescence spectrum of DPH in methylcyclohexane (solid line) with fluorescence spectra of DPH in (a) perfluoro-*n*-hexane, (b) acetonitrile, and (c) benzene.

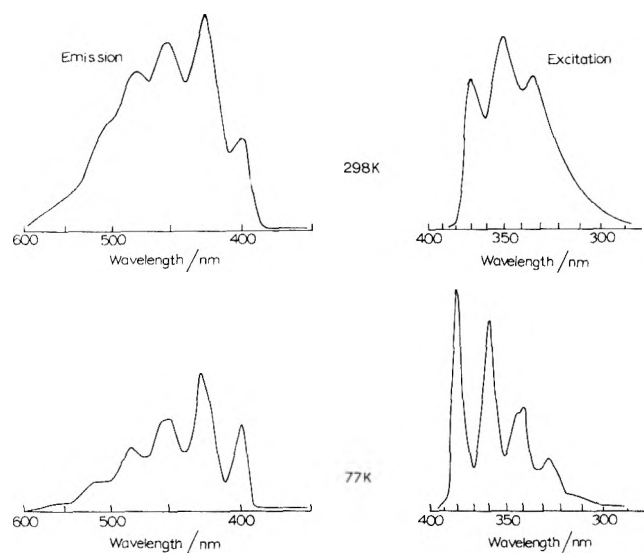


Figure 5. Effect of temperature on the excitation and emission spectra of DPH in 3-methylpentane.

ethanol were therefore obtained using fresh solutions for each measurement and the minimum exposure time.

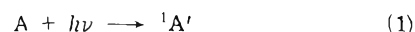
Table I shows the effect of temperature on the quantum yield and decay time for DPH in various solvents. The yields decrease with increasing temperature in all solvents, most markedly so in the polar solvents ethanol and acetonitrile. The fluorescence yields of DPH in nonpolar solvents are high and decrease slowly with increasing temperature. At low temperatures the values of  $\phi_F$  increase toward unity in the three solvents studied and achieve, within the limits of experimental error, this value in 3-methylpentane.  $\phi_F$  values are high in polar solvents also at low temperatures.

The fluorescence decay times vary with solvent. Except for ethanol and acetonitrile the decay time is constant for a given solvent at all temperatures above ambient. Unlike the other solvents investigated the fluorescence decay times in acetonitrile and ethanol decrease with increasing temperature in a manner similar to the effect on  $\phi_F$  in these solvents. Below approximately  $-30^\circ$  the decay times for DPH in 3-methylpentane and methylcyclohexane decrease and become nonexponential at temperatures below  $-110^\circ$ . In acetonitrile the fluorescence decay kinetics show evidence of nonexponential behavior below about  $0^\circ$ . The very low light levels used in the single photon counting method caused negligible photochemical reaction, even in the ethanol solutions.

The fluorescence decay time of DPH in methylcyclohexane is independent of excitation wavelength above ambient temperature and does not depend upon the emission wavelength between 395 and 550 nm.

## Discussion

**Mechanism.** The extinction coefficient for solutions of DPH in all the solvents studied is large ( $\epsilon_{\max} \approx 8 \times 10^4 M^{-1} \text{ cm}^{-1}$ ) over practically all the wavelength range in which light absorption occurs and excitation results from various allowed  $\pi-\pi^*$  transitions.<sup>23</sup> The long fluorescent lifetimes which depend upon solvent are not consistent with the emission arising from straight forward reversal of the absorption process following vibrational deactivation. The bathochromic shift observed in the position of the absorption spectrum in solvents of increasing polarizability is similar to that noted for stilbene and derivatives<sup>11</sup> and is satisfactorily explained by an increase in molecular polarizability when the solute molecule is excited.<sup>24</sup> Absorption of light by a molecule of DPH



results in an excited state possessing vibrational energy to an extent which depends upon excitation wavelength and which will, initially, have surrounding solvent molecules in a configuration appropriate to the ground state. Equilibration of vibrational energy occurs rapidly compared with the probability of emission and the independence of the fluorescence on exciting wavelength, over the experimentally studied range, shows that internal conversion of higher excited states and vibrational deactivation are very efficient. The large separation between the absorption and fluorescence bands together with the lack of mirror image symmetry and the anomalously long decay times are understandable if there are significant differences in configuration between the ground and fluorescent states.<sup>4</sup> The possibility of the absorption involving several overlapping transitions could also explain these effects.<sup>25</sup> Some comments on this

TABLE I: Fluorescence Yield and Lifetime Data for *all-trans*-1,6-Diphenyl-1,3,5-hexatriene in Various Solvents at Different Temperatures

Solvent	Fluorescence yields			Fluorescence lifetimes			Solvent	Fluorescence yields			Fluorescence lifetimes		
	$\lambda_{ex}$ , nm	$T$ , °C	$\phi_F$	$\lambda_{ex}$ , nm	$T$ , °C	$\tau_F$ , nsec		$\lambda_{ex}$ , nm	$T$ , °C	$\phi_F$	$\lambda_{ex}$ , nm	$T$ , °C	$\tau_F$ , nsec
Perfluoro- <i>n</i> -hexane								360	-103	0.923	360	0	13.4
								360	-123	0.939	360	-32	12.4
	360	63	0.48	360	60	32				360	-43	11.8	
	360	49	0.49	360	46	32				360	-51	11.5	
	360	40	0.50	360	36	31				360	-75	11.0	
	360	32	0.51	360	25	32				360	-93	10.6	
3-Methyl-pentane	360	25	0.52	360	0	32				360	-114	ne	
							Benzene						
	360	62	0.55	360	60	15.5		360	80	0.48	360	80	6.1
	360	49	0.56	360	48	15.4		360	72	0.52	360	65	6.1
	360	43	0.58	360	38	15.4		360	64	0.57	360	53	6.0
	360	34	0.60	360	30	15.5		360	57	0.60	360	40	6.1
	360	22	0.62	360	20	15.4		360	51	0.64	360	28	6.0
	360	0	0.73	360	0	15.4		360	43	0.65	360	21	6.1
	360	-33	0.88	360	-32	14.3		360	27	0.71			
	360	-63	0.96	360	-63	13.8		1,4-Dioxane					
	360	-88	0.99	360	-103	13.0		360	99	0.24	360	98	7.8
	360	-113	1.01	360	-123	12.1		360	86	0.34	360	77	7.8
	360	-153	1.05	360	-148	ne <sup>a</sup>		360	75	0.43	360	60	7.7
	360	-163	1.01	360	-168	ne		360	60	0.54	360	46	7.8
360	-183	1.00	360	-183	ne		360	48	0.58	360	31	7.8	
360	-196	1.00	360	-196	ne		360	37	0.63	360	25	7.8	
<i>n</i> -Hexane							Ethanol						
	360	68	0.56	360	66	15.7		360	74	0.07	360	75	2.1
	360	60	0.60	360	50	15.7		360	26	0.24	360	73	2.2
	360	46	0.61	360	42	15.8					360	62	2.8
	360	37	0.62	360	33	15.6					360	53	3.4
<i>n</i> -Heptane	360	25	0.64	360	25	15.7					360	40	4.2
										360	32	5.0	
	360	104	0.41	360	98	15.6				360	25	5.6	
	360	82	0.50	360	85	15.7				300	25	5.6	
	360	69	0.56	360	74	15.6				250	25	5.6	
	360	58	0.53	360	46	15.5				360	22	5.7	
	360	43	0.61	360	32	15.6				360	19	6.3	
	360	35	0.62	360	22	15.5		Acetonitrile					
Methylcyclo-hexane	360	23	0.64					360	77	0.049	360	77	1.5
								360	65	0.063	360	65	1.9
								360	55	0.078	360	47	2.6
	360	101	0.44	360	92	13.4		360	43	0.099	360	36	3.2
	360	86	0.51	300	92	13.5		360	32	0.125	360	22	4.1
	360	70	0.55	250	92	13.4		360	23	0.15	360	9	4.6
	360	54	0.59	360	81	13.6		360	9	0.23	360	0	5.2 <sup>e</sup>
	360	44	0.63	360	71	13.3		360	0	0.28			
	360	27	0.65	360	65	13.5		360	-13	0.39			
	372	25	0.65	360	52	13.4		360	-23	0.53			
	352	25	0.65	360	40	13.5		360	-33	0.62			
	338	25	0.65	360	25	13.5		360	-43	0.75			
	360	0	0.730	300	25	13.4		Ethyl iodide					
	360	-24	0.741	250	25	13.5		360	25	0.037	360	25	0.7
	360	-43	0.790	360	25	13.3 <sup>b</sup>		Carbon tetra-chloride					
	360	-63	0.871	360	25	13.5 <sup>c</sup>							
360	-81	0.885	360	25	13.5 <sup>d</sup>					360	25	0.8	

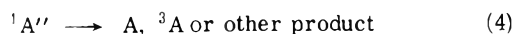
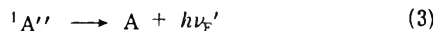
<sup>a</sup> ne = nonexponential decay curve. <sup>b</sup>  $\lambda_{emission}$  420 nm. <sup>c</sup>  $\lambda_{emission}$  550 nm. <sup>d</sup>  $\lambda_{emission}$  375 nm. <sup>e</sup> Slightly nonexponential decay curve.

possibility will be made later. The initially formed Franck-Condon state (or states) designated by  $^1A'$  undergoes solvent rearrangement and a conformational change to form another state  $^1A''$



A similar conformational change involving intramolecular twisting gives rise to cis-trans interconversions in DPH<sup>26</sup> and other stilbene derivatives.<sup>27</sup>

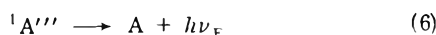
In nonpolar solvents the fluorescence yields are high and yet the fluorescence decay times vary with solvent; in particular there is a fivefold increase in  $\tau_F$  in going from benzene to perfluoro-*n*-hexane. The data are consistent neither with efficient emission nor with an effective nonradiative intersystem crossing process involving the  $^1A''$  state:



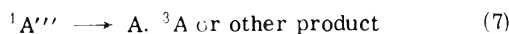
The variation in fluorescence decay times in different solvents is consistent with specific solvent-induced perturbations which lead to configurations of the excited thermalized state, or another excited state,  $^1A'''$  from which emission occurs



The fluorescence yields require that emission occurs from the  $^1A'''$  state with high efficiency.



The small decrease in fluorescence yields of DPH in nonpolar solvents with increasing temperature can be accounted for by a temperature dependent internal conversion or intersystem crossing process



The similarity of the emission spectrum for DPH in the more polar solvents such as acetonitrile and ethanol, to that in nonpolar solvents, shows that emission arises from the same state  $^1A'''$  under all conditions. The strong temperature dependence of the fluorescence yields and decay times means that in polar solvents the efficiency of nonradiative processes from  $^1A''$  and/or  $^1A'''$  states is increased.

The fluorescence behavior of DPH has previously been explained by a mechanism which involved exciplex formation<sup>28</sup> although no systematic variation of experimental conditions has been made to verify this. In all solvents used in this work the emission spectrum is virtually independent of temperature and only one emitting state of DPH is apparent. The lack of any dependence of the position of the emission spectrum on solvent is inconsistent with emission from an exciplex formed by an interaction of excited DPH with a solvent molecule. Although the formation of a nonfluorescent solvent exciplex is possible such a mechanism seems very unlikely since the experimental data would require that exciplex formation be most favored in the nonpolar media. Kinetic analysis alone does not exclude a solvent-DPH complex mechanism if the exciplex is formed during the subnanosecond period of vibrational relaxation and solvent reorganization. Formation of a nonfluorescent exciplex cannot explain the large Stokes shift and lack of mirror image symmetry between the absorption and fluorescence spectra.

*Kinetic Analysis.* A steady state treatment based on the above mechanism for the fluorescence yield  $\phi_F$  gives

$$\phi_F = \frac{k_5}{k_4 + k_5} \frac{k_6}{k_6 + k_7} \quad (i)$$

if it is assumed that only the  $^1A'''$  state can fluoresce. Since relaxation of the initially formed state  $^1A'$  is fast the concentration of the fluorescent state as a function of time after the pulse is given by

$$[^1A'''] = X \exp[-(k_4 + k_5)t] - X \exp[-(k_6 + k_7)t] \quad (ii)$$

where

$$X = \frac{k_5}{(k_4 + k_5) - (k_6 + k_7)}$$

The fluorescence decay times in methylcyclohexane and 3-methylpentane are strictly exponential over three decades of fluorescence decay down to  $-100^\circ$  and in the other nonpolar solvents over the more limited temperature range studied. Thus, either processes 4 and 5, or 6 and 7, are rate determining. At room temperature and above the fluorescence decay in nonpolar solvents is governed by a single temperature independent process which is also independent of exciting and emission wavelength. Since in methylcyclohexane and 3-methylpentane  $\phi_F$  approaches unity at the lowest temperatures  $k_4 < k_5$  and  $k_7 < k_6$  under these conditions. A temperature-dependent increase in the importance of process 4 relative to process 5, or alternatively process 7 relative to process 6, is inconsistent with the experimental facts that the fluorescence decay in nonpolar solvents is constant above and decreases below room temperature. Thus either process 5 or 6 must be rate determining.

The possibility that process 5 is fast (i.e.,  $k_5 > k_6$ ) requires the emission process 6 to be strongly solvent dependent, and process 4 the major temperature dependent nonradiative step. The data show that it is more satisfactory to assume  $k_6 > k_5$  and values of  $\tau_F$  are equal to  $k_5^{-1}$  under most conditions. Hence  $k_5 > k_4$  at all temperatures and

$$\phi_F = k_6/(k_6 + k_7) \quad (iii)$$

The decrease in the fluorescence decay times of DPH in 3-methylpentane and methylcyclohexane at temperatures below  $0^\circ$  is similar to the behavior which has been observed for the effect of temperature on the radiative lifetimes of 5-dimethylaminonaphthalene-1-sulphonamide<sup>29</sup> and some aminophthalimides.<sup>30</sup> At reduced temperatures solvent movement around the excited molecule is slowed, the state  $^1A''$  may be closer to that of the  $^1A'''$  state and  $k_5$  (or  $\tau_F^{-1}$ ) is increased. Above  $0^\circ$  the low viscosity of nonpolar solvents allows the configurational differences between the  $^1A''$  and  $^1A'''$  states to be maximized and  $k_5$  is the reciprocal of the temperature independent decay time. The extent of the differences between the  $^1A''$  and  $^1A'''$  states are governed by the properties of the individual nonpolar solvents and are reflected by the absolute values of the temperature independent decay times.

The observed deviation of the fluorescence decay kinetics from strict exponential behavior in nonpolar solvents at very low temperatures ( $< -100^\circ$ ) could be due to several different effects. A decrease in the rate of the solvent relaxation of the Franck-Condon state (process 2) at low temperature and a simultaneous increase in the rate of the configurational reorientation of the  $^1A'''$  state (process 5) would lead to nonexponential decay of fluorescence when the rates become comparable. Polarization effects as predicted theoretically by Shinitzky<sup>31</sup> can result in nonexponential decay times. It has been shown that DPH does ex-

**TABLE II: Arrhenius Parameters for the Nonradiative Process ( $k_7$ ) Occurring from the  $^1A'''$  State**

	$A, \text{sec}^{-1}$	$E, \text{kJ mol}^{-1}$
(a) Nonpolar solvents		
Methylcyclohexane	$6.6 \times 10^9$	7.1
3-Methylpentane	$7.6 \times 10^{10}$	13.4
(b) Polar solvents		
Acetonitrile	$2.3 \times 10^{13}$	22
Ethanol	$6.2 \times 10^{13}$	26.0

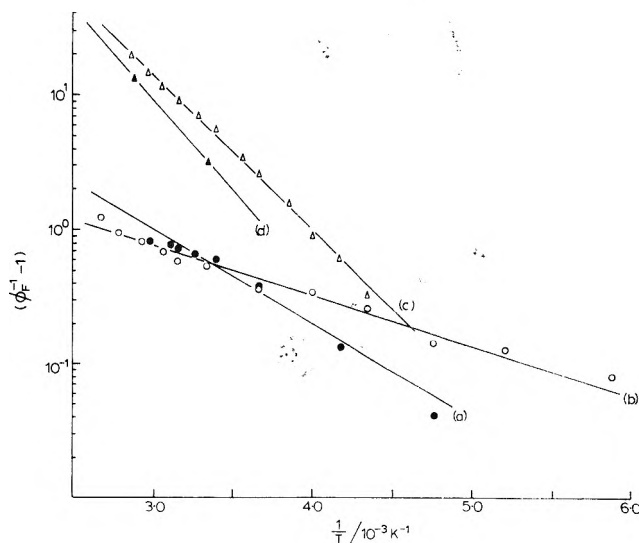
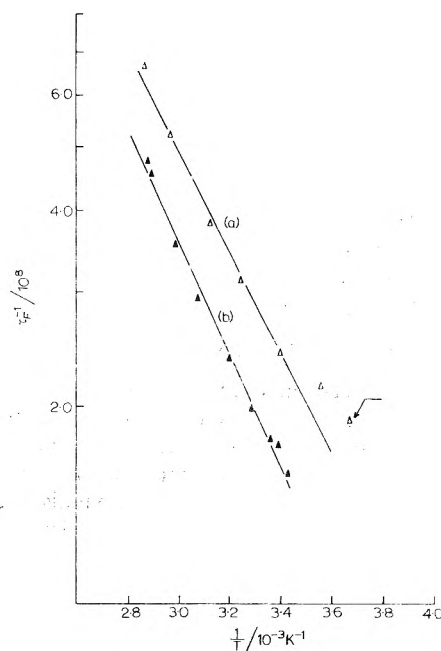
**TABLE III: Arrhenius Parameters for the Fluorescence Decay ( $k_5$ ) of DPH in Polar Solvents**

	$A, \text{sec}^{-1}$	$E, \text{kJ mol}^{-1}$
(a) Nonpolar solvents		
Perfluoro- <i>n</i> -hexane	$3.1 \times 10^7$	0
3-Methylpentane	$6.5 \times 10^7$	0
<i>n</i> -Hexane	$6.4 \times 10^7$	0
<i>n</i> -Heptane	$6.4 \times 10^7$	0
Methylcyclopropane	$7.4 \times 10^7$	0
Benzene	$1.6 \times 10^8$	0
<i>p</i> -Dioxane	$1.3 \times 10^8$	0
(b) Polar solvents		
Acetonitrile	$1.0 \times 10^{11}$	15.1
Ethanol	$1.4 \times 10^{11}$	16.7

hibit a time-dependent nonzero degree of emission anisotropy in its fluorescence decay in viscous solvents<sup>32</sup> when polarizers are placed in the excitation and emission beams. Cehelnik, Mielenz, and Velopoldi<sup>33</sup> have recently measured polarization effects on fluorescence in the steady state mode using a goniospectrofluorimeter and found them to be quite large. Since polarizers were not used in the present study the magnitude of polarization effects on the fluorescence decay times at very low temperatures remains uncertain. Furthermore the solubility of DPH in some nonpolar solvents is poor and the possibility of material coming out of solution, leading at the lowest temperatures to a two phase fluorescence, cannot be ruled out.

In accord with eq iii plots of  $\log(\phi_F^{-1} - 1)$ , which is equal to  $\log k_7/k_6$ , against  $1/T$  for DPH in methylcyclohexane and 3-methylpentane (Figure 6) are essentially linear over the whole temperature range of the experiments. An excited state of DPH which has the high radiative probability required by the kinetic scheme will have a molecular fluorescence lifetime comparable with that calculated by the Strickler-Berg or similar relationship.<sup>2</sup> The Arrhenius parameters presented in Table IIa for the nonradiative process 7 involving the  $^1A'''$  state were calculated assuming Berlmán's value<sup>2</sup> of 1.56 nsec for the radiative lifetime,  $(k_6)^{-1}$ , of DPH in cyclohexane and applying the refractive index ( $n^2$ ) correction.

A mechanism consistent with the measurements, kinetic analysis, and linearity of the Arrhenius plots which explains the pronounced temperature dependence of the fluorescence yields and decay times for DPH in ethanol and acetonitrile requires both processes 5 and 7 to be temperature dependent and enhanced by the increased solvent polarity. The plot of  $\log(\phi_F^{-1} - 1)$  against  $1/T$  for the fluorescence of DPH in acetonitrile (Figure 6) is linear over the entire

**Figure 6.** Plot of  $\log(\phi_F^{-1} - 1)$  against  $1/T$  for DPH in (a) 3-methylpentane, (b) methylcyclohexane, (c) acetonitrile, and (d) ethanol.**Figure 7.** Plot of  $\log(\tau_F^{-1})$  against  $1/T$  for DPH in (a) acetonitrile and (b) ethanol (the data point marked by an arrow refers to a fluorescence decay curve which was slightly nonexponential).

temperature range ( $-43$  to  $77^\circ$ ) studied even though  $\phi_F$  has changed by a factor of 15. It is unlikely that this plot would remain linear if both processes 4 and 7 were temperature dependent. Arrhenius parameters for  $k_7$  were calculated as for the nonpolar solvents (Table IIb) using equation iii. The measurements are consistent with the postulate that the fluorescence yields in both polar and nonpolar solvents depend only upon the relative magnitudes of the radiative and nonradiative processes from the  $^1A'''$  state.

Plots of  $\log \tau_F^{-1}$  vs.  $1/T$  for DPH in acetonitrile and ethanol (Figure 7) are linear from  $0^\circ$  up to temperatures approaching the boiling points of the solvents. The data (Table III) show that the radiative and nonradiative decay processes of the  $^1A'''$  state are faster than the solvent affected process 5 which determines the fluorescence decay

characteristics in all types of solvent. The deviation of the fluorescence decay from strictly exponential behavior in acetonitrile below 0° could be due to process 5 occurring before there is complete solvent relaxation of the initially formed state.

The effects of the various solvents on the changes in molecular configuration in processes 2 and 5 are complex. In the nonpolar solvents there is an increase in the values of  $k_5$  with decrease of temperature which is similar to the effect of solvent temperature on the fluorescence of *cis*-stilbene.<sup>12,34</sup> This may be associated with the tendency of a solvent to minimize the volume of the solute molecule, since for DPH the planar molecule occupies the minimum volume and the probability of emission is greatest for this configuration. In the polar solvents other influences must be significant. One possibility is that changes in configuration in process 2 are reduced in the more structured polar solvents.

*Assignment of the Excited States.* There is uncertainty about the identification of the lower excited states of polyenes. It has been generally assumed that the lowest excited singlet states of polyenes have  $^1B_u$  symmetry but a recent observation of a weak transition in 1,8-diphenyloctatetraene has been assigned to a forbidden  $^1A_g \rightarrow ^1A_g$  transition.<sup>35</sup> It is conceivable that  $^1A''$  could be the forbidden  $^1A_g$  excited state. This is not consistent with the decrease in fluorescence lifetime with lowering of temperature, particularly if there is an appreciable difference in energy between the  $^1B_u$  and  $^1A_g$  states, unless changes in configuration of the excited states are reduced in more rigid media.

### Conclusion

It is evident from this study that configurational changes have very marked influences on the photophysical processes of flexible molecules such as the excited states of DPH and related polyenes. Such changes are subject to strong solvent perturbations which are reflected in the independent behavior of emission efficiency and probability in these systems.

Even though DPH shows anomalous properties its use as a fluorescence lifetime standard has distinct advantages which have been demonstrated.<sup>36</sup>

*Acknowledgment.* We express our thanks to the SRC for support awards (E.D.C. and J.R.L.) and equipment grants.

### References and Notes

- (1) Th. Förster, "Fluoreszenz Organischer Verbindungen", Vandenhoeck and Rupprecht, Göttingen, 1971.
- (2) S. J. Strickler and R. A. Berg, *J. Chem. Phys.*, **37**, 814 (1962).
- (3) J. B. Birks and D. J. Dyson, *Proc. R. Soc., Ser. A*, **275**, 135 (1963).
- (4) I. B. Berlman, *J. Phys. Chem.*, **74**, 3085 (1970).
- (5) W. S. Koski and C. O. Thomas, *J. Chem. Phys.*, **19**, 1286 (1951).
- (6) R. I. T. Cromartie and J. N. Murrell, *J. Chem. Soc.*, 2063 (1961).
- (7) A. N. Nikitina, N. D. Galanin, G. S. Ter-Sarkisian, and B. M. Mikhailov, *Opt. Spectrosc.*, **6**, 226 (1959).
- (8) A. N. Nikitina, G. S. Ter-Sarkisian, B. M. Mikhailov, and L. Minchenkova, *Opt. Spectrosc.*, **14**, 655 (1963).
- (9) A. N. Nikitina and G. S. Ter-Sarkisian, *Opt. Spectrosc.*, **24**, 250 (1968).
- (10) A. N. Nikitina, G. M. Fedyunina, L. A. Yanovskaya, V. A. Dombrovskii, and V. F. Kucherov, *Opt. Spectrosc.*, **30**, 343 (1971).
- (11) R. D. Dyck and D. S. McClure, *J. Chem. Phys.*, **32**, 2326 (1962).
- (12) D. Gegiou, K. A. Muszkat, and E. Fischer, *J. Am. Chem. Soc.*, **90**, 12 (1968).
- (13) E. D. Cehelnik, R. B. Cundall, C. J. Timmons, and R. M. Bowley, *Proc. R. Soc., Ser. A*, **335**, 387 (1973).
- (14) R. B. Cundall and L. C. Pereira, *J. Chem. Soc., Faraday Trans. 2*, **68**, 1152 (1972).
- (15) J. F. Coetzee, G. P. Cunningham, D. K. McGuire, and G. P. Padmanabhan, *Anal. Chem.*, **34**, 1139 (1962).
- (16) W. R. Ware, "Creation and Detection of Excited States", A. A. Lamola, Ed., Marcel Dekker, New York, N.Y., 1971.
- (17) J. R. Lockwood and T. F. Palmer, to be submitted for publication.
- (18) R. B. Cundall and G. B. Evans, *J. Sci. Instrum., Ser. 2*, **1**, 305 (1968).
- (19) C. A. Parker, "Photoluminescence in Solution", Elsevier, New York, N.Y., 1968.
- (20) W. W. Mantulin and J. R. Huber, *Photochem. Photobiol.*, **17**, 139 (1973).
- (21) W. H. Melhuish, *J. Phys. Chem.*, **65**, 229 (1961).
- (22) J. N. Demas and G. A. Crosby, *J. Phys. Chem.*, **75**, 991 (1971).
- (23) H. H. Jaffe and M. Orchin, "Theory and Applications of Ultraviolet Spectroscopy", Wiley, New York, N.Y., 1962.
- (24) E. L. Wehry, "Fluorescence", G. G. Guilbault, Ed., Marcel Dekker, New York, N.Y., 1967.
- (25) R. M. Gavin, Jr., S. Risemberg, and S. A. Rice, *J. Chem. Phys.*, **58**, 3160 (1973); R. M. Gavin, Jr., and S. A. Rice, *ibid.*, **60**, 3231 (1974).
- (26) K. Lundi and L. Zechmeister, *J. Am. Chem. Soc.*, **73**, 2308 (1953).
- (27) S. Malkin and E. Fischer, *J. Phys. Chem.*, **68**, 1153 (1964); J. M. Pinckard, B. Wille, and L. Zechmeister, *J. Am. Chem. Soc.*, **70**, 1938 (1948); L. Zechmeister and A. L. Le Rosen, *ibid.*, **64**, 2755 (1942).
- (28) J. B. Birks, "Photophysics of Aromatic Molecules", Wiley, New York, N.Y., 1970.
- (29) M. A. El-Bayoumi, J.-P. Dalle, and M. F. O'Dwyer, *J. Am. Chem. Soc.*, **92**, 3494 (1970).
- (30) W. R. Ware, S. K. Lee, G. J. Brant, and P. P. Chow, *J. Chem. Phys.*, **54**, 4792 (1971).
- (31) M. Shinitsky, *J. Chem. Phys.*, **56**, 5979 (1972).
- (32) E. D. Cehelnik, R. B. Cundall, J. R. Lockwood, and T. F. Palmer, *J. Chem. Soc., Faraday Trans. 2*, **70**, 244 (1974).
- (33) E. D. Cehelnik, K. D. Mielenz, and R. A. Velopoldi, *J. Res. Natl. Bur. Stand. U.S., Sect. A*, **79**, 1 (1975).
- (34) K. A. Muszkat and S. Sharafy, *J. Am. Chem. Soc.*, **93**, 4119 (1971).
- (35) B. S. Hudson and B. E. Kohler, *Chem. Phys. Lett.*, **14**, 299 (1972); **23**, 13 (1973); K. Schulten and M. Karplus, *ibid.*, **14**, 305 (1972); T. A. Moore and P. Song, *ibid.*, **19**, 128 (1973).
- (36) E. D. Cehelnik, R. B. Cundall, J. R. Lockwood, and T. F. Palmer, *Chem. Phys. Lett.*, **27**, 586 (1974).



## An Investigation of Isomerization of 1,3-Pentadiene Sensitized by Solid Benzophenone Using Internal Reflection Photolysis

José S. DeGuzman and G. R. McMillan\*

Department of Chemistry, Case Western Reserve University, Cleveland, Ohio 44106 (Received September 14, 1972; Revised Manuscript Received February 7, 1975)

Publication costs assisted by the Environmental Protection Agency

Illumination by internal reflection of crystalline benzophenone deposited on a light pipe induces isomerization of *cis*- or *trans*-1,3-pentadiene vapor in contact with the solid. Triplet-triplet energy transfer is implicated. The mixture of diene isomers at the photostationary state contains 56.5% *trans*. This differs from the reported composition (58.5%) of the photostationary state for homogeneous excitation in solution but agrees with the value obtained through surface illumination of the benzophenone crystals. If the energy transfer is treated strictly as a surface reaction, the pressure dependences of the isomerization yields lead to a value of the ratio of rate constants for energy transfer to the two isomers and to a value of the ratio of decay probabilities of diene triplet to the two isomers somewhat different from those obtained by other investigators in studies of energy transfer in homogeneous and heterogeneous systems. It is demonstrated that internal reflection photolysis applied in studies of gas-solid systems yields results of acceptable reproducibility and the quantum yields can be measured. The quantum yield of isomerization for *trans* → *cis* is about  $2 \times 10^{-4}$  at 3660 Å for a 1,3-pentadiene pressure of 2 Torr.

### Introduction

The *cis*-*trans* isomerization of 1,3-pentadiene vapor induced by energy transfer from a solid sensitizer represents a heterogeneous photochemical reaction relatively uncomplicated by side reactions.<sup>1-4</sup> In the earlier attempt,<sup>1</sup> illumination of polycrystalline benzophenone in the presence of *cis*-1,3-pentadiene vapor led to formation of the *trans* isomer through a process believed to be triplet-triplet energy transfer on the basis of comparison with sensitized isomerization in solution.<sup>5,6</sup> Interpretation of the results was somewhat uncertain because of contributions to isomerization from gas-phase photosensitization and from sensitization by pentadiene adsorbed on Pyrex.<sup>7</sup> Attempts to study quantitatively the isomerization rate yielded data with considerable scatter.<sup>4</sup> It is extremely difficult to measure the absorbed intensity in such experiments. The method used in these experiments,<sup>1,4</sup> wherein the radiation passes through the vapor layer, has limited usefulness in gas-solid photochemical studies if the gas is not transparent or if the solid has an appreciable vapor pressure. Some of these difficulties are circumvented by using the method of internal reflection photolysis (IRP).<sup>7</sup> The solid is coated on a light pipe, and the light is introduced into the pipe under conditions ensuring total internal reflection. The optical path through the vapor surrounding a thin layer of solid is negligible provided no light is scattered out of the solid. The amount of light absorbed by the solid can be monitored accurately.

This study is supposed to demonstrate the applicability of IRP to a heterogeneous photochemical reaction and to compare triplet-triplet energy transfer in the system benzophenone(s)-1,3-pentadiene vapor with other cases of energy transfer from sensitizers to 1,3-pentadiene.

### Experimental Section

Both *cis*- and *trans*-1,3-pentadiene of purity 99% were obtained from Chemical Samples Co. Purities of 99.9%

were realized by preparative gas chromatography, but a slow isomerization was observed under storage conditions. All samples used for photolysis contained <3% of the isomeric impurity. Benzophenone from Matheson Coleman and Bell was recrystallized and purified by at least 25 passes through a zone refining apparatus. The IRP cell was based on a design previously illustrated.<sup>7</sup> The internal reflection element was a 4-mm Pyrex rod passing axially through a Pyrex tube of 8 mm i.d. and joined to the tube at planar end seals at an angle of about 70°. The cell was 14.5 cm long. To coat the rod, a solution of benzophenone in ethanol was admitted to the cell, and the solvent removed slowly under vacuum. Upon gentle warming of the cell walls, the benzophenone sublimed onto the rod, giving a coating uniform in appearance with an average thickness of about 0.07 mm. During an illumination, the diene vapor occupied the space (18.6 ml) between the light pipe, the 8-mm tubing, and a side arm leading to a high vacuum stopcock.

Diene samples were outgassed by several trap-to-trap distillations, mixed by raising and lowering the mercury level in a 300-ml bulb several times, and finally expanded into the reaction cell. Diene in the connecting tubing was analyzed; this allowed correction of the isomerization yields for the small amount of isomeric impurity always present.

Light from a Hanovia 673A, 550-W mercury arc was focussed onto a 2.4-mm aperture using a combination of Pyrex lenses. All light leaving the aperture was intercepted by the entrance to the light pipe. The minimum angle of incidence was 50°; this ensured total internal reflection. With the Pyrex optics, wavelengths absorbed by the benzophenone were longer than ~2900 Å. With a Corning glass CS 7-37 filter interposed in the light beam, the intensity of 3660-Å light absorbed by the benzophenone could be measured by ferrioxalate actinometry. This allowed corrections for variations in lamp output (at 3660 Å). It was assumed that small variations in absorbed intensity at all wavelengths were proportional to that at 3660 Å, and all rates

were divided by the intensity at 3660 Å to give a quantity, herein called  $Y$ , which is proportional to the actual quantum yield through a proportionality constant called  $\kappa$ . The amount of light scattered from the coating was measured with an actinometer cell of U-shaped cross section. This was slipped over the IRP cell or the coated rod during illumination. No attempt was made to control the temperature of the cell during photolysis; ambient temperature was  $24 \pm 2^\circ$ . The benzophenone (mp  $<50^\circ$ ) was never observed to flow. The pentadiene mixture was analyzed by gas chromatography at  $0^\circ$  on a 30 ft long, 0.25-in. diameter column containing 15%  $\beta, \beta'$ -oxidipropionitrile on Chromosorb W, 60–80 mesh.

## Results

Illumination of a light pipe coated with benzophenone resulted in partial isomerization of *cis*- or *trans*-1,3-pentadiene contained in the space around the pipe. No products other than the two isomers of 1,3-pentadiene were detected. Not greater than small losses of diene were observed even upon extended photolysis. Samples of diene at an initial pressure of 2 Torr were admitted into the cell and light introduced into the light pipe for 120 hr; recovery of diene was better than 96% complete. Diene in contact with the benzophenone underwent no detectable nonphotochemical isomerization in 120 hr.

Corrected isomerization yields were reproducible over a period of at least 1 year. The pressure dependences of the corrected yields of *trans*  $\rightarrow$  *cis* and *cis*  $\rightarrow$  *trans* isomerization are presented in Figures 1 and 2 as reciprocal plots. Isomerization rates can be calculated by multiplication of  $Y$  by the reference intensity of  $1.1 \times 10^{15}$  quanta  $\text{sec}^{-1}$ . Thus the rate of *trans*  $\rightarrow$  *cis* at infinite pressure was  $1.2 \times 10^{13}$  molecules  $\text{sec}^{-1}$ . About 90% of the incident 3660-Å light was absorbed by the benzophenone. From the wavelength distribution of the lamp output,<sup>8</sup> approximate extinction coefficients,<sup>9</sup> and the transmission of the 7-37 filter, the quantum yield at infinite pressure, assumed independent of wavelength, is about 0.001. For 3660-Å radiation and a diene pressure of 2 Torr, the quantum yield for *trans*  $\rightarrow$  *cis* was  $2 \times 10^{-4}$  based on ferrioxalate actinometry. All illuminations in the pressure study were of 24 hr duration; hence, constant percentage conversion was not maintained. The amount of *cis* isomer formed by photosensitized isomerization of *trans* was measured as a function of time at a diene pressure of 2 Torr. The data are shown in Figure 3. Only after 50 hr does the *cis* diene yield vary as much as 5% from linearity. The data in Figures 1 and 2 therefore correspond to initial yields.

The composition of the mixture of diene isomers at the photostationary state was determined for a total diene pressure of 2 Torr, starting both with mixtures that were *trans* rich and *cis* rich relative to the photostationary state. The percentages of *trans* obtained in those runs where the photostationary state was probably reached within experimental error were 56.5, 56.3, and 56.1 (starting *trans* rich) and 56.9 and 56.6 (starting *cis* rich).

Experiments with the sheath-type actinometer cell showed that scattering of light out of the benzophenone layer is negligible.

## Discussion

Since the light path through the rarefied phase in an internal reflection experiment is extremely small<sup>10</sup> ( $<10^{-3}$  cm for the estimated number of reflections in this case),

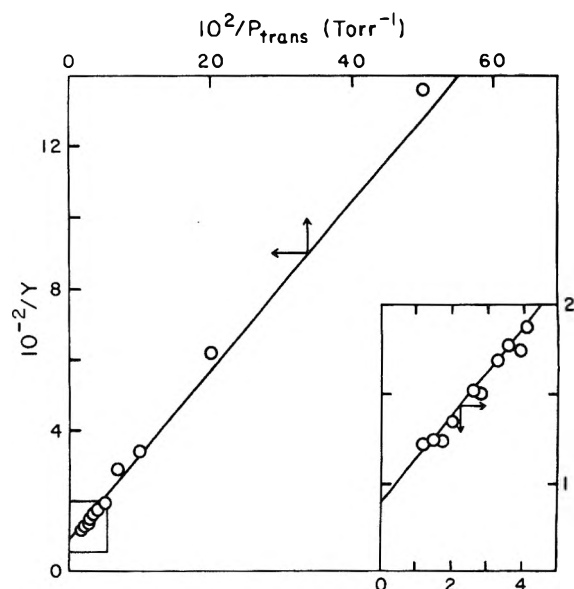


Figure 1. Isomerization of 1,3-pentadiene, *trans*  $\rightarrow$  *cis*. Plot of  $Y_{\text{cis}}^{-1}$  vs. reciprocal of pressure of *trans* diene. The quantity  $Y$ , explained in the Experimental Section, is proportional to the quantum yield of *cis*. The inset shows the high-pressure region.

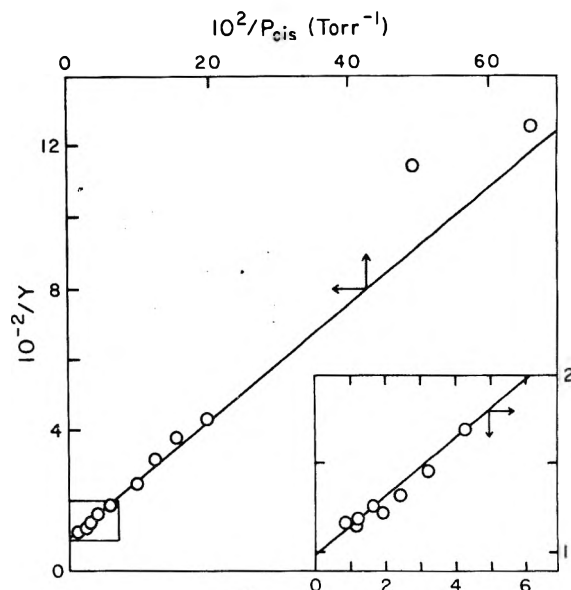


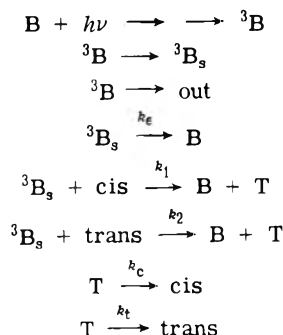
Figure 2. Isomerization of 1,3-pentadiene, *cis*  $\rightarrow$  *trans*. Plot of  $Y_{\text{trans}}^{-1}$  vs. reciprocal of pressure of *cis*. The quantity  $Y$ , explained in the Experimental Section, is proportional to the quantum yield of *trans*. The inset shows the high-pressure region.

and since no scattering into the vapor phase was observed, homogeneous excitation of the diene is probably not important in the present experiments. Pentadiene is transparent at  $\lambda > 2900$  Å.<sup>11</sup> Pentadiene strongly adsorbed on Pyrex absorbs at 3660 Å, leading to isomerization.<sup>7</sup> It may therefore be considered that the photoisomerization found in the present study is induced on areas of the light pipe which might be bare of benzophenone. Isomerization was indeed observed in IRP experiments with an uncoated light pipe, but the rate at comparable diene pressure was only 1% of that on the coated rod. Furthermore, the composition of the photostationary state for the benzophenone-sensitized reaction, 56.5% *trans*, differs markedly from the 65–70%

trans reported for the Pyrex-1,3-pentadiene system.<sup>7</sup> Shifts in the absorption spectrum of 1,3-pentadiene relative to vapor upon adsorption on crystalline benzophenone are similarly expected, possibly permitting a direct photoisomerization. This possibility is excluded by the following considerations. When crystalline sensitizers are surface illuminated in the presence of 1,3-pentadiene vapor, the photostationary state compositions<sup>1,4</sup> correlate roughly with those recorded for solutions.<sup>5,6</sup> The photostationary state established in the IRP experiment at 2 Torr, 56.5% trans, agrees with the 56% at 25 Torr obtained by surface illumination.<sup>4</sup> These comparisons suggest that, in the IRP experiment, excitation of the diene arises by triplet-triplet energy transfer from the benzophenone sensitizer.

An upper limit to the quantum yield of isomerization is fixed by the quantum yield of the intersystem crossing process populating the triplet in the benzophenone crystal together with the probabilities that energy transfer to one diene isomer will lead to the other isomer. The ratio of probabilities for the two isomers will be shown to be near 0.5. The quantum yield of intersystem crossing is not known for our conditions, but from data<sup>12</sup> on luminescence of pure and doped benzophenone at 77 and 300°K, it is inferred to be at least an order of magnitude greater than the quantum yield of isomerization calculated for infinite diene pressure. This may indicate that only triplet excitons reaching the crystal surface transfer energy to diene. The data could probably be as well explained by a reaction in the crystal bulk, but with a given diene molecule experiencing repeated excitation and isomerization or deactivation.

If energy transfer is assumed to occur only at the surface, the data may be manipulated to give some rate constant ratios which may be compared with results of energy transfer under other conditions. A possible simplified mechanism follows, with B a ground state benzophenone molecule, <sup>3</sup>B a triplet exciton in the crystal bulk, <sup>3</sup>B<sub>s</sub> a surface triplet, and T a diene triplet.



Various processes removing surface triplets are assumed to be first order with respect to triplet. The mechanism leads to the following expressions for low conversions:

$$Y_{\text{cis}}^{-1} = (k_t + k_c)/k_c\kappa\phi^t + [(k_t + k_c)/k_c\kappa\phi^t](k_c/k_2[\text{trans}]) \quad (\text{I})$$

$$Y_{\text{trans}}^{-1} = (k_t + k_c)/k_t\kappa\phi^c + [(k_t + k_c)/k_t\kappa\phi^c](k_c/k_1[\text{cis}]) \quad (\text{II})$$

The first equation applies to the trans → cis isomerization and the second equation to cis → trans, with  $Y_{\text{cis}} = \kappa\Phi_{\text{cis}}$  and  $Y_{\text{trans}} = \kappa\Phi_{\text{trans}}$ . The quantities  $\phi^t$  and  $\phi^c$  are the presumably pressure independent quantum yields of surface excitons accessible to trans and cis diene, respectively. Weighted least-squares plots of the equations are shown in Figures 1 and 2. The ratio of intercepts gives:<sup>13</sup>

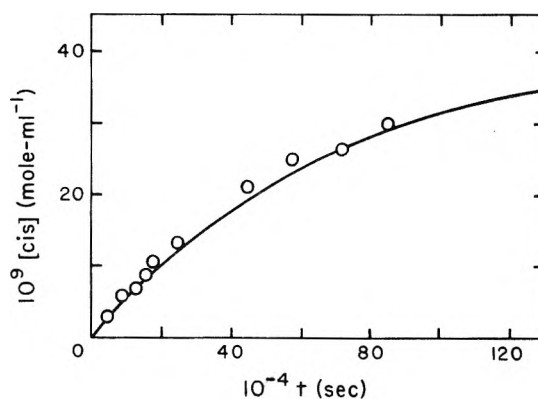


Figure 3. Time dependence of the concentration of *cis*-1,3-pentadiene in photosensitized reaction of *trans* in experiments with an initial pressure of *trans* of 2 Torr. Points are experimental results. The line represents the solution to eq V.

$$k_t\phi^c/k_c\phi^t = 0.90 \pm 0.20 \quad (\text{III})$$

The ratio of slopes divided by the ratio of intercepts gives:

$$k_1/k_2 = 1.57 \pm 0.46 \quad (\text{IV})$$

The composition of the photostationary state gives another relationship among the constants:

$$([\text{trans}]/[\text{cis}])_{\text{pss}} = k_1k_t/k_2k_c = 1.30 \pm 0.02 \quad (\text{V})$$

Dividing (V) by (IV) gives  $k_t/k_c = 0.83 \pm 0.26$ . Comparison with (III) shows that  $\phi^c/\phi^t \sim 1$ .

Values of the constants reported here differ appreciably from values reported for other systems in which isomerization of 1,3-pentadiene was induced by energy transfer from benzophenone and other high-energy triplet sensitizers. The decay ratio  $k_t/k_c$  is 1.4 for energy transfer from benzophenone in benzene solution<sup>6</sup> and in the solid-gas system of cyclohexadiene photopolymer-1,3-pentadiene vapor.<sup>3</sup> The ratio of 0.8–0.9 found for the present system may reflect the different decay probabilities for an adsorbed diene triplet. In homogeneous solution, benzophenone and other high-energy sensitizers are supposed to undergo energy transfer to *cis*- and *trans*-1,3-pentadiene with equal rate constants.<sup>5</sup> The same may apply to some other phases.<sup>14</sup> The value of  $k_1/k_2$  reported here,  $1.57 \pm 0.46$ , may be influenced by adsorption equilibria.

In photolysis starting with pure *trans* diene, the formation of the *cis* isomer is expressed by

$$d[\text{cis}]/dt = \{K_0K_1k_1 - K_0k_1\}[\text{cis}] + K_0K_1k_2[\text{trans}]\{k_1[\text{cis}] + k_2[\text{trans}] + k_c\}^{-1} \quad (\text{VI})$$

In this expression,  $K_0 = \kappa\phi^tI_a$  and  $K_1 = k_c/(k_t + k_c)$ . The integrated equation is plotted in Figure 3. The quantity  $K_0$  was obtained from the experimental initial rate. A value of  $1.50 \times 10^{-6}$  mol ml<sup>-1</sup> for  $k_c/k_2$  was obtained from the plot of eq I (Figure 1) by dividing the slope by the intercept. The value of  $k_1/k_2$  is given in eq IV. The value of  $k_t/k_c$  was taken to be 0.90; that is,  $\phi^t/\phi^c$  in eq III is assumed to be 1.0. From comparison of the experimental points with the theoretical curve (Figure 3), it is concluded that the approach to the photostationary state can be satisfactorily described using only information obtained from initial rate measurements.

This study illustrated that internal reflection photolysis applied to gas-solid photochemical reactions can give data as precise as that typical of studies of photochemical kinetic

ics in homogeneous phases. The rate of light absorption by the solid can be in principle determined accurately, with no complications due to scattered light entering the gas phase. In the benzophenone(s)-pentadiene system, interpretation of the electronic energy transfer in terms of molecular processes is pressed with many difficulties at this stage.

*Acknowledgments.* We are grateful for support through a grant from the Environmental Protection Agency and to Dr. R. L. Daubendiek for construction of the IRP cells.

## References and Notes

- (1) R. L. Daubendiek, H. Magid, and G. R. McMillan, *Chem. Commun.*, 218 (1968).
- (2) G. R. DeMaré, M.-C. Fontaine, and P. Goldfinger, *J. Org. Chem.*, **33**, 2528 (1968).
- (3) M. Sapr, Mémoire de Licence, Université de Bruxelles, Sept 1969.
- (4) H. Magid, Ph.D. Thesis, Case Western Reserve University, 1973.
- (5) G. S. Hammond, J. Saltiel, A. A. Lamola, N. J. Turro, J. S. Bradshaw, D. O. Cowan, R. C. Counsell, V. Vogt, and C. Dalton, *J. Am. Chem. Soc.*, **86**, 3157 (1964).
- (6) L. D. Weis, B. W. Bowen, and P. A. Leermakers, *J. Am. Chem. Soc.*, **88**, 3176 (1966).
- (7) R. L. Daubendiek and G. R. McMillan, *J. Am. Chem. Soc.*, **95**, 1374 (1973).
- (8) J. G. Calvert and J. N. Pitts, Jr., "Photochemistry", Wiley, New York, N.Y., 1966, p 696.
- (9) Reference 8, p 378.
- (10) N. J. Harrick, "Internal Reflection Spectroscopy", Interscience, New York, N.Y., 1967, p 30.
- (11) American Petroleum Institute Project 44, Serial No. 46 and 48.
- (12) R. M. Hochstrasser, *J. Chem. Phys.*, **39**, 3153 (1963); R. M. Hochstrasser and S. K. Lower, *ibid.*, **40**, 1091 (1964); A. S. Gaevskii, V. G. Roskolod'ko, and A. N. Faidsh, *Opt. Spektrosk.*, **22**, 232 (1967).
- (13) Errors represent 95% confidence limits throughout.
- (14) The photostationary state isomer ratio is the same in systems with benzophenone adsorbed on silica gel<sup>6</sup> or with benzaldehyde in the gas phase<sup>15</sup> as that observed with benzophenone in solution.<sup>8</sup> This may mean that  $k_1/k_2$  is the same in all these systems. It should be noted that the composition of the photostationary state reported here (56.5%) is close to that (58.5%) reported for the other cases, but the agreement arises because here an increase in  $k_1/k_2$  compensates for a decrease in  $k_1/k_c$  (cf. eq V).
- (15) Unpublished work by M.-C. Fontaine, quoted in G. R. DeMaré, P. Goldfinger, G. Huybrechts, E. Jonas, and M. Toth, *Ber. Bunsenges, Phys. Chem.*, **73**, 867 (1969).

## Dye Binding and Its Relation to Polyelectrolyte Conformation

J. S. Tan\* and R. L. Schneider

Research Laboratories, Eastman Kodak Company, Rochester, New York 14650 (Received June 20, 1974; Revised Manuscript Received March 26, 1975)

Publication costs assisted by Eastman Kodak Company

Polymer-dye interaction and its relation to the chain conformation of the hydrophobic polyelectrolyte, sodium copoly(ethyl acrylate-acrylic acid) (mole ratio 3:1) have been investigated by measuring the binding of a fluorescent dye, 6-*p*-toluidinonaphthalene-2-sulfonate (TNS), and a cationic dye, Acridine Orange (AO), to this copolymer. Data on the relative fluorescence intensity of TNS, spectrophotometric titration, sedimentation, and dialysis of the AO-polymer system suggest that dye binding is a sensitive function of polymer chain conformation. A change in the conformation of this copolymer, from an extended coil at low ionic strength to a compact coil at high ionic strength, has been found to occur in the region from 0.1 to 0.5 M NaCl.

### Introduction

A hydrophobic polyelectrolyte, copoly(ethyl acrylate-acrylic acid) (mole ratio 3:1) was studied previously by light scattering and intrinsic viscosity.<sup>1</sup> This copolymer, in its acid form, dissolves easily in tetrahydrofuran, methanol, and methyl butyrate (a  $\Theta$  solvent), but does not dissolve in aqueous medium unless it is fully ionized. Our earlier studies of this copolymer in aqueous NaCl solutions suggest that this random copolymer undergoes a conformational change from a swollen, extended coil at low ionic strength to a compact coil at high ionic strength. The transition region was found to occur in the range from 0.1 to 0.3 M NaCl. The occurrence of this transition has been interpreted as being due to the simultaneous decrease in the electrostatic repulsion between the charged groups and the onset of hydrophobic attraction between the ester groups along the chain as the ionic strength of the medium is increased. In the present study, dye binding data were employed to further substantiate this finding. Polymer-dye interaction

was investigated and related to the change in chain conformation of this copolymer as a function of ionic strength. Although detailed analyses of the binding data as a function of free dye concentration are useful in order to extract binding parameters, they are not intended in this work. We are mainly interested in detecting the change in polymer conformation by changes in ionic strength at a constant [polymer]/[dye] value.

The fluorescent dye, 6-*p*-toluidinonaphthalene-2-sulfonate (TNS), which has been used extensively to study hydrophobic sites in proteins,<sup>2</sup> was used as a probe for the existence of hydrophobic clusters of this copolymer in aqueous media. When excited with ultraviolet radiation, this dye shows an intense luminescence peak in the range of 410-480 nm in organic solvents or when it is bound to hydrophobic sites of proteins. Its emission is completely quenched in water or in aqueous NaCl solutions. Consequently, this dye can be used as a sensitive probe for the existence of hydrophobic clusters in aqueous polyelectro-

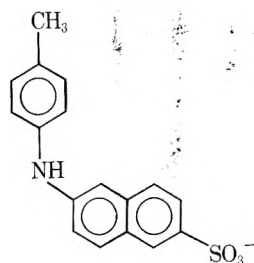
lyte solutions, and the relative fluorescence intensity of this probe in solution will measure the extent of hydrophobic interaction within the polyion coil in aqueous media. This technique has been employed to study the conformational transition proposed for poly(methacrylic acid) using Crystal Violet<sup>3</sup> and Auramine-O.<sup>4</sup>

The cationic dye, Acridine Orange (AO), has been used extensively to study the polymer-dye and dye-dye interactions in biopolymers and in synthetic polyelectrolytes.<sup>5-9</sup> The extent of binding of this dye to polymers and its stacking tendency in the presence of polyelectrolytes should yield information about the chemical and physical nature of the binding sites and the chain conformations of the polymers. In this work, data from spectrophotometric titrations, sedimentation, and dialysis of the copolymer-AO system, as a function of added salt concentration, are used to investigate polymer-dye interaction and are correlated with a weight-average molecular weight of 680,000 in its acid form was used throughout the present work.

### Experimental Section

**Materials.** Synthesis, fractionation, and characterization of the fractions of copoly(ethyl acrylate-acrylic acid), as well as the preparation of the aqueous stock solution of the sodium salt of this copolymer (fully ionized at pH 7.0-7.5), have been described in detail previously.<sup>1</sup> One fraction with a weight-average molecular weight of 680,000 in its acid form was used throughout the present work.

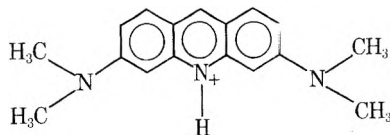
The dye, 6-*p*-toluidinonaphthalene-2-sulfonic acid (Eastman Organic Chemicals, TNS) was recrystallized



TNS

from a 2% NaOH solution, and the sodium salt was dried under vacuum at 25° for 24 hr. A stock solution made up by weight and adjusted to pH 7.0 was stored at 4°.

Acridine Orange hydrochloride (Eastman Organic Chemicals) was recrystallized twice as the free base from methanol-water solution by the addition of 1 *N* NaOH. The precipitate was washed repeatedly with distilled water and was dried under vacuum at 105° for 24 hr. A stock solution of the dye was prepared by weight in a polyethylene bottle by adding 1.05 equiv of HCl to convert the base to the cationic dye (AO)



to which distilled water was added to obtain a dye concentration of  $1 \times 10^{-4}$  *M*. The stock solution was kept at 4° at pH 7.0. The molar extinction coefficient of the solution at the absorption peak 492 nm was  $62,500 \pm 1000$  at infinite dilution and at zero ionic strength at 23°, in good agreement with results of other measurements.<sup>10-12</sup>

**Fluorescence Intensity Measurements.** Fluorescence

measurements were made with a spectrofluorimeter built in these laboratories.<sup>13</sup> The excitation unit is a 150-W xenon source coupled with a Bausch and Lomb, Model 33-86-45, monochromator. The sample cell is positioned for 45° excitation. The detection unit consists of a Beckman DK-2A spectrophotometer, equipped with a Hamamatsu R136 photomultiplier tube.

Although absolute luminescence spectra can be obtained with this spectrofluorimeter, only relative fluorescence intensities were recorded in this work. Relative fluorescence intensities were measured at 23° for 11 polymer-TNS-NaCl solutions at salt concentrations [ $C_s$  (*M*)] ranging from 0 to 1.2 *M*, where  $C_s = 1.2$  is the  $\theta$  solvent for this copolymer.<sup>1</sup> The concentration of the copolymer was held constant at 0.2 g/dl (equal to  $0.56 \times 10^{-2}$  *M* in the carboxylate moiety) and the dye concentration was kept at  $3 \times 10^{-6}$  *M* (the mole ratio of the carboxylate moiety to dye, P/D, was 1850). The sample solutions were excited at 325 nm and the fluorescence emission spectra were recorded in the range 360-650 nm. The spectrum for each sample exhibited a peak at 440 nm without a peak shift. In addition, the wavelength of the absorption maximum (440 nm) and the peak height were constant for the entire series of samples. In no case did the absorption and emission bands overlap.

**Spectrophotometric Titrations.** Titrations of AO with the polymer were carried out in a Cary Model 14 spectrophotometer and in a Perkin-Elmer Model 402 spectrophotometer with a stoppered 1-cm quartz cell. Measurements were made of solutions at values of  $C_s$  ranging from 0.01 to 1.2 *M*. An initial volume of 3 ml of dye solution ( $[D] = 1 \times 10^{-5}$  *M*) at a given added salt concentration was placed in the cuvet and aliquots of polymer solution (0.2 g/dl) with the same salt concentration were added stepwise into the cuvet with a precision microsyringe (Shandon). The absorption spectrum in the range 410-590 nm was recorded for each addition of polymer. To achieve reproducible spectra, repeated rinses of the cell with dye solution were necessary to saturate the cell walls prior to titration. The absorbance thus measured was essentially constant for 30 min.

**Sedimentation.** Sedimentation experiments were carried out in a Beckman Model E analytical ultracentrifuge with electronic speed control. Frictional heating was balanced with refrigeration to control the temperature at  $24 \pm 2^\circ$ . Three freshly prepared 5-ml polymer-AO-NaCl samples were sedimented at 48,000 rpm ( $1.0$  to  $2.25 \times 10^5$  g) for 15 hr in a SW65L titanium rotor which was then allowed to coast to rest. The polyethylene bucket liners were pre-soaked with AO dye solution at the appropriate  $C_s$ . The radial velocity chosen was adequate to sediment the average polymer molecule in the 5-cm length of the sample tube (from  $r = 4$  to  $r = 9$  cm). After sedimentation, the uppermost 3 ml of the supernatant dye solution was removed for spectrophotometric analysis. Only the monomeric dye absorption was observed for absorbances  $\leq 0.3$ . Contamination with unsedimented polymer would have caused the dimeric peak to occur at all optical densities.

**Dialysis.** Dialysis experiments were carried out in cellulose dialysis bags (average round diameter 1.5 cm) supplied by VWR Scientific Co. Two procedures have been employed. In the first method, a 10-cm bag was filled with a 10-ml polymer-AO-NaCl sample and a magnetic stirring bar. The bag was clamped at both ends and was immersed in 10 ml of NaCl solution in a wide-mouth bottle. After 24 hr of stirring at 23° in a dark room, equilibrium had been reached, as indicated by constant absorbance in the exter-

nal solution. In the second method, a 10-ml polymer-NaCl sample was placed inside the bag and was immersed in 10-ml AO-NaCl solution. The absorbance of the external solution after dialysis equilibrium was found to be identical with that observed in the first method. Therefore, the first procedure was used throughout the experiments. Because of the occurrence of precipitation at high concentration of dye, all of the runs were made with an initial  $2 \times 10^{-5} M$  dye solution.

Corrections for the substantial adsorption of AO dye to the dialysis bags were accomplished by experiments with a polymer-free AO-NaCl solution inside the bag and a NaCl solution outside the bag. At equilibrium, the values of absorbance of the external and internal solutions were found to be equal within experimental error. Details in the corrections are shown in the following section.

## Result and Discussion

**Fluorescence Measurements.** The relative fluorescence intensities at the emission peak (440 nm) for 11 polymer-TNS-NaCl solutions ( $P/D = 1850$ ,  $C_s = 0$  to 1.2) are plotted against  $\log C_s$  in Figure 1. A high value for  $P/D$  was used to ensure that the presence of the probe molecules would not appreciably perturb the conformation of the polymer. The points shown in Figure 1 are average values of two identical runs, with  $\pm 2\%$  reproducibility. Similar runs with  $P/D = 3700$  were also performed. The change in fluorescence intensity with  $\log C_s$  gave essentially the same results as those shown in Figure 1 when normalized to the same peak height at  $C_s = 1.2$ . Finally, several solutions of monomeric ethyl acrylate with TNS and NaCl ( $[\text{ethyl acrylate}]/D = 1850$ ) also yielded no emission spectra.

Consequently, we conclude that the appearance of fluorescence observed for the polymer-TNS-NaCl systems is attributed to the interaction of the probe molecules with the polymer molecules. The change in intensity as a function of  $C_s$  may be caused by two effects: an increase in the amount of TNS molecules bound or an increase in the quantum yield of the probe due to the change in the microenvironment. Either of these mechanisms suggests that it is the change in conformation of the polymer which causes the change in intensity.

The proposed model for a conformational change in this copolymer<sup>1</sup> very suitably explains the shape of the curve in Figure 1. The zero intensity at  $C_s = 0$  suggests that there is no interaction between the dye molecules and the polymer, and the fluorescence of the probe is completely quenched in the aqueous medium. In this solution ( $C_s = 0$ ), the interaction between the TNS probes and the hydrophobic parts of the polymer, if present, is overridden by the strong repulsion between the similarly charged sulfonate groups on the dye molecule and the carboxylate sites on the copolymer. This repulsion is decreased gradually by an increase in  $C_s$  due to the shielding effect of the counterions around the polyion. Hence, the interaction between TNS and the polymer backbone is increased with  $C_s$  as indicated by the increase in fluorescence intensity (Figure 1). This increase in intensity is expected to level off once the polymer sites are completely shielded by the counterions. The intensity shown by the dotted line extrapolation near  $C_s = 0.2-0.3$  would be a measure of maximum interaction between the TNS probe and the shielded polymer backbone.

However, a rapid increase in intensity beyond this region was observed. Additional modes of dye binding must have occurred to account for this increase. The proposed model

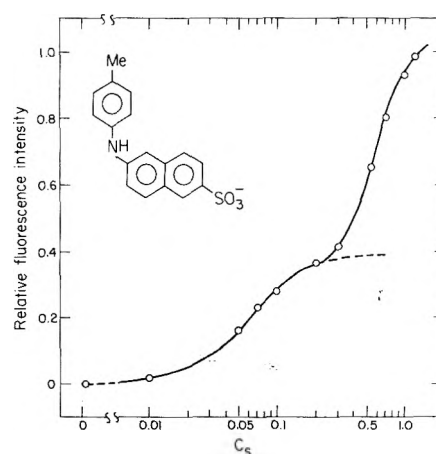


Figure 1. Relative fluorescence intensity of TNS in aqueous solutions of sodium copoly(ethyl acrylate-acrylic acid) + NaCl vs.  $\log C_s$ .

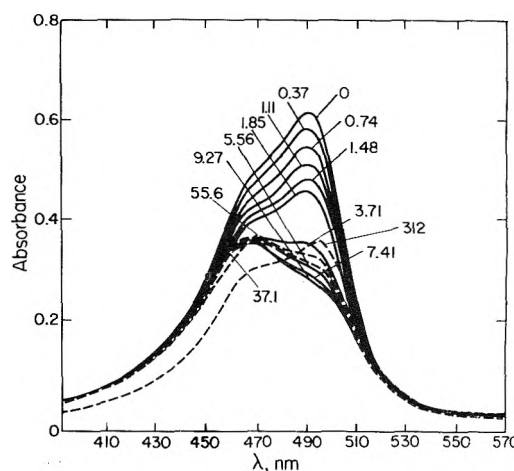


Figure 2. Absorption spectra of AO in copolymer + NaCl (0.05 M). The numbers designate the values for  $P/D$ . These spectra were not corrected for a constant dye concentration.

for the conformational change of this copolymer suggests that the range in  $C_s$  from 0.1 to 0.3 is a conformational transition region where the polymer changes from an extended coil to a compact coil.<sup>1</sup> This region marks the simultaneous occurrence of a reduction of electrostatic repulsion between the carboxylate sites and the onset of hydrophobic attraction between the ester side groups. It is this conformational change which probably causes the rapid increase in the fluorescence intensity of TNS. In this region, the strength of hydrophobic clustering is increased rapidly with  $C_s$  and hence, the interaction between the probe molecules and the hydrophobic parts of the copolymer is increased.

The foregoing results suggest that the fluorescence intensity of TNS is a sensitive measure of the chain conformation of this copolymer in aqueous NaCl solutions and that the shape of the curve can be used to identify the region in which the change in conformation occurs.

**Spectrophotometric Titration.** Typical spectra of a pure AO solution and of the polymer-AO solutions are shown in Figure 2. Curve 0 is the spectrum of a 3-ml dye solution ( $[AO] = 1 \times 10^{-5} M$ ) containing 0.05 M NaCl. Other spectra below curve 0 (Figure 2) are those for polymer-AO solutions after the addition of polymer to the dye solution. These spectra were not corrected for a constant dye con-

centration. The free monomer and dimer peaks appear at 492 and 465 nm, respectively. The molar extinction coefficients of  $1 \times 10^{-5} M$  dye solution in various added salt concentrations are listed in Table I.

Titration data were analyzed in the same manner as those reported elsewhere.<sup>5-7,9</sup> At an early stage in the titration, the spectra have a predominant peak at 492 nm. This peak corresponds to the absorption of three species: free monomer, free dimer, and bound dye. No isosbestic points were observed because the extinction coefficients of these species are different. Upon the addition of polymer sites, more free dye molecules are bound to the polymer. At saturation, the bound dye is in equilibrium with the free dye molecules. The spectra show a major peak at 470 nm indicating that the dimer is the dominant form of all dye species. Addition of excess polymer beyond this point creates a new equilibrium. The peak at 492 nm increases in intensity and shifts to a longer wavelength (496 nm). These results are thought to be attributed to the redistribution of the bound dye molecules among the polymer sites and to the increase of the bound dye monomers at the expense of other bound dye dimers.<sup>5,6,14</sup>

Since the largest absorption change occurs at 492 nm, the absorption data at this wavelength were used to determine the stoichiometry of the polymer-AO complex formation. Each absorbance value at 492 nm in Figure 2 was converted to an apparent extinction coefficient of the dye solution, including free and bound dye molecules, by using the initial dye concentration and the volume of the solution after each addition of polymer. These values of  $\epsilon_{492}$  are plotted against P/D in Figure 3a. The value of  $\epsilon_{492}$  is a maximum for a pure dye solution and it decreases with the addition of polymer binding sites. A minimum in  $\epsilon_{492}$  is reached when enough polymer sites are added to the dye solution to form the polymer-AO complexes. Further increase in polymer sites leads to redistribution of the bound dye among the polymer sites, and  $\epsilon_{492}$  increases. The titration end point,  $(P/D)_e$ , defined as the number of polymer carboxylate sites bound to one dye molecule, was obtained by extrapolation of the linear portion of the titration curve<sup>6</sup> as shown in Figure 3. Generally, the end points for the present systems were sharper ( $\pm 2\%$ ) and easier to locate at low  $C_s$  than end points ( $\pm 4\%$ ) at high  $C_s$  (as shown in Figure 3b for data in 0.7 M). The values of  $(P/D)_e$  thus obtained are plotted against  $\log C_s$  in Figure 4.

In the region  $0.01 \leq C_s \leq 0.2$ ,  $(P/D)_e$  is approximately 4. It increases very slightly with an increase in  $C_s$ . Beyond the region 0.2-0.3,  $(P/D)_e$  increases very rapidly with increasing  $C_s$ . A conformational change of the polymer induced by the change in  $C_s$  can be used to interpret these results. In the low  $C_s$  region, interaction between polymer sites and dye molecules is essentially electrostatic. As the effective charge on each polymer site decreases with the increase in  $C_s$  up to 0.2-0.3, the electrostatic attraction between a polymer site and the dye molecule is gradually decreased, and hence more polymer sites can be accommodated around a given dye molecule. Analogous to the data from fluorescence measurements (Figure 1),  $(P/D)_e$  would eventually reach a constant level once the charges on the polymer sites were completely shielded. It is the change in chain conformation or the increase in chain flexibility in the region  $C_s = 0.1-0.3$  which causes the rapid increase in  $(P/D)_e$  beyond  $C_s = 0.3$ . The simultaneous occurrence of the reduction in electrostatic interaction of the charged sites and the onset of hydrophobic clustering of the ester

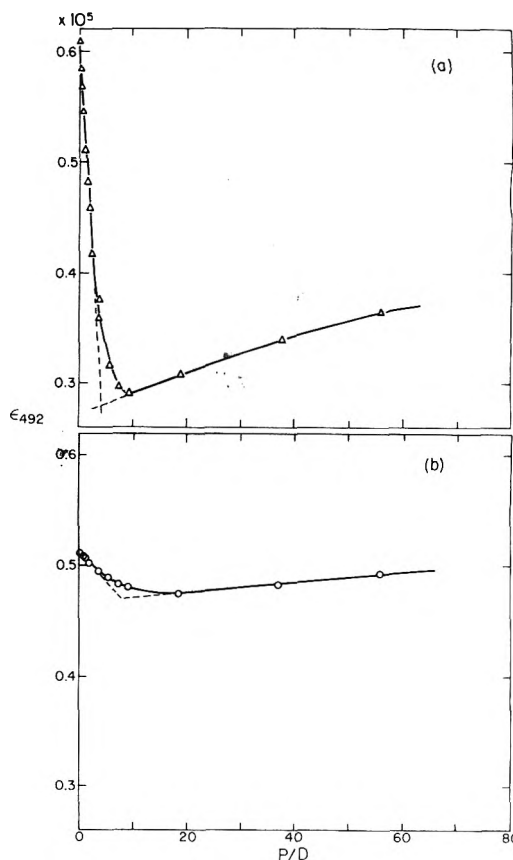


Figure 3. Extinction coefficients of AO-polymer solutions at 492 nm vs. P/D: (a) in 0.05 M NaCl, (b) in 0.7 M NaCl.

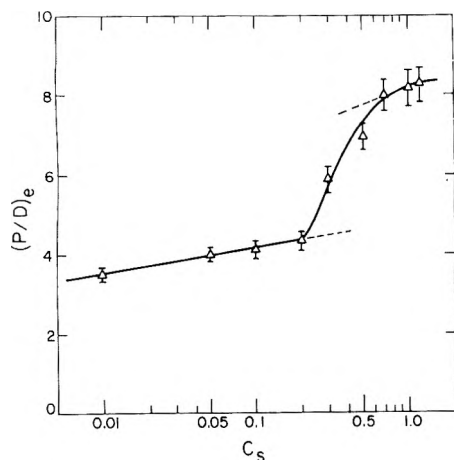
groups has caused the coil to collapse. Hence several carboxylate sites on the chain, which are partially shielded by the counterions, can be accommodated around a given dye molecule. Alternatively, it is also possible that the increase in  $C_s$  may have decreased the polymer-AO binding strength and hence fewer dye molecules are required to bind to a given number of polymer sites. Beyond the  $C_s = 0.5-0.7$  region,  $(P/D)_e$  begins to level off as  $C_s$  is increased. This is attributed to the approximately unchanged conformation of the polymer.

It is to be noted that the values for  $(P/D)_e$  obtained from the present fully ionized polymer (between 4 and 8) are much higher than the value of unity observed for the systems DNA-AO<sup>5-7</sup> and polystyrenesulfonate-AO.<sup>9</sup> The polymers used in the latter cases are rigid and extended, and the charged sites are only slightly shielded in low  $C_s$  media (water or below 0.05 M), so that a 1:1 complex is expected. The copolymer used in our titration is more coiled owing to the presence of hydrophobic ester groups, which facilitate the coiling of the backbone around a given dye molecule in aqueous media. In addition, the salt concentrations used in our measurements are relatively high so that the charged sites are partially or totally shielded. Hence, the change in  $(P/D)_e$  caused by the change in  $C_s$  can be used to probe the conformational change of the polymer.

While the polymer size decreases drastically with an increase in  $C_s$ <sup>1</sup> up to  $C_s = 0.2$  these titration data, as well as the results from sedimentation and dialysis discussed later, indicate only a slight change in polymer-dye interaction with  $C_s$  increasing up to 0.3. A probable explanation is that, although the size of the coil is a sensitive function of the

TABLE I: Molar Extinction Coefficients of Acridine Orange in NaCl Solutions at 492 nm

$C_s, M$	0	0.01	0.05	0.1	0.3	0.7	1.2
$\epsilon_{492} \times 10^{-5}, \text{cm}^{-1} M^{-1}$	$0.62_5 \pm .01$	0.62	0.61	0.60	$0.54_5$	0.50	0.48

Figure 4. Titration end points,  $(P/D)_e$ , vs.  $\log C_s$ .

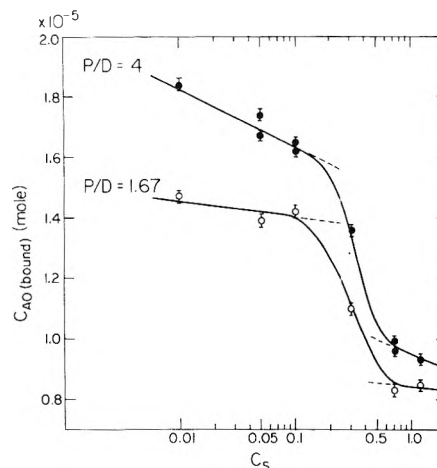
electrostatic interaction between the charged groups, the polymer-dye interaction changes only slightly with this quantity. It is only the onset of hydrophobic clustering in the coil in the region  $C_s = 0.1-0.3$  which will enhance the polymer-TNS interaction or reduce the polymer-AO interaction. Nevertheless, it should be pointed out that the origin of polymer-TNS interaction is essentially hydrophobic and that of the polymer-AO is essentially electrostatic.

**Sedimentation.** Data from sedimentation experiments are compiled in Table II. Two P/D ratios were chosen for these measurements. The absorbance of the supernatant liquids at 492 nm is tabulated under  $A_{sup}$ . The corresponding dye concentrations,  $C_{AO}$  (free), were calculated using these absorbance data and the data for the absorbance of dye-NaCl solution as a function of dye concentration. The concentrations of the bound dye,  $C_{AO}$  (bound), were obtained by subtracting  $C_{AO}$  (free) values from the initial dye concentration,  $C_{AO}^0$  ( $2 \times 10^{-5} M$ ). Figure 5 shows the plots of  $C_{AO}$  (bound) ( $\pm 2-3\%$ ) vs.  $\log C_s$ .

Similar to the discussion presented above for the titration data, the results shown in Figure 5 can be interpreted in terms of the change in chain conformation of this copolymer as a function of  $C_s$ . The number of dye molecules bound to a given number of polymer sites is maximum for a solution at  $C_s = 0$ , but decreases slightly with an increase in  $C_s$  up to 0.1. The binding between the dye molecules and the polymer sites is essentially electrostatic in this region. In the region of the change in conformation, i.e.,  $C_s = 0.1-0.5$ , a marked decrease in  $C_{AO}$  (bound) was observed. The asymptotic level beyond  $C_s = 0.5$  is due to the relatively unchanged conformation of the polymer.

Comparison of the calculated ratios of polymer sites per bound dye molecule with those obtained from the spectrophotometric titrations will be discussed later with the results obtained from dialysis.

**Dialysis.** Data from equilibrium dialysis experiments at various P/D ratios are listed in Table III. Section 1 in Table III lists the data for the blank runs without polymer and sections 2, 3, and 4 list those for the runs with polymer present inside the dialysis bag. An initial concentration of

Figure 5. Concentrations of bound AO measured from sedimentation experiments vs.  $\log C_s$ .

Acridine Orange,  $C_{AO}^0$ , of  $2 \times 10^{-5} M$  was used for all the runs, and hence the total amount of dye present in each experiment,  $M_{AO}^0$ , (6-ml dye-polymer-NaCl solution inside the bag and a 10-ml NaCl solution free of polymer and dye outside the bag) was  $(2 \times 10^{-5} M) \times (6 \text{ ml})$  or  $12 \times 10^{-8} \text{ mol}$ . The numbers listed under  $A_{out}^0$  are the absorbances of the outside solution for the blank runs after the systems reached dialysis equilibrium, while those listed under  $A_{out}$  are the corresponding values for the runs with polymer inside the bags. Because of the presence of the polymer, the spectra of the inside solutions are complicated by the appearance of a bound dimer peak. Therefore, it is more convenient to analyze the outside solution. The apparent amount of the dye molecules bound to the polymer,  $M_{AO}$ , was calculated from the quantity  $A_{out}^0 - A_{out}$  using the absorbance data for dye-NaCl as a function of dye concentration, assuming that the amounts of dye adsorbed to the bags were approximately the same for the blank and the actual runs.

Since a substantial amount of dye which would have been free and available to the polymer sites was adsorbed to the bag (this amount varies with  $C_s$ ), a correction to each apparent  $M_{AO}$  (bound) was necessary. First, we assumed that the free dye concentration was equal inside and outside the bag after dialysis equilibrium. The total amount of free dye,  $M_{AO}$  (free), was estimated from  $A_{out}$  and the total volume of the solutions inside and outside the bag. By also assuming that the amount of dye adsorbed to the bag would have been free and available to the polymer sites, corrections for  $M_{AO}$  (bound) could be made according to the following equation:

$$\frac{M_{AO}(\text{bound})}{M_{AO}^c(\text{bound})} = \frac{M_{AO}(\text{bound}) + M_{AO}(\text{free})}{\text{total amount of dye including that lost to the bag}} \quad (1)$$

( =  $12 \times 10^{-8} \text{ mol}$  )

where  $M_{AO}^c$  (bound) is the corrected  $M_{AO}$  (bound). The



TABLE II: Data from Sedimentation Experiments

$C_s, M$	$A_{sup}$		$C_{AO}(\text{free}) \times 10^5, M$		$C_{AO}(\text{bound}) \times 10^5, M$	
(1) $P/D = 1.67$ ( $C_{AO}^0 = 2 \times 10^{-5} M$ )						
0.01	0.33		(0.53 $\pm$ 0.03)		(1.47 $\pm$ 0.03)	
0.05	0.37		0.61		1.39	
0.1	0.35		0.58		1.42	
0.3	0.49		0.90		1.10	
0.7	0.58		1.17		0.83	
1.2	0.55		1.15		0.85	
	(a) <sup>a</sup>	(b) <sup>a</sup>	(a)	(b)	(a)	(b)
(2) $P/D = 4$ ( $C_{AO}^0 = 2 \times 10^{-5} M$ )						
0.01	0.11	0.10	0.18	0.16	1.82	1.84
0.05	0.16	0.20	0.26	0.33	1.74	1.67
0.1	0.22	0.21	0.37	0.35	1.63	1.65
0.3	0.35	0.35	0.64	0.64	1.36	1.35
0.7	0.52	0.50	1.04	1.00	0.96	1.00
1.2		0.51		1.06		0.94

<sup>a</sup> (a) and (b) designate two individual runs.

TABLE III: Data from Dialysis Experiments

$C_s, M$	$A_{out}^0$	$C_s, M$	$A_{out}^0$	$C_s, M$	$A_{out}^0$
1. Blank					
0	0.048 $\pm$ 0.005				
0.01	0.14 <sub>0</sub>	0.1	0.30 <sub>0</sub>	0.7	0.22 <sub>3</sub>
0.05	0.28 <sub>3</sub>	0.3	0.28 <sub>1</sub>	1.2	0.19 <sub>0</sub>
$C_s, M$	$A_{out}$	$A_{out}^0 - A_{out}$	$M_{AO}(\text{bound}) \times 10^8, \text{mol}$	$M_{AO}(\text{free}) \times 10^8, \text{mol}$	$M_{AO}^c(\text{bound}) \times 10^8, \text{mol}$
(2) $P/D = 2$ ( $C_{AO}^0 = 2 \times 10^{-5} M$ ; $M_{AO}^0 = 12 \times 10^{-8} \text{mol}$ )					
0					
0.01	0.082	0.058	1.4 <sub>7</sub>	2.1 <sub>2</sub>	4.9 <sub>1</sub>
0.05	0.17 <sub>1</sub>	0.11 <sub>2</sub>	2.9 <sub>4</sub>	4.4 <sub>8</sub>	4.7 <sub>5</sub>
0.1	0.19 <sub>0</sub>	0.11 <sub>0</sub>	2.9 <sub>3</sub>	5.0 <sub>7</sub>	4.4 <sub>0</sub>
0.3	0.21 <sub>1</sub>	0.07 <sub>0</sub>	2.0 <sub>6</sub>	6.1 <sub>9</sub>	3.0 <sub>0</sub>
0.7	0.21 <sub>5</sub>	0.008	0.2 <sub>6</sub>	6.8 <sub>8</sub>	0.4 <sub>3</sub>
1.2	0.19 <sub>2</sub>	~0	~0	6.4 <sub>0</sub>	~0
(3) $P/D = 4$ ( $C_{AO}^0 = 2 \times 10^{-5} M$ ; $M_{AO}^0 = 12 \times 10^{-8} \text{mol}$ )					
0	0.010	0.038	0.97	0.25 <sub>6</sub>	9.4 <sub>9</sub>
0.01	0.035	0.10 <sub>5</sub>	2.7 <sub>1</sub>	0.90 <sub>3</sub>	9.0 <sub>0</sub>
0.05	0.090	0.19 <sub>3</sub>	5.0 <sub>6</sub>	2.3 <sub>6</sub>	8.1 <sub>8</sub>
0.1	0.11 <sub>0</sub>	0.19 <sub>0</sub>	5.0 <sub>7</sub>	2.9 <sub>3</sub>	7.6 <sub>1</sub>
0.3	0.21 <sub>0</sub>	0.071	2.0 <sub>8</sub>	6.1 <sub>6</sub>	3.6 <sub>3</sub>
0.7	0.194	0.02 <sub>9</sub>	0.9 <sub>3</sub>	6.2 <sub>1</sub>	1.5 <sub>6</sub>
1.2	0.17 <sub>0</sub>	0.02 <sub>0</sub>	0.67	5.6 <sub>7</sub>	1.2 <sub>7</sub>
(4) $P/D = 25$ ( $C_{AO}^0 = 2 \times 10^{-5} M$ ; $M_{AO}^0 = 12 \times 10^{-8} \text{mol}$ )					
0	0.007	0.041	1.0 <sub>5</sub>	0.17 <sub>9</sub>	10.2 <sub>5</sub>
0.01	0.024	0.11 <sub>6</sub>	2.9 <sub>9</sub>	0.61 <sub>9</sub>	9.9 <sub>4</sub>
0.05	0.052	0.23 <sub>1</sub>	6.0 <sub>6</sub>	1.3 <sub>6</sub>	9.8 <sub>0</sub>
0.1	0.070	0.23 <sub>0</sub>	6.1 <sub>3</sub>	1.8 <sub>7</sub>	9.2 <sub>0</sub>
0.3	0.16 <sub>0</sub>	0.12 <sub>1</sub>	3.5 <sub>5</sub>	4.7 <sub>0</sub>	5.1 <sub>6</sub>
0.7	0.18 <sub>0</sub>	0.04 <sub>3</sub>	1.3 <sub>8</sub>	5.7 <sub>6</sub>	2.3 <sub>2</sub>
1.2	0.15 <sub>8</sub>	0.03 <sub>2</sub>	1.0 <sub>7</sub>	5.2 <sub>7</sub>	2.0 <sub>3</sub>

quantity  $M_{AO}(\text{bound}) + M_{AO}(\text{free})$  is the total amount of dye present less the amount lost to the bag, i.e., the apparent amount available to the polymer sites. Values for  $M_{AO}^c$

(bound) thus obtained were then plotted against  $\log C_s$  in Figure 6, with an accuracy of  $\pm 2-3\%$  in  $M_{AO}^c(\text{bound})$ .

The shape of the curve in Figure 6 once again supports

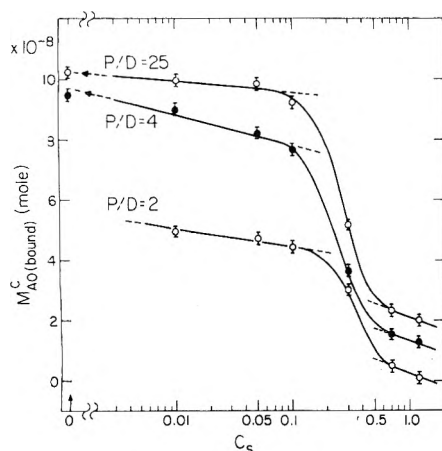


Figure 6. Amounts of bound AO measured from dialysis experiments vs.  $\log C_s$ .

the hypothesis of a conformational change proposed for this copolymer.<sup>1</sup> In the low  $C_s$  region ( $0 \leq C_s \leq 0.1$ ), the amount of dye bound is a maximum at  $C_s = 0$  and decreases slowly with an increase in  $C_s$ . At  $C_s = 0$ , the charged sites are not shielded by counterions and interaction between the sites and dye molecules is greatest. Hence, a smaller number of polymer sites is required to bind to a dye molecule. As the shielding effect is increased by an increase in  $C_s$ , the electrostatic interaction is decreased. Therefore, more polymer sites are required to bind each dye molecule, as observed previously in Figure 4, or inversely, fewer dye molecules are bound to a given number of polymer sites, as shown in Figure 5. The decrease in  $M^c_{AO}$  (bound) becomes large in the region  $0.1 \leq C_s \leq 0.5$ . This is attributed to the conformational change previously proposed for this region. Beyond  $C_s = 0.5$ , the flexibility of the chain does not change appreciably and the amount of bound dye has leveled off. Although bold assumptions had to be made in the dialysis experiments in order to derive these results, agreement between these data and those shown in Figures 1, 4, and 5 is remarkable, supporting the correctness of the assumptions.

At first glance, the results shown in Figure 1 seem to be contradictory to those shown in Figures 4–6. The interaction between the TNS molecules and the copolymer increases with ionic strength, whereas the amount of AO bound to a given number of polymer sites decreases with ionic strength. Different binding mechanisms must be considered for these findings. In the case of TNS binding, the origin of binding between the negatively charged TNS and the polyanion is hydrophobic. The hydrophobicity of this copolymer increases with an increase in  $C_s$ , and hence the fluorescence intensity of TNS increases with an increase in  $C_s$ .

In the case of AO binding, the origin of the binding may

be attributed to both the electrostatic and hydrophobic attractions between the polymer and dye molecules with the former predominantly prevailing. This is borne out by the continuously decreasing binding strength with increasing  $C_s$  (Figures 5 and 6), in spite of the increase in hydrophobic clustering with increasing  $C_s$ . The occurrence of the transition curve shape in the binding curves also suggests that, although the onset of hydrophobic clustering in the transition region has caused a rapid decrease in binding strength, hydrophobic attraction between the hydrophobic parts of the polymer and dye molecules may not contribute significantly to the AO binding.

## Conclusion

Polymer–dye-binding studies have revealed not only the nature of the polymer–dye interaction but also the change in polymer chain conformation as a function of the nature of the solvent. The region of the conformational change of sodium copoly(ethyl acrylate–acrylic acid) in NaCl solutions was identified with the data on dye binding. While it is realized that the chain conformation in the absence and in the presence of dye molecules may differ slightly, particularly in the case of solutions without an excess amount of low-molecular-weight electrolytes, a gross change in conformation as a function of ionic strength was observed and the transition region has been located. Finally, the data suggest that in the case of TNS binding, the source of binding strength is essentially hydrophobic, and in the case of AO binding, it is predominantly electrostatic.

*Acknowledgments.* The authors are indebted to Messrs. L. F. Costa and J. E. Forero for suggestions and technical assistance in the operation of the spectrofluorimeter. Discussions with Dr. R. L. Reeves were also helpful. Comments from Drs. R. S. Moore and G. L. Beyer are appreciated.

## References and Notes

- (1) J. S. Tan and S. P. Gasper, *J. Polym. Sci., Polym. Phys. Ed.*, **12**, 1785 (1974).
- (2) G. M. Edelman and W. O. McClure, *Acc. Chem. Res.*, **1**, 65 (1968).
- (3) W. H. Stork, P. L. deHasseth, W. B. Schippers, C. M. Kormeling, and M. Mandel, *J. Phys. Chem.*, **77**, 1772 (1973).
- (4) T. M. Birshtein, E. V. Anufrieva, T. N. Nekrasova, O. B. Ptitsyn, and T. V. Sheveleva, *Polym. Sci. USSR*, **7**, 412 (1965).
- (5) D. F. Bradley and M. K. Wolf, *Proc. Natl. Acad. Sci. U.S.A.*, **45**, 944 (1959).
- (6) A. L. Stone and D. F. Bradley, *J. Am. Chem. Soc.*, **83**, 3627 (1961).
- (7) B. C. Myhr and J. G. Foss, *Biopolymers*, **10**, 425 (1971).
- (8) G. Barone, V. Crescenzi, F. Quadrioglio, and V. Vitagliano, *Ric. Sci.*, **36**, 503 (1966).
- (9) V. Vitagliano, L. Costantino, and A. Zagari, *J. Phys. Chem.*, **77**, 204 (1973).
- (10) V. Zanker, *Z. Phys. Chem.*, **199**, 225 (1952).
- (11) M. E. Lamm and D. M. Neville, Jr., *J. Phys. Chem.*, **69**, 3872 (1965).
- (12) B. H. Robinson, A. Löffler, and G. Schwarz, *J. Chem. Soc., Faraday Trans. 1*, **69**, 56 (1973).
- (13) L. Costa, F. Grum, and D. J. Paine, *Appl. Opt.*, **8**, 1149 (1969).
- (14) W. Appel and V. Zanker, *Z. Naturforsch. B*, **13** (2), 126 (1958); W. Appel and G. Scheibe, *ibid.*, **13** (6), 359 (1958).

## Effects of Ion Association upon the Solubilities of the Cyclooctatetraene Dianion

Gerald R. Stevenson\* and Ignacio Ocasio

University of Puerto Rico, Department of Chemistry, Rio Piedras, Puerto Rico 00931

(Received October 21, 1974; Revised Manuscript Received April 4, 1975)

Publication costs assisted by the University of Puerto Rico

The solubilities of disodium cyclooctatetraeneide and dipotassium cyclooctatetraeneide have been accurately determined in hexamethylphosphoramide (HMPA) and tetrahydrofuran (THF) as a function of temperature. For the THF systems the dianion was considered to exist as a quadruple ion (associated with two cations) as previously reported, and the enthalpies of solution were found to be 1.09 and 5.13 kcal/mol for the potassium and sodium salts, respectively. The fact that  $\Delta H^\circ$  of solution is positive indicates that the crystal lattice energies are larger than the solvation energies of the quadruple ions. In HMPA the dianion was considered to exist as a free ion. However, considerable curvature was observed in a plot of  $\ln K_{sp}$  vs.  $1/RT$ . This curvature was attributed to the formation of ion pairs between the cyclooctatetraene (COT) dianion and one potassium cation. Addition of KI to solutions of the COT dianion and anion radical in HMPA shift the observed reverse disproportionation (comproportionation) equilibrium constant to smaller values confirming the formation of ion pairs. The sodium salt did not exhibit curvature in the van't Hoff plot, and the comproportionation equilibrium constant was invariant with the addition of  $\text{NaClO}_3$  to solutions of the COT dianion and anion radical in HMPA.

The disproportionation of the cyclooctatetraene (COT) anion radical to form the COT dianion and neutral molecule is of particular chemical interest, since it represents one of the very few reversible chemical reactions in which a compound is interchanged between an aromatic and anti-aromatic system. For this reason, the thermodynamic parameters controlling the reverse disproportionation reaction (eq 1) should yield a lot of information concerning the



resonance energy of the dianion and anion radical, the electron-electron repulsion energy in the dianion, and other intramolecular effects. Unfortunately much of this information is obscured by the fact that ion pairing strongly perturbs these thermodynamic parameters and even the stoichiometry of the reaction.<sup>1-6</sup> Despite this, some information has been obtained concerning the relative electron-electron repulsion energies in some substituted COT's in hexamethylphosphoramide (HMPA).<sup>7,8</sup>

The nature of ion pairing of the anion radical of COT has been studied in some detail in the etheral solvents and in ammonia by electron spin resonance (ESR).<sup>1-4</sup> Ion pairing of the dianion is, however, much more difficult to observe directly. These difficulties were overcome by Cox and co-workers,<sup>9</sup> who described the NMR spectra of the COT dianion with several different alkali metal cations and solvents. They found that in tetrahydrofuran (THF) the dianion of COT exists as a quadruple ion, where the dianion is ion paired to two cations.<sup>9</sup>

These ion pairing effects not only alter the disproportionation thermodynamics but considerably change the solubility of the dianion, as evidenced by the fact that the observation of precipitated dianion was found to be a function of both the solvent and the counterion.<sup>1</sup> Our intention in this report is in part to describe the thermodynamic parameters controlling the solubility of the COT dianion in

THF and HMPA and use this information to gain insight into the nature of ion pairing of the dianion in HMPA.

It has been previously observed that most anion radicals in HMPA are fully dissociated.<sup>10,11</sup> Only a few anions of highly polar nature where a large charge density exists in a localized area form ion pairs in HMPA.<sup>12</sup> This ion pairing can be increased by the addition of alkali metal salts to the anion radical solution.<sup>12,13</sup> To date there are no known ion pairs of hydrocarbon anion radicals in HMPA.

There is some evidence that the COT dianion is ion paired even in HMPA.<sup>6</sup> This evidence comes from the fact that the  $K_{eq}$  for the reverse disproportionation reaction (eq 1) varies with the cation.<sup>6</sup> This observation, however, seems to be inconsistent with the fact that  $K_{eq}$  was found to fit the stoichiometry of eq 1. If the anion radical was free of ion pairing and the dianion was associated with one cation,  $K_{eq}$  would be expected to be given by

$$K_{eq} = \frac{[\text{COT}^{2-}]^2 [\text{M}^+]}{[\text{COT}^{2-}, \text{M}^+][\text{COT}]} \quad (2)$$

Here we wish to report the thermodynamic parameters controlling the solubility of the COT dianion as a function of the solvent and counterion and the role ion pairing plays in determining these solubilities.

### Experimental Section

The solubility studies were carried out with the use of the apparatus shown in Figure 1. About 10 ml of THF was distilled from the solvated electron through the vacuum line into bulb C of the apparatus, which contained a weighed portion of alkali metal. A little less than 0.5 equiv of COT was then distilled into bulb C via a break seal. This mixture was stirred at room temperature until all of the COT was converted into the dianion. The ESR spectrum of

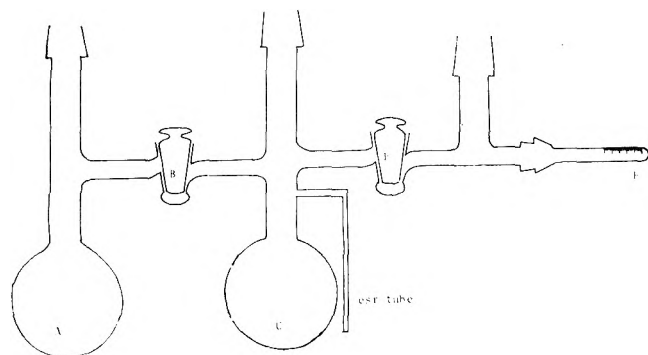


Figure 1. Apparatus used for the solubility determinations.

this solution could be monitored during the reaction with the extending ESR tube. When the reaction mixture failed to yield an ESR signal the reaction was considered to be complete. This normally took about 6 hr. After completion of the reaction the mixture was checked for dianion precipitate. If a precipitate could not be observed, some of the THF was distilled from the mixture. Once the dianion precipitate was observed, the entire apparatus was taken from the vacuum line and immersed into a constant temperature bath and allowed to come to equilibrium for a period of 1 hr. Stopcock E was then opened and a portion of the saturated solution was allowed to pass through the frit and into the graduated tube F. The apparatus was then removed from the bath and the graduated tube separated from the rest of the apparatus. The solution in bulb F was rinsed into a volumetric flask and diluted to 100 ml with distilled water. This solution was then divided into three parts, which were subsequently titrated to a phenolphthalein end point with standardized HCl solution. The number of moles of COT dianion passed into bulb F was considered to be one-half of the number of moles of hydroxide in the THF-water solution.

For the determination in HMPA, the dianion was formed in THF in bulb A. After completion of the reaction, the THF solution was separated from the excess alkali metal by passing this solution into bulb C. The THF was then distilled off and the dry salt was kept under vacuum for a period of 1 hr. HMPA was then dried in bulb A with potassium metal and was distilled into bulb C, which was kept in liquid nitrogen. The saturated HMPA solutions were then treated in a manner identical with that for the THF solutions.

The effect of dissolved salt upon the disproportionation equilibrium was studied with the use of the apparatus shown in Figure 1. The dianion anion radical solution was formed in HMPA bulb A, and the apparatus was sealed off from the vacuum system at point C. An ESR sample of this solution was taken and the remainder of the solution was allowed to pass into bulb D, which contained a known portion of either potassium iodide or sodium chlorate. The apparatus was sealed at point E, and the solution was stirred until all of the salt had dissolved. An ESR sample was taken in the remaining ESR tube.

X-Band ESR spectra were recorded on a Varian E-9 spectrometer equipped with a dual cavity. The temperature was controlled using a Varian V-4557 variable-temperature controller, which was calibrated with a copper-constantan thermocouple. Spin concentrations were compared using the dual cavity technique.

The HMPA was distilled from calcium hydride under re-

duced pressure before use. The inorganic salts were dried in a vacuum oven at 100° for 24 hr before use.

## Results and Discussion

In THF the COT dianion is known to be ion paired with two alkali metal cations,<sup>9</sup> thus  $\Delta G^\circ(\text{soln}) = -RT \ln (\pi^{2-}, M^+_2)$  where  $(\pi^{2-}, M^+_2)$  represents the concentration of the quadruple ion in the saturated solution. The solubility results at the temperatures investigated are given in Table I.

As the solubility data were obtained over a range of temperatures the standard enthalpy of solution was obtained from a plot of  $\ln (\pi^{2-}, M^+_2)$  vs.  $1/RT$ , Figure 2. Since the values for the enthalpy determined in this manner depend upon the fact that only quadruple ions remain in solution, there could be considerable error in the enthalpies if the quadruple ion dissociates at the lower temperatures. This dissociation, however, would result in curvature of the van't Hoff plot. Since no curvature is noted in Figure 2, it is safe to assume that the dianion exists in the form of the quadruple ion at all of the temperatures investigated. It is interesting to note that the solubility of the potassium salt is about two orders of magnitude greater than that for the sodium ion, and the enthalpy of solution of the potassium salt is less endothermic, Table II. Both  $\Delta S^\circ$  and  $\Delta H^\circ$  represent differences in the solution state and the crystal. Thus, crystal lattice energies and entropies are very important in the enthalpy and entropy of solution. It would be difficult to try and distinguish between the importance of solvation and that of crystal lattice effects at this point; but if we consider the third law entropies for the sodium and potassium salts to be about the same, it is clear that there is less solvent ordering for the potassium system. The theoretical entropy and enthalpy of solution of either salt from the gas phase are necessarily negative numbers due to the interactions between the solvent and the salts. The fact that both  $\Delta H^\circ$  and  $\Delta S^\circ$  are positive indicates that both of these salts have rather large crystal lattice energies.

The situation for the COT dianion in HMPA is more complicated since the extent of ion pairing of the dianion is unknown in this solvent. If the COT dianion is free of ion pairing in HMPA, the standard free energy of solution is equal to

$$\Delta G^\circ = -RT \ln \gamma_{\pi^{2-}} m_{\pi^{2-}} \gamma_{M^+}^2 m_{M^+}^2 \quad (3)$$

where  $\gamma_{\pi^{2-}}$  and  $\gamma_{M^+}$  are the mean molal activity coefficients for the dianion and cation, respectively, and  $m_{\pi^{2-}}$  and  $m_{M^+}$  are the molalities of these ions in the saturated solution. For the experiments described here the concentrations are too large for the use of Debye-Hückel theory for the estimation of the activity coefficients. Further, the possibility of ion pairing exists and eq 3 should include another parameter representing the degree of dissociation of the ion pair.<sup>14</sup>

Since the concentrations were not sufficiently low for the use of Debye-Hückel theory and the ion association constants are unknown,  $\Delta G^\circ$  for the dissolution of the salts could only be roughly estimated from

$$\Delta G^\circ = -RT \ln K_{sp} \quad (4)$$

where  $K_{sp}$  was assumed to be equal to the product of the dianion and the square of the total solution cation concentration. The solubilities could be accurately determined, Table III.

The enthalpies of solution were estimated from plots of

**TABLE I: Solubility (*M*) of the COT Dianion (Quadruple Ion) in THF at Various Temperatures**

Na <sub>2</sub> COT		K <sub>2</sub> COT	
Solubility × 10 <sup>3</sup>	<i>T</i> , °C	Solubility × 10 <sup>1</sup>	<i>T</i> , °C
3.00	-23.20	3.92	-21.0
2.34	-22.0	4.26	-15.7
5.48	0.5	4.62	-4.5
8.04	7.8	4.80	1.0
8.15	8.0	5.14	11.2
9.38	11.8	5.30	18.7
9.57	16.1	5.59	26.1
12.2	24.9		
19.2	35.0		

**TABLE II: Thermodynamic Parameters Controlling the Solubility of the COT Dianion in THF at 25°**

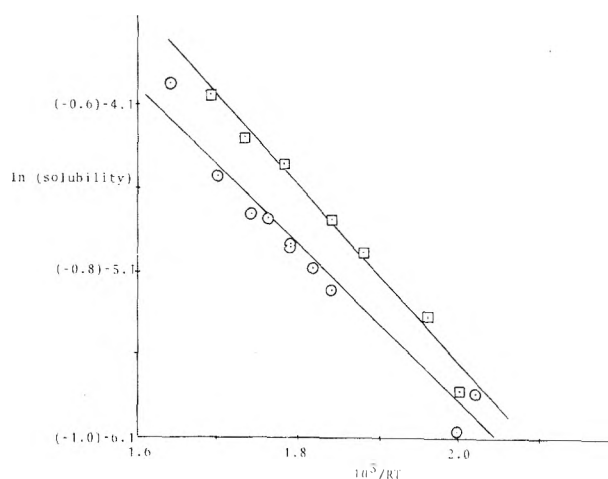
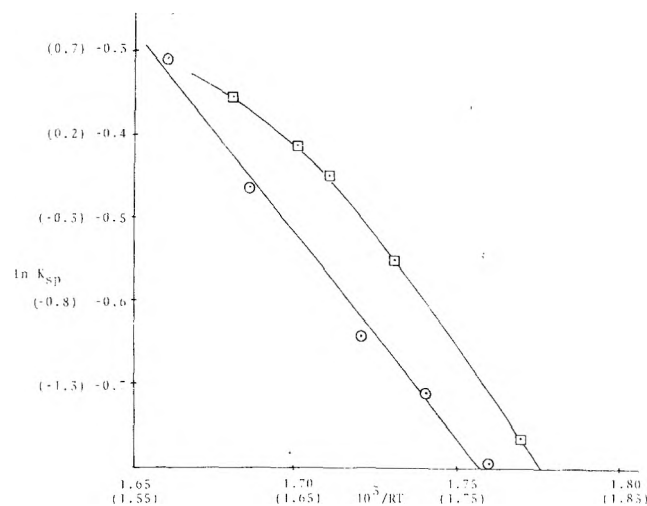
Salt	Δ <i>G</i> <sup>o</sup> , kcal/mol	Δ <i>H</i> <sup>o</sup> , kcal/mol	Δ <i>S</i> <sup>o</sup> , eu
K <sub>2</sub> COT	0.35 ± 0.02	1.09 ± 0.05	2.5
Na <sub>2</sub> COT	2.59 ± 0.02	5.13 ± 0.3	8.5

**TABLE III: Solubility (*M*) of the COT Dianion in HMPA at Various Temperatures**

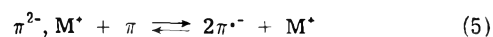
Na <sub>2</sub> COT		K <sub>2</sub> COT	
Solubility × 10 <sup>1</sup>	<i>T</i> , °C	Solubility × 10 <sup>1</sup>	<i>T</i> , °C
1.68	11.7	4.65	12.6
2.56	18.4	5.78	18.1
3.62	25.8	6.40	22.4
8.99	39.1	6.63	24.3
19.4	48.6	7.02	27.3

In  $K_{sp}$  vs.  $1/RT$ , Figure 3. It must be noted here that although the solubilities of the COT dianion salts are accurate to within 0.5% at the various temperatures, there are errors (possibly large errors) in the thermodynamic parameters due to the simplification of eq 3 and the neglect of ion pairing. Curvature of the van't Hoff plot for the potassium system indicates that ion pairs with the dianion are forming.

From Table III it is clear that the potassium salt is more soluble in HMPA than is the sodium salt, but the difference in solubilities is much less than it is in THF. The solubility of the potassium salt is about the same in the two solvents, but the sodium salt is about 18 times more soluble in HMPA. Since the dielectric constant of HMPA at 25° is 30.5 and that for THF is 8.2,<sup>15,16</sup> it is expected that these salts would be more soluble in the more polar solvent (HMPA). It is surprising that the potassium salt is not more soluble in HMPA than it is in THF, but we must remember that many poorly understood factors go into determining solubility such as the number of molecules that sterically fit into the first solvation shield, the number of molecules in each succeeding solvation sheath, and the spatial relationship between the anion and the cation in systems that undergo ion pairing.

**Figure 2.** Plots of  $\ln(\text{solubility})$  vs.  $10^3/RT$  for the disodium cyclooctatetraene and dipotassium cyclooctatetraene systems in THF. For the potassium system the numbers are given in parentheses, and the plot is represented by  $\square$ . The line represented by  $O$  is for the sodium system.**Figure 3.** Plots of  $\ln K_{sp}$  vs.  $10^3/RT$  for the disodium cyclooctatetraene and the dipotassium cyclooctatetraene systems in HMPA. For the sodium system the numbers are given in parentheses and the plot is represented by  $O$ . The line represented by  $\square$  is for the potassium system.

In order to gain more information as to the extent of ion pairing in these systems, we have determined the effect of added salt upon the reverse disproportionation (comproportionation) equilibrium. If the COT dianion exists free of ion pairing, the comproportionation equilibrium is defined by eq 1. However, if the dianion is ion paired with one alkali metal cation, the equilibrium is given by eq 5. The possi-



bility of the existence of the quadruple ion or the ion pair of the anion radical was ruled out in HMPA.<sup>10,11</sup> The equilibrium constant for this reaction is given by eq 2. If the observed equilibrium constant ( $K_{obsd}$ ) is taken as

$$K_{obsd} = (\pi^{\cdot-})^2 / (\pi)(\pi^{2-})_t \quad (6)$$

where  $(\pi^{2-})_t$  is the total dianion concentration  $\{(\pi^{2-}, M^+) + (\pi^{2-})\}$ , then

$$K_{obsd} = K_f / \{1 + (M^+)(K_{diss})^{-1}\} \quad (7)$$

where  $K_f$  represents the disproportionation equilibrium constant for the system containing only free ions and  $K_{\text{diss}}$  is the dissociation constant for the ion pair (eq 8).

$$K_{\text{diss}} = (\pi^{2-})(\text{M}^+)/(\pi^{2-}, \text{M}^*) \quad (8)$$

From eq 7 it is clear that the addition of alkali metal salts (KI or NaClO<sub>3</sub>) to solutions of the COT dianion and anion radical in HMPA should result in a decrease in  $K_{\text{obsd}}$ .

For the over modulated ESR spectra of the anion radical the anion radical concentration is proportional to the amplitude of the ESR line ( $A$ ), and  $K_{\text{obsd}}$  can be expressed as shown in eq 9 where  $B$  is simply a proportionality con-

$$K_{\text{obsd}} = (BA)^2/(\pi)(\pi^{2-})_t \quad (9)$$

stant.<sup>6</sup> Using the dual cavity technique, a simple comparison of  $A$  for samples with and without added salt allows us a comparison of  $K_{\text{obsd}}$  for the samples with various sodium and potassium cation concentrations.

No change in  $K_{\text{obsd}}$  could be observed upon addition of NaClO<sub>3</sub> from 0 to 0.3  $M$ . In order for  $K_{\text{obsd}}$  to remain constant within experimental error,  $K_{\text{diss}}$  must be very large. With the dual cavity technique used here, a change in  $K_{\text{obsd}}$  by more than about 5% would certainly be observed. For the change in  $K_{\text{obsd}}$  to be less than 5% with the addition of 0.3  $M$  salt,  $K_{\text{diss}}$  must be greater than 6. Thus, we are probably correct in assuming that  $\Delta G^\circ$  of solution is equal to  $-RT \ln K_{\text{sp}}$  for the sodium system. Addition of KI to the COT-HMPA-K system does result in a decrease in  $K_{\text{obsd}}$  indicating that there is extensive ion pairing of the dianion and the thermodynamic parameters controlling the solubility of the dipotassium cyclooctatetraeneide cannot be calculated in this simple manner.

All of the data presented to this point indicate that the COT dianion is completely free of ion pairing with the sodium cation, but it is ion paired with the potassium ion. It has been previously reported that the thermodynamic parameters controlling the disproportionation reaction (eq 1) are dependent upon the alkali metal cation in HMPA, which means that some ion pairing must exist.<sup>7</sup> These parameters were measured again in the same manner<sup>7</sup> but utilizing the more accurate dual cavity technique.  $K_{\text{obsd}}$

TABLE IV: Thermodynamic Parameters for Eq 1 in HMPA at 25°

Metal	$10^5 K_{\text{obsd}}$	$\Delta H^\circ$ , kcal/mol	$\Delta S^\circ$ , eu
Na	230 ± 100	-5.3 ± 0.3	-30
K	2.3 ± 1	-4.7 ± 0.3	-37

and  $\Delta H^\circ$  were found to be within experimental error of those previously reported, Table IV (the entropy terms are multiplied by a constant in ref 7 and are corrected in Table IV). The fact that  $K_{\text{obsd}}$  for the Na system is larger than that for the K system by a factor of 100 indicates that  $K_{\text{diss}}$  for the potassium system is ca.  $10^{-2}$ . This explains the curvature in Figure 3 for the potassium system.

*Acknowledgments.* We are grateful to Research Corporation for the support of this work.

### References and Notes

- (1) H. L. Strauss, T. J. Katz, and G. K. Fraenkel, *J. Am. Chem. Soc.*, **85**, 2360 (1963).
- (2) F. J. Smentowski and G. R. Stevenson, *J. Am. Chem. Soc.*, **89**, 5120 (1967).
- (3) R. D. Allendolfer and P. H. Rieger, *J. Am. Chem. Soc.*, **87**, 2336 (1965).
- (4) F. J. Smentowski and G. R. Stevenson, *J. Phys. Chem.*, **73**, 340 (1969).
- (5) H. van Willigen, *J. Am. Chem. Soc.*, **94**, 7966 (1972).
- (6) G. R. Stevenson and J. G. Concepción, *J. Phys. Chem.*, **76**, 2176 (1972).
- (7) G. R. Stevenson and J. G. Concepción, *J. Am. Chem. Soc.*, **95**, 5692 (1973).
- (8) G. R. Stevenson, I. Ocasio, M. Colon, and A. McB. Block, *J. Am. Chem. Soc.*, submitted for publication.
- (9) R. H. Cox, L. Harrison, and W. K. Austin, *J. Phys. Chem.*, **77**, 200 (1973).
- (10) G. Levin, J. Jagur-Grodzinski, and M. Szwarc, *J. Am. Chem. Soc.*, **92**, 2268 (1970).
- (11) (a) A. Cserhegyi, J. Chaudhuri, E. Franta, J. Jagur-Grodzinski, and M. Szwarc, *J. Am. Chem. Soc.*, **89**, 7129 (1967); (b) A. Cserhegyi, J. Jagur-Grodzinski, and M. Szwarc, *ibid.*, **91**, 1892 (1969).
- (12) (a) G. R. Stevenson and A. E. Alegria, *J. Phys. Chem.*, **77**, 3100 (1973); (b) G. R. Stevenson, L. Echegoyen, and L. R. Lizardi, *ibid.*, **76**, 1439 (1972).
- (13) (a) G. R. Stevenson and L. Echegoyen, *J. Phys. Chem.*, **77**, 2339 (1973); (b) G. R. Stevenson, L. Echegoyen, and H. Hidalgo, *ibid.*, **77**, 2649 (1973).
- (14) J. Strong and T. R. Tuttle, Jr., *J. Phys. Chem.*, **77**, 533 (1973).
- (15) J. E. Dubois and H. Vill, *J. Chim. Phys.*, **62**, 699 (1965).
- (16) N. E. Hill, *Proc. R. Soc. (London), Ser. A*, **240**, 101 (1957).

## Thermodynamic Quantities for the Transfer of Urea from Water to Aqueous Electrolyte Solutions

Martha Y. Schrier, Peter J. Turner, and Eugene E. Schrier\*

Department of Chemistry, State University of New York at Binghamton, Binghamton, New York 13901 (Received January 29, 1975)

Publication costs assisted by the State University of New York

Enthalpies of solution of urea (*c*) were determined at 25° in water and in solutions of electrolytes, mainly alkali and alkaline earth halides, over a range of salt molalities at urea molalities below 0.03 *m*. Slopes of the plots of enthalpy of transfer of urea vs. salt molality were obtained at infinite dilution of both solutes. Gibbs free energies of transfer of urea from water to solutions containing one of the salts, LiCl, NaCl, KCl, or CsCl, were obtained by potentiometric and isopiestic measurements. Entropies of transfer were calculated. Enthalpy-entropy compensation is observed with a compensation temperature of  $T^* = 280^\circ\text{K}$ . An interpretation of the trends in the data is given based on the Friedman cosphere model. No conclusions can be drawn from data at low molalities regarding the effectiveness of amide group-salt interaction in the mechanism of isothermal protein denaturation.

### Introduction

Urea-water solutions have been the subject of intense experimental<sup>1</sup> and theoretical investigation.<sup>2</sup> The polarity of urea, its hydrogen-bonding ability, and its consequent high solubility in water provides intrinsic interest. The protein-denaturing ability of urea in aqueous solutions has also attracted attention.

Thermodynamic quantities for the transfer of solutes from water to urea-water mixtures have been determined recently in the hope of elucidating the structural features of the mixed solvent which cause it to differ from water. Studies involving nonpolar solutes<sup>3</sup> have suggested that the addition of urea to water destabilizes water structure leading to the disruption of hydrophobic bonds in proteins. Recently, Ben-Naim and Yaacobi<sup>4</sup> have reached a different conclusion regarding hydrophobic interactions based on their studies of hydrocarbon solubilities in aqueous urea solutions. They suggested that urea strengthens the hydrophobic interaction rather than weakens it. Quantities for the transfer of electrolytes from water to water-urea mixtures have been obtained by a number of investigators, among them Wen and his collaborators,<sup>5</sup> Stern and Kulluk,<sup>6</sup> Desrosiers et al.,<sup>7</sup> and Cassel and Wood.<sup>8</sup> The results of these workers again suggested the reduction of structure in water-urea mixtures as compared to pure water.

The work to be described here was initiated with a somewhat different point of view than that of previous studies. We required a compound to use in modeling the interaction between an ion and an amide linkage in aqueous solution. This interaction appears to be significant in the mechanism of the denaturation of proteins by salts.<sup>9</sup> Recently, enthalpies of transfer of formamide from water to salt solutions were obtained<sup>10</sup> over a limited range of salt molalities. The greater stability of urea makes it better suited than formamide to be a model for the amide linkage in aqueous salt solutions.

The program which we have established for this work calls initially for the development of thermodynamic information which can be accurately extrapolated to limiting molalities of both salt and urea. In this way, parameters are obtained for the interaction of a urea molecule with a particular pair of ions in the aqueous medium. The availability

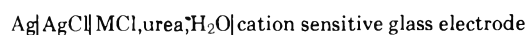
of these parameters allows us to assess the various factors which influence this interaction. The next phase of the work, more pertinent to protein denaturation, will be directed to solute-solute interaction at higher solute concentrations.

### Experimental Section

**Materials.** Urea (Fisher) was twice recrystallized from anhydrous methanol and dried under vacuum for 72 hr at room temperature. Tris(hydroxymethyl)aminomethane obtained from Sigma Chemical Co. as Trizma Base was dried at 80° under vacuum. Tetramethylammonium bromide (Eastman), recrystallized twice from a 3:1 methanol-ethanol mixture, was dried under vacuum at 60°. The remaining salts were reagent grade and were dried overnight at 110° before use. Concentrated stock solutions were prepared of hydrated salts and of other salts which were difficult to weigh directly in air. These stock solutions were passed through a 1.2- $\mu$  Millipore filter and analyzed for halide using  $\text{AgNO}_3$  in a potentiometric method. All solutions were made up with glass distilled water on a molality basis, i.e., moles of solute per kilogram of water as the solvent.

**Calorimetry.** Enthalpies of solution were measured using an LKB Model 8700-1 precision calorimeter in conjunction with a potentiometric recorder. Electrical calibrations were performed before and after the solution experiments. All calibrations and solution reactions were carried out at equal intervals on either side of the mean temperature,  $25.000 \pm 0.005^\circ$ . The corrected resistance change was determined by linear extrapolation of the before and after drift curves to that time which corresponded to 63% of the heat absorption for the solution experiments and to 50% of the heat evolution for the calibrations.

**Potentiometry.** The technique for obtaining the data has been described.<sup>11,12</sup> In general, potential differences were measured between two cells of the form



where the glass electrode is common to each cell. Each cell contained the same salt molality but different urea molalities. Monovalent cation electrodes (Beckman no. 39137 and Corning no. 476220) were used for the LiCl-urea and

KCl-urea solutions while a Corning sodium electrode (no. 476210) and the Beckman cation electrode were used to measure potentials for the NaCl-urea system. An Electronics Instruments Limited (EIL) ammonium-potassium electrode was used in CsCl-urea mixtures. Silver chloride reference electrodes were prepared from Beckman silver billet electrodes by electrolysis in 0.1 M HCl for 3 min with a 15-mA current. Cell potentials were read to  $\pm 0.02$  mV with a Keithley 630 potentiometric electrometer. All runs were carried out at  $25.0 \pm 0.1^\circ$  under a nitrogen atmosphere.

The pH range of optimum electrode response to each salt was determined potentiometrically by titrating a 0.1 M salt solution (pH 11-12) with 0.1 M HCl. Because of the limited pH range in which the electrode responded to metal ion for CsCl-urea solutions and because of low electrode sensitivity to the metal ion in this system and in LiCl-urea, the apparent slow hydrolysis of urea presented more difficulty in these systems than in the others. Frequent adjustment of the solution pH was necessary. Potential readings were made only when the pH values of both urea solutions were the same.

For the NaCl-urea and KCl-urea solutions, the potential differences were reproducible to  $\pm 0.1$  mV for two or three electrode transfers between the cells. Results for LiCl-urea and CsCl-urea were less reliable ( $\pm 0.2$  mV) for the reasons mentioned above.

Separate studies on pure salt solutions confirmed that the electrodes obeyed the Nernst equation within experimental error. Consequently, the theoretical Nernst slope, 118.3 mV, was used in all calculations.

*Isopiestic Measurements.* The technique and apparatus have been described.<sup>13</sup> Urea was used throughout as the reference solute. Generally, the solutions were allowed to equilibrate at  $25.0 \pm 0.1^\circ$  for 1 week or less. The experimental results consisted of a set of molalities of the reference solute plus a set of molalities of various mixtures of urea and the salt of interest.

## Results

*Calorimetry.* The accuracy of the calorimeter was determined by measuring the enthalpy of reaction of tris(hydroxymethyl)aminomethane with 0.1000 N HCl. Our enthalpy of  $-7113 \pm 3$  cal/mol was in good agreement with that of Prosen and Kilday,<sup>14</sup>  $-7115 \pm 1$  cal/mol. The uncertainty of our value is the standard deviation of the mean of eight determinations.

The enthalpy of solution of urea in water,  $\Delta H_{\text{soln}}^{\text{w}}$ , was measured as  $3654 \pm 1$  cal/mol for the molality range, 0.01-0.03 *m*. The uncertainty is the standard deviation of the mean of 22 determinations. This value is in good agreement with that of Egan and Luff<sup>15</sup> who obtained a value of  $3656 \pm 1$  cal/mol by extrapolation of their data to infinite dilution. Our value also agrees within experimental error with that determined by Subramanian et al.,<sup>16</sup>  $3686 \pm 33$  cal/mol.

The enthalpies of solution of urea in a variety of salt solutions,  $\Delta H_{\text{soln}}^{\text{ws}}$ , were determined as a function of salt molality at urea molalities between 0.01 and 0.03 *m*. These data are given in Table 1M.<sup>17</sup> In separate experiments with NaCl at fixed salt molality, it was shown that  $\Delta H_{\text{soln}}^{\text{ws}}$  was independent of urea molality in the range considered. These  $\Delta H_{\text{soln}}^{\text{ws}}$  values are, therefore, assumed to refer to infinite dilution with respect to the urea molality.

The enthalpy of transfer of 1 mol of urea from water to a salt solution of a given salt molality

TABLE I: Coefficients for the Representation of  $\Delta H_{\text{tr}}/m_1$  by Eq 3

Salt	No. of data points	Range of $m_1$ , mol kg <sup>-1</sup>	Coefficients	
			$h_{21}^{(0)}$ , cal kg mol <sup>-2</sup>	$h_{21}^{(1)}$ , cal kg <sup>3/2</sup> mol <sup>-5/2</sup>
LiCl	26	0.26-3.0	$-237 \pm 5$	$38 \pm 5$
NaCl	14	0.40-3.0	$-302 \pm 3$	$88 \pm 3$
NaBr	10	0.25-3.0	$-370 \pm 6$	$106 \pm 6$
NaI	11	0.25-3.0	$-394 \pm 10$	$109 \pm 8$
KCl	17	0.25-4.0	$-292 \pm 5$	$77 \pm 4$
CsCl	7	0.27-2.0	$-398 \pm 4$	$122 \pm 4$
MgCl <sub>2</sub>	8	0.10-2.0	$-533 \pm 8$	$103 \pm 9$
CaCl <sub>2</sub>	17	0.20-3.0	$-644 \pm 11$	$157 \pm 10$
CaBr <sub>2</sub>	8	0.10-1.5	$-748 \pm 5$	$187 \pm 7$
CaI <sub>2</sub>	8	0.10-1.6	$-778 \pm 7$	$190 \pm 9$
SrCl <sub>2</sub>	8	0.05-1.5	$-684 \pm 5$	$180 \pm 7$
BaCl <sub>2</sub>	6	0.20-1.4	$-805 \pm 8$	$278 \pm 10$
LaCl <sub>3</sub>	7	0.09-0.8	$-824 \pm 22$	$119 \pm 37$
Me <sub>4</sub> NBr	6	0.20-1.5	$-417 \pm 5$	$134 \pm 6$
Na <sub>2</sub> SO <sub>4</sub>	4	0.10-1.0	$-987 \pm 21$	$637 \pm 31$

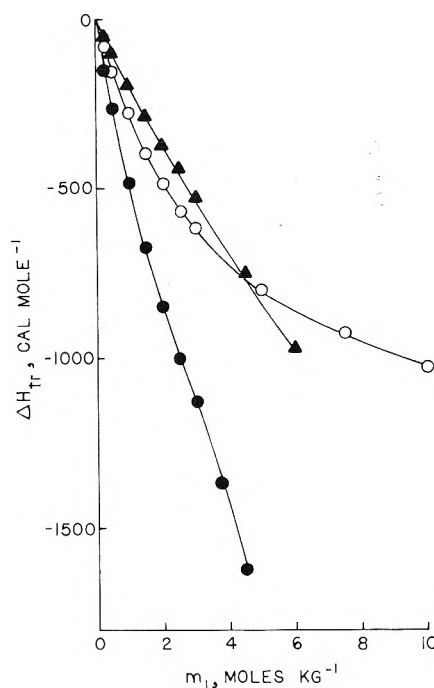


Figure 1. Enthalpies of transfer vs. salt molality for the transfer of urea to solutions of:  $\blacktriangle$ , LiCl;  $\circ$ , NaI;  $\bullet$ , CaCl<sub>2</sub>.

$$\Delta H_{\text{tr}} = \Delta H_{\text{soln}}^{\text{ws}} - \Delta H_{\text{soln}}^{\text{w}} \quad (1)$$

was calculated from the data at different salt molalities for each salt studied. Figure 1 shows the enthalpies of transfer of urea from water to solutions of NaI, LiCl, and CaCl<sub>2</sub> as a function of salt molality. Plots of this kind suggested that the dependence of  $\Delta H_{\text{tr}}$  on salt molality was of the form

$$\Delta H_{\text{tr}} = h_{21}^{(0)}m_1 + h_{21}^{(1)}m_1^{3/2} + h_{21}^{(2)}m_1^2 + \dots \quad (2)$$

where the  $h_{21}^{(i)}$  are empirical constants and  $m_1$  is the salt molality.<sup>18</sup> At sufficiently low salt molalities higher sensitivity in the extrapolation was obtained by ignoring all but the first two terms and rewriting eq 2 as



TABLE II: Coefficients and Their Standard Deviations for the Representation of  $(\partial \log \gamma_2/\partial m_1)_{m_2}$  by Eq 4

System	No. of data points	Solute molality ranges		Coefficients		
		$m_1$ , mol kg <sup>-1</sup>	$m_2$ , mol kg <sup>-1</sup>	$g_{21}^{(0)}$ , kg mol <sup>-1</sup>	$g_{21}^{(1)}$ , kg <sup>3/2</sup> mol <sup>-3/2</sup>	$g_{21}^{(2)}$ , kg <sup>2</sup> mol <sup>-2</sup>
LiCl-urea	70	0.0056-3.0	0.15-5.7	-0.0652 ± 0.0043	0.0114 ± 0.0045	0.00527 ± 0.0014
NaCl-urea	38	0.0013-2.6	0.24-7.6	-0.0429 ± 0.0021	0.0223 ± 0.0027	0.00336 ± 0.00065
KCl-urea	45	0.0028-3.1	0.43-4.8	-0.0288 ± 0.0013	0.0146 ± 0.0012	0.00298 ± 0.00046
CsCl-urea	24	0.0012-3.2	0.95-6.8	-0.0359 ± 0.0028	0.0148 ± 0.0017	0.00250 ± 0.00084

$$\Delta H_{tr}/m_1 = h_{21}^{(0)} + h_{21}^{(1)}m_1^{1/2} \quad (3)$$

The coefficients,  $h_{21}^{(0)}$  and  $h_{21}^{(1)}$ , were then obtained from a plot of  $\Delta H_{tr}/m_1$  vs.  $m_1^{1/2}$ . In practice, a least-squares routine was utilized to obtain the best fit of the data. Table I gives (1) the salt molality ranges for which the fit was obtained, (2) the number of points utilized, (3) the coefficients, and (4) their uncertainties (standard deviations) for all salts studied. Plots of  $\Delta H_{tr}/m_1$  vs.  $m_1^{1/2}$  for NaCl-urea and for CsCl-urea are shown in Figure 2. The lines were calculated from eq 3 and the coefficients of Table I.

The coefficient,  $h_{21}^{(0)}$ , represents the enthalpy of transfer of 1 mol of urea at infinite dilution in water to a salt solution of unit molality which has ion-ion interactions equivalent to those at infinite dilution. As such,  $h_{21}^{(0)}$  is a useful measure of the primary enthalpy of interaction of a urea molecule with a given pair of ions in the aqueous environment. Extraneous concentration dependences are absent.

One may question whether the extrapolation to give  $h_{21}^{(0)}$  (see Figure 2) is valid, i.e., whether the extension of the line to  $m_1 = 0$  should be linear rather than curved. We tested this extrapolation procedure using the system Me<sub>4</sub>NBr-urea. Cassel and Wen<sup>5</sup> obtained enthalpies for the transfer of 1 mol of Me<sub>4</sub>NBr at infinite dilution from water to urea solutions of various molalities. Extrapolation of their data to zero urea molality gives the coefficient,  $h_{12}^{(0)}$ , for this system as  $-392 \pm 20$  cal/mol. Stern and co-workers<sup>19</sup> have shown that  $h_{12}^{(0)}$  must equal  $h_{21}^{(0)}$  at infinite dilution. Our value of  $h_{21}^{(0)}$  from Table I is  $-417 \pm 5$  cal/mol which agrees with the value of Cassel and Wen for  $h_{12}^{(0)}$  within experimental error. Since the dependence of the enthalpies of transfer on solute molality must be different in the respective systems, it would be an unlikely accident to obtain numerical agreement within experimental error from two incorrect extrapolations. We suggest that this agreement supports the validity of our extrapolation procedure.

**Potentiometry.** Table 2M gives the measured potential differences between the cells at various salt and urea molalities for the systems LiCl-urea, NaCl-urea, KCl-urea, and CsCl-urea.<sup>17</sup> These data were analyzed by methods previously described<sup>11,12</sup> to give values of the quantity  $(\partial \log \gamma_2/\partial m_1)_{m_2}$  for each data point. Here  $\gamma_2$  is the molal activity coefficient of urea. For each salt-urea system, correlation was accomplished by means of an equation of the form<sup>20</sup>

$$(\partial \log \gamma_2/\partial m_1)_{m_2} = g_{21}^{(0)} + g_{21}^{(1)}m_1^{1/2} + g_{21}^{(2)}m_2 \quad (4)$$

and a least-squares routine. Table II gives for each system the molality ranges in which data were obtained, the num-

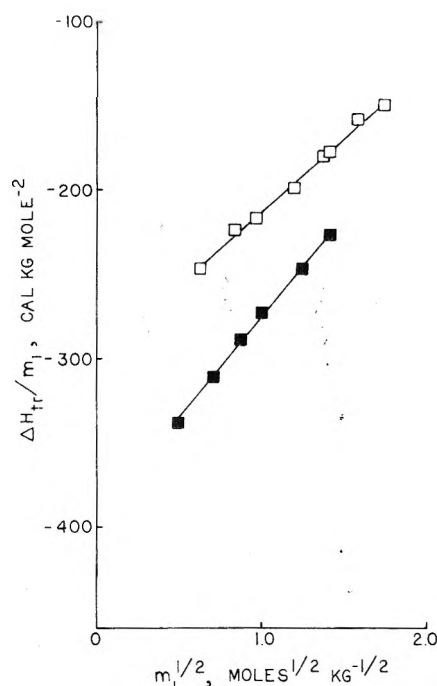


Figure 2. Enthalpies of transfer divided by the salt molality vs. the square root of the salt molality for the transfer of urea to solutions of: □, NaCl; ■, CsCl.

ber of data points taken, the values of the coefficients, and their standard deviations.

**Isopiestic Measurements.** Table 3M gives the solute molalities of solutions in isopiestic equilibrium and the values of  $\Delta/m_1m_2$ <sup>13</sup> for the systems LiCl-urea and CsCl-urea.<sup>17</sup> The osmotic coefficients of aqueous solutions of urea, LiCl, and CsCl required in the calculation of  $\Delta/m_1m_2$  were obtained from the literature.<sup>21-23</sup>

The values of  $\Delta/m_1m_2$  were correlated using a least-squares routine by means of an equation of the form<sup>20</sup>

$$\Delta/m_1m_2 = 2.303\{g_{21}^{(0)} + g_{21}^{(1)}m_1^{1/2} + g_{21}^{(2)}m_2\} \quad (5)$$

For the two systems, Table III gives the molality ranges in which data were obtained, the number of data points taken, the values of the coefficients, and their standard deviations.

**Comparison of Potentiometric and Isopiestic Results.** In principle, the numerical values of the coefficients of eq 4 and 5 should be the same. Comparison of the coefficients in Tables II and III indicates that the agreement is good in the case of the urea-LiCl system and poor for CsCl-urea. Some variation in the parameters is produced by the different ranges over which the data are fit.

A better test of the agreement of the data from the two

TABLE III: Coefficients and Their Standard Deviations for the Representation of  $\Delta/m_1m_2$  by Eq 5

System	No. of data points	Solute molality ranges		Coefficients		
		$m_1$ , mol kg <sup>-1</sup>	$m_2$ , mol kg <sup>-1</sup>	$g_{21}^{(0)}$ , kg mol <sup>-1</sup>	$g_{21}^{(1)}$ , kg <sup>3/2</sup> mol <sup>-3/2</sup>	$g_{21}^{(2)}$ , kg <sup>2</sup> mol <sup>-2</sup>
LiCl-urea	16	0.12-1.45	0.24-3.33	-0.0541 ± 0.0020	0.00889 ± 0.0023	0.00439 ± 0.0065
CsCl-urea	23	0.11-2.13	0.23-4.14	-0.0572 ± 0.0043	0.0322 ± 0.0044	0.00377 ± 0.0013

TABLE IV: Comparison of the Values of  $-\log \gamma_2/\gamma_2^0$  Obtained from Potentiometric and Isopiestic Measurements<sup>a, b</sup>

$m_2$	LiCl-urea: $-\log \gamma_2/\gamma_2^0$			NaCl-urea: <sup>c</sup> $-\log \gamma_2/\gamma_2^0$			CsCl-urea: $-\log \gamma_2/\gamma_2^0$		
	$m_1$			$m_1$			$m_1$		
	1	2	3	1	2	3	1	2	3
0	0.0576 (0.0481)	0.1088 (0.0914)	0.1560	0.0280 (0.0130)	0.0437 (0.0192)	0.0515 (0.0208)	0.0261 (0.0357)	0.0439 (0.0537)	0.0564
1	0.0523 (0.0437)	0.0983 (0.0826)	0.1402	0.0247 (0.0113)	0.0370 (0.0167)	0.0414 (0.0184)	0.0236 (0.0320)	0.0389 (0.0461)	0.0489
2	0.0470 (0.0394)	0.0878 (0.0738)	0.1244	0.0213 (0.0097)	0.0303 (0.0145)	0.0313 (0.0162)	0.0210 (0.0282)	0.0339 (0.0386)	0.0414
3	0.0418 (0.0350)	0.0772 (0.0650)	0.1086	0.0179 (0.0083)	0.0236 (0.0124)	0.0212 (0.0143)	0.0185 (0.0244)	0.0289 (0.0311)	0.0339
4	0.0365	0.0667	0.0928	0.0146 (0.0070)	0.0169 (0.0106)	0.0111 (0.0127)	0.0160 (0.0206)	0.0239 (0.0235)	0.0264
5	0.0312	0.0562	0.0770	0.0112 (0.0058)	0.0101 (0.0090)	0.0011 (0.0112)	0.0135	0.0189	0.0189
6	0.0260	0.0456	0.0612	0.0079 (0.0048)	0.0034 (0.0077)	-0.0090 (0.0101)	0.0110	0.0139	0.0114
7				0.0045 (0.0039)	-0.0033 (0.0065)	-0.0191 (0.0091)	0.0085	0.0089	0.0039

<sup>a</sup> Isopiestic results are in parentheses. <sup>b</sup> Units of  $m_1$  are moles of salt per kilogram of water; units of  $m_2$  are moles of urea per kilogram of water. <sup>c</sup> Values in parentheses are from ref 25.

methods is provided by comparing the values of  $-\log \gamma_2/\gamma_2^0$  calculated from the coefficients by means of the equation

$$-\log \gamma_2/\gamma_2^0 = m_1\{g_{21}^{(0)} + \frac{2}{3}g_{21}^{(1)}m_1^{1/2} + g_{21}^{(2)}m_2\} \quad (6)$$

where  $\gamma_2^0$  is the activity coefficient of urea in a solution of molality  $m_2$  which contains no salt. The comparison between the potentiometric and isopiestic results is shown in Table IV. The values calculated from the isopiestic data are indicated in parentheses.

The quality of the agreement between the two sets of values in the LiCl-urea and CsCl-urea systems is now comparable and is satisfactory. It does not approach what can be achieved (see the recent study of Phang and Steel<sup>24</sup> on glycine-NaCl) but (1) the slow hydrolysis of urea, (2) the possible attack of the silver electrodes by urea, (3) the low level of the response of the electrodes to Li<sup>+</sup> and Cs<sup>+</sup>, and (4) the generally small deviations from ideality in these systems tend to limit the quality of the data.

The isopiestic data of Bower and Robinson<sup>25</sup> are compared with our potentiometric data for NaCl-urea in Table IV. The agreement is poorer than in the other cases. In addition to the points just given, another possible explanation is the lack of emphasis in their isopiestic study on the low solute molality region. In further discussion, we shall employ the potentiometric values of  $g_{21}^{(0)}$  for all systems investigated here.

## Discussion

The set of  $h_{21}^{(0)}$  and  $g_{21}^{(0)}$  coefficients obtained in this work together with the  $g_{21}^{(0)}$  value from the Na<sub>2</sub>SO<sub>4</sub>-urea system<sup>13</sup> and the  $h_{12}^{(0)}$  and  $g_{12}^{(0)}$  values obtainable from the data of Wen and collaborators<sup>4,5</sup> for the Me<sub>4</sub>NBr-urea and Bu<sub>4</sub>NBr-urea systems comprise the most complete set of limiting interaction coefficients available for a given nonelectrolyte in various salt solutions. Although a quantitative interpretation of these results is well beyond the present level of theoretical understanding of these interactions, a useful working perspective can be developed.

The trends in the  $h_{21}^{(0)}$  values in Table I are marked. As with the formamide-salt systems studied previously,<sup>10</sup> the exothermicity of the  $h_{21}^{(0)}$  values increases with increasing ion size for a given series of alkali or alkaline earth halides. There is also a roughly 1:2:3 ratio of the numerical values of  $h_{21}^{(0)}$  from the alkali halides to the alkaline earth halides to lanthanum chloride.

A few values of  $h_{21}^{(0)}$  for formamide-salt systems are available. They are,  $h_{21}^{(0)} = -275, -305,$  and  $-281$  cal/mol for NaCl, NaBr, and KCl, respectively. The uncertainties for these numbers are ±15 cal/mol. The average 10% difference between these numbers and those for urea given in Table I is in keeping with the 12% difference in dipole moments between urea, 4.20 D, and formamide, 3.71 D.<sup>26</sup> Alternatively, this difference could be the effect of the addi-

**TABLE V: Values of the Limiting Thermodynamic Quantities of Transfer of Urea from Water to Various Salt Solutions at 25°**

Salt	$RT \ln g_{21}^{(0)}$ , cal kg mol <sup>-2</sup>	$h_{21}^{(0)}$ , cal kg mol <sup>-2</sup>	$s_{21}^{(0)}$ , gibbs kg mol <sup>-2</sup>
LiCl	-89 ± 6	-237 ± 5	-0.50 ± 0.04
NaCl	-59 ± 3	-302 ± 3	-0.81 ± 0.02
KCl	-39 ± 2	-292 ± 5	-0.85 ± 0.02
CsCl	-49 ± 4	-398 ± 4	-1.17 ± 0.03
Me <sub>4</sub> NBr <sup>a</sup>	-148	-392 ± 20	-0.82
Bu <sub>4</sub> NBr <sup>a</sup>	-166	466 ± 17	2.12
Na <sub>2</sub> SO <sub>4</sub> <sup>b</sup>	-86	-987 ± 21	-3.02

<sup>a</sup> Data from ref 5. <sup>b</sup>  $RT \ln g_{21}^{(0)}$  data from ref 13.

tional -NH<sub>2</sub> group present in urea. In any case, urea appears to be quite similar to formamide in its interactions with salts, an important consideration in these model studies.

In our discussion of the differences between  $h_{21}^{(0)}$  for formamide and urea, we suggested the possible significance of ion-dipole interactions in these systems. In our view, the contributions of terms involving the work of cavity formation, ion-dipole interactions, dispersion interactions, etc. to the numerical magnitude of the parameters are of real importance. Limited correlations<sup>27</sup> which can be made involving  $h_{21}^{(0)}$  as a function of the ionic radii and the ionic polarizabilities add strength to this contention. There seems little doubt, however, that the trends in these parameters and the companion entropy of transfer values are due to perturbations of the structure of water produced by the solutes.

Table V collects the values and their uncertainties of  $h_{21}^{(0)}$ ,  $RT \ln g_{21}^{(0)}$ , and  $s_{21}^{(0)}$  calculated from the data of the various investigators. The quantity  $RT \ln g_{21}^{(0)}$  represents the Gibbs free energy of transfer while  $s_{21}^{(0)}$  is the entropy of transfer of 1 mol of urea at infinite dilution in water to a salt solution of unit molality which has ion-ion interactions equivalent to those at infinite dilution. A plot of  $h_{21}^{(0)}$  vs.  $s_{21}^{(0)}$  is shown in Figure 3. The slope of the line,  $T^*$ , is  $280 \pm 8^\circ\text{K}$  and the intercept is  $104 \pm 13$  cal/mol. The fit standard deviation is 15%. This type of enthalpy-entropy compensation behavior with  $T^* \approx 280^\circ\text{K}$  appears to be characteristic<sup>28,29</sup> of water structure related processes.

Friedman's cosphere model<sup>29</sup> provides a useful framework with which to rationalize the trends in the data. In this model, a cosphere may be thought of as a layer of water molecules around a solute particle which is perturbed by the presence of the solute. The distinction is made in considering these cospheres between hydration of the first and second kind.<sup>29</sup> While hydration of the first kind arises from ionic or polar field effects, hydration of the second kind refers to a perturbation produced in water by the presence of a solute particle but without the influence of a directional solute-solvent force. For ions and other polar molecules, two, more or less distinct cospheres might correspond to these levels of hydration. They are type I and type II cospheres.

We deal only with type II cospheres. Urea is assumed to possess a type II<sub>sb</sub> cosphere. The subscript, sb, stands for structure breaking meaning that the water in this cosphere contains fewer hydrogen bonds than bulk water. The ions we consider fall into three categories. They may have no

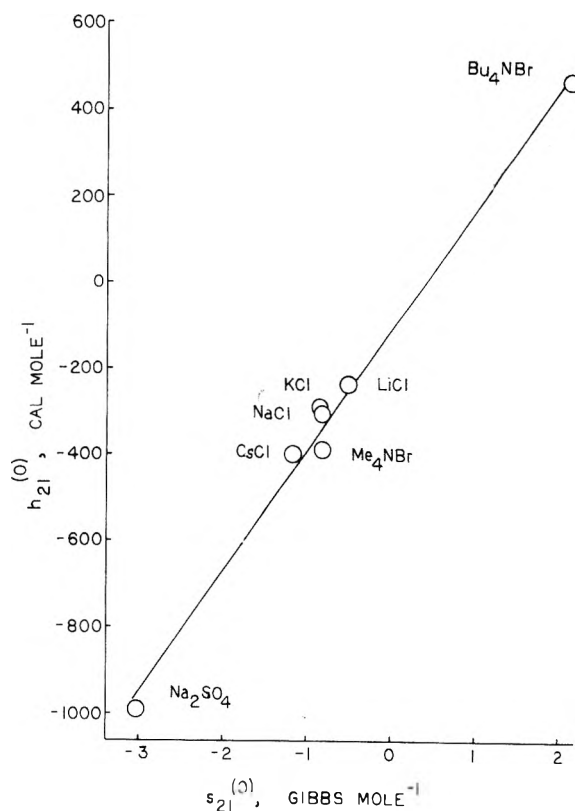


**Figure 3.** Enthalpy-entropy compensation plot for the transfer of urea from water to salt solutions.

type II cosphere, may have a type II<sub>sb</sub> cosphere, or may have a type II<sub>rg</sub> cosphere. The subscript, rg, stands for rare gas. The structure in this cosphere may be considered analogous to that surrounding a rare gas molecule, i.e., there are more hydrogen bonds than in bulk water.

In discussing ion-urea interactions, we assume that overlap of the cospheres of urea with those of the ions leads to destruction of some of the cosphere material of one or both of the ions. Starting with the interactions at the upper right hand corner of Figure 3, overlap of the type II<sub>sb</sub> cosphere of urea with the type II<sub>rg</sub> cosphere of Bu<sub>4</sub>N<sup>+</sup> leads to a net destruction of some of the type II<sub>rg</sub> cosphere, a relaxation of the structured water to bulk water, and a concomitant gain of enthalpy and entropy. Overlap of the type II<sub>sb</sub> cosphere of Br<sup>-</sup> with that of urea will lead to a net destruction of some of the type II<sub>sb</sub> cosphere, a relaxation of unstructured water to bulk water, and a concomitant loss of enthalpy and entropy. The sum of the effects in the solution leads to a net gain of enthalpy and entropy in the transfer process.

Apparently,<sup>29</sup> cosphere II for Li<sup>+</sup> may also be thought of as the rare gas type. For the interaction of LiCl with urea, one obtains a negative enthalpy and entropy of transfer. The processes involving the urea-Li<sup>+</sup> interaction are similar to those discussed above for urea-Bu<sub>4</sub>N<sup>+</sup> but the effect is smaller and (1) the interaction of urea with Cl<sup>-</sup> and (2) the influence of hydration of the first kind lead to negative values in this case. We next consider NaCl. Since Na<sup>+</sup> does not appear to give rise to hydration of the second kind, the enthalpy and entropy values are more nearly the sum of contributions of directional interactions and a cavity term in this case than for any of the other salts considered. While the enthalpies and entropies of transfer for KCl are similar to those for NaCl, the values for CsCl are more negative than for NaCl because of the overlap of the type II<sub>sb</sub>

cospheres of the ions with that of urea resulting in the loss of some of the ionic cosphere material.

Although the position of  $\text{Me}_4\text{NBr}$  may be partially the result of the  $\text{Br}^-$  ion, it does suggest some structure-breaking character to the  $\text{Me}_4\text{N}^+$  cosphere. Finally,  $\text{SO}_4^{2-}$  exhibits either exceptionally large structure-breaking tendencies or a strong H-bonding interaction with urea.

We next consider the effectiveness of these electrolytes as protein denaturants. Denaturation by electrolytes<sup>9</sup> has been thought of in terms of interactions of the electrolyte-water medium with groups which are buried (not exposed to the solvent) in the native state of the protein but which become exposed as the protein is denatured. The free energy of denaturation is comprised of opposite contributions from the unfavorable salting out of nonpolar groups and the favorable interactions of the amide linkage with the salt medium. Ying et al.<sup>30</sup> have obtained data describing the isothermal denaturation of ribonuclease by different salts at 25°. They included  $\text{LiCl}$ ,  $\text{LiBr}$ ,  $\text{LiClO}_4$ ,  $\text{NaClO}_4$ ,  $\text{NaSCN}$ , and  $\text{CaCl}_2$ . Other alkali chlorides and  $\text{Me}_4\text{NBr}$  did not act as denaturants in the concentration range investigated. Although  $\text{Na}_2\text{SO}_4$  was not studied, it is well known to be an *antidenaturant* both from thermal denaturation results<sup>9</sup> and general experience.

Urea may be thought of as a model for the amide linkages which are exposed to the solvent as the protein denatures. Although we hoped that the values of  $RT \ln g_{21}^{(0)}$  would be helpful in determining the denaturing ability of salts, they provide little assistance. The value of  $\text{LiCl}$  is more negative than that for the other alkali chlorides but is the same as that for  $\text{Na}_2\text{SO}_4$ . There is, of course, the difficulty here of accounting for the larger salting out of nonpolar groups by  $\text{Na}_2\text{SO}_4$  than by  $\text{LiCl}$ . The case of  $\text{Me}_4\text{NBr}$  is unambiguous, however. The large negative value of  $RT \ln g_{21}^{(0)}$  for  $\text{Me}_4\text{NBr}$  suggests that it should be a strong denaturant but it is not. Since Wen and Hung<sup>31</sup> have shown that  $\text{Me}_4\text{NBr}$  salts in nonpolar compounds, there would be no loss of denaturing ability through interaction with nonpolar groups.

The concentration of effort by various investigators<sup>9,32</sup> on limiting interaction coefficients<sup>33</sup> has come about because of the desire to interpret the thermal denaturation of proteins, a process which can be described by parameters obtained at low salt concentrations. However, high salt concentrations are required for isothermal denaturation by salts, e.g., 6.2 *m*  $\text{LiCl}$  is the midpoint concentration in the denaturation of ribonuclease at 25°.<sup>30</sup>

Many workers have assumed that the sign and magnitude of the limiting interaction coefficients determine the salt-nonelectrolyte interaction up to high molalities of the solutes. Examination of available Gibbs free energy data for higher solute molalities than those studied here<sup>4,13,25,30</sup> indicate that the situation is more complex. In the systems,  $\text{Me}_4\text{NBr}$ -urea,<sup>5a</sup>  $\text{Bu}_4\text{NBr}$ -urea,<sup>5a</sup> and  $\text{NaCl}$ -urea,<sup>25</sup> at  $m_1 > 1$ ,  $m_2 < 3$ , the quantity,  $(\partial^2 \log \gamma_2 / \partial m_1^2)_{m_2}$ , is positive. In  $\text{Na}_2\text{SO}_4$ -urea,  $\log \gamma_2$  even changes sign from negative to positive at  $\text{Na}_2\text{SO}_4$  molalities greater than 0.75 *m*. In contrast, in the  $\text{LiCl}$ -urea system  $(\partial^2 \log \gamma_2 / \partial m_1^2)_{m_2}$  is positive up to 3 *m*  $\text{LiCl}$  but is negative thereafter. This observation may be significant both for the thermodynamic description

of isothermal protein denaturation and with regard to the controversy which has grown up regarding the interaction of lithium salts with amide linkages in aqueous solution. Thermodynamic studies of both the  $\text{LiCl}$ -urea system and other urea systems containing denaturing salts at high solute molalities will be the subject of a later publication.

*Acknowledgment.* This work was supported in part by Grant No. GM 11762 from the Institute of General Medical Sciences, U.S. Public Health Service.

*Supplementary Material Available.* Tables 1M, 2M, and 3M will appear following these pages in the microfilm edition of this volume of the journal. Photocopies of the supplementary material from this paper only or microfiche (105 × 148 mm, 24× reduction, negatives) containing all the supplementary material for the papers in this issue may be obtained from the Journals Department, American Chemical Society, 1155 16th St. N.W., Washington, D.C. 20036. Remit check or money order for \$4.00 for photocopy or \$2.50 for microfiche, referring to code number JPC-75-1391.

## References and Notes

- (1) R. H. Stokes, *Aust. J. Chem.*, **20**, 2087 (1967).
- (2) H. S. Frank and F. Franks, *J. Chem. Phys.*, **48**, 4746 (1968).
- (3) D. B. Wetlaufer, S. K. Malik, L. Stoller, and R. I. Coffin, *J. Am. Chem. Soc.*, **86**, 509 (1964).
- (4) A. Ben-Naim and M. Yaacobi, *J. Phys. Chem.*, **78**, 170 (1974).
- (5) (a) W. Y. Wen and C. M. L. Chen, *J. Phys. Chem.*, **73**, 2895 (1969); (b) R. B. Cassel and W. Y. Wen, *ibid.*, **76**, 1369 (1972).
- (6) J. H. Stern and J. D. Kulluk, *J. Phys. Chem.*, **73**, 2795 (1969).
- (7) N. Desrosiers, G. Perron, J. G. Mathieson, B. E. Conway, and J. E. Desnoyers, *J. Solution Chem.*, **3**, 789 (1974).
- (8) R. B. Cassel and R. H. Wood, *J. Phys. Chem.*, **78**, 2460 (1974).
- (9) P. H. von Hippel and T. Schleich in "Structure and Stability of Biological Macromolecules", S. Timasheff and G. Fasman, Ed., Marcel Dekker, New York, N.Y., 1969, p 417.
- (10) E. R. Stimson and E. E. Schrier, *J. Chem. Eng. Data*, **19**, 354 (1974).
- (11) M. Y. Spink and E. E. Schrier, *J. Chem. Thermodyn.*, **2**, 821 (1970).
- (12) F. L. Wilcox and E. E. Schrier, *J. Phys. Chem.*, **75**, 3757 (1971).
- (13) E. E. Schrier and R. A. Robinson, *J. Biol. Chem.*, **245**, 2432 (1970).
- (14) E. J. Prosen and M. V. Kilday, *J. Res. Natl. Bur. Stand. U.S., Sect. A*, **77**, 581 (1973).
- (15) E. P. Egan, Jr., and B. B. Luff, *J. Chem. Eng. Data*, **11**, 192 (1966).
- (16) S. Subramanian, T. S. Sarma, D. Balasubramanian, and J. C. Ahluwalia, *J. Phys. Chem.*, **75**, 815 (1971).
- (17) See paragraph at end of text regarding supplementary material.
- (18) Throughout this paper, the subscript 1 will refer to the salt while the subscript 2 will indicate urea.
- (19) J. H. Stern, J. Lazartic, and D. Fost, *J. Phys. Chem.*, **72**, 3053 (1968).
- (20) The coefficients,  $g_{21}^{(0)}$ , replace the coefficients designated A, B, C... or a, b, C... in earlier papers.<sup>11-13</sup>
- (21) H. David Ellerton and P. J. Dunlop, *J. Phys. Chem.*, **70**, 1831 (1966).
- (22) H. F. Gibbard, Jr., G. Scatchard, R. A. Rousseau, and J. L. Creek, *J. Chem. Eng. Data*, **18**, 293 (1973).
- (23) R. A. Robinson and R. Stokes, "Electrolyte Solutions", 2nd ed, Butterworths, London, 1965, p 485.
- (24) S. Phang and B. J. Steel, *J. Chem. Thermodyn.*, **6**, 537 (1974).
- (25) V. Bower and R. A. Robinson, *J. Phys. Chem.*, **67**, 1524 (1963).
- (26) A. L. McClellan, "Tables of Experimental Dipole Moments", W. H. Freeman, San Francisco, Calif., 1963, p 44, 45.
- (27) E. E. Schrier, unpublished calculations.
- (28) R. Lumry and S. Rajender, *Biopolymers*, **9**, 1125 (1970).
- (29) H. Friedmann in "Water, A Comprehensive Treatise", Vol 3, F. Franks, Ed., Plenum Press, New York, N.Y., 1973, p 50.
- (30) A. Ying, D. Blazej, M. Y. Schrier, and E. E. Schrier, unpublished results.
- (31) W. Y. Wen and J. H. Hung, *J. Phys. Chem.*, **74**, 170 (1970).
- (32) P. K. Nandi and D. R. Robinson, *J. Am. Chem. Soc.*, **94**, 1299 (1972).
- (33) The parameter,  $g_{21}^{(0)}$ , is equivalent to the conventional Setschenow parameter when a correction is made for the change of concentration scale.

## Wave-Damping and Film-Pressure Studies of Polydimethylsiloxane Monolayers on Organic Liquid Substrates

R. L. Shuler and W. A. Zisman\*

Naval Research Laboratory, Laboratory for Chemical Physics, Washington, D.C. 20375 (Received June 3, 1974; Revised Manuscript Received March 17, 1975)

Publication costs assisted by the Naval Research Laboratory

The behavior and structure of polydimethylsiloxane films have been investigated on the following five organic liquid substrates: propylene carbonate, tetrahydronaphthalene, hexachloro-1,3-butadiene, 1,4-dichlorobutane, and hexadecane. Systematic measurements were made of (a) the damping of capillary waves by thin films of polydimethylsiloxane, and (b) the film pressure  $F$  as a function of the area per monomer  $A$ . Although stable films were formed on each organic liquid, compression caused some of the film to dissolve once a critical area per monomer was reached. This critical area varied with the nature of the substrate. Before dissolving, each monolayer went through at least one conformational change. The type of structural change which occurred during film compression, as well as the conformation adopted by the polymer chain when first spread on a specific organic liquid, depended to a large degree on the polarity of the organic substrate. Some of the wave-damping results on both clean and film-covered surfaces conformed rather well with predictions derivable from theory. The reasons for this agreement, as well as exceptions, will be discussed.

### Introduction

Ever since Fox, Taylor, and Zisman<sup>1</sup> reported in 1947 that polydimethylsiloxanes could be spread spontaneously as monolayers over the clean surface of water, the subject of the surface activity of these liquid polymers has been a source of wide interest, application, and further research. The subsequent paper by Fox, Solomon, and Zisman<sup>2</sup> generated further interest as they described the remarkable effects of both the pH of the water and the time of contact on the rate of hydrolysis of these synthetic polymers. Later, Banks<sup>3</sup> reported the existence of stable polydimethylsiloxane monolayers on such organic liquid substrates as glycol, oleic acid, and olive oil, and this was followed by the evolution of the all-Teflon film balance by Ellison and Zisman.<sup>4</sup> The Teflon balance permitted a wide variety of studies of the surface activity of the polyorganosiloxanes on organic liquids and really opened an entirely new field of surface chemistry.

### Experimental Section

**Apparatus.** The basic experimental apparatus used to determine the wave-damping coefficient  $k$  and the film pressure  $F$  was the same as that described earlier.<sup>5</sup> However, some experimental modifications were necessary for investigations in which organic liquids, rather than water, were used as substrates. The principal changes were: (a) a new trough was made entirely from one piece of Pyrex glass to prevent contamination from joint-bonding materials; (b) the stroboscope was placed above and to the side of the experimental apparatus (rather than under it as was done in previous work) and its light was reflected up through the organic liquid from a mirror in the floor of the trough because the bottom of the new trough was so thick that not enough light would penetrate it; and (c) a thin film of very low surface energy fluoropolymer, poly-1 H, 1-H-pentadecafluorooctyl methacrylate which was supplied by the Minnesota Mining and Manufacturing Co. and had been de-

scribed by Bennett and Zisman,<sup>6</sup> instead of paraffin wax, was used to coat the walls of the trough to keep the organic liquid from spilling over the sides.

Surface pressures were measured with a Langmuir-Adam type of film balance described earlier.<sup>7</sup> However, since organic liquid substrates were used instead of water, the "end loops" were made of 12- $\mu$  thick strips of Teflon instead of polyethylene. The sensitivity of the film balance was 0.120 dyn cm<sup>-1</sup> (degree of rotation)<sup>-1</sup> of the torsion head, and film pressures could be measured with a precision of 0.1 dyn cm<sup>-1</sup>. The film balance and the wave generator were mounted on an excellent vibration-proof table and were enclosed in a Lucite box to minimize contamination by airborne particles. All measurements reported here were made at room temperature (22  $\pm$  1°).

**Materials Used.** An ethoxy end-blocked polydimethylsiloxane, C<sub>2</sub>H<sub>5</sub>O[Si(CH<sub>3</sub>)<sub>2</sub>O]<sub>110</sub>C<sub>2</sub>H<sub>5</sub>, obtained from the Dow Corning Corp. was used to form the monolayer films. It was percolated through an adsorption column of activated Florisil to remove any polar impurities prior to use and was spread on the substrate in a solution containing about 0.5 mg of polymer per milliliter of freshly distilled isopropyl alcohol (ACS reagent grade). The pure organic liquids used are listed in Table I. All were obtained from the Fisher Scientific Co. Just before each experiment, the particular liquid was percolated slowly through adsorption columns of activated alumina and silica gel to remove water and surface-active contaminants. In order to compare theoretical and experimental wave-damping coefficients, the surface tension, viscosity, and density of each purified liquid substrate were determined. (These are listed in Table I.) Kinematic viscosities were obtained with a calibrated Cannon-Fenske viscometer according to ASTM method D 445-61. The viscometer was immersed in a water bath maintained at 22.0  $\pm$  0.1°. Surface tensions were determined by the Du Nouy method with a Cenco interfacial tensiometer and the correction factors of Harkins and Jordan.<sup>8</sup> Densities were determined in a standard pycnometer.

**TABLE I: Comparison of Observed and Theoretical Wave-Damping Coefficients for Polydimethylsiloxane Films on Pure Organic Substrates**

Substrate liquid	Density at 22° g/cc	Surface tension $\gamma_{22}^\circ$	Kinematic viscosity $\eta$ , cP	Wave-damping coefficient of pure liquid $k_e$			Wave-damping coefficient of film-covered surface		Ratio $k_{\max}/k_i$
				Theory	Expt	Diff, %	$k_i^a$	$k_{\max}^b$	
Dichlorobutane (highest purity grade; bp 153–154°)	1.137	35.12	1.36	0.252	0.245	3	0.425	0.863	2.0
Tetrachloroethane (reagent grade; bp 144–150°)	1.595	34.81	1.69	0.234	0.219	6			
Tetrahydronaphthalene (purified grade; bp 205–207°)	0.969	35.87	2.17	0.310	0.283	9	0.474	0.890	1.9
Propylene carbonate (practical grade; bp 121–123° (17 mm))	1.204	41.84	2.66	0.300	0.262	13	0.454	0.903	2.0
Hexadecane (practical grade; m.p 17–18°)	0.772	27.18	3.27	0.582	0.458	21	0.633		
Hexachlorobutadiene (practical grade; 210–212°)	1.680	35.68	3.30	0.441	0.350	21	0.632	1.190	1.9
Tetrabromoethane (purified grade)	2.962	48.73	10.20	0.882	0.561	36			

<sup>a</sup> Calculated from eq 5. <sup>b</sup> Obtained experimentally.

**Procedure.** In a typical experiment the polydimethylsiloxane was spread by means of a microburet to a predetermined area per monomer by carefully placing small drops of the polymer-alcohol spreading solution over the surface of the freshly percolated organic liquid. When the film had equilibrated (about 10 min), it was compressed by slowly moving the barrier forward a definite distance, usually 1 or 2 cm, by means of a variable-speed motor drive. After the film pressure had stabilized (invariably within 2 min), wave-damping and film-pressure measurements were made. All  $F$  vs.  $A$  and  $k$  vs.  $A$  plots presented are taken from a specific run, but each experiment was repeated at least twice; the results were reproducible as shown by the duplicated experiments. On at least one occasion, a film on each organic liquid was left under a high surface pressure for 1 hr with no significant decrease in  $F$ .

## Results and Discussion

**Films on Propylene Carbonate. Wave Damping and Film Pressure.** Figure 1 shows both the damping coefficient  $k$  and the film pressure  $F$  plotted vs. the area per monomer  $A$  for a polysiloxane film compressed and expanded on a propylene carbonate substrate. As the film was compressed, the  $k$  vs.  $A$  curve had maxima at about 20 and 12 Å<sup>2</sup>/monomer, with a minimum in between at about 16 Å<sup>2</sup>/monomer. This result is almost identical, down to the second maximum, with that obtained<sup>9</sup> for the same film compressed on water. Since polydimethylsiloxanes are known to adsorb on water, this immediately suggested that the film was adsorbing water from either the atmosphere or the substrate. Therefore, the experiment was repeated with precautionary measures to minimize that possibility. The experimental chamber was flushed with dehumidified air until the water in the atmosphere reached a low minimum of 26 ppm. The resistivity of the propylene carbonate measured 1.62 megohms before and 1.80 megohms after the experiment; the near agreement between these two values

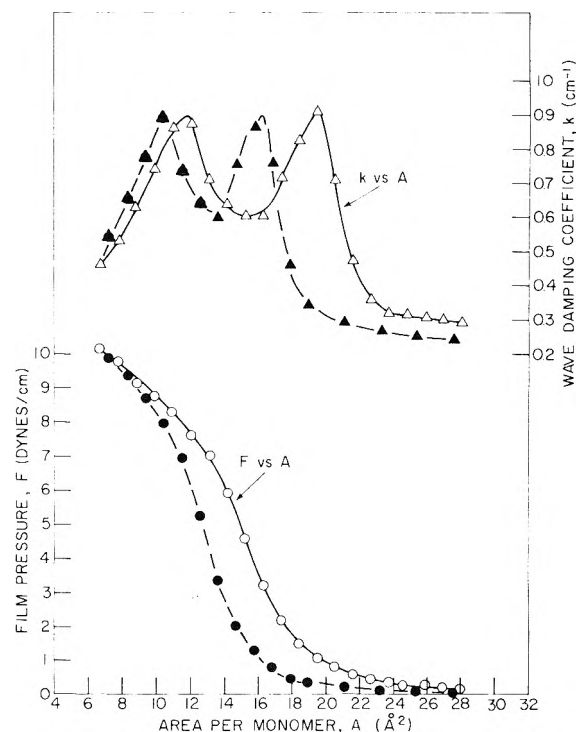


**Figure 1.** Damping coefficient and film pressure vs. area per monomer for polydimethylsiloxane film on propylene carbonate at 22.0°: open symbols, compression; filled symbols, expansion.

was good evidence that the substrate adsorbed little water during the experiment. The resulting wave-damping and film-pressure values were, within experimental error, the same as those obtained in an atmosphere of 30–50% relative humidity. Thus, it appeared that the films did, in fact, behave similarly on propylene carbonate and water when compressed to 12 Å<sup>2</sup>/monomer. However, at smaller areas

per monomer, the film behavior was obviously different on the two substrates as evidenced by the difference in the  $k$  vs.  $A$  curves and by the hysteresis that occurred in films on propylene carbonate. (Those compressed on water to very low monomer areas by Fox, Taylor, and Zisman<sup>1</sup> were reversible when expanded.) In the film compressed on water,  $k$  passed through a low value of about  $0.1 \text{ cm}^{-1}$  at approximately  $10 \text{ \AA}^2/\text{monomer}$ , then rose rapidly to pass through a third maximum at about  $8 \text{ \AA}^2/\text{monomer}$ . As the film was compressed on propylene carbonate (Figure 1), the value of  $k$  progressively decreased below its value at  $12 \text{ \AA}^2/\text{monomer}$  with no hint of a change in the slope of the curve.

As a first step in interpreting the experimental results, it was assumed that whenever a maximum or minimum appeared in the  $k$  vs.  $A$  curve, all of the polymer chains were in one structure and were packed to the utmost at that point. Therefore, Stuart and Briegleb molecular models were used to find plausible polydimethylsiloxane conformations with monomer areas of 12, 16, and  $20 \text{ \AA}^2$ . The polymer was put initially in a regular zigzag arrangement; this should be a stable structure for the siloxane chain and had already been proposed by Fox, Taylor, and Zisman,<sup>1</sup> as the one assumed on water at a certain level of compression. By use of a molecular model, these workers found that, if the zigzag chain was oriented so that the silicon and oxygen atoms were vertical to each other, a monomer unit occupied  $16 \text{ \AA}^2/\text{monomer}$  and was about  $7.9 \text{ \AA}$  high. The latter value was the same as the average film thickness calculated from the bulk density ( $0.984 \text{ g/cm}^3$ ).<sup>10</sup> Therefore, the minimum in the  $k$  vs.  $A$  curve at  $16 \text{ \AA}^2/\text{monomer}$  was ascribed to a fully packed film with the chains in the zigzag structure oriented as described above. A simplified molecular model of this conformation is shown in Figure 2.

This interpretation became more probable after it was found that when a molecular model of this structure was rotated  $90^\circ$  about its long axis (so that the Si-O-Si groups were oriented horizontally), each monomer now occupied about  $20 \text{ \AA}^2$  (the area at which the first peak appeared in the  $k$  vs.  $A$  curve). The height of the chain in the new orientation was estimated to be  $6.2 \text{ \AA}$ , the same as the calculated film thickness at  $20 \text{ \AA}^2/\text{monomer}$ . Thus, the horizontal zigzag conformation seems an excellent choice for the structure of the polymer molecules when they are spread at the higher areas per monomer. According to this interpretation, compression of the film from  $20$  to  $16 \text{ \AA}^2/\text{monomer}$  merely causes the film molecules to turn about their main axes while the chains remain horizontal to the liquid surface. At  $16 \text{ \AA}^2/\text{monomer}$ , all of the chains have been rotated exactly  $90^\circ$  and the film is packed to the utmost with the molecules in the new orientation.

It is uncertain whether the methyl or the Si-O-Si groups serve to anchor the polymer chains to the substrate. However, if the zigzag structure is in either of the orientations described above, and if the Si-O-Si groups are in or near the plane of the liquid surface, half of the methyl groups must be beneath the surface in the bulk liquid, and these groups would probably interact readily with the organic substrate.

It was postulated that further compression of a polydimethylsiloxane film with the chains in the zigzag conformation ( $16 \text{ \AA}^2/\text{monomer}$ ) on water forms helices with an average of six monomers per turn.<sup>1</sup> The same change probably occurred on propylene carbonate because a peak appeared in the  $k$  vs.  $A$  curve at  $12 \text{ \AA}^2/\text{monomer}$  which is, according to molecular models, about the monomer area to be expect-

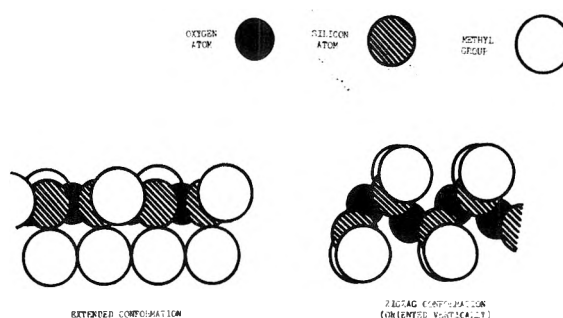


Figure 2. Simplified molecular models for the polydimethylsiloxane chain.

ed for such a helix. The height of the helix was estimated to be  $11 \text{ \AA}$ , which compares reasonably with the calculated film thickness of  $10.5 \text{ \AA}$  at  $12 \text{ \AA}^2/\text{monomer}$ .

The rise in the value of  $k$  in the region of  $16$  to  $12 \text{ \AA}^2/\text{monomer}$  indicates that the formation of the helices strengthens the interaction between the film molecules and substrate. This result is plausible if one considers the general orientation of the atoms in the six-membered helix. When this structure is formed from the zigzag conformation, the Si-O-Si groups are pulled toward the interior of the helix, leaving the hydrophobic methyl groups on the outside. This shielding of the polar silicon and oxygen atoms and the easy accessibility of the hydrocarbon groups to the organic substrate should greatly strengthen the film-substrate interaction. This would cause  $k$  to increase, as observed, probably because the surface viscosity becomes greater as the helices are formed. On the other hand, on water, the value of  $k$  decreases as helices are being formed because the oxygen and silicon atoms are being removed from the surface in the process.<sup>9</sup>

No further transitions occur in films compressed below  $12 \text{ \AA}^2/\text{monomer}$  since, as Figure 1 shows,  $k$  decreases steadily from that point down to low monomer areas. Nevertheless, compression beyond  $12 \text{ \AA}^2/\text{monomer}$  must drastically change the film because at that area it becomes irreversible when the pressure is relieved.

**Hysteresis Effects.** The expansion curves shown in Figure 1 provide a strong clue as to what causes hysteresis in these films. Both curves are very similar in shape to the compression curves, the main difference being that the expansion curves are shifted to lower areas per monomer. A simple interpretation is that compression beyond  $12 \text{ \AA}^2/\text{monomer}$  causes some of the film molecules to disappear into the propylene carbonate, a good possibility since, as mentioned earlier, the helical structure should enhance the solubility of polydimethylsiloxane in organic liquids. If this is true, the values of  $A$  in the expansion curves are all too low, of course, since they were calculated on the assumption that the film still contains all of the polymer initially spread on the substrate. The actual number of monomers left in the film can be calculated if it is assumed that expansion involves the same transformations as occur during compression, but in reverse order, that is, the transformations are reversible. Then, the first peak in the  $k$  vs.  $A$  expansion curve at an apparent area per monomer of  $10 \text{ \AA}^2$  actually represents a close-packed film of helices which have a monomer area of  $12 \text{ \AA}^2$ . By using  $12 \text{ \AA}^2$  as the true area per monomer when  $k$  passed through the first expansion maximum and knowing the area of the liquid surface, the number of monomers in the liquid surface can be easily

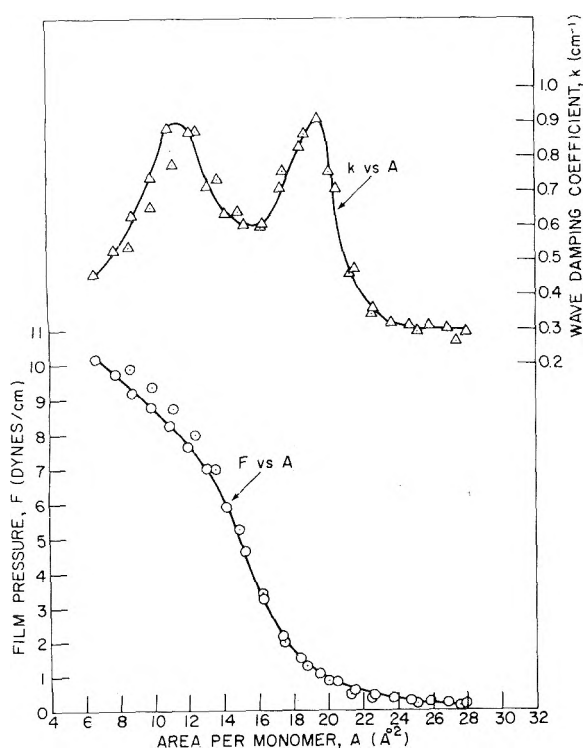


**Figure 3.** Damping coefficient and film pressure vs. area per monomer for polydimethylsiloxane film on propylene carbonate: open symbols, points reproduced from compression of film shown in Figure 1; dots within symbols, points recalculated as explained in text for the expansion of film shown in Figure 1.

calculated. This gives  $21.5 \times 10^{16}$  monomers on the liquid surface at the end of the compression as compared to  $25.8 \times 10^{16}$  monomers initially deposited.

By use of this new value, the areas per monomer were recalculated for the expansion data and the results are shown in Figure 3 compared with the unmodified compression curves. The new points fall quite close to the compression curve, although there are some deviations at the lower values of  $A$ . These deviations can be explained by assuming that at the end of the compression some of the long chains were partially immersed in the substrate and that the energy necessary to bring them back into the liquid surface was different from that required to force them into the bulk phase by compression. This difference in energies would naturally be reflected in different  $k$  and  $F$  values until all of the formerly immersed chain segments were once more in the liquid surface. When this occurred, the film would be fully packed with helices and the expanded film would be strictly comparable to the film when it was compressed to that point. Accordingly, Figure 3 shows that the recalculated  $k$  and  $F$  values fell much closer to the compression curves at  $A > 12 \text{ \AA}^2$ .

Thus we conclude that, if compression does not expel some of the polymer molecules from the liquid surface after the film becomes fully packed with helices, polydimethylsiloxane films will be completely reversible on propylene carbonate just as they are on water. The observed experimental difference is due to the organic methyl groups on the outside of the helix favoring solubility of the film in propylene carbonate but hindering its dissolution in water. Compression of a film past  $12 \text{ \AA}^2/\text{monomer}$  causes more and more of the polymer molecules to be lost into propylene carbonate, whereas on water it merely rearranges the film

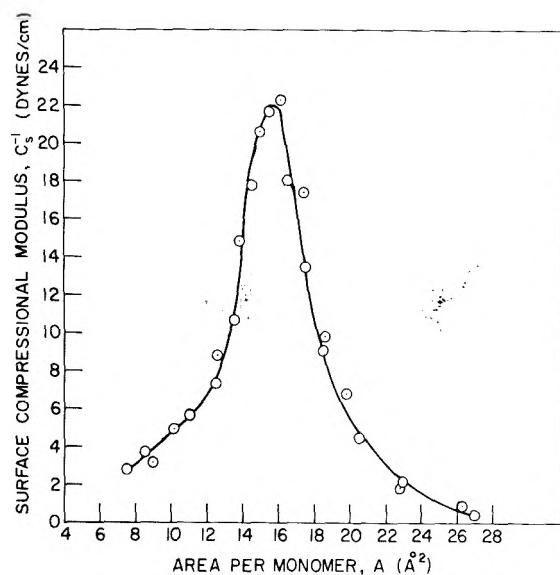


**Figure 4.** Compressibility curve of polydimethylsiloxane film on propylene carbonate: open symbols, compression of film shown in Figure 1; symbols with dots, expansion of film shown in Figure 1 but points recalculated as explained in text.

molecules in the surface into a more upright position.<sup>1</sup> Because of the low interaction energy between the helix and the underlying water, this can occur reversibly.

**Compressibility Studies.** The compressibility of the monolayers was studied by calculating the modulus of compressibility, defined by  $C_s^{-1} = -A dF/dA$ , from the slope of the  $F$  vs.  $A$  curves. In Figure 4 the  $C_s^{-1}$  values obtained from the compression and expansion  $F$  vs.  $A$  curves in Figure 3 are plotted vs.  $A$ ; all of the points are seen to fall close to the same curve.

The sharp peak in the curve coincides with a minimum in  $k$  (this means that the film was most incompressible when it was closely packed with the chains in the zigzag conformation oriented so that each monomer occupied  $16 \text{ \AA}^2$ ). However, somewhat surprisingly, the curve gives no indication of any transitions occurring in the film at either 20 or  $12 \text{ \AA}^2/\text{monomer}$  which were so apparent in the  $k$  vs.  $A$  curve. However, it may be noted that at both of these  $A$  values,  $C_s^{-1}$  was  $6.3 \text{ dyn/cm}$ . This is particularly noteworthy because Dorrestein's<sup>11</sup> theory of the damping of capillary waves by insoluble films predicts that  $k$  should pass through a maximum when  $C_s^{-1}$  is  $6.4 \text{ dyn/cm}$  (quoted by Davies and Vose<sup>12</sup>). This point will be discussed further in this article.

**Summary.** A picture can now be proposed for the behavior of polydimethylsiloxane films compressed and expanded on propylene carbonate. At higher values of  $A$ , the monolayer is composed of chains lying flat in the liquid surface in a zigzag conformation oriented so that a monomer unit occupies  $20 \text{ \AA}^2$ . The film probably interacts with the substrate through half of the methyl groups which form one side of the chain. As the liquid surface is decreased, the chains are gradually pushed closer together, causing  $k$  to rise, until at  $20 \text{ \AA}^2/\text{monomer}$  the film is fully packed with zigzag chains. Further compression causes them to rotate axially by  $90^\circ$  until, at  $16 \text{ \AA}^2/\text{monomer}$ , the film is fully packed with rotated (edge-on) zigzag chains and is least compressible. Compression past  $16 \text{ \AA}^2/\text{monomer}$  causes the chains to coil up into horizontally oriented helices until, at  $12 \text{ \AA}^2/\text{monomer}$  (where  $k$  passes through a second maxi-



mum), the film is fully packed with helical chains. Further compression forces some of the chains down into the substrate where they dissolve because the organic methyl groups located on the outside of the helix not only make the polymer more soluble in the propylene carbonate but also shield the polar Si-O-Si groups from the organic substrate. It is not clear why dissolution of the film causes  $k$  to decrease. After the liquid surface becomes fully occupied with helices at  $12 \text{ \AA}^2/\text{monomer}$ , the sole effect of further compression should be the displacement of chain segments, and eventually whole chains, into the substrate, with the packing and orientation of the chains remaining in the surface being essentially constant. If this be true,  $k$  should be constant also, as was observed when polysiloxane films started to dissolve in other substrates used in this study. The experimental results show unambiguously, however, that more and more of the film is lost by compression beyond  $12 \text{ \AA}^2/\text{monomer}$ , resulting in film hysteresis. The polymer molecules left in the liquid surface at the end of compression experience the same transitions when expanded as when compressed, but in reverse order.

*Films on Tetrahydronaphthalene, Hexachlorobutadiene, and Dichlorobutane. Wave Damping and Film Pressure.* The  $k$  vs.  $A$  and  $F$  vs.  $A$  curves, obtained for polydimethylsiloxane films on 1,2,3,4-tetrahydronaphthalene, on hexachloro-1,3-butadiene, and on 1,4-dichlorobutane are very similar. The results shown in Figure 5 for a film on tetrahydronaphthalene are typical.

Assuming, as in the propylene carbonate case, that the peak in the  $k$  vs.  $A$  curve is caused by a closely packed film of polymer molecules in a definite conformation, a polydimethylsiloxane structure was sought (with the aid of molecular models) which had a monomer area of about  $23.5 \text{ \AA}^2$  and a height of approximately  $5.3 \text{ \AA}$ , the calculated film thickness at that  $A$  value. Such a conformation results from putting one of the two methyl groups on adjacent silicon atoms as closely together as possible in the same plane to form one surface of the chain. Figure 2 shows a simplified molecular model of this structure, hereafter called the "extended conformation". The oxygen and silicon atoms are located on the other side so that the chain has a hydrophilic and oleophilic surface. The other half of the methyl groups alternate outwardly from both sides of the chains; neighboring chains would be expected to interact principally through these groups. The closely enmeshed row of methyl groups at the bottom of the chains would undoubtedly associate with the organic substrate to anchor the film to it. According to the molecular model, this structure has an area per monomer of  $23.6 \text{ \AA}^2$  and a height of  $5.2 \text{ \AA}$ , which match the experimental values very well.

The extended conformation model became more plausible when it was found that, by rotating the molecular model about the Si-O bonds, it could be twisted easily into the regular zigzag conformation having a monomer area of  $20 \text{ \AA}^2$ , which is where the flat plateau begins in the  $k$  vs.  $A$  curve. Hence, we interpret the region of  $23.5$  to  $20 \text{ \AA}^2/\text{monomer}$  as one in which the polymer molecules are being composed from the extended into the zigzag conformation. The chain loses a lot of its hydrophilic/hydrophobic character during the transformation because the Si-O-Si groups which form the predominantly polar surface of the extended conformation are now in the middle of the chain (Figure 2). This, of course, tends to make the chain more soluble in organic liquids; reference will be made to this point later. Films on tetrahydronaphthalene and hexachlo-

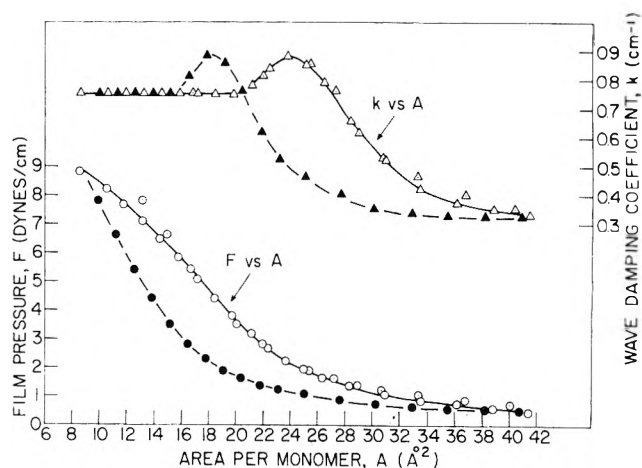


Figure 5. Damping coefficient and film pressure vs. area per monomer for a polydimethylsiloxane film on tetrahydronaphthalene at  $21.5^\circ\text{C}$ : open symbols, compression; filled symbols, expansion; dots within symbols, points recalculated as explained in text.

robutadiene, and inferentially on dichlorobutane as well, are fully reversible down to  $20 \text{ \AA}^2/\text{monomer}$ , reflecting the ease with which the extended structure can be changed into the zigzag conformation, but there is hysteresis in films compressed beyond that point. The level plateau in the  $k$  vs.  $A$  curve extends to a low monomer area, indicating that the polymer chain does not form a helical structure on these liquids. This is in contrast to its behavior on propylene carbonate in this study and on water.<sup>1</sup>

The film's preference for the extended structure on these liquids rather than the zigzag conformation assumed on propylene carbonate at high areas per monomer can be attributed to the much lower polarity of this group of liquids. As will be brought out, polydimethylsiloxane assumes the same extended structure on hexadecane, the most nonpolar substrate used here. The dielectric constants of tetrahydronaphthalene, hexachlorobutadiene, and dichlorobutane are 2.76 at  $20^\circ$ , 2.55 at  $25^\circ$ , and 8.90 at  $25^\circ$ , respectively,<sup>13</sup> compared to 65 at  $25^\circ$  for propylene carbonate.<sup>14</sup> It follows that these nonpolar liquids have a greater affinity for the organic portion of the siloxane chain than does propylene carbonate. Apparently the attraction is so strong that the methyl groups which bind the film to the substrate are pulled into positions perpendicular to the liquid surface until they are packed to the utmost. The resistance to immersion of the polar Si-O-Si groups on the other side of the chain prevents the whole molecule from being drawn into the substrate. Conversely, the adhesive forces between propylene carbonate and the same methyl groups are relatively weak and, as a result, the conformation of least energy on that substrate is the regular zigzag structure in which the methyl groups anchoring the chain are separated and tilted at a slight angle to the vertical.

*Hysteresis Effects.* To determine if the hysteresis observed in films compressed beyond  $20 \text{ \AA}^2/\text{monomer}$  is due to solution of some of the film, the  $A$  values at which  $k$  and  $F$  measurements were made were recalculated, as described earlier, for the expansion data on tetrahydronaphthalene and hexachlorobutadiene. Typical results are shown in the original plot (Figure 5) for the film on tetrahydronaphthalene. The peak in the expansion  $k$  vs.  $A$  curve is attributed to a close-packed film of chains in the extended conformation so that the actual area per monomer is  $23.5 \text{ \AA}^2$  at that

point. The close correspondence of the corrected points to the compression curves leaves little doubt that, just as with propylene carbonate, the hysteresis is caused by the loss of some of the polymer molecules by compression. The divergence of some of the new  $F$  points from the compression curve can again be ascribed to displaced chain segments returning to the liquid surface. There is no corresponding deviation in the new  $k$  points, because  $k$  is independent of  $F$  once the film starts to dissolve. In contrast to the propylene carbonate case,  $k$  is constant, as would be expected if compression beyond  $A = 20 \text{ \AA}^2$  only forced polymer molecules into the underlying liquid and left unaltered the packing and orientation of those chains remaining in the liquid surface.

On propylene carbonate the films start to dissolve only after the zigzag chains have been compressed into molecular helices. This is attributed to the increased solubility of the helices due to the methyl groups on the exterior of the chain which shield the Si-O-Si groups from the organic substrate. The situation seems to be entirely analogous in these films, except that they start to dissolve earlier when the chains are in the zigzag conformation. This difference in behavior can be explained on the basis of the low polarity of these liquids compared to propylene carbonate, just as it was used earlier to account for the difference in the conformations. As pointed out earlier, the extended conformation has a polar surface of Si-O-Si groups on one side of the chain and a nonpolar surface of close-packed methyl groups on the other. However, when the chain is compressed into the zigzag structure (Figure 2), it loses much of its polar-nonpolar character because the Si-O-Si groups move into the middle of the molecule and become surrounded by methyl groups, somewhat similar to what occurs when the zigzag molecular chains are compressed into helices on propylene carbonate. This removal of the Si-O-Si groups from the exterior of the chain apparently increases the solubility of the polymer in these relatively nonpolar liquids so much that, once all of the chains are in zigzag conformation, some of the film dissolves upon further compression. On the other hand, the energy barrier for solution of the same zigzag chains in propylene carbonate is expected to be much higher because of the high polarity of the liquid. Therefore, compression causes the chains in that conformation to reorient rather than dissolve. Furthermore, polydimethylsiloxane films on water, an even more polar liquid, do not dissolve even after molecular helices are formed.<sup>9</sup> Thus we conclude that the surface activity of polydimethylsiloxane films at liquid-air interfaces is strongly dependent on the polarity of the substrate.

**Compressibility Studies.** The film compressibility curves ( $C_s^{-1}$  vs.  $A$ ) are similar to those obtained on propylene carbonate (Figure 4), except that the maximum occurs at 20 rather than at  $16 \text{ \AA}^2/\text{monomer}$ . Thus, the film becomes least compressible at the same area per monomer that  $k$  becomes constant, i.e., when the monolayer becomes closely packed with zigzag chains. The films on propylene carbonate are also least compressible when they are fully packed with chains in the zigzag conformation (although in a different orientation). However, compression beyond the point of least compressibility affects the films on the two substrates in entirely different ways: a conformational change occurs on propylene carbonate, whereas the film on tetrahydronaphthalene starts to dissolve. As in the propylene carbonate case, there is no sign of a break in the compressibility curve where  $k$  passes through a maximum (ap-

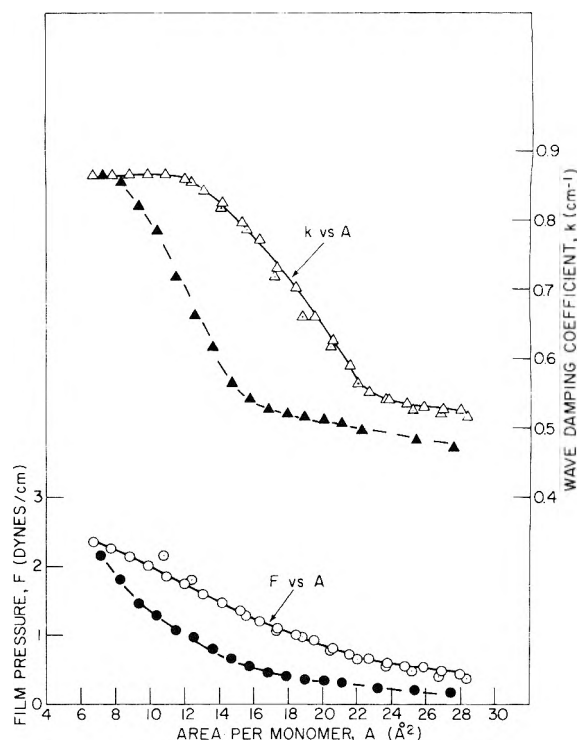


**Figure 6.** Damping coefficient and film pressure vs. area per monomer for a polydimethylsiloxane film on hexadecane at  $22.2^\circ$ : open symbols, compression; filled symbols, expansion; dots within symbols, points recalculated as explained in text.

proximately  $23.5 \text{ \AA}^2/\text{monomer}$ ). Interestingly, at that point,  $C_s^{-1}$  is equal to  $6.3 \text{ cm/dyn}$ , which is exactly the value at which the first maximum in  $k$  occurs in films on propylene carbonate. This apparent correlation between  $C_s^{-1}$  and  $k$  will be dealt with later.

**Films on Hexadecane. Film Pressure and Wave Damping.** The most notable difference between the  $k$  vs.  $A$  curves of films compressed on hexadecane (Figure 6) and those shown earlier is that  $k$  never passes through a maximum. Significantly, however, there are two abrupt changes in slope at approximately  $23.5$  and  $12 \text{ \AA}^2/\text{monomer}$ . These are the same monomer areas at which  $k$  maxima occurred on the other substrates in his study (e.g., see Figures 1 and 5). Therefore, it is easy to interpret the behavior of films on this substrate: the polymer chains are in the extended structure at high values of area per monomer, become closely packed at  $23.5 \text{ \AA}^2/\text{monomer}$ , and are converted into a helical structure in the region of  $23.5$  to  $12 \text{ \AA}^2/\text{monomer}$ .

As in the propylene carbonate case, the monolayer on hexadecane is reversible only to  $A = 12 \text{ \AA}^2$ , where the liquid surface was fully occupied with helical chains, and the hysteresis results from some of the film dissolving. This is shown by the closeness of the recalculated  $k$  and  $F$  points to the compression curve in Figure 6. The new points were obtained by assuming that at  $8 \text{ \AA}^2/\text{monomer}$ , where the expansion value of  $k$  dropped rapidly, the film was closely packed with all of the chains in the helical conformation and that the actual area per monomer at that point was therefore  $12 \text{ \AA}^2$ .

As might be anticipated from the low surface tension of hexadecane, the film pressures exhibited on that substrate are lower (at comparable areas per monomer) than on any of the other substrates in this study.

**Compressibility Studies.** The shape of a  $C_s^{-1}$  vs.  $A$  plot

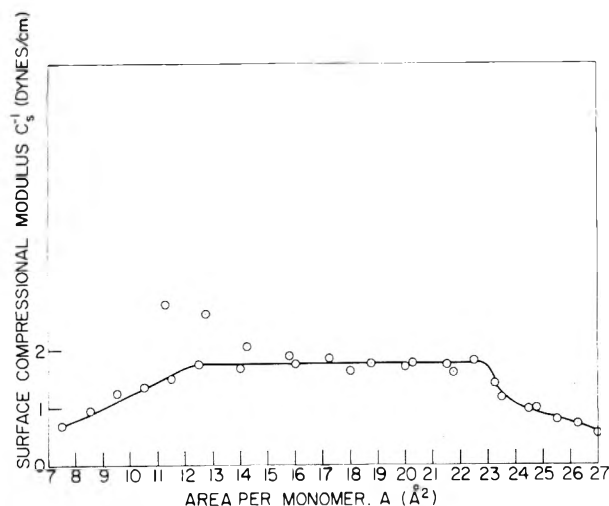


**Figure 7.** Compressibility curve of polydimethylsiloxane film on hexadecane: open symbols, compression of film shown in Figure 7; symbols with dots, expansion of film shown in Figure 7 but points recalculated as explained in text.

of a film on hexadecane (Figure 7, obtained from Figure 6) is unique in this study in that  $C_s^{-1}$  is constant over a wide range of  $A$  values, rather than showing a maximum as in all the other cases. Actually, the other compressibility curves do not correlate well with the wave-damping data since, as was noted, there are no inflections of any kind in the curves at some values of area per monomer where distinct peaks appeared in the  $k$  vs.  $A$  curve. On the other hand, the compressibility and wave-damping results of films on hexadecane are in good accord because film transitions were indicated at the same values of area per monomer in both  $k$  and  $C_s^{-1}$  vs.  $A$  curves.

It is seen from Figure 7 that  $C_s^{-1}$  initially rises because the extended chains are being pushed closer together, as would be expected, and then becomes constant at the onset of the formation of helices. In contrast to the propylene carbonate case, the compressibility of these films does not change while helices are formed. No straightforward explanation of this difference is apparent, although the conditions under which the polymer chains are converted into the helical structure are not strictly comparable in the two cases. Not only are the helices formed from different polymer conformations, but the forces binding the film to the substrate should be different because of the large difference in polarity between propylene carbonate and hexadecane. Thus, different energies may be required to compress the chains into helices on hexadecane and propylene carbonate and this could affect the compressibilities of the films. Figure 7 shows that  $C_s^{-1}$  decreases steadily as the film is dissolved in the substrate.

In light of the other compressibility data obtained in this study, one might assume that no peak appears in the  $k$  vs.  $A$  curve simply because  $C_s^{-1}$  does not reach a value of at least 6.3 dyn/cm. It was noted earlier that in all of the other films  $C_s^{-1}$  is equal to 6.3 dyn/cm each time  $k$  passes through a maximum; this point will be discussed in the next section.

The behavior of a polydimethylsiloxane film on hexadecane, outlined above, may be compared with the interpretations of other investigators who based their conclusions on force-area relationships. Ellison and Zisman's account<sup>4</sup> agrees for the most part with that given here; the main dif-

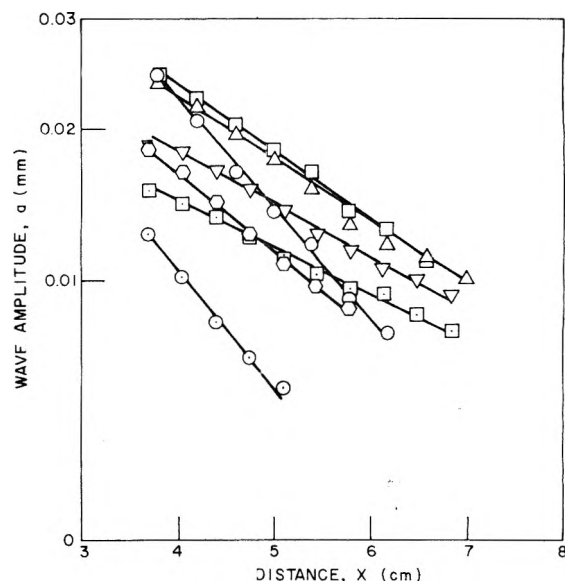


**Figure 8.** Amplitude of capillary waves on pure organic liquids as a function of the distance from the wave source:  $\square$ , tetrahydronaphthalene;  $\Delta$ , propylene carbonate;  $\circ$ , hexadecane;  $\nabla$ , dichlorobutane;  $\diamond$ , hexachlorobutadiene;  $\square$ , tetrachloroethane;  $\circ$ , tetrabromoethane.

ference is that they did not account for what happened after the film became close packed with helices. The present results provide the answer that the film begins to dissolve if compressed beyond that point, causing hysteresis upon expansion. The subsequent investigation by Jarvis<sup>15</sup> led him to believe that the polymer chains are in the helical form at high values of area per monomer and that they retain that structure regardless of the degree of compression. A similar conclusion was reached earlier by Noll, Steinbach, and Sucker<sup>16</sup> for polydimethylsiloxane films compressed on paraffin oils and other nonhydrogen-bonding liquids. However, in view of the sharp breaks in the  $k$  and  $C_s^{-1}$  vs.  $A$  curves observed here, the idea seems untenable that polydimethylsiloxane films do not undergo transitions when compressed on hexadecane and similar nonpolar liquids.

#### Comparison of Wave-Damping Results with Some Theoretical Predictions

*Wave Damping on Clean Surfaces.* In this investigation we intended to use  $k$  vs.  $A$  relationships to elucidate the way polydimethylsiloxane films behave at the organic liquid-air interface. However, the appearance of the peaks in the  $k$  vs.  $A$  curves at precisely the value of  $C_s^{-1}$  predicted by Dorrestein<sup>11</sup> encouraged us to compare other wave-damping results with theoretical predictions.

According to theory, the wave-damping coefficient can be determined from the slope of the line obtained when the log of the wave amplitude ( $a$ ) is plotted against the distance ( $x$ ) from the first wave (of amplitude  $a_0$ ):

$$\ln a = \ln a_0 - kx \quad (1)$$

Such plots are shown in Figure 8 for seven pure organic liquids differing widely in their physical properties. In addition to the five organic liquids used as substrates, wave-damping data were obtained for two other liquids (1,1,2,2-tetrabromoethane and 1,1,2,2-tetrachloroethane) which were considered and not used as substrates. Since these

two liquids are chemically similar but have greatly different physical properties which affect capillary wave damping (see Table I), we hoped to compare the wave-damping properties of polysiloxane films on them. Unfortunately, when a monolayer is compressed on tetrabromoethane, the high viscosity of the liquid causes the capillary waves to decay so quickly that usually only three wave amplitudes can be measured. Consequently, a reliable plot of wave amplitude  $a$  vs. distance  $x$  cannot be obtained, although enough wave amplitudes (five) can be measured for the pure liquid to give a satisfactory plot. A good plot was obtained also for pure tetrachloroethane, but this liquid was not used further because of its noxious vapors. The wave-damping coefficients  $k_c$  obtained from the slopes of the lines in Figure 8 are given in Table I along with the experimentally determined values of the physical properties which affect the damping of the capillary waves (see equations below).

The theoretical values of  $k_c$  for the organic liquids were calculated from hydrodynamic theory which was developed by solving Lamb's equations describing liquid motion.<sup>17</sup> According to theory, the value of  $k_c$  is given by

$$k_c = 8\pi^2\eta/\rho V_g\lambda^2 \quad (2)$$

where  $\eta$  is the kinematic viscosity (measured in poises),  $\rho$  is the density (in g/cc),  $V_g$  is the group velocity of the wave train (in cm/sec), and  $\lambda$  is the wavelength (in cm). The group velocity of the wave train is given by

$$V_g = v - \lambda \frac{dv}{d\lambda} \quad (3)$$

Here  $v$  is the wave velocity obtained from the well-known Thomson equation,<sup>20</sup> which gives the wave velocity under the combined forces of gravity  $g$  (gravitational constant) and surface tension  $\gamma$  as

$$v^2 = \frac{g}{2\pi} + \frac{2\pi\lambda}{\rho\lambda} \quad (4)$$

The values of  $k_c$  calculated from eq 2 are compiled in Table I along with the experimental values and the percentage differences between the two. All of the observed values are lower than those predicted by the theory by as much as 36%. The fact that the percentage difference increases with the viscosity of the liquid suggests that viscosity has a greater effect on capillary-wave damping than is provided for in the theoretical equations.

For example, the surface tension and density of tetrachloroethane and hexachlorobutadiene are not very different, but the latter is much more viscous and has an observed  $k_c$  21% lower than the calculated value, compared with a 6% difference for tetrachloroethane. Conversely, the surface tension and, particularly, the density of hexachlorobutadiene are appreciably different from those of hexadecane. However, their viscosities are practically the same, and their experimental  $k_c$  values differ from the theoretical values by the same percentage. Since the theoretical and observed  $k_c$  values of dichlorobutane, which is slightly more viscous than water, agree so well, we might anticipate good agreement for water also if, as indicated here, viscosity is the principal factor. In fact, other workers<sup>19,20</sup> have found excellent agreement between experimental and theoretical  $k_c$  values for water. However, on the basis of the large discrepancies between theory and experiment ob-

served here, eq 2 must be judged not to be applicable to the more viscous liquids.

*Wave Damping on Film-Covered Surfaces.* Some of our experimental data agree very well with Dorrestein's<sup>11</sup> theoretical treatment of the damping of capillary waves by monolayers (the peak in the  $k$  vs.  $A$  curve at the predicted value of  $C_s^{-1}$  has already been mentioned), but other results seem to go outside the framework of the theory. For this reason a brief summary will be given of the main points of his theory.

Dorrestein expressed capillary-wave damping by insoluble films as a function of the compressibility, which can be measured by  $C_s^{-1}$ , and of the surface viscosity  $\nu_s$  of the monolayer. He defined the two limiting cases: (a) the effect of the film on the motion of the liquid surface is negligible ( $C_s^{-1}$  and  $\nu_s \rightarrow 0$ ) and the theoretical value of  $k$  in this case is that of a clean surface and is given by eq 2; and (b) the liquid surface is completely immobilized by the film, i.e., the film practically prevents any horizontal motion in the liquid surface. According to hydrodynamic theory,<sup>17</sup> the damping coefficient  $k_i$  in this latter situation is given by

$$k_i = \left(\frac{\pi}{V_g\lambda}\right) \left(\frac{\eta\sigma}{2\rho}\right)^{1/2}$$

where

$$\sigma = \left(\frac{2\pi g}{\lambda} + \frac{8\pi^3\gamma}{\lambda^3\rho}\right)^{1/2} \quad (5)$$

The values of  $k_i$  for the five substrate liquids in this study are shown in Table I.

In going from case a toward case b the mathematics of the theory predicts that, if the viscosity of the film is negligible,  $k$  should pass through a maximum when  $C_s^{-1}$  reaches 6.4 dyn/cm, as was observed in the films on all of the substrates in this study except on hexadecane. The maximum in  $k$  has been observed previously, but this is the first time that it has occurred so near the compressibility value predicted by theory.<sup>21</sup>

The absence of a peak in the  $k$  vs.  $A$  curve for films on hexadecane might be attributed to the fact that the films are so readily compressible that  $C_s^{-1}$  never reaches the necessary 6.4 dyn/cm. However, if Dorrestein's theory is further considered, another explanation presents itself. According to theory,  $k$  should not pass through a maximum if the viscosity of the film contributes much more to the damping of the capillary waves than does the incompressibility of the film. This situation may occur in films on hexadecane because of the closer association of the hydrocarbon groups in the siloxane chain with the highly nonpolar hexadecane. The fact that  $k$  passed through a maximum at the predicted value of  $C_s^{-1}$  for the other substrates implies that the viscosity of those films was not appreciable.

Another prediction of the Dorrestein theory<sup>11</sup> is that when the damping coefficient  $k$  passes through the maximum  $k_{\max}$ , it should have about twice the value that it has when the liquid surface is fully immobilized by a film (that is to say, about twice the value  $k_i$  calculated from eq 5). As shown in the last column of Table I, this clearly holds true for films in this study.

The good quantitative agreement between our experimental results and the predictions of Dorrestein suggests that his theory can be generally applied to the films studied here. An apparent exception is the behavior of the film on propylene carbonate because there are two peaks in the  $k$  vs.  $A$  curve, whereas only one is theoretically predicted.

However, even the wave-damping properties of that film can be rationalized in terms of the theory if we make the following two assumptions: first, when the film becomes least compressible at  $16 \text{ \AA}^2/\text{monomer}$  (where  $k$  passes through a minimum) the state of the liquid surface corresponds to limiting case b described above; and second, the film when compressed beyond  $16 \text{ \AA}^2/\text{monomer}$  affects the liquid surface in the same way as when it was compressed to that point, or, in the language of the theory, the process  $a \rightarrow b$  is reversible. If these assumptions are valid, compression of the film past  $16 \text{ \AA}^2/\text{monomer}$  would cause  $k$  to rise and pass through a second maximum of the same magnitude as the first when  $C_s^{-1}$  again was  $6.4 \text{ dyn/cm}$ , as was observed experimentally.

Although some of our results definitely are compatible with and lend some support to Dorrestein's theoretical analysis, we have used a different basis for explaining the observed changes in the wave-damping properties as a monolayer is compressed. Our approach has been to identify each extremum in the  $k$  vs.  $A$  curve with a well-defined state of the film molecules. For example, in this study we propose that the first peak represents the point where the film first becomes close packed with every polymer molecule in the same configuration and orientation. To verify this proposal, plausible chain conformations are assigned to the area per monomer at which the peaks appear. It follows from this that the location of the first peak depends upon the structure of the surfactant molecules when they become close packed, and as a consequence, our wave-damping results are interpreted on an ad hoc basis. On the other hand, Dorrestein relates the maximum in the  $k$  vs.  $A$  curve to the compressibility of the film and attributes it to localized oscillations at the liquid surface. Reconciling his approach with ours, which is largely empirical in nature, would apparently require an understanding of how the structure and properties (e.g., elasticity and solubility) of a given film affect its compressibility. Information of so complex a situation would undoubtedly be very difficult to obtain.

### Conclusions

The main conclusions reached in this investigation can be summarized as follows.

(1) On all five of the organic liquids investigated here, the polydimethylsiloxane monolayers form stable and reversible films which dissolve on compression, causing hysteresis upon expansion. Before dissolving, however, a film undergoes a conformational change, and when propylene carbonate is the substrate a change occurs in the orientation of the polymer chain on the liquid surface as well.

(2) The type of structural transformation which occurs as a film is compressed and the conformation assumed when it is first spread both depend to a large degree upon the matchings of polarities of the organic substrate and film.

(3) Hydrodynamic theory is not applicable to the more viscous ( $\nu_s > 3 \text{ cP}$ ) pure organic liquids studied here; however, the agreement between the observed and theoretical wave-damping coefficients is satisfactory for the less viscous ( $< 2 \text{ cP}$ ) liquids.

(4) Dorrestein's theory<sup>11</sup> of the damping of capillary waves by these compatible monolayers is especially satisfactory for these particular substrates.

### References and Notes

- (1) H. W. Fox, P. Taylor, and W. A. Zisman, *Ind. Eng. Chem.*, **39**, 1401 (1947).
- (2) H. W. Fox, E. M. Solomon, and W. A. Zisman, *J. Phys. Colloid Chem.*, **54**, 723 (1950).
- (3) W. H. Banks, *Nature (London)*, **174**, 365 (1954).
- (4) A. H. Ellison and W. A. Zisman, *J. Phys. Chem.*, **60**, 416 (1956).
- (5) R. L. Shuler and W. A. Zisman, *Macromolecules*, **5**, 487 (1972).
- (6) M. K. Bennett and W. A. Zisman, *J. Phys. Chem.*, **66**, 1207 (1962).
- (7) R. L. Shuler and W. A. Zisman, *J. Phys. Chem.*, **74**, 1523 (1970).
- (8) W. D. Harkins and H. F. Jordan, *J. Am. Chem. Soc.*, **52**, 1751 (1930).
- (9) W. D. Garrett and W. A. Zisman, *J. Phys. Chem.*, **74**, 1796 (1970).
- (10) C. B. Hurd, *J. Am. Chem. Soc.*, **68**, 364 (1946).
- (11) R. Dorrestein, *Proc. Acad. Sci. Amst.*, **B54**, 260, 350 (1951).
- (12) J. T. Davies and R. W. Vose, *Proc. R. Soc. (London)*, *Ser. A*, **286**, 218 (1965).
- (13) National Bureau of Standards, Circular no. 514, Aug 10, 1951.
- (14) L. Simeral and R. L. Amey, *J. Phys. Chem.*, **74**, 1443 (1970).
- (15) N. L. Jarvis, *J. Colloid Interface Sci.*, **29**, 647 (1969).
- (16) W. Noll, H. Steinbach, and C. Sucker, *Bunsengesell. Phys. Chem.*, **67**, 407 (1963).
- (17) H. Lamb, "Hydrodynamics", Cambridge University Press, New York, N.Y., 1959.
- (18) W. Thompson, *Phil. Mag.*, **42**, 368 (1871).
- (19) W. D. Garrett and J. D. Bultman, NRL Report No. 6003, Oct 1963.
- (20) J. T. Davies, *Chem. Ind. (London)*, 906 (1962).
- (21) Davies and Vose<sup>12</sup> had observed a maximum at  $C_s^{-1} = 5.2 \text{ dyn/cm}$  for films of lauryl sulfate adsorbed on water.

## Conjugation between Unsaturated Systems through a Heteroatom. II. Molecular Stereolability of Reacting Para-Substituted Phenyl Isobutenyl Ethers

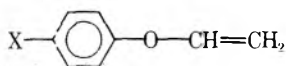
R. H. Donnay, F. Garnier, and J. E. Dubois\*

Laboratoire de Chimie Organique Physique de l'Université de Paris VII, associé au CNRS, 75005, Paris, France (Received July 25, 1974; Revised Manuscript Received February 7, 1975)

The  $h\nu$  electronic transitions associated with the charge-transfer complexes between para-substituted phenyl isobutenyl ethers,  $XPh-O-CH=C(Me)_2$  ( $X = H, Me, MeO, Cl, Br, NO_2$ ) (donors), and tetracyanoethylene (acceptor) have been determined. The linear relationship between  $h\nu$  and  $\sigma^+$  substituent constants,  $h\nu_{eV} = 0.56\sigma_p^+ + 2.39$ , shows that there is transmission of conjugation through the oxygen atom in the ground state of these molecules, thus confirming our previous theoretical calculations. However, the  $\sigma_p$  linear free-energy relationship observed for the electrophilic bromination of these ethers,  $\log(k/k_0) = -3.13\sigma_p$ , indicates that conjugation between the two  $\pi$  systems is weakened in the course of a reaction. The theoretical INDO analysis of the conformation and electronic structure of the carbonium ion,  $XPh-O-CH^+CH_3$ , chosen as a model of transition state of the reaction, shows that this weakening is due to a conformational modification of the molecule when it goes over the reaction energy barrier.

### Introduction

In the preceding paper,<sup>1</sup> we presented theoretical results on the conformational analysis and electronic structures of para-substituted phenyl vinyl ethers as calculated by the INDO method



$X = H, Me, MeO, OH, F, NO_2$

All these compounds show the same conformation, in which the trend to maximum conjugation by coplanarity of the two unsaturated systems is blocked by steric hindrance between hydrogen atoms. Analysis of the electronic structure of the ground state demonstrates the transmission of the conjugative effect through the oxygen atom to the ethylenic bond, as shown by the linear relationship between the energy of the highest occupied molecular orbital  $E_{HOMO}$  and the  $\sigma_p^+$  para-substituent constants<sup>2</sup> of the X substituent:

$$E_{HOMO} = 0.58\sigma_p^+ + 10.92 \quad (1)$$

The work presented here concerns the experimental study of this transmission of the conjugative effect on two kinds of molecular properties, spectroscopy and kinetics. These properties are commonly associated with the energy of the highest occupied molecular orbital. As pointed out by Jaffé<sup>3</sup> and Streitwieser,<sup>4</sup> the energy of the HOMO of a compound is directly related to its spectroscopic behavior and chemical reactivity.

### Spectroscopic Results

In order to compare the experimental properties with the theoretical analysis, we studied first spectroscopic properties related to this conjugation. As a spectroscopic observable of the energy of the highest occupied molecular orbital  $E_{HOMO}$ , we chose the charge-transfer type electronic transition associated with donor-acceptor complexes. These transitions involve the overlap of the highest occupied mo-

lecular orbital of the donor and the lowest empty molecular orbital of the acceptor.<sup>5</sup> As shown by the molecular orbital treatment of these complexes by Dewar and Lepley,<sup>6</sup> the energy of this electronic transition is linearly related to  $E_{HOMO}$ .

The absorption spectra corresponding to the charge-transfer complexes between para-substituted phenyl isobutenyl ethers (donors) and tetracyanoethylene (acceptor) in methylene chloride were determined. The results are listed in Table I, together with the  $\sigma_p^+$  para-substituent constants which were used previously in the  $E_{HOMO}$  structure effect correlation. As shown in Figure 1, a linear relationship exists between the  $h\nu$  transition energies of the charge-transfer complexes and the  $\sigma_p^+$  constants:

$$h\nu_{eV} = 0.56\sigma_p^+ + 2.39 \quad (R = 0.990) \quad (2)$$

The linearity of the correlation and the fact that the same slope is observed in the calculated<sup>1</sup> and experimental<sup>2</sup> relations indicate that  $E_{HOMO}$  is highly sensitive to substituent effect. This molecular orbital is mostly localized on the oxygen and alkene carbon atoms,<sup>1</sup> thus confirming the existence of conjugation between the  $\pi$  systems through the oxygen atom. The observation that the conjugative effect is transmitted through the heteroatom is in agreement with spectroscopic work done by Jaffé<sup>7</sup> on phenyl rings linked by N and P atoms and by Koch<sup>8</sup> on phenyl rings linked by a S atom.

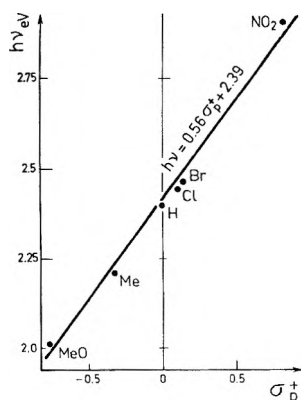
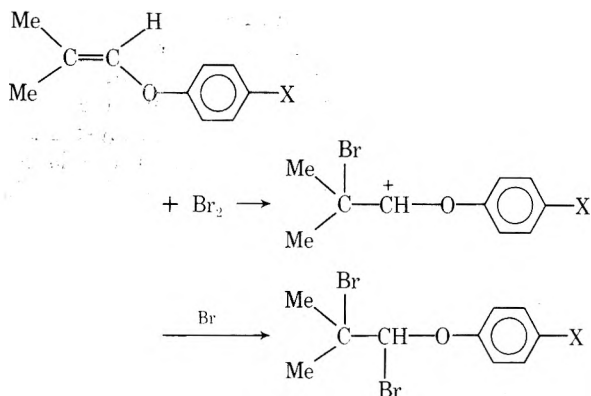
In order to analyze the transmission of the substituent effect on the reactivity of the ethylenic double bond we have performed a kinetic study of an electrophilic reaction of these compounds.

### Kinetic Results

The reaction considered is the electrophilic bromination of the para-substituted phenyl isobutenyl ethers, whose rate-determining step involves the formation of an ionic intermediate.

**TABLE I: Charge Transfer Energy of the TCNE-Phenyl Isobutenyl Ether Complexes**

X	$h\nu_{eV}$	$\sigma_p^+$
H	2.393	0
Me	2.202	-0.311
MeO	2.016	-0.778
Cl	2.408	0.114
Br	2.442	0.15
NO <sub>2</sub>	2.901	0.790

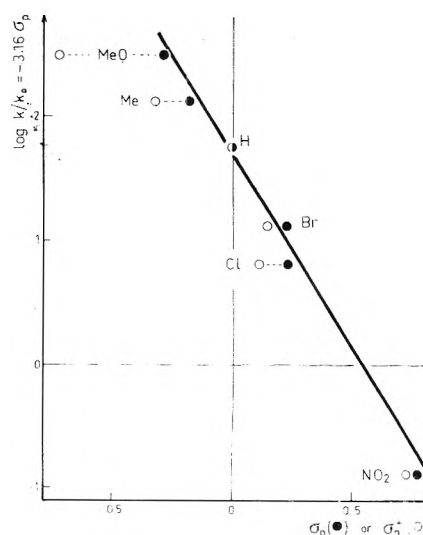
**Figure 1.** Linear relationship between the  $h\nu_{eV}$  charge-transfer transition energy and the  $\sigma_p^+$  substituents constants.

The experimental rate constants are reported in Table II.

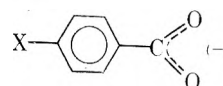
Our previous theoretical calculations led us to propose a linear relationship<sup>1</sup> between the  $E_{HOMO}$  energy and the  $\sigma_p^+$  substituent constants, defined by the solvolysis rate of para-substituted *tert*-cumyl chlorides. In this reference reaction, a positive charge  $X-Ph-C^+(Me)_2$  is created  $\alpha$  to the phenyl ring in direct resonance interaction with the para substituent. Taking the quantity  $E_{HOMO}$  as representative of the chemical reactivity,<sup>4</sup> we may expect a linear free-energy relationship  $\log k = f(\sigma_p^+)$  which would express the strong conjugation between the two unsaturated systems. This kind of relationship has been observed, for instance, for electrophilic hydration<sup>9</sup> or bromination<sup>10</sup> of para-substituted styrenes, in which there is conjugation between the para substituent and the positively charged  $\alpha$  carbon atom  $X-Ph-C^+-C$ . However, as shown in Figure 2, the rate data do not fit this relationship well at all, the largest deviations being observed for the substituents with strong conjugative effect (MeO, NO<sub>2</sub>). This suggests that the  $\sigma_p^+$  parameters are unsuitable since they overestimate the importance of resonance in this reaction.

**TABLE II: Kinetic Constants for the Bromination Reaction of Para-Substituted Phenyl Isobutenyl Ethers in  $CFCl_2CF_2Cl$  at 25°**

X	$k, M^{-1} sec^{-1}$
H	$1.09 \pm 0.03$
Me	$1.95 \pm 0.05$
MeO	$4.93 \pm 0.12$
Cl	$3.37 \times 10^{-1} \pm 0.18 \times 10^{-1}$
Br	$2.67 \times 10^{-1} \pm 0.06 \times 10^{-1}$
NO <sub>2</sub>	$2.38 \times 10^{-3} \pm 0.05 \times 10^{-3}$

**Figure 2.** Structure effect on reactivity of para-substituted phenyl isobutenyl ethers linearly related to  $\sigma_p$  substituent constants.

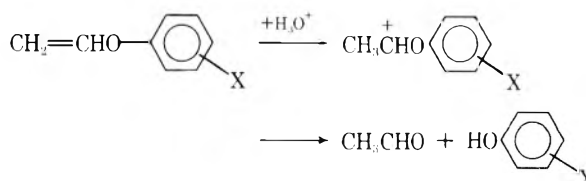
In order to understand how this structural effect operates on the reactivity of these enol ethers, we tried Hammett substituent constants  $\sigma_p$ <sup>11</sup> which are defined from the dissociation of benzoic acids



and so contain a smaller contribution from resonance than do  $\sigma_p^+$  constants. As shown in Figure 2, the correlation with  $\sigma_p$  is now satisfactorily linear

$$\log(k/k_0) = -3.16\sigma_p \quad (R = 0.987)$$

The value of the slope,  $\rho = -3.16$ , may be compared to that obtained by Fueno<sup>12</sup> for the acidic hydrolysis of substituted phenyl vinyl ethers ( $\rho = -2.14$ )



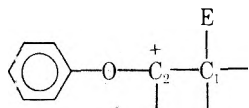
in which the rate-determining step involves the electrophilic protonation of the carbon atom.

This result, in apparent contradiction with theoretical calculations and spectroscopic data for the ground state, clearly indicates that the reactivity of the ethylenic double bond does not depend greatly on the conjugative part of the substituent effect. The height of the activation energy

barrier of the reaction is in fact directly related to the energy level of the highly polarized transition state. In order to understand the origin of this substituent effect modification we will now consider the structural stabilization of the transition state.

### Theoretical Analysis of a Transition State Model

Taking into account the partial charges born by the  $C_1$  and  $C_2$  atoms in the ground state of the molecule, the approach of an electrophilic reagent  $E^+$  to the ethylenic bond leads to a carbonium ion intermediate.



This assumption has been experimentally confirmed by reaction product studies in the case of acidic hydrolysis.<sup>13,14</sup> We shall consider this ion as a limiting model for the transition state and undertake a theoretical study of the conformation and electronic structure in the case of  $E = H$ . As in the study of the phenyl vinyl ether molecule, the INDO method of Pople<sup>15</sup> has been used.

**Computing Conditions.** The bond lengths and bond angles used in the calculations are standard values given by Pople.<sup>16</sup> The conformation of the carbonium ions, derived from the phenyl vinyl ether, has been determined by the minimization of the total molecular energy with respect to the two torsional angular parameters,  $\Phi_1$  and  $\Phi_2$ , shown in Figure 3. The  $\Phi_1$  angle corresponds to the  $C_3-O$  internal rotation angle, with positive clockwise rotation looking inward from  $C_3$  to  $O$ . The  $\Phi_2$  angle corresponds to the  $C_2-O$  internal rotation angle with positive clockwise rotation looking inward from  $C_2$  to  $O$ . The variation intervals considered for the two internal rotation angles are the following:  $0 < \Phi_1 < 180^\circ$  and  $-90^\circ < \Phi_2 < 90^\circ$  with the values  $\Phi_1 = \Phi_2 = 0$  corresponding to the planar form. These two intervals take into account the symmetry of the para-substituted phenyl ring and do not consider the sterically hindered structure in which the phenyl ring would be "inside" the  $C_2-C_1$  bond (Figure 4).

**Conformation of the Transition State Model.** The potential surfaces for the unsubstituted carbonium ion ( $X = H$ ) are represented in Figure 5. One can first note that, compared with the original phenyl vinyl ether molecule, there is no longer symmetry with respect to the origin. This loss of symmetry is due to the change of hybridization of the  $C_1$  carbon atom from  $sp^2$  to  $sp^3$  when the molecule goes to the ion.

The minimum energy conformation corresponds to the values  $\Phi_1 = 22.5^\circ$  and  $\Phi_2 = -22.5^\circ$ . Just as in the case of the ground state molecules, we have considered the possibility of a modification of the minimum energy conformation of the ion with respect to the substituent. For the two substituents  $MeO$  and  $NO_2$  of opposite electronic effect, a variation of the  $\Phi_1$  and  $\Phi_2$  angles was performed around the minimum determined for the unsubstituted ion. The potential energy curves obtained, presented in Figure 6, show that a similar wide potential well is obtained for all substituents. Thus, as for the molecules from which they are derived, a same conformation can be considered for the carbonium ions whatever the substituent.

However, the important fact is that the new conformation obtained for the ion is quite different from that found for the molecular ground state. A spatial representation of

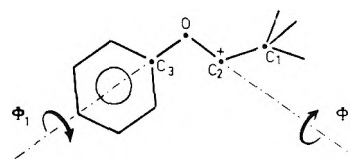


Figure 3. Internal rotation parameters for the conformational analysis.

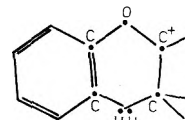


Figure 4. Forbidden structure: phenyl ring "inside" the  $C_1-C_2$  bond.

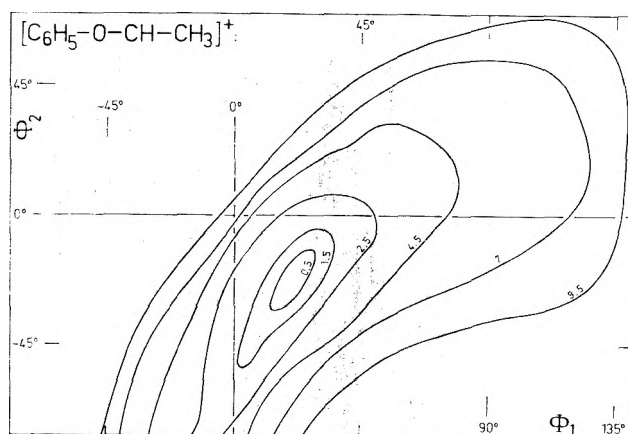


Figure 5. Conformational map of  $C_6H_5-O-CH-CH_3^+$ .

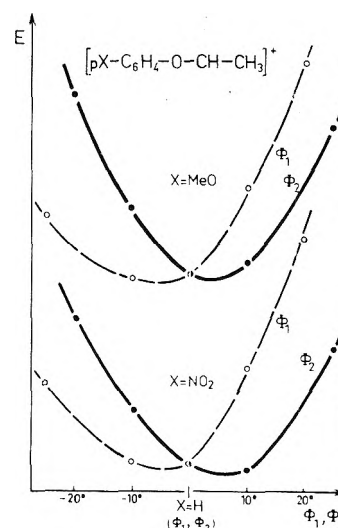


Figure 6. Potential well for substituted ethers as a function of  $\Phi_1$  and  $\Phi_2$ .

this modification cannot be easily performed and may be better visualized through the analysis of the H--H distance of Figure 7. In the molecule the calculated H--H distance, 2.2 Å, corresponds to the sum of the van der Waals radii of two hydrogen atoms; the system cannot therefore attain maximum conjugation because of this steric constraint. In the case of the carbonium ion this steric interaction is no longer operating as shown by the value of 2.6 Å calculated for this H--H distance. The difference between the two calculated H--H distances (2.2 and 2.6 Å) leads us to consid-



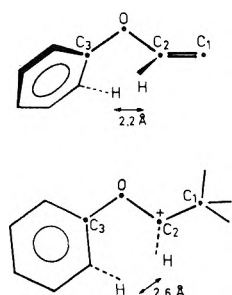
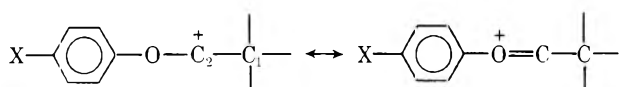


Figure 7. Comparison of H-H interactions in molecular and ionic species.

er that in the carbonium ion there is only a weak conjugative interaction between the phenyl ring and the vacant p orbital of the  $C_2$  carbon atom. This leads to a conformation where the sterically hindered position present in the ether molecule no longer exists.

As mentioned previously,<sup>1</sup> this weakening of the conjugation is in agreement with the cationic mesomeric forms



The electron demand of the electron deficient  $C_2$  carbon is partly satisfied by the neighboring oxygen electron pair, leaving little valency available for conjugation between the substituent and the side-chain group. These assumptions are confirmed by analysis of the differences of the calculated charges on the  $C_1$ ,  $C_2$ , and O atoms, for the molecule and the ion. These differences  $\Delta q_{\text{atom}} = q^{\text{mol}} - q^{\text{ion}}$ , Table III, are positive and reflect the electron loss which occurs when the carbonium ion is formed. The contributions, other than those from  $C_1$ ,  $C_2$ , and O, are very small and can be neglected. These values show that the main contributions to the electron deficiency of the molecule involve both the  $C_2$  and the oxygen atoms. The participation of the oxygen atom in the stabilization of the carbonium ion emphasizes its weakened conjugation transmitter role in the ion. The substituent effect on the transition state being mostly responsible for reactivity, it now becomes clear why the reactivity of the molecule cannot be represented by the  $\sigma_p^+$  substituent constants associated with strong conjugation.

## Conclusion

The experimental results presented here show two different types of structural effects on the physical and chemical behavior of para-substituted phenyl isobutenyl ethers. This phenomenon can be understood by considering that these two properties are related to two different states of the molecular system.

The spectroscopic properties are directly associated to the ground state of the molecule. Owing to the Franck-Condon principle, an electronic transition lasting  $10^{-14}$  to  $10^{-15}$  sec is too fast to allow any conformational modification of the molecule. Thus, the theoretical or experimental determination of the conformation and the electronic structure of the molecular ground state describe these properties adequately.

Concerning the reactivity, the crossing of a potential energy barrier is slow enough with respect to the rotation time constants around a chemical bond ( $10^{-12}$  to  $10^{-13}$  sec) for the molecule to adopt the most stable conformation in the transition state (Figure 8). As we showed experimental-

TABLE III: Charge Variation from Molecular to Ionic Species for the  $C_1$ ,  $C_2$ , and O Atoms

X	$\Delta q$		
	$C_1$	$C_2$	O
H	0.084	0.223	0.109
Me	0.083	0.224	0.107
MeO	0.087	0.209	0.116
$\text{NO}_2$	0.078	0.234	0.103

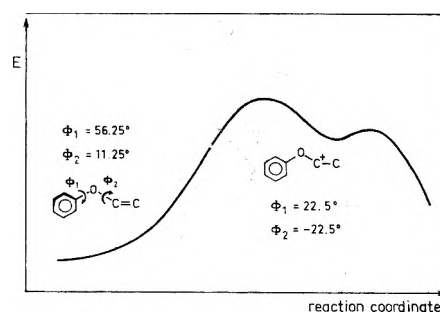
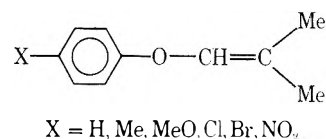


Figure 8. Molecular stereolability in the course of a reaction: conformational change from the molecule to the ion.

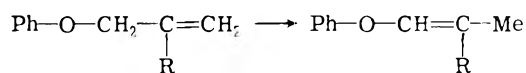
ly and theoretically, this molecular stereolability leads to a modification of the substituent effect on reactivity. This modification cannot be accounted for by a mere analysis of the ground state of the molecule.

## Experimental Section

*Organic Synthesis. Identification.* The vinyl ethers have the general formula



These ethers were prepared by allylpropenyl transposition, described in the literature.<sup>17</sup>



which was followed in each case by infrared spectroscopic observation of the disappearing methylene band. Structures of all compounds have been checked by NMR spectroscopy. X (melting point or boiling point): H ( $199^\circ$ , 760 mm); Me ( $100^\circ$ , 15 mm); MeO ( $130^\circ$ , 15 mm); Cl ( $29^\circ$ ); Br ( $40^\circ$ );  $\text{NO}_2$  ( $39^\circ$ ).

*Kinetics.* The bromination of the para-substituted phenyl isobutyl ethers was studied in Freon 113,  $\text{CFCl}_2\text{CF}_2\text{Cl}$  as solvent, at  $25 \pm 0.1^\circ$ . The rate constants were determined by means of a Cary 16 spectrophotometer.

A bromine solution,  $[\text{Br}_2] \approx 10^{-3} M$ , was placed into a 1-cm optical path-length thermostated cell and stirred by a small Teflon-coated magnetic bar. The wavelength was fixed at  $\lambda$  410 nm, corresponding to the bromine absorption maximum. The enol ether was then injected into the cell with a microsyringe; the mixing time did not exceed 0.5 sec. The absorbance variation was recorded as function of time. The data were handled by a Digital Equipment Corpora-

tion PDP 11 computer, to obtain rate constants and error values. Each rate constant is the mean of five measurements.

*Acknowledgment.* Technical assistance provided by N. Pedrono is gratefully acknowledged.

### References and Notes

- (1) R. H. Donnay and F. Garnier, *J. Phys. Chem.*, **78**, 440 (1974).
- (2) H. C. Brown and Y. Okamoto, *J. Am. Chem. Soc.*, **80**, 4979 (1958).
- (3) H. H. Jaffe and M. Orchin in "Theory and Application of UV Spectroscopy", Wiley, New York, N.Y., 1962, p 474.
- (4) A. Streiwieser, Jr., H. A. Hammond, R. H. Jagow, R. M. Williams, R. G. Jesaitis, C. J. Chang, and R. Wolf, *J. Am. Chem. Soc.*, **92**, 5141 (1970).
- (5) R. S. Mulliken, *J. Am. Chem. Soc.*, **83**, 4560 (1961).
- (6) M. J. S. Dewar and A. R. Lepley, *J. Am. Chem. Soc.*, **83**, 4560 (1961).
- (7) H. H. Jaffe, *J. Chem. Phys.*, **22**, 1430 (1954).
- (8) H. Koch, *J. Chem. Soc.*, 387 (1949).
- (9) W. M. Schubert, B. Lamm, and J. R. Keefe, *J. Am. Chem. Soc.*, **86**, 4727 (1964).
- (10) (a) J. H. Rolston and K. Yates, *J. Am. Chem. Soc.*, **91**, 1477 (1969); (b) J. E. Dubois and A. Schwartz, *Tetrahedron Lett.*, 2167 (1964).
- (11) L. P. Hammett, "Physical Organic Chemistry", McGraw-Hill, New York, N.Y., 1940.
- (12) T. Fueno, I. Matsumura, T. Okuyama, and J. Furukawa, *Bull. Chem. Soc. Jpn.*, **41**, 818 (1968).
- (13) A. J. Kresge and Y. Chiang, *J. Chem. Soc. B*, 58 (1967).
- (14) T. H. Fife, *J. Am. Chem. Soc.*, **87**, 1084 (1965).
- (15) J. A. Pople, D. L. Beveridge, and P. A. Dobosh, *J. Chem. Phys.*, **47**, 2026 (1967).
- (16) J. A. Pople and D. L. Beveridge, "Approximate Molecular Orbital Theory", McGraw-Hill, New York, N.Y., 1970, p 111.
- (17) M. Julia and M. Baillarge, *Bull. Soc. Chim. Fr.*, 734 (1966).

## Deuteron Nuclear Magnetic Resonance in Amphiphilic Liquid Crystals. Alkali Ion Dependent Water and Amphiphile Orientation

Nils-Ola Persson\* and Björn Lindman

Department of Physical Chemistry 2, Chemical Center, S-22007 Lund 7, Sweden (Received November 6, 1974; Revised Manuscript Received March 21, 1975)

From deuteron magnetic resonance spectra of mesophases composed of anionic amphiphile, decanol, and heavy water, information about the degree of orientation of both water and decanol is provided. The dependence of the deuteron quadrupole splitting on counterion, surfactant end group, sample composition, and phase structure was investigated. The degree of water orientation with respect to the amphiphilic aggregates was found to be considerably greater with  $\text{Li}^+$  as counterion than with the other alkali ions. The relative effects of  $\text{Na}^+$ ,  $\text{K}^+$ , and  $\text{Rb}^+$  vary in a complicated way with sample composition. From the dependence of water orientation on molar fraction of water it was found that only a small number of water molecules is oriented with respect to the amphiphilic aggregates and, thus, that no long-range ordering effect can be detected. Changes in water quadrupole splitting with phase structure and sample composition are discussed in terms of phase anisotropy and amphiphile hydration. The degree of decanol-OD orientation increases with decreasing water content and increasing soap concentration but is approximately independent of counterion and surfactant end group. For the alkali octanoate-decanol- $\text{D}_2\text{O}$  systems the sign of the order parameter is the same for  $\text{D}_2\text{O}$  and decanol deuterons whereas there are strong indications that for the alkali octanoate-octanoic acid- $\text{D}_2\text{O}$  systems the order parameters of octanoic acid-COOD and water deuterons are of opposite signs.

### Introduction

The complex self-association of amphiphilic substances in aqueous solutions has for a long time attracted considerable interest. It is now well known that micelle formation is preceded by the formation of smaller complexes and that micellar shape and size changes often take place at higher amphiphile concentrations.<sup>1</sup> Above the amphiphile saturation concentration in water there is generally liquid crystal formation; it is now well documented that a large number of different mesomorphic phases may occur for a single amphiphile-water system. If a third component is added, phase equilibria frequently become very complex, as illustrated in Figure 1 where the phase diagram, taken from the work of Ekwall and coworkers,<sup>2</sup> for the system sodium oc-

tanoate-decanol-water is outlined. In Figure 1 the structures of the mesophases are also schematically given. (All of the structures are not definitely established.) Mainly through the work of Ekwall and coworkers, several systems have now been elucidated concerning the region of stability of the different phases. As can be seen from a recent review by Ekwall,<sup>3</sup> phase equilibria may depend markedly on counterion, on surfactant end group, on temperature, etc. While the general picture of the successive amphiphile association is thus provided, an understanding of the underlying molecular interactions is to a great extent lacking. Obviously, amphiphile-amphiphile interactions as well as amphiphile-counterion (in the case of ionic amphiphiles), amphiphile-water, water-water, and counterion-water interactions are important; it has, however, proved difficult



formed by Dr. Krister Fontell for a number of samples. We are also grateful to Dr. Fontell for the preparation of a number of samples in the systems  $C_7COONa-C_{10}OH-D_2O$  and AOTI- $D_2O$ .

The deuteron NMR spectra were recorded using a Varian V-4200 wide-line spectrometer equipped with a 12-in. V-3603 magnet. The magnetic field and the radio frequency were 1.403 T (tesla) and 9.1786 MHz and were controlled, respectively, by a Varian Mark II Fieldial unit and a crystal oscillator circuit. A Varian V-4540 temperature controller was used for controlling sample temperature. The actual sample temperature was measured by a copper-constantan thermocouple. Unless otherwise stated, the measurements were performed at  $20 \pm 0.3^\circ$ . Except for very small deuteron splittings the derivatives of the NMR absorption curves were recorded using a modulation frequency of 20 or 40 Hz. The modulation amplitude, the amplitude of the radiofrequency field, and the sweep rate were chosen small enough to give no detectable distortion of the spectra.

For those cases where the peaks arising from the hydroxylic deuterons were recorded (cf. below), larger sample tubes, which did not fit into the temperature controller, had to be used owing to the low signal intensities. In these cases the temperature was  $26 \pm 2^\circ$ ; furthermore, these signals had to be recorded under conditions of some overmodulation and saturation. While this markedly affected signal shape, the change in splitting is probably not more than 5%.

The experiments were generally performed with powder samples, i.e., samples without macroscopic alignment. For some samples, kindly supplied by Dr. Göran Lindblom, the effect of macroscopic alignment was investigated. In most cases orientation was achieved by inserting a bundle of parallel glass plates into a powder sample whereupon the temperature was increased to produce an isotropic solution which entered between the glass plates. In this way, spectra for powder sample and aligned sample could be obtained simultaneously and effects of evaporation during preparation of aligned samples were eliminated.

The deuteron quadrupole splitting is defined as the distance between the two peaks in the NMR absorption spectrum. An empirical correction of the splittings for peak broadening was employed.<sup>10</sup> In each case, at least two spectra were recorded. The error in the reported splittings is estimated to be less than 5% except for the separate amphiphile splittings and for those cases where the peaks are extensively broadened due to chemical exchange.

### Theory and General Considerations

All nuclei with spin quantum numbers  $I \geq 1$  have electric quadrupole moments which couple to an inhomogeneous electric field. In an environment with noncubic symmetry, as in most solids and liquid crystals, the interaction between the quadrupole moment and the electric field gradients is not averaged out by the molecular motion. The residual interaction, which is rather small for water deuterons or counterions in a liquid crystal, leads to a splitting of the NMR signal into  $2I$  equidistant peaks. The general theory of quadrupole splittings is described by Cohen and Reif<sup>22</sup> and a useful general description of NMR of liquid crystals is given by Luckhurst.<sup>4</sup> A theoretical treatment of quadrupolar effects in lyotropic systems has recently been given.<sup>17</sup> (Cf. also ref 23.)

It may be shown that the hamiltonian for quadrupolar

interaction averaged over the molecular motion may be written<sup>17</sup>

$$\bar{H}_Q = \beta_Q \sum_{qq'} (-1)^q V_{-q}^M A_q^L \overline{D^{(2)}_{0q}(\Omega_{DM})} D^{(2)}_{q'0}(\Omega_{LD}) \quad (1)$$

In the derivation of eq 1 it has been assumed that the system has a threefold or higher symmetry around the director. (The director is defined by the symmetry of the mesophase and is usually coincident with the optical axis.) The following symbols are used in eq 1:  $\beta_Q = eQ/2I(2I-1)\hbar$  ( $eQ$  is the quadrupole moment);  $V_q$  and  $A_q$  are irreducible components of the electrical field gradient tensor and the spin tensor operator, respectively;  $M, L$ , and  $D$  denote the different coordinate systems where the quantities are to be taken, molecular, laboratory, and director frames, respectively;  $D^{(2)}_{qq'}$  denotes a second rank Wigner rotation matrix element; and  $\Omega_{ij}$  denotes the eulerian angles that specify the transformation from coordinate system  $j$  to system  $i$ .

The quadrupole term is usually small compared to the Zeeman term and, to first order, it is only the secular part of  $\bar{H}_Q$  that contributes to the time-independent hamiltonian,  $H_0$ . For deuterons with  $I = 1$

$$H_0 = -\nu_0 I_z + \frac{\nu_Q S}{6} (3 \cos^2 \theta_{LD} - 1) (3I_z^2 - 2) \quad (2)$$

The order parameter,  $S$ , is given by

$$S = \frac{1}{2} \{ \overline{3 \cos^2 \theta_{DM} - 1} + \eta \overline{\sin^2 \theta_{DM} \cos 2\phi_{DM}} \}$$

and  $\nu_Q$  by

$$\nu_Q = \frac{3}{4} \frac{e^2 q Q}{\hbar}$$

Here  $\eta$  is the asymmetry parameter and  $eq$  twice the largest component of the electric field gradient tensor.  $\theta$  and  $\phi$  correspond to the eulerian angles  $\beta$  and  $\gamma$ , respectively.

From the hamiltonian in eq 2 one obtains a quadrupole splitting

$$\Delta(\theta) = |\nu_Q S (3 \cos^2 \theta_{LD} - 1)| \quad (3)$$

Equation 3 applies for an oriented sample where the director orientation is uniform throughout the sample. For a powder sample, where all values of  $\cos \theta_{LD}$  are equally probable, the NMR spectrum consists of a broad absorption curve with two marked peaks separated by

$$\Delta = |\nu_Q S| \quad (4)$$

and, in the derivative studied in the present work, two further less pronounced maxima separated by  $2\Delta$ . In contrast to solid crystals, the shape of the powder spectrum of lamellar or hexagonal mesophases is, as a result of the cylindrical symmetry around the director, not affected by the asymmetry parameter. On the other hand, the magnitude of the splitting may depend on  $\eta$  as can be seen from the expression for  $S$ .<sup>24</sup>

In the presence of chemical exchange, either exchange of  $D_2O$  molecules between different environments or deuteron exchange between  $D_2O$  and an amphiphilic molecule, the above equations should be modified. The effect of chemical exchange on spectral shape depends primarily on the ratio between the exchange rate and the difference in splitting between the different deuteron sites. In the limit of very slow exchange the observable spectrum is simply a superposition of the spectra of the different sites and for each site the equations given above are separately valid. In the limit of very fast exchange only a single quadrupole-split

spectrum is obtained with a splitting given by

$$\Delta = \left| \sum p_i \nu_Q^i S_i \right| \quad (5)$$

Here  $p_i$  is the fraction of deuterons in site  $i$  and  $S_i$  and  $\nu_Q^i$  characterize the properties of this site. If it is possible to observe the deuteron spectrum in both the exchange limits the relative signs of the order parameter<sup>15</sup> of two different sites may be determined.

Exchange rates of intermediate magnitude (residence times of the order of  $10^{-5}$  sec) result in broadened peaks. A treatment<sup>15</sup> of the effect of chemical exchange on quadrupole-split spectra has recently been presented and it has been shown how deuteron exchange rates may be obtained from spectral shape.

In the present work, it appears that the fast exchange limit (eq 5) pertains for the soap-carboxylic acid-D<sub>2</sub>O systems at all temperatures studied, while the soap-alcohol-D<sub>2</sub>O systems are close to the slow exchange limit around room temperature and not too high pH's.<sup>15</sup> By increasing either the temperature or pH, deuteron exchange can be accelerated so as to produce the fast exchange limit. In the present study, the decanol-OD and D<sub>2</sub>O deuteron splittings were assumed to be those measured directly from the spectrum; the water deuteron splitting was additionally determined from the collapsed (after addition of hydroxide) D<sub>2</sub>O-decanol signal by means of eq 5. In the case of soap-decanol-water systems, the  $S_i$ 's of water and alcohol were found to have the same sign.

Under certain conditions, in addition to the quadrupole-split signal, a central peak at the resonance Larmor frequency may be observed in the D<sub>2</sub>O powder spectrum of a liquid crystal.<sup>16</sup> Evidently, such a phenomenon may occur for a two-phase sample with some isotropic phase present or phase inhomogeneities providing an isotropic environment of the water molecules, in both cases with a slow exchange between the different parts of the sample. However, a central peak may be obtained also when the effect of phase inhomogeneities is minimized and this was recently demonstrated<sup>16</sup> to be a result of double quantum transitions and not of slow water exchange<sup>25</sup> in a homogeneous phase.

The nature of the central peak may be deduced from the changes of spectrum with radiofrequency field amplitude.<sup>16</sup> In the present work the radiofrequency field strength was kept low enough so as to avoid double quantum peaks in the spectra.

We will assume in our discussion of water deuteron splittings that water exchange between different binding sites is always in the fast exchange limit. We adopt as a simple model for water binding in lyotropic mesophases the existence of two types of water binding sites:<sup>23</sup> one (denoted b) corresponding to water molecules bound to the amphiphilic molecules and one (denoted f) to "free" water molecules. In some parts of the regions of existence of the lamellar mesophases, addition of water has been shown to cause no dimensional changes in the amphiphilic lamellae.<sup>26</sup> For this one-dimensional swelling case it may be assumed that water addition only changes the amount of free water. By means of eq 5 we obtain for this model

$$\Delta_{D_2O} = \left| p_f(\nu_Q S)_f + p_b(\nu_Q S)_b \right| + \left| (\nu_Q S)_f + \frac{nX_A}{X_{D_2O}}((\nu_Q S)_b - (\nu_Q S)_f) \right| \quad (6)$$

Here  $X_{D_2O}$  is the mole fraction of water,  $X_A$  the total mole

fraction of amphiphile, and  $n$  the average hydration number of the amphiphile. According to this model, a plot of  $\Delta_{D_2O}$  against the molar ratio of amphiphile to water should give a straight line with an intercept amounting to  $(\nu_Q S)_f$  and a slope given by  $n((\nu_Q S)_b - (\nu_Q S)_f)$ .

From the above considerations it appears that quadrupole splittings, except for distribution over different binding sites, give information on the product  $\nu_Q S$ , where  $\nu_Q = (3/4)(e^2qQ/h)$ . For water  $e^2qQ/h$  has been determined to be 215 kHz for solid D<sub>2</sub>O<sup>27</sup> and to 305 kHz for gaseous D<sub>2</sub>O.<sup>28</sup> We expect  $\nu_Q$  for the liquid state to be slightly above that for solid D<sub>2</sub>O (cf. ref 29 and 30) and to be relatively insensitive<sup>31</sup> to changes in composition and temperature. We assume, therefore, that changes in  $\Delta_{D_2O}$  may to a good approximation be referred to changes in the order parameter. Asymmetry parameters have been determined to be 0.100<sup>27</sup> (solid) and 0.115<sup>28</sup> (gas); these values are small enough so that the neglect of the second term in the expression for  $S$  is, for most cases, permissible. For decanol no determination of the quadrupole coupling constant has been performed but the value for gaseous methanol<sup>32</sup>  $e^2qQ/h = 303$  kHz makes the use of the same value of  $\nu_Q$  as for liquid water reasonable (cf. below). In the calculations we have used the value<sup>30</sup> of  $e^2qQ/h = 220$  kHz for both water and decanol.

Except for interactions and anisotropies on the molecular level, the deuteron spectrum is also affected by phase anisotropy and by macroscopic alignment. For example, if regions with a uniform director orientation are small, translational diffusion between sites with different  $\theta_{LD}$  may cause a total or partial elimination of the static quadrupole interactions. Similar effects enter in the comparison of different phase structures. Thus it can be shown<sup>17</sup> that the splitting for a hexagonal phase should be half that of a lamellar phase provided (i) the lamellae show no appreciable curvature, (ii) the local interactions and structure are the same for the two phases, and (iii) translational diffusion around cylinders in the hexagonal structure occurs in a time shorter than the inverse splitting. For cubic phases no splittings are observed<sup>8,9</sup> since translational motion may average out the quadrupole interactions.<sup>33</sup>

For a number of lamellar mesophase samples, the effect of macroscopic alignment as described above was investigated. In all cases, spectra of oriented samples gave two peaks separated by an amount proportional to  $3 \cos^2 \delta - 1$  where  $\delta$  is the angle between the normal to the glass plates and the static magnetic field. It appears, therefore, that the director is normal to the glass plates and, consequently, that the lamellar phase is aligned with the lamellae and the glass surfaces parallel. (In other systems, more complicated alignment phenomena may occur.<sup>23</sup>) Furthermore, in all cases we observed with the macroscopically aligned samples  $\Delta(90^\circ)$  to equal the powder splitting within the experimental error. It would appear, therefore, that the lamellae are not appreciably curved, since lamellar curvature would cause  $\Delta$  of the powder sample to be smaller than  $\Delta(90^\circ)$ .

## Results

For lamellar mesophase samples composed of soap, decanol, and D<sub>2</sub>O the deuteron NMR spectrum at low temperatures consists of two quadrupole-split signals, one due to D<sub>2</sub>O and one due to -OD of decanol.<sup>15</sup> For samples composed of soap, octanoic acid, and D<sub>2</sub>O, due to rapid deuteron exchange, only a single splitting is observed, even at low temperatures.

For the three-component systems, the composition of the samples was varied within the limits of stability of the lamellar phases, either by changing the molar fraction of  $D_2O$ ,  $X_{D_2O}$ , at a constant ratio between the two other components or by changing this ratio at a constant molar fraction of  $D_2O$ . The molar ratio of ionic amphiphile to total amphiphile is denoted  $R_{ionic}$ .

The variation of the water deuteron splitting with  $R_{ionic}$  for the systems  $C_7COOM$  ( $M = Li, Na, K, \text{ or } Rb$ )- $C_{10}OH-D_2O$  was investigated at two constant mole fractions of water. As can be seen from Figures 2 and 3, where  $\Delta_{D_2O}$  (obtained by the two procedures described above) is given, the variation of  $\Delta_{D_2O}$  with  $R_{ionic}$  is rather small with  $K^+$  or  $Rb^+$  as counterion. With  $C_7COONa$  a slight decrease in  $\Delta_{D_2O}$  with increasing  $R_{ionic}$  is observed while for  $C_7COOLi$  a maximum in  $\Delta_{D_2O}$  is observed when the amphiphile composition corresponds approximately to two  $C_7COOLi$  per three  $C_{10}OH$ . Of interest, is that the water deuteron splitting depends considerably on the alkali ion present, the sequence of splittings in general being  $Li^+ > Rb^+ \gtrsim K^+ > Na^+$ .

The data given in Figures 2 and 3 refer to the right-hand side of the lamellar phase region (Figure 1). At a value of  $R_{ionic}$  of 0.27 the dependence of  $\Delta_{D_2O}$  on the molar fraction of  $D_2O$  was investigated up to the highest water contents where the lamellar phase exists. The data are plotted in Figure 4 as a function of the molar ratio of total amphiphile to  $D_2O$ . The experimental results agree closely with the behavior predicted by eq 6 and in all cases we obtain within experimental error  $(\nu_Q S)_f = 0$ . The values of  $n|(\nu_Q S)_b|$  obtained from the slopes in Figure 4 are listed in Table I. Approximately the same values as those given in Table I were obtained for  $Li^+$  and  $Na^+$  at higher values of  $R_{ionic}$ . Also in the water-rich part of the lamellar phase region  $\Delta_{D_2O}$  is higher with  $Li^+$  as counterion than with  $Na^+$ ,  $K^+$ , or  $Rb^+$ . With  $C_7COONa$ ,  $\Delta_{D_2O}$  appears to be slightly greater than with  $C_7COOK$  or  $C_7COORb$ . A number of lamellar mesophase samples composed of alkali octanoate, decanol, and heavy water were also investigated using an equimolar mixture of two octanoates. It was found that with respect to the deuteron splittings these mixtures behaved regularly.

For the system  $C_7COONa-C_{10}OH-D_2O$ , more extensive studies of the lamellar phase were performed and other liquid crystalline phases were investigated. Representative data are inserted in Figure 1. For the normal (E) and reversed (F) hexagonal phases the splittings are close to those for the lamellar phase with the same  $X_{D_2O}$ . (Cf. also Figure 4 where some data for the E phase are included.) In the E phase  $\Delta_{D_2O}$  increases with increasing  $R_{ionic}$  at a constant  $X_{D_2O}$ . A comparison between results for E phase samples composed of alkali octanoate and  $D_2O$  gave the following sequence of splitting:  $Rb^+ \approx K^+ > Na^+$ . (See Table II.) The temperature dependence was also investigated for E phase samples composed of sodium octanoate and  $D_2O$ . In contrast to samples containing decanol, there is no detectable temperature dependence. Thus, for a sample with  $X_{D_2O} = 0.90$ ,  $\Delta_{D_2O}$  varies between 0.81 kHz at  $20^\circ$  and 0.79 kHz at  $53^\circ$ .

The phases denoted B and C in the phase diagram of the system  $C_7COONa-C_{10}OH-H_2O$  (see Figure 1) are not as well documented as the other phases and to the earlier given structure<sup>2</sup> an alternative has recently been proposed.<sup>34</sup> A detailed investigation of these phases by different methods is being performed together with Drs. G. J. T. Tiddy and K. Fontell. While a detailed report of this study

TABLE I: Values of  $n|(\nu_Q S)_b|$  for Various Systems Obtained from the Slopes in Figures 4 and 7<sup>a</sup>

System	Phase	$R_{ionic}$	$n (\nu_Q S)_b $ , kHz
$C_7COOLi-C_{10}OH-D_2O$	D	0.27	9.8
$C_7COONa-C_{10}OH-D_2O$	D	0.27	8.2
$C_7COONa-D_2O$	E	1.00	~7.5
$C_7COOK-C_{10}OH-D_2O$	D	0.27	7.4
$C_7COORb-C_{10}OH-D_2O$	D	0.27	7.9
AOT- $D_2O$	D	1.00	23
AOT- $D_2O$	F	1.00	7.4

<sup>a</sup> Phase notations according to Figure 1. Temperature  $20^\circ$ .

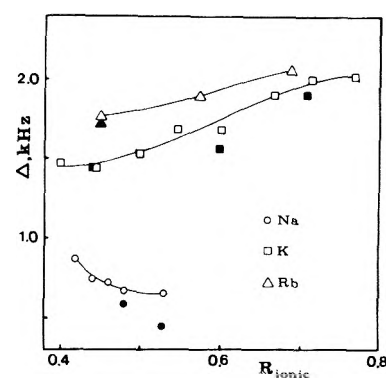


Figure 2. Directly observed (open symbols) and calculated as described in the text (filled symbols) water deuteron quadrupole splittings,  $\Delta$  in kHz, at  $20^\circ$  for lamellar mesophase samples in the  $C_7COOM-C_{10}OH-D_2O$  systems: (O, ●)  $M = Na$ ; (□, ■)  $M = K$ ; and (Δ, ▲)  $M = Rb$ .  $R_{ionic}$  is varied and  $X_{D_2O}$  is held constant at 0.77.

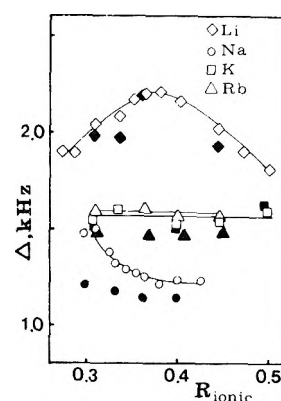


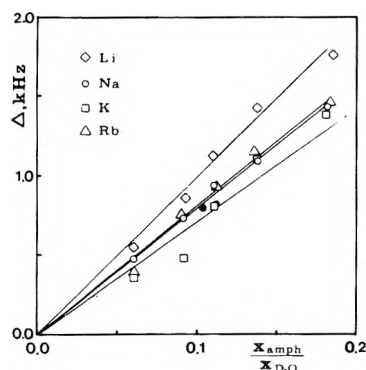
Figure 3. Observed and calculated (symbol convention as in Figure 2) water deuteron quadrupole splittings,  $\Delta$  in kHz, for lamellar mesophase samples in the  $C_7COOM-C_{10}OH-D_2O$  systems as a function of  $R_{ionic}$ .  $\diamond$  and  $\blacklozenge$  denote samples with  $M = Li$ , the others are as in Figure 2. Molar fraction of water is held constant at 0.83. Temperature  $20^\circ$ .

will be given later the following preliminary results on  $\Delta_{D_2O}$  are worth mentioning.

(a) For the C phase we have so far not been able to eliminate a central peak (not due to double quantum transitions) present in the spectra in addition to a normal quadrupole-split spectrum. The spectra correspond, therefore, to a two-phase system with one isotropic and one anisotropic phase. The splitting obtained is close to that expected for the D phase if it extended to this concentration region.

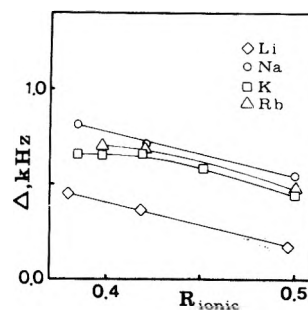
**TABLE II: Observed Deuteron Splittings for Selected Samples in Various Ternary and Binary Systems at 20°**

System	Phase	$X_{D_2O}$	$R_{ionic}$	$\Delta_{D_2O}$ kHz
$C_8SO_4Li-C_{10}OH-D_2O$	D	0.83	0.361	1.36
	D	0.83	0.300	1.32
$C_8SO_4Na-C_{10}OH-D_2O$	D	0.83	0.361	0.95
	D	0.83	0.300	1.00
$C_7COONa-D_2O$	E	0.91	1.000	0.79
$C_7COONa-C_7COOH-D_2O$	E	0.91	0.902	0.56
	E	0.90	0.843	0.45
$C_7COONa-C_{10}OH-D_2O$	E	0.90	0.771	0.76
$C_7COOK-D_2O$	E	0.91	1.000	1.01
$C_7COORb-D_2O$	E	0.91	1.000	1.01

**Figure 4.** Observed water deuteron quadrupole splittings for lamellar mesophase samples in the  $C_7COOM-C_{10}OH-D_2O$  systems as a function of the molar ratio of amphiphile to water ( $X_A/X_{D_2O}$ ).  $R_{ionic}$  was held constant at 0.27. Open symbols as in Figures 2 and 3, the filled circles denote samples in the normal hexagonal phase of the binary system  $C_7COONa-D_2O$ . Temperature 20°.

(b) For the B phase we have not been able to resolve any splitting and the maximal splitting (given by the line width) is considerably smaller than that obtained by extrapolating the D phase splittings to the higher  $X_{D_2O}$  values.

The observed splittings (which contain contributions from both  $D_2O$  and  $-COOD$  of octanoic acid) of the systems  $C_7COOM$  ( $M = Li, Na, K, \text{ or } Rb$ )- $C_7COOH-D_2O$  are given in Figure 5. In all cases the splitting increases with decreasing  $R_{ionic}$ . Also, for this system the splitting depends strongly on the counterion, the sequence being  $Na^+ > Rb^+ > K^+ > Li^+$ . Since the splittings for these systems are much smaller than the water deuteron splittings of the soap-decanol- $D_2O$  systems, the possibility of different signs of the contributions to the splittings of  $D_2O$  and  $-COOD$  must be examined (cf. eq 5). Therefore, the effect on the splitting of addition of octanoic acid to hexagonal phase samples composed of alkali octanoate and  $D_2O$  was investigated. An observed rapid decrease in splitting (see Table II) supports the assumption of different signs of the two contributions and from the rate of decrease it could be estimated that in the lamellar phase the absolute amphiphile contribution is greater than that of water. This conclusion is supported by estimates based on observations for systems where amphiphile and water contributions could be separately determined. Therefore, what we observe for the lamellar phases of the alkali octanoate-octanoic acid-water systems is essentially the difference between the

**Figure 5.** Observed deuteron quadrupole splittings as a function of  $R_{ionic}$  for samples in the  $C_7COOM-C_7COOH-D_2O$  systems. The molar fraction of water was 0.83: ( $\diamond$ )  $M = Li$ ; ( $\circ$ )  $M = Na$ ; ( $\square$ )  $M = K$ ; and ( $\triangle$ )  $M = Rb$ . Temperature 20°.

splitting of octanoic acid and that of water weighted by the deuteron population numbers. If we assume, in analogy with the alkali octanoate-decanol-water systems (see below), that the amphiphile contribution to the splitting is approximately independent of counterion, we obtain for the water splitting the sequence  $Li^+ > K^+ \approx Rb^+ > Na^+$ . Thus we obtain for the dependence of the water splitting on counterion essentially the same result as for the alkali octanoate-decanol-water systems.

$\Delta_{D_2O}$  values obtained at a constant  $R_{ionic}$  but varying  $X_{D_2O}$  are presented in Figure 6 for the systems  $C_8SO_4Li-C_{10}OH-D_2O$ ,  $C_8SO_4Na-C_{10}OH-D_2O$ ,  $C_8SO_3Na-C_{10}OH-D_2O$ , and  $C_7COONa-C_7COOH-D_2O$ . In the latter case the observed total splitting of  $-COOD$  and  $D_2O$  is given whereas for the other cases the observed water deuteron splitting is shown. Because of hydrolysis at high pH values the procedure used for the other surfactants to obtain  $\Delta_{D_2O}$  could not be employed with octyl sulfates and octylsulfonates. It can be inferred from Figure 6 and from Table II where additional data for these systems are presented, that at not too high water contents greater splittings are obtained with  $C_8SO_4Li$  than with  $C_8SO_4Na$  and that only in the case of the  $C_7COONa-C_7COOH-D_2O$  system do the data follow the simple model of water binding considered above (eq 6).

Aerosol OT contains no exchangeable deuterons and, therefore, experiments give  $\Delta_{D_2O}$  directly for the Aerosol OT- $D_2O$  systems. As can be seen from Figure 7 data follow over wide concentration ranges approximately the behavior predicted by eq 6 with  $(\nu_Q S)_f \approx 0$  and the product  $n(\nu_Q S)_b$  given in Table I. It can be seen that  $n(\nu_Q S)_b$  of the lamellar phase is more than twice that of the reversed hexagonal phase. The difference between the two Aerosol OT compounds is small.

Decanol-OD splittings were obtained for the systems  $C_7COOM-C_{10}OH-D_2O$  with  $M = Li, Na, K, Rb$ , and these are given in Figure 8 at two constant molar fractions of water as a function of  $R_{ionic}$ . As can be seen the decanol splitting increases with decreasing water content and increasing  $R_{ionic}$  but is within the experimental error independent of the counterion. Some data obtained for the system  $NaC_8SO_4-C_{10}OH-D_2O$  included for comparison in Figure 8 show that the decanol splitting is not markedly dependent on surfactant end group.

## Discussion

Our goal in studying deuteron quadrupole splittings of amphiphilic mesophases was to obtain information on the degree of water and amphiphile orientation under various conditions. In turn these results, which were given above,

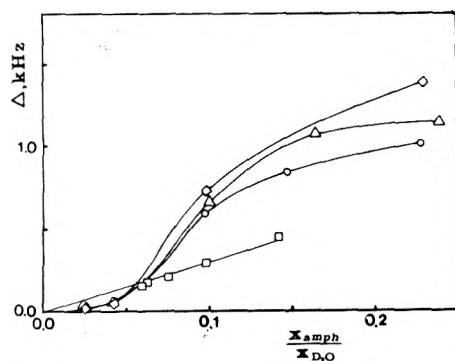


**Figure 6.** Observed water quadrupole splittings as a function of the molar ratio of amphiphile to  $D_2O$  for lamellar mesophase samples with a constant  $R_{ionic}$  of 0.31 in various systems: ( $\diamond$ )  $C_8SO_4Li-C_{10}OH-D_2O$ ; ( $\circ$ )  $C_8SO_4Na-C_{10}OH-D_2O$ ; ( $\Delta$ )  $C_8SO_3Na-C_{10}OH-D_2O$ ; and ( $\square$ )  $C_7COONa-C_7COOH-D_2O$ . For the latter system both water and octanoic acid contribute to the splitting (cf. text). Temperature  $20^\circ$ .

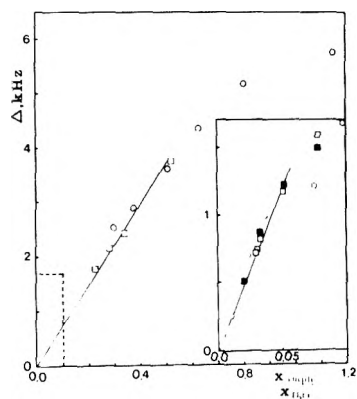


**Figure 7.** Observed water deuteron quadrupole splittings in the systems sodium di-(2-ethylhexyl)sulfosuccinate ( $\circ$ ) and sodium dioctylsulfosuccinate ( $\square$ ). The main figure shows results for the reversed hexagonal phase whereas the insert refers to lamellar samples. Temperature of measurements was  $25 \pm 2^\circ$ ; filled squares denote results for lamellar sodium dioctylsulfosuccinate  $D_2O$  samples obtained at  $20^\circ$ .

should contain information on the molecular interactions in the systems and this will now be considered.

Let us start with some general observations for the water deuteron splittings. As can be seen from Figures 4, 6, and 7 the simplified model leading to eq 6 gives, for many systems, a good rationalization of the data. Accordingly, a division into bound and free water molecules seems meaningful. For the number of water molecules bound per amphiphilic molecule no direct information is provided, since only the product of the hydration number ( $n$ ) and the order parameter is obtained. However, an upper limit of  $n$  is given from the extensions of the linear plots. In this way, upper limits of  $n$  of about 5 are obtained for the alkali octanoate-decanol-water systems; in contrast for the Aerosol OT-water systems an upper limit of  $n = 2$  is indicated. Using these upper limits of  $n$ , lower limits of  $|S|$  in the lamellar phases are obtained of ca. 0.01 for the octanoate-decanol-water systems and 0.07 for the Aerosol OT-water system. Since we obtain the order parameter of the "free" water molecules to be zero within experimental error we may conclude that there appears to be no long-range ordering of the water molecules with respect to the amphiphilic lamellae; only a small number of water molecules per amphiphilic molecule are detectably oriented.

Since in all cases investigated,  $S_f$  appears to be close to zero we have approximately

$$\Delta_{D_2O} = \left| \frac{X_A}{X_{D_2O}} n(\nu_Q S)_b \right|$$

By multiplying the experimental water deuteron splittings by the molar ratio of water to amphiphile we obtain  $n|(\nu_Q S)_b|$ . We give in Table III  $n|(\nu_Q S)_b|$  for a number of representative samples. Clearly, in discussions of molecular interactions  $n|(\nu_Q S)_b|$  is more appropriate than the observed splitting. The nonlinear plots obtained for some systems (Figure 6) can probably be referred to changes in the amphiphile hydration numbers with sample composition.

Before using the splitting parameters to obtain information on molecular interactions, we will briefly consider the dependence of the splitting on phase structure. As argued above we expect under certain conditions the order parameter of a lamellar phase to be greater by a factor of 2 than that of a phase built up of long parallel rod-shaped aggregates.<sup>17</sup> From Figure 7 and Table I it can be seen that for the Aerosol OT- $D_2O$  systems the ratio of  $n|(\nu_Q S)_b|$  between the lamellar and reversed hexagonal phases is about three. For the other systems the ratio in splitting between the lamellar and normal hexagonal phases was observed to be considerably less than two. Clearly one (or more) of the necessary assumptions given above does not apply. A considerable curvature of the lamellae does not seem to be consistent with the splittings observed for macroscopically aligned samples (see above). Thus for all samples investigated  $\Delta(0^\circ)$  divided by the powder splitting is in the range 1.8–2.0. A second possible explanation is that water diffusion around the cylinders is not fast enough to produce the partial averaging of the static quadrupole interactions. However, the required translational diffusion coefficients, estimated using cylinder radii of the order of the length of the amphiphilic molecules, are unrealistically small and therefore this explanation is most probably not correct. The remaining possibility is that the water binding to the aggregate surfaces is so affected by aggregate shape alteration and composition variation between the phases that this considerably affects the splitting. In fact we expect on purely geometrical grounds the area per polar group, and as a consequence also  $n$ , to follow the sequence  $E > D > F$ . For the sodium octanoate-decanol-water system changes in the area per polar group are considerable,<sup>35</sup> while they are less pronounced for the AOT I-water system.<sup>36</sup> For three-component systems, different hydration numbers of the two amphiphiles have to be taken into account; for example, we expect the hydration number of octanoate to be greater than that of decanol. Also in data given by other workers<sup>8,12</sup> it appears that the 2:1 ratio in splitting between the two types of phases is not obtained. It appears that conclusions on mesophase structure from water deuteron splittings are for many systems made impossible by the sensitivity of the water splitting to changes in other factors. The amphiphile splitting, changing very slowly with sample composition (Figure 8), should, on the contrary, be more useful in connection with phase structure elucidation.

For all the cases studied it appears that  $\Delta_{D_2O}$ , as well as  $n|S_b|$ , is considerably greater with  $Li^+$  as the counterion than with the other alkali ions. Since the lithium ions, having a great surface charge density, are strongly hydrated an obvious explanation for the great degree of water orientation in the presence of  $Li^+$  ions is that the water of hydration of the bound lithium counterions is oriented with re-



**TABLE III: Values of  $n|(\nu_Q S)_b|$  Obtained by Multiplying the Observed Water Deuteron Quadrupole Splitting by  $X_{D_2O}/X_A^a$** 

System	$X_{D_2O}$	$R_{ionic}$	$n (\nu_Q S)_b $
Lamellar Phases (D)			
$C_7COOLi-C_{10}OH-D_2O$	0.83	0.499	8.8
	0.83	0.443	9.9
	0.83	0.380	10.8
	0.83	0.335	10.2
	0.83	0.273	9.3
$C_7COONa-C_{10}OH-D_2O$	0.775	0.529	2.3
	0.775	0.460	2.5
	0.775	0.440	2.6
	0.775	0.420	3.0
	0.85	0.346	7.1
	0.83	0.455	5.9
	0.83	0.400	6.0
	0.83	0.380	5.9
	0.83	0.343	6.3
	0.83	0.316	6.7
	0.83	0.298	7.2
$C_7COOK-C_{10}OH-D_2O$	0.77	0.769	6.8
	0.77	0.500	5.1
	0.77	0.400	4.9
	0.83	0.497	7.8
	0.83	0.398	7.4
	0.83	0.307	7.5
	$C_7COORb-C_{10}OH-D_2O$	0.77	0.688
0.77		0.450	5.9
0.83		0.445	7.6
0.83		0.309	7.7
$C_8SO_4Li-C_{10}OH-D_2O$	0.83	0.361	6.7
	0.83	0.300	6.4
$C_8SO_4Na-C_{10}OH-D_2O$	0.77	0.424	1.6
	0.77	0.295	2.6
	0.83	0.361	4.6
	0.83	0.300	4.9
$C_8SO_3Na-C_{10}OH-D_2O$	0.77	0.500	1.2
	0.77	0.360	3.9
Normal Hexagonal Phases (E)			
$C_7COONa-C_{10}OH-D_2O$	0.90	1.000	7.2
	0.90	0.755	6.6
	0.91	1.000	7.7
$C_7COOK-C_{10}OH-D_2O$	0.91	1.000	9.8
$C_7COORb-C_{10}OH-D_2O$	0.91	1.000	9.8
Reversed Hexagonal Phases (F)			
$C_7COONa-C_{10}OH-D_2O$	0.75	0.171	2.3

<sup>a</sup> Cf. text. Temperature 20°.

spect to the lamellae. The data obtained with the other alkali ions show, however, that the correlation between degree of water orientation and strength of hydration does not apply in all cases. For example, the relative effects of  $Na^+$ ,  $K^+$ , and  $Rb^+$  appear to depend in a complex way on mesophase composition. A definite explanation to this intricate behavior may not be given at present, but possibly

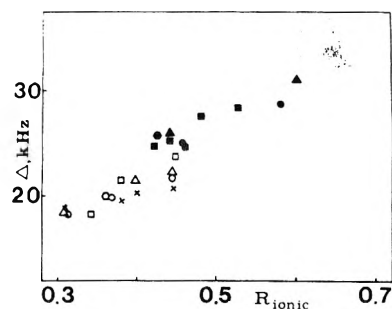


**Figure 8.** Composition dependence of decanolic deuteron quadrupole splittings of lamellar mesophase samples. Filled and open symbols denote samples with  $X_{D_2O} = 0.77$  and  $0.83$ , respectively. The following systems were studied: (X)  $C_7COOLi-C_{10}OH-D_2O$ ; (□, ■)  $C_7COONa-C_{10}OH-D_2O$ ; (Δ, ▲)  $C_7COOK-C_{10}OH-D_2O$ ; (○, ●)  $C_7COORb-C_{10}OH-D_2O$ ; (○, ●)  $C_8SO_4Na-C_{10}OH-D_2O$ . Temperature 20°.

the reason why the degree of water orientation may be smaller with  $Na^+$  as the counterion than with  $K^+$  or  $Rb^+$  is that the water of hydration of bound sodium ions is oriented with respect to the lamellae only under certain conditions.

The details of the variation of the splitting,  $\Delta\nu_{D_2O}$ , as well as the quantity  $n|(\nu_Q S)_b|$ , within the lamellar phase regions are rather complex and cannot be fully discussed; only a few interesting points will be taken up.

For the system most thoroughly investigated, the sodium octanoate-decanol-water system, it is interesting to note (see Tables I and III) that over most of the region of existence of the lamellar phase, changes in  $n|(\nu_Q S)_b|$  are rather small. However, at the lowest water contents,  $n|(\nu_Q S)_b|$  drops to quite low values. Since  $\Delta\nu_{D_2O}$  takes on low values in this part of the phase and since the degree of orientation in the amphiphilic lamellae increases (Figure 8) with decreasing water content, it appears reasonable to attribute this observation to a decreased hydration number of the amphiphilic molecules. Thus as the water content is decreased below the value compatible with complete hydration of both the amphiphilic molecules and the counterions, there appears first to be a dehydration of the amphiphiles. If the water of counterion hydration is not markedly oriented with respect to the lamellae a significant decrease in the degree of water orientation results. In part our interpretation parallels that of X-ray diffraction data.<sup>35</sup> Such changes in amphiphile hydration numbers may also be the explanation to the nonlinear plots of  $\Delta\nu_{D_2O}$  vs.  $X_A/X_{D_2O}$  obtained for some systems (see Figure 6).

An interesting observation with the lithium octanoate-decanol- $D_2O$  system is the observed maximum in  $\Delta\nu_{D_2O}$  displayed in Figure 3. This indicates that the interaction between the water and amphiphile layers is particularly strong at this amphiphile composition. Possibly, as discussed by Fontell et al.,<sup>35</sup> this may be due to the formation of hydrogen-bonded complexes between octanoate and decanol. Complex formation involving hydrogen bonding to water may be particularly important in the case of lithium due to its ability to markedly polarize the surrounding water molecules. Fontell et al.<sup>35</sup> have also proposed that when  $R_{ionic}$  is reduced below ca. 0.43 the ability of water to form bridges between octanoate and decanol and between octanoate and counterion is reduced. This leads to a partial release of counterions achieved by a Donnan equilibrium when the charge density of the aggregates becomes sufficiently low. (The counterion release with decreasing  $R_{ionic}$

has been verified by  $^{23}\text{Na}$  NMR studies.<sup>37</sup> The opposite variation with  $R_{\text{ionic}}$  at high decanol contents of  $\Delta_{\text{D}_2\text{O}}$  (Figure 3) for the lithium and sodium octanoates tends to support our assumption that the whole  $\text{Li}^+$ -water complex is oriented with respect to the amphiphilic lamellae while this is not the case for  $\text{Na}^+$ .

In previous work (e.g., ref 10, 11, 38, 39) the relation  $\Delta_{\text{obsd}} = \sum p_i \Delta_i$  has generally been used instead of eq 5. The systems alkali octanoate-octanoic acid-water appear to provide the first experimental verification of the correctness of eq 5. What we observe for these systems is the difference between the contributions of octanoic acid and of  $\text{D}_2\text{O}$ . Support for this conclusion is provided by the effect of addition of octanoic acid on the deuteron splitting for the hexagonal phase, by the very small splitting of the lamellar phase compared to the other systems, and by the variation of the splitting with  $R_{\text{ionic}}$ . If together with this result we assume that the contribution of octanoic acid to the observed deuteron splitting is independent of alkali ion present, it follows that in line with the other systems  $\text{Li}^+$  ions give a markedly greater order parameter for water than the other alkali ions.

As can be inferred from Figure 8, the decanol-OD deuteron splittings of the lamellar soap-decanol- $\text{D}_2\text{O}$  mesophase samples are in the range 20–30 kHz. Estimating  $e^2Qq/h$  for the liquid state to be 220 kHz (see above) we obtain for the order parameter  $|S| = 0.12$ – $0.18$ . A comparison with the  $S$  values obtained for water shows that the degree of amphiphile orientation is considerably greater than that of water and also than that of the water molecules bound to the amphiphile end groups. In contrast to  $\Delta_{\text{D}_2\text{O}}$  the decanol splitting is not appreciably dependent on either counterion or surfactant end group. The independence of amphiphile orientation on counterion, together with the considerable variation of  $\Delta_{\text{D}_2\text{O}}$  with counterion, is in line with  $^{23}\text{Na}$  NMR investigations<sup>40,41</sup> indicating that for the systems considered the counterions are, in general, extensively hydrated. With decreasing water content and increasing molar ratio of octanoate to decanol there is a slow increase in the degree of decanol orientation. The increase in  $|S|$  with increasing  $R_{\text{ionic}}$  may be due to a stabilization of the surfaces of the lamellae with increasing charge density or an enhanced orientation arising from hydrogen bonding between octanoate and decanol. The increased degree of amphiphile orientation with decreasing water concentration is in line with the dehydration of the amphiphilic end groups proposed above.

*Acknowledgments.* Several enlightening discussions on static quadrupolar effects with Dr. H. Wennerström are

gratefully acknowledged. During this work we also had helpful discussions with Drs. K. Fontell, G. Lindblom, and G. J. T. Tiddy. Dr. W. Egan kindly made a linguistic revision of the manuscript.

## References and Notes

- (1) P. Ekwall and P. Stenius, *MTP Int. Rev. Sci.: Phys. Chem., Ser. Two*, **7**, in press.
- (2) P. Ekwall, L. Mandell, K. Fontell, and H. Lehtinen, *Acta Polytech. Scand., Chem. Incl. Metall. Ser.*, **74** I-III (1968).
- (3) P. Ekwall, *Adv. Liquid Crystals*, **1**, 1 (1975).
- (4) G. R. Luckhurst in "Liquid Crystals and Plastic Crystals", G. W. Gray and P. A. Winsor, Ed., Ellis Horwood, 1974, p 144.
- (5) Å. Johansson and B. Lindman in ref 4, p 192.
- (6) S. Meiboom and L. C. Snyder, *Acc. Chem. Res.*, **4**, 84 (1970).
- (7) R. C. Long, Jr., and J.-M. Goldstein, *Mol. Cryst. Liquid Cryst.*, **23**, 137 (1974).
- (8) K. D. Lawson and T. J. Flautt, *J. Phys. Chem.*, **72**, 2066 (1968).
- (9) J. Charvolin and P. Rigny, *Chem. Phys. Lett.*, **18**, 575 (1973).
- (10) Å. Johansson and T. Drakenberg, *Mol. Cryst. Liquid Cryst.*, **14**, 23 (1971).
- (11) N.-O. Persson and Å. Johansson, *Acta Chem. Scand.*, **25**, 2118 (1971).
- (12) N.-O. Persson, G. Lindblom, B. Lindman, and G. Arvidsson, *Chem. Phys. Lipids*, **12**, 261 (1974).
- (13) G. Lindblom and B. Lindman, *Mol. Cryst. Liquid Cryst.*, **22**, 45 (1973).
- (14) G. Lindblom, H. Wennerström, and B. Lindman, *Chem. Phys. Lett.*, **8**, 489 (1971).
- (15) N.-O. Persson, H. Wennerström, and B. Lindman, *Acta Chem. Scand.*, **27**, 1667 (1973).
- (16) H. Wennerström, N.-O. Persson, and B. Lindman, *J. Magn. Resonance*, **13**, 348 (1974).
- (17) H. Wennerström, G. Lindblom, and B. Lindman, *Chem. Scr.*, **6**, 97 (1974).
- (18) D. Park, I. Rogers, R. W. Toft, and P. A. Winsor, *J. Colloid Interface Sci.*, **32**, 81 (1970).
- (19) P. Ekwall, *Wiss. Z. Friedrich-Schiller-Univ., Jena, Math. Naturwiss. Reihe*, **14**, 181 (1965).
- (20) P. Ekwall and L. Mandell, *Acta Chem. Scand.*, **22**, 699 (1968).
- (21) K. Fontell in ref 4, p 80.
- (22) M. H. Cohen and F. Reif, *Solid State Phys.*, **5**, 321 (1957).
- (23) H. Wennerström, N.-O. Persson, and B. Lindman, *Am. Chem. Soc., Symp. Ser.*, **9**, 253 (1975).
- (24) G. Lindblom, *Acta Chem. Scand.*, **26**, 1745 (1972).
- (25) J. Charvolin and P. Rigny, *J. Phys. (Paris) Colloq.*, **30**, C4-76 (1969).
- (26) P. Ekwall, L. Mandell, and K. Fontell, *Acta Chem. Scand.*, **22**, 1543 (1968).
- (27) P. Waldstein, S. W. Rabideau, and J. A. Jackson, *J. Chem. Phys.*, **41**, 3407 (1964).
- (28) D. W. Poesner, *Austr. J. Phys.*, **13**, 168 (1960).
- (29) H. G. Hertz, *Prog. Nucl. Magn. Reson. Spectrosc.*, **3**, 159 (1967).
- (30) J. A. Glasel in "Water a Comprehensive Treatise", Vol. 1, F. Franks, Ed., Plenum Press, New York, N.Y., 1972, p 215.
- (31) C. Deverell, *Prog. Nucl. Magn. Reson. Spectrosc.*, **4**, 235 (1969).
- (32) K. H. Castleton and S. G. Kukulich, *Chem. Phys. Lett.*, **22**, 331 (1973).
- (33) T. E. Bull and B. Lindman, *Mol. Cryst. Liquid Cryst.*, **28**, 155 (1975).
- (34) G. J. T. Tiddy, *J. Chem. Soc., Faraday Trans. 1*, **68**, 369 (1972).
- (35) Reference 2, part III.
- (36) P. Ekwall, L. Mandell, and K. Fontell, *J. Colloid Interface Sci.*, **33**, 215 (1970).
- (37) H. Gustavsson, G. Lindblom, B. Lindman, N.-O. Persson, and H. Wennerström in "Liquid Crystals and Ordered Fluids", Part 2, J. F. Johnson and R. S. Porter, Ed., Plenum Press, New York, N.Y., 1974, p 161.
- (38) B. Ellis, A. S. C. Lawrence, M. P. McDonald, and W. E. Peel in "Liquid Crystals and Ordered Fluids", J. F. Johnson and R. S. Porter, Ed., Plenum Press, New York, N.Y., 1970, p 277.
- (39) E. G. Finer, *J. Chem. Soc., Faraday Trans. 2*, **69**, 1590 (1973).
- (40) B. Lindman and P. Ekwall, *Mol. Cryst.*, **5**, 79 (1968).
- (41) H. Gustavsson and B. Lindman, *J. Am. Chem. Soc.*, in press.

# Electron Spin Resonance Studies of Phenyl and Pyridyl Radicals in Aqueous Solution<sup>1</sup>

Haya Zemel and Richard W. Fessenden\*

Radiation Research Laboratories and Department of Chemistry, Mellon Institute of Science,  
Carnegie-Mellon University, Pittsburgh, Pennsylvania 15213 (Received November 27, 1974)

Publication costs assisted by Carnegie-Mellon University and the U.S. Energy Research and Development Administration

ESR spectra of a number of phenyl and 2-pyridyl radicals have been detected in aqueous solution. Two methods of radical production were used, namely, reaction of  $\text{SO}_4^{\cdot-}$  produced by photolysis of  $\text{S}_2\text{O}_8^{2-}$  with aromatic carboxylate ions and reaction of  $e_{\text{aq}}^-$  produced by radiolysis with aromatic bromides. Most radicals had only carboxyl groups as further substituents. The proton hyperfine constants of the phenyl radicals,  $a_o \sim 17$ ,  $a_m \sim 6$ , and  $a_p \sim 2$  G, are readily assigned on the basis of effects of the various substitutions and agree well with previous determinations for radicals in the solid state. With four phenyl radicals containing two to four carboxyl groups it was also possible to detect all of the possible  $^{13}\text{C}$  containing isomers at natural abundance. A hyperfine constant of  $\sim 135$  G for the carbon at the radical site confirms the  $\sigma$  nature of phenyl radical. The other ring  $^{13}\text{C}$  hyperfine constants are  $a_o^{\text{C}} \sim 7.5$ ,  $a_m^{\text{C}} \sim 13$ , and  $a_p^{\text{C}} \sim 1.5$  G. Both  $^{14}\text{N}$  and proton hyperfine constants were determined for the 2-pyridyl radicals. Only the  $^{14}\text{N}$  value ( $\sim 27$  G) was known previously. The  $g$  factors of phenyl and 2-pyridyl radicals are low (near or below the free electron value) reflecting their  $\sigma$  nature. The presence of carboxyl groups in a phenyl radical affects the  $g$  factor in an additive fashion with increments of 13,  $-2$ , and  $-3$  units in the fifth decimal place for ortho, meta, and para substituents, respectively. The observation of phenyl and 2-pyridyl radicals demonstrates in a direct way that these radicals are formed in the two above-mentioned reactions. (One example each of a 4-pyridyl and a pyrazyl radical were also produced and studied.) Phenyl and 2-pyridyl radicals with no ortho carboxyl group were found to be very reactive toward addition to another aromatic molecule and were best detected using low concentrations ( $5 \times 10^{-4} M$ ) of aromatic bromide. Spectra of the unsubstituted phenyl and 2-pyridyl radicals were obtained in this way from the corresponding bromides. At higher solute concentrations such as used for the decarboxylation reactions these radicals react further to form adducts of the cyclohexadienyl type. Radicals with an ortho carboxyl group (for example, 2-carboxylphenyl radical produced from phthalate) are much less reactive toward addition and could be studied at higher concentrations of the starting compound. Reaction of  $\text{SO}_4^{\cdot-}$  with acids in which three (or more) adjacent carboxyl groups are present leads preferentially to loss of a central or interior carboxyl group. To provide data for comparison with earlier indirect studies, a number of adducts of phenyl and pyridyl radicals to  $\text{CH}_2=\text{NO}_2^-$  and trimesate were studied and their hyperfine constants determined. In the latter cases it was found that the ortho and meta protons in the phenyl radical which has added (i.e., the side group in the final cyclohexadienyl radical) can produce splittings of  $\sim 0.05$  and  $\sim 0.3$  G, respectively. The radicals detected in experiments in which  $\text{SO}_4^{\cdot-}$  reacts with terephthalate and trimesate are thus shown to be adducts of phenyl type radicals to the starting molecule and not  $\text{SO}_4^{\cdot-}$  adducts as previously suggested.

## Introduction

The ESR spectra of phenyl radical<sup>2-6</sup> and the related pyridyl radicals<sup>6-9</sup> have been known for some time from studies in the solid phase. Indirect ESR evidence for the formation of phenyl radicals in aqueous solution has been found in studies of the reactions of reducing species with diazonium ions<sup>10</sup> and of  $\text{SO}_4^{\cdot-}$  with benzoate<sup>11</sup> but no direct ESR observations of phenyl radicals in solution have been reported. In the present paper we wish to present ESR spectra for a number of phenyl, pyridyl, and pyrazyl radicals in aqueous solution as prepared by several types of reactions.

The present work was initiated because of a desire to explore further the reactions of  $\text{SO}_4^{\cdot-}$  with aromatic compounds. The reactions of a number of oxidizing radicals are being used to probe enzyme deactivation<sup>12</sup> and it is important to understand in more detail the nature of the reactions. Norman et al.<sup>13</sup> have reported that 1,3,5-benzenetricarboxylate (trimesate) and terephthalic acid form adducts with  $\text{SO}_4^{\cdot-}$  while benzene yields the OH adduct<sup>13</sup> and benzoate appears to be decarboxylated.<sup>11</sup> It was because of this

apparent variety of reactions that we began with  $\text{SO}_4^{\cdot-}$  and aromatic acids. The results to be described help considerably in eliminating much of the previous confusion regarding these reactions.

## Experimental Section

The radicals were prepared using previously described techniques by radiolysis directly in the ESR cavity with 2.8-MeV electrons<sup>14</sup> or by photolysis with a 1-kW mercury-xenon lamp.<sup>15</sup> Magnetic field measurements were made by means of a field-tracking NMR unit and frequency counter.<sup>14</sup> The  $g$  factors were determined by reference to the peak from the irradiated silica cell in the radiolysis experiment or directly from field and microwave frequency measurements in the photolysis work. The estimates of experimental accuracy as given in footnote a, Table I are based on the reproducibility of splittings that occur several times in a given spectrum and upon comparisons of parameters from different spectra. The results refer to solutions within a few degrees of room temperature, about 24°. Most of the aromatic precursors were from the Aldrich Chemical Co.

TABLE I: ESR Parameters of Phenyl Radicals<sup>a</sup>

Radical	Substituent	Position <sup>b</sup>	Method <sup>c</sup>	$a_{2,6}^H$ (ortho)	$a_{3,5}^H$ (meta)	$a_4^H$ (para)	$g$
I <sup>d</sup>	None		$e_{aq}^-$	17.43 (2)	6.25 (2)	2.04	2.00227
II	O <sup>-e</sup>	3	$e_{aq}^-$	20.13, 15.77	9.12	1.32	2.00226
III	OH <sup>f</sup>	4	$e_{aq}^-$	(16.8) <sup>g</sup> (2)	4.90 (2)		(2.00226) <sup>g</sup>
IV	CO <sub>2</sub> <sup>-</sup>	2	$e_{aq}^-$ , SO <sub>4</sub> <sup>-</sup>	18.11	7.85, 5.87 <sup>h</sup>	1.71	2.00240
V	CO <sub>2</sub> <sup>-</sup>	4	$e_{aq}^-$	17.06 (2)	5.88 (2)		2.00224
VI	CO <sub>2</sub> <sup>-</sup>	2, 6	SO <sub>4</sub> <sup>-</sup>		7.41 (2)	1.39	2.00254
VII	CO <sub>2</sub> <sup>-</sup>	2, 5	$e_{aq}^-$ , SO <sub>4</sub> <sup>-</sup>	18.71	7.66	1.44	2.00238
VIII	CO <sub>2</sub> <sup>-</sup>	2, 4	$e_{aq}^-$ , SO <sub>4</sub> <sup>-</sup>	17.66	7.45, 5.59 <sup>h</sup>		2.00237
IX	CO <sub>2</sub> <sup>-</sup>	2, 3, 6	SO <sub>4</sub> <sup>-</sup>		7.47	1.17	2.00251
X	CO <sub>2</sub> <sup>-</sup>	2, 4, 6	SO <sub>4</sub> <sup>-</sup>		7.10 (2)		2.00251
XI	CO <sub>2</sub> <sup>-</sup>	2, 3, 5	SO <sub>4</sub> <sup>-</sup>	18.14		1.23	2.00236
XII	CO <sub>2</sub> <sup>-</sup>	2, 4, 5	SO <sub>4</sub> <sup>-</sup>	18.04	7.37		2.00237
XIII	CO <sub>2</sub> <sup>-</sup>	2, 3, 5, 6	SO <sub>4</sub> <sup>-</sup>			0.95	2.00246
XIV	CO <sub>2</sub> <sup>-</sup>	2, 3, 4, 6	SO <sub>4</sub> <sup>-</sup>		7.43		2.00249
XV	CO <sub>2</sub> <sup>-</sup>	2, 3, 4, 5, 6	SO <sub>4</sub> <sup>-</sup>				2.00246

<sup>a</sup> Hyperfine constants are given in gauss and are accurate to  $\pm 0.03$  G. The number of nuclei exhibiting the splitting are given in parentheses if different than one. The  $g$  factors were determined from field and frequency measurements in photolysis experiments and by reference to the peak from the silica cell in radiolysis experiments. Second-order corrections have been made. The relative values are believed accurate to  $\pm 1$  in the fifth decimal place and the absolute values to about  $\pm 3$  in the fifth place. <sup>b</sup> Positions are numbered according to



<sup>c</sup> Radicals were produced by removal of Br<sup>-</sup> from the appropriate bromide by reaction with  $e_{aq}^-$  (reaction 4) or by removal of a carboxyl group from the appropriate carboxylate ion by reaction with SO<sub>4</sub><sup>-</sup> (reaction 1). <sup>d</sup> Values observed for this radical in an argon matrix are  $a_o = 17.4$ ,  $a_m = 5.9$ ,  $a_p = 1.9$  G,  $g = 2.0023$ . <sup>e</sup> Observed at pH 12. If the pK of the radical is similar to that of phenol (9.9) then the OH proton should be dissociated at this pH. <sup>f</sup> Observed at pH 7. The OH proton should not be dissociated. <sup>g</sup> Only the high-field line group (a triplet) was observed because of CIDEP effects.<sup>22</sup> The  $g$  factor given in the table was assumed to allow determination of the ortho proton splitting. <sup>h</sup> As described in the text, the value of  $\sim 7.5$  G can be assigned to the proton at the 3 position.

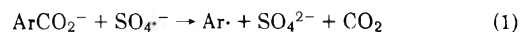
The 1,2,3- and 1,2,4-benzenetricarboxylic acids and benzenepentacarboxylic acid were from EGA-Chemie, KG (W. Germany), phthalic acid from Eastman Chemical Co., and bromobenzene and *p*-bromophenol from Baker. The samples of 1,2,3,5- and 1,2,3,4-benzenetetracarboxylic acids were kindly supplied by Dr. Klaus Eiben.<sup>16</sup> The pH was adjusted with KOH, H<sub>2</sub>SO<sub>4</sub>, Na<sub>2</sub>B<sub>4</sub>O<sub>7</sub>, Na<sub>2</sub>HPO<sub>4</sub>, and NaH<sub>2</sub>PO<sub>4</sub> which were all Baker Analyzed Reagents. The Na<sub>2</sub>S<sub>2</sub>O<sub>8</sub> was obtained from Sigma Chemical Co. and *tert*-butyl alcohol from Mallinckrodt.

Typical solutions used in the photolysis experiments contained 30–70 mM Na<sub>2</sub>S<sub>2</sub>O<sub>8</sub> and 1–5 mM of the aromatic acid. The pH was maintained with  $\sim 10$  mM of the appropriate buffer (phosphate or borate) in the range 6–10. Flow rates varied from 5 to 40 cm<sup>3</sup>/min. Solutions for radiolysis experiments contained 0.5–5 mM of the desired compound (bromide) and were in the pH range 11–12. In most cases no other solute was present. Where an OH scavenger was needed, *tert*-butyl alcohol was used. Solutions were deoxygenated by bubbling with N<sub>2</sub> or N<sub>2</sub>O.

## Results and Discussion

**Direct Observation of Phenyl and Related Radicals.** Because the radicals produced by reaction of SO<sub>4</sub><sup>-</sup> with terephthalate and 1,3,5-benzenetricarboxylate (trimesate) had already been reported,<sup>13</sup> the initial experiments were carried out with phthalate, 1,2,4,5-benzenetetracarboxylate, and benzenepenta- and hexacarboxylates. Solutions containing these compounds and S<sub>2</sub>O<sub>8</sub><sup>2-</sup> at pH 7–10 were photolyzed and new ESR spectra characterized by relatively low  $g$  factors were found. With phthalate only this set of lines with the parameters  $a^H$  (1) = 18.11, 7.85, 5.87, and

1.71 G,  $g = 2.00240$  was present, while in the other cases a mixture of radicals occurred. The new spectra are ascribed to phenyl radicals formed by decarboxylation of the carboxylate ion by SO<sub>4</sub><sup>-</sup>, (eq 1). The magnetic parameters are



similar to those reported by Kasai et al.<sup>4</sup> for phenyl radical itself in an argon matrix ( $a_o = 17.4$ ,  $a_m = 5.9$ ,  $a_p = 1.9$  G,  $g = 2.0023$ ) with the low  $g$  factor reflecting the  $\sigma$  nature of the radical. As was mentioned in the Introduction, such a decarboxylation reaction has been demonstrated indirectly in the case of benzoate by observation of the phenyl adduct to  $\dot{\text{C}}\text{H}_2=\text{NO}_2^-$ .<sup>11</sup> Phenyl radicals were also successfully produced in photolytic experiments with 1,2,3- and 1,2,4-benzenetricarboxylates, 1,2,3,4-, 1,2,3,5-, and 1,2,4,5-benzenetetracarboxylates, benzenepentacarboxylate, and benzenehexacarboxylate. The spectrum obtained with benzenepentacarboxylate is shown in Figure 1. ESR parameters for all phenyl radicals observed are summarized in Table I where they are also assigned an identifying Roman numeral. Further discussion of the magnitudes of the hyperfine constants is given in a later section. From the fact that no changes in the spectra assigned to phenyl radicals with carboxyl substituents occurred to pH 10 we assume the acid protons are dissociated as shown.

In each case the observed radicals can be identified as resulting from decarboxylation of the parent carboxylate. The proton hyperfine constants are assignable to specific positions by comparison with those for the unsubstituted radical. Thus in the case of phthalate (radical IV) there is one ortho proton, two meta protons, and one para proton. The 18.11- and 1.71-G splittings are correspondingly as-

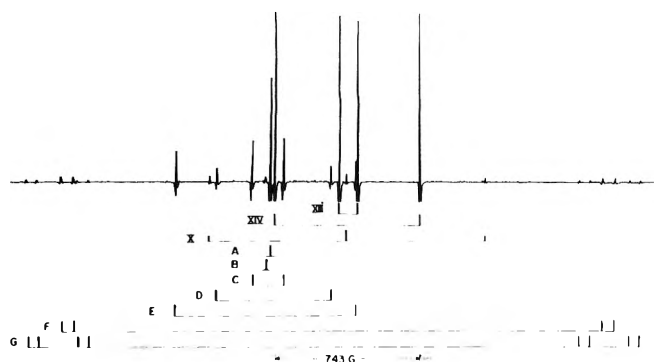


**Figure 1.** Second-derivative ESR spectrum obtained upon photolysis of a solution of 5 mM benzenepentacarboxylic acid and 70 mM  $\text{Na}_2\text{S}_2\text{O}_8$  at pH 6.7 (phosphate buffer). The main intensity is from the phenyl radicals XIII and XIV formed by loss of an "internal" carboxyl group. Weak lines are observed from phenyl radical X which is produced in secondary reactions. Spectrum A is attributed to the pentacarboxyphenoxy radical and spectra C, D, and E to tetracarboxyphenoxy radicals with single ring protons in the meta, ortho, and para positions, respectively. Spectrum B may come from the ortho or para tetracarboxybenzosemiquinone ion. Spectra F and G are hydroxycyclohexadienyl radicals formed by OH addition to the unsubstituted position in benzenepentacarboxylate and 1,2,3,5-benzenetetracarboxylate.

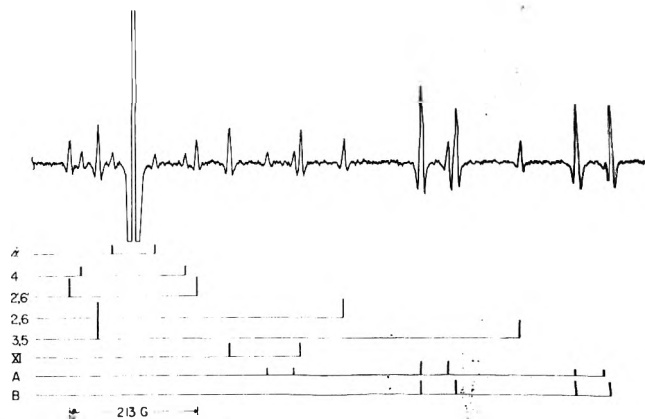


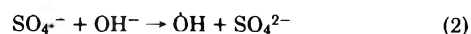
**Figure 2.** A portion, recorded at high gain, of the spectrum obtained upon photolysis of a solution of 2 mM 1,2,3,5-benzenetetracarboxylate and 60 mM  $\text{Na}_2\text{S}_2\text{O}_8$  at pH 7.3. The off-scale peak is the high-field line of the 7.10-G triplet of 2,4,6-tricarboxyphenyl radical. Lines corresponding to radicals containing  $^{13}\text{C}$  are labeled with the position of that atom according to the scheme used in Table II. (The primes represent the carboxyl carbons.) Weak lines of phenyl radical XI formed by loss of a carboxyl group at the 1 or 3 positions are also observed as are lines from the hydroxycyclohexadienyl radicals produced by OH addition to the tetracarboxylate (B) and to trimesate (A).

signed to the ortho and para protons while the 7.85- and 5.87-G values must belong to the meta protons. In a number of other cases more than one radical can be produced but the pattern of splittings allows identification. With 1,2,3-benzenetricarboxylate two radicals are possible but only VI produced by loss of the central carboxyl group is found. Similarly the two radicals XIII and XIV resulting from the loss of an internal carboxyl group from benzenepentacarboxylate were found with no trace of the third radical which would result from loss adjacent to the unsubstituted position. With 1,2,3,5-benzenetetracarboxylate the main intensity is from radical X caused by loss of the carboxyl group at position 2 and only weak lines of radical XI formed by loss at positions 1 or 3 occur at  $\sim 1\%$  of the intensity of those of the previous radical (see Figure 2). No evidence was found for loss of the carboxyl group at the 5 position. Again loss of a central carboxyl group is preferred. (With 1,2,4-benzenetricarboxylate only the phenyl radicals produced by loss of carboxyl groups at positions 1 (VIII) or 2 (VII) are observed but loss at the 4 position also occurs and leads to an adduct to another molecule as will be discussed in the next section.) The high degree of selectivity for loss of a particular carboxyl group can be interpreted as demonstrating oxidation by  $\text{SO}_4^{\cdot-}$  of the molecule as a whole followed by loss of the most labile  $\text{CO}_2$  group rather than attack of  $\text{SO}_4^{\cdot-}$  at a particular site.

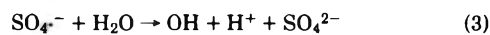
No lines attributable to phenyl radicals were found for benzoate, isophthalate, terephthalate, and trimesate. In the latter two cases, spectra of radicals identifiable as of the cyclohexadienyl type as reported by Norman et al.<sup>13</sup> were obtained. These spectra will be discussed in more detail in the next section. Similar radicals were detected for 1,2,4-benzenetricarboxylate in addition to the phenyl radicals VII and VIII. With benzoate and isophthalate only weak lines which could not be analyzed were detected.

The spectra obtained with all of the compounds yielding phenyl radicals (with the exception of phthalate) were complex to varying degrees in that lines from other types of radicals were also present. These complex spectra were analyzed by grouping together the lines with similar intensity

and a common spectral center and then looking for acceptable patterns of splitting. All of the spectra for which parameters are reported in the tables were identified by means of most, if not all, of the lines and are known with a high degree of certainty. The radicals responsible for the additional lines could be identified as of the hydroxycyclohexadienyl, phenoxy, and semiquinone ion types. The intensity of these spectra depended upon pH, flow rate, and reactant concentration becoming more intense at higher pH, lower flow rate, and lower concentration. Hydroxycyclohexadienyl radicals were identified by the  $\sim 30\text{-G}$  proton splitting by the CHOH ring proton and the parameters were checked against results of studies specifically of this type of radical.<sup>17,18</sup> These radicals can be formed at pH  $> 10$  as a result of the conversion of  $\text{SO}_4^{\cdot-}$  to OH by



with a rate constant of  $6.5 \times 10^7 \text{ M}^{-1} \text{ sec}^{-1}$ .<sup>19</sup> At lower pH values (7–9), this reaction cannot be significant and some other mechanism must exist for producing hydroxycyclohexadienyl radicals. From the fact that the lines of these radicals are less intense at higher solute concentrations it seems likely that the reaction of  $\text{SO}_4^{\cdot-}$  with water (eq 3) is

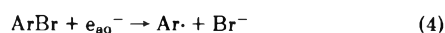


a source of OH which subsequently adds to the aromatic. The rate constant for this reaction has been reported to be  $10^3\text{--}10^4 \text{ sec}^{-1}$ <sup>19,20</sup> which is sufficiently fast to contribute. The phenoxy and semiquinone ion radicals are probably secondary products and were identified by the high  $g$  factors and by reference to the parameters reported for a number of such radicals<sup>21</sup> (some of which were also observed in this study).

The spectrum obtained with benzenepentacarboxylate and given in Figure 1 illustrates the large number of radicals possible. In addition to lines of the two main phenyl radicals there are lines from the phenyl radical X, two hydroxycyclohexadienyl types, from four radicals which can reasonably be identified as of the phenoxy type, and from one semiquinone ion. (See the figure caption for the identi-

fication.) At higher gain it was possible to observe lines from the  $^{13}\text{C}$  containing phenyl radicals (XIII, XIV) and weak lines of the phenyl radical XII and the OH adduct to 1,2,4,5-benzenetetracarboxylate. Exactly the same spectrum was observed from a sample of the pentacarboxylic acid which had been recrystallized and which showed no impurities in experiments<sup>18</sup> which allowed observation of the  $^{13}\text{C}$  containing OH adduct. The two minor phenyl radicals, two of the hydroxycyclohexadienyl radicals, and three of the phenoxyl radicals each appear to be produced from acids with one less carboxyl group than the starting compound. Somewhat similar behavior was found for benzenehexacarboxylate and 1,2,3,5-benzenetetracarboxylate. With the former compound both major phenyl radicals, the OH adduct, and the phenoxyl radical produced from the pentacarboxylate were observed as well as three phenoxyl radicals with only four carboxyl groups. With the 1,2,3,5-tetracarboxylate the OH adduct to trimesate was observed (as shown in Figure 2) as was the 2,4,6-tricarboxyphenoxyl radical. These radicals formed from compounds with one carboxyl group less than the starting compound must originate in secondary processes and not from impurities. This argument is supported by the fact that the radicals of concern are more prominent at lower flow rates. From the appearance of phenyl and hydroxycyclohexadienyl radicals as well as the phenoxyl radicals it is clear that there must be some source of the acids themselves. One possibility is that the bimolecular disappearance of at least the highly substituted phenyl radicals proceeds by an electronic disproportionation which yields a positive and negative ion and ultimately, after reaction with water, the corresponding substituted benzene and phenol.

A common feature of all of the phenyl radicals produced by reaction of  $\text{SO}_4^{\cdot-}$  is a carboxyl group ortho to the radical site. It is clear that such a structure must stabilize the radical against further reaction such as addition to another ring. If this conclusion is correct then the same radicals should be observable when produced by other routes such as the reaction of  $e_{\text{aq}}^-$  with phenyl bromides. This type of reaction does indeed occur and in radiolytic experiments (eq 4) with *o*-bromobenzoate, 2-bromoterephthalate, and



4-bromoisophthalate, the spectra of radicals IV, VII, and VIII were readily observed. Although no OH scavenger was employed in these experiments no other radicals were observed. Apparently adducts of OH to the bromo compounds did not give sufficient intensity to be detected. It is important to note that in each case the spectrum is identical with that obtained by  $\text{SO}_4^{\cdot-}$  reaction with the appropriate acid.

This same reaction also allowed observation of the unsubstituted phenyl radical from bromobenzene as well as the phenyl radicals II, III, and V from *p*-bromophenol, *m*-bromophenol, and *p*-bromobenzoate. In these three cases the concentration of the aromatic compound was kept low to prevent addition of the phenyl radical to a second molecule. The optimum concentration of the halide was about  $5 \times 10^{-4} \text{ M}$  with both higher and lower concentrations giving less signal. Such a low concentration can be used because of the high rate constant for reaction with  $e_{\text{aq}}^-$ . The presence of up to 10 mM *tert*-butyl alcohol as an OH scavenger had little effect on signal intensity although 50 mM decreased the signals by about a factor of 2. Apparently, at this concentration the reaction of the phenyl radical with *tert*-

butyl alcohol becomes important. The spectra of these radicals showed a strong intensity anomaly as the result of CIDEP<sup>22</sup> with the low-field lines weak and inverted. This fact shows that a major disappearance pathway under these conditions is by radical-radical reaction.

The intensity of the spectra of the phenyl radicals increased markedly in going to the more highly substituted compounds as a result of slower radical-radical reactions for these multiply charged radicals as well as the simpler spectra. The intensity was so great with 1,2,3-benzenetricarboxylate, 1,2,3,5-benzenetetracarboxylate, and benzene-pentacarboxylate that lines from the naturally occurring  $^{13}\text{C}$  containing phenyl radicals could be observed. With the latter compound both phenyl radicals could be studied. In each case all of the possible  $^{13}\text{C}$  hyperfine constants could be determined. The values are given in Table II.

Figure 2 illustrates some of the lines for the  $^{13}\text{C}$  containing radicals in the case of 1,2,3,5-benzenetetracarboxylate. Shown here is the region around the high-field line of the 1:2:1 triplet for the  $^{12}\text{C}$  form. Both of the lines in the pairs split around the  $^{12}\text{C}$  line are evident for the three smallest  $^{13}\text{C}$  hyperfine constants (0.73, 1.77, and 2.13 G). The peak heights are, starting with the smallest splitting, 0.5, 0.5, and 1% of that of the  $^{12}\text{C}$  radical. Only the high-field satellite is evident for the radicals with the 7.08- and 13.06-G constants but in the latter case the high-field satellite of the central line of the 1:2:1 triplet is also in the portion shown. The lines for the radical with  $^{13}\text{C}$  at the radical site ( $a^{\text{C}} = 137.1 \text{ G}$ ) are far away and are not shown. Also evident in this figure are lines from radical XI formed by loss of a carboxyl group from the 1 or 3 position and OH adducts to 1,2,3,5-benzenetetracarboxylate (A) and to trimesate (B).

Assignment of the hyperfine constants of the ring carbons was made by reference to the INDO calculations<sup>23</sup> (see Table II). In each radical a large splitting of  $\sim 135 \text{ G}$  occurs which is assigned to the carbon atom at the radical site. The relative intensities of the other lines with the various  $^{13}\text{C}$  splittings (0.5% of the  $^{12}\text{C}$  species for one carbon atom per radical or 1% for two equivalent atoms) together with the pattern which occurs upon changing the position of the carboxyl groups allows all of the other values to be assigned with reasonable certainty. The splittings assigned to ortho, meta, and para positions remain quite constant for the four radicals as is found for the proton splittings. A similar behavior is found for the splittings assigned to the carboxyl carbons and the assignment is quite certain except in the case of radical XIV where it is possible that the 1.58- and 2.10-G splittings could be reversed. The existence of  $\sim 0.7\text{-G}$  splittings only for radicals X and XIV assures that this value belongs to the para carboxyl carbon.

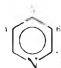
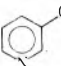
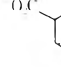
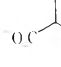
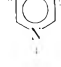
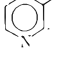
Similar reactions could be carried out with several pyridine and pyrazine derivatives. Thus the 2-pyridyl radical (XVI, see Table III) could be produced from 2-bromopyridine and the radicals XVII-XXI could be produced from the appropriate carboxylic acids. As with the benzenecarboxylic acids there occurred lines of other radicals in some of these spectra which could be assigned to OH adducts (by means of the large proton splitting at the attachment site) and phenoxyl or semiquinone ion radicals (by means of high *g* factors and small splittings). The proton hyperfine constants of XVI-XIX were assigned to the specific positions by noting the effects of changing the position of substitution. Those of XX and XXI could be assigned by reference to the phenyl and 2-pyridyl radicals, respectively.

TABLE II:  $^{13}\text{C}$  Hyperfine Constants for Phenyl Radicals<sup>a</sup>

Radical	Carboxyl position	Hyperfine constants <sup>b</sup>						
		1	2,6	3,5	4	2',6'	3',5'	4'
VI	2, 6	135.31	7.42 (2)	12.56 (2)	1.27	1.57 (2)		
X	2, 4, 6	137.15	7.08 (2)	13.06 (2)	1.77	2.13 (2)		0.73
XIII	2, 3, 5, 6	132.93	7.64 (2)	12.78 (2)	1.54	1.42 (2)	4.42 (2)	
XIV	2, 3, 4, 6	135.55	7.76	12.88	1.58	2.90	4.06	0.70
			6.94	12.28		2.10		
I (INDO) <sup>c</sup>	None	151.3	-4.8	10.7	-2.6			

<sup>a</sup> Values in gauss. The number of nuclei displaying the splitting are given in parentheses if different than one. <sup>b</sup> Unprimed positions are numbered as in Table I (see footnote *b*). Primed numbers refer to the carboxyl carbon at the corresponding position. <sup>c</sup> Values calculated by the INDO method as given by Pople et al.<sup>23</sup>

TABLE III: ESR Parameters of Pyridyl and Pyrazyl Radicals<sup>a</sup>

Radical	Method <sup>b</sup>	$a^{\text{N}}$	$a_3^{\text{H}}$	$a_1^{\text{H}}$	$a_5^{\text{H}}$	$a_6^{\text{H}}$	$g$
XVI 	$e_{\text{aq}}^-$	26.95	1.28	4.12	8.56	4.99	2.00202
XVII 	$\text{SO}_4^-$	27.73	1.56	3.70	9.68		2.00219
XVIII 	$\text{SO}_4^-$	27.58	1.48		8.08	4.84	2.00207
XIX 	$\text{SO}_4^-$	28.84		4.09	8.24	4.43	2.00206
XX 	$\text{SO}_4^-$	0.95	9.99 <sup>c</sup>		8.16 <sup>c</sup>	18.94	2.00245
XXI 	$\text{SO}_4^-$	28.38 (o) 0.27 (m)	2.39	7.32			2.00232

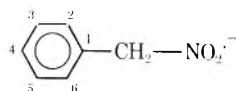
<sup>a</sup> Hyperfine constants in gauss, see footnote *a*, Table I. <sup>b</sup> See footnote *c*, Table I. <sup>c</sup> These values were assumed to show the same asymmetry as is apparent for some of the phenyl radicals in Table I.

Decarboxylation could potentially occur at two sites in the cases of 2,3-, 2,5-, and 3,4-pyridinedicarboxylates but only the product radicals XVII, XVIII, and XX, respectively, were observed. Thus no spectrum of a 3-pyridyl radical was obtained. With 3,5-pyridinedicarboxylate a 3-pyridyl radical was formed but added to another molecule to form an adduct such as that observed with terephthalate. (This radical will be discussed in the next section.)

*Indirect Detection of Phenyl Radicals.* The observation of decarboxylation in the many cases discussed in the previous section suggests that this reaction occurs generally with all benzene carboxylates. In support of this idea, Gilbert et al.<sup>11</sup> have already observed such a reaction with benzoate by use of nitromethane trapping. Further experiments of this type were carried out here. The spectrum obtained with phthalate and nitromethane and showing lines of the adduct of *o*-carboxyphenyl to nitromethane (radical XXVI) is illustrated in Figure 3. The results are summarized in Table IV. Phenyl radicals were prepared either by reaction of  $\text{SO}_4^-$  with a carboxylate or  $e_{\text{aq}}^-$  with a bromide. In several instances both methods were used to prepare a given phenyl radical and the same adduct was found. Several cases are included in which the phenyl radical has been detected directly as described in the previous section.

These various arguments together with the observation that the parameters of the adducts are all quite similar establish the radicals in Table IV very clearly as adducts of phenyl type radicals. In most cases, the lines of the adducts were wider than is usually encountered with simpler adducts suggesting unresolved hyperfine structure. The parameters for the phenyl adduct (XXII) agree with those reported by Gilbert et al.<sup>11</sup>

Lines from three other adducts are evident in Figure 3. Two of these spectra, A and C, are known to arise from the attack of  $\text{SO}_4^-$  on nitromethane. Spectrum A is that of the dinitroethane radical anion produced by trapping of  $\dot{\text{C}}\text{H}_2\text{NO}_2$ <sup>24,25</sup> and spectrum C with the parameters  $a^{\text{N}} = 23.62$ ,  $a^{\text{H}} = 7.15$  G, and  $g = 2.00504$  is that assigned to the  $\text{SO}_4^-$  adduct to nitromethane.<sup>26</sup> Spectrum B with the approximate parameters  $a^{\text{N}} = 23.7$ ,  $a^{\text{H}} = 7.3$ , and  $g = 2.0051$  seems to belong to a radical analogous to that observed by Gilbert et al.<sup>11</sup> and identified by them as the adduct of  $\text{C}_6\text{H}_5\text{CO}_2$ . Adducts with similar parameters were also found in experiments with benzoate and terephthalate. The parameters for these adducts, which are similar to those of the  $\text{SO}_4^-$  adduct in having a small nitrogen splitting of about 23.5 G, cannot be determined accurately in our spectra because of overlap of those lines with other lines in the

TABLE IV: ESR Parameters of Phenyl Radical Adducts to  $\text{CH}_2=\text{NO}_2^-$ <sup>a</sup>

Radical	Substituent on phenyl	Position	Method <sup>b,c</sup>	$a^N$	$a^H(\text{CH}_2)$	$g$
XXII	None		$e_{aq}^-$ , $\text{SO}_4^-$	25.87	9.38	2.00494
XXIII	$\text{O}^-$	2	$e_{aq}^-$	25.65	10.34	2.00501
XXIV	$\text{O}^-$	3	$e_{aq}^-$	25.67	9.47	2.00494
XXV	$\text{O}^-$	4	$e_{aq}^-$	26.10	9.60	2.00497
XXVI	$\text{CO}_2^-$	2	$e_{aq}^-$ , $\text{SO}_4^-$	25.68	9.97	2.00498
XXVII	$\text{CO}_2^-$	3	$\text{SO}_4^-$	25.91	9.42	2.00495
XXVIII	$\text{CO}_2^-$	4	$e_{aq}^-$ , $\text{SO}_4^-$	25.87	9.28	2.00497
XXIX	$\text{CO}_2^-$	3, 5	$\text{SO}_4^-$	25.94	9.73	2.00495
XXX	$\text{CH}_2-\text{NO}_2^-$		$e_{aq}^-$ , $\text{SO}_4^-$	25.81	9.93	2.00496

<sup>a</sup> Hyperfine constants in gauss, see footnote a, Table I. <sup>b</sup> Method of production of the phenyl or pyridyl radical, see footnote c, Table I. <sup>c</sup> For radiolysis experiments starting with  $e_{aq}^-$  the solutions contained 1 mM each of the bromide and nitromethane at pH 11. For photolysis experiments with  $\text{SO}_4^-$  the solutions contained 3 mM of the carboxylate, 3 mM of nitromethane, and 70 mM  $\text{Na}_2\text{S}_2\text{O}_8$  at pH 9–10.5.

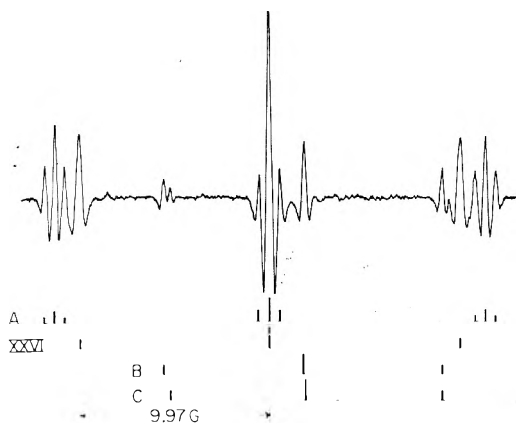


Figure 3. The low-field third of the ESR spectrum produced by photolysis of a solution containing 3 mM phthalate, 3 mM  $\text{CH}_3\text{NO}_2$ , and 70 mM  $\text{Na}_2\text{S}_2\text{O}_8$  at pH 10.5 and showing lines of the adduct of *o*-carboxyphenyl radical to  $\text{CH}_2=\text{NO}_2^-$  (XXVI). Other lines are from the adducts of  $\cdot\text{CH}_2\text{NO}_2$  (spectrum A),  $\text{SO}_4^-$  (C), and what is believed to be *o*- $\text{C}_6\text{H}_4(\text{CO}_2^-)\text{CO}_2^-$  (B).

spectra. We agree that these adducts are probably formed from radicals of the type  $\text{C}_6\text{H}_5\text{CO}_2^-$ .

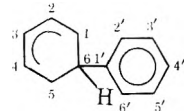
The data of Table IV show that phenyl radicals are produced from terephthalate, isophthalate, and trimesate even though those radicals could not be observed directly. An experiment to reexamine the reactions of  $\text{SO}_4^-$  with terephthalate and trimesate gave spectra typical of cyclohexadienyl radicals which matched those reported by Norman et al.<sup>13</sup> except that small triplet splittings (not previously reported) of 0.29 and 0.05 G, respectively, were found. In these cases the radicals cannot be  $\text{SO}_4^-$  adducts because all protons are accounted for without considering the small triplets. It is clear now that these radicals must be the adducts of *p*-carboxy- and 3,5-dicarboxyphenyl radicals to a parent molecule. Further proof of this idea is provided by experiments using mixtures with two different carboxylates. A photolysis experiment with 3 mM terephthalate and 1 mM trimesate showed clearly the presence of the four possible radicals produced by addition of the two phe-

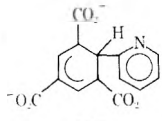
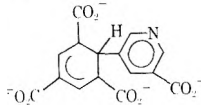
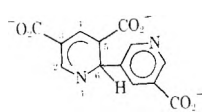
nyl types to the two starting compounds (i.e., radicals XXXIV, XXXIII, and XXXV in Table V and the adduct of 3,5-dicarboxyphenyl to terephthalate). Considerable spectral overlap occurs because adducts to the same carboxylate ion produce similar spectra and so it was not possible to get a complete analysis of this spectrum. Only the parameters of radical XXXIII could be accurately determined from this spectrum while those of XXXIV and XXXV are known from experiments on terephthalate and trimesate alone. No parameters for the fourth radical (with the weakest spectrum) were determined. Parameters for some other adducts of this type are shown in Table V. Experiments in which radicals were added to trimesate gave the best intensity. The radicals XXXVIII and XXXIX show that radicals of the 2- and 3-pyridyl type (produced from the appropriate bromides) also add to trimesate. Radical XL obtained in experiments with  $\text{SO}_4^-$  and 3,5-pyridinedicarboxylate shows that a radical of the 3-pyridyl type can be produced in this way but that it is reactive toward addition so only the adduct is observed.

The parameters for phenyl radical adducts in Table V are very similar to those reported by Beckwith and Norman<sup>10</sup> who formed the initial phenyl radicals by reducing diazonium ions. In the one case where the same radical is reported (XXXIII) in both studies the parameters agree within experimental error (including the 0.29-G triplet). As mentioned above the parameters for radicals XXXV and XXXIV (see in Table V) formed in solutions of terephthalate and trimesate, respectively, agree (except for the smallest splittings) with those assigned by Norman et al.<sup>13</sup> to  $\text{SO}_4^-$  adducts. On the basis of the present work there is no evidence in any case for formation of an  $\text{SO}_4^-$  adduct.

The origin of the  $\sim 0.3$ -G splitting in phenyl adducts is demonstrated very clearly by the portions of spectra shown in Figure 4. Here phenyl radicals with zero, one, and two meta protons formed by decarboxylation of trimesate, isophthalate, and benzoate, respectively, have added to trimesate to produce radicals XXXIV, XXXII, and XXXI with a singlet (at this level of resolution) and doublet and triplet splittings of about 0.3 G. This result illustrates very graphically that the meta protons are responsible for this split-

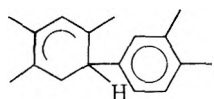


TABLE V: ESR Parameters of Phenyl Radical Adducts to Aromatic Acids<sup>a,b</sup>


Radical	Substituent	Position	$a_2^H$	$a_3^H$	$a_4^H$	$a_5^H$	$a_6^H$	$a_{2',6'}^H$	$a_{3',5'}^H$	$g$
XXXI	CO <sub>2</sub> <sup>-</sup>	1, 3, 5	2.52		2.52		31.52		0.29(2)	2.00317
XXXII	CO <sub>2</sub> <sup>-</sup>	1, 3, 5, 3'	2.52		2.52		31.78		0.28	2.00317
XXXIII <sup>c</sup>	CO <sub>2</sub> <sup>-</sup>	1, 3, 5, 4'	2.52		2.52		31.66		0.29(2)	2.00318
XXXIV <sup>d</sup>	CO <sub>2</sub> <sup>-</sup>	1, 3, 5, 3', 5'	2.52		2.52		31.95	0.05(2)		2.00317
XXXV <sup>e</sup>	CO <sub>2</sub> <sup>-</sup>	1, 4, 4'	2.86	12.49		7.88	37.01		0.29(2)	2.00277
XXXVI	CO <sub>2</sub> <sup>-</sup>	1, 3, 3'	2.67 <sup>f</sup>		2.20 <sup>f</sup>	7.78	36.80		0.28	2.00305
XXXVII <sup>g</sup>	CO <sub>2</sub> <sup>-</sup> ; OH	1, 3, 5; 3'	2.52		2.52		31.23		0.34	2.00319
XXXVIII <sup>h</sup>			2.47		2.47		34.17			2.00311
XXXIX <sup>h</sup>			2.48		2.48		31.83			2.00312
XL			1.39 <sup>f</sup>		2.82 <sup>f</sup>		37.37	$a_1^N = 4.06$		2.00349

<sup>a</sup> Hyperfine constants in gauss. see footnote a, Table I. <sup>b</sup> Except where noted phenyl radicals were produced in photolytic experiments from SO<sub>4</sub><sup>-</sup>. Typical solutions contained 1–5 mM of the acid or acids and 30–70 mM Na<sub>2</sub>S<sub>2</sub>O<sub>8</sub> at pH 7–9. <sup>c</sup> Hyperfine constants reported for this radical by Beckwith and Norman<sup>10</sup> are 32.0, 2.55(2), and 0.25(2) G. They prepared the initial phenyl radical by reduction of the diazonium ion. <sup>d</sup> Hyperfine constants reported by Norman et al.<sup>13</sup> are 31.8 and 2.55(2) G. The initial phenyl radical was prepared by reaction of trimesate with SO<sub>4</sub><sup>-</sup> as was done here but the final radical was incorrectly identified as the SO<sub>4</sub><sup>-</sup> adduct to trimesate. <sup>e</sup> Hyperfine constants reported by Norman et al.<sup>13</sup> are 36.8, 12.5, 7.9, 2.8 G. The 0.29(2) G splitting was not resolved and the radical was incorrectly identified as the SO<sub>4</sub><sup>-</sup> adduct to terephthalate. <sup>f</sup> These two proton splittings were assigned to specific positions under the assumption that the asymmetry is similar to that found in hydroxycyclohexadienyl radicals.<sup>18</sup> The alternative assignment with these two values interchanged is possible. <sup>g</sup> The *p*-hydroxyphenyl radical was produced at pH 9 by reaction of e<sub>aq</sub><sup>-</sup> with *p*-bromophenol. <sup>h</sup> Pyridyl radicals were produced by reaction of e<sub>aq</sub><sup>-</sup> with the appropriate bromides at pH 11.7.

ting. The further very small triplet splitting of 0.05 G in the case of radical XXXIV, where no meta protons are present, shows the magnitude of the splitting by ortho protons. All of the radicals in Table V follow this rule for the 0.3-G splitting with the exception of XXXVIII for which this splitting could not be resolved. (The lines were correspondingly broad, however.) With 1,2,4-benzenetricarboxylate a spectrum of eight line groups corresponding to an adduct (or adducts) at the 5 position was observed in addition to the two phenyl radicals VII and VIII. Based on the reactivity observed for phenyl radicals with no ortho carboxyl group it is expected that decarboxylation at the 4 position will produce a radical which can add to another molecule. This adduct is presumed to be



Addition at the 5 position is shown by the presence of an ortho (8 G) and a meta (2.5 G) splitting in the adduct. The eight line groups are complex but can be interpreted as arising from two radicals with common major parameters of  $a^H = 37.58$ ,  $a^H = 7.30$ ,  $a^H = 2.80$  G, and  $g = 2.00302$  but with two small additional splittings each of 0.21 and 0.15 and 0.46 and 0.20 G. The radical with splittings of 0.21 and 0.15 G is present at roughly three times the intensity of the other form. The presence of other unidentified weak lines

caused the eight line groups to be somewhat dissimilar in appearance. To explain the existence of two very similar radicals it is necessary to invoke two isomers with restricted rotation about the bond between the two rings. Such behavior has been proposed previously by Beckwith and Norman<sup>10</sup> for the *o*-chlorophenyl adduct to trimesate but in that case a large difference in the methylene splitting of the two isomers was observed contrary to the present example. The small splittings in our spectrum are different than the rather uniform value of ~0.3 G assigned to the meta protons in Table V and if the radical structure is indeed as suggested then it must be concluded that the ortho splittings in the secondary ring can be as large as 0.15–0.20 G in certain instances.

#### Discussion of the Hyperfine Constants

The proton hyperfine constants found here for phenyl radical agree very well with those reported by Kasai et al.<sup>4</sup> for the radical in an argon matrix. The values also agree with those calculated by the INDO method<sup>23</sup> for the  $\sigma$  structure ( $a_o = 18.7$ ,  $a_m = 6.1$ ,  $a_p = 3.9$  G) with the calculated value for  $a_p$  about twice that observed. The assignment to specific positions is completely supported by the pattern of splittings for the various substituted radicals in Table I. In each case the splittings of the remaining protons are similar to those in the unsubstituted radical. The largest deviations are for radical II in which the presence of

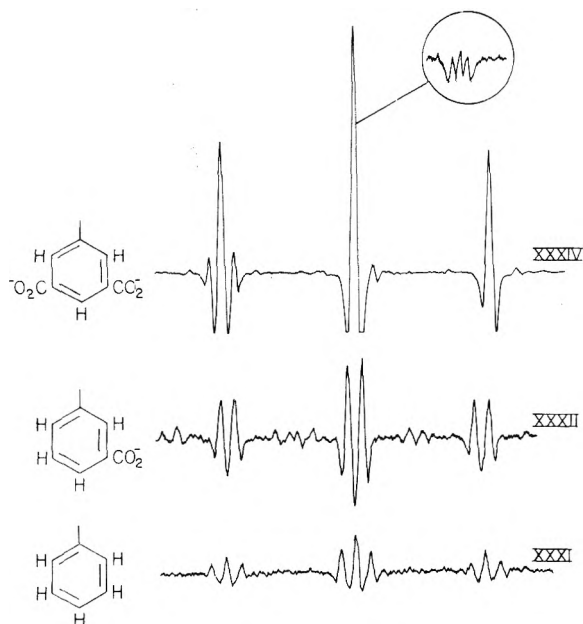


**Figure 4.** The high-field halves of the ESR spectra of the cyclohexadienyl-type radicals produced by trapping several phenyl radicals with trimesate. The three radicals trapped are given on the left and were obtained in experiments with trimesate itself and in mixtures with isophthalate and benzoate. In each case the major structure of the spectrum is the same with one large doublet splitting of  $\sim 32$  G and a triplet of 2.52 G both from the protons on the cyclohexadienyl ring. The structure on the next finer scale of (from top to bottom) singlet, doublet, and triplet clearly is caused by the meta protons in the added radicals (illustrated). At higher resolution (lower microwave power and modulation amplitude) the lines obtained with trimesate itself appear as 0.05-G triplets as shown above the upper trace. This further splitting must come from the ortho protons.

the meta  $O^-$  group introduces asymmetry into the ortho splittings and raises the value of  $a^m$  to 9.12 G. A similar asymmetry is seen for radical IV and it is possible to conclude by comparison of the values for IV, V, VI, and VII, for example, that the presence of an ortho carboxyl group raises the splitting by the meta proton on the same side of the ring to about 7.5 G. The splitting by the meta proton on the other side of the ring is affected very little.

The  $g$  factors of the radicals in Table I vary in a systematic fashion. A comparison of the values shows that carboxyl groups in ortho, meta, and para positions change the value by +13, -2, and -3 units in the fifth decimal place, respectively, and that the effects are additive. The root mean square of the deviations between the measured values and those calculated using these increments and a value of 2.00227 (as observed) for the unsubstituted radical is 1.1 units in the fifth decimal place. Because of the  $\sigma$  character of the radical, which localizes the unpaired electron at the radical site, only a carboxyl group near the radical site (ortho position) can participate significantly in the singly occupied orbital and thereby shift the  $g$  factor.

The  $^{13}C$  hyperfine constants in Table II were assigned to specific ring positions by reference to the INDO calculations of Pople et al.<sup>23</sup> for unsubstituted phenyl radical (also included in the table for reference). The values for the carboxyl carbons were assigned by means of the intensities and pattern of splittings obtained upon changing the position and number of substituent carboxyl groups. The largest splitting of  $\sim 135$  G is clearly that of the carbon at the radical site and the large magnitude demonstrates the  $\sigma$  na-

ture of phenyl radical (i.e., that a direct carbon 2s contribution to the singly occupied orbital is present to the extent of about 12%). The values found here agree with those determined for phenyl radical itself as prepared in the solid on silica gel (about 140 G)<sup>5</sup> and by a deposition method in solid benzene (129 G)<sup>6</sup> thus confirming the interpretation of those solid state spectra in terms of the large  $^{13}C$  hyperfine constant. The splittings of 7 and 13 G found here for two carbons each correspond well with the ortho and meta values predicted by calculation. The para values of 1.3–1.7 G are somewhat smaller than the predicted 4.8 G. Unfortunately INDO calculations give little help with a "mechanistic" interpretation of the origin of these latter  $^{13}C$  interactions and so cannot supply much insight into why the magnitudes of the  $^{13}C$  splittings at ortho and meta positions are reversed from the proton splittings. Because of the  $\sigma$  nature of the radicals it is difficult to anticipate the size of the splittings by the carboxyl carbons but values smaller than those of the carbons to which the carboxyl groups are attached seem likely. The values found conform to this idea and the relative magnitudes for the carboxyl carbons parallel in rough fashion the values for the corresponding ring carbons.

Both Bower et al.<sup>7</sup> and Kasai and McLeod<sup>8,9</sup> have discussed the structure of 2-pyridyl radical and Bower et al.<sup>7</sup> have reported from studies on a frozen system observation of a 170-G  $^{13}C$  splitting which establishes this radical as of the  $\sigma$  type. The large value of the nitrogen splitting ( $\sim 27$  G) was observed in all studies but the proton hyperfine constants were not known before the present work because of the limited resolution available in the solid state studies.<sup>6-9</sup> The INDO calculations in this case are not very helpful because they predict three proton splittings of comparable magnitude. Fortunately the pattern of splittings in Table III allows assignment to the various positions on the assumption that the position of the carboxyl group has little effect on the remaining splittings (as was observed for the phenyl radicals). The pattern of proton splittings is very different than that found with the phenyl radicals.

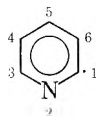
INDO calculations on 2-pyridyl radical were carried out for two geometries; calculated hyperfine constants are given in Table VI. The first (geometry A) used standard bond lengths<sup>23</sup> but ignored the difference between C–C and C–N bonds (i.e., a regular hexagon of bond length 1.40 Å) while the second (geometry B) used the geometry of pyridine following Kasai and McLeod.<sup>9</sup> The results are quite similar except for smallest proton splitting,  $a_3^H$ , which changes sign. The nitrogen splitting (17 G) is not in particularly good agreement with the observed 27 G. The results given by Kasai and McLeod<sup>9</sup> which show a calculated 29-G value were obtained by using the INDO 2s spin density and the theoretical value of splitting for 100% 2s spin density. Although good agreement with observation is obtained, this procedure is questionable and use of the empirical parameter from the original INDO study should logically be preferred.

The origin of the very large nitrogen splitting for 2-pyridyl radical has been, in part, attributed<sup>7</sup> to an in-plane  $\pi$  bond (involving the nitrogen lone-pair electrons) between the radical carbon and the nitrogen. We wish to point out that the spin densities given by the INDO calculation do not support such an effect. In particular one would expect large spin densities in the nitrogen in-plane p orbitals while the calculation for geometry A gives values of 0.011 and  $-0.003$  for the orbitals along the 1–4 direction and at right

**TABLE VI: Results of INDO Calculations on 2-Pyridyl Radical<sup>a-c</sup>**

	$a_2^N$	$a_3^H$	$a_4^H$	$a_5^H$	$a_6^H$
Geometry A <sup>c</sup>	17.67	-0.61	6.73	8.49	7.26
Geometry B <sup>d</sup>	18.66	0.35	5.64	9.51	7.70
Experimental	26.95	1.28	4.12	8.56	4.99

<sup>a</sup> Positions numbered as



<sup>b</sup> Values in gauss. <sup>c</sup> Ring structure taken as a regular hexagon with all bond lengths 1.40 Å with CH bond length 1.08 Å. <sup>d</sup> Following Kasai and McLeod<sup>9</sup> this structure was taken as for pyridine (*J. Rastrop-Anderson, J. Mol. Spectrosc.*, 2, 361 (1958)) with CH bond lengths 1.08 Å.

angles, respectively, while the 2s density is 0.047 (geometry B is similar). Thus a direct mixing of the nitrogen 2s orbital is mainly predicted. It should be pointed out in addition, however, that the small spin densities in the nitrogen p orbitals predicted by the INDO calculations probably cannot explain the relatively large anisotropy found for the <sup>14</sup>N hyperfine interaction in both solid phase studies.<sup>6,7</sup> Further study of this point is in order.

The one example of a 4-pyridyl radical (XX) has hyperfine constants similar to those of the phenyl radicals as might be expected and the assignment was made accordingly. The nitrogen splitting of 0.95 G can be compared with the para <sup>13</sup>C splitting for phenyl radical VIII. It is usually found that <sup>13</sup>C hyperfine constants are about twice those of <sup>14</sup>N in a similar position.<sup>27</sup> Thus a value of around 2 is expected for the para carbon in a phenyl radical. The observed values are 1.3–1.8 G.

## Summary

The present work provides, for the first time, solution spectra of phenyl and 2-pyridyl radicals and has allowed accurate measurement of the hyperfine constants. In the case of 2-pyridyl radical the proton splittings were not previously well known. It has also proved possible to determine the <sup>13</sup>C hyperfine constants for four substituted phenyl radicals. The observation of a very large (~135 G) splitting by <sup>13</sup>C at the radical site in these radicals has substantiated the  $\sigma$  nature of phenyl radical. The values of the  $g$  factors for both phenyl and 2-pyridyl radicals are below the free electron value as commonly observed for  $\sigma$  radicals. The other ring <sup>13</sup>C hyperfine constants ( $a_o \sim 7.5$ ,  $a_m \sim 13$ ,  $a_p \sim 1.5$  G) are in approximate agreement with those predicted by INDO calculations. Hyperfine constants were also determined for <sup>13</sup>C in the substituent carboxyl groups.

The observation of phenyl and 2-pyridyl radicals demonstrates in a direct way their formation in the two types of reaction used, namely, the decarboxylation of aromatic carboxylate ions by SO<sub>4</sub><sup>-</sup> and the dissociative attachment of e<sub>aq</sub><sup>-</sup> to aromatic bromides. The radicals with no ortho substituents are very reactive toward addition to another aromatic ring and are best studied at starting material concentrations of <1 mM. Such low concentrations can readily be used with the bromides because of the high rate constant for reaction with e<sub>aq</sub><sup>-</sup>. The unsubstituted phenyl radical, for example, was produced in this way from  $5 \times 10^{-4}$  M

bromobenzene. At higher concentrations of starting material (1–10 mM), such as used in the decarboxylation reactions, only the secondary adduct to another ring (a radical of the cyclohexadienyl type) is detected as with terephthalate or trimesate. This reaction, in part, explains the failure of Beckwith and Norman<sup>10</sup> to directly observe phenyl radicals. When the radical has at least one ortho carboxyl group the secondary addition reaction is much slower and the phenyl radical is observed in the presence of 10 mM or more of aromatic. With compounds such as 1,2,3-benzenetricarboxylate there is a very marked preference for loss of the central CO<sub>2</sub><sup>-</sup> upon reaction with SO<sub>4</sub><sup>-</sup>. A similar result is observed with 2,3-pyridinedicarboxylate in that loss at the 2 position is much more likely. In the case of 1,2,4-benzenetricarboxylate decarboxylation occurs at all three positions and direct observation of the two ortho-substituted phenyl radicals is possible while loss of the carboxyl group at the 4 position leads to a more reactive radical which adds to another molecule. The resulting adducts are observed.

NOTE ADDED IN PROOF: A. L. J. Beckwith, in a review paper [*Intra-Sci. Chem. Rep.*, 4, 127 (1970)], has given hyperfine constants for two ortho-substituted phenyl radicals but gives no other details.

## References and Notes

- (1) Supported in part by the U.S. Atomic Energy Commission.
- (2) V. A. Tolkachev, I. I. Chkheidze, and N. Ya. Buben, *Zh. Strukt. Khim.*, **3**, 709 (1962).
- (3) J. E. Bennett, B. Mile, and A. Thomas, *Chem. Commun.*, 265 (1965).
- (4) P. H. Kasai, E. Hedaya, and E. B. Whipple, *J. Am. Chem. Soc.*, **91**, 4364 (1969); P. H. Kasai, P. A. Clark, and E. B. Whipple, *ibid.*, **92**, 2640 (1970).
- (5) S. Nagai, S. Ohnishi, and I. Nitta, *J. Phys. Chem.*, **73**, 2438 (1969).
- (6) J. E. Bennett and B. Mile, *J. Phys. Chem.*, **75**, 3432 (1971).
- (7) H. J. Bower, J. A. McRae, and M. C. R. Symons, *Chem. Commun.*, 542 (1967); *J. Chem. Soc. A*, 2696 (1968).
- (8) P. H. Kasai and D. McLeod, Jr., *J. Am. Chem. Soc.*, **92**, 6085 (1970).
- (9) P. H. Kasai and D. McLeod, Jr., *J. Am. Chem. Soc.*, **94**, 720 (1972).
- (10) A. L. J. Beckwith and R. O. C. Norman, *J. Chem. Soc. B*, 403 (1969).
- (11) B. C. Gilbert, J. P. Larkin, and R. O. C. Norman, *J. Chem. Soc., Perkin Trans. 2*, 1272 (1972).
- (12) See, for example, G. E. Adams in "Advances in Radiation Chemistry", Vol. 3, M. Burton and J. Magee, Ed., Wiley-Interscience, New York, N.Y., 1972, p 125.
- (13) R. O. C. Norman, P. M. Storey, and P. R. West, *J. Chem. Soc. B*, 1087 (1970).
- (14) K. Eiben and R. W. Fessenden, *J. Phys. Chem.*, **75**, 1186 (1971).
- (15) D. Behar and R. W. Fessenden, *J. Phys. Chem.*, **75**, 2752 (1971).
- (16) The 1,2,3,4- and 1,2,3,5-benzenetetracarboxylic acids were prepared by the permanganate oxidation of 1,2,3,4-tetramethylbenzene and 2,4,6-trimethylbenzoic acid, respectively. The resulting samples were recrystallized from water and showed elementary analyses in accord with their empirical formulae. Studies of the OH adducts to samples of these compounds (see ref 18) showed no evidence of other polycarboxylic acids under a sensitivity sufficient to give the lines of the <sup>13</sup>C containing radicals derived from the stated compound.
- (17) G. Filby and K. G. Günther, *J. Phys. Chem.*, **78**, 1521 (1974).
- (18) K. Eiben and R. H. Schuler, *J. Chem. Phys.*, **62**, 3093 (1975).
- (19) E. Hayon, A. Treinin, and J. Wolf, *J. Am. Chem. Soc.*, **94**, 47 (1972).
- (20) D. E. Pennington and A. Haim, *J. Am. Chem. Soc.*, **90**, 3700 (1968).
- (21) P. Neta and R. W. Fessenden, *J. Phys. Chem.*, **78**, 523 (1974).
- (22) Chemically induced dynamic electron polarization or abnormal ESR signal intensities has been shown to arise in systems of homogeneously reacting radicals because the recombination rates of particular pairs of radicals depend upon the nuclear spin states. (R. W. Fessenden, *J. Chem. Phys.*, **58**, 2489 (1973).)
- (23) J. A. Pople, D. L. Beveridge, and P. A. Dobosh, *J. Am. Chem. Soc.*, **90**, 4201 (1968).
- (24) D. J. Edge, R. O. C. Norman, and P. M. Storey, *J. Chem. Soc. B*, 1096 (1970).
- (25) D. Behar and R. W. Fessenden, *J. Phys. Chem.*, **76**, 1710 (1972).
- (26) O. P. Chawla and R. W. Fessenden, to be submitted for publication; O. P. Chawla, Ph.D. Dissertation, Carnegie-Mellon University, 1973.
- (27) For instance, the <sup>14</sup>N splitting in NH<sub>3</sub><sup>+</sup> is 19.5 G [T. Cole, *J. Chem. Phys.*, **35**, 1169 (1961)] while that for <sup>13</sup>C in CH<sub>3</sub> is 38 G [R. W. Fessenden, *J. Phys. Chem.*, **71**, 74 (1967)].

## The Nature of the Potential Function for Internal Rotation about Carbon–Sulfur Bonds in Disulfides<sup>1</sup>

H. E. Van Wart,<sup>2a</sup> L. L. Shipman,<sup>2b</sup> and H. A. Scheraga\*

Department of Chemistry, Cornell University, Ithaca, New York 14853 (Received December 2, 1974)

The CNDO/2 semiempirical molecular orbital method has been used to calculate the variation in the conformational energy of methyl ethyl disulfide as a function of the SS–CC dihedral angle for various values of the CS–SC dihedral angle and for several different conformations of the methyl hydrogen atoms. Similar calculations were carried out on diethyl, methyl isopropyl, and methyl *tert*-butyl disulfides. The results indicate that, in contrast to internal rotation about the central C–C bond in *n*-butane, which results in *gauche* and *trans* rotational isomers, internal rotation about the C–S bond in methyl ethyl disulfide results in *cis* and *trans* rotational isomers. In addition, the *cis* rotamer of methyl ethyl disulfide is found to have lower energy than the *trans*. This is also in contrast to the case for *n*-butane and other saturated hydrocarbons in which *trans* rotamers generally have lower energy. The calculated low-energy *cis* conformations about C–S bonds in disulfides in which the carbon atom is a primary, secondary, or tertiary one can be rationalized in terms of an attractive interaction between the rotating methyl group(s) and the distal sulfur across the C–S bond. Evidence for the existence of such an interaction is the short nonbonded van der Waals contact distance between sulfur atoms and CH groups, observed in the crystal structures of many disulfides, as discussed in the accompanying paper. The presence of *cis* minima in the calculated potential functions is thought to arise from an underestimation of repulsive interactions in the CNDO/2 method. As discussed in the accompanying paper, it is believed that, while the CNDO/2 method leads to correct qualitative interactions across the C–S bond, the *cis* minima in the calculated potential functions should probably lie at somewhat larger values of the dihedral angle, intermediate between those of the *cis* and *gauche* conformations.

### I. Introduction

In order to be able to assess the effects of internal rotation about single bonds on the vibrational spectra of flexible molecules, it is necessary to know the nature of the potential function describing such rotations. In principle, rotational isomers of a given molecule need not have the same vibrational spectrum. In fact, Raman and infrared spectra of molecules for which rotational isomers are known to coexist commonly show bands characteristic of each of the species in equilibrium.<sup>3</sup> The potential function for internal rotation provides information about the equilibrium conformations, relative energies, and barriers for interconversion of these rotational isomers.

The conformation of a rotational isomer is described by the dihedral angles for rotation about the bonds in question. The minima in the potential function for this rotation occur at dihedral angles which correspond to stable conformations (rotational isomers) of the molecule. It has become common practice to designate rotational isomers that have certain characteristic ranges of dihedral angles as *cis*, *gauche*, or *trans* conformations. For example, internal rotation about the central C–C bond in *n*-butane results in stable conformations of the molecule in which the terminal methyl groups are *gauche* and *trans* (CC–CC dihedral angles of  $\pm 68$  and  $180^\circ$ ,<sup>4</sup> respectively)<sup>5–8</sup> to each other. The *gauche* and *trans* terminology has evolved predominantly from the study of internal rotation about C–C bonds in alkanes (principally 1,2-disubstituted ethanes) and other simple molecules.<sup>3,9</sup> The presence of *gauche* and *trans* rotamers in these systems has been supported by evidence from gas-phase electron diffraction studies, dipole moment measurements, and other experimental data.<sup>3</sup> In most cases, either the *gauche* or the *trans* conformations are also

the ones that prevail in the solid state, as found in X-ray and neutron diffraction studies. As a result of the consistent body of knowledge that has accumulated from the study of internal rotation about C–C bonds, the concept that internal rotation about single bonds in saturated molecules produces stable rotational isomers with characteristic dihedral angles in only the *gauche* and *trans* regions has evolved.

The application of this concept for the interpretation of the vibrational spectra of alkanes and certain substituted alkanes is probably on firm ground, since these are the systems from which this concept was developed. However, it has become more common to apply this concept to the analysis of problems related to internal rotation about single bonds (with saturated groups at each end) in more complex molecules in which direct experimental evidence for the existence of *gauche* or *trans* rotamers is lacking. In particular, we are interested here in ascertaining the nature of the stable conformations for rotation about C–S bonds in alkyl disulfides. This information is necessary for interpreting Raman spectra of these molecules and for establishing correlations between frequency and conformation. The Raman spectra of these molecules have already been interpreted by assuming that *gauche* and *trans* rotamers coexist about their C–S bonds.<sup>10,11</sup> In particular, it has been proposed that the *gauche* rotamers are lower in energy than the *trans*. The purpose of this paper is to investigate the nature of the potential function governing rotations about C–S bonds in disulfides, and hence to determine the conformations and relative energies of the rotamers present.

The most straightforward way of determining the conformations of the rotational isomers of various alkyl disul-

**TABLE I: Bond Lengths and Bond Angles Used for Calculations<sup>a,b</sup>**

	Methyl ethyl disulfide	Diethyl disulfide	Methyl isopropyl disulfide	Methyl <i>t</i> -butyl disulfide
$R(S-S)$ , Å	2.038	2.038	2.038	2.038
$R(C-S)$ , Å	1.832	1.832	1.832	1.832
$R(C-C)$ , Å	1.533	1.533	1.533	1.533
$R(C-H)$ , Å	1.090	1.090	1.090	1.090
$\tau(SSC)$ , deg	103.70	103.70	103.70	103.70
$\tau(SCC)$ , deg	114.70	114.70	109.47	109.47
$\tau(SC_\alpha H)$ , deg	109.30	107.40	109.47	109.47
$\tau(S'C_\alpha'H)$ , deg	107.40	107.40	109.47	
$\tau(CCH)$ , deg	109.30	109.30	109.47	109.47

<sup>a</sup> The type of atom (e.g., C<sub>α</sub>, C<sub>β</sub>, etc.) is specified only where needed to prevent ambiguity. See Figure 1 for the significance of the α, β, and the prime. <sup>b</sup> Taken from ref 16 and 18.

fides would be a direct experimental study of their structures. No such determination has yet been achieved, although techniques such as gas-phase electron diffraction and solid-phase X-ray diffraction are, at least in principle, applicable. On the other hand, a variety of theoretical techniques are readily applicable to the study of the potential function for internal rotation about C-S bonds. Approximate molecular orbital methods have been successful in calculating, for example, the experimentally observed conformations of rotational isomers of *n*-butane.<sup>12,13</sup> Using the semiempirical CNDO/2 method, we have recently examined the potential function for rotation about the S-S bond in dimethyl disulfide,<sup>14</sup> and were able to calculate the experimentally observed equilibrium CS-SC dihedral angle, and obtained qualitatively good agreement between calculated and experimentally observed trends in equilibrium S-S bond length and S-S stretching frequency with CS-SC dihedral angle. In this paper, we apply the CNDO/2 method to the study of rotation about C-S bonds in some alkyl disulfides.

An essential structural feature that will influence the potential function for rotation about a given bond (computed by any type of molecular orbital procedure) is the bond length. Molecules with larger bond lengths would tend to have lower repulsive energies in, e.g., cis conformations. Considering C-S bonds (1.83 Å) and C-C bonds (1.53 Å), one would expect to have a greater probability of finding a cis conformation about C-S bonds compared to C-C bonds. This effect emerges from the CNDO/2 calculations reported here, and leads to unusually short nonbonded C...S distances in cis conformations. This is verified by the existence of short nonbonded C...S distances in various crystal structures, as described in the accompanying paper;<sup>7</sup> the motivation for examining nonbonded C...S distances in crystals arose from the results of the CNDO/2 calculations reported here.

## II. Nuclear Geometry Used for Calculations

Calculations were carried out on methyl ethyl, diethyl, methyl isopropyl, and methyl *tert*-butyl disulfides. No

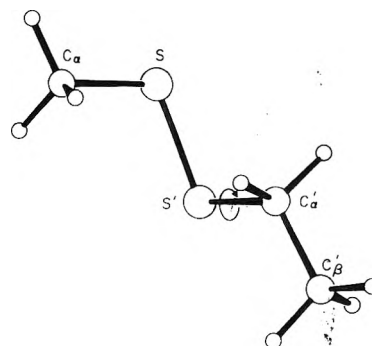


**Figure 1.** An ORTEP diagram of methyl ethyl disulfide with the C<sub>α</sub>S-S'C<sub>α'</sub> dihedral angle equal to 90° and SS'-C<sub>α'</sub>C<sub>β'</sub> dihedral angle equal to 180°. The C<sub>α</sub> and C<sub>β'</sub> hydrogen atoms are in the staggered conformation, as explained in the text. The direction of positive rotation about the S'-C<sub>α'</sub> bond is that in which the C<sub>α'</sub>-C<sub>β'</sub> bond is rotated clockwise when looking from C<sub>α'</sub> toward S'.

structural determinations are available for any of these molecules. However, neutron and X-ray diffraction structures have been determined for the structurally related molecule, L-cystine hydrochloride.<sup>15-17</sup> We used the bond lengths and bond angles from the recent neutron diffraction study by Jones et al.<sup>16</sup> on L-cystine hydrochloride (with the slight modifications discussed below) for our calculations, as shown in Table I. These parameters are in good agreement with those reported from other studies on this molecule.<sup>15,17</sup> In all cases, a C-H bond length of 1.090 Å was used. The S'C<sub>α</sub>H, SCC, and CCH bond angles of methyl ethyl and diethyl disulfides, the SC<sub>α</sub>H bond angle of diethyl disulfide, the SCC bond angles and all of the bond lengths of all of the molecules studied here were taken from the neutron diffraction structure of L-cystine hydrochloride.<sup>16</sup> The SC<sub>α</sub>H bond angle of methyl ethyl disulfide, however, was taken from the microwave structure of dimethyl disulfide.<sup>18</sup> Since no data were available on molecules similar to methyl isopropyl and methyl *tert*-butyl disulfides, for these molecules tetrahedral values were assumed for the SCC, SCH, and CCH bond angles. Calculations were carried out for a few different conformations of the methyl hydrogen atoms (e.g., staggered or eclipsed with respect to either the S-S bond or the methylene hydrogen atoms), and these will be specified below for each molecule as it is discussed.

## III. CNDO/2 Method

CNDO/2 is a semiempirical SCF-LCAO-MO theory developed by Pople and coworkers.<sup>19,20</sup> In the present study,<sup>21</sup> standard CNDO/2 parameterization was used, and all calculations were done in double precision. The d orbitals of the sulfur atoms were included in the basis set. The SCF procedure was considered to have converged when the electronic energy changed by less than 10<sup>-6</sup> atomic unit between one iteration and the next.

## IV. Results of Calculations

**Potential Energies.** Figure 1 shows an ORTEP diagram of methyl ethyl disulfide, and illustrates some geometrical features important in the calculations. The atoms are labeled in such a way that the primed side of the molecule rotates clockwise when looking from C<sub>α'</sub> toward S' about the S'-C<sub>α'</sub> bond as the SS'-C<sub>α'</sub>C<sub>β'</sub> dihedral angle is increased from 0 to 360°. In the conformation shown in this figure, the C<sub>α</sub>S-S'C<sub>α'</sub> and SS'-C<sub>α'</sub>C<sub>β'</sub> dihedral angles are 90

and  $180^\circ$ , respectively. In these calculations, only values of the  $C_\alpha S-S'C_\alpha'$  dihedral angle between  $0$  and  $180^\circ$  will be considered, since the energy of the molecule is the same for positive and negative values of the pairs of dihedral angles ( $C_\alpha S-S'C_\alpha'$ ,  $SS'-C_\alpha'C_\beta'$ ). Hence, the potential function for rotation about the C-S bond of a disulfide with  $C_\alpha S-S'C_\alpha'$  dihedral angle of  $+x$  is the mirror image of the potential function for a  $C_\alpha S-S'C_\alpha'$  dihedral angle of  $-x$ . Values of the  $SS'-C_\alpha'C_\beta'$  dihedral angle of about  $0$ ,  $\pm 60$ , and  $180^\circ$  define the commonly referred to cis, gauche, and trans positions,<sup>5</sup> respectively, for the rotation of the  $C_\alpha'-C_\beta'$  moiety about the  $S'-C_\alpha'$  bond with respect to the S atom. It should be noted that the  $C_\beta'$  and  $C_\alpha$  methyl groups are in closest proximity (for a  $C_\alpha S-S'C_\alpha'$  dihedral angle of  $90^\circ$ ) when the  $SS'-C_\alpha'C_\beta'$  dihedral angle is approximately  $250$ – $300^\circ$ , and that their separation also depends on the values of the  $C_\alpha S-S'C_\alpha'$  dihedral angle. In the conformation shown in Figure 1, the  $C_\alpha$  hydrogen atoms are staggered with respect to the S-S' bond and the  $C_\beta'$  hydrogen atoms are staggered with respect to the  $C_\alpha'$  hydrogen atoms.

The first set of calculations was carried out on methyl ethyl disulfide. This is the smallest molecule for which rotation about the  $S'-C_\alpha'$  bond is thought to affect the S-S' stretching frequency. It has been observed experimentally<sup>10,11</sup> that, while dimethyl disulfide shows a single S-S stretching band at  $508\text{ cm}^{-1}$ , methyl ethyl and diethyl disulfides show bands at about  $508$  and  $524\text{ cm}^{-1}$ . Providing that rotations about the  $C_\alpha-S$  and  $S'-C_\alpha'$  bonds do not interfere greatly with each other (i.e., that they are pairwise additive), the potential function for rotation about the  $S'-C_\alpha'$  bond in methyl ethyl disulfide should be a good approximation to that in diethyl disulfide.

The three curves shown in Figure 2 represent the variation in the energy of methyl ethyl disulfide as a function of the  $SS'-C_\alpha'C_\beta'$  dihedral angle for three different conformations of the  $C_\alpha$  and  $C_\beta'$  methyl hydrogen atoms. The energy (here, and in subsequent calculations) was computed in  $20^\circ$  intervals, except near the minima, where the interval was reduced to  $10^\circ$ . The  $C_\alpha S-S'C_\alpha'$  dihedral angle was held fixed at  $90^\circ$ . The equilibrium  $C_\alpha S-S'C_\alpha'$  dihedral angle for dimethyl disulfide is about  $85^\circ$ . Since this dihedral angle is expected to increase slightly as bulkier alkyl groups are attached to the sulfur atoms,<sup>24</sup> and since it was not known at the start of the calculations whether or not rotations about the S-S' and  $S'-C_\alpha'$  bonds were independent, we thought it reasonable to perform the initial calculations with a value of  $90^\circ$  for this dihedral angle. The effects of variation of this angle are considered later (in Figures 3, 4, and 8). For curves SS, SE, and ES, the  $C_\alpha$  hydrogen atoms were staggered, staggered, and eclipsed, respectively, with respect to the S-S' bond, and the  $C_\beta'$  hydrogen atoms were staggered, eclipsed, and staggered, respectively, with respect to the  $C_\alpha'$  hydrogen atoms. The methylene hydrogens on the  $C_\alpha'$  atoms, of course, rotated as the  $SS'-C_\alpha'C_\beta'$  dihedral angle was changed. The energy has been normalized to zero for the SE hydrogen conformation with an  $SS'-C_\alpha'C_\beta'$  dihedral angle of  $0^\circ$ .

The most striking features of all three curves are the distinct minima near the cis and trans positions. This is in direct contrast to the well-known result for internal rotation about the central C-C bond in *n*-butane, where minima are observed at the gauche and trans positions.<sup>4</sup> The conformation of methyl ethyl disulfide in which all the hydrogen atoms are staggered (SS) is the most stable one, except near  $0^\circ$ , where the molecule prefers to eclipse the  $C_\beta'$  hy-

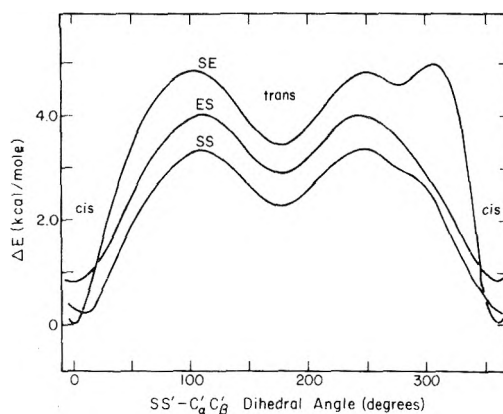


**Figure 2.** Variation of the energy of methyl ethyl disulfide with  $SS'-C_\alpha'C_\beta'$  dihedral angle for a  $C_\alpha S-S'C_\alpha'$  dihedral angle of  $90^\circ$  and for various conformations of the hydrogen atoms. In cases SS, SE, and ES, the  $C_\alpha$  hydrogen atoms were staggered, staggered, and eclipsed, respectively, with respect to the S-S bond, and the  $C_\beta'$  hydrogen atoms were staggered, eclipsed, and staggered, respectively, with respect to the  $C_\alpha'$  hydrogen atoms. The energy has been normalized to zero for the cis form with the SE hydrogen conformation.

drogen atoms with respect to the  $C_\alpha'$  hydrogen atoms (SE). In this eclipsed conformation, one of the  $C_\beta'$  hydrogen atoms points down directly over the S atom. This stable SE conformation at  $0^\circ$  in methyl ethyl disulfide would not be a disallowed conformation in cystine (which would have its  $\alpha$  hydrogen pointing directly over a sulfur atom), despite the substitution of two  $C_\beta'$  hydrogens by bulky amino and carboxyl groups, because these bulky groups do not provide steric overlap with other atoms in this SE conformation. It is observed experimentally that diisobutyl disulfide (which is analogous to cystine, but with the carboxyl and amino groups replaced by methyl groups) also exhibits S-S stretching bands at about  $508$  and  $524\text{ cm}^{-1}$ ,<sup>10,11</sup> hinting that it also is able to adopt conformations about the  $C_\alpha'-S'$  bond similar to methyl ethyl and diethyl disulfides.

The trans energy minima for these three curves all fall very close to  $180^\circ$ . The cis minima fall at  $0^\circ$  for the SE and ES conformations, but at  $10^\circ$  for the low-energy SS conformation. Examination of a space-filling model of this molecule shows that, in the SS conformation, one of the  $C_\beta'$  hydrogen atoms is very close to one of the  $C_\alpha$  hydrogen atoms when the  $SS'-C_\alpha'C_\beta'$  dihedral angle is  $0^\circ$ ; this is not so for the other conformations. Hence, the displacement of the minimum for the SS curve to  $10^\circ$  is probably due to some steric repulsion between a  $C_\beta'$  and a  $C_\alpha$  hydrogen atom. The bumpy region of these curves near  $SS'-C_\alpha'C_\beta'$  dihedral angles of  $250$ – $300^\circ$  can also be shown, with the aid of models, to coincide with close contacts between the hydrogen atoms on the  $C_\alpha$  and  $C_\beta'$  methyl groups. This interpretation is supported by the results of Figure 4, which will be discussed below.

The differences in energy between the cis and trans rotamers for the SS, ES, and SE conformations are 2.05, 2.06, and 3.37 kcal/mol, respectively. Sugeta et al.<sup>11</sup> have determined the enthalpy difference between the rotamers for methyl ethyl disulfide from the effect of temperature on its Raman spectrum and report a value of  $0.9 \pm 0.2$  kcal/mol. It is difficult to compare this value directly with our results since we have calculated the relative potential energy of these two rotational isomers by assuming rigid rotation about the  $S'-C_\alpha'$  bond. That is, all degrees of freedom of the molecules (except for the  $SS'-C_\alpha'C_\beta'$  dihedral angle)

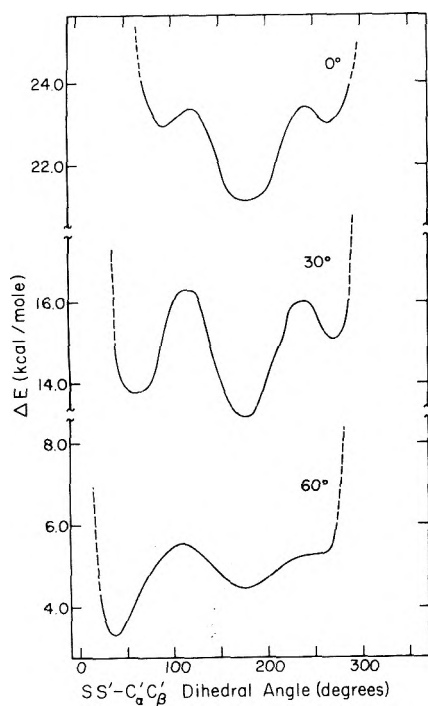


**Figure 3.** Variation of the energy of methyl ethyl disulfide with  $SS'-C_\alpha'C_\beta'$  dihedral angle for values of the  $C_\alpha S-S'C_\alpha'$  dihedral angle of 0, 30, and 60°. The hydrogen atoms were held fixed in the SS (completely staggered) conformation. The dashed lines indicate high energy regions. The zero of energy is that for the SE conformation, as shown in Figure 2.

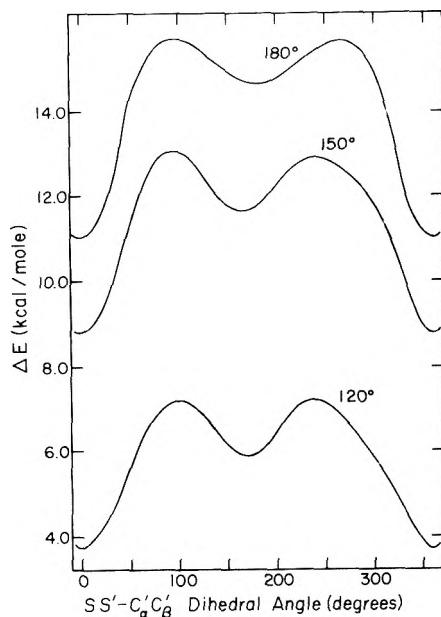


**Figure 4.** Same as Figure 3, but for  $C_\alpha S-S'C_\alpha'$  dihedral angles of 120, 150, and 180°.

were held fixed during the calculation. It is not unreasonable to assume, for example, that changes in the SCC or SSC bond angles could accompany such rotations. Furthermore, variations in the  $SS'-C_\alpha'C_\beta'$  and  $C_\alpha S-S'C_\alpha'$  dihedral angles are not always independent, as will be evident from the data shown in Figures 3 and 4. The experimentally determined enthalpy difference between these two rotational isomers, on the other hand, reflects potential energy differences (including those due to bond angle bending) as well

as conformational differences due to zero-point and thermal vibrational energies and intermolecular effects. The discrepancy between our calculated  $\Delta E'$  and the  $\Delta H$  of Sugeta et al.<sup>11</sup> is probably due both to the factors cited above and to the errors inherent in the CNDO/2 method.

It should be pointed out that, while the calculations presented here indicate that the cis rotamer is of lower energy, the relative entropies of these two rotamers must also be taken into consideration before it can be ascertained which species predominates under a given set of experimental conditions. For example, it may happen that the rotational entropy of the  $C_\beta'$  methyl group is greatly diminished because of its proximity to the sulfur atom in the cis conformation; this would lead to an increased population of the trans relative to the cis conformations.

The variation in the energy of methyl ethyl disulfide with  $SS'-C_\alpha'C_\beta'$  dihedral angle for other values of the  $C_\alpha S-S'C_\alpha'$  dihedral angle from 0 to 180° are shown in Figures 3 and 4. The zero of energy is the same as for Figure 2. The broken lines in Figure 3 represent high energy regions caused by atomic overlaps between the  $C_\beta'$  and  $C_\alpha$  methyl groups. The energy of the molecule increases as the  $C_\alpha S-S'C_\alpha'$  dihedral angle departs from about 90°, as was shown for dimethyl disulfide.<sup>14</sup> In all of these calculations, the stable SS conformation for the  $C_\alpha$  and  $C_\beta'$  hydrogen atoms was used.

A comparison of the curves plotted in Figures 2 and 3 shows that lowering the  $C_\alpha S-S'C_\alpha'$  dihedral angle from 90° changes both the positions and relative stability of their energy minima. The cis conformation for the  $C_\beta'$  methyl group ( $SS'-C_\alpha'C_\beta'$  dihedral angle = 0 to 10°) is a high energy conformation for low values of the  $C_\alpha S-S'C_\alpha'$  dihedral angle because of severe atomic overlap between the  $C_\beta'$  and  $C_\alpha$  methyl groups. There is, however, a definite tendency for the  $C_\beta'$  methyl group to approach the S atom as closely as the  $C_\alpha$  methyl group will allow. This manifests itself as energy minima (in roughly the gauche regions) on both sides of the cis position. These two minima approach each other and coalesce at the cis position as the  $C_\alpha S-S'C_\alpha'$  dihedral angle is increased to 90° (i.e., as the  $C_\alpha$  methyl group gets out of the way of the  $C_\beta'$  methyl group). The position of the trans minimum is not affected by changes in the  $C_\alpha S-S'C_\alpha'$  dihedral angle. The relative stabilities of the minima do, however, vary monotonically with the  $C_\alpha S-S'C_\alpha'$  dihedral angle. As this angle is increased from 0 to 90°, the trans rotamer becomes increasingly less stable than the other two. This trend persists as the disulfide dihedral angle is increased from 90 to 180°, as shown in Figure 4. This is illustrated further in Figure 5 in which the energy difference between the trans (t) and the more stable of the remaining rotamers (c') is plotted as a function of  $C_\alpha S-S'C_\alpha'$  dihedral angle.

The minima in the cis region shown in Figure 4 are at  $SS'-C_\alpha'C_\beta'$  dihedral angles of 0° as opposed to the value of 10° for the SS conformation with a  $C_\alpha S-S'C_\alpha'$  dihedral angle of 90° (Figure 2). Hence, the cis  $SS'-C_\alpha'C_\beta'$  dihedral angle of 10° (rather than 0°) is probably due to the steric repulsion between the  $C_\alpha$  and  $C_\beta'$  methyl groups. These calculations indicate then that, in the absence of other influences, the potential function for rotation about the C-S bond in methyl ethyl disulfide has minima at the cis and trans positions. We now use this information as a starting point for the calculations on diethyl disulfide.

Figure 6 shows an ORTEP diagram of diethyl disulfide with a  $C_\alpha S-S'C_\alpha'$  dihedral angle of 90°. The  $C_\beta C_\alpha-SS'$  di-

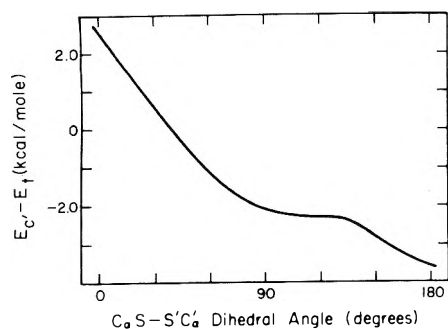


**Figure 5.** Variation of the relative energies of *c'* and *t* rotamers (for rotation about  $S'-C_{\alpha}'$  bond) in methyl ethyl disulfide with  $C_{\alpha}S-S'C_{\alpha}'$  dihedral angle, where the *t* rotamer is always the trans form and the *c'* the most stable of the remaining rotamers.

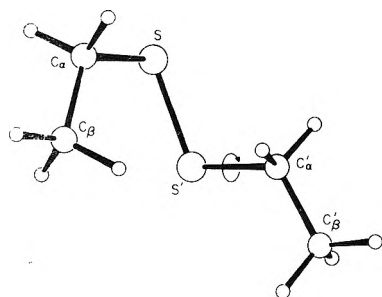


**Figure 6.** An ORTEP diagram of diethyl disulfide with  $C_{\beta}C_{\alpha}-SS'$  dihedral angle equal to  $10^{\circ}$  (cis),  $C_{\alpha}S-S'C_{\alpha}'$  dihedral angle equal to  $90^{\circ}$ , and  $SS'-C_{\alpha}'C_{\beta}'$  dihedral angle equal to  $180^{\circ}$  (trans). The direction of positive rotation about the  $S'-C_{\alpha}'$  bond is that in which the  $C_{\alpha}'-C_{\beta}'$  bond is rotated clockwise when looking from  $C_{\alpha}'$  toward  $S'$ . The  $C_{\beta}$  and  $C_{\beta}'$  hydrogens are in the SS conformation.

hedral angle is  $10^{\circ}$  and the  $C_{\beta}$  and  $C_{\beta}'$  hydrogen atoms are in the SS conformation. The energy of this molecule was calculated as a function of the  $SS'-C_{\alpha}'C_{\beta}'$  dihedral angle in the same manner as for methyl ethyl disulfide. The results of this and three other calculations on diethyl disulfide are shown in Figure 7. For curves 1 and 2, the  $C_{\alpha}C_{\beta}-SS'$  dihedral angle was  $180^{\circ}$  while for curves 3 and 4 this angle was  $10^{\circ}$ . These are the minima found for rotation about the  $S'-C_{\alpha}'$  bond in methyl ethyl disulfide. For curves 1 and 3, the  $C_{\beta}$  or  $C_{\beta}'$  hydrogen atoms were eclipsed with respect to the  $C_{\alpha}$  or  $C_{\alpha}'$  hydrogen atoms, respectively. In cases 2 and 4, these hydrogen atoms were staggered. The energy is normalized to zero for curve 4 at a  $SS'-C_{\alpha}'C_{\beta}'$  dihedral angle of  $10^{\circ}$ .

The results shown in Figure 7 indicate that the most stable form of this molecule is the conformation in which the  $C_{\beta}$  and  $C_{\beta}'$  methyl groups are cis to the  $S'$  and  $S$  atoms, respectively, and in which the  $C_{\beta}$  and  $C_{\beta}'$  hydrogen atoms are staggered. This is essentially the same result as for methyl ethyl disulfide. The energy difference between the cis and trans rotamers in curve 4 (Figure 7) is 2.12 kcal/mol. Sugata et al.<sup>11</sup> have determined the energy difference between these rotamers in diethyl disulfide to be  $0.6 \pm 0.2$  kcal/mol, which is within experimental error of the analogous value reported for methyl ethyl disulfide. The calculated value of 2.12 kcal/mol is almost equal to the calculated value of 2.05 kcal/mol for methyl ethyl disulfide (Figure 2). These results indicate that, for a  $C_{\alpha}S-S'C_{\alpha}'$  dihedral angle of  $90^{\circ}$ , rotations about the C-S bonds are essentially pairwise additive. Other features of the curves shown in Figure 7, such as the bumpy region near  $SS'-C_{\alpha}'C_{\beta}'$  equal to  $250-300^{\circ}$ , are

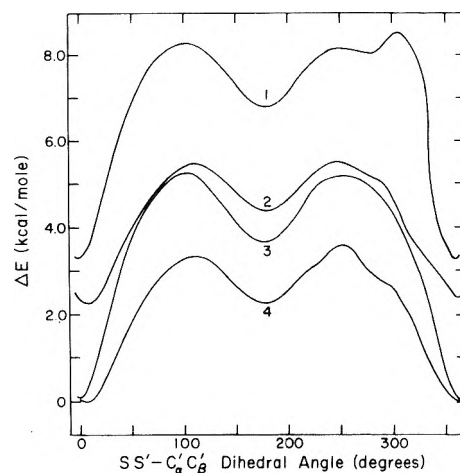


**Figure 7.** Variation of the energy of diethyl disulfide with  $SS'-C_{\alpha}'C_{\beta}'$  dihedral angle. The  $C_{\alpha}$  and  $C_{\alpha}'$  hydrogen atoms were held staggered with respect to the  $S-S'$  bond. In curves 1 and 2, the  $C_{\beta}C_{\alpha}-SS'$  dihedral angle was  $180^{\circ}$  while in curves 3 and 4 this angle was  $10^{\circ}$ . In curves 1 and 3, the  $C_{\beta}$  or  $C_{\beta}'$  hydrogen atoms were eclipsed with respect to the  $C_{\alpha}$  or  $C_{\alpha}'$  hydrogen atoms, respectively. In curves 2 and 4, these hydrogen atoms were staggered. The energy is normalized to zero for curve 4 with an  $SS'-C_{\alpha}'C_{\beta}'$  dihedral angle of  $10^{\circ}$ .

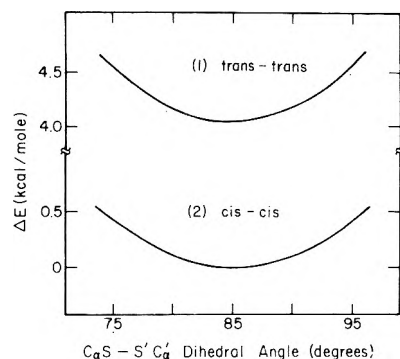


**Figure 8.** Variation of the energy of diethyl disulfide in the (1) trans-trans and (2) cis-cis forms (for rotation about the  $C_{\alpha}-S$  and  $C_{\alpha}'-S'$  bonds) with  $C_{\alpha}S-S'C_{\alpha}'$  dihedral angle. The energy is normalized to zero for the cis-cis form.

due to the same factors as discussed previously for Figure 2.

In order to investigate the effects of rotations about the C-S bonds on the equilibrium value of the  $C_{\alpha}S-S'C_{\alpha}'$  dihedral angle in diethyl disulfide, the following calculations were carried out. Holding the  $C_{\beta}C_{\alpha}-SS'$  and the  $SS'-C_{\alpha}'C_{\beta}'$  dihedral angles (1) both at  $180^{\circ}$  and (2) both at  $10^{\circ}$  with staggered  $C_{\beta}$  and  $C_{\beta}'$  hydrogen atom conformations, the energy was calculated as a function of the  $C_{\alpha}S-S'C_{\alpha}'$  dihedral angle near the expected minimum of  $85-90^{\circ}$ . The results, shown in Figure 8, confirm that the equilibrium value of the  $C_{\alpha}S-S'C_{\alpha}'$  dihedral angle is independent of the conformation about the C-S bonds and is close to the value of  $85^{\circ}$  found for dimethyl disulfide. This shows that the equilibrium  $C_{\alpha}S-S'C_{\alpha}'$  dihedral angle is not affected even though the low energy conformations about both C-S bonds are cis; i.e., there is no steric overlap between the ethyl ends of the molecule which could cause the  $C_{\alpha}S-S'C_{\alpha}'$  dihedral angle to depart from  $85^{\circ}$ .

The variation of the energy of methyl isopropyl disulfide with  $SS'-C_{\alpha}'C_{\beta}'$  dihedral angle is shown in Figure 9. The  $SS'-C_{\alpha}'C_{\beta}'$  dihedral angle is defined in such a way that with the  $C_{\alpha}'$  hydrogen in Figure 1 pointing out toward the



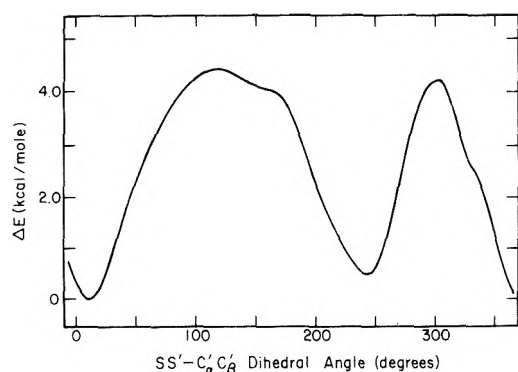


**Figure 9.** Variation of the energy of methyl isopropyl disulfide with  $SS'-C_{\alpha}'C_{\beta}'$  dihedral angle for a  $C_{\alpha}S-S'C_{\alpha}'$  dihedral angle of  $90^{\circ}$  and a staggered hydrogen conformation. The manner in which the  $SS'-C_{\alpha}'C_{\beta}'$  dihedral angle is defined is discussed in the text.

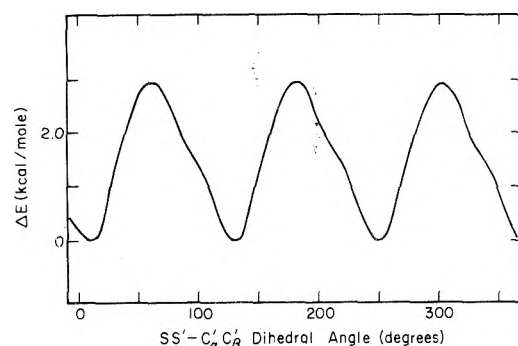


**Figure 10.** Variation of the energy of methyl *tert*-butyl disulfide with  $SS'-C_{\alpha}'C_{\beta}'$  dihedral angle for a  $C_{\alpha}S-S'C_{\alpha}'$  dihedral angle of  $90^{\circ}$  and a staggered hydrogen conformation. The manner in which the  $SS'-C_{\alpha}'C_{\beta}'$  dihedral angle is defined is discussed in the text.

reader replaced by a methyl group (we will refer to this as the  $C_{\beta}''$  methyl group), the  $SS'-C_{\alpha}'C_{\beta}'$  dihedral angle shown would still be  $180^{\circ}$ . The  $C_{\alpha}S-S'C_{\alpha}'$  dihedral angle was held fixed at  $90^{\circ}$ . The  $C_{\alpha}$  methyl hydrogen atoms were staggered with respect to the S-S' bond and the  $C_{\beta}'$  and  $C_{\beta}''$  methyl hydrogen atoms were staggered with respect to the S'- $C_{\alpha}'$  bond. For values of the  $SS'-C_{\alpha}'C_{\beta}'$  dihedral angle of 0 and  $240^{\circ}$ , the  $C_{\beta}'$  and  $C_{\beta}''$  methyl groups, respectively, are situated cis to the S atom. The energy minima in Figure 9 are at 10 and  $250^{\circ}$ , and are conformations in which the  $C_{\beta}'$  and  $C_{\beta}''$  methyl groups are situated  $10^{\circ}$  from the S atom (away from the side of the molecule with the  $C_{\alpha}$  methyl group) as in the lower energy conformations of methyl ethyl disulfide. The energy difference between these two minima is 0.46 kcal/mol. Values of the  $SS'-C_{\alpha}'C_{\beta}'$  dihedral angle of 60 and  $180^{\circ}$  place the  $C_{\beta}''$  and  $C_{\beta}'$  methyl groups, respectively, in the trans position. These, however, are high energy regions, presumably because the methyl groups prefer the cis positions much more than the trans positions.

Figure 10 shows the variation of the energy of methyl *tert*-butyl disulfide as a function of  $SS'-C_{\alpha}'C_{\beta}'$  dihedral angle. Since there is local  $C_3$  symmetry for rotation about the S'- $C_{\alpha}'$  bond, there is no ambiguity in the way the  $SS'-C_{\alpha}'C_{\beta}'$  dihedral angle is defined. Here, again, the  $C_{\alpha}S-S'C_{\alpha}'$  dihedral angle has been held fixed at  $90^{\circ}$  and the  $C_{\alpha}$  hydrogen atoms staggered with respect to the S-S' bond. The hydrogen atoms on the three  $C_{\beta}'$  methyl groups were staggered with respect to the S'- $C_{\alpha}'$  bond. The minima in this potential function are at  $SS'-C_{\alpha}'C_{\beta}'$  dihedral angles of

10, 130, and  $250^{\circ}$ , and correspond, again, to conformations in which one of the  $C_{\beta}'$  methyl groups is nearly cis to the S atom.

**Vibrational Frequencies.** It has been observed experimentally that internal rotation about both C-S and S-S bonds affects the S-S stretching frequency in disulfides.<sup>10,11</sup> In a previous paper,<sup>14</sup> it was shown that torsion about the S-S bond away from the equilibrium dihedral angle of  $85^{\circ}$  in the model compound dimethyl disulfide is accompanied by an increase in the equilibrium bond length of the disulfide group, with a concomitant decrease in the force constant for a pure S-S stretching motion. While this motion is undoubtedly not a pure S-S stretch, it probably is predominantly so. Hence, the observed variation in S-S stretching frequency due to rotations about the S-S bond can, at least in part, be attributed to changes in the force constant due to the bond weakening associated with this torsion. In order to investigate whether or not rotations about C-S bonds affect the force constant for a pure S-S stretching motion similarly, the following calculation was performed on diethyl, methyl isopropyl, and methyl *tert*-butyl disulfides. With the  $C_{\alpha}S-S'C_{\alpha}'$  dihedral angle held fixed at  $90^{\circ}$  (and, in the case of diethyl disulfide, with the  $C_{\beta}C_{\alpha}-SS'$  dihedral angle held fixed at either 10 or  $180^{\circ}$ ), a value of the  $SS'-C_{\alpha}'C_{\beta}'$  dihedral angle was first selected. Then four values of the energy were calculated by varying the S-S bond length,  $R_{S-S}^{eq}$ , in 0.01-Å steps close to its CNDO/2 equilibrium value. These energies were then used to calculate the equilibrium energy,  $E_0$ , the equilibrium S-S bond length,  $R_{S-S}^{eq}$ , the disulfide stretching force constant,  $K_{S-S}$ , and the anharmonicity constant,  $K_a$ , shown in the following equation:

$$E = E_0 + (\frac{1}{2})K_{S-S}(R_{S-S} - R_{S-S}^{eq})^2 + (\frac{1}{6})K_a(R_{S-S} - R_{S-S}^{eq})^3 \quad (1)$$

This calculation was performed at  $20^{\circ}$  intervals in the  $SS'-C_{\alpha}'C_{\beta}'$  dihedral angle. The values of  $K_{S-S}$  obtained were then translated into stretching frequencies using the following equation:

$$\omega_{S-S} = [1/(2\pi c)](K_{S-S}/\mu)^{1/2} \quad (2)$$

where  $c$  is the speed of light and  $\mu$  is the reduced mass for the pure S-S stretching motion. The results of these calculations are shown in Figure 11 where  $\omega_{S-S}$  is plotted as a function of  $SS'-C_{\alpha}'C_{\beta}'$  dihedral angle.

Curve 1 represents the results of calculations on methyl *tert*-butyl disulfide and curves 2 and 3 the results for diethyl disulfide with  $C_{\beta}C_{\alpha}-SS'$  dihedral angles of 10 and  $180^{\circ}$ , respectively. The curve for methyl isopropyl disulfide is not shown, but is also relatively flat and lies essentially on top of curves 1-3. For comparison, the results of an earlier study on dimethyl disulfide<sup>14</sup> showing the variation in  $\omega_{S-S}$  with CS-SC dihedral angle is plotted as curve 4. The magnitudes of these stretching frequencies are too large by about a factor of 2. The variations in  $\omega_{S-S}$  with  $SS'-C_{\alpha}'C_{\beta}'$  dihedral angle shown by curves 1-3 show that rotation about C-S bonds does not affect the S-S stretching force constant significantly.

This and the previous<sup>14</sup> calculations of the variation of the S-S stretching frequency with dihedral angles were made by assuming the character of the S-S stretching normal mode and then calculating the vibrational frequency for that assumed mode by use of the CNDO/2-calculated  $K_{S-S}$ . The normal mode considered was a "pure" S-S stretch in which the parts of the molecule at each end of

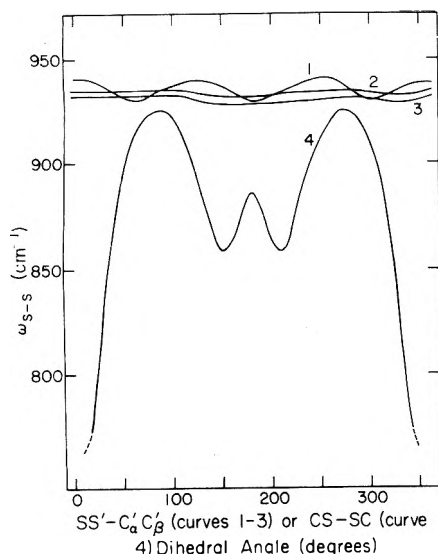


**Figure 11.** Variation of S-S stretching frequency with  $SS'-C_{\alpha}'C_{\beta}'$  dihedral angle for: (1) methyl *tert*-butyl disulfide, (2) diethyl disulfide with  $C_{\beta}'C_{\alpha}-SS'$  dihedral angle equal to  $10^{\circ}$ , (3) diethyl disulfide with  $C_{\beta}'C_{\alpha}-SS'$  dihedral angle equal to  $180^{\circ}$ , and (4) variation of S-S stretching frequency with CS-SC dihedral angle for dimethyl disulfide (this curve was taken from ref 14). The curve for the variation of  $\omega_{S-S}$  with  $SS'-C_{\alpha}'C_{\beta}'$  dihedral angle for methyl isopropyl disulfide was calculated but is not shown since it is also relatively flat and lies essentially on top of curves 1-3.

the S-S bond moved as rigid units during the S-S stretching motion. It is of interest to consider the problem in terms of a more general model for harmonic vibrations, viz., the GF method.<sup>25</sup> The **F** matrix is the force constant matrix in terms of the internal coordinates (bond stretches, bond angle bends, torsions, etc.) and the **G** matrix contains both atomic mass and molecular structural information. The normal modes are obtained by diagonalizing the product **GF**, so that the variation (with dihedral angles) of the character (viz., the contribution of each internal coordinate to the normal mode identified as the S-S stretching mode) is determined by variations in both the **F** and **G** matrices. The **G** matrices for the molecules studied here are calculable and the **F** matrices could be calculated (with the expenditure of a considerable amount of computer time) using the CNDO/2 method. However, after analysis of the results of the initial studies reported here, it was felt that the accuracy of the CNDO/2 internal potential energy surface was not good enough to justify going ahead with the full **GF** calculation.

It has been observed experimentally<sup>10,11</sup> that the frequencies of bands, which have been identified as S-S stretching bands, in alkyl disulfides vary with SS-CC dihedral angle. Since the preceding calculation has shown that the force constant for a pure S-S stretching motion does not vary with SS-CC dihedral angle, we conclude that the observed bands are not due to pure S-S stretching motions, but are due to a mixture of at least two motions, of which the S-S stretching motion is predominant. These experimentally observed bands, then, are most likely S-S stretching motions mechanically coupled with C-S stretches, SCC bends, etc. The effects of vibrational coupling cannot show up in this calculation of the force constants since we have constrained the calculated  $\omega_{S-S}$  to arise from a pure S-S stretching motion by allowing changes in only the S-S bond length.

## V. Discussion

The results of the calculations presented here indicate that energy minima in the potential function for rotation about C-S bonds in disulfides (where the carbon atom is a primary one) are at the cis and trans positions and that the cis rotamer is of lower energy. Furthermore, the positions of the energy minima for such rotations involving secondary and tertiary carbons can be understood by considering the dominant tendency to position a rotating methyl group cis to the distal sulfur across the C-S bond. It seems to be this tendency that differentiates this potential function from that describing rotations about the central C-C bond in *n*-butane. If the results of the calculations presented here are confirmed experimentally, the vibrational spectra of these alkyl disulfides<sup>10,11</sup> will require reinterpretation.

It is difficult to abstract from an approximate molecular orbital calculation physical insight concerning the origins of the observed trends. One conclusion, however, that is worthy of consideration in light of the present results is that there is an attractive interaction between the rotating methyl group and the distal sulfur. This would account for the occurrence of the cis minima and for the fact that they are lower in energy than the trans minima. On the other hand, it is commonly believed that the terminal methyl groups in *n*-butane prefer to be apart from each other and from the methylene hydrogen atoms on the central carbons, accounting for the gauche and trans minima. The physical origin of an attractive methyl group-sulfur atom interaction in sulfur-containing compounds is not obvious. The CNDO/2 partial charges on both sulfur atoms are negative while the charge on the  $C_{\beta}'$  carbon atom in methyl ethyl disulfide is slightly positive (typically  $-0.05$  and  $+0.02$ , respectively, when the  $C_{\alpha}S-S'C_{\alpha}'$  dihedral angle is  $90^{\circ}$ ). Hence, an attractive electrostatic interaction between these atoms is feasible. If this were the only factor responsible for the cis minimum, one might expect the trend in the stability of the cis relative to the trans rotamer shown in Figure 5 to follow the trend in the partial charges. This is not the case, however, since the CNDO/2 partial charge on the sulfur atoms becomes more negative as the  $C_{\alpha}S-S'C_{\alpha}'$  dihedral angle departs from  $90^{\circ}$  (about  $-0.07$  at  $180^{\circ}$  and about  $-0.06$  at  $0^{\circ}$ ), while the partial charge on the  $C_{\beta}'$  carbon atom remains fairly constant. It may be that the cis form becomes more stable as the  $C_{\alpha}S-S'C_{\alpha}'$  dihedral angle increases from  $0$  to  $180^{\circ}$  because the positive  $C_{\beta}'$  methyl "sees" the two sets of lone-pair electrons on the S atom better. It is noteworthy that the disposition of the  $C_{\beta}'$  hydrogen atoms is not crucial for the relative stability of the cis and trans rotamers, as can be seen from Figure 2. At no time during rotation are the sulfur,  $C_{\beta}'$  carbon atom, and one of the  $C_{\beta}'$  hydrogen atoms colinear. Hence, this interaction would seem to lack the directionality commonly attributed to a hydrogen bond.

The results of the present study should be considered along with the known tendency of the CNDO/2 method to underestimate overlap repulsions in mind. For example, this underestimation of overlap repulsions consistently leads to calculated hydrogen bond distances that are too short.<sup>28</sup> As another example, calculations carried out on *n*-butane using the CNDO/2 method give the experimentally observed dihedral angles for the gauche and trans rotamers for rotation about the central C-C bond but, because of the underestimation of overlap repulsions between terminal methyl groups, they do not yield the experimentally ob-

served relative energies of these rotamers; i.e., these calculations indicate that the gauche form is more stable than the trans form by 70 cal/mol,<sup>13</sup> whereas it is observed experimentally that the trans form is more stable than the gauche by about 800 cal/mol.<sup>9</sup> It is, therefore, conceivable that the occurrence of the cis minima in the calculations described in this paper may be due, in part, to a similar underestimation of repulsions between nearby groups in the cis conformations. If this turns out to be the case, the potential function for rotation about the S'-C $\alpha$ ' bond in methyl ethyl disulfide may have an energy minimum at a dihedral angle intermediate in value between those which we have defined for the cis and gauche conformations instead of at the cis conformation. This possibility is discussed in detail in the accompanying paper.<sup>7</sup>

Even if this turns out to be the case, however, these CNDO/2 calculations have been valuable in that they have pointed to an attractive interaction between carbon and sulfur atoms across C-S bonds which explains why the trans rotamer is not the one of lowest energy.

With proper allowance for the expected underestimation of overlap repulsions, the calculated CNDO/2 potential energy curves are a good starting point for the understanding of the conformations of alkyl disulfides; these CNDO/2 calculations have provided useful information for the interpretation of existing spectroscopic data on disulfides and for the optimum design of future experimental and theoretical studies using more sophisticated methods than CNDO/2.

As mentioned earlier, no direct experimental evidence is available on the nature of the rotamers present in the compounds studied here. The only available data are diffraction data on crystals of structurally related disulfides. A survey of these data has revealed many examples of short intramolecular nonbonded carbon-sulfur contact distances. These results are presented in the accompanying paper<sup>7</sup> in which the implications of an attractive carbon-sulfur interaction for the conformations of organosulfur molecules are considered and in which the effect of a reduced repulsion in the CNDO/2 method on the calculated potential functions is discussed in detail.

NOTE ADDED IN PROOF: Recently, Yokozeki and Bauer<sup>29</sup> and Van Wart et al.<sup>30</sup> have completed an electron diffraction and Raman spectral study, respectively, of methyl ethyl disulfide. The Raman spectra indicated the existence of three rotamers about the S'-C $\alpha$ ' bond. The electron diffraction data indicated that one of these is trans, but the conformations of the other two rotamers could not be specified uniquely.

## References and Notes

- (1) This work was supported by research grants from the National Institute of General Medical Sciences of the National Institutes of Health, U.S. Public Health Service (GM-14312), and from the National Science Foundation (BMS71-00872 A04).
- (2) (a) NIH Predoctoral Trainee, 1970-1974. (b) NIH Postdoctoral Fellow, 1972-1974.
- (3) S. Mizushima, "Structure of Molecules and Internal Rotation", Academic Press, New York, N.Y., 1954, Chapters I and II.
- (4) K. Kuchitsu, *Bull. Chem. Soc. Jpn.*, **32**, 748 (1959).
- (5) Considerable ambiguity can result from use of the terms cis, gauche, and trans. Even though it has been suggested<sup>6</sup> that the term trans be reserved for the specification of steric relationships across double bonds, and that the term anti be used for specifying conformation about single bonds, we will retain the term trans in this paper, since this is the one that has been used in the interpretation of the vibrational spectra of the molecules of interest here. The terms gauche and skew are often used interchangeably to specify conformation and seldom is the range of dihedral angles which define these conformations specified. In this paper, we will consider a rotational isomer to be cis, gauche, or trans if its dihedral angles lie within 15° of 0, 60, and 180°, respectively. Using these definitions of rotational isomers, there are certain ranges of dihedral angles for which there is no designation. This will not lead to any confusion in this paper, since the present definitions cover the regions of interest. However, in the accompanying paper,<sup>7</sup> the steric relationships across single bonds will be specified in accordance with the terminology of Klyne and Prelog.<sup>6</sup>
- (6) E. Eliel, *J. Chem. Educ.*, **37**, 126 (1960).
- (7) H. E. Van Wart, L. L. Shipman, and H. A. Scheraga, *J. Phys. Chem.*, following paper in this issue.
- (8) W. Klyne and V. Prelog, *Experientia*, **16**, 521 (1960).
- (9) E. Eliel, "Stereochemistry of Carbon Compounds", McGraw-Hill, New York, N.Y., 1962, Chapter 6.
- (10) H. Sugeta, A. Go, and T. Miyazawa, *Chem. Lett. Jpn.*, **83** (1972).
- (11) H. Sugeta, A. Go, and T. Miyazawa, *Bull. Chem. Soc. Jpn.*, **46**, 3407 (1973).
- (12) R. Hoffmann, *J. Chem. Phys.*, **39**, 1396 (1963).
- (13) R. B. Davidson, W. L. Jorgensen, and L. C. Allen, *J. Am. Chem. Soc.*, **92**, 749 (1970).
- (14) H. E. Van Wart, L. L. Shipman, and H. A. Scheraga, *J. Phys. Chem.*, **78**, 1848 (1974).
- (15) L. K. Steinrauf, J. Petersen, and L. H. Jensen, *J. Am. Chem. Soc.*, **80**, 3835 (1958).
- (16) D. D. Jones, I. Bernal, M. N. Frey, and T. F. Koetzle, *Acta Crystallogr., Sect. B*, **30**, 1220 (1974).
- (17) S. C. Gupta, A. Sequeira, and R. Chidambaram, *Acta Crystallogr., Sect. B*, **30**, 562 (1974).
- (18) D. Sutter, H. Dreizler, and H. D. Rudolph, *Z. Naturforsch. A*, **20**, 1676 (1965).
- (19) J. A. Pople and D. L. Beveridge, "Approximate Molecular Orbital Theory", McGraw-Hill, New York, N.Y., 1970.
- (20) D. P. Santry and G. A. Segal, *J. Chem. Phys.*, **47**, 158 (1967).
- (21) We are indebted to Professor R. Hoffmann for making the CNDO/2 computer program available to us.
- (22) It should be noted that the dihedral angles in this paper inadvertently, but consistently, have been defined to be opposite in sign from the IUPAC-IUB Commission Convention.<sup>23</sup> This in no way affects any of the results presented here since the steric relationships between the various atoms are identical in either sign convention.
- (23) IUPAC-IUB Commission on Biochemical Nomenclature, *Biochemistry*, **9**, 3471 (1970).
- (24) D. B. Boyd, *J. Am. Chem. Soc.*, **94**, 8799 (1972).
- (25) E. B. Wilson, J. C. Decius, and P. C. Cross, "Molecular Vibrations", McGraw-Hill, New York, N.Y., 1955, p 64.
- (26) H. E. Van Wart, A. Lewis, H. A. Scheraga, and F. D. Saeva, *Proc. Natl. Acad. Sci.*, **70**, 2619 (1973).
- (27) E. J. Bastian and R. B. Martin, *J. Phys. Chem.*, **77**, 1129 (1973).
- (28) P. A. Kollman and L. C. Allen, *J. Am. Chem. Soc.*, **92**, 753 (1970).
- (29) A. Yokozeki and S. H. Bauer, *J. Phys. Chem.*, submitted for publication.
- (30) H. E. Van Wart, F. Cardinaux, and H. A. Scheraga, *J. Phys. Chem.*, submitted for publication.

## Theoretical and Experimental Evidence for a Nonbonded 1,4 Carbon-Sulfur Interaction in Organosulfur Compounds<sup>1</sup>

H. E. Van Wart,<sup>2a</sup> L. L. Shipman,<sup>2b</sup> and H. A. Scheraga\*

Department of Chemistry, Cornell University, Ithaca, New York 14853 (Received December 2, 1974)

The suggestion in an earlier paper that an attractive nonbonded carbon-sulfur interaction exists in organosulfur compounds has been investigated further. The potential functions for internal rotation about single bonds between carbon and sulfur atoms in methyl *n*-propyl sulfide and methyl *n*-propyl disulfide have been calculated using the CNDO/2 semiempirical molecular orbital method. The results of these calculations are consistent with the existence of an attractive nonbonded interaction between a methylene or methyl group and a sulfur atom. When there are three intervening single bonds, this interaction is referred to as a 1,4 carbon-sulfur interaction, although hydrogen atoms bonded to the carbon are thought to participate in the interaction. A summary of short 1,4 carbon-sulfur contacts taken from crystal structures of organosulfur compounds in the literature has been compiled. On the basis of these contact data, it can be inferred that there is an attractive nonbonded 1,4 carbon-sulfur interaction that is comparable in strength to a weak hydrogen bond, but with less directionality. The existence of such an interaction is consistent with independent thermodynamic evidence which gives a value for the enthalpy of formation of such an interaction of  $-1$  to  $-2$  kcal/mol. It is concluded that, although the CNDO/2 calculations are qualitatively correct in that they point to the existence of this 1,4 carbon-sulfur interaction, they overestimate its strength. The effect of this overestimate on the calculated potential functions is discussed.

### I. Introduction

In the preceding paper,<sup>3</sup> the potential function for internal rotation about C-S bonds in several alkyl disulfides was studied using the semiempirical molecular orbital CNDO/2 method. The results indicated that, in contrast to internal rotation about the central C-C bond in *n*-butane, which leads to stable gauche and trans rotational isomers,<sup>4</sup> rotation about the C-S bond in methyl ethyl disulfide results in stable cis and trans rotational isomers. These two results are depicted schematically in Figure 1. The Newman projections show the relative positions of the atoms for the stable cis, gauche, and trans rotamers mentioned above (and defined earlier<sup>3</sup>), as seen by viewing *n*-butane and methyl ethyl disulfide along the <sup>2</sup>C-<sup>3</sup>C and <sup>2</sup>C-<sup>3</sup>S bonds, respectively.

In this paper, the cis, gauche, and trans terminology will be replaced by the more systematic nomenclature of Klyne and Prelog.<sup>5-7</sup> This change allows one to specify more precisely the steric relationship between groups in the 1 and 4 positions which are separated by three single bonds. The relationship between these two terminologies can be visualized by superimposing the Newman projections of the cis, gauche, and trans rotamers shown in the lower part of Figure 1 on the schematic diagram at the top. In order to designate the relative positions of groups in the 1 and 4 positions in the Klyne and Prelog terminology, one views the molecule along the 2 → 3 bond with the group in the 4 position at 12 o'clock. The steric relationship between groups in the 1 and 4 positions is then designated by the symbols<sup>6</sup> in the sector of the circle in which the group in the 1 position lies. In the Klyne-Prelog system, the two conformationally equivalent gauche rotamers of *n*-butane are said to have their terminal methyl groups  $\pm$  syn-clinal ( $\pm$ sc) to each other.

The reason for the occurrence of stable  $\pm$ sc and ap conformations for *n*-butane but of +sp and ap conformations

for methyl ethyl disulfide, as shown in Figure 1, can be rationalized in terms of the differences between the interactions of the groups across the <sup>2</sup>C-<sup>3</sup>C and <sup>2</sup>C-<sup>3</sup>S bonds, respectively. For *n*-butane, the interactions between each methyl group in the 1 or 4 positions and the methylene hydrogen atoms across the 2-3 bond are repulsive when their nonbonded internuclear distances are smaller than the sum of their van der Waals radii. This leads to energy minima at the  $\pm$ sc and ap positions at which these repulsions are minimized by having these groups as far apart as possible.<sup>4</sup> The stability of the +sp conformation for internal rotation about the <sup>2</sup>C-<sup>3</sup>S bond of methyl ethyl disulfide, on the other hand, can be explained<sup>3</sup> by an attractive nonbonded interaction between the methyl group in the 1 position and the sulfur atom in the 4 position when the molecule adopts the +sp conformation. The sum of the van der Waals radii of the sulfur atom and the methyl group varies from 3.45<sup>8</sup> to 3.85<sup>9</sup> Å, depending on which set of van der Waals contact distances one chooses. Hence, if the results of the CNDO/2 calculations<sup>3</sup> are correct, the attractive nonbonded interaction between the sulfur atom and the methyl group is stronger than can be accounted for by van der Waals interactions alone since these calculations lead to nonbonded carbon-sulfur distances less than 3.45 Å. We will refer to this interaction as a 1,4 carbon-sulfur interaction. For the moment, the role that the hydrogen atoms play in this attractive interaction will not be specified (but will be discussed in section III E).

The primary aim of this paper is to investigate further the possible existence of the nonbonded 1,4 carbon-sulfur interaction proposed previously<sup>3</sup> and to determine how such an interaction would influence the conformation of organosulfur compounds, in general. In particular, it is of interest to determine (by CNDO/2 calculations) whether such an interaction can affect the potential function for rotation about bonds other than C-S bonds, in which the bond in question lies between the 2 and 3 positions relative

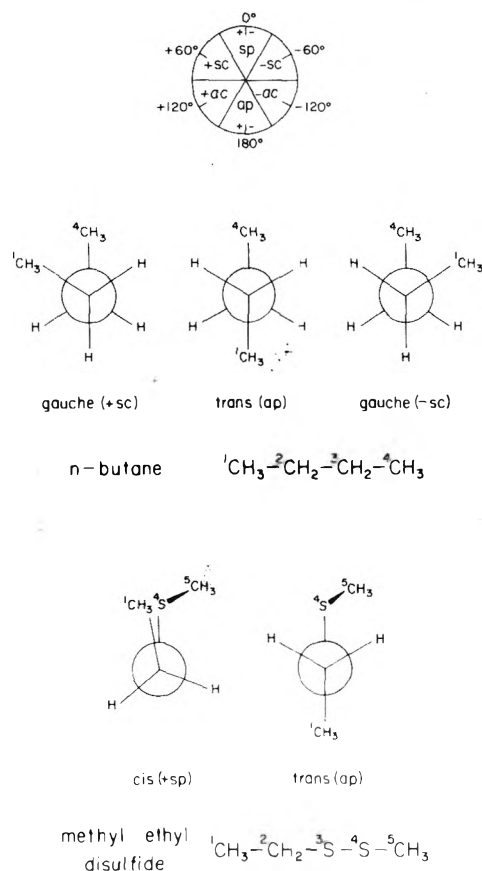


**Figure 1.** Newman projections showing known conformations of the rotational isomers of *n*-butane<sup>4</sup> and the calculated conformations of the rotational isomers of methyl ethyl disulfide<sup>3</sup> due to rotations about the  ${}^2\text{C}-{}^3\text{C}$  and  ${}^2\text{C}-{}^3\text{S}$  bonds, respectively. The schematic diagram at the top can be used to relate the well-known *cis*, *gauche*, and *trans* terminology for rotational isomers to that of Klyne and Prelog,<sup>5-7</sup> as explained in the text.

to the 1,4 carbon-sulfur interaction. In addition, the crystal structures of a number of organosulfur compounds will be examined for experimental evidence supporting the existence of such an interaction. Finally, the results of the calculations and the available experimental evidence will be discussed in light of the known limitations of the CNDO/2 method. Conclusions can then be drawn about the manner in which such an interaction influences the conformation of organosulfur compounds.

## II. Theoretical Evidence for a Nonbonded 1,4 Carbon-Sulfur Interaction from Molecular Orbital Calculations

**A. Nuclear Geometry Used for CNDO/2 Calculations.** Calculations were carried out on methyl *n*-propyl sulfide and methyl *n*-propyl disulfide. The bond lengths and bond angles used for the calculations are shown in Table I. Since no structural determinations are yet available for either of these molecules, these parameters were obtained from structurally related molecules. The parameters listed in Table I for methyl *n*-propyl sulfide were taken from the recent crystal structure determination of *L*-methionine,<sup>10</sup> since methyl *n*-propyl sulfide can be considered to be a model compound for the methionine side chain. *L*-Methionine crystals contain two conformationally nonequivalent sets of molecules per unit cell (which are referred to as the A and B conformations<sup>10</sup>). Calculations were carried out on

**TABLE I: Bond Lengths and Bond Angles Used for Calculations<sup>a</sup>**

	Methyl <i>n</i> -propyl sulfide <sup>b</sup>		Methyl <i>n</i> -propyl disulfide
	A	B	
$R(\text{S}-\text{S}), \text{Å}$			2.038
$R(\text{C}_\alpha-\text{S}), \text{Å}$	1.810	1.758	1.832
$R(\text{S}-\text{C}_{\alpha'}), \text{Å}$	1.863	1.798	1.832
$R(\text{C}_\alpha-\text{C}_\beta), \text{Å}$	1.535	1.546	1.533
$R(\text{C}_\beta-\text{C}_\gamma), \text{Å}$	1.536	1.561	1.533
$R(\text{C}-\text{H}), \text{Å}$	1.090	1.090	1.090
$\tau(\text{SSC}_\alpha), \text{deg}$			103.7
$\tau(\text{SC}_\alpha\text{C}_\beta), \text{deg}$	107.3	113.4	114.7
$\tau(\text{C}_\alpha\text{C}_\beta\text{C}_\gamma), \text{deg}$	111.1	117.8	109.47
$\tau(\text{C}_\alpha\text{SC}_{\alpha'}), \text{deg}$	99.8	101.8	
$\tau(\text{SCH}) = \tau(\text{CCH}), \text{deg}$	109.47	109.47	109.47
$\chi(\text{SC}_{\alpha'}-\text{C}_\beta-\text{C}_\gamma'), \text{deg}$	174.2	73.6	<i>d</i>

<sup>a</sup> The type of atom (e.g.,  $\text{C}_\alpha$ ,  $\text{C}_\beta$ , etc.) is specified only where needed to prevent ambiguity. See Figures 2, 4, and 6 for the significance of the  $\alpha$ ,  $\beta$ ,  $\gamma$ , and the prime. <sup>b</sup> These data were taken from ref 10. <sup>c</sup> These data were taken from ref 3. <sup>d</sup> Varied in the calculations.

both nuclear geometries with the coordinates shown in columns A and B, respectively, of Table I. The conformation of methyl *n*-propyl sulfide that is the analog of the B conformation of *L*-methionine is shown in Figure 2. This molecule has an  $\text{SC}_{\alpha'}-\text{C}_\beta-\text{C}_\gamma'$  dihedral angle of  $73.6^\circ$ . The analog of the A conformation differs from the B mainly in that its  $\text{SC}_{\alpha'}-\text{C}_\beta-\text{C}_\gamma'$  dihedral angle is  $174.2^\circ$ . The SCH and CCH bond angles were assumed to have the tetrahedral value of  $109.47^\circ$ . The bond lengths and bond angles used for methyl *n*-propyl disulfide were the same as those used in the earlier calculations on disulfides<sup>3</sup> except that the CCC bond angle for the *n*-propyl group (which was not encountered in earlier calculations) was assumed to have the tetrahedral value of  $109.47^\circ$ . In all cases, a C-H bond length of  $1.090 \text{ Å}$  was used. Other conformational constraints made in these calculations will be discussed where appropriate.

**B. CNDO/2 Method.** The CNDO/2 calculations were carried out as described earlier.<sup>3</sup>

**C. Results of Calculations.** The CNDO/2 method has been shown to yield dihedral angles that are in good agreement with the observed rotational isomers of *n*-butane<sup>11</sup> and dimethyl disulfide<sup>12</sup> due to rotations about the central C-C and S-S bonds, respectively. Using this method, +sp and ap conformations were found to be energy minima for rotation about the C-S bond in methyl ethyl disulfide; however, no direct experimental evidence was available with which to check this result. In order to test further the reliability of the CNDO/2 method for calculating the conformations of organosulfur compounds, the potential function for rotation about the S-C $_{\alpha'}$  bond (Figure 2) of methyl *n*-propyl sulfide was investigated. If the results of the calculations are reliable, the calculated positions of the energy minima in this potential function should be in agreement with the experimentally observed  $\text{C}_\alpha\text{S}-\text{C}_\alpha-\text{C}_\beta'$  dihedral angles for the *L*-methionine side chains in the crystalline state.

Figure 2 shows an ORTEP diagram of methyl *n*-propyl

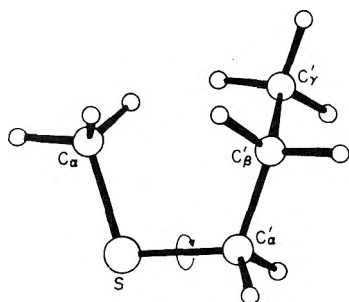


**Figure 2.** An ORTEP diagram of methyl *n*-propyl sulfide with  $C_{\alpha}S-C_{\alpha}'C_{\beta}'$  and  $SC_{\alpha}'-C_{\beta}'C_{\gamma}'$  dihedral angles equal to 0 and  $73.6^{\circ}$ , respectively. The  $C_{\alpha}$  and  $C_{\gamma}'$  hydrogen atoms are staggered with respect to the  $S-C_{\alpha}'$  and  $C_{\alpha}'-C_{\beta}'$  bonds, respectively. The direction of positive rotation about the  $S-C_{\alpha}'$  bond is that in which the primed side of the molecule is rotated clockwise when looking from  $C_{\alpha}'$  toward  $S'$ .

sulfide with the B conformation about the  $C_{\alpha}'-C_{\beta}'$  bond. In this conformation, the  $C_{\alpha}S-C_{\alpha}'C_{\beta}'$  and  $SC_{\alpha}'-C_{\beta}'C_{\gamma}'$  dihedral angles are 0 and  $73.6^{\circ}$ , respectively. In conformations A and B, the  $C_{\gamma}'$  methyl group is ap and sc, respectively, to the S atom across the  $C_{\alpha}'-C_{\beta}'$  bond. The  $C_{\alpha}S-C_{\alpha}'C_{\beta}'$  dihedral angle is defined in such a way that the primed side of the molecule rotates clockwise (viewed with the  $C_{\alpha}'$  atom in front) about the  $S-C_{\alpha}'$  bond as this dihedral angle is increased from 0 to  $360^{\circ}$ .<sup>13</sup> This brings the  $C_{\alpha}$  and  $C_{\gamma}'$  groups in closest proximity when the  $C_{\alpha}S-C_{\alpha}'C_{\beta}'$  dihedral angle is about  $250$  to  $300^{\circ}$ . The  $C_{\alpha}$  hydrogen atoms were held staggered with respect to the  $S-C_{\alpha}'$  bond and the  $C_{\gamma}'$  hydrogen atoms were held staggered with respect to the  $C_{\beta}'$  hydrogen atoms during the calculations. The energies of both the A and B conformations were calculated as a function of the  $C_{\alpha}S-C_{\alpha}'C_{\beta}'$  dihedral angle in  $20^{\circ}$  intervals, except near the minima, where the intervals were reduced to  $10^{\circ}$ . The results of these calculations are shown in Figure 3.

The minima for curve A are at values of the  $C_{\alpha}S-C_{\alpha}'C_{\beta}'$  dihedral angles of about  $65$ ,  $180$ , and  $285^{\circ}$ ; for curve B, they are at about  $65$ ,  $180$ , and  $270^{\circ}$ . The  $C_{\alpha}S-C_{\alpha}'C_{\beta}'$  dihedral angles found crystallographically in the side chains of the two forms of L-methionine are  $179.7$  and  $73.6^{\circ}$  for conformations A and B, respectively.<sup>10</sup> The lowest-energy conformation found in the calculations using either the A or the B geometries of Table I has a  $C_{\alpha}S-C_{\alpha}'C_{\beta}'$  dihedral angle of  $180^{\circ}$ . This is in good agreement with the observed  $C_{\alpha}S-C_{\alpha}'C_{\beta}'$  dihedral angle of the A crystal conformation of the methionine side chain, but in disagreement with the observed B crystal conformation. We presume that intermolecular packing forces (not included in the calculation) influence the B conformation. These additional interactions force the B molecule into the next lowest-energy calculated minimum (with a  $C_{\alpha}S-C_{\alpha}'C_{\beta}'$  dihedral angle of about  $65^{\circ}$ ).

The broken lines for curve B near  $C_{\alpha}S-C_{\alpha}'C_{\beta}'$  dihedral angles of 0 and  $300^{\circ}$  indicate high-energy regions caused by steric overlap between the  $C_{\alpha}$  and  $C_{\gamma}'$  groups. The shoulder on curve A near  $330^{\circ}$  can be shown, with the aid of space-filling models, to correspond to a close contact between hydrogen atoms attached to the  $C_{\alpha}$  and  $C_{\gamma}'$  atoms.

The  $C_{\gamma}'$  group and the S atom are in 1,4 positions across the  $C_{\alpha}'-C_{\beta}'$  bond. In order to investigate the effect, if any, of this 1,4 carbon-sulfur interaction on the potential function for rotation about the  $C_{\alpha}'-C_{\beta}'$  bond, the following calculation was performed. Using the bond lengths, bond angles, and  $C_{\alpha}S-C_{\alpha}'C_{\beta}'$  dihedral angle from the A conformation ( $179.7^{\circ}$ ) of L-methionine, the energy of methyl *n*-pro-

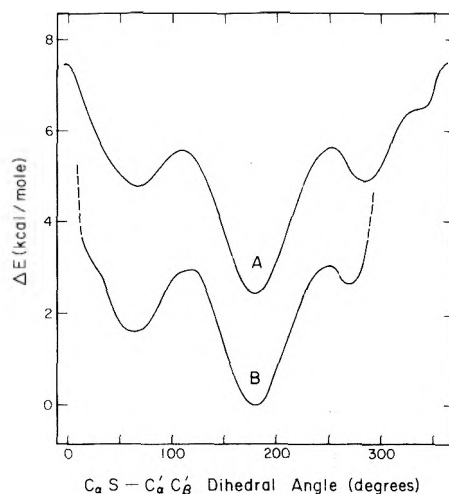


**Figure 3.** Variation of the energy of methyl *n*-propyl sulfide with  $C_{\alpha}S-C_{\alpha}'C_{\beta}'$  dihedral angle for the sets of geometrical parameters A and B listed in Table I. The energy has been normalized to zero for the ap conformation of curve B.

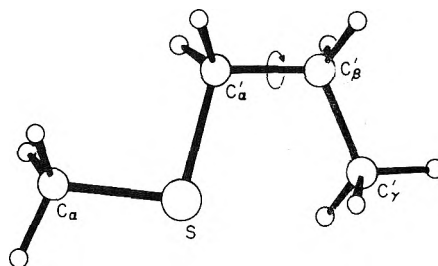


**Figure 4.** An ORTEP diagram of methyl *n*-propyl sulfide with  $C_{\alpha}S-C_{\alpha}'C_{\beta}'$  and  $SC_{\alpha}'-C_{\beta}'C_{\gamma}'$  dihedral angles of  $179.7$  and  $0^{\circ}$ , respectively. The  $C_{\alpha}$  and  $C_{\gamma}'$  hydrogen atoms are staggered with respect to the  $S-C_{\alpha}'$  and  $C_{\alpha}'-C_{\beta}'$  bonds, respectively. The direction of positive rotation about the  $C_{\alpha}'-C_{\beta}'$  bond is that in which the  $C_{\beta}'-C_{\gamma}'$  bond is rotated clockwise when looking from  $C_{\beta}'$  toward  $C_{\alpha}'$ .

pyl sulfide was calculated as a function of the  $SC_{\alpha}'-C_{\beta}'C_{\gamma}'$  dihedral angle. The A geometry was chosen because in this conformation the  $C_{\alpha}$  group is trans to the  $C_{\beta}'$  and  $C_{\gamma}'$  groups and will not interfere with rotation about the  $C_{\alpha}'-C_{\beta}'$  bond. An ORTEP diagram of this molecule with a  $SC_{\alpha}'-C_{\beta}'C_{\gamma}'$  dihedral angle of  $0^{\circ}$  is shown in Figure 4. The  $C_{\alpha}$  hydrogen atoms are staggered with respect to the  $S-C_{\alpha}'$  bond, and the  $C_{\gamma}'$  hydrogen atoms are staggered with respect to the  $C_{\alpha}'-C_{\beta}'$  bond. The direction of positive rotation about the  $C_{\alpha}'-C_{\beta}'$  bond is that in which the  $C_{\beta}'-C_{\gamma}'$  bond is rotated clockwise when looking from  $C_{\beta}'$  to  $C_{\alpha}'$ .

The results of this calculation are shown in Figure 5. The minima in this potential function correspond to sp and ap conformations with the sp more stable by more than 12 kcal/mol. The energy has been normalized to zero for the sp conformation. This potential function has minima at the same dihedral angles as the potential function for internal rotation about the C-S bond in methyl ethyl disulfide.<sup>3</sup> In both cases, there were carbon and sulfur atoms in the 1 and 4 positions, respectively. One striking difference between these two calculated potentials, however, is the relative energy differences between the minima. In methyl ethyl disulfide, the sp form is more stable than the ap form by only about 2 kcal/mol.<sup>3</sup> Another important difference between the two calculations that should be pointed out is that the nonbonded carbon-sulfur internuclear distance in the sp

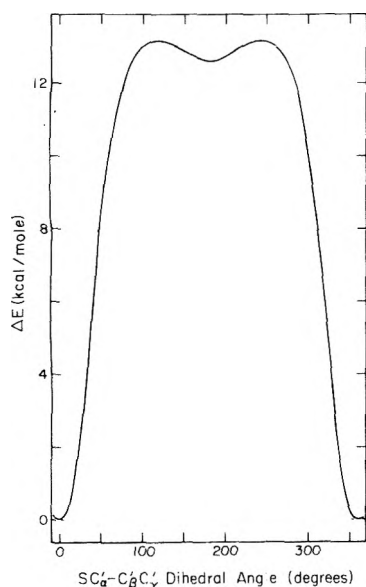


Figure 5. Variation of the energy of methyl *n*-propyl sulfide with  $S'C_{\alpha'}-C_{\beta'}C_{\gamma}'$  dihedral angle for the conformation shown in Figure 4. The energy has been normalized to zero for the *sp* conformation.

conformation is 3.01 Å for methyl ethyl disulfide, but 2.63 Å for methyl *n*-propyl sulfide. The calculated difference in the relative energies of the *sp* and *ap* conformations of these two molecules is probably related to the differences in these nonbonded carbon-sulfur distances. It seems natural to conclude that the carbon-sulfur interaction, which is thought to be responsible for the *sp* minima in these potential functions, is more favorable at a carbon-sulfur internuclear distance of 2.66 Å than 3.01 Å. The fact that a nonbonded carbon-sulfur distance as short as 2.66 Å is associated with a conformation of low energy in these calculations, however, suggests that the tendency toward carbon-sulfur interaction is being exaggerated. One well-recognized characteristic of the CNDO/2 method is that, while it generally gives correct qualitative trends for interatomic interaction, it tends to overestimate the magnitudes of attractive interactions. For example, for attractive intermolecular interactions (such as hydrogen bonds), the CNDO/2 method has been found to systematically overestimate the stabilization energy and allow contact distances that are too short.<sup>14</sup> Hence, the large energy difference between the *sp* and *ap* conformations found here for methyl *n*-propyl sulfide is probably related to this deficiency of the CNDO/2 method. The manner in which this deficiency may be affecting the calculated potential functions is discussed in section IIIH.

It should be kept in mind that these calculations were carried out using the assumption of rigid rotations (i.e., by calculating the energy as a function of a dihedral angle alone and not allowing for other simultaneous changes in bond lengths, bond angles, etc.). Hence, the nonbonded carbon-sulfur internuclear distance is determined completely by the three bond lengths, two bond angles, and dihedral angle of the valence bonds connecting atoms 1-4. It is the differences in the values of these structural parameters that makes the nonbonded carbon-sulfur internuclear distances and relative energies of the *sp* conformations of methyl ethyl disulfide and methyl *n*-propyl sulfide discussed above different.

The last set of calculations that were carried out were on

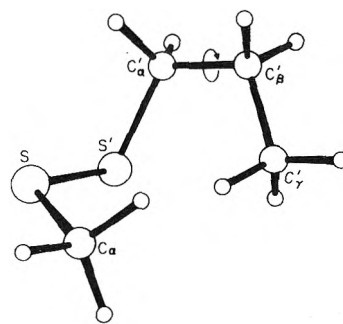


Figure 6. An ORTEP diagram of methyl *n*-propyl disulfide with  $C_{\alpha}S-S'C_{\beta'}$ ,  $SS'-C_{\alpha'}C_{\beta}'$ , and  $S'C_{\alpha'}-C_{\beta'}C_{\gamma}'$  dihedral angles of 90, 270, and 0°, respectively. The  $C_{\alpha}$  and  $C_{\gamma}'$  hydrogen atoms are staggered with respect to the  $S-S'$  and  $C_{\alpha'}-C_{\beta}'$  bonds, respectively. The direction of positive rotation about the  $C_{\alpha'}-C_{\beta}'$  bond is that in which the  $C_{\beta}'-C_{\gamma}'$  bond is rotated clockwise when looking from  $C_{\beta}'$  toward  $C_{\alpha}'$ .

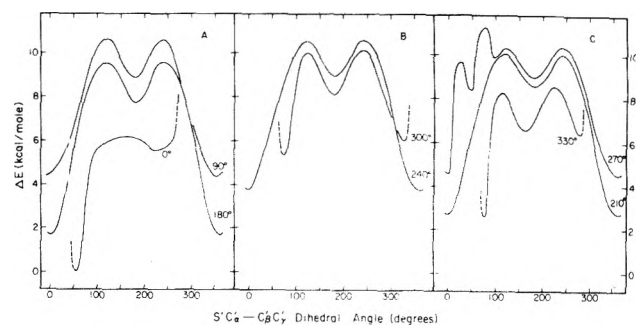


Figure 7. Variation of the energy of methyl *n*-propyl disulfide with  $S'C_{\alpha'}-C_{\beta'}C_{\gamma}'$  dihedral angle, with various values of the  $SS'-C_{\alpha'}C_{\beta}'$  dihedral angle. The value of the  $SS'-C_{\alpha'}C_{\beta}'$  dihedral angle is shown next to each curve. The energy is normalized to zero for the minimum in the 0° curve near  $S'C_{\alpha'}-C_{\beta'}C_{\gamma}' \sim 50^\circ$ .

methyl *n*-propyl disulfide. An ORTEP drawing of this molecule is shown in Figure 6. This molecule is of interest because of the possibility of two different 1,4 carbon-sulfur interactions. The  $S$  and  $C_{\beta}'$  atoms as well as the  $S'$  and  $C_{\gamma}'$  atoms are in the 1,4 positions relative to one another across the  $S'-C_{\alpha'}$  and  $C_{\alpha'}-C_{\beta}'$  bonds, respectively. The energy of the molecule was calculated as a function of the  $S'C_{\alpha'}-C_{\beta'}C_{\gamma}'$  dihedral angle for various values of the  $SS'-C_{\alpha'}C_{\beta}'$  dihedral angle. The  $C_{\alpha}S-S'C_{\alpha'}$  dihedral angle was held fixed at 90°. The  $C_{\alpha}$  hydrogen atoms were held staggered with respect to the  $S-S'$  bond and the  $C_{\gamma}'$  hydrogen atoms were held staggered with respect to the  $C_{\alpha'}-C_{\beta}'$  bond. The direction of positive rotation about the  $C_{\alpha'}-C_{\beta}'$  bond is that in which the  $C_{\beta}'-C_{\gamma}'$  bond is rotated clockwise when looking from  $C_{\beta}'$  to  $C_{\alpha}'$ . In the conformation of the molecule shown in this figure, the  $SS'-C_{\alpha'}C_{\beta}'$  dihedral angle is 270° and the  $S'C_{\alpha'}-C_{\beta'}C_{\gamma}'$  dihedral angle is 0°. It should be noted that the  $C_{\alpha}$  and  $C_{\beta}'$  groups come into closest proximity when the  $SS'-C_{\alpha'}C_{\beta}'$  dihedral angle is around 300°, and that certain pairs of  $SS'-C_{\alpha'}C_{\beta}'$  and  $S'C_{\alpha'}-C_{\beta'}C_{\gamma}'$  dihedral angles will result in severe atomic overlaps between the  $C_{\gamma}'$  group and either the  $S$  atom or  $C_{\alpha}$  group. The resulting high energy regions in the potential energy curves will be indicated by broken lines in Figure 7.

The results of the calculations on methyl *n*-propyl disulfide are shown in Figure 7. The value of the  $SS'-C_{\alpha'}C_{\beta}'$  dihedral angle used for each calculation is shown next to each curve. The energy has been normalized to zero for the minimum of the 0° curve near the  $S'C_{\alpha'}-C_{\beta'}C_{\gamma}'$  dihedral angle

of  $\sim 50^\circ$ . One conclusion that follows from the results shown in Figure 7 is that the energy minima for rotation about the  $C_{\alpha'}-C_{\beta'}$  bond correspond to conformations in which the  $C_{\gamma'}$  and S' atoms are sp and ap to each other, except for those values of the  $SS'-C_{\alpha'}C_{\beta'}$  dihedral angle in which there are steric overlaps for the sp conformation about the  $C_{\alpha'}-C_{\beta'}$  bond (and for the bumpy region of the  $270^\circ$  curve near  $S'C_{\alpha'}-C_{\beta'}C_{\gamma'}$  dihedral angles of  $20-80^\circ$ , which will be discussed at the end of this section). In those cases where atomic overlaps prevent the sp form from being a low-energy conformation, energy minima appear at values of the  $S'C_{\alpha'}-C_{\beta'}C_{\gamma'}$  dihedral angle which are as close to the sp conformation as these atomic overlaps will allow. That is, minima still appear for conformations in which the carbon and sulfur atoms in the 1 and 4 positions are as close to one another as they can get before severe overlap results in high energies. Minima of this sort which are found very close to regions of severe steric overlap occur for curves whose  $SS'-C_{\alpha'}C_{\beta'}$  dihedral angles are 0, 300, and  $330^\circ$ .

The two conformations of lowest energy are those in which the  $SS'-C_{\alpha'}C_{\beta'}$  dihedral angles are 0 and  $180^\circ$  and in which the  $S'C_{\alpha'}-C_{\beta'}C_{\gamma'}$  dihedral angles are  $50$  and  $0^\circ$ , respectively. These are conformations in which close carbon-sulfur contacts occur. In the lowest-energy conformation, the S atom and the  $C_{\beta'}$  methylene group are sp to one another and the  $C_{\gamma'}$  group lies in contact with the S atom (at an  $S'C_{\alpha'}-C_{\beta'}C_{\gamma'}$  dihedral angle of  $50^\circ$ ). Hence, this lowest-energy conformation of methyl *n*-propyl disulfide obtains some of its stability from a 1,5  $C_{\gamma'}-S$  interaction. The  $C_{\gamma'}\cdots S$  nonbonded internuclear distance in this conformation is about 2.5 Å. Distances shorter than this lead to high energies. Hence, it appears that in these calculations carbon-sulfur nonbonded distances as short as 2.5 Å are allowed.

The second-lowest energy conformation found is one in which the S atom and  $C_{\beta'}$  methylene groups are ap and in which the S' and  $C_{\gamma'}$  groups are sp. These two lowest-energy conformations have the same values of the  $SS'-C_{\alpha'}C_{\beta'}$  dihedral angles as the two lowest-energy conformations of methyl ethyl disulfide.<sup>3</sup> Hence, it seems that the 1,4  $C_{\beta'}-S$  interaction determines the conformation about the  $S'-C_{\alpha'}$  bond. The low-energy position of the  $C_{\gamma'}$  group is then found by rotation about the  $C_{\alpha'}-C_{\beta'}$  bond until this group comes into contact with either the S atom (when the  $SS'-C_{\alpha'}C_{\beta'}$  dihedral angle is  $0^\circ$ ) or the S' atom (when the  $SS'-C_{\alpha'}C_{\beta'}$  dihedral angle is  $180^\circ$ ).

With the aid of space-filling models, the double minimum in the  $270^\circ$  curve between  $S'C_{\alpha'}-C_{\beta'}C_{\gamma'}$  dihedral angles of  $20$  and  $80^\circ$  can be shown to be due to two of the hydrogen atoms on the  $C_{\gamma'}$  methyl group brushing past one of the hydrogen atoms on the  $C_{\alpha'}$  group. This feature does not appear on the  $90^\circ$  curve because, in this conformation, the  $C_{\alpha'}$  group is on the side of the molecule opposite from the  $C_{\gamma'}$  group.

### III. Experimental Evidence for a Nonbonded 1,4 Carbon-Sulfur Interaction from Short Intramolecular Nonbonded Carbon-Sulfur Contacts in Crystals

*A. Definition of and Criterion for an Attractive Nonbonded Carbon-Sulfur Interaction.* It has been shown in section II of this paper and in a previous paper<sup>3</sup> that the form of the potential functions for rotations about C-S and C-C bonds can be rationalized in terms of an attractive nonbonded carbon-sulfur interaction, in cases where there are carbon and sulfur atoms in the 1 and 4 positions. The

TABLE II: Sets of van der Waals Contact Distances

Atomic contact	van der Waals contact distance, Å		
	Ref 9	Ref 8	This work <sup>a</sup>
CH $\cdots$ CH <sup>b</sup>	4.0	3.5	3.5
C <sub>ar</sub> $\cdots$ C <sub>ar</sub> <sup>c</sup>	3.4	3.4	3.4
C' $\cdots$ C' <sup>d</sup>		2.9	2.9
S $\cdots$ S	3.7	3.4	3.3
OH $\cdots$ OH		3.2	3.2
O $\cdots$ O <sup>e</sup>	2.8	2.4	2.4
NH $\cdots$ NH		3.4	3.4
N $\cdots$ N	3.0	2.6	2.6

<sup>a</sup> Only the S $\cdots$ S contact distance in this column differs from those of Nemethy and Scheraga.<sup>8</sup> <sup>b</sup> CH is used for CH, CH<sub>2</sub>, and CH<sub>3</sub> groups without correction for the deviation of these groups from a spherical shape. <sup>c</sup> This is the radius of an aromatic carbon and takes into account the thickness of an aromatic molecule. <sup>d</sup> C' is used for contacts involving a carbonyl carbon. <sup>e</sup> This refers to an alcohol oxygen atom. This contact distance was not given by Nemethy and Scheraga,<sup>8</sup> but is obtained by subtracting 0.4 Å from the van der Waals radius of an OH group. Similarly, the van der Waals radii of the NH group and N atom differ by 0.4 Å.

value of the internuclear distance (in this case, the nonbonded C $\cdots$ S distance) at which the usual nonbonded attractive (dispersion, etc.) and repulsive (overlap repulsions, etc.) forces between the atoms involved balance one another is referred to as the van der Waals contact distance of the two groups. When the observed equilibrium internuclear distance between the two groups is shorter than their van der Waals contact distance, an additional attractive interaction (besides the van der Waals attractive forces) must exist between the two groups. The origin of the additional 1,4 carbon-sulfur attractive interaction proposed here has not yet been identified, but the strength of this force can, and will, be compared with those in other interactions, such as hydrogen bonds. Having defined what is meant by a carbon-sulfur interaction and having established a criterion for its existence (viz., observed carbon-sulfur contact distances less than their van der Waals contact distances), we turn now to the problem of choosing a reasonable set of van der Waals contact distances to be used for comparison with those observed in crystals of organosulfur compounds.

*B. Choice of van der Waals Contact Distances.* The concept of a van der Waals contact distance between two groups is not a rigorously defined one, but is a measure of the space occupied by the groups due to the mutual repulsion of their electron clouds. Because of the qualitative nature of this concept, there is a wide variation in the accepted values for these contact distances. A comparison and discussion of several sets of these contact distances has been made<sup>15</sup> (see Table II).

The van der Waals contact distances given in the second column of Table II are those of Pauling,<sup>9</sup> while those in the third column are the values used by Nemethy and Scheraga<sup>8</sup> to calculate the sterically allowed conformations of peptides. These two sets of van der Waals contact distances represent a "long" and a "short" set, respectively. The contact distances listed in the fourth column are those to be used in this paper for comparison with crystallographically observed nonbonded carbon-sulfur contacts. These values are essentially the "short" values used by Nemethy and Scheraga,<sup>8</sup> except that the van der Waals contact distance



between two sulfur atoms has been reduced even further from the value given by Pauling to a value of 3.3 Å. The shortest nonbonded sulfur-sulfur contact distance that has been observed is 3.25 Å.<sup>16</sup> This short set of values was chosen intentionally so that one could have confidence that experimentally observed nonbonded distances shorter than those calculated from this set would point to the presence of nonbonded attractive interactions over and above the van der Waals attractive forces.

It should be noted that three different types of contact distances involving carbon atoms appear in Table II. The values taken for contacts with CH<sub>3</sub>, CH<sub>2</sub>, and CH groups are shown as CH values in this table. C' values are used for carbon atoms in a carbonyl group and C<sub>ar</sub> values are used for aromatic carbon atoms, and take into account the thickness of an aromatic molecule. Since there may be differences in the nature of the attractive interactions between a sulfur atom and each of these three types of carbon atoms, experimentally observed short carbon-sulfur contacts will be listed separately according to the type of carbon involved in the interaction.

In order to obtain a feeling for how experimentally observed nonbonded distances compare with those calculated from the van der Waals contact distances listed in Table II for cases in which the atoms in question are hydrogen bonded,<sup>17</sup> the data in Table III were assembled. The values in the second column of Table III are the nonbonded contact distances calculated from Pauling's values shown in Table II. The numbers in the parentheses in the second column, which are explained in footnote *a* of the table, take into account the effect of the hydrogen atom. These are to be compared with the other two sets of contact distances (which also take the hydrogen into account) listed in Table II and with the representative crystallographically observed hydrogen bonded distances taken from ref 17.

From a comparison of the last four columns in Table III, it can be seen that van der Waals contact distances calculated using Pauling's<sup>9</sup> values are generally a few tenths of an ångström larger than the crystallographically observed hydrogen bonded distances. The contact distances calculated on the basis of the Nemethy and Scheraga values,<sup>8</sup> on the other hand, are comparable to, or smaller than, those found in hydrogen bonds. The C-H...O contact distance is particularly short by the Nemethy and Scheraga criterion. The data shown in this table serve two purposes. First, they illustrate that the set of contact distances to be used in this paper is, indeed, a "short" set. Second, the data give one a basis on which to assess the strength of an interaction from the difference in calculated and observed contact distances by showing how these calculated and observed distances are related for interactions such as the hydrogen bonds (of various strengths) shown in this table.

*C. Geometrical Parameters that Determine the Nonbonded 1,4 Carbon-Sulfur Distance.* Before presenting examples of short nonbonded carbon-sulfur distances, it is of interest to reiterate the degrees of freedom in the <sup>1</sup>CXY<sup>4</sup>S unit that determine the <sup>1</sup>C...<sup>4</sup>S distance. A diagram of the <sup>1</sup>CXY<sup>4</sup>S fragment is shown in Figure 8. The <sup>1</sup>C...<sup>4</sup>S nonbonded internuclear distance is a function of the <sup>1</sup>C-X, X-Y, and Y-<sup>4</sup>S bond lengths, <sup>1</sup>CXY and XY<sup>4</sup>S bond angles, and <sup>1</sup>CX-Y<sup>4</sup>S dihedral angle, as indicated in this figure. Hence, a favorable <sup>1</sup>C...<sup>4</sup>S contact distance can be achieved by the simultaneous variation of any or all six of these degrees of freedom.

*D. Crystallographically Observed Short Nonbonded In-*

**TABLE III: Comparison of Some Calculated Contact Distances with Crystallographically Observed Hydrogen-Bonded Distances**

Atomic contact	Calculated contact distances, Å			Observed H-bonded distances, <sup>b</sup> Å
	Pauling <sup>a</sup>	Nemethy and Scheraga	This work	
(1) OH...O	2.8 (3.1)	2.8	2.8	2.7
(2) OH...N	2.9 (3.1)	2.9	2.9	2.8
(3) NH...O	2.9 (3.1)	2.9	2.9	2.9
(4) NH...N	3.0 (3.2)	3.0	3.0	3.1
(5) NH...S	3.35 (3.55)	3.4	3.35	3.4
(6) CH...O	3.4 (3.4)	2.95	2.95	3.2
(7) CH...S	3.85 (3.85)	3.45	3.40 <sup>c</sup>	
(8) C <sub>ar</sub> ...S	3.55 (3.55)	3.40	3.35 <sup>c</sup>	
(9) C'...S		3.15	3.10 <sup>c</sup>	

<sup>a</sup> Since Pauling reports van der Waals radii only for O and N atoms and not for the OH and NH groups, contacts involving NH and OH groups in this column were calculated in two ways. The first number is simply the heavy atom contact distance calculated using Pauling's van der Waals radii for the O and N atoms. In parentheses are contact distances calculated by allowing an additional 0.2 Å for the effect of the hydrogen. The numbers in parentheses are the values to be compared with those in the other two columns since contacts in these columns have also taken the effect of the hydrogen into account. The value of 0.2 Å was chosen because it is the difference between the NH and OH values of Nemethy and Scheraga<sup>8</sup> and the N and O values of Pauling,<sup>9</sup> respectively. <sup>b</sup> These are representative crystallographically observed internuclear distances for the types of hydrogen bonds indicated. These values have been taken from ref 17. <sup>c</sup> To be compared with data in Tables IV-VI.

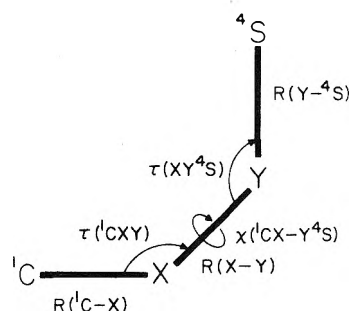


**Figure 8.** A schematic diagram defining the three bond lengths, two bond angles, and one dihedral angle that determine the <sup>1</sup>C...<sup>4</sup>S nonbonded internuclear distance.

*tramolecular Carbon-Sulfur Contact Distances.* Examples of short 1,4 carbon-sulfur contact distances<sup>10,16,18-43</sup> are shown in Tables IV-VI for each of the three types of carbon atoms defined earlier (Table VI is available in microfilm; see paragraph at end of text regarding supplementary material). The data shown in these tables require some explanation. Only intramolecular contacts involving carbon and divalent sulfur atoms which are separated by at least two other singly bonded atoms are listed. These structures can have one of several different atoms in the X and Y positions (see Figure 8). In order to illustrate how different combinations of the six independent degrees of freedom shown in Figure 8 lead to the observed contact distances, each of these six geometrical parameters are included in

**TABLE IV: Crystallographically Observed Short Intramolecular Contact Distances between Sulfur and Aliphatic CH-Type Carbon Atoms**

Compound	$R(^1C \cdots ^1S), \text{\AA}$	$R(CX), \text{\AA}$	$R(XY), \text{\AA}$	$R(YS), \text{\AA}$	$\tau(CXY),$ deg	$\tau(XYS),$ deg	$\chi(^1CX-$ $Y^1S), \text{deg}$	Ref	
Tetragonal L-cystine	$C_5 \cdots S_1$ 3.55	C-C 1.53	C-S 1.79	S-S 2.04	CCS 116.8	CSS 104.1	CC-SS 67	18	
Bis[ <i>N,N</i> -(dimethyl- amino)ethyl] disul- fide	$C_8 \cdots S_4$ 3.32	C-C 1.51	C-S 1.81	S-S 2.04	CCS 115.4	CSS 102.8	CC-CS 55	19	
	$C_{12} \cdots S_3$ 3.40	C-C 1.51	C-S 1.81	S-S 2.04	CCS 111.4	CSS 103.6	CC-CS 67		
Thiamine <i>n</i> -propyl <sup>a</sup> disulfide	$C_3 \cdots S_1$ 3.09	C-C 1.49	C-C 1.76	C-S 1.90	CCC 97	CCS 113	CC-CS 79	20	
	$C_7 \cdots S_1$ 3.31	C-C 1.54	C-S 1.79	S-S 2.04	CCS 118	CSS 107	CC-SS 34		
	$C_8 \cdots S_2$ 3.43	C-C 1.51	C-C 1.54	C-S 1.79	CCC 113	CCS 118	CC-CS 72		
L-Methionine	$C_{2R} \cdots S_{1B}$ 3.44	C-C 1.53	C-C 1.51	C-S 1.79	CCC 117.8	CCS 113.4	CC-CS 74	10	
L-Cystine·2HBr·2H <sub>2</sub> O	$C_5 \cdots S_1$ 3.44	C-C 1.52	C-S 1.82	S-S 2.04	CCS 113.1	CSS 100.1	CC-SS 70	21	
3,3,3',3'-Tetra- methyl-D-cystine· 2HCl	$C_9 \cdots S_1$ 3.37	C-C 1.52	C-S 1.87	S-S 2.05	CCS 110.1	CSS 105.5	CC-SS 55	21	
	$C_5 \cdots S_1$ 3.53	C-C 1.56	C-S 1.87	S-S 2.05	CCS 109.9	CSS 105.5	CC-SS 67		
	$C_7 \cdots S_2$ 3.42	C-C 1.51	C-S 1.87	S-S 2.05	CCS 113.8	CSS 105.5	CC-SS 53		
D,L-6,8-Thioctic acid Dicinnamyl disulfide	$C_2 \cdots S_2$ 3.51	C-C 1.47	C-S 1.87	S-S 2.05	CCS 106.8	CSS 105.5	CC-SS 70		
	$C_5 \cdots S_2$ 3.24	C-C 1.51	C-C 1.53	C-S 1.83	CCC 115.3	CCS 111.3	CC-CS 60	22	
	$C_3 \cdots S_1 =$ $C_3' \cdots S_1' =$ 2.85	C-C 1.33	C-C 1.54	C-S 1.88	CCC 122.8	CCS 105.4	CC-CS 1	23	
	$C_2 \cdots S_1' =$ $C_2' \cdots S_1 =$ 3.23	C-C 1.54	C-S 1.88	S-S 2.01	CCS 105.4	CSS 103.3	CC-SS 57		
	$C_3 \cdots S_1' =$ $C_3' \cdots S_1 =$ 2.86	} 1.5 interactions							
	<i>tert</i> -Butyl- <i>N,N</i> - dimethyl trithio- per- carbamate	$C_6 \cdots S_2$ 3.33	C-C 1.54	C-S 1.85	S-S 2.00	CCS 109.8	CSS 105.4	CC-SS 56	24
	Tetraethyl thiuram disulfide	$C_4 \cdots S_2$ 3.52	} 1,5 interactions						25
$C_{10} \cdots S_4$ 3.56									
$C_8 \cdots S_3$ 3.46									

<sup>a</sup> The structure of the *n*-propyl group was not accurately determined in this study due to its thermal mobility.

these tables for each contact cited. In a few cases, contacts are listed between atoms in the 1 and 5 positions. In these cases, only the  $^1C \cdots ^5S$  contact distance is listed.

The reference to the published crystal structure from which each contact distance was calculated is listed in the last column of these tables. The numbers on the carbon and sulfur atoms in the second column refer to the labeling scheme used for these atoms in the *published* structure. The bond lengths in these tables have been rounded to the nearest 0.01 Å, the bond angles to the nearest 0.1°, and the dihedral angles to the nearest degree. Since the contacts listed in these tables will be compared with the "short" set of calculated van der Waals contacts in the fourth column of Table III, observed contacts up to 0.2 Å larger than those shown in column 4, rows 7-9, of Table III are included in Tables IV-VI. The literature search that uncovered these examples of short carbon-sulfur contacts was by no means exhaustive and, hence, other examples (especially intermolecular ones) may have been overlooked. Unfortunately, the positions of the hydrogens bonded to the carbon atoms involved in these short contacts are seldom determined from X-ray studies, and neutron diffraction data generally are not available. Hence, while it would have been desirable to list H $\cdots$ S contact distances in these tables, only the CH $\cdots$ S distances could be calculated.

*E. Short Contacts Involving Aliphatic CH-Type Carbon Atoms.* The short carbon-sulfur contacts listed in Table IV are for CH-type carbon atoms. With the exception of dicin-

namyl disulfide,<sup>23</sup> each of the examples listed in this table involves a contact with a hydrogen atom bonded to a tetrahedral carbon atom. In the case of dicinnamyl disulfide, the contact involves a hydrogen atom bonded to a trigonal carbon. It could be argued that this example belongs in either Table V or VI with the other trigonal carbon atoms. However, the observed contact distances are short by the criteria established for any of these three types of carbon atoms.

About half of the contacts listed in Table IV are shorter than the "short" calculated CH $\cdots$ S van der Waals contact distance of 3.40 Å, and the other half are still shorter than the value of 3.85 Å calculated using Pauling's criteria (Table III). This indicates that there is an attractive interaction between these two groups. The unusually short contacts found for dicinnamyl disulfide have been attributed<sup>23</sup> to bifurcated hydrogen bonds between a methylene hydrogen atom and two sulfur atoms. A detailed discussion of the nature of each of the contacts listed would be prohibitively long and, hence, the reader is referred to the published structures for further details. *It should be pointed out that there is no indication in the papers cited that these contacts were due to other influences, such as ring closure constraints, partial double bond character between atoms in the 2-3 position, etc.*

In order to be able to assess unambiguously the role that the hydrogen atoms play in this interaction, a knowledge of the positions of the hydrogen atoms in these structures would be required. As mentioned earlier, these positions

**TABLE V: Crystallographically Observed Short Intramolecular Contact Distances between Sulfur and C<sub>ar</sub>-Type Carbon Atoms**

Compound	$R(C \cdots S)$ , Å	$R(CX)$ , Å	$R(XY)$ , Å	$R(YS)$ , Å	$\tau(CXY)$ , deg	$\tau(XYS)$ , deg	$\chi(^1CS-Y^4S)$ , deg	Ref
Diphenyl disulfide	$C_{12} \cdots S_1$ 3.25	C-C 1.38	C-S 1.81	S-S 2.03	CCS 123.7	CSS 105.8	CC-SS 18	26
	$C_2 \cdots S_2$ 3.25	C-C 1.40	C-S 1.79	S-S 2.03	CCS 124.3	CSS 106.5	CC-SS 0	
Bis( <i>o</i> -nitrophenyl) disulfide	$C_{12} \cdots S_1$ 3.14	C-C 1.38	C-S 1.81	S-S 2.05	CCS 120.8	CSS 104.6	CC-SS 11	27
	$C_8 \cdots S_2$ 3.19	C-C 1.39	C-S 1.78	S-S 2.05	CCS 122.6	CSS 104.3	CC-SS 19	
Bis( <i>p</i> -nitrophenyl) disulfide	$C_6 \cdots S' =$ $C_6' \cdots S =$ 3.28	C-C 1.41	C-S 1.77	S-S 2.02	CCS 124.7	CSS 106.2	CC-SS 22	28
	$C_6 \cdots S_2$ 3.20	C-C 1.39	C-S 1.80	S-S 2.05	CCS 121.0	CSS 105.1	CC-SS 21	29
2-(2-Pyridylmethyl-dithio)benzoic acid	$C_{10} \cdots S_2$ 3.46	C-C 1.39	C-C 1.50	C-S 1.83	CCC 122.4	CCS 111.7	CC-CS 78	
	$C_{16} \cdots S_6$ 3.21	C-C 1.38	C-S 1.80	S-S 2.05	CCS 121.4	CSS 105.4	CC-SS 22	30
2,2'-Dicarboxydi-phenyl disulfide anion	$C_{23} \cdots S_5$ 3.21	C-C 1.41	C-S 1.78	S-S 2.05	CCS 121.5	CSS 107.2	CC-SS 8	
	$C_3 \cdots S_1$ 3.44	C-C 1.38	C-C 1.49	C-S 1.84	CCC 122.6	CCS 114.3	CC-CS 70	31
Dibenzyl disulfide	$C_{10} \cdots S_2$ 3.41	C-C 1.43	C-C 1.50	C-S 1.85	CCC 119.7	CCS 112.3	CC-CS 72	
	$C_2 \cdots S_2$ 3.53	C-C 1.49	C-S 1.84	S-S 2.02	CCS 114.3	CSS 103.3	CC-SS 73	
	$C_9 \cdots S_1$ 3.49	C-C 1.50	C-S 1.85	S-S 2.02	CCS 112.3	CSS 102.9	CC-SS 72	
5,5'-Dithiobis(2-nitrobenzoic acid)	$C_4 \cdots S' =$ $C_4' \cdots S =$ 3.13	C-C 1.38	C-S 1.78	S-S 2.02	CCS 120 <sup>a</sup>	CSS 105.5	CC-SS 16	32
	$C_5 \cdots S$ 3.07	C-C 1.39 <sup>a</sup>	C-S 1.79	S-S 2.02	CCS 120 <sup>a</sup>	CSS 104	CC-SS 4	33
Tetraphenyl <i>o</i> -thio-carbonate	$C_{31} \cdots S_4$ 3.09	C-S 1.78	C-S 1.83	C-S 1.84	CSC 103.9	SCS 107.0	CS-CS 44	34
	$C_{21} \cdots S_1$ 3.20	C-S 1.78	C-S 1.83	C-S 1.81	CSC 105.1	SCS 103.9	CS-CS 57	
	$C_{41} \cdots S_2$ 3.38	C-S 1.77	C-S 1.84	C-S 1.83	CSC 105.3	SCS 105.5	CS-CS 66	
	$C_{11} \cdots S_3$ 3.39	C-S 1.77	C-S 1.81	C-S 1.83	CSC 110.3	SCS 108.8	CS-CS 55	
<i>syn</i> -2,11-Dithia-9,18-dimethyl[3,3]- <i>m</i> -cyclophane	$C_5 \cdots S_1'$ 3.28	C-C 1.41	C-C 1.52	C-S 1.80	CCC 117	CCS 117.4	CC-CS 54	35
	$C_5' \cdots S_1$ 3.25	C-C 1.40	C-C 1.52	C-S 1.79	CCC 116	CCS 115.5	CC-CS 54	

<sup>a</sup> These values were not given in the structures referenced, but were assumed for the calculation of the carbon-sulfur nonbonded distance.

are not generally determined accurately from X-ray diffraction studies. Hence, deductions made concerning the role of the hydrogen atoms in this interaction from the contacts shown are speculative. The nature of this interaction, however, is not unlike hydrogen bonding. The short values of the contact distances shown in Table IV compared with those calculated distances shown in Table III indicate that this interaction is comparable in strength with many of those hydrogen bonds listed in column 1 of Table III. Using the Lippincott-Schroeder empirical potential function, it has recently been concluded that C-H $\cdots$ S hydrogen bonds exist and that they are two to three times stronger than C-H $\cdots$ O or C-H $\cdots$ N hydrogen bonds.<sup>44</sup> This prediction is not inconsistent with the data shown in Tables III and IV.

There is also recent thermodynamic evidence for a C-H $\cdots$ S interaction with an enthalpy of formation of about -1 to -2 kcal/mol.<sup>45-47</sup>

The results of the CNDO/2 calculations carried out earlier<sup>3</sup> show that the orientation of the hydrogen atoms attached to the carbon is not crucial for this interaction. Hence, it would seem to be less directional in character than one would expect for a hydrogen bond such as N-H $\cdots$ O=C. In light of this result, and because of the lack of direct experimental evidence concerning the involvement of the hydrogen atoms in this interaction, the nonspecific term "interaction" will be retained for the description of this effect.

One other important conclusion that can be drawn from

the data shown in Table IV is that short contacts between carbon and sulfur atoms in the 1 and 4 positions, respectively, do not generally coincide with values of the  ${}^1\text{CX}-\text{Y}^4\text{S}$  dihedral angle near  $0^\circ$ . This means that, in contrast to the results of the CNDO/2 calculations, the 1,4 carbon-sulfur interaction need not lead to sp conformations about the XY bond. We will return to this point in section IIIH.

**F. Short Contacts Involving  $C_{ar}$ -Type Carbon Atoms.** The short carbon-sulfur contacts listed in Table V involve aromatic carbon atoms. More than half of the short contact distances listed are shorter than the "short" calculated  $C_{ar}$  carbon-sulfur contact distance of  $3.35 \text{ \AA}$  of Table III. The other values are still shorter than the values of  $3.55 \text{ \AA}$  calculated using Pauling's criterion. These contacts cannot be discussed in the same manner as those shown in Table IV since there is the possibility of a  $p-\pi$  interaction between an unhybridized p orbital on the sulfur and the aromatic  $\pi$  system. Hence, the possible effects of this type of interaction must be considered.

A large number of the short contacts in Table V occur in disulfides in which phenyl rings are directly bonded to the sulfur atoms. We will refer to compounds with this type of structure as aromatic disulfides. In terms of the diagram shown in Figure 8 (in which X and Y are C and S atoms, respectively), atoms C and X form part of a phenyl ring. The  $p-\pi$  interaction mentioned previously is between unhybridized p orbitals on the X and Y atoms which are perpendicular to the  ${}^1\text{CXY}$  and  $\text{XY}^4\text{S}$  planes, respectively. Maximum orbital overlap between these orbitals is achieved when the SS-CC dihedral angle is  $0^\circ$ . At the same time, this is the value of the SS-CC dihedral angle that brings the  ${}^1\text{C}$  and  ${}^4\text{S}$  atoms into closest contact. Hence, one might attribute the observed short carbon-sulfur contacts to a 2,3  $p-\pi$  interaction, to a 1,4 carbon-sulfur interaction, or to both. The data plotted in Figure 9 are helpful for choosing between these alternatives.

Figure 9 shows the variation of the SSC bond angle and C-S bond length with SS-CC dihedral angle for a series of aromatic disulfides.<sup>26-30,32,33,48-50</sup> Observed values of the SS-CC dihedral angle are clustered in two regions, near  $10^\circ$  and  $90^\circ$ ; there are no values of the SS-CC dihedral angle observed between  $25^\circ$  and  $75^\circ$ . Furthermore, the cluster of points at low SS-CC dihedral angles generally have larger SSC bond angles and longer C-S bond lengths. Since  $p-\pi$  overlap, which would be maximal at low values of the SS-CC dihedral angle, would lead to a shorter C-S bond length (because of the increased partial double bond character), in contrast to the larger values observed in Figure 9B, we conclude that there is no appreciable attractive  $p-\pi$  interaction.

Alternatively, the low values of the SS-CC dihedral angle can be considered to result from the 1,4 carbon-sulfur interaction proposed here. The SSC bond angle may increase at low values of the SS-CC dihedral angle in order to allow the hydrogen atom bonded to the  ${}^1\text{C}$  atom to have a more favorable interaction with the  ${}^4\text{S}$  atom. It has been shown that the energy required to bend the SSC bond angle by a few degrees is not large in dimethyl disulfide.<sup>12</sup> It should be noted that, for SS-CC dihedral angles near  $0^\circ$ , the hydrogen that is bonded to the carbon atom involved in the short contact must point almost directly over the sulfur atom. Hence, if the positions of these hydrogens were known accurately, the H...S contact distance would almost certainly be short. The reason for the occurrence of conformations with SS-CC dihedral angles of about  $90^\circ$  with

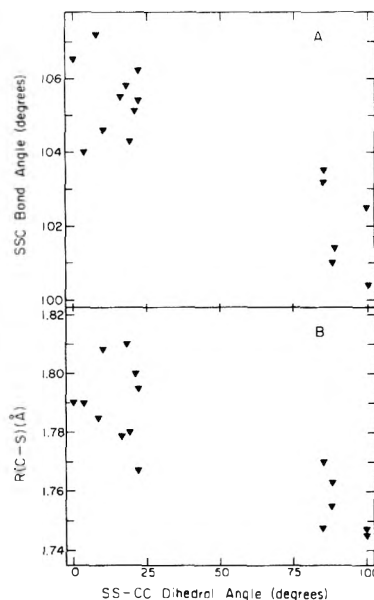
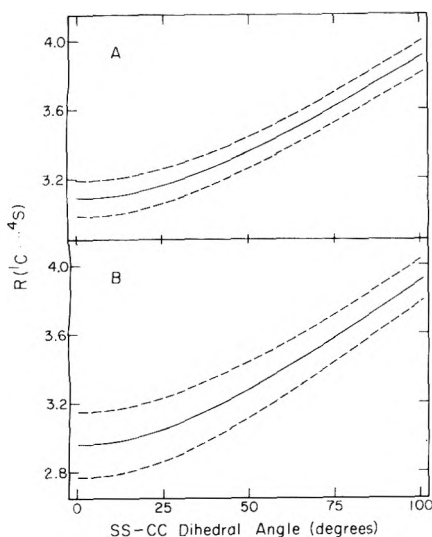


Figure 9. Variation in the (A) SSC bond angle and (B) C-S bond length with SS-CC dihedral angle for the aromatic disulfides of ref 26-30, 32, 33, and 48-50.

shortened C-S bond lengths is not clear. The absence of any orbital interaction between the phenyl ring and the sulfur to which it is bonded is supported by the very low barrier to internal rotation about the C-S bond in thiophenol. This barrier has been determined from a recent far-infrared study<sup>51</sup> to be only  $216 \text{ cm}^{-1}$ . Furthermore, the observed nonplanar structures of molecules such as thianthrene,<sup>52</sup> in which such  $p-\pi$  carbon-sulfur orbital interactions would lead to planar structures, also supports the present interpretation of these data.

**G. Short Contacts Involving  $C'$ -Type Carbon Atoms.** The short carbon-sulfur contacts listed in Table VI (which appears only in the microfilm edition of this Journal) involve  $C'$ -type carbon atoms which are encountered in the carbonyl group. In contrast to the contact distances listed in Tables IV and V, none of the contact distances listed in this table are very much shorter than the calculated van der Waals contact distance of  $3.10 \text{ \AA}$  of Table III. Hence, these contact distances are indicative of  $C'$  and S atoms that are at their van der Waals contact distance, but not closer. Therefore, it cannot be concluded that there is an attractive interaction between these atoms of the sort proposed between CH or  $C_{ar}$  groups and an S atom. This is probably related to the fact that the  $C'$ -type carbon atom does not have a hydrogen atom bonded to it. This type of carbon atom also has an unhybridized p orbital which could possibly interact with another p orbital on a sulfur atom. However, there is no evidence for such an interaction based on these contact distances. The occurrence of this many contacts at the van der Waals contact distance may be a significant observation in itself, however, in that it suggests that the crystal conformations of these molecules are partly determined by optimizing the  $C'-\cdots\text{S}$  van der Waals contacts.

**H. Relationship between the Nonbonded 1,4 Carbon-Sulfur Interaction and the SS-CC Dihedral Angle in Disulfides.** The search for experimental evidence supporting the existence of a 1,4 carbon-sulfur interaction was motivated by the results of the CNDO/2 calculations in this and the previous paper.<sup>3</sup> The existence of such an interaction



**Figure 10.** Variation in the  ${}^1\text{C}\cdots{}^4\text{S}$  nonbonded internuclear distance defined in Figure 8 calculated using the parameters shown in Table VII for (A) aromatic disulfides and (B) cystine-like disulfides. The solid and dashed lines are explained in the text in section III.

could help explain the occurrence of the  $sp$  conformations in the calculated potential functions for rotations about C-S and C-C bonds in cases where there are carbon and sulfur atoms in the 1 and 4 positions, respectively. There are indications from the calculations, however, that the CNDO/2 method is underestimating the repulsions between the  ${}^1\text{C}$  and  ${}^4\text{S}$  atoms in the  $sp$  conformation. It is the underestimation of these repulsions, for example, that is probably responsible for the abnormally short nonbonded carbon-sulfur distance of 2.5 Å discussed in section IIC. It is of interest to consider what the effect of this underestimation of interatomic repulsions is on the calculated potential functions.

These calculations lead to low-energy  $sp$  conformations with nonbonded carbon-sulfur distances that are shorter than any that have been observed experimentally; however, such conformations should have higher energies because of these steric overlaps. Presumably, if the calculations correctly accounted for interatomic repulsions, the minimum-energy  $sp$  conformations, which are stabilized by the 1,4 carbon-sulfur interaction, would occur at nonbonded 1,4 carbon-sulfur internuclear distances that are comparable to those observed experimentally (see Tables IV and V). Since these calculations were carried out using the assumption of rigid rotation, if the minimum-energy  $sp$  conformations were forced to have the larger experimentally observed values of the 1,4 carbon-sulfur internuclear distance, this would result in a change of the value of the dihedral angle of these  $sp$  minima away from  $0^\circ$ . This may even result in new minima on both sides of  $0^\circ$ , at either the  $\pm sc$  or  $\pm sc$  positions.

Figure 10 shows the relationship between the nonbonded 1,4 carbon-sulfur distance and the SS-CC dihedral angle for rigid rotation about the X-Y bond of the fragment shown in Figure 8 with X = C and Y = S. For curves A and B, different sets of C-C, C-S, and S-S bond lengths and SSC and SCC bond angles were chosen to be representative of those found in the same fragment in aromatic disulfides and in cystine-like disulfides, respectively. The values chosen were obtained by averaging those for a number of compounds of related structure. These average values are

**TABLE VII: Average Bond Lengths and Bond Angles for the SS-CC Fragment of Aromatic and Cystine-Like Disulfides<sup>a</sup>**

	A aromatic disulfides <sup>b</sup>	B cystine-like disulfides <sup>c</sup>
$R(\text{C}-\text{C})$ , Å	1.390	1.511 (16)
$R(\text{C}-\text{S})$ , Å	1.788 (34)	1.821 (37)
$R(\text{S}-\text{S})$ , Å	2.043 (26)	2.039 (8)
$\tau(\text{SCC})$ , deg	120.0	113.4 (4.5)
$\tau(\text{SSC})$ , deg	104.4 (1.9)	103.6 (8)

<sup>a</sup> Numbers in parentheses are the computed standard deviations in the last significant figures shown. No standard deviation is reported for  $R(\text{C}-\text{C})$  and  $\tau(\text{CCS})$  in column A since these parameters almost never varied within the experimental errors of the structural determinations. <sup>b</sup> The numbers in this column were obtained by averaging parameters from the structures reported in ref 26-30, 32, 44, and 45. <sup>c</sup> The numbers in this column were obtained by averaging parameters from the structures in ref 18, 19, 21, and 36-39.

shown in Table VII. The  ${}^1\text{C}\cdots{}^4\text{S}$  distance was then calculated as a function of the SS-CC dihedral angle by assuming rigid rotation about the C-S bond as in the calculations of section II. The broken lines on either side of curves A and B were calculated similarly, except that values from Table VII that differed by one standard deviation from the average values were used. These deviations were added and subtracted in such a way that the broken curves represent the maximum range of the  ${}^1\text{C}\cdots{}^4\text{S}$  distances from the solid lines due to all combinations of a variation in one standard deviation in each of five structural parameters shown in Table VII. These broken lines, then, give an indication of how the  ${}^1\text{C}\cdots{}^4\text{S}$  distance may also be influenced by variations in the parameters of Table VII. By assuming that cystine-like and aromatic disulfides actually undergo rigid rotation and that the position of one of the minima in the potential functions is determined only by the optimum 1,4 carbon-sulfur contact distance, a range of dihedral angles for this minimum can be obtained from Figure 10. Using this procedure, an experimentally observed contact distance of 3.15-3.25 Å for the aromatic disulfides leads to a predicted minimum in the potential function for rotation about the C-S bond at an SS-CC dihedral angle of about  $20$ - $35^\circ$ . Similarly, an experimentally observed contact distance of 3.3-3.4 Å for the cystine-like compounds gives minima at SS-CC dihedral angles of  $50$ - $60^\circ$ . Finally, by using the same 3.3-3.4 Å estimate for the experimentally observed contact distance (but the bond lengths and bond angles from an earlier study),<sup>3</sup> an SS-CC dihedral angle of about  $45$ - $55^\circ$  follows for methyl ethyl disulfide. These estimates may be on the high side, however, if the assumption of rigid rotation is not valid. This is illustrated by the data in Figure 9 which show that, for the aromatic disulfides, the SSC bond angle and C-S bond length both increase as the SS-CC dihedral angle is lowered, whereas the bond angles of a rigid rotor should remain constant. An increase in bond length would increase the value of the dihedral angle needed to achieve a given C...S contact distance; similarly, an increase in SSC bond angle would decrease the corresponding value of the dihedral angle. Since the effect of increasing the bond angle outweighs the effect of increasing the bond lengths in this case, the net result is that the same carbon-sulfur contact distance can be achieved only with a smaller SS-CC dihedral angle. This, indeed, is what is ob-

served experimentally, since, in Table V, contact distances of about 3.2 Å generally are associated with dihedral angles of less than 20°; i.e., since the rigid rotor is not a good approximation, the dihedral angles are decreased here.

If similar bond angle and bond length changes were to accompany the lowering of the SS-CC dihedral angle in aliphatic disulfides, then the positions of the minima estimated above would also be somewhat smaller. The curve shown in Figure 10B is very flat near low values of the SS-CC dihedral angle. Hence, a small increase in the SSC bond angle in this region can result in a large decrease in the value of the dihedral angle associated with the experimentally observed 1,4 nonbonded carbon-sulfur contact distance.

While no quantitative conclusions can be drawn from the above arguments, they serve to illustrate qualitatively that the underestimation of interatomic repulsions by the CNDO/2 method results in an energy minimum at an SS-CC dihedral angle of 0° that, in fact, should be at a somewhat larger value of this dihedral angle. The true value, however, is influenced by all of the degrees of freedom of the <sup>1</sup>CXY<sup>4</sup>S unit shown in Figure 8 and could be either an sp or an sc conformation.

#### IV. Conclusions

The results of the CNDO/2 calculations in this and the previous<sup>3</sup> paper give indications that the interaction between a methyl or methylene group and a sulfur atom is attractive, even at interatomic distances shorter than their van der Waals contact distance. This interaction seems to occur most frequently between carbon and sulfur atoms separated by two other singly bonded atoms and, hence, has been termed a 1,4 carbon-sulfur interaction, even though it is thought that the hydrogen atom bonded to the carbon atom participates in the interaction. Subsequent to the calculations, a survey of crystal structures on organosulfur compounds has uncovered a reasonably large number of short intramolecular 1,4 carbon-sulfur contacts, which supports the existence of this interaction.

The CNDO/2 method has been known to systematically overestimate interatomic stabilization energies with the result that it allows contact distances that are too short. Hence, while the CNDO/2 calculations correctly reflect qualitative tendencies for molecular interaction (such as hydrogen bonding), they overpredict the stability of these interactions. The forms of the potential functions for rotation about X-Y single bonds which are in the 2,3 position with respect to a 1,4 carbon-sulfur interaction have been calculated here to have energy minima near <sup>1</sup>CX-Y<sup>4</sup>S dihedral angles of 0°. Since the minima at these dihedral angles reflect the presence of an attractive 1,4 carbon-sulfur interaction in these systems, the positions of these minima are affected by the tendency in these calculations to bring the carbon and sulfur atoms in the 1 and 4 positions, respectively, too close together. This defect, however, can be qualitatively taken into account by shifting the minima at <sup>1</sup>CX-Y<sup>4</sup>S dihedral angles of 0° to somewhat larger values, depending on the bond lengths and bond angles of the <sup>1</sup>CX-Y<sup>4</sup>S unit.

NOTE ADDED IN PROOF: It has come to our attention [J. Donohue, A.C.A. Abstracts, No. C3, p 43, Berkeley, Calif., March 24-28 (1974)] that the structure of dicinnamyl disulfide (Table IV) may not be correct.

*Supplementary Material Available.* Table VI will appear following these pages in the microfilm edition of this volume of the journal. Photocopies of the supplementary material from this paper only or microfiche (105 × 148 mm, 24× reduction, negatives) containing all of the supplementary material for the papers in this issue may be obtained from the Journals Department, American Chemical Society, 1155 16th St., N.W., Washington, D.C. 20036. Remit check or money order for \$4.00 for photocopy or \$2.50 for microfiche, referring to code number JPC-75-1436.

#### References and Notes

- (1) This work was supported by research grants from the National Institute of General Medical Sciences of the National Institutes of Health, U.S. Public Health Service (GM-14312), and from the National Science Foundation (BMS71-00872 A04).
- (2) (a) NIH Predoctoral Trainee, 1970-1974. (b) NIH Postdoctoral Fellow, 1972-1974.
- (3) H. E. Van Wart, L. L. Shipman and H. A. Scheraga, *J. Phys. Chem.*, preceding paper in this issue.
- (4) E. Eliel, "Stereochemistry of Carbon Compounds", McGraw-Hill, New York, N.Y., 1962, Chapter 6.
- (5) W. Klyne and V. Prelog, *Experientia*, **16**, 521 (1960).
- (6) The letters c, p, s, and a represent clinal, periplanar, syn, and anti, respectively. The reader should refer to ref 5 for an explanation of these symbols. The + and - signs refer to the sign of the 1,2-3,4 dihedral angle as defined by the IUPAC-IUB Commission on Biochemical Nomenclature.<sup>7</sup>
- (7) IUPAC-IUB Commission on Biochemical Nomenclature, *Biochemistry*, **9**, 3471 (1970).
- (8) G. Nemethy and H. A. Scheraga, *Biopolymers*, **3**, 155 (1965).
- (9) L. Pauling, "The Nature of the Chemical Bond", Cornell University Press, Ithaca, N.Y., 1960, p 260.
- (10) K. Torii and Y. Iitaka, *Acta Crystallogr., Sect. B*, **29**, 2799 (1973).
- (11) R. B. Davidson, W. L. Jorgensen, and L. C. Allen, *J. Am. Chem. Soc.*, **92**, 749 (1970).
- (12) H. E. Van Wart, L. L. Shipman, and H. A. Scheraga, *J. Phys. Chem.*, **78**, 1848 (1974).
- (13) The dihedral angles in this paper inadvertently, but consistently, have been defined to be opposite in sign from the IUPAC-IUB Commission convention.<sup>7</sup> This in no way affects any of the results presented here since the steric relationships between the various atoms are identical in either sign convention. To avoid confusion, however, the + and - signs that are shown in the uppermost diagram of Figure 1 (and which refer to the IUPAC-IUB Commission sign convention) will not be used in the discussion of these calculations.
- (14) P. A. Kollman and L. C. Allen, *J. Am. Chem. Soc.*, **92**, 753 (1970).
- (15) S. J. Leach, G. Nemethy, and H. A. Scheraga, *Biopolymers*, **4**, 369 (1966).
- (16) R. E. Rosenfield and R. Parthasarathy, *J. Am. Chem. Soc.*, **96**, 1925 (1974).
- (17) W. C. Hamilton and J. A. Ibers, "Hydrogen Bonding in Solids", W. A. Benjamin, New York, N.Y., 1968, p 16.
- (18) M. O. Chaney and L. K. Steinrauf, *Acta Crystallogr., Sect. B*, **30**, 711 (1974).
- (19) T. Ottersen, L. G. Warner, and K. Seff, *Acta Crystallogr., Sect. B*, **29**, 2954 (1973).
- (20) M. Nishikawa, K. Kamiya, Y. Asahi, and H. Matsumaru, *Chem. Pharm. Bull. (Tokyo)*, **17**, 932 (1969).
- (21) R. E. Rosenfield, Ph.D. Thesis, SUNY Buffalo, May 1974.
- (22) R. M. Stroud and C. H. Carlisle, *Acta Crystallogr., Sect. B*, **28**, 304 (1972).
- (23) J. D. Lee and M. W. R. Bryant, *Acta Crystallogr., Sect. B*, **27**, 2325 (1971).
- (24) D. J. Mitchell, *Acta Crystallogr., Sect. B*, **25**, 998 (1969).
- (25) I. L. Karle, J. A. Estlin, and K. Britts, *Acta Crystallogr.*, **22**, 273 (1967).
- (26) J. D. Lee and M. W. R. Bryant, *Acta Crystallogr., Sect. B*, **25**, 2094 (1969).
- (27) J. S. Ricci and I. Bernal, *J. Chem. Soc. B*, 806 (1970).
- (28) J. S. Ricci and I. Bernal, *J. Am. Chem. Soc.*, **91**, 4078 (1969).
- (29) J. Karle, I. L. Karle, and D. Mitchell, *Acta Crystallogr., Sect. B*, **25**, 866 (1969).
- (30) T. Ottersen, L. G. Warner, and K. Seff, *Acta Crystallogr., Sect. B*, **30**, 1188 (1974).
- (31) J. D. Lee and M. W. R. Bryant, *Acta Crystallogr., Sect. B*, **25**, 2497 (1969).
- (32) E. Shefter and T. Kalman, *Chem. Commun.*, 1027 (1969).
- (33) E. Shefter and T. Kalman, *Biochem. Biophys. Res. Commun.*, **32**, 878 (1968).
- (34) V. K. Kato, *Acta Crystallogr., Sect. B*, **28**, 606 (1972).
- (35) B. R. Davis and I. Bernal, *J. Chem. Soc. B*, 2307 (1971).
- (36) J. Petersen, L. K. Steinrauf, and L. H. Jensen, *Acta Crystallogr.*, **13**, 104 (1960).
- (37) M. O. Chaney and L. K. Steinrauf, *Acta Crystallogr., Sect. B*, **24**, 1564 (1968).

- (38) S. C. Gupta, A. Sequeira, and R. Chidambaram, *Acta Crystallogr., Sect. B*, **30**, 562 (1974).
- (39) H. L. Yakel and E. W. Hughes, *Acta Crystallogr.*, **7**, 291 (1954).
- (40) R. Ramachandra Ayyar, *Z. Kristallogr.*, **126**, 227 (1968).
- (41) H. B. Dyer, *Acta Crystallogr.*, **4**, 42 (1951).
- (42) D. J. Haas, *Acta Crystallogr.*, **19**, 860 (1965).
- (43) M. M. Harding and H. A. Long, *Acta Crystallogr., Sect. B*, **24**, 1096 (1968).
- (44) J. N. Spencer, G. J. Casey, J. Buckfelder, and H. D. Schreiber, *J. Phys. Chem.*, **78**, 1415 (1974).
- (45) G. R. Wiley and S. I. Miller, *J. Am. Chem. Soc.*, **94**, 3287 (1972).
- (46) J. P. Sheridan, D. E. Martire, and Y. B. Tewari, *J. Am. Chem. Soc.*, **94**, 3294 (1972).
- (47) K. W. Jolley, L. M. Hughes, and I. D. Watson, *Aust. J. Chem.*, **27**, 287 (1974).
- (48) E. Shefter, *J. Chem. Soc. B*, 903 (1970).
- (49) E. Shefter, M. Kotick, and T. Bardos, *J. Pharm. Sci.*, **56**, 1293 (1967).
- (50) J. D. Lee and M. W. R. Bryant, *Acta Crystallogr., Sect. B*, **26**, 1749 (1970).
- (51) N. W. Larsen and F. M. Nicolaisen, *J. Mol. Structure*, **22**, 29 (1974).
- (52) H. Lynton and E. G. Cox, *J. Chem. Soc.*, 4886 (1956).

## A Statistical Thermodynamical Approach to the Distribution of Cations in Silicate Minerals

W. J. Mortier

*Centrum voor Oppervlaktische Chemie en Colloidale Scheikunde (Center for Surface and Colloidal Chemistry), De Croylaan 42, B-3030 Heverlee, Belgium (Received December 20, 1974)*

*Publication costs assisted by the Katholieke Universiteit Leuven*

The Boltzmann distribution law is introduced in the discussion of the cation distribution in silicate minerals. This allows the calculation of potential energy differences between two cation sites and the calculation of the variation of the site population with temperature. It was found that for potassium-exchanged X and Y zeolites, the energy differences between the sites varied linearly with the degree of isomorphic substitution. The temperature-dependent distribution of  $\text{Fe}^{2+}$  in orthopyroxenes also obeyed the Boltzmann distribution law.

### Introduction

Cations in silicates are mobile to a certain extent. Very high temperatures are often needed to accomplish migration. On the other hand, zeolites contain cations which are exchangeable at room temperature. The study of the migration with temperature and the distribution of the cations over different sites has repeatedly been a subject of investigation. Although the cations probably obey general rules, such rules were never clearly established. This study is an attempt to develop the more basic laws underlying the cation distribution. Results from a previous study on KX and KY zeolites,<sup>1,2</sup> and literature data on orthopyroxenes from Virgo and Hafner<sup>3</sup> will allow us to make some considerations on the cation distribution of two much differing silicates.

The zeolites X and Y are synthetic isotypes of the mineral faujasite ( $\text{M}_x^+ \text{Al}_x \text{Si}_{192-x} \text{O}_{384} \cdot y \text{H}_2\text{O}$ ), a hydrated aluminosilicate with a three-dimensional anion network. The structures of many cation exchanged forms were determined by several authors. For a general review, refer to Smith.<sup>4</sup>

For the location of the cations, to which several physicochemical properties refer, no general distribution laws could be expressed. From a structural viewpoint, the zeolite system was never considered as a whole, accounting for all the interactions which finally result in a certain cation distribution. There were some attempts at the interpretation of those distributions by considering, e.g., the mutual interaction of cations located at two sites. The Madelung poten-

tial calculations of Dempsey<sup>5</sup> was an exception of the general treatment.

Orthopyroxenes ( $\text{Mg}^{2+}, \text{Fe}^{2+}$ )<sub>2</sub>Si<sub>2</sub>O<sub>6</sub> are orthorhombic pyroxenes, i.e., chain silicates. The chains are formed by sharing two of the four corners by the SiO<sub>4</sub> tetrahedra. The chains are laterally linked by cations.

### Theoretical Approximation

The exchangeable potassium ions are located at several nonequivalent sites (I, I', II, and unlocated) in the structural framework of the zeolites X and Y. Orthopyroxenes have two nonequivalent sites, M<sub>1</sub> and M<sub>2</sub>, containing cations which are mutually exchangeable only at elevated temperatures. Several factors influence the cation location as, e.g., the Si/Al ratio and the presence of ligands. Together with the local framework environment, these factors determine the potential energy of an exchange site. As for plasmas or electrolyte solutions,<sup>6</sup> the coulombic interaction of a cation with its environment may be expressed by the potential energy of this ion in the electrostatic field ( $\Phi$ ). This electrostatic field is the result of the contribution of all charges present in the structure. The potential energy ( $\epsilon_i$ ) is then given by  $ze\Phi_i$ . The number ( $n_i$ ) of such ions at the site  $i$  is then expressed by the Boltzmann relation:

$$n_i = n_0 \exp(-ze\Phi_i/kT) = n_0 \exp(-\epsilon_i/kT) \quad (1)$$

where  $n_0$  is the number of such ions in a unit volume. This formula may be applied whenever the cations are freely mobile and includes the mutual electrostatic interaction of

**TABLE I: Distribution of the Cations among the Exchange Sites**

		Site I <sup>b</sup>	Site I'	Site II	Un-located
KF 48.2 <sup>a</sup>	Hydrated	0.0 <sup>c</sup>	13.6	17.8	16.8
	Dehydrated	6.4	14.1	26.1	1.6
KF 54.7	Hydrated	1.3	13.3	20.0	20.1
	Dehydrated	5.4	18.1	26.8	4.4
KF 69.8	Hydrated	7.0	12.0	24.3	26.5
	Dehydrated	9.4	16.6	28.9	14.9
KF 86.5	Hydrated	8.9	7.2	23.2	47.2
	Dehydrated	9.2	13.6	25.6	38.2

<sup>a</sup> The sample name indicates the exchangeable cation (K), the framework structure of faujasite (F), and the number of exchangeable cations per unit cell (for Si:Al = 1, i.e., 96). The samples KF54.7 and KF86.5 are the conventional Y and X samples, respectively. The Si/Al ratio for these samples varies from KF48.2 to KF86.5, i.e., 2.98, 2.51, 1.75, and 1.22, respectively. <sup>b</sup> The multiplicity of the sites equals 16, 32, and 32 per unit cell for the sites I, I', and II, respectively. Unlocated cations were supposed to be located at the sites III<sup>b</sup> with a multiplicity of 96.<sup>1,2</sup> <sup>c</sup> The values are the number of potassium ions per unit cell at the given site.

**TABLE II: Energy Differences ( $\epsilon_j - \epsilon_i$ ) between the Exchange Sites Given in  $kT$  Units, i.e.,  $\ln(n_i\omega_j/n_j\omega_i)$**

Sample	$n_i/n_j$			Unlocated/I'	Unlocated/II
	I/I'	I/II	I'/II		
A. Hydrated Samples					
KF48.2			-0.26	-0.89	-1.16
KF54.7	-1.64 <sup>a</sup>	-2.04 <sup>a</sup>	-0.41	-0.69	-1.10
KF69.8	0.15	-0.55	-0.71	-0.31	-1.01
KF86.5	0.90	-0.27	-1.17	0.78	-0.39
B. Dehydrated Samples					
KF48.2	-0.10	-0.72	-0.62	-3.28 <sup>b</sup>	-3.89 <sup>b</sup>
KF54.7	-0.52	-0.91	-0.39	-2.51	-2.91
KF69.8	+0.12	-0.43	-0.55	-1.21	-1.76
KF86.5	+0.30	-0.33	-0.63	-0.07	-0.70

<sup>a</sup> Subject to large error due to the very small occupancy of the site I. <sup>b</sup> Subject to large error due to the small amount of unlocated cations.

the cations as well as the cation-framework interaction. If we assume that, at all equivalent sites, the same potential energy is created, we must account for a degeneracy  $\omega_i$ , which is the multiplicity of the site under consideration. For two different sites the ratio of the occupancy numbers is then related to the energy difference by

$$\ln(n_i\omega_j/n_j\omega_i) = -(\epsilon_i - \epsilon_j)/kT \quad (2)$$

This allows us to determine ( $\epsilon_i - \epsilon_j$ ) if the ratio of the occupancy numbers in the equilibrium distribution is known. The latter can easily be calculated from X-ray structure determinations. The influence of the temperature on the site occupancy ratio is obvious.

**Results and Discussion**

(1) *Cation Distribution of Four K-Exchanged X and Y Zeolites with Varying Si/Al Ratio.* For monovalent cations no irreversibilities were observed even at room tempera-

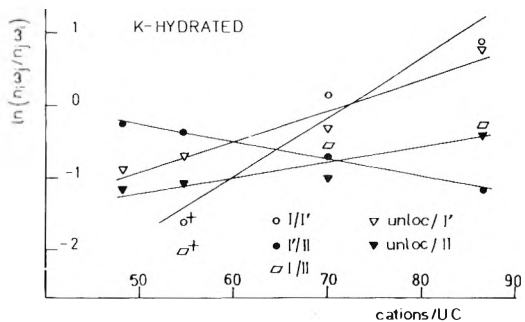


**Figure 1.** Variation of  $\ln(n_i\omega_j/n_j\omega_i)$  with the number of exchangeable cations per unit cell for the hydrated X and Y zeolites with varying Si/Al ratio. The points marked with a cross are subject to large error.

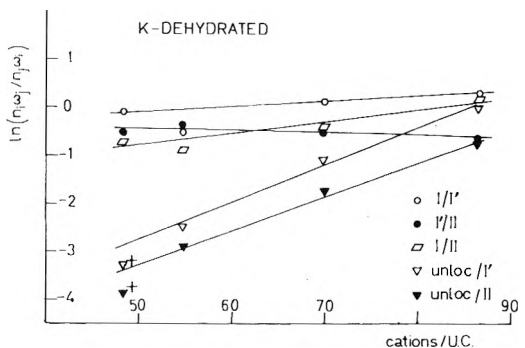


**Figure 2.** Variation of  $\ln(n_i\omega_j/n_j\omega_i)$  with the number of exchangeable cations per unit cell for the hydrated X and Y zeolites with varying Si/Al ratio. The points marked with a cross are subject to large error.

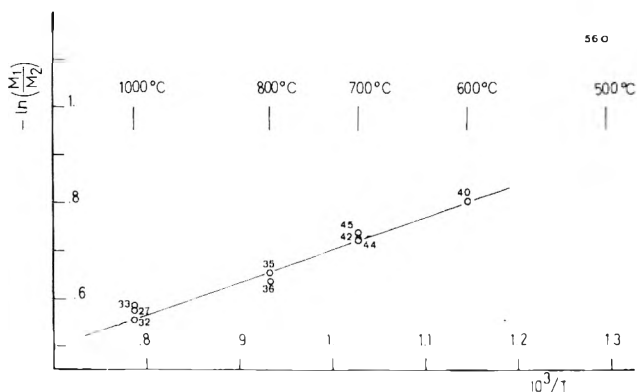


**Figure 3.** Variation with temperature of the Fe<sup>2+</sup> site occupancy number ratio in the cation sites M<sub>1</sub> and M<sub>2</sub> for orthopyroxenes. These data were obtained from Virgo and Hafner.<sup>3</sup> The figures indicate the experiment number on their sample 3209.

ture, and we assume that eq 2 is applicable. The distribution of the cations for the hydrated and dehydrated series is given in Table I. For the different sites, the energy difference between the sites, in  $kT$  units, is given in Table IIA and IIB for the hydrated and dehydrated series, respectively. A positive energy difference ( $\ln(n_i\omega_j/n_j\omega_i)$  negative) indicates a more favorable location of the cations at the sites  $j$ , i.e., a lower  $\epsilon_j$  value.

The values of the dehydrated series may be compared to the Madelung potential calculations of Dempsey.<sup>5</sup> For dehydrated X and Y zeolites exchanged with K ions, Dempsey gives the following site preference series: i.e., for X (Si:



Al = 1:1)  $I \approx I' > II > III$ ; and for Y (Si:Al = 2:1)  $II > I \approx I' > III$ . This site III may be compared to our unlocated cations, which we accept to be located at sites III'. We obtained a comparable sequence for the Y sample (KF54.7):  $II > I' > I > III'$ , but the X sample is different:  $II > I > I' > III'$ . In all cases, site III' is the least favorable site. Those differences may be due to a difference in the site occupancies accepted and the probable location of "unlocated cations" at site III' instead of site III. Site III' has a more favorable coordination from framework oxygens.<sup>1,2</sup>

Another result is the variation of energy differences with the number of cations per unit cell. For the hydrated samples (Figure 1) this energy difference seems to vary linearly with the degree of isomorphic substitution. This is also the case for the dehydrated series (Figure 2). (There are a few deviating values. For KF54.7 dehydrated, a change in the occupancy from 8.69 to 7.62  $K^+$  per unit cell for the site I and for I' from 18.11 to 15.88 fits those points to the observed variation for the other samples. Similar variations, as for KF69.8 hydrated, may be within the error since those structures were determined from powder diffraction measurements.) An important result for the potassium forms is that the potential energy at a site mainly depends on the electrostatic interactions with the framework, since a linear variation with the degree of isomorphic substitution was observed. The variation of the cation location with temperature can also be estimated if the same energy levels at the exchange sites may be accepted.

(2) *Temperature Dependence of the  $Fe^{2+}$  Distribution over Two Sites ( $M_1$  and  $M_2$ ) in Orthopyroxenes.* Using Mössbauer spectroscopic studies, Virgo and Hafner followed the variation of the site occupancy for  $Fe^{2+}$  and  $Mg^{2+}$  in the two sites. They found that at higher temperatures (above 500°) an equilibrium distribution was reached which varies with temperature. The logarithm of the  $Fe^{2+}$  occupancy ratio ( $\ln(M_1/M_2)$ ) should vary linearly with the

reciprocal absolute temperature if the difference in energy level of those sites is constant in the temperature range of their experiments. This is shown in Figure 3. This indicates that at higher temperatures, where equilibrium has been reached, their observations completely fit the Boltzmann relation. The deviation at 500° is in agreement with the conclusion of the authors that no equilibrium has been reached.

Those energy level differences however do not apply to other cations, since the size of the latter is also important. Indeed, the closer approach to the framework, the higher the attraction between framework and cations.

In conclusion we can state that the statistical thermodynamical approach is valid in cases where no irreversibilities arise and may largely contribute to the discussion of cation distributions among several sites in minerals. A static description of the cation location cannot be realistic and a small change (as, e.g., the exchange of some cations as in the case of zeolites) must have an influence on the entire system.

*Acknowledgment.* The author wishes to acknowledge the Belgisch Nationaal Fonds voor Wetenschappelijk Onderzoek (Belgian National Fund for Scientific Research) for a research grant as Aspirant. The author also thanks Dr. R. Schoonheydt for helpful discussions.

## References and Notes

- (1) W. J. Mortier and H. J. Bosmans, *J. Phys. Chem.*, **75**, 3327 (1971).
- (2) W. J. Mortier, H. J. Bosmans, and J. B. Uytterhoeven, *J. Phys. Chem.*, **76**, 650 (1972).
- (3) D. Virgo and S. Hafner, *Mineral. Soc. Am., Spec. Pap.*, **2**, 67 (1969).
- (4) J. V. Smith, *Adv. Chem. Ser.*, **No. 101**, 171 (1971).
- (5) E. Dempsey, *J. Phys. Chem.*, **73**, 3660 (1969).
- (6) L. Landau and E. Lifchitz, *Physique Statistique*, Mir, Moscou, 1967, Section 75.

## Conductivity Anomalies of Aqueous Carboxylic Acid Solutions. Dimerization or Effect of Solvent Medium?

R. B. Simpson

Laboratory of Biophysical Chemistry, National Institute of Arthritis, National Institutes of Health, Bethesda, Maryland 20014  
(Received February 8, 1973; Revised Manuscript Received November 22, 1974)

Publication costs assisted by the National Institutes of Health

The low conductivity of concentrated aqueous solutions of fatty acids cannot be explained by the model of a cyclic dimer proposed by Katchalsky, Eisenberg, and Lifson because (1) the "dimerization constants" of homologs calculated on this basis are inconsistent with the model; (2) "dimerization constants" calculated from conductivity are larger than those from other data (this includes vapor pressure data if the presence of hydrated fatty acids in the vapor phase is recognized); (3) Raman spectra published by Koteswaram and confirmed in this paper show very little cyclic dimer in predominantly aqueous solutions of fatty acids. In these solutions the dimerization constant calculated from Raman spectra is approximately  $0.01 M^{-1}$ . Most of the anomaly in the conductivity or electromotive force cannot be due to dimerization, but must be ascribed to the replacement of water by un-ionized fatty acid in the solvent medium. The medium effect must still be regarded as empirical, since attempts to calculate its value from the properties of the medium have not been successful.

### Introduction

It has long been known that fatty acids in the vapor phase and in organic solvents form dimers. Various physical methods, including electron diffraction,<sup>1</sup> leave no doubt that under these conditions the carboxyl groups form a ring by hydrogen bonding. When the activities or conductances of moderately concentrated aqueous solutions of fatty acids were found to be less than predicted from the dilute solution values, the discrepancies were at first<sup>2-4</sup> ascribed to the effect of the medium (un-ionized fatty acid replacing water); in 1933, however, MacDougall and Blumer<sup>5</sup> apparently fitted their vapor pressure data by assuming acetic acid dimers in the aqueous phase. Influenced by this and the established dimerization in nonaqueous solvents, Katchalsky, Eisenberg, and Lifson<sup>6</sup> proposed a nonionizable cyclic dimer to explain the conductances of fatty acids in aqueous solution. Their explanation has been widely quoted, and subsequent workers have usually<sup>7</sup> assumed that anomalies in conductivity and electromotive force of fatty acid solutions were due to dimerization. Actually, papers by Koteswaram<sup>8</sup> cited by Katchalsky, Eisenberg, and Lifson as support for dimerization in water gave clear spectroscopic evidence that the concentration of hydrogen-bonded dimer must be very small in the solutions for which the latter authors calculated rather large dimerization constants. In this paper Koteswaram's studies are confirmed, and the role of the un-ionized fatty acid as part of the solvent medium is recalled.

### Experimental Section

An Industrial Instruments Model RC16 conductivity bridge was used for the conductance measurements.

Solutions of the esters used were titrated with sodium hydroxide to determine impurities due to hydrolysis. It was found that newly opened reagent bottles contained negligible amounts of acid.

A Cary model 81 spectrophotometer with an argon laser of wavelength 5145 Å provided the Raman spectra. Per-

centages of water are by volume. E.g., 50% water = 1 ml of water + 1 ml of acid.

### Results and Conclusions

Katchalsky, Eisenberg, and Lifson calculated the "dimerization constants" shown in the first column of Table I by assuming that conductivities smaller than predicted by the Fuoss-Onsager theory were entirely due to a dimer which did not ionize. It will be shown here that these dimerization constants are unsatisfactory in several respects.

*I. Calculation of Dimerization Constant from Vapor Pressure.* Katchalsky, Eisenberg, and Lifson<sup>6</sup> found that their acetic acid dimerization constant of  $0.16 M^{-1}$  agreed with the value of  $0.185 M^{-1}$  obtained by MacDougall and Blumer<sup>5</sup> (MB) from measurements of the vapor pressure of acetic acid and water above aqueous solutions. The latter authors did not consider, however, an important species in the vapor, the complex of acetic acid with water. If the presence of this species is recognized, the vapor pressure data are actually fitted better with a very small value of liquid phase dimerization constant than with the large value that MacDougall and Blumer obtained.

To show this, the total acetic acid pressure  $p_X$  was calculated from the other data in MacDougall and Blumer's nine experiments with low sulfuric acid concentration ( $0.05 M$ ), using the equations (see Appendix)

$$p_{HA} = V \frac{-1 + \sqrt{1 + 8Dc}}{4D} \quad (1)$$

$$p_X = p_{HA} [1 + p_{HA}/0.325 + Hp_{H_2O}/(1 + Hp_{HA})] \quad (2)$$

where  $1/0.325$  mm is the vapor phase dimerization constant;  $c$  is the concentration from MB's Table I, column 3;  $p_{H_2O}$  is the water pressure from MB's Table III, column 3; and the three parameters  $V$ , the vapor pressure of monomeric HA per unit concentration of acetic acid,  $D$ , the dimerization constant in the liquid phase, and  $H$ , the hydration constant to form HA-H<sub>2</sub>O in the vapor phase were varied to give the best fit of the calculated  $p_X$  to the observed

**TABLE I: "Dimerization Constants" ( $M^{-1}$ ) of Carboxylic Acids Calculated from Various Types of Data**

	Conduc- tivity <sup>a</sup>	Cryoscopy <sup>b,c</sup>	Partition <sup>c</sup>
Formic	0.04	0.01-0.015 at 3 M	
Acetic	0.16	0.027-0.030 at 3 M	0.04, <sup>d</sup> 0.02, <sup>e</sup> 0.005 <sup>f</sup>
Propionic	0.23	0.05-0.17 at 4 M	0.07 <sup>g</sup>
Butyric	0.36	0.10-0.17 at 1.2 M	0.1 <sup>h</sup>

<sup>a</sup> Reference 6, calculated from data of ref 4. <sup>b</sup> E. R. Jones and C. R. Bury, *Phil. Mag.*, 4, 841 (1927). <sup>c</sup> To compare these with the conductivity results, we have calculated the data in terms of "dimerization constants" although not all the authors used this interpretation. <sup>d</sup> M. Davies and D. M. L. Griffiths, *Z. Phys. Chem., (Frankfurt am Main)*, 2, 353 (1954). <sup>e</sup> F. S. Brown and C. R. Bury, *J. Chem. Soc.*, 123, 2430 (1923). <sup>f</sup> S. D. Christian, H. E. Affsprung, and S. A. Taylor, *J. Phys. Chem.*, 67, 187 (1963). <sup>g</sup> H. W. Smith and T. A. White, *ibid.*, 33, 1953 (1929). <sup>h</sup> M. Davies and D. M. L. Griffiths, *Z. Phys. Chem. (Frankfurt am Main)*, 6, 143 (1956).

$\rho_X$ . The best fit was obtained with  $V = 3$  mm/mole fraction of acetic acid, and with  $H = 0.1$  mm<sup>-1</sup>, and  $D = 0.02$  M<sup>-1</sup>. A dihydrate model with the last term in the equation for  $\rho_X$  appropriately altered was also tested and gave the best fit with a dihydration constant 0.005 mm<sup>-2</sup> and a vanishingly small value of  $D$ . Since the standard deviation of the errors for the best fits (0.0072 mm) was not appreciably better than for the MacDougall-Blumer model (0.0084 mm), additional support for the model with large hydration constant must come from independent data.

From Levy and Davis' data<sup>9</sup> on the vapor pressure of acetic acid and water at elevated temperatures the ratio of the monohydration constant to the dimerization constant in the vapor phase is shown in Figure 1a. The value of the ratio obtained at 25° from extrapolation of their ratios to low temperatures depends on the relative enthalpies of the hydration and dimerization reactions. If, as it appears from the data in Levy and Davis' limited temperature range, the two enthalpies are about equal, the ratio of monohydration constant to dimerization constant at 25° would actually be somewhat larger than the ratio (0.03) calculated from MacDougall and Blumer's data. On the other hand, it seems plausible that the hydration reaction, with a smaller free energy change than the dimerization, should have a smaller enthalpy change, and it is easy to see that a line with sufficient slope to give a negligible value of hydration constant at 25° would also be a credible approximation to the data points. Support for the larger value of hydration constant, however, comes from the value of 0.05 for the ratio of hydration constant to dimerization constant of acetic acid in benzene at 25°.<sup>10</sup>

For the dihydrate model, the ratio of the dihydration constant to the dimerization constant is shown in Figure 1b. The average value of the ratio is 0.00018 mm<sup>-1</sup> if only Levy and Davis' most consistent series are used, and 0.00025 mm<sup>-1</sup> if all their data are used. The best fit to MacDougall and Blumer's data gives a ratio of 0.0016 mm<sup>-1</sup> at 25°. For trifluoroacetic acid at 20° the vapor phase hydration constant<sup>11</sup> was found to be 0.01 mm<sup>-2</sup>, giving a ratio of dihydration constant to dimerization constant of 0.02 mm<sup>-1</sup>.

From most of the evidence available, therefore, a large vapor phase hydration constant and a small liquid phase dimerization constant seems more reasonable than the opposite alternative in fitting the MacDougall-Blumer data.

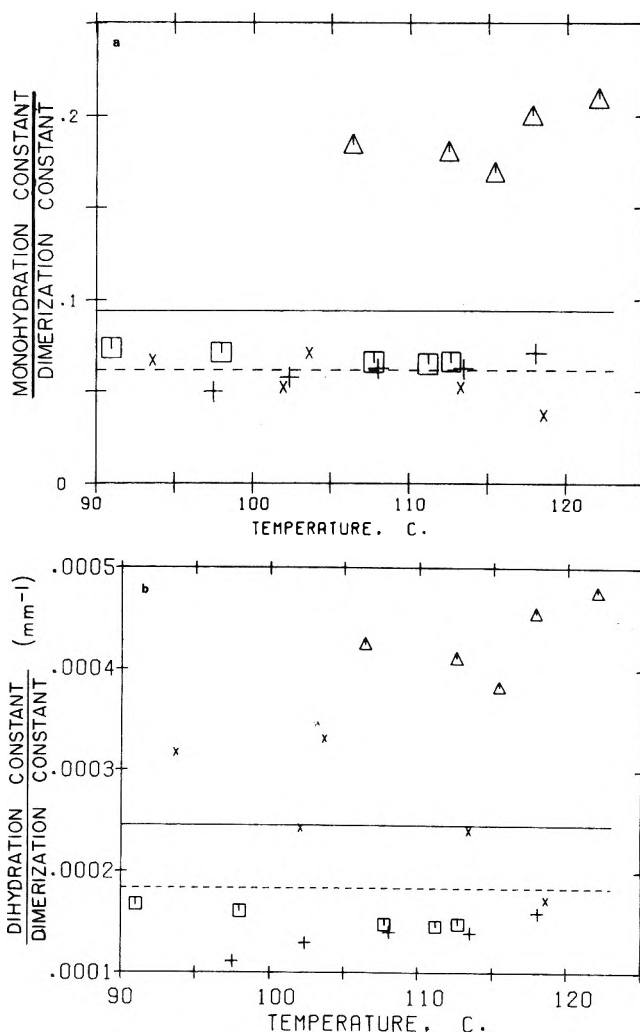


**Figure 1.** Effect of temperature on ratio of hydration constant to dimerization constant of acetic acid in the vapor phase. Calculated from the data of Levy and Davis.<sup>9</sup> Different symbols refer to their four series of experiments: X, series 1; squares, series 2; triangles, series 3; +, series 4. For the extrapolation to 25° it was assumed that the enthalpy of the two equilibria is the same, i.e., that deviations of points from a horizontal line are random, rather than indicative of a slope. Thus the ordinate of the dashed line is the average of the ordinates of series 1, 2, and 4, while the ordinate of the solid line is the average of all the ordinates. Figure 1a was calculated for monohydrate model, Figure 1b, calculated for dihydrate model.

**II. Calculation of Dimerization Constant from Raman Spectra.** Figures 2-4 show Raman spectra of acetic and butyric acid with various fractions of water added. Figure 2 agrees well with the spectra of Koteswaram.<sup>8</sup>

The hydrogen-bonded C=O vibration of fatty acid dimers has been identified in the vapor phase as a line at 1740 cm<sup>-1</sup> in the infrared.<sup>12</sup> Concomitant with the dissociation of the dimer at low pressure or high temperature this line decreases in intensity and a doublet at 1776-1799 cm<sup>-1</sup> increases in intensity.<sup>12,13</sup> The hydrogen bonded C=O line of the dimer occurs at 1660-1670 cm<sup>-1</sup> in the Raman spectra of pure liquid fatty acids. Since the intensity of this line decreases relative to a line at higher frequency (1710 cm<sup>-1</sup>) as water is added to the fatty acid (ref 8 and Figures 2 and 4), it is eminently reasonable to ascribe this phenomenon, as Koteswaram did, to dissociation of the dimer. That it is not a medium effect per se is indicated by the facts that (1) the frequencies of other lines in the spectrum remain essentially constant, and (2) as water concentration increases,

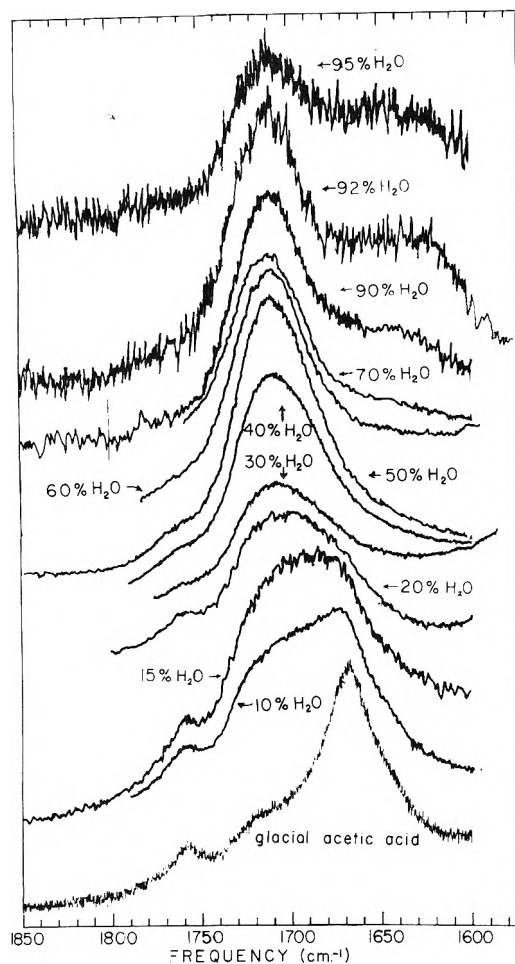


**Figure 2.** Raman spectra of acetic acid solutions. Recorded heights depend on sensitivity settings and other factors. Some solutions, e.g., 60% water, show more slope of the base line than others, probably because they were not irradiated long enough to quench fluorescence.

there is a concentration range in which the frequency changes, and then a long concentration range in which the  $1710\text{-cm}^{-1}$  line does not change in width or frequency.

If the relative intensities of these lines are considered to be proportional to the relative concentrations of C=O in the dimer and monomer species, the precipitous drop in the  $1670\text{-cm}^{-1}$  intensity as the water content increases indicates that the C=O present in dimer must extrapolate to a fraction much smaller than the 15% anomaly in conductivity observed at 1 M acetic acid (94% water).

To calculate a "dimerization constant" we must take account of the competition between water and acetic acid for the hydrogen bonding with the carboxyl group. We may combine the equation for dimerization of the anhydrous monomer

$$\text{DIM} = \frac{[(\text{HA})_2]}{[\text{HA}]^2} \quad (3)$$

with an equation for hydration of the monomer

$$\text{HYD} = \frac{[\text{HA} \cdot \text{H}_2\text{O}]}{[\text{HA}][\text{H}_2\text{O}]} \quad (4)$$

to get a dimerization equation involving the hydrated monomer

$$\frac{[(\text{HA})_2]}{[\text{HA} \cdot \text{H}_2\text{O}]^2} = \frac{\text{DIM}}{\text{HYD}^2[\text{H}_2\text{O}]^2} \quad (5)$$

*Hydration of Acetic Acid in Water.* To show, by a rough calculation, that almost all the monomeric acetic acid is hy-

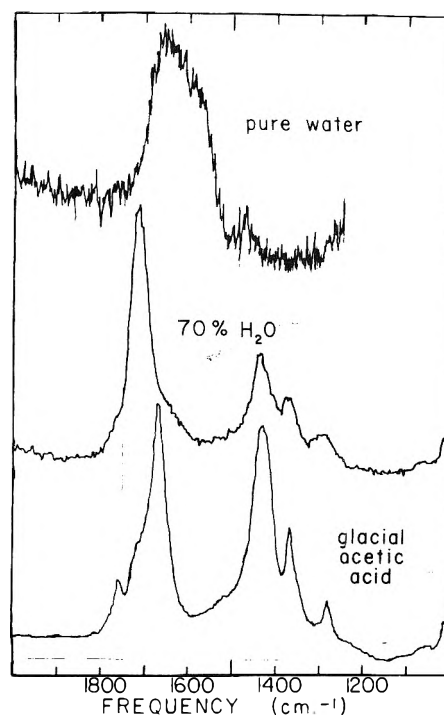


**Figure 3.** Raman spectra of acetic acid solutions and water. Recorded heights of different samples depend on sensitivity settings and other factors.

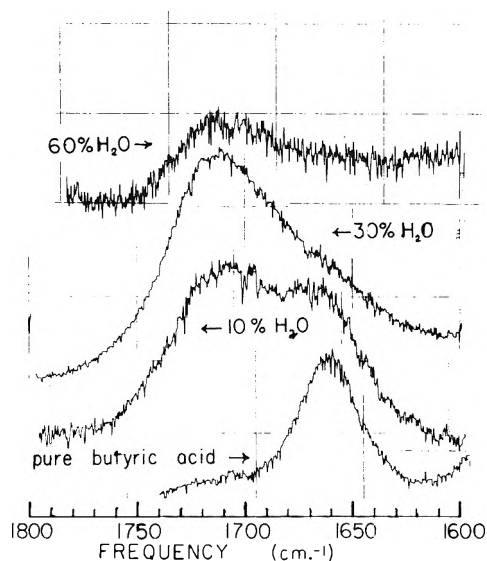


**Figure 4.** Raman spectra of butyric acid solutions. Recorded heights of different solutions depend on sensitivity settings and other factors.

drated in predominantly aqueous solutions, we first make use of Henry's law:

partial pressure of HA =

$$\text{vapor pressure (of pure HA)} \times \text{mole fraction of HA} \quad (6)$$

To get the coefficient representing the vapor pressure of pure HA we apply the equation to glacial acetic acid. The ratio of monomer to dimer decreases rapidly as acetic acid is added to organic solvents,<sup>14</sup> so that in glacial acetic acid the ratio must be very small. We shall take 0.01 as a round number for the mole fraction of monomer in glacial acetic

acid. The vapor pressure of glacial acetic acid at 25° is 15.4 mm, and using the vapor phase dimerization constant  $1/0.325$  mm yields a partial pressure of 1.5 mm for the monomer. From eq 6 therefore the hypothetical vapor pressure of pure anhydrous monomeric acetic acid is in the neighborhood of  $1.5/0.01$ , i.e., 150 mm.

From the best fit to the data of MacDougall and Blumer<sup>5</sup> we found that

partial pressure of anhydrous monomeric acetic acid =  $3(\text{mole fraction of } [\text{HA} \cdot \text{H}_2\text{O} + \text{HA}] \text{ in solution})$  (7)

Equating the two expressions (6) and (7) for the partial pressure of anhydrous monomeric acetic acid, we get:

$$150(\text{mole fraction of HA}) = 3(\text{mole fraction of } [\text{HA} \cdot \text{H}_2\text{O} + \text{HA}]) \quad (8)$$

Equation 8 shows that in the solutions with which MacDougall and Blumer worked, the ratio of hydrated to anhydrous acetic acid is in the neighborhood of 50 to 1, and therefore it may be safely assumed that the monomer represented by the Raman line at  $1710 \text{ cm}^{-1}$  is the hydrated monomer occurring in eq 5. In applying eq 6 to predominantly aqueous solutions we assumed that the activity coefficient of anhydrous monomeric acetic acid is substantially unchanged in going from glacial acetic acid to water, an approximation we consider sufficiently good for our purposes.

*Calculation of Dimerization Equilibrium.* Since the height of the recorded Raman spectrum of a particular sample is affected by several uncontrolled factors, the relative intensities of the  $1670\text{-}$  and  $1710\text{-cm}^{-1}$  lines cannot be determined by comparing the recorded heights from two different spectra. The relative intensities may, however, be obtained by comparison of each band with the methyl deformation band at  $1430 \text{ cm}^{-1}$ , since the intensity of this band should be unaffected by hydrogen bonding of the solvent. Applying this method to Figure 3, we estimate that the integrated intensity of the monomer line at  $1710 \text{ cm}^{-1}$  is intrinsically about two times that of the dimer line at  $1670 \text{ cm}^{-1}$ . In making this estimate, we attribute the  $1720\text{-}$  and  $1760\text{-cm}^{-1}$  bands in glacial acetic acid to oligomers, as Haurie and Novak suggested.<sup>15</sup>

Let us now calculate the values in eq 5 from the relative intensities of the  $1670\text{-}$  and  $1710\text{-cm}^{-1}$  bands in some particular solution, e.g., that with 50% water. If we subtract the spectrum of the pure monomer from this curve, we should get the area of the shoulder at  $1670 \text{ cm}^{-1}$  due to dimer. To get the shape of the "pure monomer" spectrum, we take the 90% water spectrum, and subtract the contribution of the water band. (The relative height of the water band is estimated by comparison of the spectra for 90 and 95% water, and the shape of the water band is obtained from the spectrum of pure water in Figure 3.) Following this procedure, we estimate the area of the shoulder near  $1670 \text{ cm}^{-1}$  as about 12% of the area of the  $1710\text{-cm}^{-1}$  band in the solution with 50% water. Multiplying this by the intrinsic area ratio 2 noted above, we calculate the ratio of C=O in the form of dimer to that of C=O in the form of monomer as about 0.24. Since there are two C=O groups per dimer, the mole ratio of  $(\text{HA})_2$  to monomer is  $0.24/2$ , i.e., 0.12. Dividing this by  $7 M$ , the approximate monomer concentration in a 50% water solution, we get  $0.017 M^{-1}$  for the left-hand side of eq 5.

From the vapor pressure data of Arich and Tagliavini<sup>16</sup> we obtain the activity coefficient of water as a function of mole fraction at  $69.7^\circ$  (Figure 5). By comparison with their

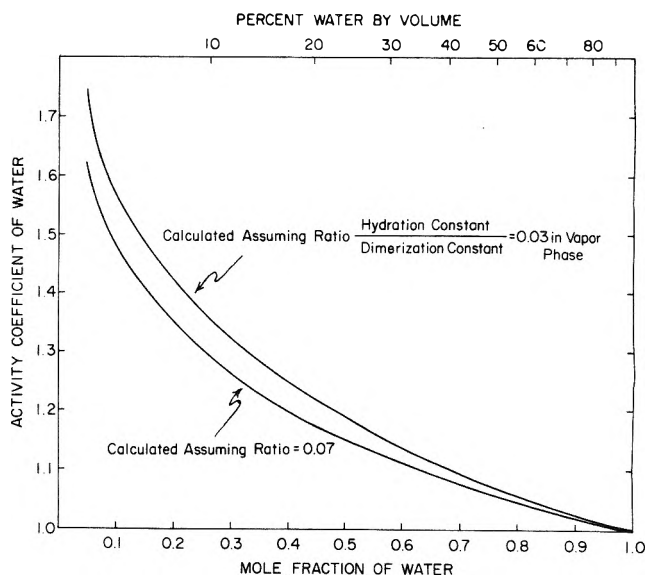


Figure 5. Activity coefficient of water in acetic acid solutions at  $69.7^\circ$ , calculated from the vapor pressure data of Arich and Tagliavini.<sup>16</sup>

data at  $89.9^\circ$  we find that there is very little variation of activity coefficient with temperature, so Figure 5 should also apply fairly well at  $25^\circ$ .

In 50% water the mole fraction of water is 0.76, and from Figure 5 the activity coefficient relative to pure water is about 1.06, so that the square of the water activity in eq 5 is  $(0.76 \times 1.06)^2$ , i.e. 0.65. Therefore the value of  $\text{DIM}/\text{HYD}^2$  is  $0.017 \times 0.65$ , equal to approximately  $0.01 M^{-1}$ . In solutions of less than  $1 M$  acid concentration, where the activity of water is greater than 0.98, this number, 0.01, would also represent the value of the left-hand side of eq 5, the conventional dimerization constant.<sup>17</sup>

The greatest uncertainty in this result comes from the uncertainty in the areas, i.e., integrated intensities, of the  $1670\text{-}$  and  $1710\text{-cm}^{-1}$  bands. If we had chosen the line at  $1100$  rather than  $1430$  as a reference intensity, we would have obtained an area ratio closer to 1 than 2, yielding a dimerization constant of about 0.005 rather than  $0.01 M^{-1}$ .

Values in the same neighborhood are obtained from solutions with other water contents. It is worth noting that the predicted rate of change in the monomer-dimer ratio with change in water activity is dependent on the exponent for water in eq 5, and this in turn is dependent on the average number of water molecules in the complex (assumed to be one in eq 4). Although an accurate number is difficult to determine because of uncertainties about the contribution of oligomers and other weak lines, our spectra fit better the assumption of a monohydrate than of an anhydrous monomer.<sup>18</sup>

Figure 4 shows that for butyric acid, the dimerization constant must also be quite small.

*III. Dimerization Constant from Cryoscopy and Partition.* Table I shows that the "dimerization constants" calculated from conductivity are much larger than those calculated from cryoscopy or partition.

*IV. Inconsistency of Values of "Dimerization Constants" Calculated from Conductivity.* (a) For a cyclic dimer the dimerization constant should be essentially independent of chain length because the planarity of the resonating ring would keep the hydrocarbon chains so far away from each other that there could be practically no interac-

tion between them. (b) The "dimerization constant" calculated from aqueous conductivity on the basis of this model (Table I) increases by a factor of 9 from formic to butyric acid. (For comparison, the dimerization constants of the acids from acetic to lauric in carbon tetrachloride show random deviations of only 21%.<sup>19</sup>) (c) Therefore the assumption that the conductivity anomalies are due to dimerization leads to results that are inconsistent with the model.

**Medium Effect.** It is clear that we must return to an explanation of the solution properties based on the medium effect,<sup>3,20</sup> i.e., that replacement of solvent water by un-ionized fatty acid will decrease the activity of organic molecules and increase the activity of ions.

**Neutral Molecules.** From the measurement of activity of un-ionized molecules, e.g., the last two columns of Table I, it is not possible to distinguish between association (a small number of solute molecules in close contact) and a generalized medium effect (a large number of solute molecules at various small but nonbonding distances from each other). In the absence of compelling structural evidence for specific bonding, it is unwarranted, or at least arbitrary, to attribute the decrease in activity coefficient of carboxylic acids in aqueous solution to dimerization. At any rate, carboxylic acids are not unique in showing decreases in activity coefficients as the concentration is increased, since some other organic compounds, e.g., the alcohols,<sup>21-24</sup> show roughly similar decreases.

Although the dimerization constant calculated from Raman spectra may be large enough to account for the numbers in the last two columns of Table I for acetic acid, this is not true for butyric acid. Thus, for the longer acids, at least, the activity coefficient changes probably involve further association or a generalized medium effect.

**Ions.** If ionization were not hindered by dimerization, there should be a negligible effect of dimerization on conductivity and on antilog (emf), which, to a first approximation, are proportional to the number of ions.

Let us consider the usual assumption that the effect of dimerization on the conductivity or emf is due to *nonionizable* dimer. We shall calculate its effect on the number of solute particles and on the number of ions. Let us suppose that 1% of the neutral solute particles are dimers. The freezing point lowering would be approximately 1% less than in the absence of dimerization. On the basis of the foregoing assumption, the fraction of molecules (or carboxyl groups) available for ionization would be about 2% less than in the absence of dimerization, i.e., the concentration of ionizable HA would be about 98% of its normal value. From the definition of the ionization constant,  $[H^+] = [A^-] = (K[HA])^{1/2}$ , so that  $[H^+]$  or  $[A^-]$  would have about  $0.98^{1/2} = 0.99$  of its value in the absence of dimerization, and, to a first approximation, the anomaly in conductivity or antilog (emf) would be 1%. It follows, on the basis of the above assumption, that the anomaly *due to nonionizable dimer* must be approximately the same, whether one uses measurements of neutral molecules (colligative properties) or measurements of ions (conductivity or emf).

However, in fact, the anomalies in conductivity and emf are much larger than in colligative properties. All of the difference must be attributed to other causes, e.g., the medium effect, and any treatments which start with the foregoing assumption, whether explicit<sup>6</sup> or implicit,<sup>7,25</sup> and ascribe a large part of the conductivity or emf anomaly to dimerization must be incorrect.

**TABLE II: Percentage Decrease in Conductivity Caused by Presence of Un-ionized Compounds**

	1 M Methyl acetate	0.16 M Methyl butyrate
0.015 M HClO <sub>4</sub>	4	3
0.1 M HAC	15	8
	1 M Acetic acid	0.16 M Butyric acid
	15 <sup>a</sup>	6 <sup>a</sup>

<sup>a</sup> These are the conductivity anomalies of the acids, i.e., the percentage differences between the observed conductivity and that calculated from the Fuoss-Onsager theory.

One cannot, even now, be much more specific about the details of the influence of organic molecules than was Owen,<sup>3</sup> whose primary medium effect was not calculated from a model as in the Debye-Hückel theory or the Katchalsky, Eisenberg, and Lifson hypothesis, but regarded merely as a parameter which fit the emf data.

This is also the situation at present with the conductivity data. Certain qualitative rules are discernible, e.g., increased viscosity decreases conductivity, and larger organic molecules are more effective than small ones in decreasing conductivity. Attempts at a quantitative explanation, however, have not been successful.

In solutions where there is no ambiguity about the difference between activity and concentration, we may define

$$\text{conductivity} = \Sigma (\text{concentration} \times \text{mobility of ions}) \quad (9)$$

Davies<sup>26</sup> found that MacInnes and Shedlovsky's<sup>27</sup> conductivity data on acetic acid could be fitted fairly well by assuming that the mobilities of the ions were inversely proportional to the viscosity of the medium. For the other fatty acids Cartwright and Monk<sup>7</sup> employed the same hypothesis, and ascribed the remainder of the anomaly to nonionizable dimer. Table II shows that the conductivity effects are more specific than the above hypothesis would indicate, and the inaccuracy of Cartwright and Monk's constant for butyric acid shows that Davies' fit<sup>26</sup> was fortuitous.

In eq 9 the substitution of activities (calculated from electromotive force data) for concentrations, either with or without the substitution of the viscosity of the medium for that of water, also does not give a quantitative fit to the conductivity data. Although a more sophisticated theory may some day be available, one must at present accept the fact that the conductivity anomaly is not simply related to any property, such as fraction of dimer, viscosity of the medium, or activity of the ions. The medium effect must still be regarded as empirical.

**Acknowledgment.** I wish to thank Ira Levin and Robert Spiker for the use of the Raman spectrophotometer, and for discussions of the interpretation of the spectra.

## Appendix

Equation 1 for the vapor pressure of monomeric acetic acid was obtained by combining the equations for the total aqueous concentration

$$c = [HA] + 2[(HA)_2]$$

the aqueous dimerization constant

$$D = [(HA)_2]/[HA]^2$$

and the definition of vapor pressure

$$p_{HA} = V[HA]$$

Equation 2 for the total acetic acid pressure was obtained by substituting into

$$p_X = p_{HA} + \dot{p}_{(HA)_2} + p_{HA \cdot H_2O}$$

the value MacDougall and Blumer used for the vapor phase dimerization constant

$$1/0.325 \text{ mm} = p_{(HA)_2}/(p_{HA})^2$$

and the vapor phase hydration constant

$$H = p_{HA \cdot H_2O}/p_{HA} \cdot p_w$$

where  $p_w$  is the pressure of uncomplexed water as distinguished from the total water pressure  $p_{H_2O}$

$$p_w = p_{H_2O} - p_{HA \cdot H_2O} = p_{H_2O} \left( 1 - \frac{p_{HA \cdot H_2O}}{p_{H_2O}} \right)$$

Since the fraction of water complexed with fatty acid is small, we may make a binomial series of the reciprocal of the expression in parentheses, and take only the first two terms, to give

$$p_w \cong p_{H_2O} \left( \frac{1}{1 + \frac{p_{HA \cdot H_2O}}{p_{H_2O}} \dots} \right)$$

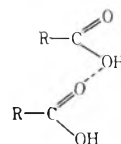
In this last expression  $p_{HA \cdot H_2O} = Hp_{HA}p_w$  is then approximated by  $Hp_{HA}p_{H_2O}$ . I.e.,  $p_w$  is approximated by  $p_{H_2O}$ , to give

$$p_w \cong p_{H_2O} \frac{1}{1 + Hp_{HA}}$$

## References and Notes

- (1) L. Pauling and L. O. Brockway, *Proc. Natl. Acad. Sci.*, **20**, 336 (1934).
- (2) W. A. Roth, *Z. Phys. Chem.*, **43**, 539 (1933).
- (3) B. B. Owen, *J. Am. Chem. Soc.*, **54**, 1758 (1932).
- (4) B. Saxton and L. S. Darken, *J. Am. Chem. Soc.*, **62**, 846 (1940).
- (5) F. H. MacDougall and D. R. Blumer, *J. Am. Chem. Soc.*, **55**, 2236 (1933).

- (6) A. Katchalsky, H. Eisenberg, and S. Lifson, *J. Am. Chem. Soc.*, **73**, 5889 (1951).
- (7) D. C. Cartwright and C. B. Monk, *J. Chem. Soc.*, 2500 (1955), pointed out the large effect of viscosity, but still calculated dimerization constants from the conductivity data.
- (8) P. Koteswaram, *Z. Phys.*, **110**, 118 (1938); **112**, 395 (1939).
- (9) B. Levy and T. W. Davis, *J. Am. Chem. Soc.*, **76**, 3268 (1954).
- (10) Reference *f* in Table I.
- (11) S. D. Christian, H. E. Aftsprung, and C. Ling, *J. Chem. Soc.*, 2378 (1965).
- (12) R. C. Herman and R. Hofstadter, *J. Chem. Phys.*, **6**, 534 (1938).
- (13) M. Haurie and A. Novak, *J. Chim. Phys.*, **62**, 139 (1965).
- (14) J. Lascombe, M. Haurie, and A. Novak, *J. Chim. Phys.*, **59**, 1217 (1962).
- (15) M. Haurie and A. Novak, *C. R. Acad. Sci., Ser. B*, **246**, 694 (1967).
- (16) G. Arich and G. Tagliavini, *Ric. Sci.*, **28**, 2493 (1958).
- (17) This is about the same as the value 0.005 estimated by I. M. Klotz and J. S. Franzen, *J. Am. Chem. Soc.*, **84**, 3461 (1962), for the aqueous dimerization constant of *N*-methylacetamide, even though the dimerization constant in carbon tetrachloride is about three orders of magnitude larger for the acid (ref 19) than for the amide (where both constants are calculated from infrared spectra).
- (18) The Raman spectra do not provide support for an extended dimer sug-



- gested by E. E. Schrier, M. Pottle, and H. A. Scheraga, *J. Am. Chem. Soc.*, **86**, 3444 (1964). Except, perhaps, in formic acid solutions, there is unlikely to be a significant fraction of this present. The ratio of this form to the cyclic dimer should be fairly independent of concentration. Pure acetic acid is nearly all cyclic dimer, so it does not seem reasonable that there would be much extended dimer in dilute acetic acid solutions. Pure formic acid, on the other hand, consists mainly of hydrogen-bonded polymers (E. Constant and A. Lebrun, *J. Chim. Phys.*, **61**, 163 (1964); R. J. Jakobsen, Y. Mikawa, and J. W. Branch, *Spectrochim. Acta, Part A*, **23**, 2199 (1967)), so it is possible that at some concentration there is an appreciable fraction of intermediate, i.e., extended dimer. In any case, this structure would not help explain why the conductivity anomaly is larger than the anomaly in colligative properties.
- (19) J. Wenograd and R. A. Spurr, *J. Am. Chem. Soc.*, **79**, 5844 (1957).
  - (20) H. S. Harned and B. B. Owen, "The Physical Chemistry of Electrolytic Solutions", 3rd ed, Reinhold, New York, N.Y., 1958, p. 462.
  - (21) G. Scatchard and S. S. Prentiss, *J. Am. Chem. Soc.*, **56**, 1486 (1934).
  - (22) F. Gölles, *Monatsh. Chem.*, **93**, 191 (1962).
  - (23) J. F. Marucco, M. Ratouis, and M. Dode, *J. Chim. Phys.*, **63**, 239 (1966).
  - (24) D. N. Chaplits, K. D. Samokhvalova, and I. Ya. Tyuryaev, *Khim. Prom.*, **41**, 653 (1965).
  - (25) G. R. Nash and C. B. Monk, *J. Chem. Soc.*, 4274 (1957).
  - (26) C. W. Davies, *J. Am. Chem. Soc.*, **54**, 3776 (1932).
  - (27) C. A. Macinnes and T. W. Shedlovsky, *J. Am. Chem. Soc.*, **54**, 1429 (1932).

## Capacitance and Conductance of Solutions of Optically Active Amino Acid Ion Pairs in 1-Octanol

Stefan Highsmith\*

Chemistry Department, Brandeis University, Waltham, Massachusetts 02154 (Received December 2, 1974)

The dipole moments ( $\mu$ ) and the equilibrium constants for proton transfer ( $K_p$ ) and ionic dissociation ( $K_d$ ) for ion pairs composed of L-phenylalanine methyl ester and *N*-acetyl-D- or L-phenylalanine in 1-octanol were determined by capacitance and conductance measurements. The nearly equal values for  $\mu$ ,  $K_p$ , and  $K_d$  for the D,L and L,L ion pairs imply that specific contacts at points other than the charge centers do not occur in this semipolar medium ( $\epsilon_0 = 9.88$ ) which roughly approximates the interior of a protein. Ion pairing and proton transfer are discussed.

### Introduction

Recent increased interest in ion pairs in solution has motivated research to obtain detailed descriptions of the association and structure of ion pairs in solvents of low permittivity by measuring the dielectric properties of the solution.<sup>1</sup> The results for salts in sufficiently apolar media, where the solvent association and conductance are negligible, have yielded highly detailed structures for ion pairs in solution. In an attempt to obtain similar information for ion pairs in a somewhat polar solvent, the capacitance and conductance of solutions of the amine L-phenylalanine methyl ester plus one of the carboxylic acids, *N*-acetyl-D- or L-phenylalanine in 1-octanol were measured.

My intent was to determine what differences exist in the equilibrium constants for proton transfer and ionic dissociation and the structures for amino acid ion pairs for which the sole difference is the optical activity of one of the ions. Any differences found would be attributable to nonelectrostatic interactions between the modified amino acids and would result from differences in the shapes of the ions. Solvation, the atomic skeleton, and the electronic distribution are identical for the D and L ions. London dispersion forces, hydrogen bonding, dipole stabilization, and ion pair solvation were expected as possible contributors to the differences, if any, between the optically active ion pairs. Model building (using Ealing CPK atomic models) showed that the closely packed L,D pair allowed favorable phenyl-phenyl interactions which were not possible for the L,L pair. Thus, if the ions were in contact at points other than the charge centers, the L,D pair would be expected to have a smaller dissociation constant and a different dipole moment from the L,L pair.

Hydrogen bonding at a second point of contact appeared, from model building, to be possible for both pairs between the amide hydrogen and the ester carbonyl oxygen. The ion pairs with the second hydrogen bond had no other possible points of contact, implying that these structures would have equal dissociation constants but dissimilar dipole moments.

The specific physical and chemical interactions which occur in the interior of a protein molecule to determine its unique three-dimensional shape, although of interest, are difficult to measure directly in a macromolecule due to the large number of such interactions which occur simulta-

\*Address correspondence to Cardiovascular Research Institute, University of California, San Francisco, Calif. 94143.

neously. The present study was motivated by a desire to devise a model system for such interactions. Octanol, with a permittivity of 9.88, offers a reasonable model for the interior of a protein<sup>2</sup> perhaps somewhat on the apolar side; so interactions between the amino acids are of interest as models for the *specific* interactions involved in determining the tertiary structure of proteins.

### Experimental Section

**Materials.** 1-Octanol (99%) was purchased from Aldrich Chemical Co. and distilled twice under reduced pressure. A center portion was collected each time and stored in the dark under nitrogen. *N*-Acetyl-L- and D-phenylalanine and L-phenylalanine methyl ester-HCl were obtained from the Sigma Chemical Co. The acid was recrystallized thrice from chloroform and stored in a desiccator at 4°. Stock solutions were prepared by weighing out samples which were dissolved in octanol. The stock solutions were stored at 4°. The base was dissolved in dilute aqueous Na<sub>2</sub>CO<sub>3</sub> and extracted with ether. The combined ether portions were dried with MgSO<sub>4</sub> and the ether was removed on a rotary evaporator. The clear viscous free base was then distilled at reduced pressure. A center portion was collected in a weighed flask and octanol was added to make a stock solution. The entire operation took about 1 hour. The stock solution was stored at 4°. Potentiometric titration of the stock solution, when the base was extracted into dilute HCl, yielded a concentration which was within 0.2% agreement with the concentration determined by weighing. The purified stock solutions were stable for several weeks. Tetraisoamylammonium nitrate was gratefully received from Dr. Adan Effio and used directly. Stock solutions were prepared as for the acid.

Solutions used for measurements were prepared by weighing out portions of the acid and the base stock solutions and octanol in a nitrogen drybox. Special care had to be taken to clean the measuring cells of the viscous octanol. The best procedure was found to be rinses with boiling hexane, acetone, and methanol, followed by several hours under vacuum.

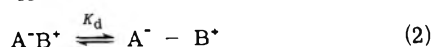
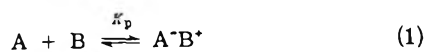
**Measurements.** The optical activity of the stock solutions was checked using a Zeiss Winkel polarimeter. Potentiometric titrations were done at 25.0° using a Corning digital 112 research pH meter. Molar volumes were measured at 25.0° using twin-necked pycnometers produced by G. Finkenbeiner, Inc. The complex admittance of the solu-



tions,  $G + j\omega C$ , was measured with a General Radio Type 1615 A transformer ratioarm bridge and guarded three terminal cells by the method of Grunwald and Effio.<sup>3,4</sup> The cells were thermostated at  $25.00 \pm 0.01^\circ$  in a dry nitrogen bath. The conductance,  $G$ , varied from 0 to  $60 \mu\text{S}$ . The capacitance,  $C$ , was about  $175 \text{ pF}$ . Air capacitance was  $18 \text{ pF}$ . Three solutions and a pure solvent reference were measured during one experiment.

## Results

**Conductance Data.** The solvent showed a conductance which varied from 0.2 to  $1.5 \mu\text{S}$  depending on the method of cleaning the cells between runs. Solutions of the base showed no increased conductance with concentration. Solutions of acid showed a small increase with  $G = 2.5 \mu\text{S}$  for the most concentrated solutions ( $1.293 \times 10^{-2} M$ ). A plot of the conductance,  $G$ , of the D acid plus L base solutions vs. the total concentration of added base is shown in Figure 1. The equilibria shown by eq 1 and 2 for proton transfer to



form the ion pairs and for dissociation of the ion pairs to free ions must be considered.<sup>5</sup> If  $c_A$  and  $c_B$  are the total concentration of acid and base,  $x$  is the concentration of free base,  $I$  is the concentration of free ions, and  $a$  is the concentration of excess acid, then the expressions for mass balance are as follows:

$$c_A = (x + a) + (c_B - x) + I \quad (3)$$

$$c_B = x + (c_B - x) + I \quad (4)$$

$$a = c_A - c_B \quad (5)$$

Thus the equilibrium constants may be written as

$$K_p = (c_B - x)/x(x + a) \quad (6)$$

and

$$K_d = I^2/(c_B - x) \quad (7)$$

where  $c_B - x$  is the concentration of the ion pairs and  $I$  is taken as stoichiometrically negligible compared to  $x$  and  $c_B - x$ . The activity coefficients have been taken as unity.

The specific conductance,  $1000L = 1000G/A$  (where  $A$  is the cell constant) is equal to  $\Lambda I$  or

$$1000L = \Lambda \sqrt{K_d}(c_B - x)^{1/2} \quad (8)$$

where  $\Lambda$  is the equivalent conductance of the free ions. The concentration of free base,  $x$ , can be obtained as a function of the known  $a$  and  $c_B$  and the parameter  $K_p$ , as shown in

$$x = \frac{\sqrt{(aK_p + 1)^2 + 4c_B K_p} - (aK_p + 1)}{2K_p} \quad (9)$$

When (9) is substituted into (8), a least-squares analysis can be done to obtain values for the parameters  $\Lambda \sqrt{K_d}$  and  $K_p$ . No data are available for  $\Lambda$  for these ions or this solvent; so the value obtained from measurements on tetraisoamylammonium nitrate in octanol, 4.0, was used. With this analysis, the concentrations of all the species in solution could be obtained and are shown in Table I along with the equilibrium constants.

**Capacitance Data.** The dielectric increments (the slopes of the plots of the change in permittivity vs. concentration) for solutions of acid and base only were found to be  $S_A = 2.44 \pm 0.29 M^{-1}$  and  $S_B = -2.74 \pm 0.48 M^{-1}$ , respectively.

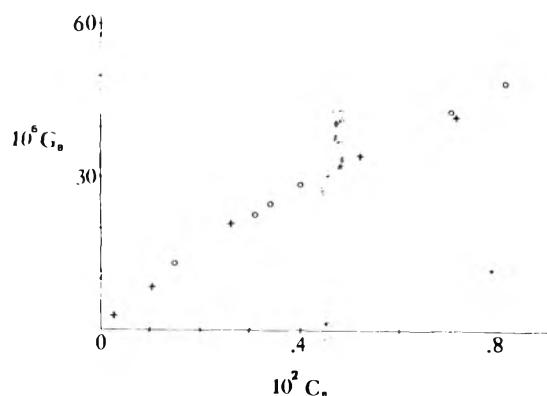


Figure 1. The conductance,  $G_B$ , in seimens, of solutions of *N*-acetyl-L- or D-phenylalanine and L-phenylalanine methyl ester in 1-octanol vs. the concentration,  $c_B$ , of base (the ester). Acid is in roughly  $0.2 \times 10^{-2} M$  excess. Circles are for the L,D solutions and crosses are for the L,L solutions.

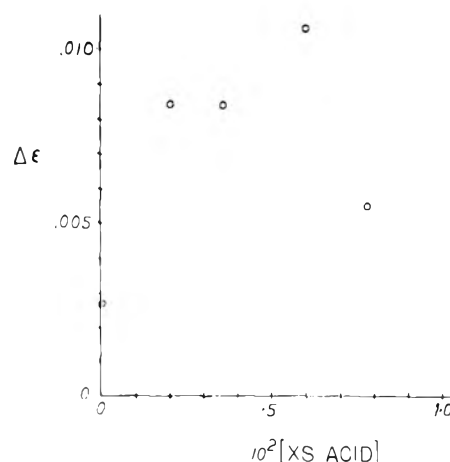


Figure 2. The change in permittivity,  $\Delta\epsilon$ , for  $0.2 \times 10^{-2} M$  solutions of the base, L-phenylalanine methyl ester, vs. the concentration of excess acid, *N*-acetyl-D-phenylalanine.

Solutions of acid and base were prepared with excess acid to drive the equilibrium toward more complete proton transfer.<sup>5</sup> Figure 2 shows the effect of increasing excess acid on the  $\Delta\epsilon$  for a  $0.2 \times 10^{-2} M$  solution of base plus acid. Experiments were done using solutions with an excess acid concentration of approximately  $0.2 \times 10^{-2} M$ .

The change in permittivity due to the ion pairs and free ions was obtained correcting the measured permittivity for the contributions due to the free acid and base (see Table II). The solutions were dilute enough to assume that  $\Delta\epsilon_{meas} = \sum S_i C_i$ , where  $S_i$  is the molar dielectric increment for species  $i$  of concentration  $C_i$ . Thus eq 10 yields (11). When the mass law is applied, assuming the free ions are stoichiometrically insignificant, one obtains eq 12. A linear least-

$$\Delta\epsilon_{meas} = \Delta\epsilon_{ions \& ion \ pairs} + \Delta\epsilon_{acid} + \Delta\epsilon_{base} + C \quad (10)$$

$$= S_{IP}(IP) + S_{FI}(FI) + S_A(A) + S_B(B) + C \quad (11)$$

$$\begin{aligned} \Delta\epsilon_{meas} - S_A(A)_{total} - S_B(B)_{total} &= \Delta\epsilon_{free \ ions \ \& \ ion \ pairs} \\ &= (S_{IP} - S_A - S_B)(IP) + S_{FI}(FI)^{1/2} + C \end{aligned} \quad (12)$$

TABLE I

Expt no.	$10^2 c_B, M$	$10^2 c_A, M$	$10^2 x, M$	$10^2(c_B - x), M$	$10^2 \sqrt{I}, M^{1/2}$	$10^6 G, S$
$K_p = 22 \pm 2 M^{-1} K_d = (2.68 \pm 0.24) \times 10^{-6} M K_p K_d = 6.0 \times 10^{-5}$ L,D						
1	0.1489	0.3554	0.1369	0.0103	0.403	13.12
2	0.2988	0.5413	0.2662	0.0297	0.531	22.79
3	0.3464	0.5465	0.3087	0.0346	0.556	24.98
4	0.4048	0.6352	0.3554	0.0458	0.595	28.57
5	0.6982	0.9072	0.5894	0.1035	0.727	42.77
6	0.8023	1.0540	0.6629	0.1334	0.775	48.51
$K_p = 19.5 \pm 2 M^{-1} K_d = (2.93 \pm 0.25) \times 10^{-6} M K_p K_d = 5.7 \times 10^{-5}$ L,L						
1	0.0261	0.1051	0.0252	0.0005	0.202	3.29
2	0.1051	0.2248	0.0997	0.0043	0.333	8.98
3	0.2611	0.5079	0.2363	0.0223	0.504	20.56
4	0.5204	0.7551	0.4549	0.0612	0.654	34.65
5	0.7063	0.8227	0.6138	0.0874	0.717	41.50
6	1.0171	1.2835	0.8318	0.1781	0.850	58.40

TABLE II

Expt no.	$10^2[\text{ion pairs}], M^a$	$\Delta \epsilon_{\text{meas}}$	$\Delta \epsilon(\text{corr for acid + base})$
L,D			
1	0.0103	0.0212	0.0158
2	0.0297	0.0319	0.0248
3	0.0346	0.0317	0.0256
4	0.0458	0.0354	0.0284
5	0.104	0.0521	0.0451
6	0.133	0.0566	0.0483
L,L			
1	0.0005	-0.0049	-0.0071
2	0.0043	0.0013	-0.0022
3	0.0223	0.0239	0.0167
4	0.0612	0.0355	0.0282
5	0.0874	0.0364	0.0319
6	0.1781	0.0661	0.0570

<sup>a</sup> Total concentrations of acid and base,  $C_A$  and  $C_B$ , are shown in Table I.

square analysis was then done to separate the contribution due to the ion pairs and the free ions (this is the 90° out-of-phase contribution due to the conductance<sup>6-9</sup>), and obtain the molar dielectric increments needed to calculate the dipole moment.  $S_{ip}$  is the molar dielectric increment due to the ion pairs,  $S_A$  is that due to the acid,  $S_B$  to the base, and  $S_{FI}(\text{free ions})^{1/2}$  is the contribution due to the free ions.  $S_{FI}$  is an empirical slope, which according to Onsager and Provencher<sup>8</sup> must lie between 10.6 and 3.6 for the given solvent. Equation 12 contains a constant term,  $C$ , to allow for the presence of free ions in the pure solvent. Although the concentration of the latter is small, their effect is not negligible since it varies as the square root of the concentration. The results are shown in Table III.

### Discussion

**Equilibrium Constants.** The equilibrium constant for proton transfer,  $K_p = 21$ , is small. This may seem surprising compared to a predicted value of about  $10^5$  based on aqueous  $pK_A$ 's. However, acidities and basicities are difficult to predict in nonaqueous solutions.  $K_p$  values from Jadzyn and Malecki<sup>10</sup> for acids and bases in solvents of low

TABLE III

Compd	$S_{ip}, M^{-1}$	$S_{FI}, M^{-1}$	$C$	$\mu, D$
L,D	12.47	5.14	-0.0068	9.9
L,L	14.74	5.87	-0.0197	10.6

permittivity ( $\epsilon_0 = 2-3$ ), where  $pK_A + pK_B$  is equal to that in this work (8.2), when extrapolated to  $\epsilon_0 = 9.88$  agree with the measured value.  $K_p$  includes two reactions: the association of the free acid and free base to form a complex, and the proton transfer step to form the ion pair. No unequivocal rationalization of the low value is possible. It could be due to strong solvation of the free acid or base or due to the unfavorable energetics of forming an ion pair in a solvent of permittivity 9.88. Jadzyn and Malecki<sup>10</sup> assumed the latter to be the case for their apolar solvents. Their data are for three solvents which are not likely to have solvating properties similar to each other or to octanol; so unfavorable energetics of ion pair formation seems to be the more reasonable explanation.

Comparisons are difficult to make with data for proton transfer in water. Ion pairs in water dissociate nearly completely and aqueous data must be compared to  $K_p K_d$ . The ratio is 11 orders of magnitude.

In applying the values reported for  $K_d$ , it should be kept in mind that our experiment does not measure  $K_d$  directly. As explained before, it measures  $\Lambda \sqrt{K_d}$ , and the accuracy of the result for  $K_d$  depends on the accuracy of the value chosen for  $\Lambda$ . However, the ratio of  $K_d$  for the enantiomers is independent of  $\Lambda$  because the free ions have the identical equivalent conductance in an optically inactive solvent. Moreover, the absolute magnitude of  $K_d$  also appears to be reasonable, based on the value of  $K_d$  for tetraisoamylammonium nitrate ( $2.88 \times 10^{-5} M$ ).<sup>9</sup> This is about one order of magnitude larger than for the amino acid ion pairs and the difference is typical for ion pairs with and without a hydrogen bond.

**Dipole Moments and Structures of the Ion Pairs.** The dipole moments for the L,D and L,L complexes were calculated by the method of Onsager.<sup>11,12</sup> Within experimental error, the dipole moments for the two enantiomers are the same. The average of the values 9.9 and 10.6 D, when treated by the method of Bauge and Smith,<sup>13</sup> which method

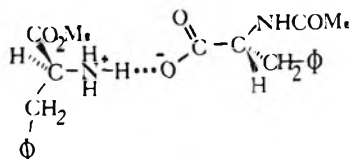


Figure 3. Favored configuration for L,D ion pair.

considers the effects of the dipole moments of the cation and anion and the mutual polarization of the ions, yields an interionic distance of 3.1 Å which is in excellent agreement with that obtained from the crystallographic data<sup>14</sup> for  $\text{NH}_4^+$  and  $\text{CO}_2^-$ , 3.2 Å. When this is combined with the apparent equality of the equilibrium constants, the following picture of the ion pairs emerges: the ions have intimate contact at the centers of charge with no other enduring specific points of contact; the ions are each free to rotate about the point of contact and about the single bonds within each ion to an extent which is comparable to that allowed in the free acid and base.

If there were stable specific secondary points of contact, there certainly would be a difference in the dipole moments and possibly in the dissociation and proton transfer equilibrium constants. If the ions were solvent separated or were not in contact at the charge centers, the dipole mo-

ment would have to be larger. Figure 3 shows the favored structure for the L,D pair.

**Acknowledgment.** Acknowledgment is made to the donors of the Petroleum Research Fund, administered by the American Chemical Society, for partial support of this work. Thanks are due also to the Rosenstiel Fund of Brandeis University and to the National Institutes of Health for postdoctoral fellowships. My special thanks to Professor Ernest Grunwald for his guidance and many helpful discussions throughout the course of this work.

## References and Notes

- (1) E. Grunwald, S. Highsmith, and T.-P. Li in "Ions and Ion Pairs in Organic Reactions", Vol. 2, M. Szwarc, Ed., Wiley-Interscience, New York, N.Y., 1974.
- (2) Y. Nozaki and C. Tanford, *J. Biol. Chem.*, **246**, 2211 (1971).
- (3) E. Grunwald and A. Effio, *J. Solution Chem.*, **2**, 373 (1973).
- (4) K. S. Pirabaldi and R. L. Kay, *Rev. Sci. Instrum.*, **40**, 726 (1969).
- (5) R. Fuoss and M. Ellicott, *J. Am. Chem. Soc.*, **61**, 294 (1939).
- (6) P. Debye and H. Falkenhagen, *Phys. Z.*, **29**, 401 (1928).
- (7) H. Falkenhagen and G. Kelbg in "Modern Aspects of Electrochemistry", Vol. 2, J. O'M. Bockris, Ed., Butterworths, London, 1959.
- (8) L. Onsager and S. W. Provencher, *J. Am. Chem. Soc.*, **90**, 3134 (1968).
- (9) S. Highsmith and E. Grunwald, *J. Phys. Chem.*, **78**, 1431 (1974).
- (10) J. Jadzyn and J. Malecki, *Acta Phys. Polon.*, **A41**, 599 (1972).
- (11) L. Onsager, *J. Am. Chem. Soc.*, **58**, 1486 (1936).
- (12) C. F. J. Bottcher, "Theory of Electric Polarization", Elsevier, Amsterdam, 1952, p 191.
- (13) K. Baugé and J. W. Smith, *J. Chem. Soc.*, 4249 (1964).
- (14) L. Pauling, "The Nature of the Chemical Bond", Cornell University Press, Ithaca, N.Y., 1944, Chapter 10.

## Evaluation of Dielectric Behavior by Time Domain Spectroscopy.

### I. Dielectric Response by Real Time Analysis

Robert H. Cole

Chemistry Department, Brown University, Providence, Rhode Island 02912 (Received February 21, 1975)

Publication costs assisted by the Material Sciences Program, Brown University, with support from the National Science Foundation

Simple formulas are derived by "real time" analysis by which the dielectric response function of a finite sample in a coaxial line may be calculated from the time integral and self convolution of the reflections produced by an incident step voltage pulse. These take account of finite amplitude of the reflection in second-order approximation and of finite rise time of the incident pulse. The cases of a sample inserted in a matched line and of a sample terminating a line are treated; the latter is shown to have several advantages. Errors in the analysis and information derivable from short time behavior are discussed. Formulas are also derived which take account of finite ohmic conductivity if this is not too large.

### I. Introduction

The availability of time domain spectroscopy (TDS) systems for generating voltage pulses with short rise times ( $<40 \times 10^{-12}$  sec) and observing reflected or transmitted signals from samples in coaxial lines has led to development of a variety of methods<sup>1</sup> for determining dielectric response behavior from these signals for a wide possible range of times ( $10^{-7}$  to  $10^{-11}$  sec at least). These methods have, however, suffered from one or more of several limitations: necessity for numerical Fourier analysis, restricted

time range (time "window"), small signals and large errors from residuals, difficulty in taking account of finite ohmic conductance, and necessity of assuming the form of the response or relaxation function.

In this first of two companion papers, we describe "real time" methods for evaluating dielectric response functions from observations of voltage waves reflected from a dielectric sample. The analyses require only simple numerical integrations without prior assumptions as to the form of the function, are applicable for a considerably wider range of

sample parameters than in previous simple methods, and permit evaluation of conductivity and dielectric properties of samples with appreciable ohmic conductance. In the second paper, we shall present "frequency domain" methods which do require numerical Fourier transformation to obtain complex permittivity  $\epsilon^*(\omega)$ , but are otherwise simple and are still more generally useful.

We here take the objective of the measurements to be determination of the time dependence of dielectric polarization, assumed linear in the sense of time superposition. For a time-dependent voltage  $V(t)$  across a sample, an appropriate response function  $\Phi(t)$  can then be defined relating electrode charge  $Q(t)$  for geometric capacitance  $C$  to  $V(t)$  by

$$Q(t) = C[\epsilon_\infty V(t) + \int_0^t dt' \dot{\Phi}(t-t')V(t')] \quad (1)$$

where  $\epsilon_\infty$  is the conventional limiting permittivity at high frequency or time short compared to the scale of  $\Phi(t)$  and resolution of the observed reflected wave. The complex permittivity  $\epsilon^*(s)$  measured by steady state methods is related to  $\Phi(t)$  by

$$\epsilon^* = \epsilon_\infty + s\phi(s) \quad (2)$$

$$\psi(s) = L\Phi(t) = \int_0^\infty dt e^{-st}\Phi(t) \quad (3)$$

$s$  being the Laplace transform variable, replaced by  $i\omega$  where  $\omega = 2\pi$  frequency to obtain  $\epsilon^*(\omega)$ .

Conventional treatments of the problem of evaluating  $\Phi(t)$  or  $\epsilon^*(s)$  from an observed reflected voltage wave  $R(t)$  for a given incident  $V_0(t)$  proceed by Laplace transformation of eq 1 and the propagation equations for the coaxial line with appropriate boundary conditions to obtain an explicit solution for  $r(s)$ , the Laplace transform  $LR(t)$ , in terms of  $v_0(s)$ ,  $\epsilon^*(s)$ , and line parameters. The difficulties with the resulting expressions can be illustrated by the solution<sup>2</sup> for a dielectric sample of length  $d$  inserted in a line terminated in its characteristic impedance

$$\begin{aligned} r(s) &= \rho^* \frac{1 - \exp(-2d\epsilon^{*1/2}s/c)}{1 - \rho^{*2} \exp(-2d\epsilon^{*1/2}s/c)} v_0(s) \quad (4) \\ \rho^* &= (\epsilon^{*1/2} - 1)/(\epsilon^{*1/2} + 1) \end{aligned}$$

Here  $c$  is the speed of propagation in the empty line (0.300 mm/psec, 1 psec =  $10^{-12}$  sec), our sign conventions for  $R(t)$ ,  $r(s)$ , and  $\rho^*$  are the negative of the usual ones to make their real parts positive, and  $v_0(s) = LV_0(t)$ .

No exact analytic solutions of eq 4 for  $\epsilon^*$  are known even in the simple case of Debye relaxation. For times preceding the first internal reflection, the exponentials can be dropped, permitting solution for  $\epsilon^{*1/2}$  and hence  $\epsilon^*$ , but long samples are required for times greater than a few nanoseconds and the relation of  $R(t)$  to  $\Phi(t)$  is not simple. Suggett<sup>3</sup> and coworkers have solved eq 4 by Newton-Raphson iteration assuming trial values for  $\epsilon^*$  starting at low frequencies, a procedure which works well but gives little insight into the relation of  $R(t)$  to  $\Phi(t)$  or of  $r(s)$  to  $\epsilon^*(s)$ .

The thin sample method proposed by Fellner-Feldegg<sup>2</sup> is an entirely different approach based on expanding the exponentials in eq 4 and retaining only the first-order terms in  $d$ . His result is

$$r(s) = (d/2c)(\epsilon^* - 1)s v_0(s) \quad (5)$$

which gives a very simple explicit solution for  $\epsilon^* - 1$ . For an applied step voltage  $V_0(t) = V_0$ ,  $t > 0$ , the reflected

voltage pulse  $R(t)$  by inverse Laplace transformation of eq 5 is

$$R(t) = L^{-1}r(s) = (d/2c)[(\epsilon_\infty - 1)\delta(t) + \dot{\Phi}(t)]V_0 \quad (6)$$

thus showing the direct proportionality of  $R(t)$  to the derivative of the response function. The results are attractively simple, but unfortunately exact only in the limit of zero sample length (and hence no signal) with no indication of errors for real samples of finite length. van Gemert has pointed out<sup>4</sup> that the  $\delta$  function at time  $t = 0$  is an idealization obtained only in the limit  $d \rightarrow 0$ . In reality a large but finite peak is observed, with duration of order  $T_\infty = 2d\epsilon_\infty^{1/2}/c$ , i.e., the time required to charge the sample during the first internal reflection, which is typically of order 10–100 psec (see Figures 5, 7, and 10 for examples). He also showed by including second-order terms in the expansion of eq 4 and numerical calculations of  $R(t)$  assuming a Debye relaxation,  $\Phi(t) \sim 1 - \exp(-t/\tau)$ , that values of  $\Phi(t)$  from eq 6 can be considerably in error for quite small lengths, calculated relaxation times being too long.

Despite the drawbacks, Fellner-Feldegg's thin sample result has, in contrast to other methods, the advantage of giving  $\Phi(t)$  directly from  $R(t)$ , although this formula is obtained by transformations to and from the frequency domain. In a review of time domain methods, Suggett<sup>5</sup> remarked that "since the first application of fast-response methods to dielectric measurements, the value of direct time-domain conversion of the data has been universally recognized. It is after all a strange paradox that, in order to obtain information about time-dependent molecular motions from the time-dependent reflection coefficient,  $P(t)$ , one must go through the stage of the frequency-dependent reflection coefficient  $\rho(j\omega)$ ".

It seemed to the writer that at least Fellner-Feldegg's first-order result should be obtainable directly without transformations. This indeed proves to be possible by a simple analysis, but more important, the analysis reveals the principal reason for errors in  $\Phi(t)$  calculated from eq 6 and provides a simple means for obtaining a considerably better approximation *without* prior assumptions as to the form of  $\Phi(t)$ . The second-order correction obtained requires only a simple numerical convolution of  $R(t)$  to evaluate  $\Phi(t)$  with useful accuracy for sample lengths and reflection signals much larger than can be used for satisfactory results from eq 6.

A similar analysis can be developed for alternative experimental arrangements. The case of a dielectric sample terminating a coaxial line, rather than being inserted in a matched line, is found to have advantages of greater simplicity and larger observed reflection signals for a given accuracy of determining  $\Phi(t)$  from the analysis. In both cases, there are no intrinsic long time limits, permitting observations of finite ohmic conductivity. If this is not too large, both its limiting value at long times and a total response function can be evaluated.

The results are particularly simple for an incident step voltage, but approximate account of finite rise time can be taken. We also discuss procedures which can be helpful in analysis of initial behavior at times less than the sum of pulse rise and internal sample reflection times.

## II. Sample in Matched Line

In this experimental arrangement, shown in Figure 1, a finite sample of length  $d$  is inserted in a coaxial line, assumed loss free, which is terminated in its characteristic

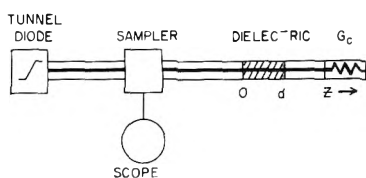


Figure 1. Experimental arrangement for sample in matched line method.

conductance  $G_c$ . We denote the incident voltage at the front surface by  $V_0(t)$  and the reflected voltage by  $R(t)$ ,  $t > 0$ , so that the voltage at  $d = 0$  is

$$V(t) = V_0(t) - R(t) \quad (7)$$

For nonmagnetic samples with permeability  $\mu = 1$ , the voltage  $V = V(t, z)$  and current  $I = I(t, z)$  at all points in the line are related by

$$\frac{\partial V}{\partial z} = -L_c \frac{\partial I}{\partial t} \quad (8)$$

where  $L_c$  is the inductance per unit length. For the empty line preceding the dielectric section,  $I$  and  $V$  are also related by

$$\frac{\partial I}{\partial z} = C_c \frac{\partial V}{\partial t} \quad z < 0 \quad (9)$$

where  $C_c$  is the geometric capacitance per unit length. The current  $I(t)$  at  $d = 0$  is then given by

$$I(t) = G_c [V_0(t) + R(t)] \quad (10)$$

where  $G_c = (C_c/L_c)^{1/2}$  and  $c = (C_c L_c)^{-1/2}$  is the speed of propagation in the empty line.

In the dielectric section,  $0 < z < d$ , the second propagation eq 9 is replaced by

$$\partial I / \partial z = -\partial Q / \partial t \quad z > 0 \quad (11)$$

where  $Q$  is given by eq 1 with  $C = C_c$  for unit length. As the line is terminated by its characteristic conductance  $G_c$ , the boundary condition at  $z = d$  in this arrangement is  $I(t, d) = G_c V(t, d)$ . We now approximate  $I(t, d)$  and  $V(t, d)$  in terms of  $I(t)$  and  $V(t)$  at  $d = 0$  by second-order Taylor series expansion in powers of  $d$ :

$$I(t, d) = I(t) + d \left( \frac{\partial I}{\partial z} \right)_{z=0} + \frac{1}{2} d^2 \left( \frac{\partial^2 I}{\partial z^2} \right)_{z=0}$$

$$V(t, d) = V(t) + d \left( \frac{\partial V}{\partial z} \right)_{z=0} + \frac{1}{2} d^2 \left( \frac{\partial^2 V}{\partial z^2} \right)_{z=0}$$

the subscript zero denoting evaluation at  $z = 0$ . Inserting values of  $I(t)$  and  $V(t)$  from eq 7 and 10, of the derivatives from eq 8, 11, and 1, and applying the boundary condition gives after rearrangement the second-order result

$$(d/2c) \frac{d}{dt} \int_0^t dt' [(\epsilon_\infty - 1)\delta(t') + \dot{\Phi}(t')] [V_0(t-t') - R(t-t')] = R(t) + (d/c)\dot{R}(t) \quad (12)$$

In this equation, there are no terms explicitly of order  $d^2$  because those of second-order involving  $V_0$  cancel, while ones involving  $R(t)$  are of third order and have been neglected. We also note that although  $V_0(t)$  and  $R(t)$  have been defined as true values in the line at  $d = 0$ , and at the sampler probe input after taking account of propagation time, the result 12 is also valid for recorded response of the sampler to  $V_0(t)$  and  $R(t)$ , because a linear superposition

function expressing the sampler response characteristic commutes with the operations in eq 12.

In commercially available TDS equipment, the incident pulse has the form shown in Figure 2a, and can be approximated by a finite ramp with linear rise to constant value  $V_0$  in time  $Tr$  (40 psec for Hewlett-Packard Type 181 TDS system):

$$V_0(t) = V_0 t / Tr \quad 0 < t < Tr \\ = V_0 \quad t > Tr \quad (13)$$

Although our principal interest is in the relation of  $\Phi(t)$  to the response  $R(t)$  for times  $t > Tr$ , analysis for  $t < Tr$  is needed to take account of the effect of finite rise time on this relation, and can be useful for situations in which the rise time is by design or necessity not small compared to times in which  $\Phi(t)$  changes significantly.

For times  $t < Tr$ , eq 12 can be written

$$(\epsilon_\infty - 1) + \Phi(t) = (2cTr/d) \frac{R(t)}{V_0} + Tr \times \\ \frac{d}{dt} \int_0^t dt' [(\epsilon_\infty - 1)\delta(t') + \dot{\Phi}(t')] \frac{R(t-t')}{V_0} + 2Tr \frac{R(t)}{V_0} \quad t < Tr \quad (14)$$

In first-order approximation for small sample lengths,  $\Phi(t)$  is given by the counterpart of Fellner-Feldegg's thin sample result

$$(\epsilon_\infty - 1) + \Phi(t) \cong (2cTr/d) \frac{R(t)}{V_0} \quad t < Tr \quad (15)$$

This is an attractively simple result, but if the sample length is not so small that  $R(t)$  is much less than  $V_0$ , the last two second-order terms in eq 14 give appreciable corrections. For  $\Phi(t)$  and  $R(t)$  of the general form shown in Figure 2b,c, the last term in  $\dot{R}(t)$  is small except at short times of order  $T_\infty$  for charging the "instantaneous" polarization  $\epsilon_\infty - 1$ . The superposition integral of  $\Phi(t)$  and  $R(t)$  can, however, be significant at all times for which  $\Phi(t)$  is. A useful approximation to its value can be obtained by using the first-order result 15, which gives after partial integration

$$(\epsilon_\infty - 1) + \Phi(t) = (2cTr/d) \frac{R(t)}{V_0} + 2cTr/d \times \\ \int_0^t dt' Tr \frac{\dot{R}(t')}{V_0} \frac{R(t-t')}{V_0} + 2Tr \frac{\dot{R}(t)}{V_0} \quad t < Tr \quad (16)$$

For times  $t > Tr$ , the solution of eq 12 for  $V_0(t)$  given by eq 13 after time integration is

$$(\epsilon_\infty - 1) + \frac{1}{Tr} \int_{t-Tr}^t dt' \Phi(t') = (2c/d) \int_0^t \frac{R(t')}{V_0} + \\ \int_0^t dt' [(\epsilon_\infty - 1)\delta(t') + \dot{\Phi}(t')] \frac{R(t-t')}{V_0} + 2 \frac{R(t)}{V_0} \quad t > Tr \quad (17)$$

The integral on the left-hand side is simply the time average of  $\Phi(t)$  over the interval  $t - Tr$  to  $t$ , which we approximate by  $\Phi(t - \frac{1}{2}Tr)$ . The first-order result is then essentially Fellner-Feldegg's thin sample formula in integrated form:

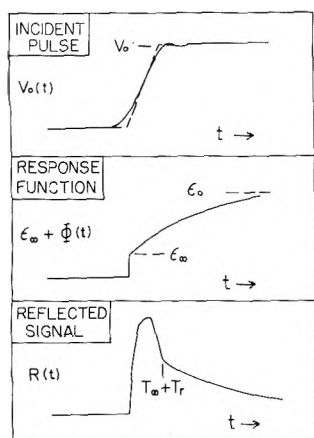


Figure 2. (a) Incident pulse  $V_0(t)$  and finite ramp approximation with rise time  $Tr$ . (b) Typical response function  $\epsilon_\infty + \Phi(t)$ . (c) Reflected signal  $R(t)$  for a finite sample in matched line.

$$(\epsilon_\infty - 1) + \Phi(t - \frac{1}{2}Tr) = (2c/d) \int_0^t dt' \frac{R(t')}{V_0} \quad t > Tr \quad (18)$$

which is again a good approximation only for sample lengths small enough that  $R(t) \ll V_0$ . To obtain a more accurate second-order result, the superposition integral in eq 17 is approximated using eq 15 for  $\Phi(t)$ ,  $t < Tr$ , and the approximation from eq 18 for  $t > Tr$  that

$$(\epsilon_\infty - 1)\delta(t) + \dot{\Phi}(t) = (2c/d) \frac{R(t)}{V_0} \quad t > Tr \quad (19)$$

With these approximations, the second-order solution for  $t > Tr$  is

$$(\epsilon_\infty - 1) + \Phi(t - \frac{1}{2}Tr) = (2c/d) \int_0^t dt' \frac{R(t')}{V_0} + (2c/d) \int_0^t dt' \frac{R(t')}{V_0} \frac{R(t-t')}{V_0} + 2 \frac{R(t)}{V_0} + (2c/d) \times \int_0^{Tr} dt' \left[ Tr \frac{R(t')}{V_0} - \frac{R(t')}{V_0} \right] \frac{R(t-t')}{V_0} \quad t > Tr \quad (20)$$

In Appendix A, we consider the evaluation of the last integral, and show that it can for most purposes be adequately approximated by  $(cTr/d)R(Tr)R(t)/V_0^2$ , giving

$$(\epsilon_\infty - 1) + \Phi(t - \frac{1}{2}Tr) = (2c/d) \int_0^t dt' \frac{R(t')}{V_0} + (2c/d) \int_0^t dt' \frac{R(t')}{V_0} \frac{R(t-t')}{V_0} + \left[ 2 + (cTr/d) \frac{R(Tr)}{V_0} \right] \frac{R(t)}{V_0} \quad t > Tr \quad (21)$$

This is the formula we propose for direct evaluation of time-dependent dielectric response from measured reflected pulses. Examples of its use are given in section IV, but some general comments are appropriate here. The evaluation of  $\Phi$  at time  $t - \frac{1}{2}Tr$  corresponds to that for an equivalent ideal step starting at time  $\frac{1}{2}Tr$ , while the last term in eq 20 or 21 vanishes for  $Tr = 0$  and is usually unimportant except for times not much greater than  $t = Tr$ . The latter is also true for the term  $2R(t)/V_0$  arising from the termination by  $G_c$ , which decreases in time for  $\phi(t)$  and  $R(t)$  of the form shown in Figure 2b,c, while the integral of  $R(t)$  in-

creases with time to a limiting value corresponding to the static permittivity (see below).

The most important correction to the first-order result is the self convolution of  $R(t)$ . It is easily seen from eq 1 and 12 that it appears because the voltage across the sample is  $V_0(t) - R(t)$  rather than  $V_0(t)$ . The integral is significant at all times for which  $R(t)$  is not very small compared to  $V_0(t)$ , reaching a maximum at times of order of a characteristic relaxation time for  $\Phi(t)$ , and falling off to zero at  $t \rightarrow \infty$ . Omission of the correction results in the thin sample approximation to  $\Phi(t)$  by the integral of  $R(t)$ . This rises more slowly than the true function, giving apparent relaxation times which are too long, by significant amounts if  $R(t)$  is more than a few percent of  $V_0$  at the beginning of the response resulting from  $\Phi(t)$ . This "nonlinear" effect evidently has nothing to do with finite propagation times in the sample, but rather results from the delay in rise of the sample voltage  $V(t)$  to the final value  $V_0$ .

Conclusions similar to ours have been reached by van Gemert<sup>4</sup> for the special case of a Debye dielectric expressed by

$$\Phi(t) = (\epsilon_0 - \epsilon_\infty)[1 - \exp(-t/\tau)] \quad (22)$$

corresponding to

$$\epsilon^*(s) = \epsilon_\infty + (\epsilon_0 - \epsilon_\infty)/(1 + \tau s) \quad (23)$$

where  $\tau$  is the relaxation time. In his analysis, he evaluated  $R(t)$  from the second-order expansion of eq 4 for  $r(s)$  using eq 23 for  $\epsilon^*(s)$  and showed that the results for  $t > T_\infty = 2d\epsilon_\infty^{1/2}/c$  could be approximated by

$$R(t)/V_0 = (d/2c) \exp(-t/\tau_{app}) \quad (24)$$

$$\tau_{app} = \tau + (d/2c)(\epsilon_0 - \epsilon_\infty) \quad (25)$$

Essentially the same result can be obtained from the present analysis. If the observed  $R(t)$  can be approximated by eq 24, evaluation of the integrals in eq 21 and neglect of the terms proportional to  $R(t)$  gives

$$\Phi(t) \cong (\epsilon_0 - \epsilon_\infty) \times \left[ 1 - \exp(-t/\tau_{app}) \left( 1 - \frac{d}{2c\tau_{app}} (\epsilon_0 - \epsilon_\infty) \frac{t}{\tau_{app}} \right) \right] \quad (26)$$

If the quantity  $\mu = (d/2c\tau_{app})(\epsilon_0 - \epsilon_\infty)$  is small compared to unity, this expression is surprisingly well approximated by  $\Phi(t) = (\epsilon_0 - \epsilon_\infty)[1 - \exp(-t/\tau)]$  with  $\tau$  and  $\tau_{app}$  related by eq 25. It is not clear analytically from eq 26 why this should be so, although at short times the approximation

$$1 - (d/2c\tau_{app})(\epsilon_0 - \epsilon_\infty)t/\tau_{app} \cong \exp(-\mu t/\tau_{app}) \quad (27)$$

valid for

$$t/\tau_{app} \ll 2c\tau_{app}/(\epsilon_0 - \epsilon_\infty) \quad (28)$$

gives  $\Phi(t) = (\epsilon_0 - \epsilon_\infty)[1 - \exp(-t/\tau)]$  with  $\tau = \tau_{app}/(1 + \mu) \cong \tau_{app} - (d/2c)(\epsilon_0 - \epsilon_\infty) + O(\mu^2)$  in agreement with eq 25.

Conditions of the form of the inequality 28 have been cited<sup>4</sup> as giving an upper limit on times for which the thin sample method is valid. These are somewhat misleading, at least if the integrated form for  $\Phi(t)$  is used, as the derived value of  $\Phi(t)$  from the integral of  $R(t)$  is correct in the limit  $t \rightarrow \infty$  for any sample length. This follows from a limit theorem for Laplace transforms:

$$\int_0^\infty dt' R(t') = \lim_{s \rightarrow 0} r(s)$$

where the Laplace transform of  $r(s)$  is given exactly by eq

4. For an incident pulse  $V_0(t)$  approaching the constant value  $V_0$  as  $t \rightarrow \infty$  and  $v_0(s) \rightarrow V_0/s$  as  $s \rightarrow 0$ , evaluation of the limit gives

$$\int_0^{\infty} dt' R(t') = (d/2c)(\epsilon_0 - 1)V_0$$

in agreement with the thin sample formula. (We note that this agreement is secured only if the area under the initial peak is included.)

From these considerations, errors in values of  $\Phi(t)$  from the thin sample formula have the form of distortions of the time scale, the calculated rise of  $\Phi(t)$  to its correct final value being slower than the true one. A useful rule of thumb is that the fractional error in time of response is of order  $R(t_1)/V_0$ , where  $t_1$  is the time at the end of the initial peak in  $R(t)$  resulting primarily from charging the instantaneous polarization, as discussed in section V. For a Debye response, this error is approximately  $(d/2c\tau_{app})(\epsilon_0 - \epsilon_\infty)$ . The self convolution of  $R(t)/V_0$  in eq 21 corrects this distortion with remaining error of order  $(R(t_1)/V_0)^2$ . Thus for 2% error of the first-order result,  $R(t_1)$  should not exceed 2% of  $V_0$ , i.e.,  $R(t_1) < 5$  mV for a 250 mV incident pulse, while for the same error after making the convolution correction  $R(t_1)$  can be as large as 35 mV. As the reflection signal seen by the sampler is superposed on  $V_0(t)$ , noise and irregularities from even small impedance mismatches have much less effect on values of  $\Phi(t)$  calculated for thicker samples using the finite sample formula 21. A further advantage of using an integrated formula for  $\Phi(t)$  rather than Fellner-Feldegg's original formula for  $\dot{\Phi}(t)$  is that irregularities are smoothed by integration, as shown by examples in section IV.

### III. Sample Terminating Line

The methods of the preceding section can be usefully applied to an alternative experimental method, proposed in one form by Iskander and Stuchly,<sup>6</sup> in which a dielectric sample is placed at the end of a coaxial line and so acts as its termination. We consider the arrangement shown in Figure 3, with a sample of length  $d$  and lumped capacitance  $C_s$  at the end, to take approximate account of either dielectric or open end effects. As shown in Figure 3, the observed signal at the sampler for an applied finite ramp is initially the same as for a sample in a matched line, but then rises to a final open circuit value  $2V_0$  as charging of the termination is completed. The voltage and current at  $d = 0$  are conveniently expressed in terms of  $P(t) = V_0(t) + R(t)$ , i.e., the difference between  $V(t)$  and the open circuit reflection voltage  $V_0(t)$ , by the relations  $V(t) = 2V_0(t) - P(t)$ ,  $I(t) = G_c P(t)$ . The boundary condition at  $z = d$  is  $I(t, d) = C_s dV(t, d)/dt$ . Using the Taylor series expansions for  $I(t, d)$ ,  $V(t, d)$  and propagation equations to evaluate the derivatives as before gives through second-order terms

$$\begin{aligned} (d/c) \frac{d}{dt} \int_0^t dt' \left[ \left( \epsilon_\infty + \frac{C_s}{dC_c} \right) \delta(t') + \right. \\ \left. \dot{\Phi}(t') \right] \left[ 2V_0(t - t') - P(t - t') \right] = P(t) + \\ \frac{1}{2} \left( \frac{d}{c} \right)^2 \frac{C_s}{dC_c} \frac{d^2}{dt^2} \left[ P(t) + \frac{C_s}{dC_c} \frac{d}{dt} V_0(t) \right] \quad (29) \end{aligned}$$

In obtaining this result, a term explicitly of order  $d^2$  has been dropped as it involves  $P(t)$  and so is third order. The stray capacitance  $C_s$  in any reasonable experimental arrangement is small (e.g., of order 0.12 pF if it represents

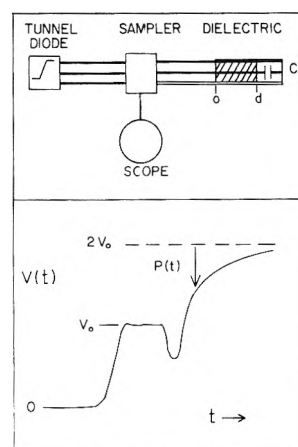


Figure 3. (Upper) Experimental arrangement for sample termination method. (Lower) Voltage observed at sampler for finite ramp voltage from generator.

the capacitance of an open ended 50-ohm coaxial line, and the correction term on the right with the factor  $(C_s/dC_c)$  can then also be neglected.

The similarity of eq 29 to eq 12 for a sample in a matched line is evident, and the differences between the two cases will be considered after solutions for a finite ramp voltage  $V_0(t)$  given by eq 13 have been developed. For times  $t < Tr$ , the dielectric response is given to second order by

$$\begin{aligned} \epsilon_\infty + (C_s/dC_c) + \Phi(t) = (cTr/d) \frac{P(t)}{2V_0} + \\ (cTr/d) \int_0^t dt' \frac{\dot{P}(t')}{2V_0} \frac{P(t-t')}{2V_0} \quad t < Tr \quad (30) \end{aligned}$$

For times  $t > Tr$ , the procedure used in the preceding section gives in second order

$$\begin{aligned} \epsilon_\infty + (C_s/dC_c) + \Phi \left( t - \frac{1}{2} Tr \right) = (c/d) \int_0^t dt' \frac{P(t')}{2V_0} + \\ (c/d) \int_0^t dt' \frac{P(t')}{2V_0} \frac{P(t-t')}{2V_0} + (c/d) \times \\ \int_0^{Tr} dt' \left[ Tr \frac{\dot{P}(t')}{2V_0} - \frac{P(t')}{2V_0} \right] \frac{P(t-t')}{2V_0} \quad t > Tr \quad (31) \end{aligned}$$

and the last integral may similarly be approximated by  $(cTr/2d)P(Tr)P(t)/4V_0^2$ .

The results in the present case differ from those for the sample in a matched line by the factor  $P(t)/2V_0$  replacing  $R(t)/V_0$  and  $c/d$  replacing  $2c/d$ . Together, these differences result in a signal  $P(t)$  which is larger than  $R(t)$  for a given sample length, by approximately a factor of 4 if the length is not too great. This gain is not realized for the same accuracy of derived response, however, as the self convolution correction is approximately twice as large for the same  $d$ . A sample half as long is thus required for comparable accuracy in the present case, with a reflected signal twice as large; these are modest but worthwhile gains. One might suppose that a shorter sample would result in a better approximation to  $\Phi(t)$  at short times, but as discussed in sections IV and V there is little difference in this respect. The present result is also simpler than eq 29 or 21 in that there is no counterpart of the term  $2R(t)/V_0$  for the sample in a matched line. That term results from the conductive termination  $G_c$  with some effect at short times, whereas in the

present case the effect of small stray capacitance  $C_s$  has been neglected.

For a Debye dielectric with response function  $\Phi(t)$  given by eq 22, the present analysis shows that an apparent relaxation time  $\tau_{app}$  of  $P(t)$  is related approximately to the true  $\tau$  of the dielectric by

$$\tau \cong \tau_{app} - (d/c)(\epsilon_0 - \epsilon_\infty)$$

and the error for a given  $d$  is thus twice as great in the present case, in agreement with the preceding discussion.

Finally, we may note that as before in the long time limit, the integrated area of the reflected wave gives the correct static result for arbitrary sample length. This follows from the exact expression for the Laplace transform  $p(s)$  of  $P(t)$ :

$$p(s) = \frac{1 + \rho^*}{2} \times \frac{(1 + zs) - (1 - zs) \exp(-2d\epsilon^{*1/2}s/c)}{(1 + zs) - \rho^*(1 - zs) \exp(-2d\epsilon^{*1/2}s/c)} 2v_0(s) \quad (32)$$

$$z = (d/c)(C_s/dC_c\epsilon^{*1/2})$$

from which

$$\int_0^\infty P(t') dt' = \lim_{s \rightarrow 0} p(s) = (d/c)[\epsilon_0 + C_s/dC_c]2V_0 \quad (33)$$

for an incident pulse approaching the limiting value  $V_0$  as  $t \rightarrow \infty$ . In addition to establishing the validity of the first-order result in this limit, the equation is useful for determining the effective length or stray capacitance correction  $C_s/dC_c$  from measurements of samples with known  $\epsilon_0$ .

#### IV. Examples of Use of the Analysis

Measurements of reflection signals from samples of various lengths in both experimental arrangements have been used to test the analysis. For the most part, liquid normal aliphatic alcohols and glycols were used, as these have been studied by a variety of time domain and steady state methods with reasonable agreement of values of dielectric parameters obtained by different workers.

The measurements were made with a Hewlett-Packard Type 181 TDS system, including Type 1105A-1106B pulse generators, Type 1811A sampling time base, and Type 181A sampling oscilloscope connected to an X-Y recorder to obtain plots of reflected voltage vs. time suitable for numerical analysis.

Very simple sample cells designed for easy construction and attachment to precision 7-mm coaxial line of the TDS system were found to give satisfactory results. For the matched line arrangement, the cells shown in Figure 4a,b are simply short sections of 3-mm rod and 7-mm i.d. tubing with one or two Kel-F disks 1.5 mm thick to confine the liquid sample. These disks were threaded on a  $\frac{1}{16}$  screw, a size which gives an approximate impedance match and small reflections in the absence of liquid sample. The version in Figure 4a can be filled to different heights and the presence of a curved meniscus, rather than confined flat surfaces, produced no apparent errors for sample lengths used.

For the sample termination arrangement, a section of 7-mm coaxial line was either closed off by a thin Kel-F washer as in Figure 4c or a metal cup 1.6 mm deep as in Figure 4d, a shell from a standard connector being used to

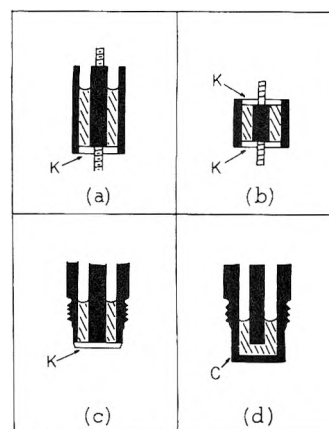


Figure 4. Schematic drawings of liquid sample cells for insertion in matched line (a,b) and for termination of the line (c,d). The symbol K denotes a Kel-F washer, the symbol C a metal cap.

secure the end piece in either case. In the former, there is an end capacitance  $C_s \approx 0.10$  pF, in the other the effective length of the cell is approximately 1.8 mm greater than the length of sample in the coaxial line.

From a variety of experiments, it was found that these arrangements gave consistent results from the appropriate analysis if the real or effective length of the cell used was greater than 3 mm, inconsistencies for shorter lengths resulting from meniscus errors, imperfections in impedance matching, or the approximation of an effective length. For strongly polar dielectrics with short relaxation times, the errors from nonlinearity using this minimum length may then be unacceptably large. As a rough criterion, if errors in derived relaxation times  $\tau$  are not to exceed 4%, the ratio  $(d/c)(\epsilon_0 - \epsilon_\infty)/\tau$  for a Debye dielectric should not exceed 0.02 for sample termination or 0.04 for sample in the matched line if  $\tau$  is in picoseconds.

All four cells were filled with known volumes of liquid by a microliter syringe and sample lengths were calculated from the cell dimensions. Measurements were made at ambient temperatures in the range 22–26° without temperature control, but thermostats for measurements at other temperatures should present no special difficulties, and should be simpler for the “single ended” cells of the sample termination method.

Numerical integrations and self convolutions of  $R(t)$  and  $P(t)$  were done by simple trapezoidal rule sums for the examples described below, with constant intervals  $\Delta$  of 40 or 100 psec between values from the recorder plots and 30 to 40 points out to reflection signals of order 1–2% of the peak value.

Results for a 3.2-mm sample of 1-propanol at 22° in the cell of Figure 4a are shown in Figure 5: the upper plot is the observed reflection  $R(t)$  and the lower shows calculated values of  $(\epsilon_\infty - 1) + \Phi(t)$  from the thin sample eq 18 and second-order eq 21. Both of the latter can be fitted at times greater than 80 psec by the Debye eq 22 for  $\Phi(t)$ . This is conveniently shown, and the relaxation time  $\tau$  determined, by Guggenheim's method of plotting logarithms of differences  $\Delta\Phi = \Phi(t + n\Delta) - \Phi(t)$  for constant difference  $n\Delta$  against  $t$ , giving a straight line of slope  $-1/2.303\tau$  if eq 22 is valid. The plot of second-order results for  $n\Delta = 640$  psec in Figure 6 gives  $\tau = 355$  psec; a similar plot of results from the thin sample formula gives  $\tau = 445$  psec. The difference of 90 psec is consistent with the value 95 psec from the approximate eq 25 using  $\epsilon_0 = 20$  from the integrated area of



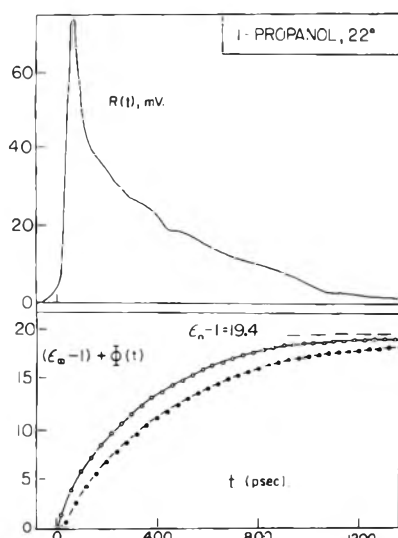


**Figure 5.** (Upper) Reflected signal  $R(t)$  from a 3.2-mm sample of 1-propanol at 22° in a matched line for incident  $V_0 = 240$  mV. (Lower) Response function  $\epsilon_\infty + \Phi(t)$  calculated from eq 21 (open circles) and from thin sample eq 18 (filled circles).

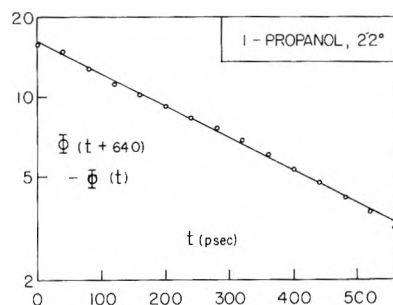


**Figure 6.** Guggenheim plot of the difference  $\Phi(t + n) - \Phi(t)$  for interval  $n\Delta = 640$  psec from data of Figure 5.

the  $R(t)$  curve and  $\epsilon_\infty = 3.7$  (from short time behavior as discussed in section V). Similar results for 1-butanol in a matched line were reported in an earlier communication.<sup>7</sup> In both cases, values of  $\epsilon_0$ ,  $\epsilon_\infty$ , and  $\tau$  from the second-order analysis agree well with ones from other sources (as tabulated, for example, in the review by Suggett<sup>5</sup>).

Results from the sample termination method with a 11.0-mm sample of 1-octanol at 23.5° in the cell of Figure 4d are shown in Figure 7: the upper plot is of the observed reflection  $P(t)$  and the lower of the differences  $\Delta\Phi$  with  $n\Delta = 1600$  psec from the second-order analysis. For times greater than 300 psec, the data are fitted by a Debye relaxation with  $\tau_1 = 1290$  psec, but the differences at shorter times cannot be accounted for by system rise time or sample propagation time and give evidence of a smaller short time relaxation process. The resolution of the data does not permit accurate definition of this process, but rough estimates indicate a relaxation time  $\tau_2$  of order 100 psec. Analysis by frequency domain methods described in part II confirms the existence of such a relaxation with  $\tau_2 = 72$  psec. Lebrun<sup>8</sup> using steady state methods found evidence of two relaxations, with relaxation times  $\tau_1 = 1490$  psec and  $\tau_2 = 240$  psec estimated from his data in qualitative agreement with our results. The static permittivity  $\epsilon_0 = 9.8$  from the area of the  $P(t)$  curve and the high-frequency limit of the primary relaxation from short time behavior of  $P(t)$  is esti-

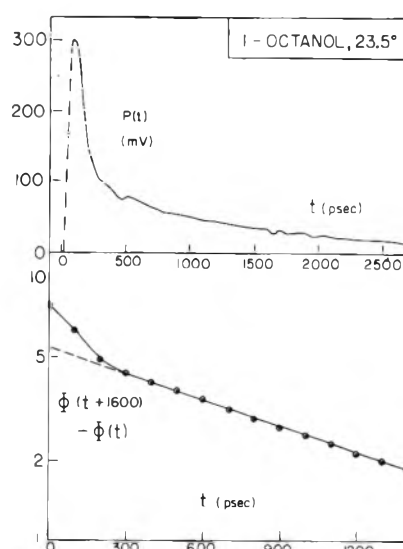


**Figure 7.** (Upper) Reflected signal  $P(t)$  from a 11.0-mm sample of 1-octanol at 23.5° terminating the coaxial line for incident  $V_0 = 250$  mV. (Lower) Guggenheim plot for  $n\Delta = 1600$  psec.

ated to be  $\epsilon_1 = 2.4$  as compared to 2.6 from the frequency domain analysis.

Results for a 3.0-mm sample of 1,2-propanediol at 25° in the cell of Figure 4d are an example of nonexponential relaxation. The calculated response curve shown in Figure 8 is fitted by an exponential with relaxation time 490 psec for times greater than 600 psec, but there are increasing deviations at shorter times of the sort found at lower temperatures (-45 to -90°) by Davidson and Cole<sup>9</sup> and fitted by a "skewed arc" relaxation function  $\epsilon^* - \epsilon_\infty (\epsilon_0 - \epsilon_\infty) / (1 + i\omega\tau)^\beta$  with  $\beta \approx 0.65$ . The response function  $\Phi(t) = (\epsilon_0 - \epsilon_\infty) \gamma(t/\tau, \beta) / \gamma(\beta)$ , where  $\gamma(t/\tau, \beta)$  is the incomplete  $\gamma$  function,<sup>10</sup> fits the present results for times greater than 100 psec, as shown by the solid curve in Figure 8 for values  $\epsilon_0 - \epsilon_\infty = 28.2$ ,  $\tau = 515$  psec, and  $\beta = 0.84$ .

## V. Short Time Behavior

Both the thin sample and second-order analysis become inaccurate at short times because of the finite times between multiple internal reflections in the dielectric sample which lead to more complicated relations between the reflected wave and dielectric response function. For such times, more detailed treatments are necessary, which can be based on the Laplace transforms of  $R(t)$  and  $P(t)$  given by eq 4 and 32, but require numerical analysis in general. If, however,  $\epsilon^*$  is not too large or frequency dependent in the range of interest, approximate analytical results for  $R(t)$  and  $P(t)$  can be obtained which provide useful insight and supplement the analysis for longer times.

Writing the complex permittivity  $\epsilon^*(s) = \epsilon_\infty + s\psi(s)$ , we consider the case that  $s\psi(s)$  is small enough to justify expansion of  $\epsilon^*{}^{1/2}$  in powers of  $s\psi(s)$  retaining only first-order terms. This gives

$$\begin{aligned} \epsilon^*{}^{1/2} &\approx \epsilon_\infty^{1/2} + s\psi(s)/2\epsilon_\infty^{1/2} \\ \rho^* &\approx \rho_\infty + s\psi(s)/\epsilon_\infty^{1/2}(\epsilon_\infty^{1/2} + 1)^2 \times \\ &\exp(-2d\epsilon^*{}^{1/2}s/c) \approx \exp(-2d\epsilon_\infty^{1/2}s/c) \times \\ &\quad [1 - s^2\psi(s)d/\epsilon_\infty^{1/2}c] \quad (34) \end{aligned}$$

As the limiting high-frequency permittivity  $\epsilon_\infty$  is assumed constant, the factor  $\exp(-2d\epsilon_\infty^{1/2}s/c)$  has the time shift

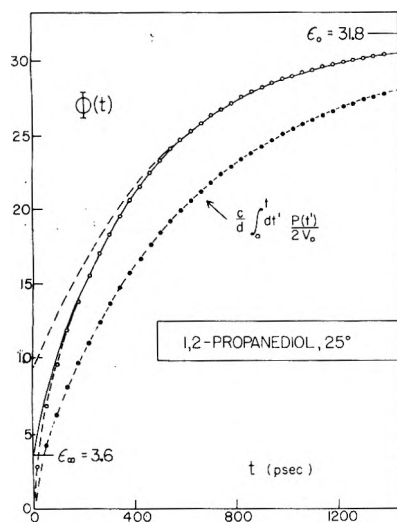


**Figure 8.** Calculated response functions for a 3.0-mm sample of 1,2-propanediol at 25° terminating a coaxial line. Solid circles calculated by the thin sample approximation, open circles by the second-order formula 31. The upper dashed curve is an exponential of time constant  $\tau = 490$  psec, the solid curve a skewed arc response function with  $\beta = 0.84$ .

property on inverse Laplace transformation to the time domain:

$$L^{-1}[f(s) \exp(-T_{\infty}s)] = \begin{cases} F(t - T_{\infty}) & t > T_{\infty} \\ 0 & t < T_{\infty} \end{cases}$$

where  $F(t)$  is the inverse transform of  $f(s)$  and  $T_{\infty} = 2d\epsilon_{\infty}^{1/2}/c$ .

We consider the case of a sample in a matched line. Expansion of the denominator  $1 - \rho^* \exp(-2d\epsilon^{1/2}s/c)$  in eq 4 for  $r(s)$  using the approximation of eq 34 results in a series of reflections at multiples of  $T_{\infty}$  in the time domain, but if  $\epsilon_{\infty}$  is in the range 2–4 as for many polar dielectrics,  $\rho_{\infty}^2 = [(\epsilon_{\infty}^{1/2} - 1)/(\epsilon_{\infty}^{1/2} + 1)]^2$  is in the range 0.03–0.09 and to a useful approximation these reflections can be neglected. For  $V_0(t)$  a finite ramp with rise time  $Tr$  as defined by eq 13,  $v_0(s) = (V_0/Tr)[1 - \exp(-Trs)]/s^2$  and eq 4 for  $r(s)$  becomes on neglecting second-order terms in  $\rho_{\infty}$  and  $s\psi(s)$

$$\frac{r(s)}{V_0} = \frac{1}{Tr s^2} \left[ \left( \rho_{\infty} + \frac{1}{\epsilon_{\infty}^{1/2}(\epsilon_{\infty}^{1/2} + 1)^2} s\psi(s) \right) \times (1 - \exp(-T_{\infty}s)) + \frac{d}{\epsilon_{\infty}^{1/2}c} s^2\psi(s) \exp(-T_{\infty}s) \right] \times [1 - \exp(-Trs)] \quad (35)$$

The reflected signal  $R(t)$  predicted from this equation has four distinct regions with discontinuities at times  $Tr$ ,  $T_{\infty}$ , and  $Tr + T_{\infty}$ . The response to instantaneous polarization characterized by  $\epsilon_{\infty}$  is a trapezoidal wave form, to which is added an algebraic sum of time shifted integrals of  $\Phi(t) = L^{-1}s\psi(s)$ , this sum approaching  $\Phi(t)$  at long times. The behavior for a Debye relaxation with  $\psi(s) = (\epsilon_0 - \epsilon_{\infty})/s(1 + \tau s) \simeq (\epsilon_0 - \epsilon_{\infty})/\tau s^2$  for  $|\tau s| \gg 1$  is shown in Figure 9 for the case  $\epsilon_0 - \epsilon_{\infty} = 9.0$ ,  $\epsilon_{\infty} = 2.25$ , and  $\tau = 10Tr$  with three sample lengths such that  $T_{\infty} = \frac{1}{2}Tr$ ,  $Tr$ , and  $2Tr$ . For convenience, calculated values of  $(2cTr/d)R(t)/V_0$  are plotted as a function of time in units of  $Tr$ , with reflected signal  $R_{\infty}(t)$  due to  $\epsilon_{\infty}$  shown as the dashed lines. We note that the integrated area of  $R_{\infty}(t)$  to time  $Tr + T_{\infty}$  is from eq 35 given by

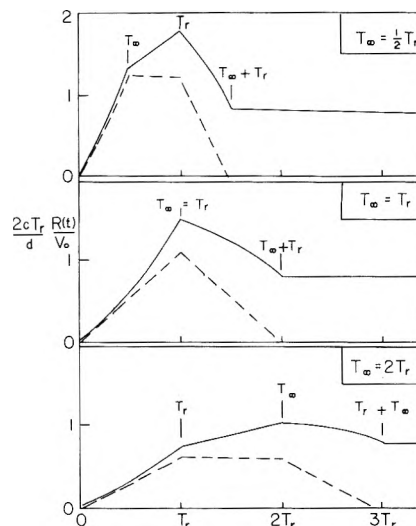


**Figure 9.** Calculated reflected pulses from a finite sample with relaxation time  $\tau = 10Tr$  in a matched line for sample lengths corresponding to  $T_{\infty} = \frac{1}{2}Tr$ ,  $Tr$ , and  $2Tr$ , where  $Tr$  is the rise of the incident finite ramp voltage pulse.

$$(2c/d) \int_0^{T_{\infty}+Tr} dt' R_{\infty}(t')/V_0 = 2c\rho_{\infty}T_{\infty}/d = (\epsilon_{\infty} - 1)(1 - \rho_{\infty}^2)$$

which for  $\rho_{\infty}^2 \ll 1$  is very nearly the value  $\epsilon_{\infty} - 1$  for the complete response integral to  $t = \infty$ . Evaluation of the integral of  $R(t)$  from eq 35 similarly shows that it quite closely approximates the assumed  $\Phi(t)$  for times  $t > Tr + T_{\infty}$ , with increasing deviations at much longer times resulting from the finite amplitude effect.

The observed short time reflection from a 7.8-mm sample of 1-butanol at 23° is shown in Figure 10. The discontinuities predicted by eq 35 are rounded somewhat because the actual incident signal  $V_0(t)$  deviates from the idealized finite ramp assumed in the approximate analysis, but values  $Tr = 40$  psec and  $T_{\infty} = 92$  psec are reasonably well defined. The latter corresponds to  $\epsilon_{\infty} = 3.13$  in agreement with other estimates in the range 3.1–3.2. Estimates of the contributions  $R_{\infty}(t)$  are shown as dashed lines in Figure 10. The difference  $R(t) - R_{\infty}(t)$  is thus attributable to initial behavior of  $\Phi(t)$  and can give useful information, but no simple general procedures have been found.

The initial behavior of the reflection  $P(t)$  from a sample termination can be worked out from eq 32, but for results to a similar approximation it is necessary to retain the first internal reflection of order  $\rho^*$  from expansion of  $[1 - \rho^* \exp(-2d\epsilon^{1/2}s/c)]^{-1}$ . When this is done with the approximations of eq 32 and neglecting  $z$ , one obtains

$$\frac{p(s)}{2V_0} = \frac{1}{2Tr s^2} [1 + \rho_{\infty} + s\psi(s)/2\epsilon_{\infty}^{1/2}(\epsilon_{\infty}^{1/2} + 1)^2 - (1 - s^2\psi(s)d/\epsilon_{\infty}^{1/2}c) \exp(-T_{\infty}s) - (\rho_{\infty} + s\psi(s)/2\epsilon_{\infty}^{1/2}(\epsilon_{\infty}^{1/2} + 1)^2 - s^2\psi(s)2\rho_{\infty}d/\epsilon_{\infty}^{1/2}c) \exp(-2T_{\infty}s)] [1 - \exp(-Trs)] \quad (36)$$

The predicted reflections have a more complicated structure than for the sample in a matched line, as a result of the added contributions beginning at times  $2T_{\infty}$  and  $2T_{\infty} + Tr$ . The behavior is shown in Figure 11 for the normalized function  $(cTr/d)P(t)/2V_0$  with the same values of param-

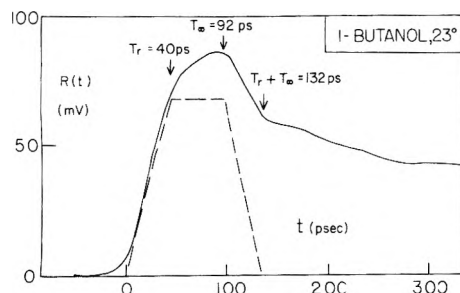


Figure 10. Short time reflected pulse from a 7.8-mm sample of 1-butanol at 23° in a matched line.

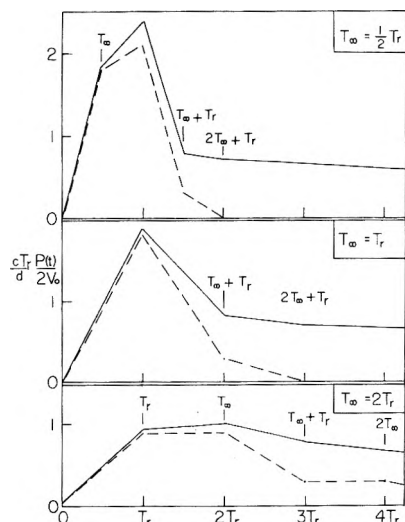


Figure 11. Calculated reflected pulses from a sample termination with relaxation time  $\tau = 10 Tr$  for sample lengths corresponding to  $T_\infty = \frac{1}{2} Tr$ ,  $Tr$ , and  $2Tr$ , where  $Tr$  is the rise time of the incident finite ramp voltage pulse.

ters as before:  $\epsilon_\infty = 2.25$ ,  $\epsilon_0 - \epsilon_\infty = 9.0$ ,  $\tau = 10 Tr$  and three sample lengths such that  $T_\infty = \frac{1}{2} Tr$ ,  $Tr$ , and  $2Tr$ . The reflections  $P_\infty(t)$  associated with  $\epsilon_\infty$ , plotted as dashed lines, are essentially complete over a time interval  $2T_\infty + Tr$ , rather than  $T_\infty + Tr$  for the matched line case, as shown by the integral

$$\left(\frac{c}{d}\right) \int_0^{2T_\infty + Tr} dt' P_\infty(t') / 2V_0 = \epsilon_\infty [1 - 2\rho_\infty^2 / (1 + \rho_\infty)]$$

The effect of the assumed Debye relaxation is shown by the solid curves, and the integrated area is found from eq 36 to approach  $\Phi(t)$  for times  $t > 2T_\infty + Tr$  (except for the finite amplitude error). Thus for short as well as long time behavior, samples terminating a line give more nearly comparable results to those from samples in a matched line for half the sample length (i.e.,  $T_\infty$  one-half as large). Although the difference between the total reflected signal  $P(t)$  and  $P_\infty(t)$  calculated for induced polarization gives information about the contributions from  $\Phi(t)$ , it is evident from eq 36 that the relation is not simple. In most cases, one expects that the principal value of analysis of short time data ( $t < 2T_\infty$ ) is for estimates of  $T_\infty$ , and hence  $\epsilon_\infty$ , plus qualitative indications of the magnitude of the relaxation function. More reliable quantitative results at short times can be obtained by Fourier transform analysis, as discussed in part II.

## VI. Conducting Dielectrics

In the preceding analysis, the dielectric sample has been

assumed to be nonconducting with finite relaxation function  $\Phi(t)$  in the limit  $t \rightarrow \infty$  and reflected signals approaching zero. The effect of finite ohmic conductivity can be taken into account by replacing eq 1 by

$$\frac{\partial Q}{\partial t} = (G/E)\sigma V + C \frac{d}{dt} \left[ \epsilon_\infty V(t) + \int_0^t dt' \dot{\Phi}(t-t') V(t') \right] \quad (37)$$

where  $\sigma$  is the specific conductance of the sample and  $E$  an appropriate conversion factor for consistency of units chosen (if  $\sigma$  is in mho  $\text{cm}^{-1}$  and  $C$  in pF,  $E = 0.0884$ ).

For sample of length  $d$  in a matched line, the counterpart of eq 12 is

$$\begin{aligned} (\sigma d/2cE V_0(t) + (d/2c) \frac{d}{dt} \int_0^t dt' [(\epsilon_\infty - 1)\delta(t') + \\ \dot{\Phi}(t')]) [V_0(t-t') - R(t-t')] = \\ (1 + \sigma d/2cE) R(t) + (d/c) \dot{R}(t) \quad (38) \end{aligned}$$

For an incident pulse  $V_0(t)$  reaching a limiting value  $V_0$  as  $t \rightarrow \infty$ , the limiting value  $R(\infty)$  of the reflected signal is no longer zero, but is given by

$$\frac{R(\infty)}{V_0} = \frac{\sigma d/2cE}{1 + \sigma d/2cE} = \frac{G_s}{2G_c + G_s} \quad (39)$$

where  $G_s = (\sigma/E)Cd$  is the ohmic sample conductance and  $G_c = cC_c$  the characteristic conductance of the coaxial line (e.g., 20 mmho). Although derived from our second-order analysis, this result is exact as can be shown from the Laplace limit theorem

$$R(\infty) = \lim_{s \rightarrow 0} s r(s)$$

using eq 4 for  $r(s)$  with  $\epsilon^*$  replaced by  $\epsilon^* + \sigma/Es$  and  $v_0(s) = V_0/s$ . (We note that eq 39 is also simply derived from the equivalent dc circuit of sample conductance  $G_s$  and line conductance  $G_c$  in parallel, with open circuit voltage  $2V_0$  applied through series conductance  $G_c$ .)

The decay to finite limiting value  $R(\infty)$  suggests that analysis to determine dielectric response  $\Phi(t)$  be expressed in terms of the difference of  $R(t)$  from this value. For simplicity, we consider an ideal step pulse  $V_0(t) = V_0$ ,  $t > 0$ , but the cases of a ramp or finite ramp present no difficulties. Defining  $\Delta R(t) = R(t) - R(\infty)$  gives on substitution in eq 38 and use of eq 39 the second-order result

$$\begin{aligned} \epsilon_\infty - 1 + \Phi(t) = (2c/d)(1 + \sigma d/2cE) \times \\ \left[ (1 + \sigma d/2cE) \int_0^t dt' \frac{\Delta R(t')}{V_0} + (1 + \sigma d/2cE)^2 \times \right. \\ \left. \int_0^t dt' \frac{\Delta R(t')}{V_0} \frac{\Delta R(t-t')}{V_0} + \frac{d}{c} \frac{R(t)}{V_0} \right] \quad (40) \end{aligned}$$

The similarity of this result to eq 21 (with  $Tr = 0$ ) for a nonconducting dielectric is apparent, and the dielectric response function can be evaluated in a similar way from  $\Delta R(t)$  if the ratio  $\sigma d/2cE = G_s/2G_c$  is not too large. For nonconducting dielectrics, we showed in II that  $\epsilon_0 - 1$  is given exactly by the integral of  $(2c/d)R(t)/V_0$  to infinite time. Its counterpart for finite conductivity  $\sigma$  can be obtained by evaluating

$$\int_0^\infty dt' [R(t') - R(\infty)] = \lim_{s \rightarrow 0} [r(s) - v_0(s)]$$

where  $v_0(s) = V_0/s$  and  $r(s)$  is given by eq 4 on replacing  $\epsilon^*$  by  $\epsilon^* + \sigma/E_s$ . This gives

$$(2c/d)(1 + \sigma d/2cE)^2 \int_0^\infty dt' \frac{\Delta R(t')}{V_0} = \epsilon_0 - 1 - \sigma d/2cE - \frac{1}{3}(\sigma d/2cE)^2 \quad (41)$$

The first-order limit of eq 40 thus does not give  $\epsilon_0 - 1$  exactly, and the error of order  $\sigma d/cE$  sets an upper limit on usable sample length. Such a restriction is also necessary because too large a value of  $R(\infty)/V_0$  makes the difference  $\Delta R(t)$  too small. As an example, a specific conductance  $\sigma = 10^{-2}$  mho  $\text{cm}^{-1}$  sets a limit  $d \leq 1.8$  mm if  $R(\infty)/V_0$  is not to exceed 0.25 and the error in  $\epsilon_0 - 1$  is then 0.81.

There is a further limitation on possibilities of evaluating the response function  $\epsilon_\infty - 1 + \Phi(t)$  from  $\Delta R(t)$ , as the ratio of  $\Delta R(t)$  to  $R(\infty)$  is determined by intrinsic properties of the sample independent of its geometry. The exact relation depends on the response function but is of the form

$$\frac{\Delta R(t)}{R(\infty)} \leq \frac{\epsilon_0 - \epsilon_\infty}{\tau\sigma/E}$$

where  $\epsilon_0 - \epsilon_\infty$  is the relaxation contribution to the total response and  $\tau$  a characteristic time for this contribution, e.g., the Debye relaxation time. As an example, for  $R(\infty) = 0.25V_0$  and  $\sigma = 10^{-2}$  mho  $\text{cm}^{-1}$ ,  $\Delta R(t)$  will be as large as  $0.25V_0$  only for  $(\epsilon_0 - \epsilon_\infty)/\tau > 0.60$  psec $^{-1}$ , which for  $\tau = 500$  psec requires  $\epsilon_0 - \epsilon_\infty > 30$ .

Similar procedures can be developed for conducting dielectrics as sample terminations. When eq 37 for  $\partial Q/\partial t$  is used, the basic eq 29 for the method becomes

$$\begin{aligned} (\sigma d/cE)2V_0(t) + (d/c) \frac{d}{dt} \int_0^t dt' [\epsilon_\infty \delta(t') + \dot{\Phi}(t')] \times \\ [2V_0(t-t') - P(t-t')] + \\ (C_s/cC_c) \frac{d}{dt} [2V_0(t) - P(t)] = (1 + \sigma d/cE)P(t) \quad (42) \end{aligned}$$

if terms involving the product  $(d/c)^2(C_s/dC_c)$  are neglected. The limiting reflection signal  $P(\infty)$  for an incident pulse approaching  $V_0$  as  $t \rightarrow \infty$  is given by

$$\frac{P(\infty)}{2V_0} = \frac{\sigma d/cE}{1 + \sigma d/cE} = \frac{G_s}{G_c + G_s} \quad (43)$$

where  $G_s$  is the sample conductance, a result again in agreement with the exact response from the Laplace transform of  $p(s)$  and with the dc equivalent circuit for this case.

Introducing the difference  $\Delta P(t) = P(t) - P(\infty)$  in eq 42 gives for a step voltage  $V_0(t) = V_0/t$  the second-order result

$$\begin{aligned} \epsilon_\infty + \Phi(t) + C_s/dC_c = (c/d)(1 + \sigma d/cE)^2 \times \\ \left[ \int_0^t dt' \frac{\Delta P(t')}{2V_0} + (1 + \sigma d/cE) \times \right. \\ \left. \int_0^t dt' \frac{\Delta P(t')}{2V_0} \frac{\Delta P(t-t')}{2V_0} \right] \quad (44) \end{aligned}$$

In the limit  $t \rightarrow \infty$ , exact analysis based on eq 32 for  $p(s)$  gives

$$(c/d)(1 + \sigma d/cE)^2 \int_0^\infty dt' \frac{\Delta P(t')}{2V_0} = \epsilon_0 + C_s/dC_c - \frac{1}{3}(\sigma d/cE)^2 \quad (45)$$

and the error in the first-order expression is of order  $(\sigma d/$

$cE)^2$ . This smaller error, as compared to  $\sigma d/cE$  for the matched line method, is negligible for acceptable values of  $P(\infty)/2V_0$ , and is a potential advantage of using the sample termination method. The working eq 44 is also simpler, and the reflected signals for a given accuracy of derived  $\Phi(t)$  larger, for the sample termination.

Finally in this section, we remark that the function  $\Phi(t)$  derived by either method of necessity represents effects of both dielectric response and of dispersion in conductivity. This is of course true of any observed electromagnetic effect, as the Maxwell field equations together with the equation of continuity for charge involve only the sum of conduction and polarization currents, and any evaluation of separate contributions must be on the basis of a theoretical model. In this section we have adopted a model only in the sense that a finite limiting response at long times is assumed and is described as the result of a finite ohmic conductance.

## VII. Discussion

In the limit of very short samples, the observed reflection of an incident step voltage is proportional to the derivative of the response function of the dielectric, as first pointed out by Fellner-Feldegg<sup>2</sup> for the case of a sample in a matched line.

The analyses presented here show that major deviations from this behavior for finite samples result from the fact that the voltage across the sample is not the incident voltage, but the sum of incident and reflected pulses. The formulas obtained in second approximation for finite samples provide simple corrections, the principal one being the self convolution of the reflected voltage, by which satisfactory response functions can be calculated for much larger samples (and observed reflections) than is possible with the thin sample approximation.

The limitations of the analysis are that approximate, rather than exact, account is taken of the finite reflected pulse and that deviations at short times as a result of finite speed of propagation in the sample are not taken into account, but simple criteria in terms of the observed reflection permit at least rough estimates of the errors. These can be made satisfactorily small for reasonable sample lengths of at least moderately polar substances with not too short relaxation time. One can, however, expect unacceptable errors for such systems as dilute solutions of polar molecules in a nonpolar solvent or strongly polar solvent, e.g., water.

Although the present analysis can be extended by carrying the expansions in powers of sample length to higher order, the resulting formulas involve multiple convolutions and time derivatives which are unattractive for numerical calculations. A more useful approach if greater accuracy is needed is to work with Laplace transforms of the incident and reflected voltage pulses. As we show in part II, the extra labor of numerical computations of the transforms makes it possible to use quite simple explicit formulas for permittivity  $\epsilon^*$  which are exact with respect to finite amplitude of the reflection signal and satisfactory up to frequencies corresponding to much shorter times than in the time domain analysis.

*Acknowledgments.* This work was supported by the Brown University Materials Science Program and the National Science Foundation.

## Appendix A

The integral correction  $I$  for finite rise time  $Tr$  in eq 20 is

$$I = (2c/d) \int_0^{Tr} dt' \left[ Tr \frac{\dot{R}(t')}{V_0} - \frac{R(t')}{V_0} \right] \frac{R(t-t')}{V_0} \quad (\text{A1})$$

We assume that  $R(t')$  and  $R(t-t')$  both vary linearly with  $t'$  in the interval  $0 < t' < Tr$ :

$$R(t') = R(Tr)t'/Tr$$

$$R(t-t') = R(t) - t'\dot{R}(t)$$

which gives

$$I = (cTr/d) \frac{R(Tr)}{V_0} \frac{R(t)}{V_0} \left[ 1 - \frac{1}{3} Tr \frac{\dot{R}(t)}{R(t)} \right] \quad (\text{A2})$$

For reflected pulses  $R(t)$  of the form shown in Figure 2c, the term  $\frac{1}{3}Tr\dot{R}(t)/R(t)$  is much less than unity for times  $t > Tr - T_\infty$ , and to a sufficient approximation

$$I = (cTr/d) \frac{R(Tr)}{V_0} \frac{R(t)}{V_0} \quad (\text{A3})$$

which is the result used to obtain eq 21. An alternative approximation is to evaluate the integral  $I$  by the trapezoidal rule using values of the integrand at  $t' = 0$  and  $t' = Tr$ , which gives the same result eq A3.

NOTE ADDED IN PROOF: After the manuscript went to the printer, a referee has pointed out to me a difficulty in the expansion of

$$\exp(-2d\epsilon^{*1/2}s/c)$$

given by the last of eq 34 if  $s^2 \psi(s)$  does not remain finite in the limit  $s \rightarrow \infty$ , as in the cases of skewed arc or circular arc relaxation functions. In such cases, the expansion of the exponential should not be made, but the approximation to  $\epsilon^{*1/2}$  given by the second of eq 34 can be used in the exponential. The predicted reflection starting at time  $T_\infty$  which permits an estimate of  $T_\infty$  has been confirmed by explicit calculations and observations.

## References and Notes

- (1) For a review, see M. J. C. van Gemert, *Philips Res. Rep.*, **28**, 530 (1973).
- (2) H. Fellner-Feldegg, *J. Phys. Chem.*, **76**, 2112 (1972).
- (3) A. H. Clark, P. A. Quickenden, and A. Suggett, *J. Chem. Soc., Faraday Trans. 2* **11**, 1847 (1974).
- (4) M. J. C. van Gemert, *J. Chem. Phys.*, **60**, 3963 (1974).
- (5) A. Suggett in "Dielectric and Related Molecular Processes", Vol. 1, Chemical Society, London, 1972, p 100.
- (6) M. F. Iskander and S. S. Stuchly, *IEEE Trans. Instrum. Meas.*, **IM-21**, 425 (1972).
- (7) R. H. Cole, *J. Phys. Chem.*, **78**, 1440 (1974).
- (8) A. Lebrun, *Cah. Phys.*, **60**, 11 (1955); *Ann. Phys.*, **10**, 16 (1955).
- (9) D. W. Davidson and R. H. Cole, *J. Chem. Phys.*, **19**, 1484 (1951).
- (10) Convenient numerical tables of  $\Phi(t)$  for  $\beta$  in intervals of 0.02 from 0.98 to 0.30 have been given by N. Koizumi and Y. Kita, *Bull. Inst. Chem. Res., Kyoto Univ.*, **50**, 499 (1972).

## Evaluation of Dielectric Behavior by Time Domain Spectroscopy. II. Complex Permittivity

Robert H. Cole

Chemistry Department, Brown University, Providence, Rhode Island 02912 (Received February 21, 1975)

Publication costs assisted by the Materials Science Program, Brown University, with support from the National Science Foundation

Simple explicit formulas are derived for evaluation of permittivity  $\epsilon^*(\omega)$  of a dielectric sample in a coaxial line from Fourier transforms of incident and reflected voltage pulses. These take exact account of finite reflected wave amplitude and provide good approximations to propagation effects for wavelengths greater than one-sixth the sample length. Use of the sample as termination of the line is shown to have several advantages over the more common method of inserting it in a matched line. Simple numerical and analytical procedures for evaluation of the Fourier transforms are given, together with a discussion of errors.

### I. Introduction

A variety of methods has been developed<sup>1</sup> for evaluating the steady state permittivity  $\epsilon^*$  from observations of the voltage pulses transmitted through or reflected from a dielectric sample in a coaxial line as a function of time after an incident pulse arrives at its front surface. The analyses have usually been based on explicit solutions for frequency components of the pulse wave forms as obtained by Laplace transformation of the basic propagation equations and current-voltage relation characterizing the dielectric. The scattering and transmission coefficients so derived

represent the combined effects of the relation of observed voltages to the sample voltage and current at the front surface, propagation effects in the sample, and boundary conditions at the back surface.

The usual expressions are better suited for calculation of the expected behavior given the dielectric properties than for evaluation of permittivity from observed voltage waveforms, as they involve reflection coefficients  $\rho^* = (\epsilon^{*1/2} - 1)/(\epsilon^{*1/2} + 1)$  and propagation functions  $\exp(-i\omega d\epsilon^{*1/2}/c)$ , where  $d$  is the sample length and  $c = 0.300$  mm psec<sup>-1</sup> the speed of propagation in vacuo. The result is that explicit

solutions for  $\epsilon^*$  cannot be obtained even for the simple case of Debye relaxation, and the effects of the several complicating factors are so to speak scrambled together.

In the preceding companion paper<sup>1</sup> (hereafter referred to as part I), a quite different approach was developed of solving the basic propagation equations without recourse to Laplace transformations by expanding the voltage and current in the dielectric in Taylor series as a function of sample length and voltage-current relations at the surface. In first order, these results confirm Fellner-Feldegg's "thin sample" result<sup>2</sup> and show simple relations of observed reflection signal to the dielectric response function in this limit of small sample length and reflected pulse amplitude.

In the second approximation, one finds that the principal difference except at short times is the consequence of the fact that the voltage at front surface of the dielectric sample is the sum of incident and reflected pulse voltages, not just the incident voltage as assumed in the first-order approximation, and that the resultant distortion of the simple relations is significant at all times for which dielectric response to the incident pulse is incomplete. Although the second analysis provides simple approximate corrections which give results of useful accuracy for considerably greater sample lengths and reflection signals, it too becomes inaccurate as these increase and no account can be simply taken of effects of finite speed of propagation in the sample.

In this paper, we formulate the problem in terms of frequency components of voltage and current at the sample surfaces as related to dielectric properties and the boundary conditions. This leads quite directly to convenient relations which take exact account of finite reflection signal amplitude and approximate propagation effects by a series expansion in powers of  $(\omega d/c)^2 \epsilon^*$ . From these relations, simple explicit solutions for  $\epsilon^*$  in terms of incident and reflected voltages are obtained which are correct to terms of order  $(\omega d/c)^4$  and  $(\omega d/c)^6$  if necessary and give results of useful accuracy up to frequencies for which the sample length is an appreciable fraction of the wavelength in the sample.

Two experimental arrangements are considered: insertion of a dielectric sample in a coaxial line terminated in its characteristic conductance, and termination of the line by a finite length of sample. The latter is shown to have advantages of larger reflected signals for comparable accuracy, simpler analysis, and simpler cell designs. In both cases, there are no intrinsic low-frequency limits and evaluation of properties of dielectrics with appreciable ohmic conductance is possible.

## II. Basic Analysis

We consider a section of uniform transmission line of length  $d$  filled with dielectric of complex relative permittivity  $\epsilon^*$ . Regarded as a symmetrical four terminal network, this section has an input admittance  $y_{in}$  given by<sup>3</sup>

$$y_{in} = \frac{y_0 + y_d}{1 + Z_s y_d} \quad (1)$$

where  $y_0$  is the open circuit admittance of the section,  $Z_s$  its short circuit impedance, and  $y_d$  the input admittance of the line or network used to terminate the section. If the geometric capacitance and inductance per unit length of line are  $C_c$  and  $L_c$ , then from transmission line theory  $y_0$  and  $Z_s$  are given by<sup>3</sup>

$$y_0 = i\omega C_c d \epsilon^* \left( \frac{\tanh x}{x} \right) \quad (2)$$

$$Z_s = i\omega L_c d \left( \frac{\tanh x}{x} \right)$$

where  $x = i\omega(L_c C_c)^{1/2} \epsilon^{*1/2} d = i(\omega d/c) \epsilon^{*1/2}$ , as the speed of propagation  $c$  in vacuo is  $c = (L_c C_c)^{-1/2}$ . (In these expressions for  $Z_s$  and  $x$ , a nonmagnetic sample with relative permeability  $\mu^* = 1$  is assumed.)

If the component of incident pulse voltage  $V_0(t)$  of frequency  $\omega/2\pi$  is denoted by  $v_0(i\omega)$ , i.e.,  $v_0(i\omega) = LV_0(t)$  where  $L$  is the Laplace transform, and the component of reflected pulse voltage  $-R(t)$  at the input of the dielectric section by  $-r(i\omega)$ , the input voltage and current are given by  $v(i\omega) = v_0(i\omega) - r(i\omega)$  and  $i(i\omega) = G_c[V_0(i\omega) + r(i\omega)]$ , where  $G_c = (C_c/L_c)^{1/2}$  is the characteristic conductance of the coaxial line, assumed loss free, connecting the sample section to the pulse generator. The input admittance of the dielectric section and termination is then related to  $v_0$  and  $r$  by

$$y_{in} = \frac{i(i\omega)}{v(i\omega)} = G_c \frac{v_0(i\omega) + r(i\omega)}{v_0(i\omega) - r(i\omega)} \quad (3)$$

Combining eq 1, 2, and 3 gives on rearrangement and using  $G_c/C_c = c$

$$\epsilon^* + \frac{y_d}{i\omega C_c d} x \coth x = \frac{c}{i\omega d} \left( \frac{v_0 + r}{v_0 - r} \right) (x \coth x + i\omega L_c y_d d) \quad (4)$$

In this equation, the relation of voltages  $v_0$  and  $r$ , calculable from observed incident and reflected pulses, to the input voltage and current of the sample is accounted for by the ratio  $(v_0 + r)/(v_0 - r)$ . The result is not an explicit solution for  $\epsilon^*$ , as  $\epsilon^*$  appears in the argument  $x = i(\omega d/c) \epsilon^{*1/2}$ , but the key to approximate solutions is that  $x \coth x$  can be expanded as a series in powers of  $x^2$  valid for  $|x| < \pi$ :

$$x \coth x = 1 + \frac{1}{3} x^2 - \frac{1}{45} x^4 + \frac{2}{945} x^6 + \dots$$

$$= 1 - \frac{1}{3} (\omega d/c)^2 \epsilon^* - \frac{1}{45} (\omega d/c)^4 \epsilon^{*2} - \frac{2}{945} (\omega d/c)^6 \epsilon^{*3} + \dots \quad (5)$$

From this expansion and eq 4, a solution correct to terms of order  $(\omega d/c)^4$  is obtained as a linear equation in  $\epsilon^*$  and to terms of order  $(\omega d/c)^6$  as a quadratic. The most convenient forms depend on the terminating admittance  $y_d$  and we consider two useful arrangements separately.

*A. Sample Inserted in Matched Line.* In this case, the terminating admittance  $y_d = G_c$ , as the output of the sample section is a coaxial line terminated in its characteristic conductance  $G_c$ . Inserting this value in eq 4 and rearranging gives

$$\epsilon^* - 1 = f [x \coth x + i(\omega d/c)] \quad (6)$$

where

$$f = \frac{(2c/d)(r/i\omega v_0)}{1 - i(\omega d/2c)[(2c/d)(r/i\omega v_0)]} \quad (7)$$

Neglecting terms of order  $\omega d/c$  gives  $\epsilon^* - 1 \approx (2c/d)(r/i\omega v_0)$ , which is essentially Fellner-Feldegg's thin sample

formula. However, the replacement of the denominator in eq 7 by unity leads to large errors in derived values of  $\epsilon^* - 1$ , except in the limit of zero frequency, unless the sample length is very small and  $|r/v_0| \ll 1$ . If this approximation is not made, but  $x \coth x$  in eq 6 is replaced by unity, thereby neglecting terms of order  $(\omega d/c)^2$ , a first approximation  $(\epsilon^*)_1$  is given by

$$(\epsilon^*)_1 = 1 + f[1 + i(\omega d/c)] \quad \frac{1}{3}(\omega d/c)^2 \epsilon^* \ll 1 \quad (8)$$

Retaining the  $x^2$  term in the expansion 5 for  $x \coth x$  gives our second approximation

$$(\epsilon^*)_2 = (\epsilon^*)_1 / \left[ 1 + \frac{1}{3}(\omega d/c)^2 f \right] \quad \frac{1}{45}(\omega d/c)^4 \epsilon^{*2} \ll 1 \quad (9)$$

and using the approximation for the  $x^4$  term in  $x \coth x$  gives to order  $(\omega d/c)^6 \epsilon^{*3}$

$$(\epsilon^*)_3 = (\epsilon^*)_2 \left[ 1 - \frac{1}{45}(\omega d/c)^4 (\epsilon^*)_2^2 \right] \quad \frac{2}{945}(\omega d/c)^6 \epsilon^{*3} \ll 1 \quad (10)$$

A series of solutions for  $\epsilon^*$  adequate to increasingly high frequencies is thus generated from the ratio  $r/i\omega v_0$  and straightforward algebra of complex numbers, the order of approximation needed depending on the sample length, value of  $\epsilon^*$ , and frequency. For a variety of examples we have considered, the approximation  $(\epsilon^*)_1$  of eq 8 has proved adequate in many cases, with the correction by the  $(\epsilon^*)_2$  formula significant only at the higher frequencies of interest and the  $(\epsilon^*)_3$  formula usually unnecessary or unjustified because of inaccuracies in values of  $r/i\omega v_0$  at very high frequencies.

Similar methods can be used to derive formulas for  $\epsilon^*$  from the transmitted pulse, but these have been found to be less useful, chiefly because of problems in choosing a proper zero of time for evaluation of the Fourier transform of the transmitted pulse.

**B. Sample Termination.** From the basic eq 4, a particularly simple formula results for the case  $y_d = 0$ , i.e., a sample terminated by an open circuit, as one has merely

$$\epsilon^* = \frac{c}{i\omega d} \frac{v_0 + r}{v_0 - r} x \coth x \quad (11)$$

An ideal open circuit cannot be realized exactly of course, as even an open ended coaxial line has an effective admittance characterizing its end capacitance, or more generally radiation into the external medium, but two close approximations to the ideal are possible. From standing wave measurements, the effective electrical length of an open ended 14 mm coaxial line is found to be about 2.5 mm greater than its physical length below a frequency of 3 GHz and to increase by about 0.2 mm at 8 GHz.<sup>4</sup> Below this range at least, the effect of an open ended 7-mm coaxial line should be well described by a fixed capacitance  $C_s$  of order 0.08 pF, corresponding to 1.2 mm length of 50-ohm coaxial line and  $y_d = i\omega C_s$ .

A second alternative is to close off the end of the dielectric section with a cap, also filled with the dielectric (cells corresponding to these cases are shown schematically in

Figure 4 of part I), and to approximate the effect of the added dielectric by an effective sample length  $d$  in eq 11 which is longer than the length in the line. This assumption is certainly valid at low frequencies and measurements with the cell of Figure 4d of part I give an extra length  $\Delta d = 1.8$  mm.

At sufficiently high frequencies, propagation effects must complicate the problem, but a variety of measurements have failed to reveal any significant errors at frequencies below 3 GHz from the simplifying assumptions. Analytic solutions of the field problem for boundary conditions in the cells shown in Figure 4c,d have not been found, but Levine and Papas<sup>5</sup> have obtained solutions for an open coaxial line ending at an infinite grounded plane at right angles to the axis and radiating into free space. Their results for driving point admittance at the end of the line correspond to a limiting capacitance  $C_s = 0.076$  pF for a 7-mm 50-ohm line increasing only slightly with frequency below 15 GHz and corresponding to an effective end length of 1.1 mm, with radiation losses increasing as  $\omega^4$  initially becoming appreciable at higher frequencies. The results are qualitatively similar to those for the end effects we assume. Exact agreement is not to be expected because of the different boundary conditions, and the differences (larger  $C_s$  and negligible radiation losses in the assumed effects) are consistent with the finite boundaries of the cells used.

If the terminating admittance  $y_d$  is either neglected or taken into account by use of an effective length  $d$ , eq 11 can be solved very simply to remarkably good approximation. We denote the difference of voltage  $v$  at the sample input from the value  $2v_0$  for an open circuit by  $p = v_0 + r$ , corresponding to observed voltage  $P(t) = V_o(t) + R(t)$  as shown in Figure 3 of part I and eq 11 can then be written

$$\epsilon^* = g(x \coth x) \quad (12)$$

where

$$g = \frac{(c/d)(p/2i\omega v_0)}{1 - i(\omega d/c)[(c/d)(p/2i\omega v_0)]} \quad (13)$$

The sequence of approximations as in A for a sample in a matched line then gives

$$(\epsilon^*)_1 = g \quad \frac{1}{3}(\omega d/c)^2 \epsilon^* \ll 1 \quad (14)$$

$$(\epsilon^*)_2 = (\epsilon^*)_1 / \left[ 1 + \frac{1}{3}(\omega d/c)^2 (\epsilon^*)_1 \right] \quad \frac{1}{45}(\omega d/c)^4 \epsilon^{*2} \ll 1 \quad (15)$$

$$(\epsilon^*)_3 = (\epsilon^*)_2 \left[ 1 - \frac{1}{45}(\omega d/c)^4 (\epsilon^*)_2^2 \right] \quad \frac{2}{945}(\omega d/c)^6 \epsilon^{*3} \ll 1 \quad (16)$$

The  $(\epsilon^*)_1$  approximation is seen to be even simpler than its counterpart in A and has likewise been found sufficient in many cases, the  $(\epsilon^*)_2$  correction becoming significant only at relatively high frequencies for examples so far studied.

The effect of residual fringing fields is easily obtained in the approximation  $y_d = i\omega C_s$  with  $C_s$  independent of frequency, for which eq 4 becomes

$$\epsilon^* + (C_s/C_c d) x \coth x = g[x \coth x - (\omega d/c)^2 (C_s/C_c d)] \quad (17)$$

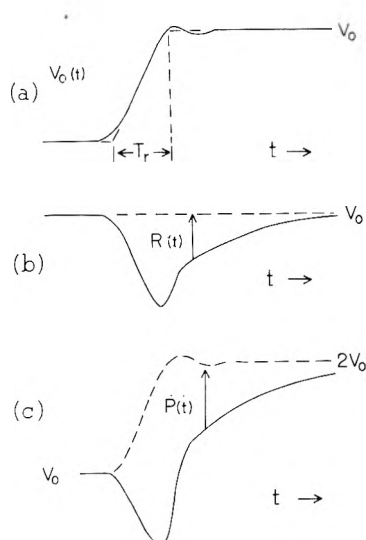


**Figure 1.** Typical incident and reflected voltage pulse forms observed in time domain spectroscopy: (a) incident pulse, (b) reflection from sample in matched line, (c) reflection from sample termination.

with  $g$  defined by eq 13. For arrangements like the cell in Figure 4c of part I,  $C_s$  is of order 0.10 pF and for sample lengths greater than 3 mm the ratio  $C_s/C_c d < 0.5$ , resulting in small corrections for its effect which can be simply approximated.

### III. Evaluation of Pulse Transforms

The principal computational problem in applying the various formulas is the evaluation of the Laplace, or one-sided Fourier, transforms of the reflected and incident pulse voltages  $R(t)$  or  $P(t)$  and  $V_0(t)$ . As these appear only in the ratio  $(2c/d)(r/i\omega v_0)$  or  $(c/d)(p/2i\omega v_0)$ , effects of linear sampler response cancel in forming the ratio, which can therefore be calculated from transforms of the observed pulses without correction for the response.

For commercial TDS equipment and representative dielectrics, the observed pulses have the relatively simple forms shown in Figure 1, permitting quite rudimentary numerical calculations of their transforms with sufficient accuracy for many purposes. Considering first reflected pulses  $P(t)$  or  $R(t)$  as in Figure 1b,c, the observed profile can be approximated by a sum of triangular pulses  $P(n\Delta)$  of width  $2\Delta$ , giving a straight line segment (trapezoid) simulation which can usually be made to give a surprisingly good fit to actual curves by judicious choice of the constant time interval  $\Delta$ .

Summing the transforms of the triangular pulses gives

$$p(i\omega) \cong \Delta [\sin(\omega\Delta/2)/(\omega\Delta/2)]^2 \sum_{n=1}^N P(n\Delta) \exp(-i\omega n\Delta) \quad (18)$$

This result, apparently first given by Tuck,<sup>6</sup> is exact for the approximation made to the actual curve. We remark that this formula without the  $[\sin(\omega\Delta/2)/(\omega\Delta/2)]^2$  factor has also been used. Although the simpler formula is exact for pulses such that  $p(i\omega) = 0$  at frequencies  $f > 1/2\Delta$  (the Shannon sampling theorem<sup>7</sup>), this condition is usually not met in cases of interest, and we believe that eq 18 is then a better approximation, but the differences are small for frequencies such that  $(\omega\Delta/2)^2 \ll 1$ .

The choice of interval  $\Delta$  and number of points  $N$  to keep

aliasing and truncation errors sufficiently small must of course be made for specific cases, but we have found for a variety of examples that some 30–40 points usually suffice, with occasional need for a finer interval at short times or some sort of analytic approximation to the behavior at longer times. In such cases, the numerical summations of eq 18 require only modest amounts of computer time, without need for fast Fourier transforms or other more elaborate algorithms.

For incident pulses  $V_0(t)$  of the form shown in Figure 1a, a simple analytic approximation suffices to evaluate  $v_0(i\omega)$  with sufficient accuracy to quite high frequencies. This consists in fitting  $V_0(t)$  by a finite ramp as indicated by the dashed curve and expressed by

$$V_0(t) = \begin{cases} 0 & t < 0 \\ V_0 t / Tr & 0 < t < Tr \\ V_0 & Tr < t \end{cases} \quad (19)$$

for which

$$V_0 = [1 - \exp(-i\omega Tr)] / (i\omega)^2 Tr$$

and

$$\frac{1}{i\omega v_0} = \frac{1}{V_0} [(\omega Tr/2) \cot(\omega Tr/2) + i\omega Tr/2] \quad (20)$$

At sufficiently low frequencies,  $\omega Tr/2 \ll 1$ , setting  $1/i\omega v_0 = 1/V_0$  suffices, while for  $(\omega Tr/2)^2 \ll 1$  the amplitude factor  $(\omega Tr/2) \cot(\omega Tr/2)$  can be replaced by unity and only the phase correction  $i\omega Tr/2$  is needed (this corresponds approximately to replacing  $V_0(t)$  by an ideal step starting at time  $Tr/2$ ).

Although the simple approximation 20 has been found to work very well at frequencies below 3 GHz, deviations of the actual pulse form from a finite ramp, such as rounding at the inflection points, irregularities from impedance mismatches, etc., cause deviations which require more elaborate calculations by numerical Fourier transformation. Because the incident pulse remains finite and nearly constant to long times, the triangular pulse approximation method is not appropriate and recourse must be had to other procedures, such as the Samulon version<sup>8</sup> of the Shannon sampling theorem or Nicolson's device<sup>9</sup> of subtracting a finite ramp with long rise time  $Tr$ .

It should also be pointed out that similar measures must be taken in applying the analysis to samples with finite ohmic conductance, as these result in reflection signals  $R(\infty)$  or  $P(\infty)$  in the limit  $t \rightarrow \infty$  which are finite and related to the conductance  $\sigma/E$  by eq 39 and 43 of part I. With this proviso, our formulas for  $\epsilon^*$  give values of  $\epsilon^* + \sigma/i\omega E$  if the total dielectric current is represented as the sum of complex permittivity and ohmic conduction effects.

Our numerical and analytical approximations to the required Fourier transforms are subject to increasing uncertainties at high frequencies as a result of error in the choice of zero of time. For a relative timing error  $\Delta t$ , a phase error in the ratio  $r/i\omega v_0$  or  $p/i\omega v_0$  results, which is given by a factor  $\exp(i\omega\Delta t)$ . We have used simple X-Y recorder plots of reflected pulses and taken the zero of time as the intercept of a linear extrapolation of the initial rise to the baseline. With the equipment we have used,  $\Delta t$  is of order 2 to 3 psec at least and the phase angle in the ratio can be in error by 0.05 radian at 3 GHz, with the effect on derived values of  $\epsilon'$  and  $\epsilon''$  depending on their relative magnitudes. Reliable re-



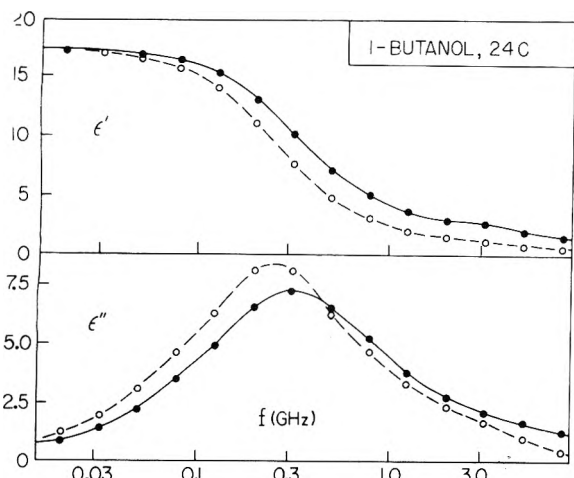


Figure 2. Dispersion ( $\epsilon'$ ) and loss ( $\epsilon''$ ) curves for a 6.0-mm sample of 1-butanol at 24° in a matched line: open circles from the thin sample approximation, filled circles from eq 8–10.

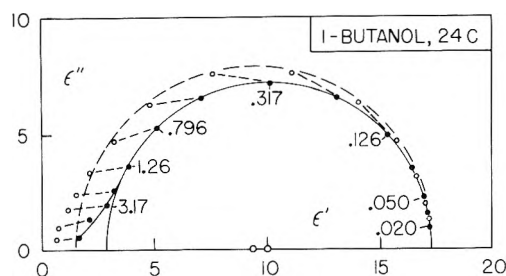


Figure 3. Complex permittivity locus for a 6.0-mm sample of 1-butanol at 24° in a matched line: open circles from the thin sample approximation, filled circles from eq 8–10.

sults at higher frequencies require better methods for time referencing of the incident and reflected pulses, such as the three-point computer-controlled scanning method of Nicolson.<sup>10</sup>

In the opposite limit of evaluations for low frequencies, deviations of the incident pulse from a limiting constant value  $V_0$  may require correction, as diode generators give a slow decay, of order 10% in 0.2  $\mu$ sec for a Hewlett-Packard Type 1105A/1106B unit. If this is represented by the initial decay of negative exponential  $V_0(t) = V_0 \exp(-t/\lambda)$ , the transform needed can be approximated by  $1/sv_0(s) = [1 + (i\omega\lambda)^{-1}]/V_0$  for  $\omega \gg 1/\lambda$ .

#### IV. Examples of Use of the Analysis

The measurement system and cell used to obtain the results presented here are described in part I. Numerical evaluations of Fourier transforms were made using the Brown University IBM 360/70 computer and a Fortran program written by T. G. Copeland.

Results from a 6.0-mm sample of 1-butanol at 24° in a matched 50-ohm line are shown as dispersion  $\epsilon'$  and absorption  $\epsilon''$  curves against logarithm of frequency in Figure 2, and as complex plane plots in Figure 3. Open circles connected by the dashed curves are values from the thin sample formula  $\epsilon^* - 1 = (2c/d)r/i\omega v_0$ ; the filled circles connected by solid curves result from use of eq 8–10. Although the results from the thin sample approximation can be fitted below 1 GHz by a semicircle and hence a Debye relaxation function, the high-frequency limit at  $\epsilon_1 = 1.5$  and fre-

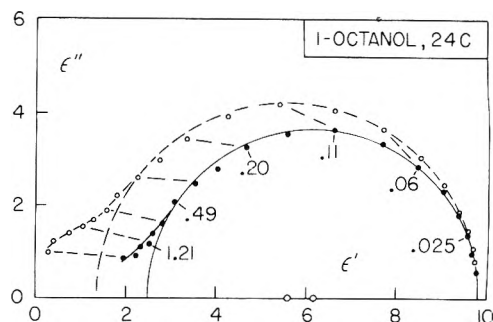


Figure 4. Complex permittivity locus for a 11.3-mm sample of 1-octanol at 24° terminating a coaxial line: open circles from the thin sample approximation,  $\epsilon^* = (c/d)(p/2i\omega v_0)$ , filled circles from eq 14–16.

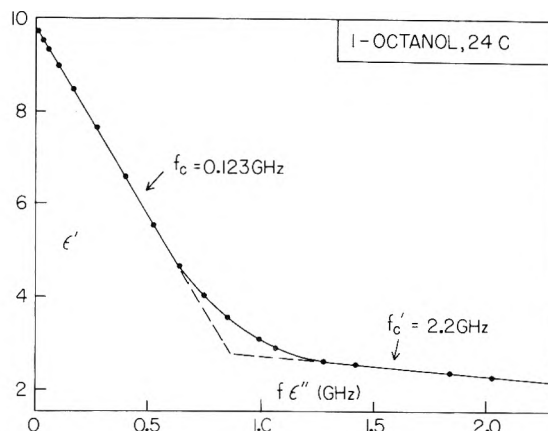


Figure 5. Plot of  $\epsilon'$  vs.  $f\epsilon''$  from the data of Figure 4 for 1-octanol.

quency  $f_c = 0.253$  GHz of maximum  $\epsilon''$  are both much too small. The corrected values are fitted to 3 GHz by a Debye function with  $\epsilon_1 = 3.0$  and  $f_c = 0.328$  GHz (relaxation time  $\tau = 484$  psec), in good agreement with other steady state and TDS results. Above 3 GHz, the corrected values show indications of a higher frequency relaxation process, but are increasingly unreliable because of timing errors and approximations in evaluations of the transforms.

Results from the sample termination method have been given for 1-propanol in a previous communication;<sup>11</sup> another example for a 11.3-mm sample of 1-octanol at 24° is shown in the complex plane locus of Figure 4. The indicated Debye relaxation at frequencies below 1 GHz has parameters  $\epsilon_1 = 1.4$  and  $f_c = 0.105$  GHz from the thin sample approximation, corrected to  $\epsilon_1 = 2.5$  and  $f_c = 0.123$  GHz by eq 14–16.

The corrected locus for 1-octanol gives definite evidence at frequencies above 0.6 GHz of a second faster relaxation process. A convenient analysis to show this more clearly is by a plot of  $\epsilon'$  against  $f\epsilon''$ , as shown in Figure 5. For a single Debye relaxation the relation of  $\epsilon'$  to  $f\epsilon''$  is a straight line of shape  $1/f_c$ ,<sup>12</sup> with transition to a second straight line of slope  $1/f'_c$  if a second Debye process with higher relaxation frequency  $f'_c$  is also present. Within their accuracy, the data have this behavior with  $f'_c = 2.2$  GHz. For two Debye relaxations described by

$$\epsilon^* - \epsilon_\infty = \frac{(\epsilon_0 - \epsilon_1)}{1 + i\omega\tau_1} + \frac{\epsilon_1 - \epsilon_\infty}{1 + i\omega\tau_2}$$

the relaxation times  $\tau_1$  and  $\tau_2$  are related to the indicated values  $\tau_a$  and  $\tau_b$  from  $f_c$  and  $f_c'$  by

$$\tau_1, \tau_2 = \frac{1}{2} \tau_a [1 \pm (1 - 4\tau_b/\tau_a)^{1/2}]$$

For  $\tau_b \ll \tau_a$ , the two roots are  $\tau_1 \approx \tau_a + \tau_b$  and  $\tau_2 \approx \tau_b$ . The values  $\tau_a = 1290$  psec,  $\tau_b = 72$  psec from the slopes of the  $\epsilon'$  vs.  $f\epsilon''$  plot in Figure 5 give  $\tau_1 = 1220$  psec and  $\tau_2 = 76$  psec, with  $\epsilon_1 = 2.8$  and  $\epsilon_2$  not determinable with any accuracy. As mentioned in part I, Lebrun<sup>13</sup> found evidence of two such dispersions in 1-octanol from steady state measurements, and the existence of higher frequency relaxation processes in aliphatic alcohols has been established by results of several workers.<sup>14</sup>

## V. Discussion

We believe the methods of analysis developed here for evaluation of complex permittivity  $\epsilon^*$  from TDS measurements are both simple and general enough to be widely useful. As compared with the direct analysis in part I to obtain dielectric response in "real time", numerical Fourier transformations rather than time integrations are required, but with these in hand exact account of finite reflection signals can be taken and satisfactory approximations obtained for the relaxation at considerably higher frequencies (shorter times) by simple algebra. The examples we have given are for liquids with principal relaxation of simple Debye form, but the analyses in no way assume this or any other time dependence, and we have obtained equally satisfactory results for glycols with "skewed arc" (Davidson-Cole) dispersion,<sup>15</sup> for example.

Our use of input admittance and properties of transmission lines considered as four terminal networks leads more directly and naturally to our working equations than the use of conventional expressions for total or multiple reflection coefficient  $r(\omega)/v_0(\omega)$  or  $p(\omega)/v_0(\omega)$ , but the two are fully equivalent and involve the same assumptions about the experimental conditions. Thus eq 4 and 32 for  $r(\omega)$  and  $p(\omega)$  given in part I are obtained from eq 4 on insertion of the appropriate  $y_d$  and rearrangement. Claassen and van Gemert have pointed out the converse by obtaining the equivalent of our eq 6, arranged in a slightly different way, from eq 4 of I for  $r(\omega)$ .

Of the two experimental arrangements considered, the sample termination method has the advantages of simpler sample conditions and working formulas, together with larger reflection signals for comparable accuracy and resolution of the derived results. Upper frequency limits for either case are set in a particular application by limitations of the instruments used and by approximations of the analysis. For pulse generators and sampling units with rise time of order 40 psec, the first limit is about 3 GHz with the methods used for evaluations of the Fourier transforms, but can be increased with more refined procedures. The other factor to be considered is accuracy of the approximations to the propagation factor  $x \coth x$ , where  $x = i(\omega d/c)\epsilon^*{}^{1/2}$ . Although the series used (eq 5) is convergent for  $|x| < \pi$ , the accuracy of approximating  $x \coth x$  by the series is increasingly sensitive to small errors for  $|x| > 1$ , which can be taken as an approximate limit beyond which the formulas should be used with increasing caution. (We may note that the first zero of  $x \coth x$  for  $\epsilon^*$  real occurs at  $|x| = \pi/2$

= 1.57, the condition for quarter wave resonance of the dielectric sample.) This limit corresponds to a frequency  $f = c/2\pi d|\epsilon|^{1/2}$ , which for a sample with  $d = 3$  mm,  $|\epsilon| = 3.2$  is 8.8 GHz. At higher frequencies, the formulas given here may still be useful, as by providing starting values of  $\epsilon^*$  for numerical solutions of eq 6 or 12 by a Newton-Raphson or other iterative methods.<sup>17</sup>

Our examples of the use of TDR, and most of those reported to date, have been for quite strongly polar substances with relatively large values of static permittivity  $\epsilon_0$  falling to much smaller values in the frequency or time range of the measurements. The evaluation of smaller changes, as for polar solutes at low concentrations, will present greater difficulties, but we believe that the present methods at least considerably extend the range of possibilities.

Finally, it should be remarked that most of the discussion has been for nonconducting dielectrics, although the possibilities for study of samples with finite conductance have been considered, and it has also been assumed that the system of interest is nonmagnetic. If the relative permeability  $\mu^*$  is appreciably different from one, our formulas for  $\epsilon^*$  are valid only at relatively low frequencies. This is because the propagation function  $x$  is given by  $x = i(\omega d/c)(\epsilon^*\mu^*)^{1/2}$  and the line inductance by  $L_c = i\omega L_c d\mu^*$  ( $(\tanh x)/x$ ). Evaluation of  $\epsilon^*$  if  $|x|$  is not much less than one then requires a knowledge of  $\mu^*$  and vice versa, and simultaneous evaluation of the two requires further information, as obtained by the simultaneous reflection-transmission method of Nicolson and Ross<sup>18</sup> for example. An alternative is to measure the reflection from a sample terminated in a short circuit, which together with the open circuit measurement can be analyzed by our methods to give both  $\epsilon^*$  and  $\mu^*$ .

*Acknowledgments.* This work was supported by the Brown University Materials Science Program and the National Science Foundation. I thank Drs. T. A. C. M. Claassen and M. J. C. van Gemert for a copy of their paper<sup>16</sup> prior to publication, and Dr. A. M. Nicolson for helpful discussion.

## References and Notes

- (1) For reviews, see ref 1 and 5 of part I (preceding paper in this issue).
- (2) H. Fellner-Feldegg, *J. Phys. Chem.*, **76**, 2116 (1972).
- (3) See, for example, W. C. Johnson, "Transmission Lines and Networks", McGraw-Hill, New York, N.Y., 1950.
- (4) From specifications for General Radio Type 900-WO precision open circuit termination, General Radio Catalog U, 1970.
- (5) H. Levine and C. Fapas, *J. Appl. Phys.*, **22**, 29 (1951).
- (6) E. O. Tuck, *Math. Comput.*, **21**, 239 (1967).
- (7) C. Shannon, *Proc. Inst. Radio Eng.*, **37**, 10 (1949).
- (8) H. A. Samulon, *Proc. Inst. Radio Eng.*, **39**, 175 (1951).
- (9) A. M. Nicolson, *Electron. Lett.*, **9**, 317 (1973).
- (10) A. M. Nicolson, WESCON Technical Paper, No. 13, 22 (1969). See also ref 18.
- (11) R. H. Cole, *J. Phys. Chem.*, **79**, 93 (1975).
- (12) R. H. Cole, *J. Chem. Phys.*, **23**, 493 (1955).
- (13) A. Lebrun, *Cah. Phys.*, **60**, 11 (1955); *Ann. Phys.*, **10**, 16 (1955).
- (14) See, for example, P. Girard and P. Abadie, *Trans. Faraday Soc.*, **42A**, 40 (1946).
- (15) D. W. Davidson and R. H. Cole, *J. Chem. Phys.*, **19**, 1484 (1951).
- (16) T. A. C. M. Claassen and M. J. C. van Gemert, submitted for publication in *J. Chem. Phys.*
- (17) S. B. Dev, A. M. North, and R. A. Pethrick, *Adv. Mol. Relax Processes*, **4**, 159 (1972).
- (18) A. M. Nicolson and G. F. Ross, *IEEE Trans. Instrum. Meas.*, **IM-19**, 377 (1970).

# COMMUNICATIONS TO THE EDITOR

## Evidence for an Exciton Interaction in the Low-Lying Singlets of Diphenyl Sulfide

Sir: A spectroscopic study was carried out on benzenethiol (PhSH), thioanisole (PhSCH<sub>3</sub>), and diphenyl sulfide (PhSPh) using the photoselection technique.<sup>1</sup> In this study the polarization experiments give the expected result that the first and second absorption bands in PhSH and PhSCH<sub>3</sub> are oppositely in-plane polarized. The low-lying weak absorption band is the <sup>1</sup>L<sub>b</sub> state while the first intense absorption band is the <sup>1</sup>L<sub>a</sub> state. This and other polarization results have been discussed in a previous paper.<sup>2</sup> The polarization results obtained for PhSPh are found to be different in some respects and suggest that an exciton type interaction occurs between each corresponding pair of low-lying ring states. These results are discussed here. Experimental details have been given elsewhere.<sup>2</sup> The Aldrich PhSPh (99+%) was vacuum distilled.

Becker et al.<sup>3</sup> first suggested that the weak fluorescence observed in PhSPh<sup>4</sup> was caused by excitonic type behavior. This was explained in the following way. The coupling between the <sup>1</sup>L<sub>b</sub> states of the phenyl groups result in two exciton states. Transitions to or from the lower state are more forbidden than in the absence of any interaction. This leads to less fluorescence, more intersystem crossing to the triplet state, and consequently to a larger ratio of phosphorescence to fluorescence. By contrast this same ratio in PhSH and PhSCH<sub>3</sub> is only one-tenth as large.<sup>2</sup>

The absorption spectra (Figure 1) and the polarization results (Table I) obtained for PhSPh provide more evidence to support the view that an exciton interaction occurs in this molecule. It appears that two allowed polarization components result from the interaction of each pair of low-lying ring states. This interaction is due to the faces of

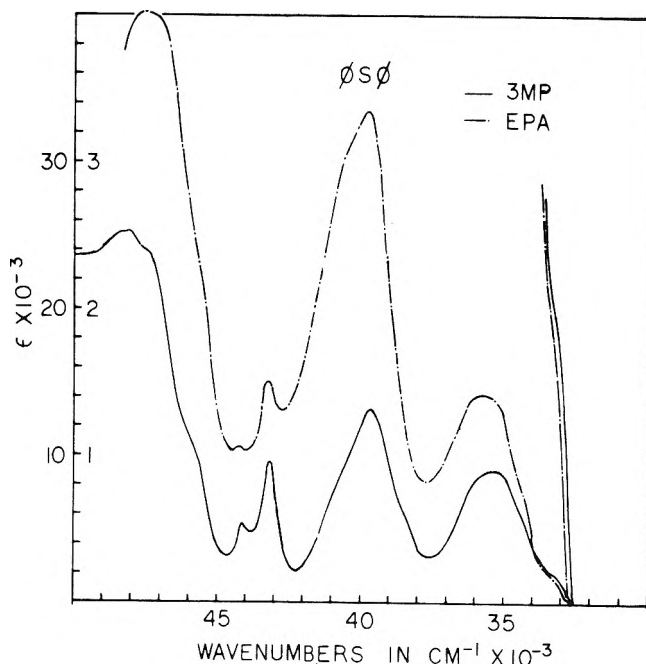
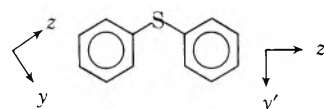


Figure 1. Low temperature absorption spectra of PhSPh in 3MP and EPA. Molar absorptivity,  $\epsilon$ .

### Chart I



the benzene rings being tilted toward each other (see Chart I). This is known to occur in *p*-tolyl sulfide where the

TABLE I: Polarization Ratios for the Fluorescence and Phosphorescence Bands Obtained in the 0-0 Region,  $\lambda_{0-0}$ , and at the Wavelength of Maximum Emission Intensity,  $\lambda_{max}$

$\lambda_{ex}$	Polarization results in PhSPh							
	EPA				3MP			
	$N_{r1}$		$N_{ph}$		$N_{r1}$		$N_{ph}$	
	$\lambda_{0-0}$ 305	$\lambda_{max}$ 320	$\lambda_{0-0}$ 387	$\lambda_{max}$ 430	$\lambda_{0-0}$ 308	$\lambda_{max}$ 325	$\lambda_{0-0}$ 390	$\lambda_{max}$ 430
296	2.29	1.92	1.73	1.68	1.87	1.92	1.79	1.78
285					1.91	1.88	1.70	1.74
282	1.89	1.91	1.61	1.65				
280	1.76	1.94	1.66	1.66				
252	2.21	2.06	1.67	2.06	2.09	1.88	1.63	1.88
250	2.14	2.16	1.71	2.07				

<sup>a</sup> Each value of  $N$  shown is the average of two or more experiments done on different sample regions. The wavelengths are given in millimicrons.

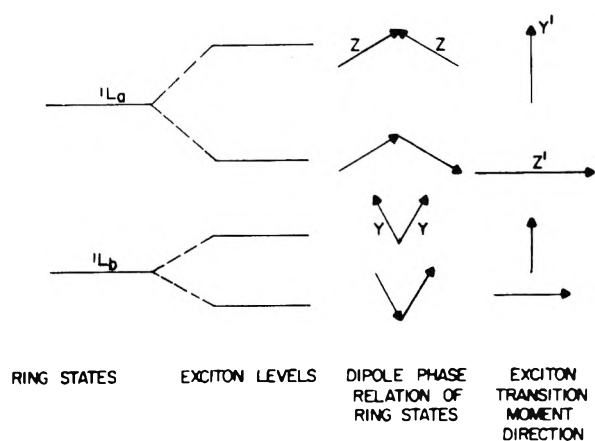


**Figure 2.** Exciton band energy diagram for a double molecule with oblique transition dipoles. The  ${}^1L_b$  and  ${}^1L_a$  ring states are  $y$  and  $z$  polarized, respectively. The presence of a distinct structured band (see Figure 1) is a result of the large exciton splitting energy (approximately  $3500\text{ cm}^{-1}$ ). This is due to the intense absorption in the  ${}^1L_a$  ring states.

C-S-C angle is found to be  $109^\circ$  in the crystal structure.<sup>5</sup> The absorption spectra of PhSPH is different than the absorption spectra of PhSCH<sub>3</sub> and PhSH in two respects. First, the near-uv band (probably composed of two states with different polarization components) is much stronger than the  ${}^1L_b$  band in these two molecules, and secondly, a structured band is found between the two strong uv bands. The near-uv band is the result of exciton formation between the lowest  ${}^1L_b$  states in each ring while the first strong absorption band and the structured one result from the interaction between the corresponding  ${}^1L_a$  states. The polarization results for PhSPH in EPA and 3MP for excitation and emission bands, respectively, give additional support to this interpretation. These results show that the absorption and emission parameters (probability for absorption and emission along individual molecular axes) in each case have the same large parallel polarization component. This is in contrast to the results found in PhSCH<sub>3</sub> and PhSH where the 0-0 region of the  ${}^1L_b$  and  ${}^1L_a$  absorption bands are  $y$  and  $z$  polarized, respectively. If one assumes that the polarization components for the phosphorescing state (this may also be a  ${}^3n,\pi^*$  state<sup>2</sup>) in PhSPH are similar to the values found in PhSH because the polarization ratios in the 0-0 and  $\lambda_{\text{max}}$  regions are very similar (for excitation in the  ${}^1L_a$  band) in each case (more so for PhSPH in EPA) then the results in Table I would be obtained if the near-uv band and the corresponding fluorescence in this molecule was  $z$  polarized ( $z'$  in the exciton state) in the 0-0 region. This would give the large values obtained for  $N^{\text{ph}}$  (for  $\lambda_{\text{ex}}$   $296\text{ m}\mu$ ) and  $N^{\text{f}}$  (for  $\lambda_{\text{ex}}$   $252\text{ m}\mu$ ) as compared to values of less than 1 found for these same ratios in PhSCH<sub>3</sub> and PhSH<sup>2</sup>. Assuming that the structure shown in Chart I of PhSPH is correct<sup>6</sup> the  $z$  direction no longer lies along the benzene ring but instead lies along the line connecting the rings ( $x$  and  $x'$  are perpendicular to the plane of the paper). This would make the  $z'$  polarized component lowest energy in each case so that the structured band should be  $y'$  polarized (see Figure 2).<sup>7</sup> The lowest value of  $N^{\text{f}}$  (1.76 in EPA) shown in Table I is obtained for excitation at  $280\text{ m}\mu$ . This value is 0.4-0.5 units less than those values obtained for excitation in a 100%  $z'$  polarized region (for  $\lambda_{\text{ex}}$  at  $296$  and  $250\text{ m}\mu$ ). This result suggests the presence of a weak  $y'$  polar-

ized exciton band (from the weaker interacting  ${}^1L_b$  states) lying under the maximum in the stronger  $z'$  polarized low-energy exciton state. Since the triplet states do not interact strongly the direction of the  $z$  axis and the  $z'$  axis must be similar in order that values greater than 2.0 can be observed for  $N^{\text{ph}}$ . This suggests that the C-S-C angle in PhSPH is larger than the value of  $109^\circ$  found in the  $p$ -tolyl sulfide single crystal.

**Acknowledgment.** The author is indebted to the Chemistry Department for most of the equipment used in these experiments. He is also grateful for a yearly NSF grant made available to him by the Research Committee. The machine shop work of Mr. Peter Amirato is appreciated.

## References and Notes

- (1) A. C. Albrecht, *J. Mol. Spectrosc.*, **6**, 84 (1961).
- (2) P. G. Russell, *J. Phys. Chem.*, **79**, 1347, 1353 (1975).
- (3) R. S. Becker, A. D. Jordan, and J. Kolc, *J. Chem. Phys.*, **59**, 4024 (1973).
- (4) In the study reported here the emission intensity in the phosphorescence was found to be approximately 100 times larger than the intensity in the fluorescence.
- (5) W. R. Blackware and S. C. Abraham, *Acta Crystallogr.*, **8**, 329 (1955).
- (6) In order to interpret the polarization results by using a simple molecular exciton model (quasiclassical vector method) the phenyl rings are assumed to be coplanar (for randomly oriented single molecules in a rigid glass) whereas in the actual molecular configuration there may be some steric hindrance preventing coplanarity. This is known to be the case in single crystals of  $p$ -tolyl sulfide where the normals to these rings form an angle of  $56^\circ$  to each other.<sup>5</sup>
- (7) M. Kasha, H. R. Rawls, and M. Ashraf El-Bayoumi, *Pure Appl. Chem.*, **11**, 371 (1965).
- (8) Address correspondence to the Department of Applied Science, Brookhaven National Laboratory, Upton, N.Y. 11973.

Department of Chemistry

C.W. Post College

P.O. Greenvale, New York 11548

Philip G. Russell<sup>8</sup>

Received March 12, 1975

## Ethylamine Behavior on 3A Zeolite Surface

Publication costs assisted by the Institute of Chemistry, Technology and Metallurgy, Beograd

*Sir:* In an attempt to dry ethylamine on 3A zeolite, adsorption of amine on the zeolite was observed. Since, according to Barrer's classification,<sup>1</sup> ethylamine is adsorbed on zeolites having dimensions greater than  $4.2\text{ \AA}$ , we considered it of interest to examine this phenomenon. The processes of amine adsorption and desorption have been studied by the method of infrared spectroscopy.

Experiments were performed on the zeolite 3A from The Union Carbide Corp., Linde Division, in  $1/8$ -in. pellets. Ethylamine, Merck p.a., was used without further purification.

Adsorption of ethylamine was performed at room temperature by the static method in a specially prepared tube. After adsorption, an ir spectrum was recorded for a part of the zeolite solid phase; the zeolite was prepared as fluorocarbon and nujol mulls between KBr disks. The remaining zeolite was then degased ( $p = 10^{-2}$  Torr) and heated from

room temperature to 773 K. At approximately 50 K intervals, the temperature was kept constant for 0.5 hr in order to establish equilibrium between the desorbed gaseous phase and the sample adsorbed on the solid phase. Desorption products were collected in a specially prepared vessel, by liquid nitrogen trapping. Ir spectra of the gaseous phase were recorded in a 6 cm long gas cell at room temperature. The pressure in the system was measured using a mercury manometer. All the spectra were recorded on a Perkin-Elmer 457 ir spectrometer.

Ethylamine was adsorbed at room temperature on hydrated zeolite. Immediately after adsorption of the amine, the ir spectrum of the solid phase, zeolite, was recorded (Figure 1, spectrum a). It is evident in this spectrum that, besides the bands characteristic of zeolite 3A,<sup>2</sup> two new bands appear in the region of OH stretching vibrations at 3695 and 3615  $\text{cm}^{-1}$  and new bands in the region of 3000 and 1400  $\text{cm}^{-1}$ .

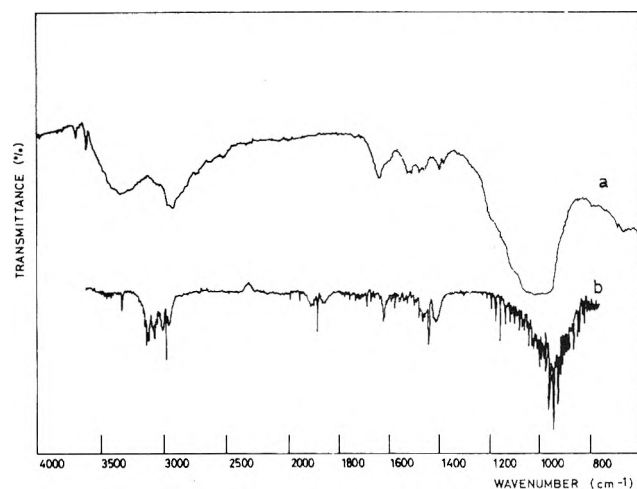


Figure 1. Infrared spectra of (a) solid phase zeolite after adsorption of ethylamine and (b) desorbed gaseous phase.

The bands in the region of 3000  $\text{cm}^{-1}$  might be due to the adsorbed amine. However, as ethylamine also has a very intense band in the region of 780  $\text{cm}^{-1}$ ; the absence of this band in the spectrum of the solid phase was taken to indicate that the bands in the region of 3000  $\text{cm}^{-1}$  do not belong to the CH stretching vibrations of the adsorbed amine. The origin of these bands was clarified by analysis of the ir spectrum of the desorbed gaseous phase, which was found to consist of ethylene and ammonia (Figure 1, spectrum b), and, therefore, bands in the region of 3000  $\text{cm}^{-1}$  have been attributed to ethylene on the solid phase.

The gaseous phase components have been identified by analyzing the bands in the region of 900–1000  $\text{cm}^{-1}$ . Ethylene was identified on the basis of the very intense band  $\nu_7$  (949.2  $\text{cm}^{-1}$ ). Although other bands of the ethylene molecule were also identified in the spectrum [ $\nu_9$  (3105.5  $\text{cm}^{-1}$ ),  $\nu_{10}$  (995  $\text{cm}^{-1}$ ),  $\nu_{11}$  (2989.5  $\text{cm}^{-1}$ ), and  $\nu_{12}$  (1443.5  $\text{cm}^{-1}$ ), as well as the combination band  $\nu_7 + \nu_8$  (1889.6  $\text{cm}^{-1}$ )],<sup>3</sup> the appearance of band  $\nu_7$  in the spectrum was assumed to prove the presence of ethylene in the sample. In order to identify ammonia we used Q branches, near 968 and 932  $\text{cm}^{-1}$ , of the band  $\nu_2$  (950.24  $\text{cm}^{-1}$ ) of the ammonia molecule, since the fundamental  $\nu_2$  has a double Q branch.<sup>4</sup> Bands corresponding to  $\nu_1$  (3336.0  $\text{cm}^{-1}$ ),  $\nu_3$  (3414.9  $\text{cm}^{-1}$ ), and  $\nu_4$  (1627.77  $\text{cm}^{-1}$ ) vibrations of the ammonia molecule are also identified in the spectra.<sup>4</sup>

The band at 1400  $\text{cm}^{-1}$  and those at 1478 and 1505  $\text{cm}^{-1}$  in the ir spectrum of the solid phase indicate the presence of the  $\text{NH}_4^+$  ion on the zeolite.<sup>3</sup> The existence of the  $\text{NH}_4^+$  ion on the solid phase after adsorption of ethylamine is probably due to subsequent interaction between ammonia and water in the zeolite, or to the water adsorbed during preparation of the sample for recording of the ir spectra, when the  $\text{NH}_4^+$  ion could also be formed.

The change of pressure in the system during heating, i.e., desorption from the solid phase, gives three peaks on the  $\Delta P/\Delta T$  vs.  $T$  plot (Figure 2, curve a). (The plot actually represents the curve of the desorption process from the zeolite as a function of temperature.) The first peak, at 433 K, and the second, at 543 K, are identified, on the basis of

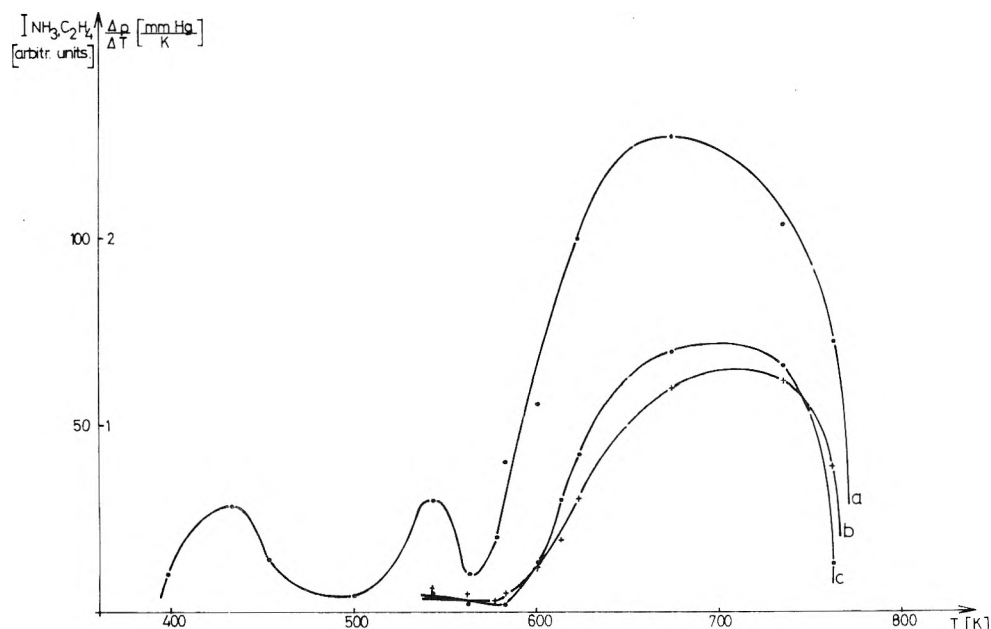


Figure 2. Plots of (a) the change of pressure in the system during desorption  $\Delta P/\Delta T = f(T)$ ; (b) the intensity of the ammonia band (arbitrary units) as a function of temperature; (c) the intensity of the ethylene band (arbitrary units) as a function of temperature.

literature data,<sup>5</sup> as the temperatures of water desorption, while the third, at 673 K, corresponds to the desorption of the ammonia and ethylene mixture. This last observation agrees with the analysis of the ir spectra of the gaseous phase, as stated above.

The intensity of the ethylene band  $\nu_7$  at 949.2  $\text{cm}^{-1}$  is stronger than the ammonia bands at 968 and 932  $\text{cm}^{-1}$  at heating temperatures below 733 K, while, at higher temperatures, the relative ratio of band intensities is reversed (Figure 2, curves b and c). At 773 K the zeolite is completely degased. Repeated adsorption of ethylamine on the same zeolite sample gives the same results as those of ethylamine adsorption on hydrated zeolite. The process of ethylamine decomposition is repeated. (We note here that no thermal decomposition of ethylamine alone into ammonia and ethylene was observed during its heating to 783 K.)

From the experimental results it can be seen that adsorption of ethylamine takes place on the 3A zeolite. On the basis of the ir spectra of both the solid phase and desorbed gaseous phase, it can be concluded that catalytic decomposition of ethylamine occurs at room temperature. Deamination was not observed in our experiments. Desorption from the zeolite gives ammonia and ethylene and not amine, as has been observed during desorption of amines from X and Y zeolites<sup>6</sup> and during deamination of the primary alkylammonium zeolites.<sup>7</sup>

The process of catalytic decomposition of ethylamine takes place on the internal zeolite surface. This was verified by ethylamine behavior on the 3A zeolite inclusion complex,<sup>8</sup> the channels of which had been blocked by alkali nitrate molecules. Amine decomposition did not occur on this solid phase. The appearance of the bands at 3695 and 3615  $\text{cm}^{-1}$ , in the ir spectrum of the solid phase, has been taken as proof of this conclusion as these bands also appear when the inclusion of molten nitrate molecules in hydrated zeolite takes place.<sup>9</sup> Therefore, ethylamine enters the channels of the zeolite and is decomposed into ammonia and ethylene. Explanation of the mechanism of ethylamine decomposition on the zeolite requires further experiments which are in the progress.

*Acknowledgment.* The authors wish to express thanks to Professor M. Šušić and Professor S. Ribnikar for their helpful suggestions and comments.

## References and Notes

- (1) V. A. Sokolov, N. S. Topochetnikov, and N. V. Keltsev, "Molekulyarnye Sita i ih Primenenie", Khimiya, Moskva, 1964, p 29.
- (2) I. E. Maxwell and A. Baks, *Adv. Chem. Ser.*, No. 121, 87 (1973).
- (3) G. Herzberg, "Infrared and Raman Spectra of Polyatomic Molecules", Van Nostrand, New York, N.Y., 1950.
- (4) N. L. Alpert, W. E. Keiser, and H. A. Szymanski, "IR Theory and Practice of Infrared Spectroscopy", Roseta Edition, Plenum Press, New York, N.Y., 1970, p 142.
- (5) V. Vucelić, D. Vucelić, D. Karaulić, and M. Susić, *Thermochim. Acta*, 7, 77 (1973).
- (6) P. A. Jacobs, B. K. G. Theng, and J. B. Uytterhoeven, *J. Catal.*, 26, 191 (1972).
- (7) P. A. Jacobs and J. B. Uytterhoeven, *J. Catal.*, 26, 175 (1972).
- (8) M. Liguornik and Y. Marcus, *J. Phys. Chem.*, 75, 2523 (1971).
- (9) N. Petranovic, Ph.D. Thesis, University of Belgrade, 1972.

Department of Physical Chemistry  
Faculty of Sciences  
Belgrade, Yugoslavia

Ubavka Mioč\*  
Nadežda Petranovic

Received July 25, 1974; Revised Manuscript Received April 28, 1975

## Chemistry of Nuclear Recoil $^{18}\text{F}$ Atoms. VII. Detection of Caging Reactions in Liquid Phase $\text{CF}_3\text{CH}_3$ and $\text{CHF}_2\text{CH}_3$

Publication costs assisted by the U.S. Energy Research and Development Administration

*Sir:* Franck and Rabinowitsch first proposed that a diffusion-limiting solvent cage could increase the efficiency of photochemically initiated radical combination under condensed phase conditions.<sup>1</sup> An extensive literature has developed on this subject in both conventional and nuclear recoil kinetics. The recent preliminary recoil  $^{18}\text{F}$  vs.  $\text{CH}_3\text{F}$  study of Richardson and Wolfgang<sup>2</sup> stimulated other applications of the density-variation technique.<sup>3-5</sup> These workers observed substantial  $\text{CH}_3^{18}\text{F}$  and  $\text{CH}_2^{18}\text{F}$  radiochemical yield enhancements at large reactant density (cf. Figure 1),<sup>6</sup> which were ascribed to Franck-Rabinowitsch caging. The initial  $\text{CH}_3^{18}\text{F}$  and  $\text{CH}_2^{18}\text{F}$  yield increases observed at small densities ( $\leq 0.4 \text{ g cm}^{-3}$ ) were attributed to collisional stabilization of internally excited primary substitution products. However, complications associated with collisional excitation-stabilization in the proposed density range associated with caging were rejected on the basis of an intuitive lifetime argument.<sup>2</sup> Within this framework it clearly follows that the density-variation technique is capable of detecting the occurrence of caging reactions in nuclear recoil systems and that caging yields can be assigned from substitution product yield data based upon excitation-stabilization corrections determined at small density. The extreme simplicity of this proposal has made it attractive for applications in other recoil systems.<sup>3-5,7</sup>

We wish to communicate our recent finding that collisional stabilization of primary energetic  $^{18}\text{F}$  substitution reaction products in  $\text{CF}_3\text{CH}_3$  and  $\text{CHF}_2\text{CH}_3$  occurs to a significant extent ( $\geq 20\%$ ) over the same reactant density range in which caging reactions take place. Our results, which consist in part of apparent hot substitution yields quite similar to those obtained by previous workers,<sup>2-5</sup> have been obtained by a novel combination of the density-variation<sup>2</sup> and full mechanism determination<sup>3,9</sup> techniques. It is our strong contention that caging reactions in hot atom systems cannot be unambiguously detected in the absence of full mechanism results unless excitation-stabilization complications have been clearly demonstrated to be unimportant.<sup>3,10</sup>

Our density-dependent radiochemical yield data for the hot F-for-F channel in  $\text{CF}_3\text{CH}_3$  are compared in Figure 1 to the corresponding  $\text{CH}_3\text{F}$  results.<sup>6,10</sup> It is evident that qualitatively similar density dependences were obtained for these systems. In our alternative and preferred method for presenting density-variation results (cf. Figure 2), the direct bulk density correlation utilized in conventional Richardson-Wolfgang caging plots<sup>2-5</sup> has been replaced by a comparison of the variation of experimental yields with the reduced length parameter ( $\lambda/\sigma$ ). This latter quantity represents the ratio of the mean intermolecular separation distance to the molecular diameter of the host substance.<sup>11</sup> Both our apparent  $\text{CF}_2^{18}\text{FCH}_3$  yields and total F-for-F mechanism yields have been shown on Figure 2. The density-independent complementary yield technique has become well established as a test of completeness for hot atom reaction mechanisms.<sup>3,9</sup> We thus regard the wide range of ( $\lambda/\sigma$ )-independence demonstrated by the present F-for-F mechanism yield data as providing very strong evi-

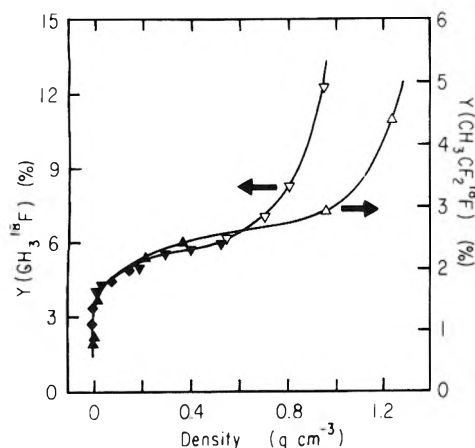


**Figure 1.** Conventional caging plots for energetic F-for-F substitution in  $\text{CH}_3\text{F}$  and  $\text{CF}_3\text{CH}_3$ :  $\blacktriangledown$ ,  $\nabla$ ,  $\text{CH}_3\text{F}$  (ref 2 and 6);  $\blacktriangle$ ,  $\triangle$ ,  $\text{CF}_3\text{CH}_3$ ;  $\blacklozenge$ , plot point overlaps ( $\blacktriangledown + \blacktriangle$ ); open points represent condensed phase results.

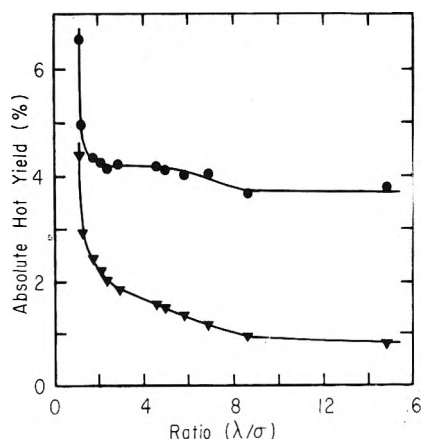


**Figure 2.** Total mechanism plot for energetic F-for-F substitution in  $\text{CF}_3\text{CH}_3$ :  $\bullet$ , total mechanism yields (ref 9 and 10);  $\blacktriangledown$ , apparent  $\text{CF}_2^{18}\text{FCH}_3$  yields.

dence favoring the essential correctness of our F-for-F mechanism. The apparent decrease in the mechanism yield at  $(\lambda/\sigma)$  values larger than 5.0 corresponds to the onset of sequential consecutive decomposition leading to the formation of unmeasured carbene products. Qualitatively similar density-independent results were obtained in this study for all nine of the available hot  $^{18}\text{F}$  substitution and alkyl replacement channels in  $\text{CF}_3\text{CH}_3$  and  $\text{CHF}_2\text{CH}_3$ .<sup>10</sup>

From the standpoint of the detection and characterization of caging reactions our relevant results correspond to  $(\lambda/\sigma)$  values ranging downward from 5.0. The F-for-F total mechanism yields shown in Figure 2 did not change over the  $(\lambda/\sigma)$  interval 2.0 to 5.0, providing strong support for the assumed mechanism.<sup>3,9,10</sup> Over this same interval, however, the  $\text{CF}_2^{18}\text{FCH}_3$  yield was a monotonically increasing function of increasing density, clearly indicating the importance of collisional stabilization in the gas phase at very high pressures. For  $(\lambda/\sigma)$  values less than 2.0 both the  $\text{CF}_2^{18}\text{FCH}_3$  and total mechanism yields exhibited significant further increases. Within the framework of the primary hot reaction hypothesis (vide supra), this increase in the total mechanism yield at densities corresponding to the 303 and 197°K liquid phases cannot be understood. A careful analysis of all the radiochemical yield data fails to cast doubt upon the validity of the primary hot reaction hy-

**TABLE I: Calculated Caging Yields in Liquid Phase  $\text{CF}_3\text{CH}_3$  and  $\text{CHF}_2\text{CH}_3$**

Reaction channel	Reactant	$Y_c, \%$	
		303 °K	197 °K
F-for-F	$\text{CF}_3\text{CH}_3$	$0.7 \pm 0.3$	$2.3 \pm 0.4$
F-for-F	$\text{CHF}_2\text{CH}_3$	$1.0 \pm 0.3$	$2.3 \pm 0.4$
F-for-H	$\text{CF}_3\text{CH}_3$	$0.1 \pm 0.2$	$1.6 \pm 0.5$
F-for- $\beta\text{H}^a$	$\text{CHF}_2\text{CH}_3$	$0.6 \pm 0.3$	$1.8 \pm 0.4$
F-for- $\alpha\text{H}^a$	$\text{CHF}_2\text{CH}_3$	$0.8 \pm 0.3$	$1.5 \pm 0.3$

<sup>a</sup> In  $\text{CHF}_2\text{CH}_3$  the methyl carbon has been designated  $\beta$ .

pothesis at large density.<sup>10</sup> We thus conclude that the present observation of a pronounced increase in the total F-for-F mechanism yield in liquid phase  $\text{CF}_3\text{CH}_3$  provides definitive evidence for the occurrence of some unspecified form of caging process. It also rather clearly follows that the density-dependent  $\text{CF}_2^{18}\text{FCH}_3$  yield data alone do not provide sufficient information to determine the onset of caging. Further discussion concerning the possible mechanism for these caging reactions will be deferred to a more detailed article. Here we merely state without further proof our experimental results that comparable total mechanism yield enhancements were observed in 303 and 197°K liquid phase experiments for all five of the available hot substitution channels in  $\text{CF}_3\text{CH}_3$  and  $\text{CHF}_2\text{CH}_3$ , that similar behavior was not observed for the alkyl replacement channels, that the caged  $^{18}\text{F}$  activity was derived exclusively in lieu of F-to-HF abstraction, and that the effect of ambient temperature at constant density was negligible over a range of more than 100°K.

Based upon these results we conclude that the observation of an intermediate density "plateau" on a Richardson-Wolfgang hot atom caging plot<sup>2,4,5</sup> (cf. Figure 1) does not constitute conclusive evidence for the onset of caging reactions. Unless the role of excitation-stabilization has been quantitatively established on experimental grounds, apparent product yield enhancements observed at large density cannot be attributed solely to caging. We suggest the following general procedure for the quantitative determination of caging yields in hot atom systems. The primary mechanism ( $Y^0$ ) and total decomposition ( $Y_d$ ) yields associated with each primary reaction channel can be determined from gas phase experiments at densities approaching the values corresponding to the onset of caging. Then the caged yield ( $Y_c$ ) follows from the apparent total stabilized yield ( $Y_T$ ):<sup>10</sup>

$$Y_c = Y_T - (Y^0 - Y_d) \quad (1)$$

Our present caging yield results estimated in this fashion have been listed in Table I.

In all of our liquid phase experiments we have consistently observed the presence of typical gas phase secondary decomposition products. Many of these (notably the olefins from HF-elimination reactions) require extensive rearrangement of the reactant precursor species. Such behavior taken together with mechanism density independence has been uniformly accepted in the unimolecular kinetics literature as indicative of a true complex, sequential reaction mechanism. Our present suggestion is merely that this same reasoning can be extended to the liquid phase. We thus conclude in apparent conflict with the cited lifetime proposal<sup>2</sup> that no a priori grounds exist for excluding the oc-

currence of "normal" hot atom excitation-stabilization processes in liquid phase experiments.<sup>12</sup>

**Acknowledgments.** We wish to acknowledge discussions with Professor D.L. Bunker and Drs. E.R. Grant and R.R. Pettijohn. Financial support has been provided by the U.S. Atomic Energy Commission,<sup>13</sup> from an N.D.E.A. Graduate Fellowship (R.G.M.), and from a John Simon Guggenheim Memorial Foundation Fellowship (J.W.R.).

## References and Notes

- (1) J. Franck and E. Rabinowitsch, *Trans. Faraday Soc.*, **30**, 120 (1934).
- (2) A. E. Richardson and R. Wolfgang, *J. Am. Chem. Soc.*, **92**, 3480 (1970).
- (3) M. D. Loberg, K. A. Kronn, and M. J. Welch, *J. Am. Chem. Soc.*, **95**, 5496 (1973).
- (4) H. J. Machulla and G. Stocklin, *J. Phys. Chem.*, **78**, 658 (1974).
- (5) R. W. Helton, W. M. Grauer, and E. P. Rack, *Radiochim. Acta*, **19**, 44 (1973).
- (6) We thank Professor A. E. Richardson for permission to reproduce the <sup>18</sup>F vs. CH<sub>3</sub>F results.
- (7) We note that ref 3 and 4 have proposed caging mechanisms other than caged primary radical combination. For definition of this terminology cf. ref 8.
- (8) D. L. Bunker and B. S. Jacobson, *J. Am. Chem. Soc.*, **94**, 1843 (1972).
- (9) K. A. Krohn, N. J. Parks, and J. W. Root, *J. Chem. Phys.*, **55**, 5771, 5785 (1971).
- (10) (a) R. G. Manning, Ph.D. Dissertation, University of California, Davis, 1975. (b) J. W. Root, U.S. Atomic Energy Commission Technical Report No. UCD-34P158-74-1, University of California, Davis, 1975. (c) R. G. Manning and J. W. Root, submitted for publication.
- (11) (a) For the close-packed sphere model the mean intermolecular separation is calculated as follows from the experimentally measured bulk density:

$$\lambda = [6M/\pi\rho L]^{1/3} \times 10^8 \text{ \AA}$$

in which the quantities  $M$ ,  $\rho$ , and  $L$  denote molecular weight (amu), bulk density ( $\text{g cm}^{-3}$ ), and Avogadro's number, respectively. The molecular diameters employed in our calculations were determined from critical data (ref 11b): CH<sub>3</sub>F, 4.06; CF<sub>3</sub>CH<sub>3</sub>, 4.98; and CHF<sub>2</sub>CH<sub>3</sub>, 4.86 \AA. (b) J. W. Root, Ph.D. Dissertation, University of Kansas, 1964; Available from University Microfilms as Dissertation No. 65-7004.

- (12) (a) Evidence favoring secondary decomposition following T-for-H substitution in liquid phase  $\text{c-C}_6\text{H}_6$  has been obtained previously (ref 12b,c). (b) E. K. C. Lee and F. S. Rowland, *J. Am. Chem. Soc.*, **85**, 897 (1963); (c) A. Hosaka and F. S. Rowland, *J. Phys. Chem.*, **75**, 3781 (1971).
- (13) This research has been supported under A.E.C. Contract No. AT-(04-3)34, project agreement 158.

Department of Chemistry and  
Crocker Nuclear Laboratory  
University of California  
Davis, California 95616

Ronald G. Manning  
John W. Root\*

Received February 24, 1975

## Selective Oxidation of Nickel in Copper-Nickel Alloys in Nitric Oxide

Publication costs assisted by Yamaguchi University

*Sir:* We found that nitric oxide (NO) selectively oxidized nickel in a Cu-Ni alloy, so that the structure of the scale formed on the alloy in nitric oxide was different from that formed in oxygen.

Figure 1 shows the oxidation curves of copper and nickel plates in nitric oxide (700°, 10 Torr) and oxygen (700°, 10

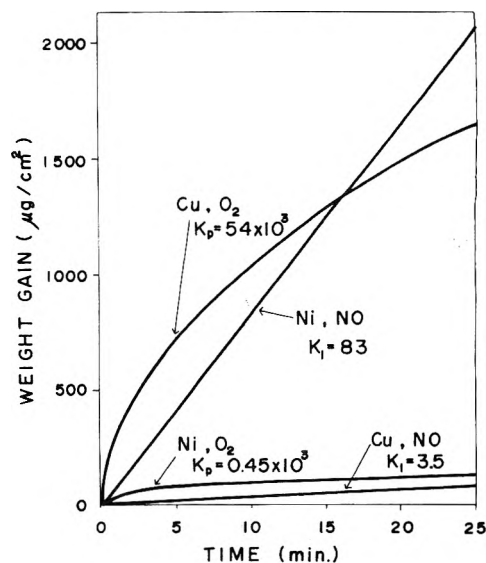


**Figure 1.** Oxidation curves for Cu and Ni at 700° at 10 Torr of nitric oxide or oxygen.  $K_1$  is the rate constant for the linear rate law,  $\mu\text{g}/\text{cm}^2 \text{ min}$ , and  $K_p$  is the rate constant for the parabolic rate law,  $\mu\text{g}^2/\text{cm}^4 \text{ min}$ .

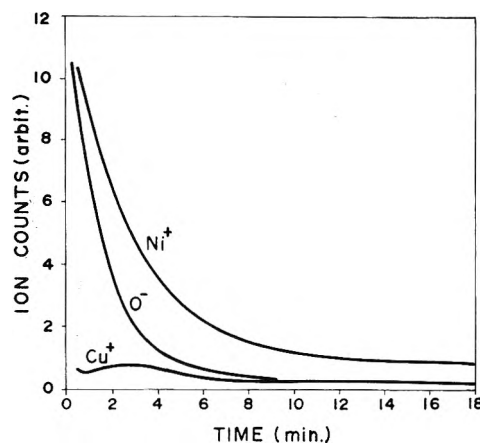


**Figure 2.** IMA spectrum of the scale on Cu-Ni alloy (35% Cu-65% Ni) formed at 700° at 10 Torr of nitric oxide for 20 sec. The abscissa is the sputtering time by argon ions (7 kV for Ni<sup>+</sup> and Cu<sup>+</sup>, 13 kV for O<sup>-</sup>; 0.6  $\mu\text{A}/0.8 \text{ mm}^2$ ).

Torr) that were measured with a microbalance. On oxidation of these metals in nitric oxide, a linear rate law was observed, though a parabolic rate law was observed in oxygen.<sup>1</sup> More remarkable is the fact that the rate of the oxidation of nickel in nitric oxide was much higher than that of copper, while, in oxygen, the rate of the oxidation of nickel was very low compared to that of copper.

These findings suggested that the oxidation of these metals in nitric oxide was related to the chemical reactivity of the surface species of the metals with nitric oxide, while that in oxygen was related to the diffusion behaviors of the metallic ions through the oxide layers.<sup>2</sup> Therefore, nickel should be preferentially oxidized on the oxidation of alloys of these metals in nitric oxide.

Figures 2 and 3 show ion microanalysis (IMA) spectra of the scales on 35% Cu-65% Ni alloys formed in nitric oxide and oxygen, respectively. Then, the abscissa is the sputtering time by argon ions (7 kV for Ni<sup>+</sup> and Cu<sup>+</sup>, 13 kV for



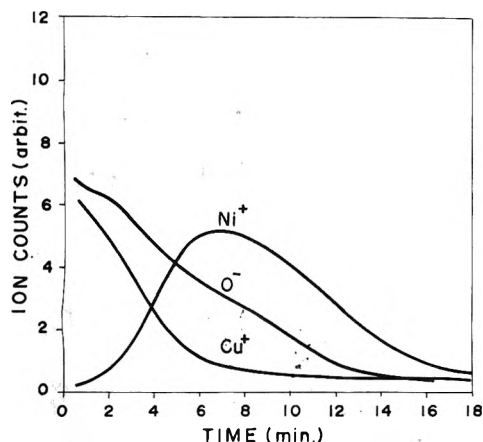


**Figure 3.** IMA spectrum of the scale on Cu-Ni alloy (35% Cu-65% Ni) formed at 700° at 10 Torr of oxygen for 20 sec.

O<sup>-</sup>; 0.6  $\mu$ A/0.8 mm<sup>2</sup>). As seen in Figure 2, the sputtered species almost entirely consisted of Ni<sup>+</sup> and O<sup>-</sup> in the initial stage of the sputtering on the scale by argon ions, and this signified the main component of the scale to be nickel oxide. On the other hand, in Figure 3, the amount of Cu<sup>+</sup> decreased rapidly with increasing sputtering time while that of Ni<sup>+</sup> was found to have a maximum at 7 min after the beginning of the sputtering. The scale formed in oxygen seemed to consist of two distinct layers: i.e., the component of the outer layer was copper oxide and that of the inner was nickel oxide. Then, the IMA spectra showed no evidence of nitrogen in these scales. The evaluations of the structures of the scales by IMA spectra cited above were confirmed by means of X-ray diffraction analysis of the scale formed at 700° at 10 Torr of nitric oxide for 30 min having given only the spectrum of NiO. However, the spectra of CuO and NiO were observed on X-ray diffraction patterns of the scale prepared in oxygen.

Thus, it is remarkable that selective oxidation of nickel occurs in the oxidation of Cu-Ni alloy by nitric oxide.

*Acknowledgment.* The authors wish to thank Mr. Masaharu Eguchi of the Faculty of Engineering, Osaka University, for obtaining the IMA spectra.

#### References and Notes

- (1) Y. Takasu, Y. Matsuda, S. Maru, and N. Hayashi, *Nature (London)*, submitted for publication.
- (2) C. Wagner, *Z. Phys. Chem. B*, **32**, 447 (1936).

Department of Industrial Chemistry  
Faculty of Engineering  
Yamaguchi University  
Tokiwadai, Ube 755  
Yamaguchi, Japan

Yoshio Takasu\*  
Yoshiharu Matsuda  
Shun-ichi Maru  
Nobutoshi Hayashi

Department of Applied Chemistry  
Faculty of Engineering  
Osaka University  
Yamadakami, Suita 565  
Osaka, Japan

Hiroshi Yoneyama  
Hideo Tamura

Received March 28, 1975

#### Absolute Viscosity of D<sub>2</sub><sup>18</sup>O between 15 and 35°

*Sir:* We have recently reported in this Journal<sup>1</sup> values for the absolute viscosity of D<sub>2</sub><sup>18</sup>O between 15 and 35°. The values reported for the pure D<sub>2</sub><sup>18</sup>O were extrapolated from viscosity values determined for our experimental sample, whose composition is given in Table I, sample 1, by applying Eyring's theory of viscosity

$$\eta = (hN/\bar{V}) \exp[\Delta G^\ddagger/RT] \quad (1)$$

where  $\eta$  is the viscosity,  $\bar{V}$  is the molar volume, and  $\Delta G^\ddagger$  is the free energy of activation for viscous flow.

Due to the nature of the isotopic composition of the sample (i.e., the relatively high concentration of H atoms) we were faced with a major difficulty in the analysis of the experimental data. The hydrogen present exists essentially (~90%) in the form of HDO. Our extrapolation procedure requires viscosity and density values corresponding to the pure species of all components present in solution whereas pure HDO does not exist. It exists only in solution and up to a concentration maximum of 50%.

We simplified the analysis by neglecting the presence of the HDO species altogether and assumed that we were involved with a quaternary solution composed of H<sub>2</sub><sup>16</sup>O, H<sub>2</sub><sup>18</sup>O, D<sub>2</sub><sup>16</sup>O, and D<sub>2</sub><sup>18</sup>O. The mole fraction of each species was assumed to be the product of the mole fraction of its components.

The validity of these assumptions was tested for a binary solution, i.e., the viscosities of H<sub>2</sub><sup>16</sup>O-D<sub>2</sub><sup>16</sup>O mixtures were calculated and compared to the experimental values available (cf. ref 1, Table V).

We have lately been able to obtain a sample with much higher concentrations of deuterium and oxygen-18, as shown in Table I, sample 3. This enabled us to test the validity of the extrapolation technique and assumptions involved when applied to a "quaternary solution".

The isotopic analysis and the viscosity measurements of the highly enriched D<sub>2</sub><sup>18</sup>O sample 3 were performed using the identical apparatus as before.<sup>1</sup> The viscosity values were extrapolated in the same manner to obtain those for pure D<sub>2</sub><sup>18</sup>O.

The experimental and extrapolated viscosity values are reported in Table II for sample 3 plus those for the two previously reported samples. We have included the data for the least enriched sample 2 to emphasize that the extrapolation is limited by the proximity to 100% purity, i.e., compare  $\Delta\%(3-1) = 0.27$  to  $\Delta\%(3-2) = 1.15$ , where  $\Delta\%(3-i)$  is the average difference between the extrapolated values

**TABLE I: Isotopic Compositions of D<sub>2</sub><sup>18</sup>O Samples**

Sample	% D	% H	% <sup>16</sup> O	% <sup>17</sup> O	% <sup>18</sup> O
1	95.94	4.06	4.711	0.462	94.827
2	93.59	6.41	7.067	0.377	92.556
3	99.50	0.50	1.360	0.396	98.244

TABLE II: Viscosity of D<sub>2</sub><sup>18</sup>O (cP)

t, °C	$\eta_{\text{D}_2^{18}\text{O}}$			100% $\eta_{\text{D}_2^{18}\text{O}}$			$\Delta\%(3 - 1)$	$\Delta\%(3 - 2)$
	1 <sup>a</sup>	2 <sup>a</sup>	3	1 <sup>a,b</sup>	2 <sup>b</sup>	3		
15	1.4764	1.4732	1.4974	1.5057	1.5358	1.5020	+0.25	+2.25
20	1.2898	1.2797	1.3000	1.3150	1.3205	1.3037	+0.87	+1.29
25	1.1245	1.1250	1.1418	1.1441	1.1591	1.1449	-0.07	+0.87
30	0.9974	0.9945	1.0124	1.0140	1.0223	1.0150	-0.10	+0.72
35	0.8929	0.8897	0.9055	0.9072	0.9136	0.9078	-0.07	+0.64

<sup>a</sup> Reference 1. <sup>b</sup> 100% D<sub>2</sub><sup>18</sup>O calculated by extrapolating experimental data by means of Eyring's theory of viscosity.

based upon sample 3 and samples 1 and 2 respectively (cf. Table II, columns 8 and 9). We believe that the agreement between the extrapolated values for samples 1 and 3 justifies the assumptions involved in our extrapolation procedure.

#### References and Notes

(1) A. I. Kudish and D. Wolf, *J. Phys. Chem.*, **79**, 272 (1975).

Isotope Department  
The Weizmann Institute of Science  
Rehovot, Israel

D. Wolf  
A. I. Kudish\*

Received March 14, 1975

# PHYSICAL PHENOMENA

spectroscopy,  
thermodynamics,  
reaction kinetics,  
and other areas  
of experimental  
and theoretical  
physical chemistry  
are covered  
completely in

## THE JOURNAL OF PHYSICAL CHEMISTRY

The biweekly JOURNAL OF PHYSICAL CHEMISTRY includes over 25 papers an issue of original research by many of the world's leading physical chemists. Articles, communications, and symposia cover new concepts, techniques, and interpretations. A "must" for those working in the field or interested in it, the JOURNAL OF PHYSICAL CHEMISTRY is essential for keeping current on this fast moving discipline. Complete and mail the coupon now to start your subscription to this important publication.

### The Journal of Physical Chemistry American Chemical Society

1155 Sixteenth Street, N.W.  
Washington, D.C. 20036

1975

Yes, I would like to receive the JOURNAL OF PHYSICAL CHEMISTRY at the one-year rate checked below:

	U.S.	Canada**	Latin America**	Other Nations**
ACS Member One-Year Rate*	<input type="checkbox"/> \$20.00	<input type="checkbox"/> \$24.50	<input type="checkbox"/> \$24.50	<input type="checkbox"/> \$25.00
Nonmember	<input type="checkbox"/> \$80.00	<input type="checkbox"/> \$84.50	<input type="checkbox"/> \$84.50	<input type="checkbox"/> \$85.00
Bill me <input type="checkbox"/>	Bill company <input type="checkbox"/>	Payment enclosed <input type="checkbox"/>		

*Air freight rates available on request*

Name \_\_\_\_\_

Street \_\_\_\_\_

Home   
Business

City \_\_\_\_\_

State \_\_\_\_\_

Zip \_\_\_\_\_

Journal subscriptions start on January '75

\*NOTE: Subscriptions at ACS member rates are for personal use only. \*\*Payment must be made in U.S. currency, by international money order, UNESCO coupons, U.S. bank draft, or order through your book dealer.

# RADIONUCLIDES IN THE ENVIRONMENT

## ADVANCES IN CHEMISTRY SERIES NO. 93

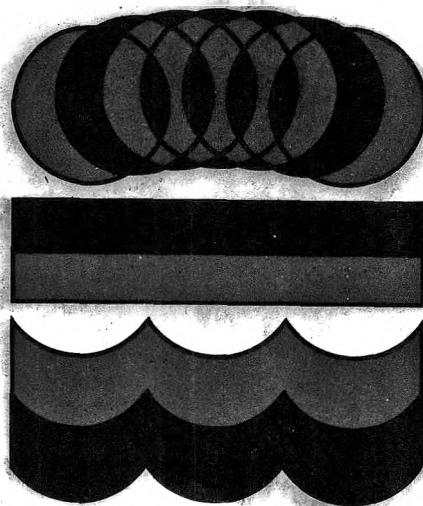
Twenty-eight papers from a symposium sponsored by the Division of Nuclear Chemistry and Technology, chaired by E. C. Freiling.

Pollution . . . a growing concern . . . a concept not generally associated with radionuclides. The successful control of this hazardous waste product of nuclear energy is essential to the continued use and development of nuclear power. Critical to this problem is an understanding of the processes by which radionuclides are produced, dispersed, and retained in the environment.

The papers in this volume discuss and evaluate the properties and problems relating to radionuclides, including

- mechanisms of release, absorption, uptake, transport
- behavior, measurement and characterization, specific weapons tests
- specific activity, public health aspects, fallout
- new methods and equipment

522 pages with index Clothbound (1968) \$15.00  
Set of L.C. cards with library orders upon request.



Other books in the ADVANCES IN CHEMISTRY SERIES OF related interest include:

No. 89 Isotope Effects in Chemical Processes. Methods of separating isotopes and labeled molecules—chemical exchange, electromigration, photochemical processes, and distillation—are examined, along with factors that suit a process to isotope separation—single stage fractionation, exchange rate, and reflux.  
278 pages cloth (1969) \$13.00

No. 82 Radiation Chemistry—II. Thirty-six papers and 17 abstracts on radiation chemistry in gases, solids, and organic liquids. Includes three plenary lectures. 558 pages cloth (1968) \$16.00

No. 81 Radiation Chemistry—I. Forty-one papers and 17 abstracts on radiation chemistry in aqueous media, biology, and dosimetry. From the international conference at Argonne National Laboratory. 616 pages cloth (1968) \$16.00. No. 81 and 82 ordered together \$30.00

No. 72 Mass Spectrometry in Inorganic Chemistry. A basic tool for chemical manipulations, the mass spectrometer is a conventional monitor for any stage in a research problem to help establish what is going on. 21 Research reports. 329 pages cloth (1968) \$12.00

No. 68 The Mössbauer Effect and Its Application in Chemistry. Ten papers that will familiarize chemists with Mössbauer spectroscopy as an analytical tool for studying chemical bonding, crystal structure, electron density, magnetism, and other properties.  
178 pages cloth (1967) \$8.00

No. 66 Irradiation of Polymers. Eighteen papers survey radiation mechanics in polymers, the chemical nature of reactive species produced, crosslinking and scission, homopolymerization, graft copolymerization, and the effects of ultraviolet light radiation.  
275 pages cloth (1967) \$10.00

No. 58 Ion-Molecule Reactions in the Gas Phase. Eighteen papers survey spectrometric and other methods for producing and studying ion-molecule reactions such as pulsed sources for studying thermal ions, reactions in flames and electrical discharges.  
336 pages cloth (1966) \$10.50

No. 50 Solvated Electron. Reviews of theory, structure, reactions of solvated and hydrated electrons; detailed papers on electrical transport properties, photochemistry, theory of electron transfer reactions, structure of solvated electrons, hydrated electron research. 304 pages cloth (1965) \$10.50

Postpaid in U. S. and Canada; plus 30 cents elsewhere.

Order from:

**SPECIAL ISSUES SALES  
AMERICAN CHEMICAL SOCIETY  
1155 SIXTEENTH ST., N.W.  
WASHINGTON, D. C. 20036**